Isotopes in Hydrology, Marine Ecosystems and Climate Change Studies

Proceedings of an International Symposium, Monaco, 27 March–1 April 2011

Vol. 1

Organized by the
International Atomic Energy Agency

Hosted by
the Principality of Monaco

ISOTOPES IN HYDROLOGY,
MARINE ECOSYSTEMS AND
CLIMATE CHANGE STUDIES

VOLUME 1

The following States are Members of the International Atomic Energy Agency:

AFGHANISTAN
ALBANIA
ALGERIA
ANGOLA
ARGENTINA
ARMENIA
AUSTRALIA
AUSTRIA
AZERBAIJAN
BAHRAIN
BANGLADESH
BELARUS
BELGIUM
BELIZE
BENIN
BOLIVIA
BOSNIA AND HERZEGOVINA
BOTSWANA
BRAZIL
BULGARIA
BURKINA FASO
BURUNDI
CAMBODIA
CAMEROON
CANADA
CENTRAL AFRICAN
  REPUBLIC
CHAD
CHILE
CHINA
COLOMBIA
CONGO
COSTA RICA
CÔTE D'IVOIRE
CROATIA
CUBA
CYPRUS
CZECH REPUBLIC
DEMOCRATIC REPUBLIC
  OF THE CONGO
DENMARK
DOMINICA
DOMINICAN REPUBLIC
ECUADOR
EGYPT
EL SALVADOR
ERITREA
ESTONIA
ETHIOPIA
FIJI
FINLAND
FRANCE
GABON
GEORGIA
GERMANY
GHANA
GREECE

GUATEMALA
HAITI
HOLY SEE
HONDURAS
HUNGARY
ICELAND
INDIA
INDONESIA
IRAN, ISLAMIC REPUBLIC OF
IRAQ
IRELAND
ISRAEL
ITALY
JAMAICA
JAPAN
JORDAN
KAZAKHSTAN
KENYA
KOREA, REPUBLIC OF
KUWAIT
KYRGYZSTAN
LAO PEOPLE'S DEMOCRATIC
  REPUBLIC
LATVIA
LEBANON
LESOTHO
LIBERIA
LIBYA
LIECHTENSTEIN
LITHUANIA
LUXEMBOURG
MADAGASCAR
MALAWI
MALAYSIA
MALI
MALTA
MARSHALL ISLANDS
MAURITANIA
MAURITIUS
MEXICO
MONACO
MONGOLIA
MONTENEGRO
MOROCCO
MOZAMBIQUE
MYANMAR
NAMIBIA
NEPAL
NETHERLANDS
NEW ZEALAND
NICARAGUA
NIGER
NIGERIA
NORWAY
OMAN
PAKISTAN
PALAU

PANAMA
PAPUA NEW GUINEA
PARAGUAY
PERU
PHILIPPINES
POLAND
PORTUGAL
QATAR
REPUBLIC OF MOLDOVA
ROMANIA
RUSSIAN FEDERATION
RWANDA
SAUDI ARABIA
SENEGAL
SERBIA
SEYCHELLES
SIERRA LEONE
SINGAPORE
SLOVAKIA
SLOVENIA
SOUTH AFRICA
SPAIN
SRI LANKA
SUDAN
SWAZILAND
SWEDEN
SWITZERLAND
SYRIAN ARAB REPUBLIC
TAJIKISTAN
THAILAND
THE FORMER YUGOSLAV
  REPUBLIC OF MACEDONIA
TOGO
TRINIDAD AND TOBAGO
TUNISIA
TURKEY
UGANDA
UKRAINE
UNITED ARAB EMIRATES
UNITED KINGDOM OF
  GREAT BRITAIN AND
  NORTHERN IRELAND
UNITED REPUBLIC
  OF TANZANIA
UNITED STATES OF AMERICA
URUGUAY
UZBEKISTAN
VENEZUELA
VIETNAM
YEMEN
ZAMBIA
ZIMBABWE

The Agency's Statute was approved on 23 October 1956 by the Conference on the Statute of the IAEA held at United Nations Headquarters, New York; it entered into force on 29 July 1957. The Headquarters of the Agency are situated in Vienna. Its principal objective is "to accelerate and enlarge the contribution of atomic energy to peace, health and prosperity throughout the world".

PROCEEDINGS SERIES

ISOTOPES IN HYDROLOGY, MARINE ECOSYSTEMS AND CLIMATE CHANGE STUDIES

PROCEEDINGS OF THE INTERNATIONAL SYMPOSIUM
HELD IN MONACO,
27 MARCH–1 APRIL 2011

In two volumes

VOLUME 1

INTERNATIONAL ATOMIC ENERGY AGENCY
VIENNA, 2013

COPYRIGHT NOTICE

All IAEA scientific and technical publications are protected by the terms of the Universal Copyright Convention as adopted in 1952 (Berne) and as revised in 1972 (Paris). The copyright has since been extended by the World Intellectual Property Organization (Geneva) to include electronic and virtual intellectual property. Permission to use whole or parts of texts contained in IAEA publications in printed or electronic form must be obtained and is usually subject to royalty agreements. Proposals for non-commercial reproductions and translations are welcomed and considered on a case-by-case basis. Enquiries should be addressed to the IAEA Publishing Section at:

Marketing and Sales Unit, Publishing Section
International Atomic Energy Agency
Vienna International Centre
PO Box 100
1400 Vienna, Austria
fax: +43 1 2600 29302
tel.: +43 1 2600 22417
email: sales.publications@iaea.org
http://www.iaea.org/books

FOREWORD

Humanity is facing many water related challenges, including access to safe water, pollution of continental and coastal waters and ocean acidification, as well as the growing impact of climate change on the hydrological cycle. Many countries are confronted by increasingly stressed water resources due to rapidly growing populations, increasing agricultural and energy production demands, industrial development, and pollution. The greatest issues of the 21st century, including competition for resources and possible related conflicts, may well focus on the role of water in food and energy security.

For more than 50 years, the IAEA has played a key role in advancing and promoting the development and use of isotope techniques to address global environmental issues, such as water resources assessment and management, the study of marine ecosystems, and more recently the impact of climate change. This symposium was jointly organized by the Water Resources Programme and IAEA Environment Laboratories to commemorate the 50th anniversary of the establishment of the IAEA laboratory in the Principality of Monaco, and represented the 13th edition of the quadrennial symposium on isotope hydrology and water resources management, which has been regularly organized by the IAEA since 1963.

The main objectives of the symposium were to review the state of the art in isotope hydrology, the use of isotopes in the study of climatic systems and in marine ecosystems and to outline recent developments in the application of isotope techniques, as well as to identify future trends and developments for research and applications. The contributions submitted by the authors are included in two volumes of proceedings with editorial corrections. These proceedings are intended to serve as an aid for those using isotopes for applied problems in hydrology as well as for the research community.

The IAEA officers responsible for this publication were H. Nies of the IAEA Environment Laboratories and B. Newman and L. Araguas of the Department of Nuclear Sciences and Applications.

CONTENTS

SYMPOSIUM SUMMARY

The International Symposium on Isotopes in Hydrology, Marine Ecosystems and Climate Change Studies was held from 27 March to 1 April 2011 in the Principality of Monaco. The symposium was jointly organized by the IAEA Water Resources Programme and the Environment Programme. The symposium was held at the Oceanographic Museum of Monaco to commemorate the 50th anniversary of the establishment of the IAEA Laboratory in the Principality of Monaco. The Symposium also represented the 13th edition of the quadrennial symposium on isotope hydrology and water resources management, which has been regularly organized by the IAEA since 1963.

The symposium attracted 278 participants and observers from 67 Member States, covering aspects related to the use and application of isotope tools to address a broad spectrum of scientific disciplines through invited talks, oral and poster presentations, and workshops. Participants from developing countries were well represented with 120 attending. There were 49 oral presentations in the morning sessions and workshops, and 142 posters were presented. Brent Newman and Luis Araguas from the IAEA Water Resources Programme and Hartmut Nies from the IAEA Marine Environment Laboratory in Monaco were the symposium scientific secretaries.

The symposium was formally opened by H.S.H Prince Albert II of Monaco, followed by an invited talk on the interaction between the science and politics of climate change by Hartmut Grassl. Afterwards participants were able to enjoy the unique venue of the museum during the evening reception.

The symposium addressed five major topics through invited talks and oral presentations during the morning sessions and poster sessions and dedicated workshops during the afternoon sessions. On Monday, the first topic addressed was the role of isotopes in understanding and modelling climate change. Oral and poster sessions explored a variety of climate related issues including paleoclimate reconstruction using groundwater and other proxies, and understanding impacts of anthropogenic activities using various isotope approaches. The poster session also included a theme on isotope hydrology where a large number of posters focused on the use of isotopes in understanding atmospheric moisture and precipitation, including isotope monitoring networks such as the IAEA Global Network of Isotopes in Precipitation (GNIP). Many isotope applications for surface water studies and water quality problems were also presented.

On Tuesday the symposium continued with a climate related theme, but was focused on isotope related aspects of carbon sequestration and carbon cycling. Interesting talks were presented on the challenges of monitoring deep geological sequestration of carbon dioxide as well as carbon cycling in groundwater and the oceans. The themes of the afternoon poster session were on analytical methods for isotope measurements and a second isotope hydrology session which had a focus on

isotope applications to flow and transport modelling as well as general groundwater studies. Methods posters discussed new developments for measuring isotopes such as argon-39 as well as ways to improve isotope measurement accuracy.

Wednesday was dedicated to isotopes and radionuclides in the marine environment where a wide variety of marine related isotope techniques and applications were presented. Isotope and radionuclide studies were used for source identification of pollutants and investigation of marine processes. The very long lived I-129, released by the European nuclear industry, was used for very wide range studies of ocean circulation and dispersion from European seas to Arctic areas. Investigations on coastal pollution areas applying both natural and artificial radionuclides were presented as a tool for the reconstruction of pollution history. A special workshop was held in the afternoon covering radionuclides in the southern hemisphere, where more data gaps occur than in other parts of the world ocean. The poster session completed the wide range of applications of isotopes and radionuclides for marine and radioecological studies.

Thursday was dedicated to hydrology and the morning session included a series of stimulating talks on groundwater assessments using satellite remote sensing and noble gases. Groundwater assessment case studies were also presented for studies in Brazil, the Democratic Republic of the Congo, Tunisia, and Turkey. The afternoon session was dedicated to a workshop on new frontiers and future directions in isotope hydrology. This session had a unique format in that a series of experts led guided discussions with conference participants on four topics.

The first workshop topic was on isotope monitoring networks and isotope mapping and George Darling led the discussion which considered the value of isotope networks and issues related to expanding and maintaining monitoring stations. Another important aspect of this topic was the increasing use of and need for isotope mapping from basin to global scales. It was clear that isotope monitoring networks and related databases such as those associated with GNIP and Global Network of Isotopes in Rivers (GNIR) are increasingly useful for a variety of applications. However, important areas lack sufficient station coverage and it was suggested that more monitoring stations are especially needed in parts of Africa, Asia, and Australia. Because running monitoring stations is voluntary, participants were encouraged to contact the IAEA Water Resources Programme to inform them of whether they can establish new precipitation or river monitoring stations in their areas. The generation of isotope maps using GIS interpolation methods was noted as a positive step for interpreting isotope data and presenting results to stakeholders. However, measurement gaps can cause large uncertainties for some regions or locations on isotope interpolation maps. Thus in addition to reducing gaps, the isotope hydrology community should strive to make map users more aware about the limitations of using interpolated data to make interpretations.

The second topic involved analytical developments and was led by Roland Purchert. New technologies and methodological improvements have been substantial.

For example, the rapid adoption of laser absorption based stable isotope analysers, satellite imaging for isotopes, and improved sampling methods for noble gases are facilitating the collection of more and better isotope data around the world. Much of the initial discussion involved issues related to new and emerging analytical methods for collecting and measuring noble gases. It was clear that argon and krypton isotopes have great potential if progress on analytical and sampling methods continues to be made. It was also noted that the IAEA can play an important role for making access to noble gas analyses (including tritium/helium-3) available to Member States. The topic finished with a discussion of the value of isotope analysers robust enough for use in the field. Laser absorption based stable isotope analysers are starting to be used in the field and the possibility to analyse for nitrogen-15 in the near future is also a welcome development. Other portable analysers such as radon-222 systems can now be used effectively to map groundwater discharges in the field.

The third topic was hydrological residence times and the discussion was led by Jay Famiglietti. Quantifying the residence time of water in a system is key for understanding the sustainability of groundwater resources and for understanding the fate of pollutants in hydrological systems. One issue of concern brought up is that many applications use a steady state assumption, however, pumping, for example, can create a situation where transient behaviour can be important. Another issue is that there has historically been a great deal of focus on determining the mean residence time, but there needs to be more focus on estimating the residence time distribution. This idea brought up the question of whether studies typically sample enough to be able to determine the distribution. As a final comment it was noted that despite their complications isotope tracer methods for estimating residence times and residence time distributions have distinct advantages over conventional hydraulic approaches and can be a very effective way of testing and constraining numerical flow and transport models.

The fourth topic was on groundwater assessments and was led by Niel Sturchio. The discussion started off with a talking point on what kind of information might be needed when starting an assessment of an aquifer about which little is known. For an initial reconnaissance it was suggested that deuterium, oxygen-18, and carbon-14 and/or tritium would be a good starting point for the isotope component of a sampling plan. It was emphasized that building and testing hydrological conceptual models is an important aspect for developing sampling plans and to identify which kinds of isotopes and which sampling locations may be the best for the initial and subsequent assessments. Numerical models can also be used effectively as part of conceptual model development. From the discussion it was clear that properly planning an initial groundwater assessment is important to efficiently develop an understanding of the system and to decide on what the best applications for future investigation might be. Such an approach provides the most useful information to water managers who need to make decisions about how to address their specific water resource concerns.

The symposium concluded on Friday morning with a series of talks on analytical methods and instrumentation. The session covered topics related to krypton-81 dating, novel cosmogenic radionuclides such as sodium-22, as well as other radionuclide methods. The talks were followed by a ceremony where five young scientists (Vasileios Salamalkis, Fria Hadj Ammar, Wen Yu, Joachim Welte, and Helene Delattre) were presented awards and bottles of champagne for their outstanding posters. The conference was then adjourned after closing comments by the Manager of the Water Resources Programme, Pradeep Aggarwal and Maria Betti, the Director of the IAEA Environment Laboratory.

In general, presentations by participants throughout the symposium illustrated the contributions of isotope tools in addressing many pressing issues in Member States regarding the need to conduct more sound assessments of water resources which will help meet sustainable management goals. In addition, it was clear that isotopes have a major role to play in understanding marine and terrestrial environments, climate change and for evaluating mitigation strategies such as carbon sequestration.

CONCLUSION

The symposium constituted an excellent opportunity to review the current status and recent developments in the application of nuclear and isotope tools in the study of the water cycle, climate change, and marine systems. The symposium brought together experts and counterparts with a wide range of expertise compared to other similar meetings and this aspect was appreciated by many of the participants.

ROLE OF ISOTOPES IN UNDERSTANDING AND
MODELLING CLIMATE CHANGE, MARINE
ECOSYSTEMS AND WATER CYCLES

A TEMPERATURE AND MONSOON RECORD DERIVED FROM ENVIRONMENTAL TRACERS IN THE GROUNDWATER OF NORTHWEST INDIA

M. WIESER, W. AESCHBACH-HERTIG, T. SCHNEIDER
Institute of Environmental Physics,
University of Heidelberg,
Heidelberg, Germany

R.D. DESHPANDE, S.K. GUPTA
Physical Research Laboratory,
Ahmedabad, India

Abstract

A quantitative palaeoclimate record was derived from the aquifer system of the Cambay Basin, Gujarat, India, a region characterised by a semi arid, monsoon dominated climate. Stable isotopes generally increase with flow distance and ^{14}C age, whereas noble gas temperatures (NGTs) show a decline with age, amounting to a difference of ~3.5°C between Holocene and last glacial samples. The paper focuses on the Holocene covariation of the climate proxies. Stable isotopes and excess air show consistent variations, confirming their interpretation as proxies for palaeohumidity. A group of early to mid Holocene samples depleted in stable isotopes and enriched in excess air indicates a phase of strong monsoon during the Holocene Climate Optimum. This is followed by a drying trend in the second half of the Holocene, and more humid conditions in the youngest part of the record. A temporary rise of NGT in the dry late Holocene may reflect a change in the soil temperature–air temperature relationship.

1. INTRODUCTION AND STUDY AREA

The monsoonal climates of Asia, e.g. the Indian summer monsoon, affect the livelihoods of billions of people and are therefore a focus of climate research. Many palaeoclimatic studies have detected a connection between northern hemisphere insolation and the intensity of the Indian summer monsoon [1], as the ITCZ is forced further towards the north with stronger insolation (e.g. Ref. [2]). Implications of such relationships for the future may be a strengthening of the monsoon as a result of global warming.

Our study region in the Cambay Basin, northern Gujarat, India, is semi arid and receives most of its precipitation from the Indian summer monsoon. Besides the monsoon months, precipitation in Gujarat originates only from isolated thunderstorm

events. Most rainfall takes place in the eastern highlands of the Cambay Basin, feeding a sedimentary aquifer system in which flow is directed towards the southwest. The sediments filling the basin descend from both fluvial and aeolian origin, the youngest layers being of Quaternary age. These young sediments have a thickness ranging from 300 to 800 m in their deeper parts [3]. Shallow aquifers in most of the region have dried up due to exploitation of the groundwater over several decades, and deeper aquifers have a greater salt content due to rock–water interaction. The geographical distribution of the chemical and isotopic properties of groundwater is reported to be related to past climate change, the topography and the tectonic framework of the study area.

The palaeoclimate of India has been described by numerous studies. In late Pleistocene times from 30 to 50 kyr BP, dune and alluvial deposits [4] near the project location indicate an enhanced monsoon that declined around peak glacial times. In the Last Glacial Maximum (LGM), little precipitation and arid conditions are indicated, as the alluvial deposits from flood plain aggradation make room for aeolian deposits. Stalagmite data support these discoveries [5, 6]. After the end of the LGM, a strong monsoon phase occurred in the early Holocene and left marks in lake [7] and river [4] sediments and their isotopic condition. Stalagmites in Oman [2, 8] China [6] and India [9] with stable isotope data also show enhanced precipitation, which is also predicted by model simulations [10]. In all these different studies, the climate optimum ranges between 10 to 12 and 5 to 8 kyr BP.

Temperature information is not provided by isotopic data in this subtropic region, where the amount effect dominates stable isotope signals [2, 11]. Noble gas temperatures (NGTs) can provide quantitative temperature information, but only few such records are available for Asia. The most adjacent studies of this type were conducted in Oman, indicating a present–LGM temperature change of 6.5°C [12] and in China with a result of 4.5°C [13] also indicating an enhanced monsoon during the early Holocene.

The wet phase is superseded by a weakening of the monsoon which set in gradually [8]. Desiccated lakes [7] and piston core data from the Arabian Sea as well as a change in vegetation and civilisation indicate this dry period with events of drought. A noble gas study from Niger [14] also provided evidence for this dry phase in the late Holocene. Several records place this time period from around 5 to 8 until 1 to 2 kyr BP. According to some records, the recent time shows more fluctuation [11] with dry phases around 1 to 2 kyr BP and a wet phase which started in about 600 year BP. The most recent increase of monsoon precipitation may among other reasons result from global warming [15].

2.   METHODS

From 2008 to 2010, three sampling campaigns along two different transects through the aquifer system of the north Cambay Basin took place (Fig. 1).

The transects running from the northeast towards the southwest follow the flow direction and slope of the basin, beginning with very shallow wells in the recharge area, where the aquifer is still unconfined and infiltration takes place, and ending with deep wells in the confined aquifer.

Parameters analysed directly in the field were water temperature, specific conductivity, alkalinity, dissolved oxygen and pH. Stable isotopes and tritium were sampled in small glass bottles. The analysis of stable water isotopes was performed on a MAT 252 Finnigan mass spectrometer and tritium was analysed radiometrically, both at the University of Heidelberg. ^{14}C samples were taken in glass bottles and poisoned to avoid biological alteration. In the lab, dissolved carbon was extracted as CO_2 and converted to graphite, which was analysed by AMS at ETH Zurich. For the noble gas samples, a copper tube fit into an aluminium rack was well flushed before being closed with steel clamps on either end. The samples were analysed on a GV 5400 noble gas mass spectrometer in Heidelberg. In this system, noble gases
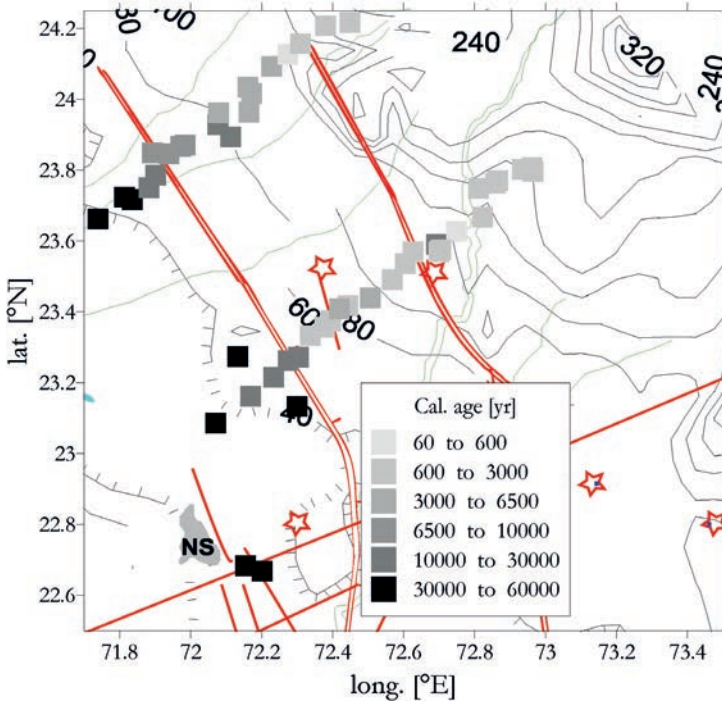
FIG. 1. Map of the study area showing the positions of the sampled wells along two transects. The ^{14}C age of the water is indicated by the shading of the symbols. It increases progressively from the recharge area in the northeast towards the confined parts of the aquifer in the southwest. Thin lines indicate isolines of hydraulic head, bold lines outline tectonic faults, in particular the east and west Cambay Basin Bounding Faults (double lines) running NW–SE, perpendicular to groundwater flow.

9

are extracted from a sample, collected, cleaned and finally measured successively in the mass spectrometer. Air aliquots are used for calibration.

Gas solubility in water depends on the equilibration temperature. For inert gases, this can be used to identify the infiltration temperature of water masses from past times, as no temporal alteration takes place. Noble gas concentrations extracted from water samples in a confined aquifer, therefore, reflect the water table temperature that prevailed in the recharge area at the time of infiltration. A complication occurs due to the trapping and (partial) dissolution of air bubbles during groundwater infiltration, leading to an excess of dissolved gas concentrations above solubility equilibrium. This so-called excess air component is usually expressed by ΔNe, which is the neon excess in relation to the equilibrium concentration of neon, given in percent: ΔNe (%) $= (Ne_{exc}/Ne_{eq}) \times 100\%$.

Various models to parameterise the excess air component have been proposed [16]. ΔNe is almost independent of the adopted model and depends mainly on the pressure exerted on the bubbles, which in turn is due to increases of the water table. In arid regions, several studies have attributed high excess air signals to a strongly fluctuating water table as a result of strong rain events between periods of aridity [14, 17]. The effect is more pronounced in regions with temporal aridity such as monsoon affected regions, but can also be observed in temperate zones [18]. Therefore, excess air appears to be an interesting climate proxy for changes in the degree of precipitation.

The equilibration temperature (NGT), the amount of excess air and its possible fractionation relative to the composition of atmospheric air are three model parameters, which can be determined by fitting the model to the observed concentrations of the four atmospheric noble gases Ne, Ar, Kr, Xe [19]. Helium is ignored in such calculations, as non-atmospheric components occur.

3.   RESULTS AND DISCUSSION

Groundwater was dated by ^{14}C, taking into account various correction models for the addition of old carbon from the sediments. The final ages were estimated as the mean of selected models, which yielded broadly consistent ages. The main characteristics of the age distributions are displayed in Fig. 1. Firstly and as expected, the ages of the wells increase with increasing distance to the recharge area in the northeast. Secondly, ages increase gradually on the northern transect, while on the southern transect the ages first increase slowly east of the west Cambay Basin Bounding Fault, but increase rather quickly west of it. Ages of all wells in the unconfined region east of the east Cambay Basin Bounding Fault are very young, as indicated by the presence of bomb-derived tritium.

Stable isotopes ratios δ^{18}O and δ^2H show a general increase with age. Higher values of δ^{18}O during the LGM are at least in part attributed to the global ice-volume
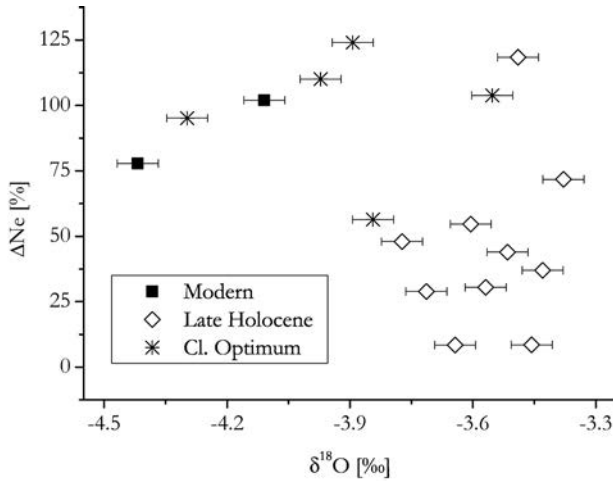
FIG. 2. Excess air (as ΔNe) versus δ^{18}O for Holocene samples. High ΔNe and depleted δ^{18}O both indicate humid conditions in the early Holocene climate optimum as well as in modern times. In contrast, the late Holocene period shows low ΔNe and enriched δ^{18}O, indicating dryer conditions.

effect. In contrast, the variability of δ^{18}O of about 1‰ during the Holocene is probably mostly due to the amount effect, indicating changes in monsoon strength [10]. This interpretation is supported by a comparable pattern of variation in the excess air (ΔNe) signal. The variation of δ^{18}O and ΔNe for the Holocene samples from the confined part of the aquifer (the unconfined area is assumed to be too strongly disturbed by effects of point recharge and pumping) is shown in Fig. 2. Based on the ^{14}C ages and the characteristics of various tracers, three groups of Holocene samples were defined, which are distinguished in this plot: samples from the early Holocene climate optimum, from the following period of the late Holocene, and a few modern samples.

High excess air signals are found in the samples from the climate optimum and the modern period. These samples also show generally lower δ^{18}O values. Both characteristics are indicative of humid conditions, i.e. phases of strong monsoon activity. Stronger precipitation and massive rain events in these times are therefore strongly suggested and agree with numerous palaeoclimate studies of the region. In contrast, the late Holocene group of intermediate age shows generally low excess air amounts and comparatively high δ^{18}O values. Weak monsoon and dry conditions are therefore expected in this period, again confirmed by other studies [7]. The independent humidity proxies provided by the stable isotopes and the noble gases thus confirm the view that a moist phase in the early Holocene was followed by dryer conditions except for the most recent part of the Holocene.

It is interesting to note that a correlation between NGT and ΔNe seems to exist for the Holocene samples (Fig. 3). Contrary to expectations, the warmest NGTs are
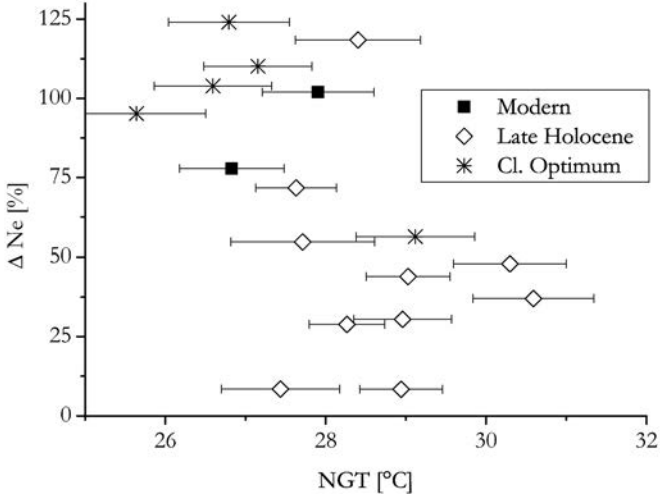
FIG. 3. Excess air (as ΔNe) versus NGT for Holocene samples. Low ΔNe values indicating dry conditions in the late Holocene period coincide with high NGTs, presumably due to a relative enhancement of soil temperatures compared to air temperatures in dry phases.

not found in the climate optimum or modern times, but during the dry late Holocene epoch. The NGTs of the late Holocene group (28.7°C on average) are somewhat higher than the present-day mean annual air temperature (MAAT) of Ahmedabad of 27.5°C. In contrast, the NGTs obtained for the two more humid Holocene phases are in good agreement with modern MAAT. We interpret the variation of NGT between the Holocene groups as a change in soil temperature rather than air temperature. The noble gas thermometer directly reflects the soil temperature at the water table, which is in general close to MAAT. However, in dry periods such as the late Holocene in our study area, soil temperatures may be significantly higher than air temperatures, producing an offset in the relationship between NGT and MAAT.

The same effect of enhanced soil and thus noble gas temperatures relative to air temperature in dry periods has been found before in a study in Niger [14]. It was explained by reduced vegetation in dry periods exposing the soil to radiative heating. That study also found a concurrent relationship between $\delta^{18}O$ and ΔNe, identifying the dry and humid phases. We conclude from these results that in warm semi arid regions such as the Sahel zone and north Gujarat, India, NGT is a good proxy for air temperature only in comparatively wet periods. In dry phases, NGT is enhanced compared to MAAT.

This result has to be taken into account in the estimation of temperature changes between the last glacial period and the Holocene from noble gas data. Based on $\delta^{18}O$ and ΔNe data, we find that the LGM in our study area was a rather dry phase, consistent with other climate records. Therefore, the NGT for this period should be

compared to the warmest NGTs from the dry late Holocene phase in order to avoid offsets due to changes in the air–soil temperature relationship. This comparison results in an estimate for the difference in mean annual air temperature between the Holocene and the last glacial period of 3.5 ± 0.5°C.

A slightly higher temperature change of 4.5°C has been observed in northeastern China [13]. As shown by palaeotemperature studies in different latitudes [16] temperature change between Holocene and the LGM was more pronounced at higher latitudes. Our result for northwest India fits into this pattern. It is, however, contradictory to a groundwater study from Oman, which suggested a temperature change between modern times and the LGM of 6.5°C [12] at a location relatively close to the present study site. It may be crucial for groundwater studies in tropical arid regions to take changes of the air–soil temperature relationship due to changing humidity into account.

REFERENCES

[1]   KUTZBACH, J.E., Monsoon Climate of the Early Holocene: Climate Experiment with the Earth's Orbital Parameters for 9000 Years Ago, Science **214** (1981) 59–61.

[2]   FLEITMANN, D., BURNS, S.J., MANGINI, A., MUDELSEE, M., KRAMERS, J., VILLA, I., NEFF, U., AL-SUBBARY, A.A., BUETTNER, A., HIPPLER, D., MATTER, A., Holocene ITCZ and Indian monsoon dynamics recorded in stalagmites from Oman and Yemen (Socotra), Quat. Sci. Rev. **26** (2007) 170–188.

[3]   DESHPANDE, R.D., Groundwater in and Around Cambay Basin, Gujarat: Some Geochemical and Isotopic Investigations, PhD Thesis, Physical Research Laboratory, Ahmedabad (2006).

[4]   JUYAL, N., CHAMYAL, L.S., BHANDARI, S., BHUSHAN, R., SINGHVI, A.K., Continental record of the southwest monsoon during the last 130 ka: evidence from the southern margin of the Thar Desert, India. Quat. Sci. Rev. **25** (2006) 2632–2650.

[5]   FLEITMANN, D., BURNS, S.J., NEFF, U., MANGINI, A., MATTER, A., Changing moisture sources over the last 330 000 years in Northern Oman from fluid-inclusion evidence in speleothems, Quatern. Res. **60** (2003) 223–232.

[6]   WANG, Y., CHENG, H., EDWARDS, L., KONG, X., SHAO, X., CHEN, S., WU, J., JIANG, X., WANG, X., AN, Z., Millennial- and orbital-scale changes in the East Asian monsoon over the past 224 000 years, Nature **451** (2008) 1090–1093.

[7]   ENZEL, Y., ELY, L.L., MISHRA, S., RAMESH, R., AMIT, R., LAZAR, B., RAJAGURU, S.N., BAKER, V.R., SANDLER, A., High-Resolution Holocene Environmental Changes in the Thar Desert, Northwestern India, Science **284** (1999) 125–128.

[8]   FLEITMANN, D., BURNS, S.J., MUDELSEE, M., NEFF, U., KRAMERS, J., MANGINI, A., MATTER, A., Holocene Forcing of the Indian Monsoon Recorded in a Stalagmite from Southern Oman, Science **300** (2003) 1737–1739.

[9]   RAMESH, R., High resolution Holocene monsoon records from different proxies: An assessment of their consistency, Current Science **81** (2001) 1432–1436.

[10] LEE, J.-E., SWANN, A.L., Evaluation of the "amount effect" at speleothem sites in the Asian monsoon region, Earth Environ. Sci. **9** (2010).

[11] YADAVA, M.G., RAMESH, R., Monsoon reconstruction from radiocarbon dated tropical Indian speleothems, Holocene **15** (2005) 48–59.

[12] WEYHENMEYER, C.E., BURNS, S.J., WABER, H.N., AESCHBACH-HERTIG, W., KIPFER, R, LOOSLI, H.H., MATTER, A., Cool glacial temperatures and changes in moisture source recorded in Oman groundwaters, Science **287** (2000) 842–845.

[13] KREUZER, A. M., VON ROHDEN, C., FRIEDRICH, R., CHEN, Z.Y., SHI, J.S., HAJDAS, I., KIPFER R., AESCHBACH-HERTIG, W., A record of temperature and monsoon intensity over the past 40 kyr from groundwater in the North China Plain, Chem. Geol. **259** (2009) 168–180.

[14] BEYERLE, U., RUEEDI, J., LEUENBERGER, M., AESCHBACH-HERTIG, W., PEETERS, F., KIPFER, R., DODO A., Evidence for periods of wetter and cooler climate in the Sahel between 6 and 40 kyr BP derived from groundwater, Geophys. Res. Lett. **30** (2003) 1173.

[15] ANDERSON, D.M., OVERPECK, J.T., GUPTA, A.K., Increase in the Asian Southwest Monsoon During the Past Four Centuries, Science **297** (2002) 596–599.

[16] KIPFER, R., AESCHBACH-HERTIG, W., PEETERS, F,. STUTE, M., "Noble gases in lakes and ground waters", Noble gases in geochemistry and cosmochemistry (PORCELLI, D., BALLENTINE, C., WIELER, R., eds), Mineralogical Society of America, Geochemical Society. Washington, DC, Rev. Mineral. Geochem. **47** (2002) 615–700.

[17] AESCHBACH-HERTIG, W., BEYERLE, U., HOLOCHER, J., PEETERS, F., KIPFER, R., "Excess air in groundwater as a potential indicator of past environmental changes", Study of Environmental Change Using Isotope Techniques (Proc. Int. Conf. Vienna), 2001, IAEA, Vienna (2002).

[18] INGRAM, R.G.S., HISCOCK, K.M., DENNIS, P.F., Noble gas excess air applied to distinguish groundwater recharge conditions, Environ. Sci. Technol. **41** (2007) 1949–1955.

[19] AESCHBACH-HERTIG, W., PEETERS, F., BEYERLE, U., KIPFER, R., Interpretation of dissolved atmospheric noble gases in natural waters, Water Resour. Res. **35** (1999) 2779–2792.

LATE PLEISTOCENE VEGETATION, CLIMATE AND RELATIVE SEA LEVEL CHANGES IN THE SOUTHEASTERN BRAZILIAN COAST, BASED ON C AND N ISOTOPES AND BIO INDICATOR ANALYSIS OF MANGROVE ORGANIC MATTER

L.C.R. PESSENDA[a], E. VIDOTTO[a], A.A. BUSO JR[a], J. PASSARINI JR[a],
P.E. DE OLIVEIRA[b], F. MACIAS[c], F. RICARDI-BRANCO[d],
J.A. BENDASSOLLI[a]

[a] Center for Nuclear Energy in Agriculture (CENA),
  University of São Paulo (USP),
  Piracicaba, São Paulo, Brazil

[b] University of Guarulhos (UNG),
  Guarulhos, São Paulo, Brazil

[c] "Luiz de Queiroz" College of Agriculture/USP,
  Piracicaba, São Paulo, Brazil

[d] University of Campinas – Geosciences Institute,
  Campinas, São Paulo, Brazil

Abstract

On the southeastern Brazilian coast, mangrove organic matter records have been studied by C and N isotopes, pollen and diatom analysis to reconstruct 40 ka of vegetation and climatic history. The $\delta^{13}C$ and $\delta^{15}N$ presented more depleted values from 40 to 19 ka BP. The high C/N ratios and depleted isotopic values indicate the predominance of C3 land plants in the location presently occupied by the mangrove vegetation, and a lower sea level than today. The presence of pollen of *Ilex*, *Weinmannia*, *Symplocos*, *Drimys* and *Podocarpus* suggest a colder and more humid climate than present. From 19 to 2.2 ka BP a sedimentary hiatus is associated with a sea level rise. The presence of mangrove in its present position since at least 2.200 a BP and the return of the marine coastline are associated with the lowest C/N ratio, more enriched $\delta^{13}C$ and $\delta^{15}N$ values and the presence of marine diatoms.

1. INTRODUCTION

The Brazilian Atlantic rainforest has the second highest biodiversity in Brazil after the Amazonian rainforest. Its present distribution has been drastically reduced due to intensive deforestation since European colonization in the 16th century and only 7% of its original distribution remains in preserved areas. The original rainforest domain included different types of forest adapted to varying ecological conditions, extending ~4000 km in the coastal region and covering an area of approximately 1.2 Mkm^2.

This study emphasizes the mangrove vegetation, a coastal ecosystem with constant influence of marine tides, which is typical of tropical and subtropical regions; it is defined by the existence of flora consisting of an association of specific arboreal taxa such as *Rhizophora mangle* and *Avicennia* sp., adapted to variations in salinity and low levels of free oxygen in the substrate. Previous studies of pollen records in Brazilian mangroves have demonstrated that palynological analysis can provide important information about the vegetation history of this particular ecosystem [1, 2].

Bulk organic carbon isotope (δ^{13}C) analysis has been used to determine the origin of organic matter in coastal sediments and reflects the relative amounts of the isotope distinctive parent source materials in the sample [3]. This is because the mean δ^{13}C value of C3 vascular vegetation and freshwater phyto-plankton is ~ –27‰, therefore distinguishable from the C4 plants and marine phytoplankton δ^{13}C signature which are ~ –20‰. Organic carbon to total nitrogen (C/N) ratios can be measured alongside δ^{13}C in an effort to distinguish between vascular vegetation and freshwater phytoplankton. Vascular vegetation has higher C/N ratios around 12 and over, in contrast to phytoplankton, which tends to be nitrogen rich and has lower ratios around 5 and 7 [3]. δ^{15}N indicate the terrestrial (~ +1‰) or phytoplankton (~ +8.5‰) constitution of the sediment organic matter [3].

The aim of this paper is to verify changes in the origin of the organic matter in the mangrove area, based on isotope, pollen and diatom analysis in order to contribute with the studies of paleo-environmental reconstruction on this area of the Brazilian Atlantic Rainforest region, southeastern Brazil, in the last 40 000 a BP.

2. STUDY AREA

Samples were collected in the Sitio Grande mangrove (MSG), 24º40´S, 47º56´W, at Cardoso Island, located at the Cananéia lagoon estuarine system on the south coast of Brazil (Fig. 1). Cardoso Island has an area of 25 500 ha and it is situated between the latitudes of 25º05´–25º15´S and longitudes of 47º53´–48º06´W. Mean annual temperature oscillates between 20ºC and 22ºC and mean annual precipitation is 2250 mm. Highest precipitations occur during the summer (December to March) and the lowest in winter (July to August), although there is no well-defined
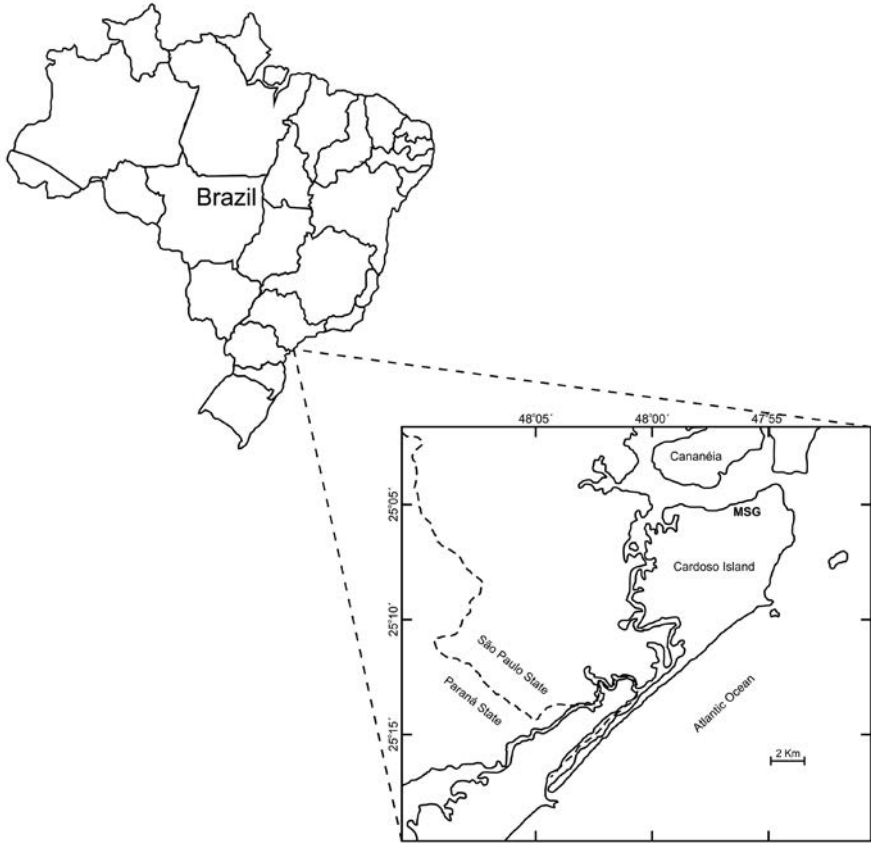
FIG. 1. Map of Brazil and the study site (MSG) at Cardoso Island.

dry season. The topography of the island is largely mountainous dominated by a massif of over 800 m. The soils of the coastal plain are classified as Spodosols. Vegetation types are pioneer dune vegetation, arboreal/shrubby restinga vegetation, coastal plain rainforest, lowland to cloud tropical rainforest and mangrove. The vegetation of the Sítio Grande mangrove is constituted by *Rhizophora mangle* (Rhizophoraceae), *Avicennia schaueriana* (Acanthaceae) and *Laguncularia racemosa* (Combretaceae) [4].

3.   MATERIALS AND METHODS

A 190 cm mangrove sediment core was collected using a vibrocorer [5] at the location identified as MSG in Fig. 1. After core opening, colour, grain size, roots and other fragments of vegetation were recorded. The samples were collected at 2 cm

depth intervals for carbon, nitrogen and pollen analyses, 10 cm depth intervals for diatoms and twelve samples collected for radiocarbon dating [6].

Chemical and isotopic analyses (total organic C, ^{13}C, total N, ^{15}N) were carried out at the Stable Isotope Laboratory of the Center for Nuclear Energy in Agriculture (CENA). Organic carbon and nitrogen results are expressed as a percentage of dry weight. Carbon and nitrogen isotopes ratios of bulk organic matter were also measured and results expressed in delta per mil notation, with an analytical precision better than 0.2‰. ^{13}C results are expressed as δ^{13}C with respect to VPDB standard and ^{15}N results are expressed as δ^{15}N with respect to atmospheric N$_2$ standard.

^{14}C analyses were carried out by Accelerator Mass Spectrometry (AMS) at the Isotrace Laboratory of the University of Toronto, Canada, and benzene synthesis liquid scintillation counting methods [6] at the ^{14}C Laboratory of CENA. Radiocarbon ages are expressed as ^{14}C years BP (before present) normalized to δ^{13}C of –25‰ VPDB.

The methodology for pollen analysis is described as follows: mineral removal with 50% HF for 18 hours, followed by a 50 % HCl treatment in a hot water bath and by a 10% KOH solution [7, 8]. Palynomorphs were extracted using a ZnCl$_2$ solution of density 2 g/cm^3 and mounted in glycerine for light microscopy. Pollen was identified by comparison with the ^{14}C Laboratory reference collections of about 5000 Brazilian forest taxa and several pollen keys [8, 9]. At least 300 arboreal pollen grains were counted at each level and the percentage diagram (Fig. 3) prepared using the Tilia and Tilia*Graph softwares [10].

Diatom analyses followed the standard technique [11] using 30% H$_2$O$_2$ solution for 24 hours for organic matter removal. Permanent slides were mounted in Zrax Mounting Medium for light microscopy analyses and identified based on published diatom keys [12, 13]. Diatom concentration (diatom per cubic centimeter) was determined by the addition of exotic *Lycopodium clavatum* spores according to the technique described in the reference [14].

4.   RESULTS AND DISCUSSION

4.1. ^{14}C age

The radiocarbon dates obtained from the mangrove samples are presented in Fig. 2. The base of the sediment core (196–190 cm) presented the age > 40 000 a BP. In the surface layers inversions were observed. The woody fragment collected in the 180–175 cm layer presented the date of 28 060 years BP whereas sediment samples from 156–150 cm, 130–123 cm and 98–93 cm depths were dated at 23 880, 25 420 and 35 900 a BP, respectively. The 130–100 cm and 97–83 cm interval indicate black clayey sediment with frequent roots and bioturbation (ichnofossils), which could have enhanced transport of allochthonous materials and thus contributed to
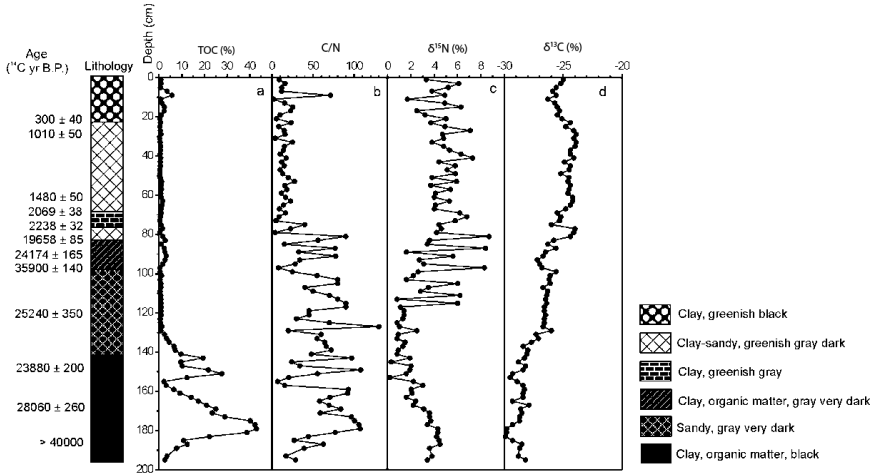
FIG. 2. ¹⁴C dating, total organic carbon (TOC), C/N, δ¹⁵N and δ¹³C of the sedimentary organic matter.

the date inversions. A hiatus of approximately 19 600 a BP is recorded within the 84–75 cm interval (19 658–2238 a BP). This could represent an erosive event associated to the RSL rise, which began at ~ 17.000 a BP, reaching the maximum at ~ 5000 a BP [15]. An age of 1010 a BP was obtained in the surface (33–23 cm) of the core. The woody fragment in the same layer showed a younger age, ~ 300 a BP, probably associated to an eventual transport of this material from surface layers due to the biological activity (crabs) found in the sampling location.

4.2. Total organic carbon, C/N, δ¹³C and δ¹⁵N values of mangrove samples

The total organic carbon (TOC) content showed a value of 2.6% in the deeper part of the profile (> 40 000 a BP) and a trend toward higher values (between 3.4 and 40.2%) to ~ 28 000 a BP (Fig. 2). A decrease in TOC content was observed from ~28 000 (29%) to ~25 000–24 000 a BP (2.1%) and an increase to 19.4‰ (~24 000 a BP). From ~24 000 to the surface (~300 a BP) the values varied between 0.3 and 5.7‰.

The C/N values varied from 17 up to 62 at >40 000 a BP (Fig. 2). A trend towards higher values (between 44 and 107) is observed at ~30 000 a BP, changing to lower values around 7 to ~28 000 a BP and reversing to higher values (~130) around 25 000 a BP, indicative of the predominance of C3 land plants in the location presently occupied by the mangrove, in consequence of the decrease of the RSL of at least 100 m during the glacial period [16]. In consequence, the present mangrove location was occupied by C3 land plants, probably arboreal species and herbs from

the Atlantic Forest. Values ranging from 2 to 27.5 are observed from ~2200 a BP to present, and are indicative of higher phytoplankton influence as a source of organic matter.

More depleted $\delta^{13}C$ values, around –28.5‰, are found in the bottom of the sediment core (Fig. 2), also suggesting the predominance of C3 land plants. A trend toward more enriched $\delta^{13}C$ values is observed from ~25 000 a BP to surface of the profile (~ –24.5‰). These values associated with C/N ratios from 2 to 27 indicate a mixture of C3 land plants and phytoplankton since at least 2220 a BP.

The $\delta^{15}N$ values from ~40 000 to ~25 000 a BP varied from ~+1.0 to +4.5‰ (Fig. 2), indicative of C3 land plants dominance and a mixture with phytoplankton. From ~25 000 to ~2200 a BP the values varied from +0.8 to +9.0‰, suggesting an increase in the phytoplankton influence. From ~2200 a BP to the present the values between +2.5 and +7.5‰ characterized the mixture of C3 land plants and phytoplankton in the organic matter composition.

4.3. Pollen analysis

The results of pollen analysis are presented in Fig. 3. Three zones may be distinguished. Zone I (~40 000 to < 24 000 a BP) is composed basically of organic rich clay and clayey-sandy sediments. The significant percentage of Myrtaceae, *Alchornea*, *Weinmannia*, Melastomataceae/Combretaceae, *Symplocos* and *Rapanea*, and the presence of *Hedyosmum* (1.4%) and *Podocarpus* (1%), associated with aquatic herbs and typical ferns of forest formations [17], suggest a colder and humid forest in the current area of the mangrove. Therefore the paleo-environmental interpretation for zone I is a tropical forest under a more humid and colder climate than the present.

The zone II (~24 000 to ~19 000 a BP) is composed basically of sandy sediments which gradually become organic rich. This interval is similar to the previous zone due to the constant presence of forest elements such as Myrtaceae, *Ilex*, Melatomataceae/Combretaceae, *Miconia, Symplocos* and *Rapanea*. The presence of Poaceae, Cyperaceae, aquatic herbs and ferns [17], suggest a humid and/or flooded environment, probably with the Poaceae being represented by C3 grasses. The presence of *Drimys*, *Hedyosmum, Cyathea* and *Podocarpus* reinforce the interpretation of a cold forest in the area. The $\delta^{15}N$ and C/N ratios indicated a phytoplankton influence in the organic matter composition. Isotopic studies developed in a peatland in the altitude Atlantic Forest, located ~170 km to the north of Cardoso Island, also revealed a cold and humid climate during the period 28 000 to 19 000 a BP [18].

Due to the sedimentary hiatus, the zone III (~19 000 to 2200 a BP) cannot be characterized. The lack of palynomorphs in the upper part of the sediment might also be explained by the presence of oxidizing conditions within the modern mangrove continuously submitted to alternating anoxic/oxic conditions, controlled by tides [19]. Palynological study conducted in marine sediments collected in Vitória, Espírito Santo State, southeastern Brazil [20], observed a larger amount of pollen grains in
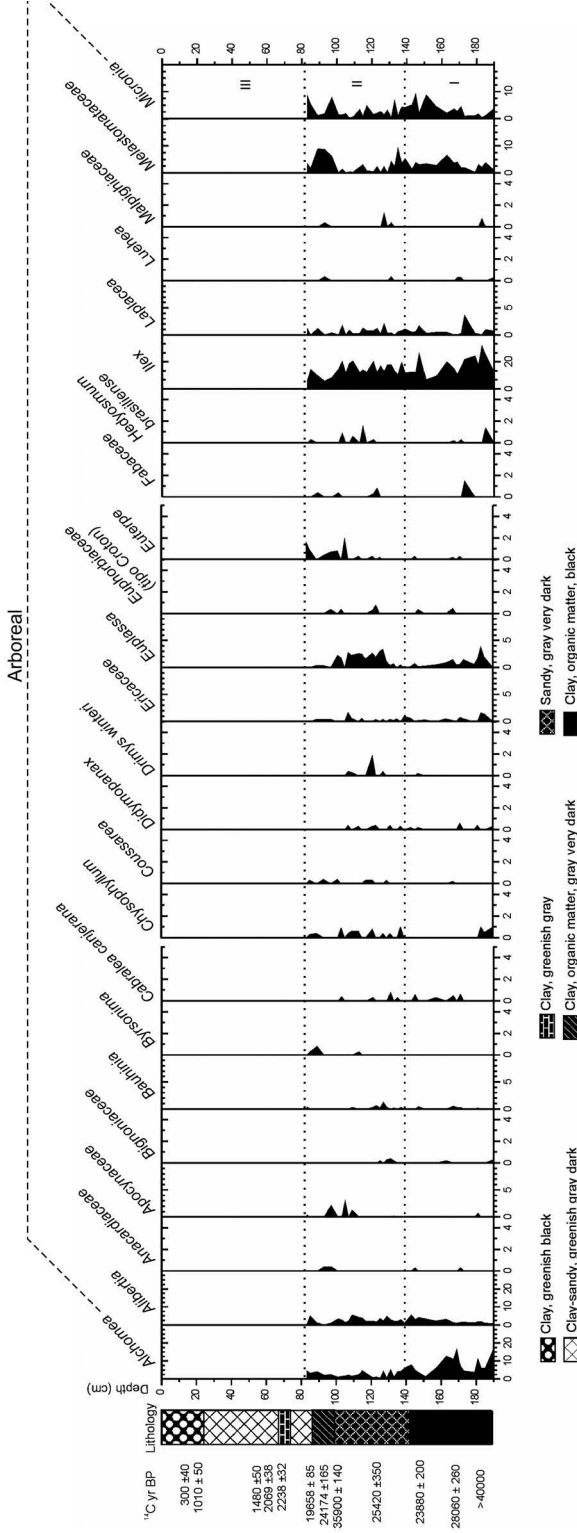
FIG. 3. Pollen diagram of the mangrove sediment samples.

21

materials of the glacial period when the sea level was lower. During the Holocene, with the highest sea level and consequent sea influence, reduced amounts of palynomorfs were observed.

4.4. Diatoms analysis

Well preserved diatoms are found only from ~2200 a BP to the present. In the period 2200 to 1.010 a BP, marine taxa *Actinoptychus splendens* (5 to 10%), *Coscinodiscus marginatus* (5 to 20%), *Cyclotella striata* (5 to 10%), *Diploneis gruendleri* (3 to 8%) and *Paralia sulcata* (10 to 25%) were found [17]. Despite the low percentage values, high concentrations of *Cocconeis disculus*, a periphytic freshwater diatom ranging from 21 600 to 14 450 valves per cm^3, indicates a source of continental waters [17]. This taxon is commonly found in water with temperature ranging from 0°C to 15°C, so it is possible to assume that the diatom community in this zone is indicative of an estuarine-lagoon system under strong marine influence. The assemblage found for the period ~1010 a BP to the present is composed of approx. 80% of marine taxa, approx. 5% of brackish water diatoms and 2% of freshwater elements. Within the marine group the best represented taxa are *Actinoptychus campanulifer* (approx. 5%), *Coscinodiscus marginatus* (approx. 10 to 15%) and *Cyclotella striata* (approx. 15%) [17].

5. CONCLUSIONS

From ~40 000 to 25 000 a BP, higher C/N and more depleted $\delta^{13}C$ and $\delta^{15}N$ values indicated the predominance of C$_3$ land plants in the location at present occupied by the mangrove ecosystem, associated with the retreatment of the modern marine coast line (decrease of the RSL). Between ~25 000 and 19 000 a BP the results suggest the dominance of C3 land plants in the sedimentary record, however they also indicate a contribution of the phytoplankton in the organic matter composition, probably characterizing a mixture of tress and herbs in a flooded environment. Pollen analysis indicated the presence of arboreal elements of cold and humid forest, as well as aquatic herbs. The climate inference is a colder and more humid climate than the present. From ~19 000 to 2200 a BP a sedimentary hiatus was observed. The presence of mangrove since at least 2200 years BP in its present position and the return of the modern marine cost line are associated with the lowest C/N and more enriched $\delta^{13}C$ and $\delta^{15}N$ values and the presence of marine diatoms.

ACKNOWLEDGMENTS

REFERENCES

[1]   GRINDROD, J., MOSS, P., VAN DER KAARS, S., "Late Quaternary mangrove pollen records from continental shelf and ocean cores in the North Australian-Indonesian region", Bridging Wallace's Line: The environmental and cultural history and dynamics of the SE-Asian-Australian region (KERSHAW, P., DAVID, B., TAPPER, N., PENNY, D., BROWN, J., Eds). CATENA Verlag, Reiskirchen, Germany (2002) 119–146.

[2]   AMARAL, P.G.C., LEDRU, M.-P., BRANCO, F.R., GIANNINI, P.C.F., Late Holocene development of a mangrove ecosystem in southeastern Brazil (Itanhaém, state of São Paulo), Palaeogeogr. Palaeoclimat., Palaeoecol. **241** (2006) 608–620.

[3]   WILSON, G.P., LAMB, A.L., LENG, M.J., GONZALEZ, S., HUDDART, H., Variability of organic $\delta^{13}C$ and C/N in the Mersey Estuary, U.K. and its implications for sea level reconstruction studies, Estuar. Coast. Shelf Sci. **64** (2005) 685–698.

[4]   SCHAEFFER-NOVELLI, Y., MESQUITA, H.S.L., CINTRON-MOLERO, G., The Cananéia lagoon estuarine system, São Paulo, Brazil, Estuaries **13** (1990) 193–203.

[5]   MARTIN, L., FLEXOR, J.M., 'Vibrotestemunhador leve: utilização e possibilidades', 2nd Congresso da Associação Brasileira de Estudos do Quaternário, ABEQUA (1989).

[6]   PESSENDA, L.C.R., CAMARGO, P.B., Datação radiocarbônica de amostras de interesse arqueológico e geológico por espectrometria de cintilação líquida de baixa radiação de fundo, Química Nova **14** (1991) 98.

[7]   FAEGRI, K., IVERSEN, J., Textbook of pollen analysis, John Wiley, Chichester, UK, (1989).

[8]   COLINVAUX, P., DE OLIVEIRA, P.E., MORENO PATIÑO, J.E.M., Amazon Pollen Manual and Atlas, Harwood Academic Publishers, Amsterdam (1999).

[9]   ABSY, M.L., Polen e esporos do Quaternário de Santos (Brasil), Hoehnea **5** (1975) 1.

[10]   GRIMM, E.C., CONISS: A Fortran 77 program for stratigraphically constrained cluster analysis by the method of incremental sum of squares, Comput. Geosci. **13** (1987) 13–35.

[11]   BATARBEE, R.W., "Diatom analysis", Handbook of Holocene palaeoecology and palaeohydrology (BERGLUND, B.E., Ed.), Wiley, Chichester (1986) 527–570.

[12]   PATRICK, R., REIMER, C.W., The diatoms of the United States, Academy of Natural Sciences, Philadelphia, Vol. 2 (1975).

[13]   FÜRSTENBERGER, C.B., Interpretações paleolimnológicas do Quaternário recente a partir da análise da comunidade de diatomáceas (Bacillariophyta) no sedimento do rio Icatu, município de Xique-Xique, estado da Bahia, Brasil, PhD Thesis, Universidade de São Paulo, São Paulo (2001).

[14]   STOCKMARR, J., Tablets with spores used in absolute pollen analysis, Pollen et Spores **13** (1971) 615.

[15]   SUGUIO, K., et al., "Paleoníveis do mar e paleolinhas de costa", Quaternário do Brasil (SOUZA, C.R.G., SUGUIO, K., OLIVEIRA, A.M.S., DE OLIVEIRA, P.E., Eds), Holos, R.Preto (2005) 114–129.

[16]   DAWSON, A.G., Ice Age Earth. Late Quaternary Geology and Climate, Routledge, London and New York (1992).

[17]   VIDOTTO, E., Reconstrução paleoambiental (vegetação e clima) no Parque Estadual da Ilha do Cardoso-SP durante o Quaternário tardio, PhD Thesis, Centro de Energia Nuclear na Agricultura, Universidade de São Paulo, Piracicaba, (2008).

[18]   PESSENDA, L.C.R., et al., The evolution of a tropical rainforest/grassland mosaic in southeastern Brazil since 28,000 ^{14}C yr BP based on carbon isotopes and pollen records, Quaternary Res. **71**(2009) 437–452.

[19]   FERREIRA, T.O., OTERO, X.L., VIDAL-TORRADO, P., MACIAS, F., Redox processes in mangrove soils under *Rhizophora mangle* in relation to different environmental conditions, Soil Sci. Soc. Am. J. **71** (2007) 484–491.

[20]   BEHLING, H., ARZ, H.W., PÄTZOLD, J., WEFER, G., Late Quaternary vegetational and climate dynamics in southeastern Brazil, inferences from marine cores GeoB 3229–2 and GeoB 3202–1, Palaeogeogr. Palaeoclimatol. Palaeoecol. **179** (2002) 227–243.

CHANGES IN HYDROLOGIC CONDITIONS AND GREENHOUSE GAS EMISSIONS IN CIRCUMPOLAR REGIONS DUE TO CLIMATE CHANGE INDUCED PERMAFROST RETREAT

M.J. WHITICAR
School of Earth and Ocean Sciences,
University of Victoria, Victoria, Canada

J. BHATTI, N. STARTSEV
Northern Forestry Centre, St Edmonton,
AB, Canada

Abstract

Thawing permafrost peatlands substantially influence Canadian northern ecosystems by changing the regional hydrology and mobilizing the vast carbon (C) reserves that results in increased greenhouse gas (GHGs) emissions to the atmosphere. With permafrost distribution controlled largely by topography and climate, our International Polar Year (IPY) study intensively monitored the local C cycling processes and GHG fluxes associated with different hydrologic and permafrost environments at 4 sites along a climatic gradient extending from the Isolated Patches Permafrost Zone (northern Alberta), to the Continuous Permafrost Zone (Inuvik, NWT). Each site encompasses a local gradient from upland forest and peat plateau to collapse scar. Our multi-year measurements of peatland profiles and flux chambers for CH_4 and CO_2 concentrations and stable isotope ratios indicate processes, including methanogenesis, methanotrophy, transport and emission that control the distribution of these GHGs. These relationships are modulated by fluctuating local soil water and corresponding ecosystem conditions. The gas geochemistry shows that significant surface CH_4 production occurs by both hydrogenotrophic and acetoclastic methanogenesis in submerged, anaerobic peats, e.g., collapse scars, whereas methane oxidation is restricted to aerobic, drier environments, e.g., upland sites and peat-atmosphere interface. The most active methanogenesis and emissions are in areas of actively thawing permafrost contrasting with sites under continuous permafrost. This degree of methanogenesis is being amplified by the increased rate of Arctic warming and the rapid retreat of permafrost in Canada's Arctic (approximately. 2.5 km/a).

1.   INTRODUCTION

Forests and peatlands in northern regions are the largest terrestrial reservoir of carbon (C) [1]. In Canada's northern region, the 304 M ha of forest and 89 M ha of peatland represent a combined estimated C pool of 186 Pg and annual C flux of 87 Tg
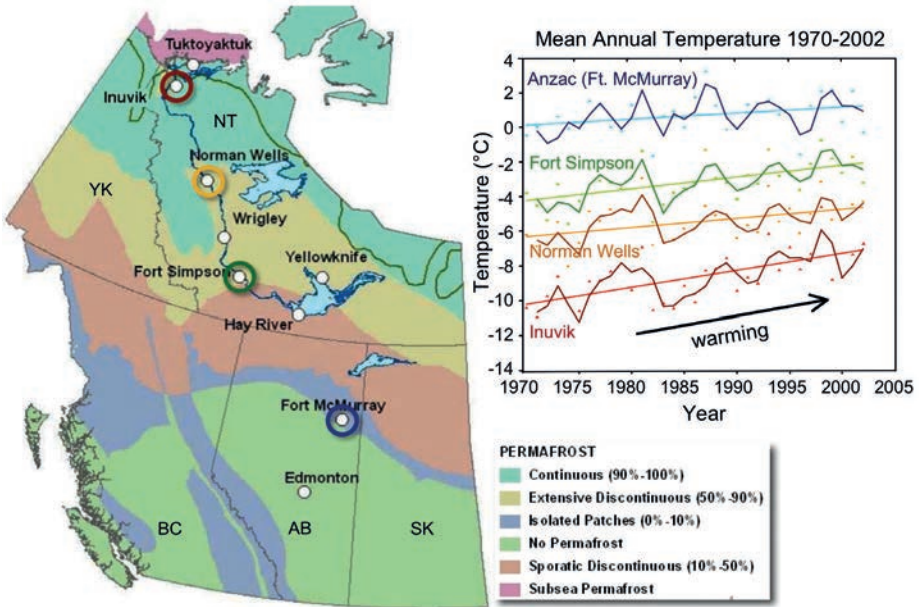
FIG. 1. Left: location map of study in different permafrost areas (with $\delta^2 H_{H2O}$). Right: record of temperature increase at Anzac, Ft. Simpson, Norman Wells and Inuvik study sites.

[2, 3]. In continental western Canada, peatlands cover ca. 365 000 km² or 20% of the land area [4, 5]. These large forest and peatland areas are the most significant potential source of terrestrial C in Canada. These northern ecosystems are also a major contributor of global, atmospheric greenhouse gases (GHGs), including CH_4, CO_2, and N_2O. Further, the global warming potential of CH_4 and N_2O are 23 and 296 times that of CO_2, respectively, and the concentrations of CO_2, CH_4 and N_2O in the atmosphere are increasing significantly [6].

Growing evidence indicates that the northern latitudes of Canada are warming more rapidly than the mid latitudes [7]. In Canada's northern region this trend has increased to a rate of 1.8°C/century during the past 25 to 30 years and is associated with drier conditions. The Mackenzie Valley region of northwestern Canada (Fig. 1) has undergone the most warming (1.7°C) over the last century in Canada [7]. Moreover, general circulation models predict that for climate warming resulting from a doubling of CO_2, the region will experience increases in mean annual air temperature of up to 5°C.

In the event of such predicted climate change, forest and peatland ecosystems in the Mackenzie valley region will also be affected by changes in the key disturbance regimes of permafrost and wildfire. Regional studies including ECMBIS [8] and NRCanPEMV [9] predict that permafrost will partially or completely disappear over large areas in the Mackenzie Valley.

Climate change may lengthen growing seasons, change mineralization rates, increase fire frequencies, and lead to widespread thawing of permafrost. It is estimated that since 1960 about 2600 km^2 of permafrost has thawed in the peatlands of boreal western Canada [10], and the projections are for this to increase spatially and temporally. Recent analysis projected a 74–118% increase in area burned in northwestern Canada by end of this century under $3 \times CO_2$ scenarios [11].

It is uncertain how the above-mentioned changes will affect the distribution, composition and C source–sink capacity of forests and peatlands, i.e., balance between organic matter production, heterotrophic mineralization, and GHG emissions, especially CH_4 [12–16]. Because of the relatively large changes in climate and associated disturbances occurring in this region, our IPY project was designed to improve our understanding of the potential effects of recent climate change, as well as natural and anthropogenic disturbances, on the total C storage and source–sink relationships, and GHG emissions of forests and peatlands in the Mackenzie Valley.

Quantifying the C source/sink nature and GHG emissions budgets of forests and peatlands represents a substantial challenge. Yet even more difficult is predicting future C and GHG balances under climate change and associated disturbances such as fire and permafrost melting. The warming and drying predicted for the Mackenzie Valley is expected to lead to increased area burned [11]. Fire also indirectly controls longer term patterns of C accumulation by initiating secondary succession [17–19] and altering site environmental conditions [20, 21]. Fire has a strong influence on patterns of net primary production [22] and soil respiration [23], which cumulatively influence long term patterns of soil C storage [24, 25]. In addition to soil CH_4 release with melting permafrost, increased fires are a potential source of GHGs and were important during enhanced warming periods in the Holocene [12, 26, 27, 15]. Considering these interactions, the role of fires in long term C cycling in the region is complex and remains little understood.

In forest and peat ecosystems, soil organic C can be assimilated, immobilized, leached and emitted to the atmosphere as CO_2 via aerobic, or CH_4 via anaerobic, microbial respiration. To estimate the microbial mediated fluxes of CO_2 and CH_4 to the atmosphere, we need to identify the types of microbes and establish the linkages with GHGs formation. At present, there has been very little research linking specific the types of microbes and GHGs dynamics in northern ecosystems.

During the Younger Dryas-Preboreal (YD-PB) transition (ca. 11.5 kyBP), warming, similar to that expected in this century, led to the retreat of ice cover and permafrost. New CH_4 C isotope measurements from Greenland ice over this YD-PB period [28, 29] strongly suggest that this CH_4 rise was not from marine gas hydrates (Clathrate Gun Hypothesis, [30]) or from tropical wetlands. Rather, permafrost modulated CH_4 emissions are the most probable, yet poorly characterized, cause of the rise.

In the subarctic region of Sweden [31] between 1970 and 2000 there was a 22–66% increase in CH_4 emissions on a landscape scale attributed to climate change

influence on permafrost and bog vegetation. It is conceivable that climate change and its associated disturbances could tip C balances from net sinks to net sources over the next 20 to 60 years.

Overall, the most important controls of C cycling in forests and peatlands are plant communities, soil temperature, hydrology, and the chemistry of peat and plant tissues [32]. Limited data and understanding of how changing environmental conditions and disturbances (including fires and permafrost thawing) influences the C cycle of forests and peatlands over short and medium timescales (10–100 years), poses a great challenge to predict changes in C sink–source relationships and GHG dynamics under a changing climate. Given the complexity of climate–disturbance–C cycle interactions, there is a strong need for across-scale and across-ecosystems studies.

Our research focuses on soil profiles of GHG (CH_4, CO_2) concentrations and their corresponding isotope ratios ($\delta^{13}CO_2$ and $\delta^{13}CH_4$) to determine and track the different processes of methanogenesis, methylotrophy and microbial respiration, e.g., Ref. [33]. This is possible due to the distinctive isotope effects (and resultant isotope ratio signatures) that are characteristic of these various microbial processes, e.g., Ref. [33]. By comparing co-existing isotope pairs, i.e., $\delta^{13}CO_2$–$\delta^{13}CH_4$, it is possible to distinguish between different methanogenic pathways, i.e., acetoclastic fermentation vs hydrogenotrophic (CO_2-reduction) [33]. This information reveals the state of organic substrate availability and 'reserve', which could be expected to shift in type or stratigraphic depth as the climate changes. For example our previous work in Fluxnet [34] and elsewhere has shown that acetoclastic fermentation is a dominant methanogenic process until the labile organic pool (LOC, e.g., acetate, formate, TMA, DMS etc.) is exhausted. The methanogenic pathway then shifts, typically in older and deeper soils and sediments, to hydrogenotrophic methanogenesis.

We test with concentration and isotope information whether the acetoclastic methanogenic pathway diminishes during dryer conditions with lowered water tables (less LOC), with a resultant drop in longer-term CH_4 fluxes. It is important to note that measurements on soil profiles, not just flux chamber studies, are vital to understand the spatial and temporal (seasonal and decadal) variations in diagenesis and GHG systematics.

Furthermore, C-isotope information is critical to identify the presence and degree of aerobic methane oxidation occurring in soils [33]. Characteristic isotope shifts are diagnostic of this process [33, 34]. We use isotopes to test the hypothesis that decreased water table leads to enhanced microbial oxidation of CH_4 and enhanced CO_2 formation.

2. STUDY AREA

The study area is a 1500 km transect from northern Alberta along the Mackenzie Valley to the Beaufort Sea coast (Fig. 1). The transect covers the latitudinal
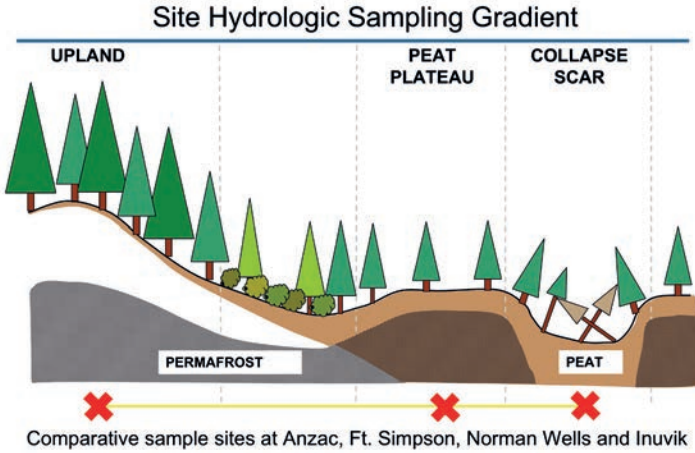
FIG. 2. Comparative sampling sites along hydrologic gradient (UL – Upland, PP – Peat Plateau, CS – Collapse Scar) at Anzac, Ft. Simpson, Norman Wells and Inuvik.

gradient of Boreal, Subarctic and Arctic ecoclimatic regions. Its general south-north orientation offers representative permafrost distributions from the southern fringe of the discontinuous permafrost zone, where the Mackenzie River begins at Great Slave Lake, to the continuous permafrost zone on the Arctic Ocean coast and the Mackenzie Delta. In May 2007 intensive monitoring sites were selected throughout the Mackenzie Valley and northern Alberta. Each study site was chosen to reflect a gradient from upland to peatland conditions. Individual plots are located within the upland forest (UL), peat plateau (PP), and collapse scar (CS), as shown in Fig. 2.

3.   SAMPLING AND METHODS

Passive gas flux chambers using permanent soil collars inserted in the ground were deployed at all sites to determine the net CH_4 and CO_2 fluxes. Soil gas samples are collected using thin metal tubes (SAS tubes) permanently inserted in the soil to pre-determined depths from 5 to approx. 200 cm and. Soil water or gases are sampled seasonally by aspirating with a syringe (CH_4 in water samples is extracted by shaking the water with air). CH_4 and CO_2 concentrations are measured in the field using a portable optical spectrometer system (GYRO™) developed by Isometric Instruments, Victoria. Stable isotope ratios are measured by Continuous Flow-Isotope Ratio Mass Spectrometry (CF-IRMS) methods at the BF-SEOS UVic [35]. The carbon isotope ratios are expressed as $\delta^{13}C$ in per mil (‰) using standard δ-notation:

$$\delta(\text{‰})= \frac{R_{\text{sample}} - R_{\text{standard}}}{R_{\text{standard}}} 10^3$$

where R is the molar ratio of heavy to light isotope, i.e., $^{13}C/^{12}C$ for the sample and standard. Carbon isotope ratios are referenced to Vienna Pee Dee Belemnite (V-PDB).

4. RESULTS AND DISCUSSION

CH_4 emissions varied significantly between study sites with the highest values in the Ft Simpson collapse scar (CS) even though Anzac has the highest annual soil temperature. Ft Simpson is located in the zone of most active permafrost thawing. The highest CH_4 emissions are consistently observed in the submerged or water saturated features of the landscape at all study sites (Fig. 3). Both peatland and upland landscape features showed very low efflux or even negative influx of CH_4 from the boundary layer into the soil, i.e., CH_4 concentration was continually dropping with time in the chamber (Fig. 3). This indicates significant CH_4 uptake and microbial oxidation in these soils.

Although the peatlands (PP, UP) had no surface flux of CH_4, soil CH4 concentrations in water-saturated layers at depth reached several hundred ppm, indicating that the drained soil effectively oxidized produced CH_4.

Methane concentration soil depth profiles in water saturated areas of the CS show sharp increases in CH_4 concentration with depth (Fig. 4). Overall, CH_4 production was greatest in early summer across all sites. In midsummer, CH_4 production was minimal in all study sites despite the fact that the water table remained high (within 10 cm from the surface) (Fig. 4). This can be attributed to the increased O_2 concentration throughout the profile and was observed in mid-July to mid-August.
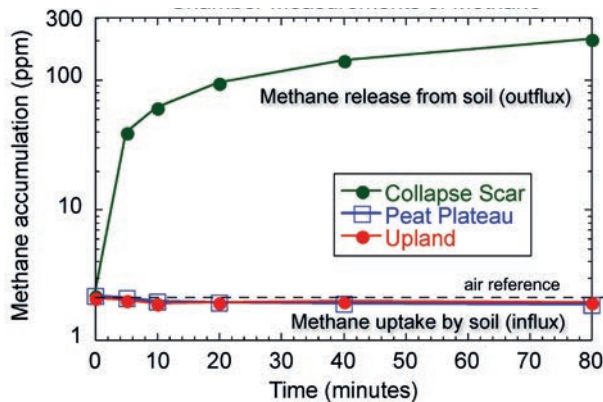
FIG. 3. Comparison of methane concentration build-up in flux chambers at CS, PP and UL sites along the hydrologic gradient at Anzac.
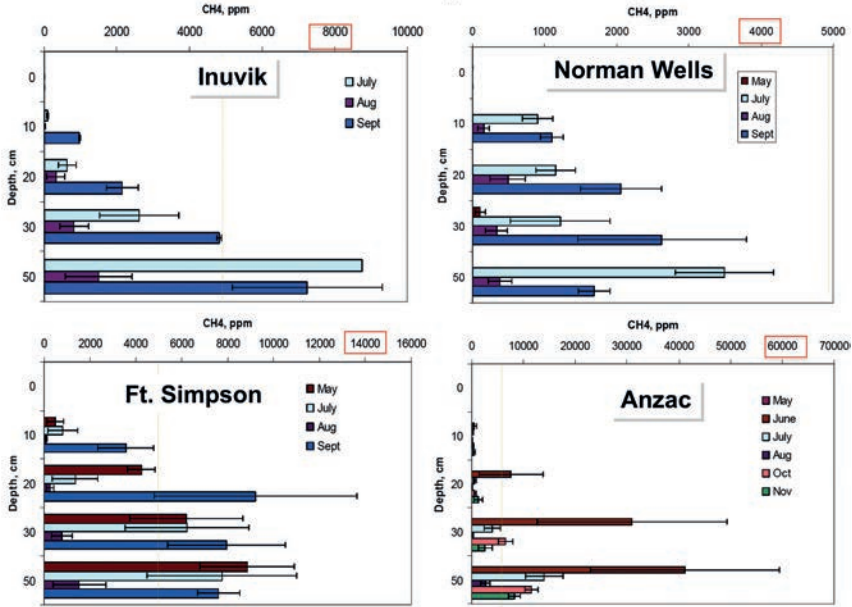
FIG. 4. Comparison of soil methane concentration depth profiles in collapse scars (CS) at Anzac, Ft. Simpson, Norman Wells and Inuvik.

We hypothesize that the increase in O_2 concentration is due to the activity of herbaceous roots, capable of transporting O_2 down the profile of anaerobic soils [36].

The $\delta^{13}CH_4$ from collapse scar soil samples in the 4 study areas (Fig. 5) show considerable range from –83.7‰ to –47.8‰, the latter a value similar to atmospheric air (–47.6‰). The soil samples show remarkably little variation in $\delta^{13}CH_4$ with depth at any specific site, but large differences between sites. In particular, at Ft Simpson the $\delta^{13}CH_4$ varied about –52‰, whereas it was more ^{12}C-enriched around –66‰ at the southern Anzac site (Fig. 5). This isotopic homogeneity is rather unexpected based on the soil methane concentration gradients observed in Fig. 4. Isotope effects due to methane production, consumption or even diffusion, should lead to a vertical partitioning of the $\delta^{13}CH_4$ [33], but this is not observed in this soil profile dataset. The surface soil chamber $\delta^{13}CH_4$ measurements at Anzac are similar to the soil profile, whereas at Ft Simpson the chambers $\delta^{13}CH_4$ are about 8‰ ^{12}C-enriched relative to the soil (Fig. 5).

A possible explanation for the vertical $\delta^{13}CH_4$ homogeneity could be that the methane in collapse scars is generated rapidly and in relatively large amounts once the soil becomes anoxic. Vertical migration may smear the isotope signature so that there is no change in $\delta^{13}CH_4$ with depth. The consistent $\delta^{13}CH_4$ offset between Ft. Simpson and Anzac (ca. 14‰) could be due to differences in the methanogenic pathway. If so, then Ft Simpson expresses a $\delta^{13}CH_4$ signature that is more characteristic
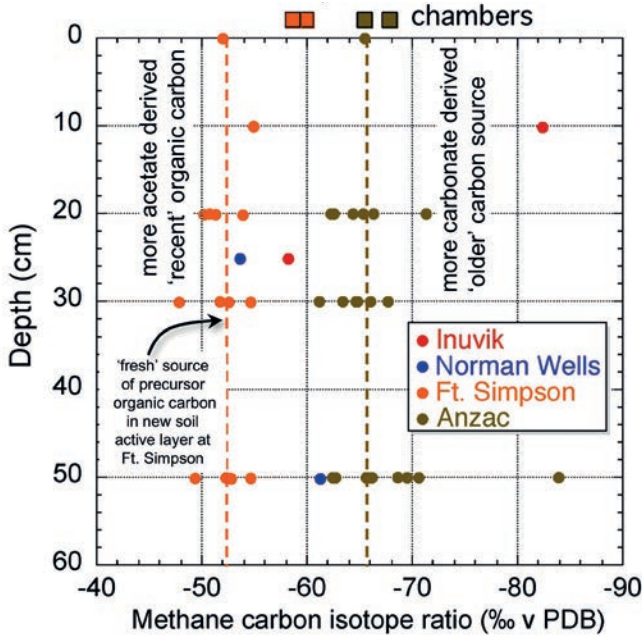
FIG. 5. *Comparison of soil $\delta^{13}CH_4$ depth profiles and chambers in collapse scars at Anzac, Ft. Simpson, Norman Wells and Inuvik.*

of acetoclastic methanogenesis [33]. In contrast, Anzac has a $\delta^{13}CH_4$ signature more representative of hydrogenotrophic methanogenesis [33].

The comparison of the soil $\delta^{13}CO_2$ and $\delta^{13}CH_4$ values as shown in Fig. 6 [33] can be useful to determine the methanogenic/methanotrophic pathways and process-es. Although the soil $\delta^{13}CO_2$-$\delta^{13}CH_4$ database is currently limited, it does appear from these data that the northern permafrost sites, including Ft Simpson, are dominated by acetoclastic methanogenesis. In contrast, Anzac, the southern permafrost-free site, is dominated by hydrogenotrophic methanogenesis. A possible explanation is related to the carbon precursors. The northern sites may have more labile organic material pre-sent, e.g. organic acids, that support acetoclastic methanogenesis. These labile sub-strates have only recently, and to a limited degree, become active due to the exposure of the active layer (especially at Ft Simpson) because of the retreat and loss of per-mafrost at these sites (Fig. 1). In comparison the Anzac site has been permafrost-free for thousands of years and the labile carbon pool has been exhausted. Under these conditions, the methanogenic pathway shifts from acetoclastic to hydrogenotrophic methanogenesis (as observed).

Overall, our study reveals that there is a net emission of CH_4 and CO_2 from the soils at all 4 sites (Fig. 7). In particular, CO_2 from the upland soils is the larg-est source of GHG emissions observed up to 1 g CO_2 m^{-2} hr^{-1}. The emissions follow
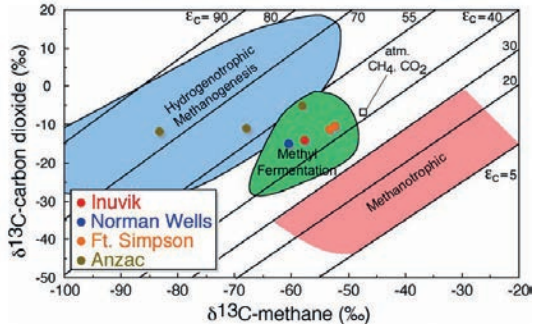
FIG. 6. Comparison of soil $\delta^{13}CO_2$ and $\delta^{13}CH_4$ at Anzac, Ft. Simpson, Norman Wells and Inuvik.
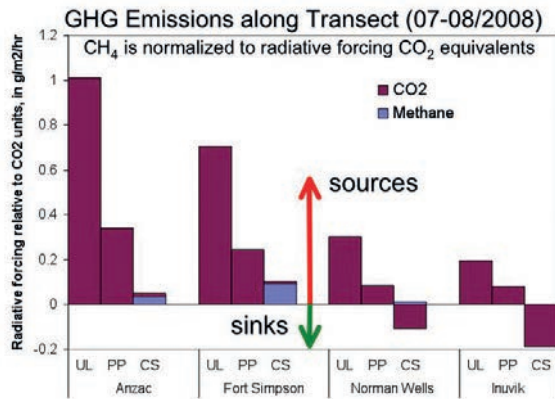
FIG. 7. Comparison of CH_4 and CO_2 emissions at Anzac, Ft. Simpson, Norman Wells and Inuvik.

a clear trend to lower values as we move down the hydrologic gradient to peat plateau (PP) and then collapse scar (CS) (Fig. 7). Only in the collapse scar at the northern sites is there net uptake of CO_2 by the soils. Methane is only a minor contributor at all sites compared with CO_2 (CH_4 converted by GWP to CO_2 equivalents [36] and is relevant only in the collapse scar settings (Fig. 7).

5.   CONCLUSIONS

This study indicates that in permafrost-related peatlands, increased CH_4 production by anaerobic methanogenesis is associated with water saturated areas, such as the collapse scars. The greatest CH_4 production takes place in the regions with

the most recently thawed permafrost. This illustrates the potential for increased GHG emissions under climate warming.

Based on initial stable isotope measurements, the soils with an active layer most recently thawed (Ft Simpson) appear to be dominated by acetoclastic methanogenesis, whereas the 'aged' soils, e.g., Anzac, appear to have depleted the labile organic material and have transitioned to hydrogenotrophic methanogenesis.

In the upland forest and peat plateau methanogenesis is absent or low. In these aerated, oxic soils there is evidence for methane uptake and consumption by methylotrophs in the soil.

At the height of the growing season, increased oxygenation of the soil profile, possibly due to root activity, led to decreasing CH_4 concentrations throughout the soil profile.

The effect of temperature (Q10 factor) for CH_4 emissions decreased from southern to northern sites, indicating differences in methanogenic microflora adaptation and possibly available methanogenic substrates.

ACKNOWLEDGEMENTS

REFERENCES

[1]   INTERGOVERNMENTAL PANEL ON CLIMATE CHANGE, "Observed Climate Variability and Change", Climate Change 2001, Working Group I: The Scientific Basis, Cambridge University Press, Cambridge, UK (2001) 99–182.

[2]   APPS, M.J., KURZ, W.A., LUXMOORE, R.J., NILSSON, L.O., SEDJO, R.A., SCHMIDT, R., SIMSON, I.G., VINSON, T.S., Boreal forest and tundra, Water Air Soil Poll. **70** (1993) 39–53.

[3]   WEBER, M.G., FLANNIGAN, M.D., Canadian boreal forest ecosystem structure and function in a changing climate: impact on fire regimes, Environ. Rev. **5** (1997) 145–166.

[4]   VITT D.H., HALSEY, L.A., ZOLTAI, S.C., The changing landscape of Canada's western boreal forest: the current dynamics of permafrost, Can. J. For. Res. **30** (2000) 283–287.

[5]   ZOLTAI, S.C., POLLET, F.C., "Wetlands in Canada: their classification distribution, and use", Mires: Swamp, Bog, Fen, and Moor, Vol. 4B, Regional Studies (GORE, A.J., Ed.), Elsevier, Amsterdam (1983) 245–268.

[6]   BHATTI, J.S., LAI, R., APPS, M.J., PRICE, M.A., (Eds), Climate Change and Managed Ecosystems, CRC Press, Boca Raton, FL (2006) 464.

[7]   HENGEVELD, H. WHITEWOOD B., Understanding climate change: A synthesis of climate change science, Meteorological Service of Canada, Ottawa (2005) 72.

[8]   COHEN, S.J., Mackenzie basin impact study (MBIS): Final report, Ottawa, Environment Canada (1997) 372.

[9]   DYKE L.D., BROOKS, G.R., (Eds), Northwest Territories: a baseline for the assessment of environmental change, Geol. Surv. Canada Bull. **547** (2000) 189.

[10]   ROBINSON, S.D., Carbon accumulation in peatlands, southwestern Northwest Territories, Canada, Can. J. Soil Sci. **86** (2006) 305–319.

[11]   FLANNIGAN M.D., LOGAN, K.A., AMIRO, B.D., SKINNER, W.R., STOCKS, B.J., Future Area Burned in Canada, Climatic Change **72** 1–2 (2005) 1–16.

[12]   CARCAILLET, C., at al., Holocene biomass burning and global dynamics of the carbon cycle, Chemosphere **49** 8 (2002) 845–863.

[13]   ROULET, N.T., Peatlands, carbon storage, greenhouse gases and the Kyoto Protocol: Prospects and significance for Canada, Wetlands **20** (2000) 605–615.

[14]   THONICKE, K., PRENTICE, I.C., HEWITT, C., Modelling glacial–interglacial changes in global fire regimes and trace gas emissions, Global Biogeochemical Cycles **19** (2005) 3008.

[15]   TURETSKY M., WIEDER, R.K., VITT, D.H., Boreal peatland C fluxes under varying permafrost regimes, Soil Biol. Biochem. **34** (2002) 907–912.

[16]   BOURGEAU-CHAVEZ, L.L., KASISCHKE, E.S., BRUNZELL, S.M., MUDD, J.P., SMITH, K.B., FRICK, A.L., Analysis of spaceborne SAR data for wetland mapping in Virginia riparian ecosystems, International Journal of Remote Sensing **22** (2001) 3665–3687.

[17]   ROWE, J.S., SCOTTER, G.W., Fire in the boreal forest, Quat. Res. 3 (1973) 444–464.

[18]   VIERECK, L.A., VAN CLEVE, K., DYRNESS, C.T., "Forest ecosystem distribution in the taiga environment", Forest ecosystems in the Alaskan taiga: A synthesis of structure and function (VAN CLEVE, K., et al., Eds), Springer, New York (1986) 22–43

[19]   KASISCHKE, E.S., BRUHWILER, L.M., Emissions of carbon dioxide, carbon monoxide and methane from boreal forest fires in 1998, J. Geophys. Res. **107** D1 8146 (2003).

[20]   O'NEILL, K.P., KASISCHKE, E.S., RICHTER, D.D., Environmental controls on soil CO_2 flux following fire in black spruce, white spruce, and aspen stands of interior Alaska. Can. J. For. Res. **32** (2002) 1525–1541.

[21]   HICKE, J.A., ASNER, G.P., KASISCHKE, E.S., FRENCH, N.H.F., RANDERSON, J.T., COLLATZ, G.J., STOCKS, B.J., TUCKER, C.J., LOS, S.O., FIELD, C.B., Postfire response of North American boreal forest net primary productivity analyzed with satellite observations, Glob. Change Biol. **9** (2003) 1145–1157.

[22]   KIM, Y., TANAKA, N., Effect of forest fire on the fluxes of CO_2, CH_4 and N_2O in boreal forest soils, interior Alaska, J. Geophy. Res. **108** (2003) 8154.

[23] HARDEN, J.W., TRUMBORE, S.E., STOCKS, B.J., HIRSCH, A., GOWER, S.T., O'NEILL, K.P., KASISCHKE, E.S., The role of fire in the boreal carbon budget. Global Change Biology **6**, suppl. 1 (2000) 174–184.

[24] ZOLTAI. S.C., MORRISSEY, L.A., LIVINGSTON, G.P., GROOT, W.J., Effects of fires on carbon cycling in North American boreal peatlands, Environ. Rev. **6** 1 (1998) 13–24.

[25] CHAPPELLAZ, J.A., FUNG, I.Y., THOMPSON, A.M., The atmospheric CH4 increase since the Last Glacial Maximum, Tellus **45 B** (1993) 228–241.

[26] FERRETTI, D.F., et al., Unexpected changes to the global methane budget over the past 2000 years, Science **309** (2005) 1714–1717.

[27] SCHAEFER, H., Stable carbon isotopic composition of methane from ancient ice samples, PhD thesis, University of Victoria (2005) 213.

[28] SCHAEFER H., ET AL., Ice record of $\delta^{13}C$ for atmospheric CH_4 across the Younger Dryas–Preboreal transition, Science **313** (2006) 1109–1112.

[29] BEHL, R.J., HILL, T M., KENNETT, J.P., Recent advances in understanding of the methane hydrates in quaternary climate change, (Proc. 5th, Int. Gas. Hydrate. Conf. Trondheim, 2005) **3** (2005) 3008.

[30] CHRISTENSEN T.R., JOHANSSON, T., ÅKERMAN, J., MASTEPANOV, M., MALMER, N., FRIBORG, T., CRILL, P., SVENSSON, B.H., Thawing sub-arctic permafrost: Effects on vegetation and methane emissions, Geophys. Res. Lett. **31** 4 (2004) L04501.

[31] BHATTI, J.S., ERRINGTON, R.C., BAUER, I.E., HURDLE, P.A., Carbon stock trends along forested peatland margins in central Saskatchewan. Can. J. Soil Sci. **86** (2006) 321–333.

[32] WHITICAR M.J., Carbon and hydrogen isotope systematics of bacterial formation and oxidation of methane, Chem. Geol. **161** 1–3 (1999) 291–314.

[33] ALSTAD, K.P., WHITICAR, M.J., Carbon and hydrogen isotope ratio characterization of methane dynamics for Fluxnet Peatland Ecosystems, Org. Geochem. **42** 5 (2011) 548–558.

[34] WHITICAR, M.J., EEK, M., "Challenges of $^{13}C/^{12}C$ measurements by CF-IRMS of biogeochemical samples at sub-nanomolar levels", New approaches for stable isotope ratio measurements, IAEA-TECDOC-1247 (2001) 75–95.

[35] STARTSEV, N., BHATT, J., The Influence of Climatic Gradient and Permafrost on Surface Net Ecosystem Exchange (NEE) and Soil Respiration along Mackenzie Valley (CC-029), International Polar Year Quebec 2008 (2009).

STABLE ISOTOPE MASS BALANCE OF THE LAURENTIAN GREAT LAKES TO CONSTRAIN EVAPORATIVE LOSSES

S. JASECHKO [a,b], J.J. GIBSON [b,c], A. PIETRONIRO [d], T.W.D. EDWARDS [a]

[a] Department of Earth and Environmental Sciences,
   University of Waterloo, Waterloo,
   Ontario, Canada

[b] Alberta Innovates – Technology Futures,
   Victoria, British Columbia, Canada

[c] Department of Geography, University of Victoria,
   Victoria, British Columbia, Canada

[d] National Water Research Institute,
   Environment Canada, Saskatoon,
   Saskatchewan, Canada

Abstract

Evaporation is an important yet poorly constrained component of the water budget of the Laurentian Great Lakes, but is known historically to have a significant impact on regional climate, including enhanced humidity and downwind lake effect precipitation. Sparse over lake climate monitoring continues to limit ability to quantify bulk lake evaporation and precipitation rates by physical measurements, impeded by logistical difficulties and costs of instrumenting large areas of open water (10^3–10^5 km^2). Measurements of stable isotopes of oxygen and hydrogen in water samples of precipitation and surface waters within the Great Lakes basin are used to better understand the controls on the region's water cycle. A stable isotope mass balance approach to calculate long term evaporation as a proportion of input to each lake is discussed. The approach capitalizes on the well understood systematic isotopic separation of an evaporating water body, but includes added considerations for internal recycling of evaporated moisture in the overlying atmosphere that should be incorporated for surface waters sufficiently large to significantly influence surrounding climate.

1.   INTRODUCTION

Evaporation is an important component of the water budget for the Laurentian Great Lakes of North America; it is the least understood control on lake levels, and

has a significant influence on lake and local climates. The Great Lakes contain roughly 20% of the global reservoir of unfrozen fresh surface water, and support a robust binational regional economy. Evaporation estimates by the Great Lakes Environmental Research Laboratory (GLERL) lumped heat storage model estimate the evaporation flux to be similar in magnitude to catchment runoff or direct precipitation into each Great Lake. This model utilizes lakeshore climate station data and satellite measurements, but does not incorporate temperature and humidity data from over lake monitoring buoys [1]. Further, Lake Superior's residence time is greater than a century, and necessary data for the GLERL model does not extend sufficiently far back in time to produce a long term evaporation estimate. Evaporation for the Great Lakes ranges from roughly 600 mm to 900 mm. Evaporation is highly seasonal, weighted to fall and early winter months.

2. CONSIDERATION OF LAKE EFFECTS ON THE ATMOSPHERE AND THE USE OF AN ISOTOPE MASS BALANCE TO CALCULATE EVAPORATION

Use of stable isotopes of oxygen and hydrogen in water is a cost efficient method of determining evaporation as a proportion of inflow (E/I) for small lake systems, particularly for regions in which it is difficult and expensive to set up instrumentation [2]. Also, this approach is shown to rapidly assess small scale spatial variability in evaporation as a proportion of input to lake systems [3, 4]. A synchronized approach using two conservative tracers, namely $\delta^{18}O$ and δ^2H, is used to calculate *E/I* and allows for a calculation check to ensure that the model realistically captures the physical characteristics of the lake evaporation process. Evaporation calculations have been described for large systems such as the Caspian Sea, the eastern Mediterranean Sea and Lake Titicaca [5–7]; however, a unifying approach to calculating *E/I* for large surface water bodies that accounts for effects on the overlying atmosphere, and matches outputs for both $\delta^{18}O$ and δ^2H has yet to be described.

The evaporation as a proportion of hydrologic inputs to a surface water body (*E/I*) can be calculated for $\delta^{18}O$ and δ^2H by equation 1.

$$\frac{E}{I} = \frac{\delta_I - \delta_L}{\delta_E - \delta_L} \tag{1}$$

where a δ symbol represents a value for either $\delta^{18}O$ or δ^2H, and the subscripts represent the isotope composition of inputs, outgoing evaporate, and the lake (δ_I, δ_E, δ_L, respectively). The application of an isotope mass balance model to calculate evaporation is reliant upon an accurate determination of δ_E, as all other values can be well approximated and readily measured. δ_E is best estimated as a function of air temperature, relative humidity, the isotope composition of the lake surface (δ_L) and of moisture in the overlying atmospheric (δ_A) following a linear resistance model [8].

2.1. Appropriate weighting of calculation inputs

Hydrologic inputs to the Great Lakes are direct precipitation, catchment runoff, and input from another Great Lake by connecting channel inflow, or interlake mixing in the special case of Great Lakes Michigan and Huron that share a common lake level. In order to produce a representative estimate for the isotope composition to a lake, the isotope composition of each lake input must be weighted to water amount. In the case of precipitation (P), runoff (R) and inflows (C), this is completed at a monthly time step following equation 2.

$$\delta_{\text{P, R, or C}} = \frac{\sum_{i=1}^{n} \delta_i Q_i}{\sum_{i=1}^{n} Q_i} \tag{2}$$

where i is a month (n = 1, 2... 12), δ is a measured value for $\delta^{18}O$ or δ^2H, and Q represents the monthly mean precipitation flux, runoff flux, or connecting channel discharge. Results for the three possible inputs to each Great Lake are weighted against one another to produce a single value for $\delta^{18}O$ and δ^2H for the input to the Great Lake (δ_I) following Eq. 3.

$$\delta_I = \frac{\delta_P P + \delta_R R + \delta_C C}{P + R + C} \tag{3}$$

Fluxes of precipitation, runoff, and interlake input correspond to P, R and C, respectively. Subscripts attached to δ symbols represent the flux weighted $\delta^{18}O$ or δ^2H value for each flux. The Great Lakes are a chain lake system, and the contribution of connecting channel inflow is the dominating input to the lower Great Lakes, Erie and Ontario, but is non-existent for Lake Superior.

Finally, since evaporation is a seasonal occurrence, atmospheric and lake condition inputs to the calculation of *E/I* must be weighted to months when evaporation dominates as established by [9]. This is completed at a monthly time step using GLERL monthly evaporation estimates. As a result, winter and fall conditions dominate the calculation inputs for the Great Lakes. Weighting by evaporation to winter weighting conditions opposes isotope mass balance studies for smaller lake systems in seasonal climates. For these lake systems, weighting by evaporation commonly results in a greater influence of warmer temperatures and generally higher δ_A values of summer months than the annual mean values.

2.2. Calculating $\delta_{E:}$ considerations for the Great Lakes

The immense areas of open water covered by the Great Lakes and the known effects the lakes have on the atmosphere encourage modifications to the formulation of the isotope value for evaporating water. Since evaporated moisture in an upwind

area of a Great Lake modifies the downwind over lake atmosphere, it is reasonable to include a certain proportion of evaporated moisture in the isotope value for the overlying atmosphere (δ_A).

Other considerations include the choice of a kinetic fractionation factor for either smooth or rough conditions. In many studies, fractionation factors developed in wind tunnel experiments are applied. However, in the case of the oceans smooth conditions best represent the kinetic fractionation process. Due to the large areas covered by the North American Laurentian Great Lakes, smooth kinetic fractionation factors are worth considering for use in calculating value for the isotope value of outgoing evaporate (δ_E).

REFERENCES

[1]   CROLEY, T.E., II. Verifiable evaporation modelling on the Laurentian Great Lakes,Water Resources Research **25** (1989) 781–792.

[2]   GIBSON, J.J., EDWARDS, T.W.D., BURSEY, G.G., PROWSE, T.D., Estimating evaporation using stable isotopes: quantitative results and sensitivity analysis for two catchments in northern Canada, Nordic Hydrology **24** (1993) 79–94.

[3]   GIBSON, J.J., BIRKS, S.J., JEFFRIES, D.S., KUMAR, S., SCOTT, K.A., AHERNE, J., SHAW, P., Site-specific estimates of water yield applied in regional acid sensitivity, J. Limnology **69** Suppl. 1 (2010) 67–76.

[4]   GIBSON, J.J., JASECHKO, S., YI, Y., BIRKS, S.J., "Stable isotope balance of lakes and reservoirs: a Canadian perspective", Paper presented at conference on Roles of Stable Isotopes in Water cycle Research, Keystone, Colorado, March 29–31 (2011).

[5]   FROEHLICH, K., Evaluating the water balance of inland seas using isotopic tracers: the Caspian Sea experience, Hydrol. Process. **14** (2000) 1371–1383.

[6]   ZUBER, A., On the environmental isotope method for determining the water balance components of some lakes, J. Hydrol. **61** (1983) 409–427.

[7]   GAT, J.R., SHEMESH A., TZIPERMAN E., HECHT A., GEOGOPOULOS D., BASTURK O., The stable isotope composition of waters of the Eastern Mediterranean Sea, J. Geophys. Res. 101 C3 (1996) 6441–6451.

[8]   CRAIG, H., GORDON, L.I., "Deuterium and oxygen-18 variations in the ocean and the marine atmosphere" (TONGIORGI, Ed.), Proc. Conf. on Stable Isotopes in Oceanographic Studies and Paleotemperatures, Spoleto, Italy (1965) 9–130.

[9]   GIBSON, J.J., A new conceptual model for predicting isotope enrichment of lakes in seasonal climates, IGBP PAGES News **10** 2 (2002)10–11.

GAMMA SPECTROMETRY FOR CHRONOLOGY OF RECENT SEDIMENTS
Tracing human induced climate change in NW Africa

D. PITTAUEROVÁ [a], S. MULITZA [b], H.W. FISCHER [a]

[a] Institute of Environmental Physics,
University of Bremen,
Bremen, Germany

[b] MARUM — Center for Marine Environmental Sciences,
University of Bremen,
Bremen, Germany

Abstract

Gamma spectroscopy was used for the determination of radionuclides in sediment cores from the continental shelf off northwest Africa to provide age control of the sediment record used for a study of aridification of the Sahel zone. ^{210}Pb, ^{226}Ra and ^{137}Cs were measured in the upper part of a gravity core and the associated multicorer and used for aligning these cores. This provided information about the amount of sediment loss due to the sampling procedure in the upper part of the gravity core. The age model based on the matched profiles extended to 140 years B.P. and the rest of the gravity core was dated by ^{14}C. The ^{210}Pb age allowed the estimation of the local radiocarbon reservoir age. Application of ^{210}Pb and ^{137}Cs chronology helps to significantly extend paleoclimatic proxy data into the Anthropocene, thereby allowing the comparison of human induced climate change with natural climate variability.

1.   INTRODUCTION

Gamma spectroscopy is a widely used method for studying sediment samples. A number of radioisotopes which can be used for dating young sediment sequences or tracing changes in recent parts of sediment cores are routinely analysed. These most often include:

- U/Th decay series members: ^{210}Pb, ^{226}Ra (via ^{214}Pb and ^{214}Bi), ^{234}Th, ^{228}Th (via ^{212}Pb, ^{212}Bi and ^{208}Tl), ^{228}Ra (via ^{228}Ac);
- Primordial isotope: ^{40}K;
- Cosmogenic isotope: ^{7}Be;
- Artificial isotopes: ^{137}Cs, ^{241}Am.

[210]Pb (half-life 22.3 a) is a part of [238]U series. It enables the relative dating of ages between 20–150 a and is used for estimation of sedimentation rates in lakes, estuaries and marine sediments as part of environmental, pollution and climate change studies [1]. [210]Pb in sediments consists of two components: supported [210]Pb ([210]Pb$_{sup}$), which is present due to authigenic material of the sediment and is usually assumed to be in radioactive equilibrium with its parent nuclide [226]Ra (half-life 1600 a) and unsupported (or excess) [210]Pb ([210]Pb$_{xs}$), which originates from atmospheric deposition. Unsupported lead is then determined by subtracting supported activity from the total activity and used for estimation of accumulation rates and age models.

Measurement techniques of the total signal of [210]Pb ([210]Pb$_{tot}$) include alpha spectroscopy via [210]Po with assumption of radioactive equilibrium between [210]Po and ^{210}Pb, or gamma spectroscopy. Advantages of gamma spectroscopy over alpha spectroscopy of [210]Pb [2] are that gamma spectroscopy is non-destructive, several isotopes can be measured simultaneously in one spectrum (including [210]Pb$_{sup}$), only physical preparation of the samples (no time consuming chemical separation) is needed and the detection efficiency is only dependent on physical parameters. On the other hand, this method has certain disadvantages. It requires a large amount of sample (minimum 1 g d m., optimum about 50 g d m) for the analysis, gamma spectra have a higher and more complicated background, detection efficiency varies with gamma energy and self absorption of gamma radiation in the sample itself must be considered.

[137]Cs, an artificial radionuclide introduced to the atmosphere by nuclear bomb tests, nuclear accidents and routine discharges from nuclear installations and has a half-life of 30 a. It is often used as a complementary independent and also as an absolute chronometer for the last 60 a. Its onset in the environment can be observed since early 1950s, with maximum nuclear test fallout occurring in 1963. In Europe, the 1986 Chernobyl accident represents another important input of [137]Cs.

2.   METHODS

2.1. Sampling

Terrigenous sediments deposited at the marine site GeoB9501 were sampled by high resolution gravity core (GC) GeoB9501–5 (16°50.44'N, 16°43.97'W, 323 m depth) and multicore (MUC) GeoB9501–4 (16°50.38'N, 16°43.96'W, 330 m depth) on the northern rim of the Mauritania Canyon in the Senegal mud belt during the METEOR Cruise M65/1 in June 2005 (Fig. 1). A multicorer deployed to recover sediment-water interface, the undisturbed sediment surface to the depth of 42 cm and the overlaying water, was equipped with 8 large and 4 small plastic tubes, each of 60 cm length and 10 and 6 cm in diameter, respectively. A core recovered using one of the larger tubes was used for radiometric analysis. A gravity corer was deployed to
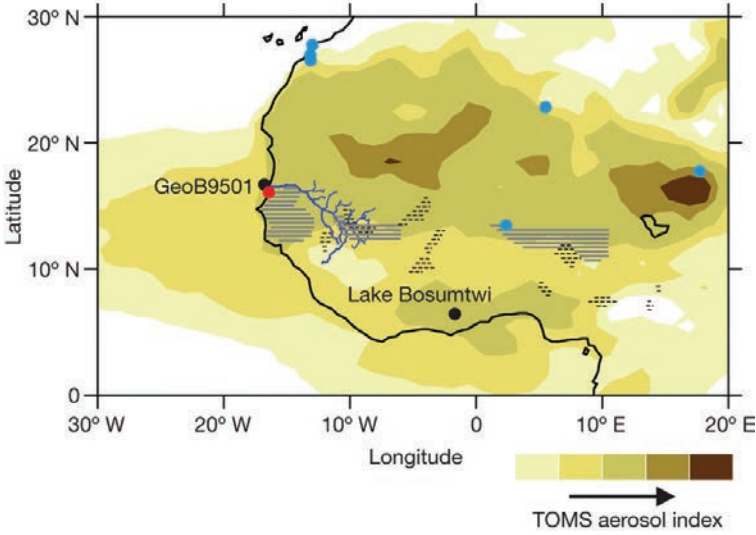
FIG. 1. Location of the marine site GeoB950 (from [3]). The averaged TOMS 1997–2005 aerosol (http://toms.gsfc.nasa.gov/) shows the Sahara-Sahel dust corridor. Aeolian dust together with Senegal river suspension is the main constituent of the GeoB950 sediment. Horizontal hatching indicates agricultural areas with groundnut (solid) and cotton (dashed) production in AD 1914. (Reprinted by permission from Macmillan Publishers Ltd: Nature (Mulitza et al.), copyright (2010)).

recover longer sediment sequences of a total of 532 cm. This set of cores was used as a sediment archive for interpreting a history of 3200 a of Sahel droughts [3].

2.2. Sample preparation

Material of each 1 cm slice of MUC and every other 1 cm slice of GC (upper 42 cm long part of the core – 21 slices) was placed wet into cylindrical plastic containers with a diameter of 69 mm and height of 20 mm. The MUC samples (total 42 slices) were filled in variable heights in the measurement dishes in order to use the maximal amount of the material, while the GC samples were filled to a uniform height of 10 mm. All measurement dishes were sealed in radon proof foil for a minimum of 3 weeks to establish radioactive equilibrium between ^{226}Ra and ^{222}Rn (and its daughter products).

2.3. Gamma spectroscopy

The samples of both GC and MUC were analysed by low level low background gamma spectroscopy using a coaxial HPGe detector (Canberra Industries) of 50% rel. efficiency housed in a 10 cm Pb shielding with Cu, Cd and plastic lining, operated under Canberra Genie 2000 software. Activity concentrations in Bq/kg in the wet

mass sediment of ^{210}Pb, ^{137}Cs, ^{214}Bi, ^{214}Pb and ^{40}K were determined. Activity concentrations in Bq/cm^3 were calculated by multiplying with measured wet densities for MUC. For GC, sediment volume could not be estimated reliably, therefore activity concentrations in Bq/kg dry mass were used instead. The latter quantity was also used for aligning of MUC and GC profiles.

^{210}Pb$_{xs}$ activity concentrations were calculated for each sample as a difference between ^{210}Pb$_{tot}$ and ^{210}Pb$_{sup}$. For estimation of ^{210}Pb$_{sup}$, ^{214}Pb in equilibrium with ^{226}Ra was used. Additionally, self attenuation corrections for low energy ^{210}Pb (45.6 keV, I$_\gamma$ 4.25%) for the MUC were necessary due to varying sample geometries. They were calculated using a modification of the Hurtado et al. method [4], combining both experimental transmission measurements and mathematical Monte Carlo simulations. In this study, the full energy peak efficiencies for samples of zero density with different heights in measurement containers were generated using the Monte Carlo based LabSOCS Genie 2000 calibration tool [5]. For the associated GC no individual self-attenuation corrections were applied for ^{210}Pb due to the constant geometry of the samples. Instead, efficiency values experimentally obtained with test sources of similar geometry were used.

3.   RESULTS AND DISCUSSION

3.1. ^{210}Pb$_{xs}$ and ^{137}Cs age model

The age model for MUC and GC was developed using a combination of two independent radiometric methods. A ^{210}Pb$_{xs}$ and ^{137}Cs pair was employed for the upper part of the cores and AMS radiocarbon dating of planktonic Foraminifera for the rest of the GC [3].

For the ^{210}Pb$_{xs}$ age model of MUC, the classical constant rate of supply (CRS) model was applied [6]. The absolute chronology extends to AD 1915 ± 7 in the depth of 42.5 cm. ^{137}Cs activity concentrations were compared to the expected ^{137}Cs bomb fallout atmospheric input. The ^{137}Cs data show a broad maximum in approximately AD 1962–81. The onset of ^{137}Cs in the profile in AD 1947 ± 3 is in a relatively good agreement with atmospheric bomb testing initiation in the early 1950s. Due to rather low ^{137}Cs values, the measurement uncertainties are high and do not provide fine resolution. It was not possible to clearly identify the AD 1963 nuclear fallout peak or the contribution of the four geographically close French atmospheric nuclear tests in Algeria, performed in AD 1960–61. Nevertheless, the shape of the ^{137}Cs profile is compatible with the bomb fallout chronology, possibly followed by a terrestrial erosion component, especially when the activities are decay corrected using ages derived from the ^{210}Pb$_{xs}$ chronology (Fig. 2).
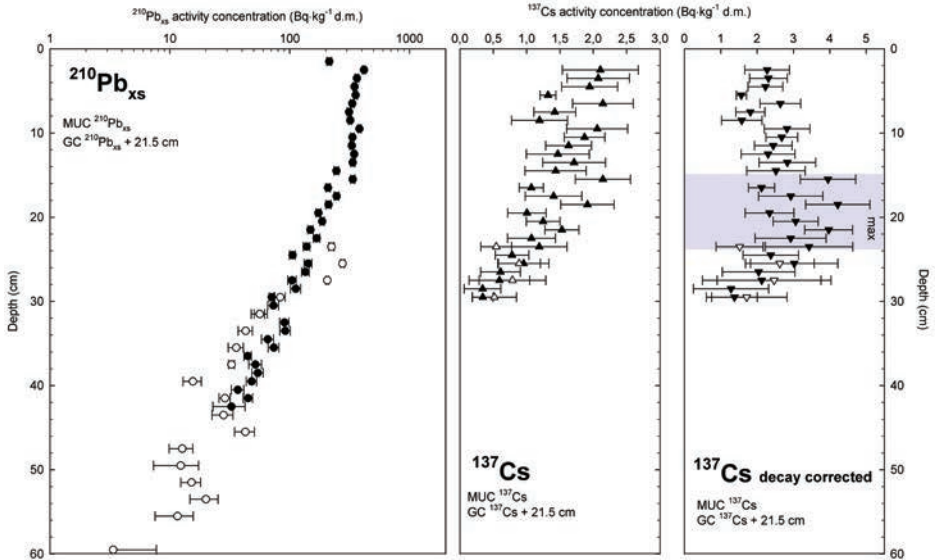
FIG. 2. Depth matching of the MUC and GC records for $^{210}Pb_{xs}$ (log-scale, left) and ^{137}Cs (linear scale, middle and right) profiles. The error bars for all data are 1 standard deviation (they include counting statistics and calibration of the measuring device). ^{137}Cs under 30 cm depth are below detection limit. ^{137}Cs profile in the right is decay corrected to the date of analysis using ages derived from $^{210}Pb_{xs}$ model. A broad maximum in approximately AD 1962–81 is shaded.

3.2. Matching the cores and extending the chronology

During sampling using a gravity corer, usually some loss of material on the top of the core is inevitable. It is thus important to determine how much material was lost during the sampling procedure. Obtaining a continuous profile by aligning GC and MUC is also desirable. Routinely this is done by colour, physical properties, stable isotopes or main elements content. Our approach suggests using radionuclide data for matching MUC and GC.

Depth aligning of the GC and the MUC was performed using the corresponding $^{210}Pb_{xs}$ and ^{137}Cs profiles using a method based on least square fitting described in [7]. The onset of ^{137}Cs corresponds to a depth of 29.5 cm in MUC and to a depth of 8 cm GC. An upper segment of about 21.5 cm long sediment material was lost during gravity coring (Fig. 2). The correctness of the matching was independently validated by profiles of the main element composition (Al, Si, K, Fe, Ti) and their ratios, which were also variable [7]. The $^{210}Pb_{xs}$ profile appears to be disturbed in the uppermost part of the GC (not an unusual finding due to the mechanical impact applied during the coring procedure), but it shows a very good continuity to the MUC-B profile from the composite depth of 43 cm downwards, which enables the extension of the chronology.

Following the aligning of MUC and GC, the age model for the MUC could be extended to the GC based on an average sedimentation rate obtained from a combined record of MUC $^{210}Pb_{xs}$ data from the depths of 16.5–42.5 cm with the follow-up part of the GC (depth 43.5–63.5 cm) (Fig. 3). This part of the composite profile showed an exponential decrease, which enabled the expression of a mean sedimentation rate based on an exponential fit obtained by the least squares method. The average sedimentation rate was then used for dating the upper part of the GC to the composite depth of 63.5 cm, corresponding to AD 1864 $\pm$ 9.

The combined MUC and GC chronology based on gamma spectroscopy covered the youngest, 140 year old, part of the core. The interconnection of the combined $^{210}Pb_{xs}$ and ^{137}Cs model to the radiocarbon model of the GC (Fig. 3) was constructed by fitting a weighted four-order polynomial function to the pooled $^{210}Pb_{xs}$ and calibrated radiocarbon ages by the least square method [3].

3.3. Radiocarbon reservoir age

The $^{210}Pb_{xs}$ age model allowed the estimation of the local radiocarbon reservoir age using the AMS ^{14}C-date of a Foraminifera sample from the bottom of a parallel core (45.5 cm) from the same MUC cast. From the $^{210}Pb_{xs}$-based age model, it was estimated that this core depth corresponds to AD 1907. The calculated local reservoir effect of 140 years [3] was used for the calibration of the conventional AMS radiocarbon dates of GC. A constant reservoir age was assumed throughout the time period covered by the sediment record.
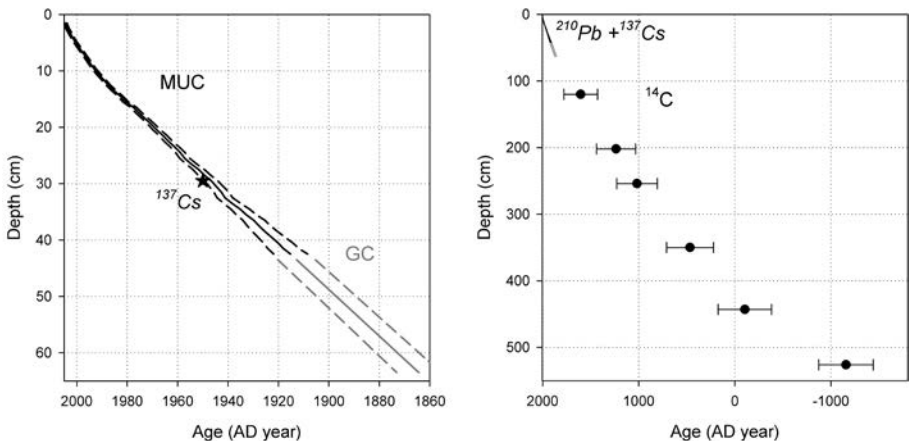
FIG. 3. Left: Extended $^{210}Pb_{xs}$ chronology for aligned MUC and GC. The dashed lines stand for 1σ confidence limit of $^{210}Pb_{xs}$ age. ^{137}Cs onset in the depth of 29.5 cm is in a good agreement with $^{210}Pb_{xs}$ chronology. Right: Radiocarbon ages [3] (error bars indicating 2 standard deviations) together with $^{210}Pb_{xs}$ chronology from the left figure.

3.4. Use of the age model for paleoclimatological interpretations

Further sediment sample parameters were determined, including bulk geochemistry of Si, Al, Ti, K, Ca, and grain size analysis was performed by the team at MARUM. The data were analysed and interpreted in Mulitza et al. [3]. The main constituents of the studied sediment material are aeolian dust (Si rich, with particles up to 200 mm) and fine Senegal river suspension (Al and Fe rich, 95% < 10 mm). The relative proportions of riverine, aeolian and marine contributions were evaluated by endmember analysis. Dust and fluvial endmembers were constructed using the normalized relative abundances of Si, Al, Ti, K and Ca from modern aeolian and riverborne materials and the marine endmember was constructed theoretically (98% Ca, 2% Si) [3]. Knowing sedimentation rates enabled the expression of dust fluxes in the past (Fig. 4).
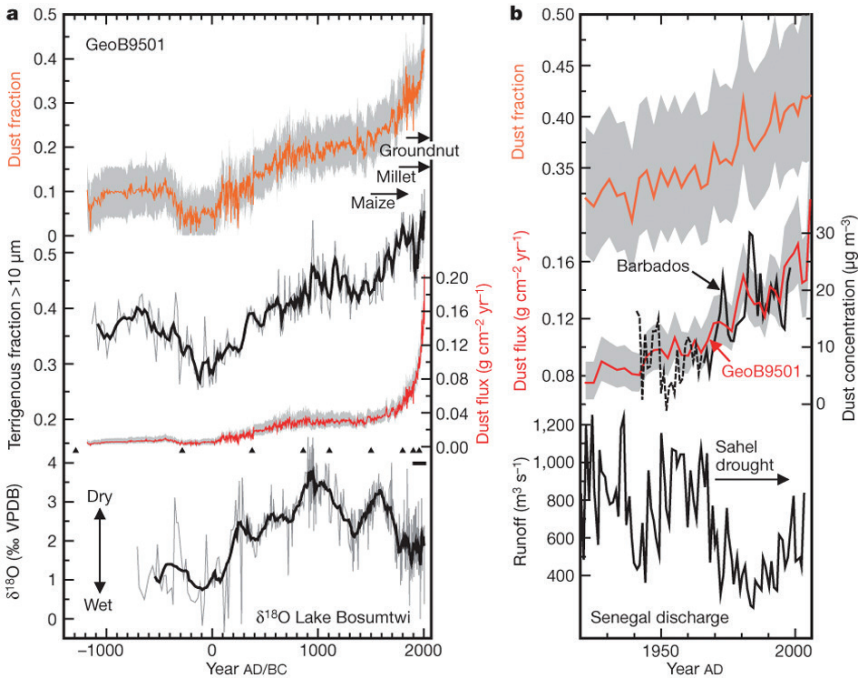
FIG. 4. Left (from [3]): The mean dust fraction, terrigenous grain size fraction > 10 μm and dust deposition flux records were compared to literature data on $\delta^{18}O$ authigenic carbonate from Lake Bosumtwi (Ghana), indicating dry and wet periods in Sahel history. The triangles indicate radiocarbon age control and the horizontal bar the time period dated by the $^{210}Pb_{xs}$ and ^{137}Cs method.

Right (from [3]): Recent records of mean dust fraction and dust deposition flux compared to instrumental measurements of airborne African dust concentrations at Barbados from mid–1960s (the pre-1968 record is estimated from regression with Sahel precipitation) and Senegal river discharge.

4. CONCLUSIONS

The reconstruction of the history of African dust generation showed that the onset of commercial agriculture about 200 years ago started to contribute to the overall dust budget (Fig. 4). Corn was introduced to the Sahel in the early 18th Century. It was gradually replaced by millet and sorghum in the mid 18th Century. The steepest dust deposition increase can be observed in the period of commercial peanut production in Senegal, Nigeria and Gambia starting in the 1840s. It was suggested that deforestification and the expansion of agriculture use of the land in the Sahel zone contributed extensively to wind erosion in the region [3].

REFERENCES

[1]   APPLEBY, P.G., Three decades of dating recent sediments by fallout radionuclides: a review, Holocene **18** (2008) 83–93.

[2]   ZABORSKA, A., CARROLL, J., PAPUCCI, C., PEMPKOWIAK, J., Intercomparison of alpha and gamma spectrometry techniques used in ^{210}Pb geochronology, J. Env. Rad. **93** (2007) 38–50.

[3]   MULITZA, S., et al., Increase in African dust flux at the onset of commercial agriculture in the Sahel Region, Nature **466** (2010) 226–228.

[4]   HURTADO, S., VILLA, M., MANJÓN, G., GARCÍA-TENORINO, R., A self-sufficient and general method for self-absorption correction in gamma-ray spectrometry using GEANT4, Nucl. Instrum. Meth. A **580** 1 (2007) 234–237.

[5]   BRONSON, F.L., Validation of the accuracy of the LabSOCS software for mathematical efficiency calibration of Ge detectors for typical laboratory samples, J. Radioanal. Nucl. Ch. **255** 1 (2004) 137–141.

[6]   APPLEBY, P.G., OLDFIELD, F., The calculation of lead–210 dates assuming a constant rate of supply of unsupported ^{210}Pb to the sediment, Catena **5** (1978) 1–8.

[7]   PITTAUEROVÁ, D., FISCHER, H.W., MULITZA, S., "Using ^{210}Pb and ^{137}Cs record for matching sediment cores", Proc. International Topical Meeting on Polonium and Radioactive Lead Isotopes, Seville, Spain, October 2009.

MULTI-TRACER APPROACH FOR SHELF WATER MIXING STUDIES IN BRAZILIAN REGIONS UNDER DIFFERENT CLIMATES

L.D. LACERDA[a], M.L.D.P. GODOY[b], R.V. MARINS[a], J.M. GODOY[c],
T.A. SOUZA[c], F.J.S. DIAS[a], C.E. REZENDE[d]

[a] Instituto de Ciências do Mar,
Universidade Federal do Ceará,
Fortaleza, CE, Brazil

[b] Instituto de Radioproteção e Dosimetria,
Comissão nacional de Energia Nuclear,
Rio de Janeiro, RJ, Brazil

[c] Departamento de Química,
Pontifícia Universidade Católica,
Rio de Janeiro, RJ, Brazil

[d] Centro de Biociências e Biotecnologia,
Universidade Estadual do Norte Fluminense,
Campos dos Goytacazes, RJ, Brazil

Abstract

Fresh water and sediment supply at estuary and plume regions has dramatically changed due to land use changes, mostly damming, in river basins. The resulting impact, however, may vary significantly depending on climate and hydrology. The seasonal differences in shelf, plume, estuarine and river waters of two watersheds located under contrasting climates in the Brazilian coast are reported using a multi-tracer approach (salinity, barium, silica, uranium, deuterium and ^{18}O) to characterize the mixing processes. At the Paraíba do Sul River, SE Brazil, in a wet tropical coast, all results showed similarity between dry and wet seasons; at the Jaguaribe River under semi arid climate in NE Brazil, the results showed a moving freshwater plume depending on season, with freshwater at the estuary in the rainy season and shelf water intrusion upstream in the estuary in the dry season. Most tracers used were able to consistently characterize water masses even in the wide range of latitudes studied, confirming their importance as a tool for modelling mixing processes at the continent–ocean boundary. Barium, however, still needs better studies on its seashore chemistry, since in the semi arid site, Ba distribution could not be directly related to conservative mixing behaviour, at least during the rainy season.

1. INTRODUCTION

Rivers are the major route of transfer of dissolved and particulate continental materials to the ocean. During transport, several physical, chemical and biological factors can quantitatively and qualitatively modify the original geochemical forms and source signatures along the continent–ocean axis. The longitudinal distribution of these factors is a function of the regional climate, resulting in multiple situations of complex hydrodynamics that makes the assessing of water and materials flows through conventional techniques difficult, in particular in medium and small catchments, which, although generally disregarded, can represent a large contribution for certain elements, especially in areas with dense human occupation. Under humid climates, rivers always have a positive flux towards the ocean, meaning that varying proportions of freshwater can be identified in over continental shelf areas. Under semi arid climates, however, fluvial fluxes can be zero or even negative, meaning that seawater may move upstream into rivers. The mixing zones in estuaries and river plumes are highly dynamic milieus where sorption/desorption processes, biological uptake, sedimentation and erosion combine to give typical hydrochemical signatures, which once identified can be used to monitor alterations in flux dimensions due to changes in land use along river basins and due to global climate changes.

Different tracers have been used in many studies; however, few compared significantly large latitudinal gradients. Among these, the most used so far for estuarine mixing process studies were Ba, U, Si, and more recently ^{18}O and Deuterium. Barium distribution at the continent–ocean interface suggests desorption from river-borne sediments, which effectively increases Ba flux to the ocean [1]. Desorption of elements bound to particles presumably occurs owing to a decrease in their adsorption coefficients with increasing ionic strength [2]. Ba behaviour in estuarine waters is dominated by the release from particle phases in the low to moderate salinity ranges. Most of the release is attributed to ion exchange between major cations of seawater and Ba bound to the fluvial suspended particle load. Uranium behaviour in estuarine waters is frequently characterized as a conservative mixing of the enriched seawater with U-poor freshwater. In continental surface waters, U mainly comes from the presence of naturally occurring radioactive materials in the Earth's crust. Its release is primarily controlled by the weathering rates of the source rocks. Uranium forms various soluble complexes with ions, such as bicarbonate. In estuaries, dissolved uranium behaves in a globally conservative manner and shows a linear relationship with salinity [3]. Silicon as well as barium derives from the weathering of continental rocks, and being relatively inert along the mixing zone of estuaries, save for eventual uptake by the biota, Si has been successfully used as a tracer of the river water in mixing studies of the continent–ocean interface. Along estuaries, the δ^2H vs $\delta^{18}O$ plot should be a straight line between the two water endmembers: sea and river water. The relative distance to the endmembers represents the percentage of mixture. Deviation of

the expected behaviour indicates the presence of an additional water source — under natural conditions generally groundwater discharge.

The result of the adsorption/sorption process, however, will result in different settings depending on the actual location of the mixing zones within estuaries. Therefore if sedimentation or solubilization will be the end processes they can either occur inside the river proper or outside in the continental shelf. This study examines the dominant water mixing patterns using different stable and radionuclide tracer distributions in surface waters along a continuum from the river to the continental shelf, during different seasons and under contrasting climates in the humid southeastern and the semi arid NE sectors of the Brazilian coast. Our main objective is to propose a set of tracers to be used for the monitoring of eventual changes in the extension and intensity of the mixing processes at the continent–ocean interface and changing environmental scenarios due to land use modifications and global climate changes. The chosen tracers will be tested for their validity over a wide range of latitudes.

2. MATERIAL AND METHODS

2.1. Study area and sampling strategy

Sampling campaigns were carried out in two sectors of the Brazilian coast. At the humid southeast coast at the Paraíba do Sul River (PSR) surface water samples from the river plume and the adjacent continental shelf were collected from two day-long cruises conducted in August 2007 (winter, dry season), when the river discharge averaged 330 m^3/s and in March 2008 (summer, rainy season) when the average river discharge was a maximum of 780 m^3/s (details of the region and its environmental characteristics can be found in Ref. [4]). Sampling points were distributed along perpendicular transects from the river mouth to about 30 km away in the continental shelf (Fig. 1a).

The other campaigns were carried out at the semiarid northeastern coast off the Jaguaribe River (JR), where surface water samples were collected from the river proper, estuary, plume and the adjacent continental shelf. Cruises were conducted during the rainy season (May 2009) when the river discharge was a maximum of 160 m^3/s and the dry season (October 2009) when the river discharge may approach zero (details of the region and its environmental characteristics can be found in Ref. [5]). Each cruise from these campaigns lasted an average of 10 days and consisted of hydrographic stations distributed in five transects of 3 nautical miles each totalling 16 stations at the inner shelf region off the mouth of the Jaguaribe River. The middle and external continental shelf off the Jaguaribe River were represented by five transects of about 25 nautical miles each, totalling 25 hydrographic stations. In the river and estuary fixed stations representative of each section were established and 6 samples were collected at 2 hour intervals through an entire tidal cycle (Fig. 1b).
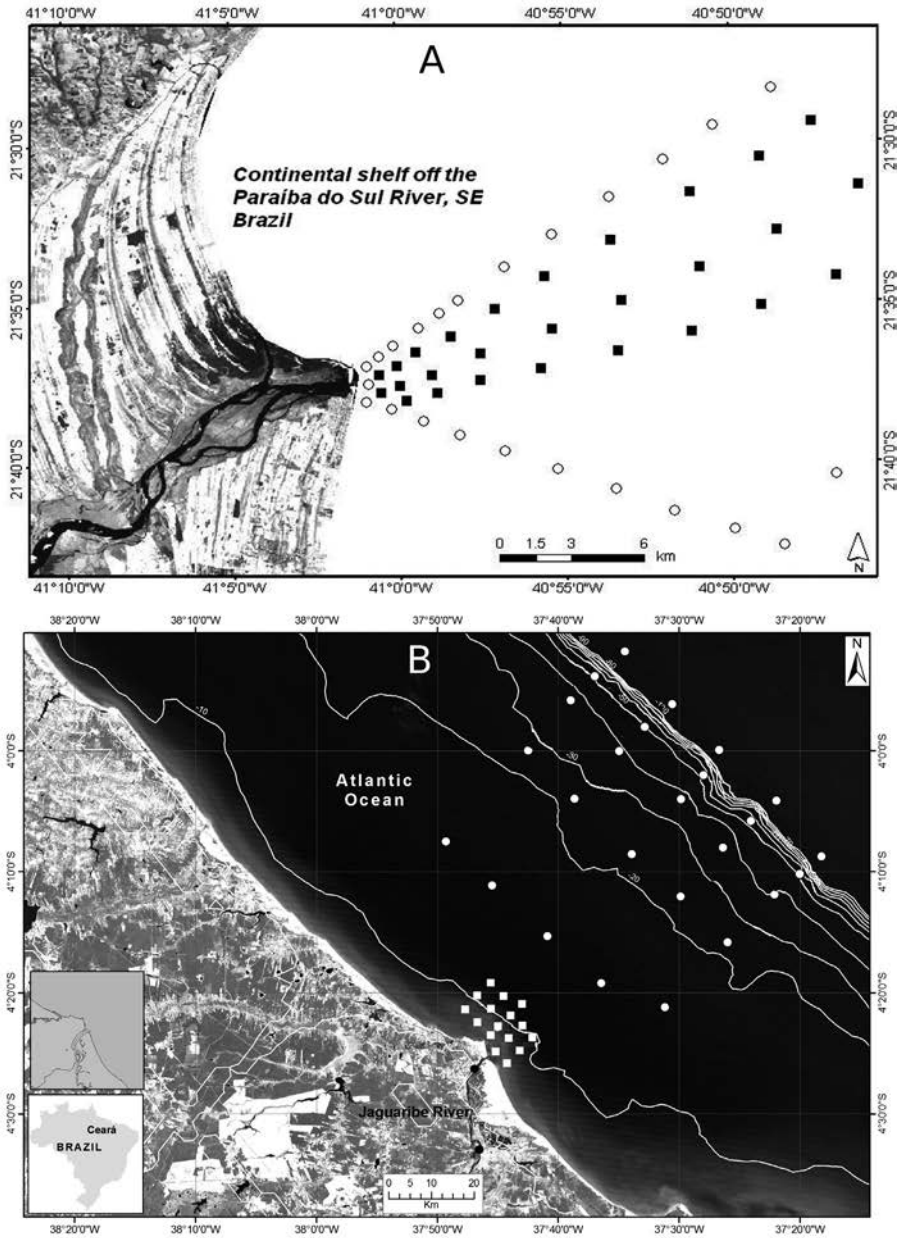
FIG. 1. Satellite imaging showing the 4 study transects (2 for each season) at the Paraíba do Sul River (1a). Continental shelf off the Jaguaribe River showing sampling grid (16 stations five transects in the plume region) and the 25 stations grid in five shelf transects between the 10–100 m isobaths, during dry and rainy seasons. At the river and estuary the two fixed stations are shown as dots in the river (1b). Maps were laid over images provided by the National Institute of Space Research of Brazil (INPE, www.inpe.gov.br).

2.2. Hydrochemistry

At the PSR only water temperature and salinity/conductivity were measured with a pH/conductivity pocket meter (WTW, model: pH/Cond 340i), which was calibrated with a solution of KCl (35 g/kg). All salinity measurements were performed at 25°C. At the JR CTD data (pressure, temperature and salinity) were collected along 10 m isobaths in the inner shelf and along 10 m, 20 m, 30 m, 50 m and 100 m isobaths in the middle and external shelf. Based on calibration, the final precision of CTD data was ± 0.05 SU and ± 0.02°C. The sampling rate of the CTD was 15 Hz.

2.3. Silicon, barium, uranium, $\delta^{18}O$ and δ^2H

Concentrations of silicon and barium in seawater samples were determined by Inductively Coupled Plasma-Optical Emission Spectroscopy (ICP–OES; Perkin Elmer, model: Optima 4300 DV). Direct analysis was used without dilution and scandium was applied as an internal standard. During the second sampling campaign, the ^{238}U concentration in seawater samples was determined by Inductively Coupled Plasma Mass Spectrometry (ICP–MS; Varian, model: 820 MS). Analysis was performed after dilution by 1:100 and thallium (Tl) was applied as an internal standard.

δ^2H and $\delta^{18}O$ were determined by applying a PICARRO isotope water analyser L1120i with an auto sampler. IAEA standards, VSMOW2, GISP and SLAP2, were
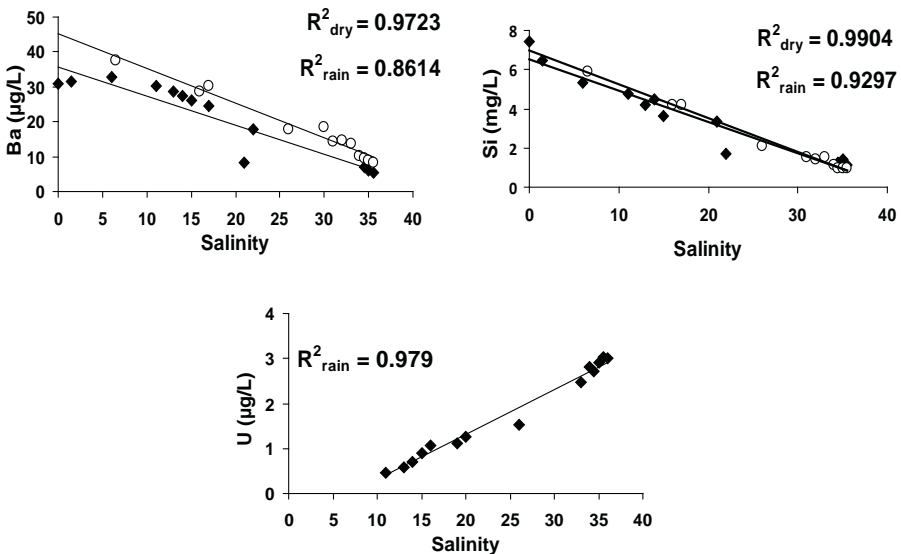
FIG. 2. Tracer (Ba, Si and U) concentrations distributions in dry and rainy seasons along the salinity gradient at the continent-ocean interface in the Paraíba do Sul region, humid coast of SE Brazil. Only rainy season samples were available for U.

measured in six samples each. Samples and standards were injected six times and only the last three injections were used to calculate the results. Each batch of twelve unknown samples also contains control samples.

3.   RESULTS AND DISCUSSION

Concentration distributions of Ba, Si and U in the Paraíba do Sul area is presented in Fig. 2. There is no significant difference between tracer distributions in the rainy and the dry season. The three tracer elements presented expected distributions with straight lines strongly suggesting dilution of the fluvial waters (enriched in Ba and Si) into marine waters (enriched in U).
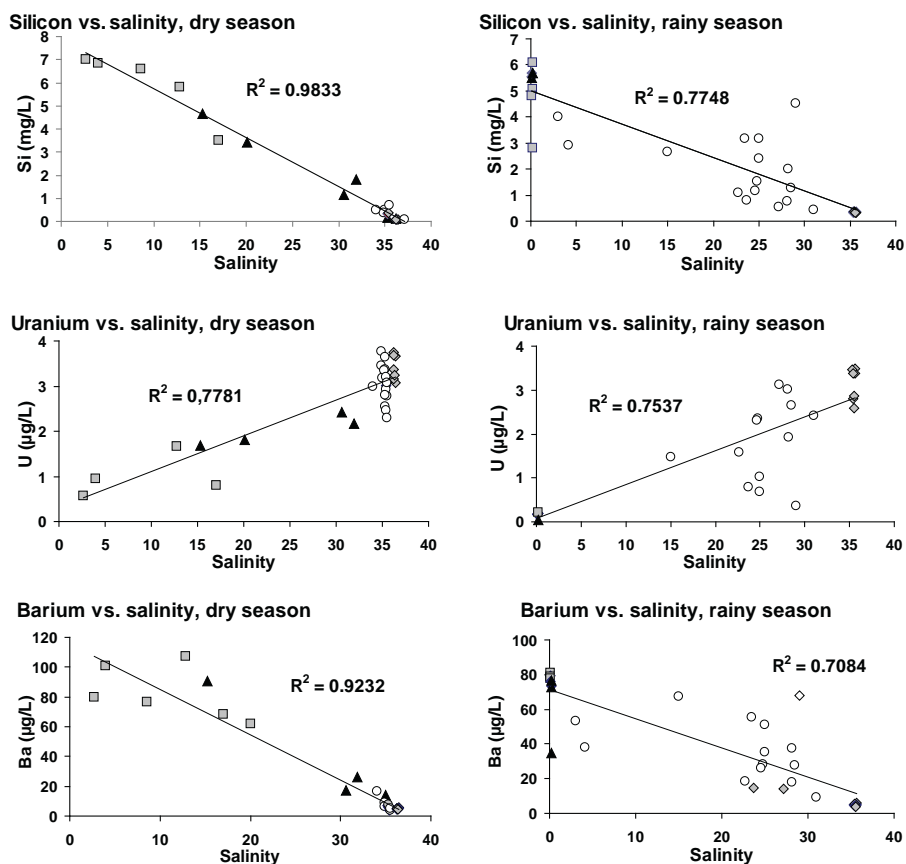
FIG. 3. Tracer concentrations distributions in dry and rainy seasons along the continent-ocean interface in the Jaguaribe River region, semi arid coast of NE Brazil.

54

At the Paraíba do Sul River, under a humid climate, Ba, Si and U presented significantly linear correlations with salinity, suggesting diffusion and dilution as the major controls of the final tracer concentrations along the continent–ocean interface. The only seasonal difference noted at this site was the occurrence of a certain displacement in the seaward reach of freshwater into the shelf. Therefore, the tracers used can be consistently applied irrespective of the season.

At the semi arid coast, off the Jaguaribe River, the distribution of the tracers (Fig. 3) also followed the salinity gradient. However, seasonal differences were most striking. During the dry season shelf waters invade the estuary and river sites, whereas in the rainy season river waters invade the estuary. Comparing the two sites, Si and U presented similar concentrations, since their geological sources and dissolution processes are similar in both areas. However, Ba concentrations were much higher in the semi arid NW, at almost twice the level. Also, during the rainy season when Ba is particularly enriched in plume waters it shows a poorer correlation with salinity. The local continental geology is particularly enriched in calcareous rocks. Also,
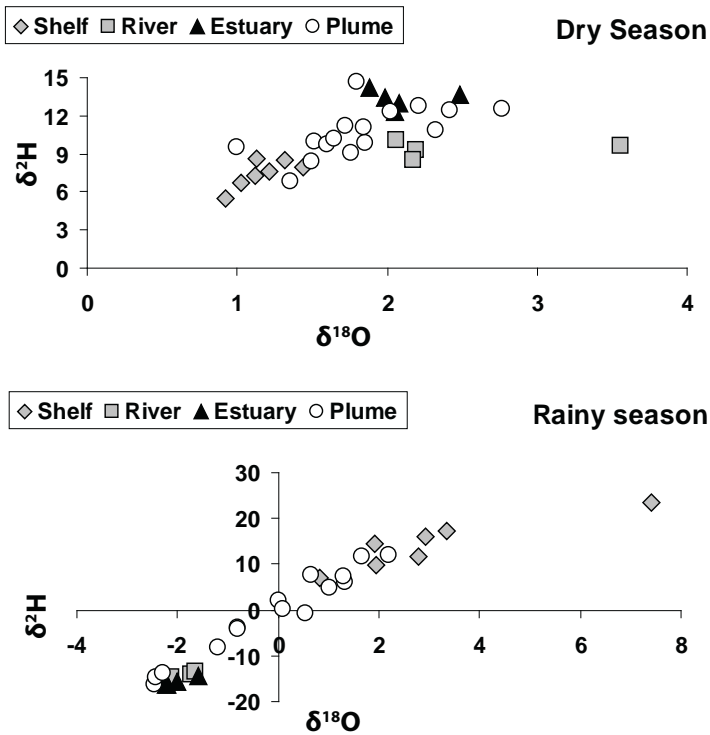
FIG. 4. Seasonal distribution of δ^2H and $\delta^{18}O$ along the continent–ocean interface at the Jaguaribe River, semi arid coast of NE Brazil.

continental shelf and near shore bottom sediments may reach up to 98% of biogenic carbonates. Previous work in this region's continental shelf showed the control of Ba concentrations by carbonate chemistry [6]. Therefore, autogenous control of Ba concentrations may affect its concentration gradient, reducing its application as a consistent tracer in this region.

Fig. 4 presents the seasonal distribution of δ^2H and δ^{18}O along the continent–ocean interface at the Jaguaribe River site. During the rainy season river water is dominated by precipitation showing typical distribution patterns. However, during the dry season the distribution suggests another source of freshwater, probably subterranean as shown by the outlier of river water within the marine endmember. This agrees with Ba distribution, also suggesting that careful analysis of Ba distribution should be made when using this tracer in semi arid climates.

Based on the results, it was possible to conclude that the multitracers used in this study (salinity, Si, and U, as well as δ^{18}O and δ^2H) presented satisfactory results defining the plume reach and determining the positioning of the estuarine mixing zone in different seasons and along a large latitudinal gradient, which includes humid and semi arid climates. Barium, however, should be used with care, at least in semi arid littorals and during specific seasons.

REFERENCES

[1]   LI, Y.H., CHAN, L.-H., Desorption of Ba and ^{226}Ra from river-borne sediments in the Hudson estuary, Earth Planet. Sci. Let. **43** (1979) 343–350.

[2]   NOZAKI, Y., et al., Dissolved barium and radium isotopes in the Chao Phraya River estuarine mixing zone in Thailand, Cont. Shelf Res. **21** (2001) 1435–1448.

[3]   SAARI, H.-K., et al., Spatiotemporal variation of dissolved ^{238}U in the Gironde fluvial-estuarine system (France), J. Environ. Radioact. **99** (2008) 426–435.

[4]   SOUZA, T.A., et al., Use of multitracers for the study of water mixing in the Paraíba do Sul River estuary, J. Environ. Radioact. **101** (2010) 564–570.

[5]   DIAS, F.J.S., et al., Hydrology of a well-mixed estuary at the semi arid Northeastern Brazilian coast, Acta Limnol. Brasil. **21** (2009) 377–385.

[6]   LACERDA, L.D., MARINS, R.V., Geoquímica de sedimentos e o monitoramento de metais na plataforma continental Nordeste Oriental do Brasil, Geochim. Brasil. **20** (2006) 120–132.

APPLICATION OF RADIOTRACER METHODOLOGY FOR UNDERSTANDING THE INFLUENCE OF GEOCHEMICAL FRACTIONATION ON METAL BIOAVAILABILITY IN ESTUARINE SEDIMENTS

N.S. FISHER, Z. BAUMANN
School of Marine and Atmospheric Sciences,
Stony Brook University,
Stony Brook, New York USA

Abstract

To evaluate the extent to which contaminated sediments could introduce metals into marine food chains, gamma emitting radioisotopes of arsenic, cadmium and chromium were used to study their geochemical fractionation in estuarine sediments and bioavailability to deposit feeding polychaetes. Radioisotopes were added to sediments directly or via planktonic debris and were then fractionated with a sequential extraction scheme after aging for up to 90 days. The assimilation of ingested metals was positively related to their partitioning in the two most readily extractable (labile) sediment fractions and negatively related to refractory organic fractions, oxides, and pyrite. In comparison to uptake from ingested sediment, metal uptake from pore water was negligible. A metal bioaccumulation model, modified to consider their geochemical fractionation, was found to quantitatively predict metal concentrations in benthic polychaetes better than total metal concentrations in sediment. Metals need to desorb from ingested particles into gut fluid within the polychaete gut before they can be assimilated.

1. INTRODUCTION

Coastal and estuarine sediments are greatly enriched in particle reactive metals relative to overlying waters [1, 2], and they can serve as important sources of metals for benthic animals [3–5]. Deposit feeding animals ingest sediments to acquire nutrients and have been shown to assimilate potentially toxic metals from ingested sediments [6, 7]. Benthic animals can also acquire metals released from sediments into pore water and overlying water, although the aqueous phase typically represents a much smaller source of metals for benthic animals than dietary sources [8, 9]. Despite the importance of sediments as a source of metal contaminants for marine food chains, there remain many uncertainties with respect to the extent to which sediment-bound metals are biologically accessible to benthic animals. In particular, it is known that metals can partition into different geochemical fractions in sediments [10], and the bioavailability of metals from these distinct fractions can vary significantly [7, 11]. Moreover, differences are to be expected among different kinds of sediments,

with varying grain sizes and organic contents and among metals, each with its own characteristic binding patterns to different sediment phases and its own ability to cross the gut lining of deposit feeding animals. Differences are also to be expected among animal species, whose gut characteristics, including gut fluid composition, acidity, and redox conditions all may influence the fate of ingested metals [12]. Previously, it was concluded that a metal must be solubilized from ingested sediment into gut fluid before it can be assimilated across the gut lining [13]. This issue was further explored here.

2.   DESCRIPTION OF EXPERIMENTS

In this study, we present the results of controlled experimental studies involving radiotracers, in which the fractionation of radioisotopes of three different metals (arsenic, cadmium, and chromium) introduced to sediments collected from three different estuaries was assessed. The fractionation patterns of the radiotracers were related to their assimilability in the deposit-feeding polychaete, *Nereis succinea*, a ubiquitous worm which can serve as a source of metal for bottom feeding fish and crabs. Three different sediments were used in these experiments. Two sample sites were from Chesapeake Bay: Baltimore Harbor (salinity 8.5) and Elizabeth River, Norfolk, Virginia (salinity 19.5). A third site was from Mare Island in San Francisco Bay (salinity 23). The organic carbon and nitrogen contents of the sediments were 5.0 and 0.3%, respectively (by wt) for Baltimore, 2.0 and 0.1% for Elizabeth River, and 1.5 and 0.1% for Mare Island.

Gamma emitting isotopes of arsenic (^{73}As, $t_{1/2}$ = 80.3 d), cadmium (^{109}Cd, $t_{1/2}$ = 461.4 d), and chromium (^{51}Cr, $t_{1/2}$ = 27.7 d) were used to follow the fate of these metals. Tracer concentrations (typically amounting to $<<1\%$ of background metal concentrations in the sediments) were added directly to the surface of sediments or added via radiolabelled algal debris. These labelling methods simulated sorption of metals from overlying waters (direct addition method) or addition of metals through settling planktonic debris (algal debris method). To add the metals directly to the sediments, the isotopes were injected directly onto the surface of sediments so the isotopes could sorb to the sedimentary particle surfaces. To add the metals via algal debris, diatom cells were exposed to dissolved radioisotopes for up to one week and, after becoming uniformly radioactive, were harvested by filtration and centrifugation; this radioactive algal paste of radiolabelled cells was mixed in with the sediments. The isotope additions resulted in concentrations of 1–11 kBq/g or 3–12 kBq/g (wet wt) sediment for ^{73}As added directly or via algal debris, respectively, from 9–169 kBq/g or 4–72 kBq/g (wet wt) sediment for ^{109}Cd added directly or via algal debris, respectively, and from 2–28 or 2–31 kBq/g (wet wt) sediment for ^{51}Cr added directly or via algal debris, respectively. The radiolabelled sediments were then incubated at 21°C
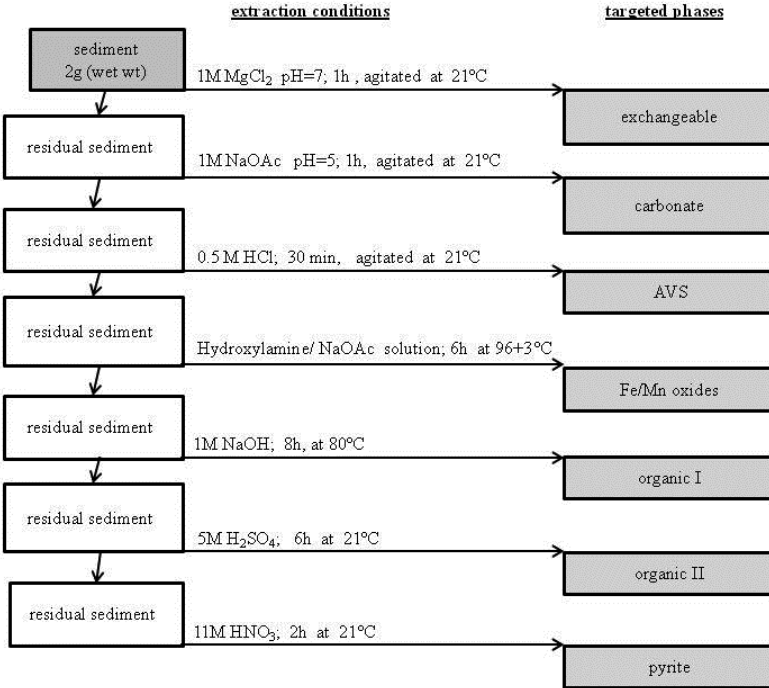
FIG. 1. Scheme showing the steps of the sequential extraction procedure used in this study.

for 2, 30 or 90 days, after which they underwent a sequential extraction procedure (Fig. 1) or were presented to *N. succinea* for feeding and assimilation studies.

The assimilation of radioisotopes by the worms was determined using a pulse-chase feeding approach for polychaetes described by Wang et al. [14] and Baumann and Fisher [7]. Calculations of radioisotope assimilation efficiencies were made by regressing the retention of each isotope in the worms over time following the radio-active feeding, specifically by determining the *y*-intercept of the slowly exchanging pool of isotope retained by the worms [8]. The efflux rate constant of a radioisotope, reflecting the physiological turnover of the assimilated radioisotope, was determined by calculating the slopes of the slowly exchanging pool of each isotope in the worm. Metal uptake from pore water, extracted from sediments by centrifugation at 7500 g, was also determined with these radioisotopes for worms exposed for 2–4 hours and depurated for up to 14 days [9]. These parameters were used in a widely-used bioki-netic (or biodynamic) model of metal bioaccumulation in animals, in which the metal concentration at steady state in the animal tissue (C_{ss}) is determined as:

$$C_{ss} = \frac{k_u}{k_{ewslow} + g} C_w + \frac{AE \times IR}{k_{ef} + g} C_f \tag{1}$$

where k_u = the metal uptake rate constant from the aqueous phase, C_w = the concentration of metal dissolved in pore water, AE = assimilation efficiency, IR = wet-specific ingestion rate, C_f = metal concentration in the food, k_{ew} and k_{ef} = metal efflux rate constants from the worms following uptake from water and food, respectively, and g = growth rate constant of the animal (typically negligible for adult animals compared to k_e values). This model has been shown to accurately reflect metal body burdens measured independently in marine animals on a site-specific basis [15, 16] and can be used to delineate metal uptake from dietary and aqueous sources [8]. In the case of deposit feeding worms feeding on sediments, we further refined the metal concentration in the sediments (C_f) to reflect the fractionation of the metal in them, specifically in the two most labile fractions (nominally, the 'exchangeable' and 'carbonate' phases, dubbed here 'carbonex').

$$C_{ss} = \frac{k_u}{k_{ewslow} + g} C_w + \frac{z_i \times b_i \times IR}{k_{ef} + g} C_f \tag{2}$$

$$C_{ss,f} = \frac{z_i \, b_i \, IR}{k_{ef} + g} C_f \tag{3}$$

This modification took into consideration the % of metal in the carbonex sedimentary fraction ($z_{carbonex}$) and the regression slope between the metal AEs and % of metal in a given sedimentary fraction ($b_{carbonex}$) [9].

To better understand the process of metal assimilation from ingested sediment, the assimilation of [73]As in *N. succinea* was compared with the release of [73]As from ingested sediment (radiolabelled with or without added algae) into gut fluid. Radiolabelled sediments were immersed in extracted gut fluid for up to 4 hours (to simulate typical gut passage times) and the [73]As release into gut fluid was compared with the AE of [73]As from those sediments in intact worms.

3.   RESULTS AND DISCUSSION

The fractionation of As, Cd, and Cr radioisotopes in the different sediments after 30 days of exposure is shown in Table 1. For the directly labelled sediments, As was predominant in the organic phases, AVS and residual phases, whereas in the sediments labelled via algal debris Fe/Mn oxides also accounted for about 20% of the As. Cd was most prominent in the exchangeable phases of the different sediments, followed by Fe/Mn oxides. Cr was predominantly in the pyrite fraction in directly labelled sediment and in the Fe/Mn oxide fraction in the sediments labelled with algal
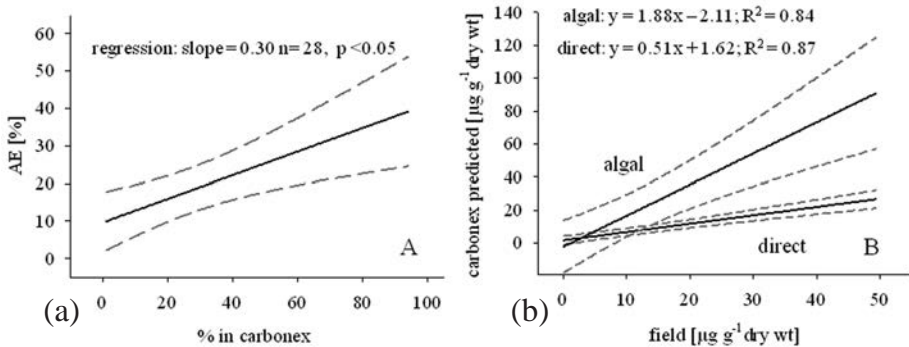
FIG. 2. (a) Significant regression of As, Cd and Cr AEs in Nereis succinea and their concentration in the carbonex pool. (b) Relationships between metals measured in deposit feeding polychaetes collected from contaminated sediments in Elizabeth River, Baltimore Harbor and Mare Island, and metal body burdens predicted by the biokinetic model in which metal concentrations in sediments used the carbonex metal fraction as a measure of the bioavailable metal pool in sediments. Sediments labelled directly and via algal debris are compared. Dashed lines indicate 95% confidence intervals. The r² values for AEs vs total metal in sediments ranged from 0.11 for sediments labelled via algal debris to 0.50 for directly labelled sediment [9].

debris. Fig. 2a shows the significant positive relationship — across all metals and sediments — of metal AEs in *N. succinea* with their distribution in the carbonex pool. The slope (0.30) suggests that about one third of the metal in the carbonex fraction was assimilable by this polychaete. By contrast, there was a significant ($p < 0.05$) negative correlation between metals associated with more refractory sediment phases and AEs (slopes ranging from –0.4 to –0.2) [7], indicating that metals associated with these phases are generally not bioavailable to deposit feeding polychaetes. Uptake rate constants (k_u) for metals from pore water (L/(g·d)) ranged from 0.02 to 0.18 for ^{73}As at the 3 sites, from 0.2 to 3.4 for ^{109}Cd, and from 0.8 to 2.3 for ^{51}Cr [9].

The model predictions of metal concentrations in polychaetes that considered the labile (carbonex) fractions in sediments using Eq. 3 were compared with independent field measurements of metal concentrations in field collected polychaetes from these same estuarine sites [9] (Fig. 2b). Model predictions for sediments directly labelled underestimated metal body burdens by a factor of about 2, while those for sediments labelled with algal debris overestimated body burdens by a factor of almost 2 (Fig. 2b). The underprediction associated with the directly labelled sediment suggests that sediments in situ at the sites we considered have some freshly added planktonic debris that could more efficiently deliver metal to resident polychaetes. Model predictions that considered only total metal concentrations in sediments or other sediment fractions showed no significant positive relationship to field measured metal concentrations in polychaetes, indicating that the labile phases are the best

TABLE 1. FRACTIONATION PATTERNS OF [73]AS, [109]CD, AND [51]CR AFTER 30 DAYS IN SEDIMENTS FROM THREE ESTUARINE SITES: BALTIMORE HARBOR, ELIZABETH RIVER, AND MARE ISLAND.

Label	Location:	Direct			Algal Debris		
		Baltimore Harbor	Elizabeth River	Mare Island	Baltimore Harbor	Elizabeth River	Mare Island
Sedimentary fraction		Mean±SD [%]					
[73]As	Exchangeable	2.7±1.6	1.7±0.6	4.3±1.5	3.4±1.2	21.2±5.6	2.6±0.5
	Carbonate	2.4±1.8	1.0±0.4	3.6±1.6	4.2±0.7	9.2±1.4	8.6±3.6
	AVS	12.2±2.0	10.4±6.3	25.1±16.4	5.6±1.2	11.1±3.8	18.1±1.3
	Fe/Mn oxides	5.0±1.5	13.9±1.9	7.6±5.7	19.6±1.3	20.9±3.3	19.7±3.0
	Organic I	39.3±12.8	29.5±1.1	33.8±15.9	38.0±2.9	17.0±1.7	29.4±3.5
	Organic II	11.1±6.3	11.3±3.6	10.0±2.1	11.7±3.3	2.7±0.3	8.2±2.8
	Pyrite	4.5±5.0	7.1±2.1	3.7±0.7	0.0±0.0	0.0±0.0	0.0±0.0
	Residue	22.8±4.9	25.0±4.7	11.8±2.3	17.5±6.6	17.8±3.6	13.5±2.4
[109]Cd	Exchangeable	32.1±13.3	88.5±4.6	36.9±7.0	43.7±2.3	68.7±3.6	24.1±4.0
	Carbonate	16.3±5.7	3.7±1.5	21.1±3.1	8.7±1.1	9.6±1.4	16.8±6.5
	AVS	20.4±7	1.2±0.3	20.7±3.0	5.1±6.6	4.1±0.4	3.3±4.1
	Fe/Mn oxides	30.4±1.2	6.3±5.9	20.5±3.4	37.8±7.2	13.0±2.5	39.4±14.5
	Organic I	0.4±0.1	0.2±0.2	0.3±0.0	0.75±0.07	0.6±0.03	2.0±0.4
	Organic II	0.0±0.0	0.0±0.0	0.0±0.0	2.7±0.4	2.5±0.3	8.0±3.1
	Pyrite	0.4±0.1	0.2±0.1	0.5±0.0	1.1±0.6	1.5±0.3	6.4±2.0
	Residue	0.0±0.0	0.0±0.0	0.0±0.0	0.0±0.0	0.0±0.0	0.0±0.0

TABLE 1 cont.

	51Cr					
Exchangeable	1.5±0.7	1.1±0.5	1.4±0.4	0.91±0.11	1.6±0.3	1.25±0.5
Carbonate	2.5±1.3	1.6±0.3	2.2±0.2	1.4±0.6	2.7±0.6	2.09±0.7
AVS	14.9±4.4	7.4±2.1	8.1±0.9	10.2±1.5	11.6±3.1	14.7±2.7
Fe/Mn oxides	11.9±8.2	11.3±6.9	15.4±3.6	65.8±1.8	53.8±5.1	41.2±2.3
Organic I	7.7±4.0	18.2±5.6	23.3±11.3	1.4±0.1	2.5±0.4	3.50±0.2
Organic II	2.9±0.9	4.2±2.5	8.1±1.0	11.6±4.2	15.6±2.1	20.1±4.9
Pyrite	56.7±1.8	55.7±10.7	40.9±15.8	7.3±3.3	10.8±2.4	15.5±7.1
Residue	1.9±1.8	0.50±0.3	0.61±0.2	1.5±0.3	1.4±0.4	1.6±1.5

Note: Sediments radiolabelled directly or via radioactive algal debris are compared. Nominal sediment fractions are operationally defined, as indicated in Fig. 1.

TABLE 2. ARSENIC ASSIMILATION EFFICIENCIES AND % RELEASED FROM SEDIMENT PARTICLES INTO THE NATURAL GUT FLUID OF *Nereis succinea*[*]

	Sediment labelled with algae	Sediment directly labelled	Radiolabelled goethite
[73]As AE (%)	50.7 ± 9.0	10.2 ± 6.8	2.5 ± 0.7
[73]As released (%)	33.7 ± 11.7	17.4 ± 5.7	14.7 ± 3.0

[*] (means ± 1 SD, n = 5–8)

predictors of bioavailable metals in estuarine sediments. Further, the model showed that in all but one case, >97% of the metal body burden in these polychaetes was obtained from ingested sediment as opposed to pore water (the exception being for As in one of the sediments, in which 86% was from ingested sediment) [9]. Thus, the ingestion pathway is critical for understanding metal bioaccumulation in these worms and understanding the geochemical fractionation of the metals is essential for understanding the metal uptake from sediments.

Table 2 shows that release of [73]As from ingested sediment into *N. succinea* gut fluid was significantly greater from sediments labelled with algal debris than from sediments that were directly radiolabelled (p < 0.05). The pattern of As AEs paralleled the desorption of [73]As from the sediments, suggesting that desorption of metals from ingested sediment into gut fluid is a necessary step for metals to be ultimately assimilated in these polychaetes.

4. CONCLUSIONS

The release of [73]As from radiolabelled goethite into gut fluid was significantly greater than the resulting AE (14.7 vs 2.5%) in worms, suggesting that metal release into gut fluid alone cannot explain AEs and indicating that metals tightly bound to organic compounds that are nutritionally useful to the polychaete are most likely to cross the gut lining and become assimilated.

REFERENCES

[1]   KENNISH, M.J., Practical Handbook of Estuarine and Marine Pollution, CRC Press, Boca Raton, FL (1996).
[2]   INTERNATIONAL ATOMIC ENERGY AGENCY, Sediment Distribution Coefficients and Concentration Factors for Biota in the Marine Environment, IAEA, Vienna (2004).

[3]   CASADO-MARTINEZ, M.C., SMITH, B.D., DELVALLS, T.A., LUOMA, S.N., RAINBOW, P.S., Biodynamic modelling and the prediction of accumulated trace metal concentrations in the polychaete *Arenicola marina*, Environ. Pollut. **157** (2009) 2743–2750.

[4]   CROTEAU, M.-N., LUOMA, S.N., Delineating copper accumulation pathways for the freshwater bivalve *Corbicula* using stable copper isotopes, Environ. Toxicol. Chem. **24** (2005) 2871–2878.

[5]   LEE, B.G., et al., Influences of dietary uptake and reactive sulfides on metal bioavailability from aquatic sediments, Science **287** (2000) 282–284.

[6]   GRISCOM, S.B., FISHER, N.S., Bioavailability of sediment-bound metals to marine bivalve molluscs: an overview, Estuaries **27** (2004) 826–838.

[7]   BAUMANN, Z., FISHER, N.S., Relating the sediment phase speciation of As, Cd and Cr with their bioavailability for the deposit-feeding polychaete *Nereis succinea*, Environ. Toxicol. Chem. **30** (2011) 747–756.

[8]   WANG, W.-X., FISHER, N.S., Assimilation efficiencies of chemical contaminants in aquatic invertebrates: a synthesis, Environ. Toxicol. Chem. **18** (1999) 2034–2045.

[9]   BAUMANN, Z., FISHER, N.S., Modelling metal bioaccumulation in a deposit-feeding polychaete from labile sediment fractions and from pore water, Sci. Total. Environ. **409** (2011) 2607–2615.

[10]   TESSIER, A., CAMPBELL, P.G.C., BISSON, M. Sequential extraction procedure for the speciation of particulate trace metals, Anal. Chem. 51 (1979) 844–851.

[11]   DIKS, D.M., ALLEN, H.E., Correlation of copper distribution in a freshwater-sediment system to bioavailability, Bull. Environ. Contam. Toxicol. 30 (1983) 37–43.

[12]   GRISCOM, S.B., FISHER, N.S., ALLER, R.C., LEE, B.G., Effects of gut chemistry in marine bivalves on the assimilation of metals from ingested sediment particles, J. Mar. Res. 60 (2002) 101–120.

[13]   CHEN, Z., MAYER, L.M., Mechanisms of Cu solubilization during deposit feeding, Environ. Sci. Technol. 32 (1998) 770–775.

[14]   WANG, W.-X., STUPAKOFF, I., FISHER, N.S., Bioavailability of dissolved and sediment-bound metals to a marine deposit-feeding polychaete, Mar. Ecol. Prog. Ser. 178 (1999) 281–293.

[15]   WANG, W.-X, FISHER, N.S., LUOMA, S.N., Kinetic determinations of trace element bioaccumulation in the mussel *Mytilus edulis*, Mar. Ecol. Prog. Ser. 140 (1996) 91–113.

[16]   LUOMA, S.N., RAINBOW, P.S., Why is metal bioaccumulation so variable? Biodynamics as a unifying concept, Environ. Sci. Technol. 39 (2005) 1921–1931.

SHORT TERM vs LONG TERM ENVIRONMENTAL RECONSTRUCTION FROM CARBONATED DEPOSITS OF THE LIMAGNE AREA (MASSIF CENTRAL, FRANCE)

F. BARBECOT[a], E. GIBERT[a], B. GHALEB[b], Y. AMOKRANE[a],
M. MASSAULT[a], A. NORET[a]

[a] Centre National de la Recherche Scientifique
Interaction et Dynamique des Environnements de Surface,
Université Paris, France

[b] GEOTOP, Université du Québec à Montréal,
Montréal, Canada

Abstract

A 80 cm sequence has been cored from carbonated travertine in the Limagne area (French Massif Central, France) in order to document recent environmental fluctuations (0–100 a) of gaseous springs, in relation to the environmental and geochemical parameters that control the isotopic signatures of modern carbonate deposits. The chronology of these finely laminated deposits that are ideal for reconstructing hydrological conditions at very narrow time steps is determined through AMS-^{14}C and ^{210}Pb/^{226}Ra radiometric methods. Preliminary results highlight a high enrichment in stable isotopes (eg up to +8‰ *vs* VPDB for δ^{13}C), likely linked to both recharge temperature and degassing processes. Moreover, two general trends are superimposed: the first one, cyclic, may be correlated to the hydrologic annual/biannual budget while the second one, linear, implies a long term environmental trend.

1.   INTRODUCTION

The T-RIP project (Travertine-Reconstruction of Isotopical Palaeo-environ-ment) focuses on the understanding of the hydrogeochemical processes related to carbo-gaseous springs in the area of the Limagne Plain (French Massif Central) in relation with recent environmental changes (0–100 a), including evolution of recharge areas and fluxes for surrounding aquifers. Some of the springs are producing fine, laminated carbonated deposits that are ideal for the reconstruction of hydrological fluctuations at very narrow time steps.

Stratigraphic log of the SO-08 core
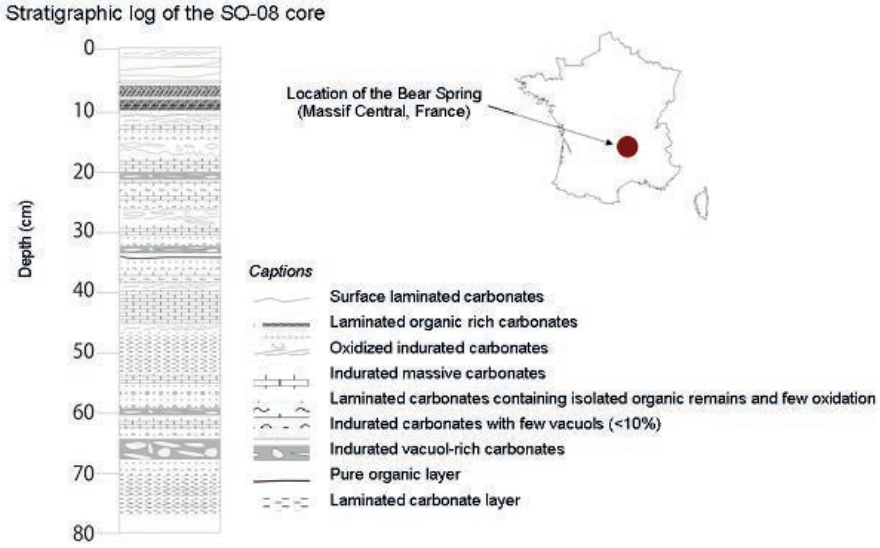
FIG. 1. Location and geological profile of the core.

2. GENERAL CONTEXT

The main factors determining groundwater resources in the study area are (1) the morphological aspects of the relief, sedimentary facies and basin superstructure, (2) the continental climate characterised by important thermic gaps and abundant summer rainfall, and (3) the piezometric level. The study area can be divided in two distinct zones [1, 2]: the granitic and metamorphic domain in the east and south-east, and the sedimentary infilling of the Limagne basin everywhere else [1].

The Médagues springs group formed one of the most important networks in Central France. Among all the springs referenced in this area, the Bear Spring is the most important since its flow is over 80 L.mn^{-1} (more that 100 m^3 per day). It is a CO_2-rich sparkling spring of 13.8 °C mean annual temperature. In the 1970s, the society of the 'Eaux du Bassin de Vichy' bought the spring area and protected it through the definition of a 'strategic reserve' protocol. The Bear spring is now part of the 'Conservatoire des Espaces et Paysages d'Auvergne' as it presents protected halophyte flora.

3. THE GEOCHEMICAL SYSTEM

3.1. Description

A 80 cm long core was drilled on a flat zone located approximately 200 m under the emerging spring. Sediments consist of indurated carbonate, alternating from finely laminated to massive layers. In situ organic remains (leaves) have been found sandwiched in the laminated sections.

Samples were taken every 1 to 2 cm in relation to the induration degree of the core. Leaves were carefully hand-picked and prepared for the establishment of the ^{14}C chronology.

3.2. Analytical methods

For stable isotope content analyses, water, gas and carbonate samples were converted into CO_2 by direct acidification, and the ^{13}C contents of carbon species were measured by mass spectrometry (SIRA) at the IDES Laboratory (University of Paris Sud, France). The ^{13}C content is reported using conventional δ notation, as a deviation from the V-PDB (*Vienna-Belemnitela* from the Pee Dee formation, North Carolina, USA).

Concerning ^{14}C measurements, all the dating was performed on in situ deposited left remains. The specific treatment for organic samples was applied following the standard alkali-acid-alkali protocol to avoid any contamination either by humic acids or by atmospheric CO_2. The CO_2 gas produced after burning was reduced on iron powder (IDES Laboratory) and graphite sources were measured with the accelerator mass spectrometry (ARTEMIS) of the UMS LMC14 in Gif-sur-Yvette (INSU-CNRS France). The ^{14}C activities are expressed as percentages of modern carbon (pMC) normalized to a $\delta^{13}C = -25$‰.

4.   RESULTS

The stable isotopic composition of the spring water is –9.6‰ and –62.8‰ vs V-SMOW for [18]O and ^{2}H respectively.

Stable isotope contents of finely laminated carbonates comprise between 5.8‰ and 7.6‰ for ^{18}O, and from –7.9‰ to –6.7‰ for ^{13}C, with mean values of +6.6‰ and –7.2‰ respectively. These results display a ^{13}C enrichment (up to +8‰) with respect to the isotopic composition of the spring TDIC (Total Dissolved Inorganic Carbon). This enrichment may be due to either degassing of the dissolved CO_2 from the running spring water, the temperature during the deposition and/or to precipitation fractionation during the solid carbonates deposits [1].
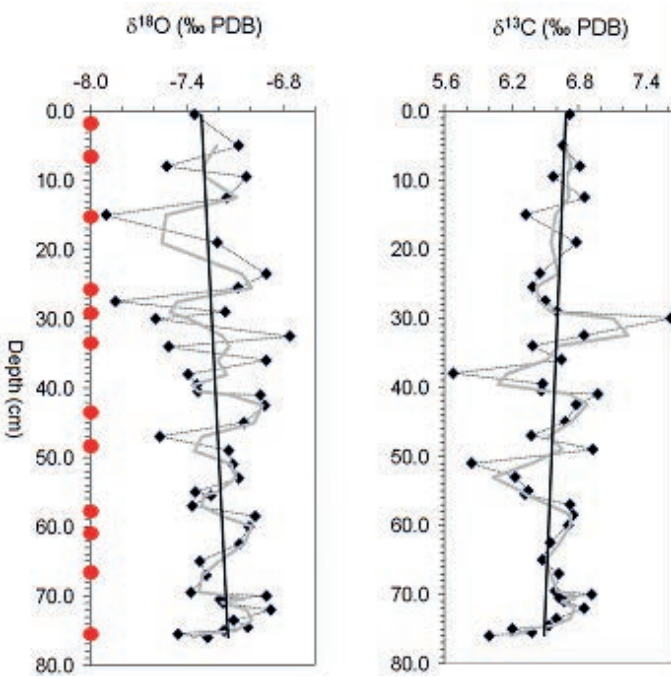
FIG. 2. Evolution of the stable isotope contents of carbonated deposits from the Bear Spring with depth. Plain circles represent sampled levels for $^{238}U/^{234}U/^{226}Ra$ analyses (ongoing). The grey line indicates the variability of the data after a two-step running mean calculation.
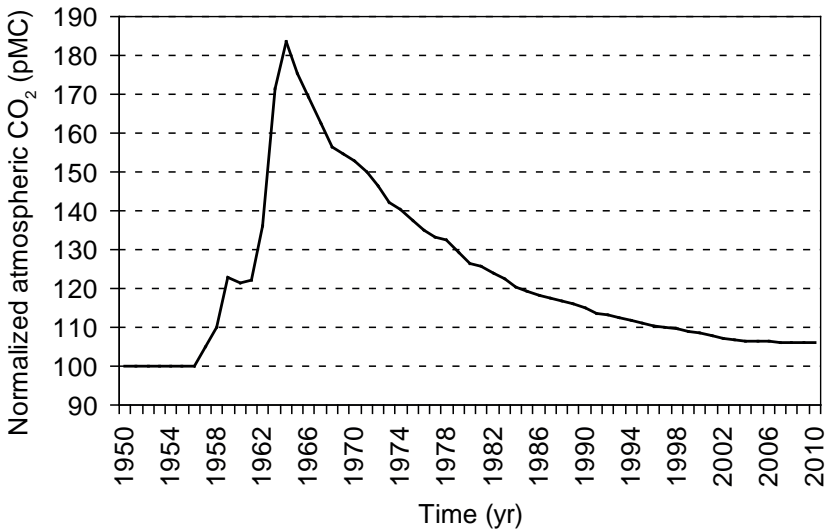
FIG. 3. Evolution of the ^{14}C activity in atmospheric CO_2 (normalized at 25‰) since 1950.

Preliminary results indicate that the organic residues come from C3-plants, with a mean $\delta^{13}C$ of –26‰ vs PDB [3]. A first ^{14}C activity of 118 pMC performed on in situ leaves at 65 cm depth indicate that the time period covered by our core is of a few decades (Figure 3).

5.   DISCUSSION AND CONCLUSION

For carbo gaseous waters, the quantity of CO_2 dissolved at great depth controls the carbonate system during water recovery to the surface through the calcareous deposits of the Limagne plain. It evolves according to the equilibria of the calco carbonic system. The increase of Ca^{2+} during the rising up of the water is accompanied by a progressive saturation of the solution with respect to calcium carbonate.

The solid carbonates precipitates along the surface flowpath originate from water with a nearly constant ^{18}O isotopic composition, highlighting the inertia of the system that gives rise to the springs. In such a geochemically homogenized water system, the stable isotope contents of the carbonates issued from precipitation reflect the mean isotopic composition of water, with respect to the thermodependant fractionation factors. The deviation between isotopic compositions of water and carbonates, taking into account the water-calcite fractionation and its related variability, can give information on the temperature during carbonate precipitation.

Preliminary calculations indicate a temperature significantly lower than the mean annual temperature of this area for carbonate precipitation, which is an aberration for the time lag covered. Other processes have then to be considered to explain this anomaly such as (1) a biofilm intimately mixed with carbonates, (2) kinetic fractionation, (3) the evolution of the isotope signature of the water between the emergence and the zone of precipitating carbonates, due to either evaporation, impact of hydroxide precipitation preceding carbonate precipitation, or the variability of the aquifer reservoir, and/or (4) the recrystallisation or mixing of different carbonated phases.

Whatever the processes involved, a significant evolution in the environmental signal is highlighted on $\delta^{13}C$ signatures. This is clearly related with the geochemical process of Rayleigh distillation during water degassing and carbonate precipitation [4–6]. We may infer two superimposed fluctuations: the first one, cyclic, is probably annual to biannual, while the second one, linear, implies geochemical processes in relation with a long term evolution of the system.

As a conclusion, the chronology needs to be more deeply investigated through the comparison of ^{14}C activity measurements and of $^{210}Pb/^{226}Ra$ dating [7–8], in order to discriminate short hydrological events/peaks. Moreover, associated stable isotope contents of these finely laminated carbonated samples will be compared with historical records such as temperature and precipitation, in order to identify the key parameters of the geochemical differentiation footprinted in the solid carbonates.

REFERENCES

[1]   BELKESSA, R., Données Hydrogéologiques acquises en Limagne, Rapport 78 SGN 087 MCE (1978) 29.

[2]   BUREAU DE RECHERCHES GÉOLOGIQUES ET MINIÈRES, DIVISION NA-TIONALE DES EAUX MINÉRALES ET THERMALES, Les eaux minérales et le gaz carbonique, Note technique DNEMT n°10 (1997) 23.

[3]   DEINES, P., "The isotopic composition of reduced organic carbon", Handbook of Environmental Isotope Chemistry, Vol. 1 (FRITZ, P., FONTES, J.Ch., Eds), Elsevier, New York (1980) 329–406.

[4]   CLARK, I., FRITZ, P., Environmental isotopes in Hydrogeology, Lewis Publishers Boca Raton, FL (1997).

[5]   ASSAYAG, N., BICKLE, M., KAMPMAN, N., BECKER, J., Carbon isotopic con-straints on CO_2 degassing in cold-water Geysers, Green River, Utah, Energy Procedia **1** (2009) 2361–2366.

[6]   SCOTT, K.M., LU, X., CAVANAUGH, C.M., LIU, J.S., Optimal methods for esti-mating kinetic isotope effects from different forms of the Rayleigh distillation equa-tion, Geochim. Cosmochim. Acta **68** 3 (2004) 433– 442.

[7]   CONDOMINES, M., RIHS, S., First [226]Ra–[210]Pb dating of a young speleothem, Earth Planet. Sci. Lett. **250** (2006) 4–10.

[8]   CONDOMINES, M., BROUZES, C., RHIS, S., Radium and its daughters in hy-drothermal carbonates from Auvergne (French Massif Central): Origin and dating applications, CRAS Serie II-A (1999), Vol. 328–1, 23–28.

MATRIX PORE WATER IN LOW PERMEABLE CRYSTALLINE BEDROCK: AN ARCHIVE FOR THE PALAEOHYDROGEOLOGICAL EVOLUTION OF THE OLKILUOTO INVESTIGATION SITE

F. EICHINGER [a, b], H.N. WABER [b], J.A.T. SMELLIE [c]

[a] Hydroisotop GmbH,
Schweitenkirchen, Germany

[b] Rock–Water Interaction,
Institute of Geological Sciences, University of Bern,
Bern, Switzerland

[c] Conterra AB,
Stockholm, Sweden

Abstract

Matrix pore water in the connected inter- and intragranular pore space of low permeable crystalline bedrock interacts with flowing fracture groundwater predominately by diffusion. Based on the slow exchange between the two water reservoirs, matrix pore water acts as an archive of past changes in fracture groundwater compositions and thus of the palaeohydrological history of a site. Matrix pore water of crystalline bedrock from the Olkiluoto investigation site (SW Finland) was characterised using the stable water isotopes ($\delta^{18}O$, δ^2H), combined with the concentrations of dissolved chloride and bromide as natural tracers. The comparison of tracer concentrations in pore water and present day fracture groundwater suggest for the pore water the presence of old, dilute meteoric water components that infiltrated into the fractures during various warm climate stages. These different meteoric components can be discerned based on the diffusion distance between the two reservoirs and brought into context with the palaeohydrological evolution of the site.

1.   INTRODUCTION

In low permeable bedrock, pore water resides in the connected inter- and intragranular pore space of the rock matrix where solute transport may be dominated by diffusion. The amount of pore water present in the rock matrix is significant and its influence on fracture groundwater needs to be understood for the long term safety of future deep repositories for radioactive waste, for example. Here, pore water will be the first water that will interact with the various technical barriers (e.g. bentonite

backfill, Cu-canister). Such interaction may modify the chemical and physical properties of the barrier materials and possibly lead to a deterioration of their functionality.

Within fractured bedrock, pore water in the tight rock matrix and groundwater in the transmissive fracture network are connected systems that will tend to reach chemical and isotopic equilibrium. The driving force for the interaction between pore water and fracture groundwater are the chemical and isotopic gradients established between these two reservoirs. Such interaction can be quantified as a function of time and space by comparing the signatures of stable water isotopes ($\delta^{18}O$, δ^2H) and chemically conservative elements (Cl, Br) in pore water and fracture groundwater.

An isotopic and chemical signal established in the pore water at a specific time in the hydrogeological evolution of a site might be preserved over long geological time periods. For chemically conservative tracers, the preservation of such signatures depends on: (1) the distance between the pore water sample and the nearest water conducting feature in three dimensions, (2) the solute transport properties of the rock matrix (i.e. diffusion coefficient, porosity), and (3) the boundary conditions given by the initial pore water and the fracture groundwater compositions. The interpretation of an observed pore water signature is greatly facilitated if it has been transmitted from constant boundary conditions in the fracture(s). In reality, however, superimposed signatures as a result of changing boundary conditions as a function of time are more common.

Unravelling complex, superimposed signatures can be approached by comparing data sets of different tracers that carry different information with respect to the groundwater infiltration conditions. Thereby, the stable water isotopes will provide information about the climate and the water origin (e.g. meteoric vs marine). The pore water Cl concentration will provide information about the groundwater salinity, and the Br/Cl ratio about the salinity source. The interpretation of an observed signature in the pore water needs to be consistent for all tracers taking into account compositional differences in fracture groundwaters as a function of time and differences in the diffusion behaviour of the tracers.

Within this study, pore water of crystalline rocks from the Olkiluoto investigation site (SW Finland) was investigated and compared to fracture groundwater that circulates in the local and regional fracture systems. Core samples for pore water extraction were collected from two subvertical deep drillings located in the centre of the island (KR39: 500 m length) and directly on the shore line (KR47: 1000 m length) and from one horizontal drillhole (PH9: 150 m length) drilled from the ONKALO access tunnel at a depth of 306 m below sealevel (b.s.). In the deep drillholes, pore water samples were collected at intervals of 10 to 40 m, whereas sampling in the horizontal drillhole consisted of a 10 m long continuous profile away from a water conducting fracture into the rock matrix.

The present contribution focusses on the palaeohydrogeological implications of the water isotope compositions $\delta^{18}O$ and δ^2H of pore water. Pore water concentrations of the chemical tracers chloride and bromide including the chloride isotope

composition are used in support of the $\delta^{18}O$ and δ^2H data where needed, but extensive discussions of these tracers are given elsewhere [1–4].

2. GEOLOGY AND HYDROGEOLOGY OF THE OLKILUOTO INVESTIGATION SITE

Olkiluoto bedrock consists of Precambrian metasedimentary, supracrustal rocks. It mainly comprises fine to medium grained foliated gneisses with intercalated coarse-grained granitic pegmatites [5]. The crystalline rocks mainly consist of quartz, feldspar, biotite and cordierite [1–3, 5]. They show variable degrees of hydrothermal alteration resulting in a large range of connected porosity between 0.32 and 2.62 Vol.% [1–3].

Groundwater flow in the Olkiluoto bedrock is limited to the connected fracture network created by brittle deformation of the bedrock. This fracture network is subdivided into two domains which are the hydrogeologically active deformation zones and the sparsely fractured rock between these zones [6]. In both domains, more or less large portions of undisturbed, non-fractured rock matrix occur. Hydrogeologically active deformation zones have high fracture transmissivities (10^{-7} m²/s to $> 10^{-5}$ m²/s) and seem to form subhorizontal to moderately dipping flow planes [6]. In contrast, fractures detected in the sparsely fractured bedrock domains have low transmissivities ($< 10^{-7}$ m²/s [6]) and show no preferential orientation and angle of dip. At Olkiluoto, the fracture frequency and transmissivity decrease with increasing depth corresponding approximately to the shallow (0–150 m b.s), intermediate (150–400 m b.s) and deepest zone (400–800 m b.s).

Fracture groundwaters at the Olkiluoto site are of variable composition and represent mixtures of different components suggesting a complex evolution [6, 7]. A general increase in salinity with depth becomes especially pronounced below about 400 m and fracture groundwaters reach brine compositions at around 1000 m depth. Oxygen and hydrogen isotope compositions combined with the chemical compositions suggest the presence of meteoric cold climate and glacial components that interact with older non-marine saline (brine) components and younger marine components (Littorina and Baltic Sea) besides the present day meteoric infiltration [6, 7]).

3. METHODS

Pore water residing in the rock matrix cannot be sampled by conventional groundwater sampling techniques. The isotopic and chemical composition of pore water has, therefore, to be derived by indirect extraction techniques based on rock material. The stable water isotopes are determined by the diffusive isotope exchange technique developed for sedimentary rocks [8] and adapted to crystalline rocks [4, 9].

In this technique the pore water of originally saturated rock pieces is equilibrated with a test water of known isotopic composition over the vapour phase. The pore water $\delta^{18}O$ and δ^2H values are then derived by isotope mass balance calculations with the error being determined by Gaussian error propagation. Chemical pore water tracers are derived by out-diffusion experiments in which an originally saturated, intact core is immersed in deionised water for equilibration [4, 9]. Periodic sampling from the out-diffusion experiment for tracer time series allows the derivation of transport properties of the rock matrix by modelling the tracer breakthorugh curves by radial diffusion [1–3]. These methods require thoroughly tested core preservation techniques and a concerted logistical effort to minimise the time from drilling through sampling to commencement of the laboratory investigations [4, 9]. The obtained data have to be carefully evaluated for potential perturbations induced by drilling activities and rock stress release [10] in the field, and sample treatment in the laboratory, in order to derive the degree to which the samples represent *in situ* conditions [4].

4. RESULTS

4.1. Transport properties of the rock matrix

Chloride breakthrough curves of out-diffusion experiments conducted on Olkiluoto bedrock can be adequately described by diffusion indicating that in the connected pore space of the rock matrix the transport of Cl occurs by diffusion [2–4]. For the different lithologies, pore diffusion coefficients of chloride vary between 1.8 and 8.1×10^{-11} m²/s at 10 °C [2–4]. Applying these results to the site scale, the isotopic and chemical concentrations of pore water samples can be brought into an evolutionary context as a function of time and space using the fracture groundwater compositions as boundary conditions for the diffusion domain. For different time periods, Figure 1 shows schematically the relative concentration change, C/C_0, in a pore water composition induced by fracture groundwater as a function of the distance to the nearest water conducting fracture.

4.2. Pore water tracer composition and their palaeohydrogeological implications

The water isotope composition of pore water in rocks of the Olkiluoto bedrock covers a large range of $\delta^{18}O$ values between –13.1‰ and –4.3‰ V–SMOW (Fig. 2) and δ^2H values between –105‰ and –17‰ V–SMOW. The general trends described by the oxygen and hydrogen isotopes with depth correlate so that only the $\delta^{18}O$ signatures of pore water are discussed. Large concentration ranges are also obtained for the Cl and Br concentrations in the pore water, which vary between 60 and 13 000 mg/kg H₂O (Fig. 2) and between <0.5 and 82 mg/kg H₂O.
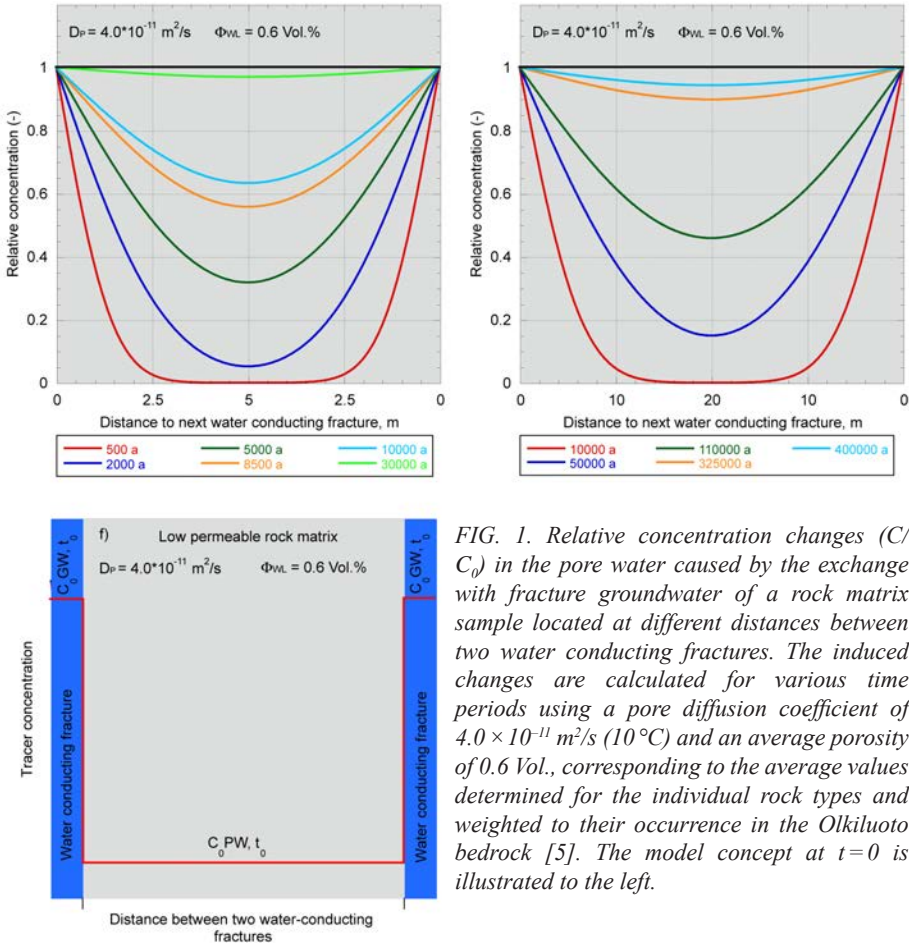
FIG. 1. Relative concentration changes (C/C_0) in the pore water caused by the exchange with fracture groundwater of a rock matrix sample located at different distances between two water conducting fractures. The induced changes are calculated for various time periods using a pore diffusion coefficient of 4.0×10^{-11} m²/s (10 °C) and an average porosity of 0.6 Vol., corresponding to the average values determined for the individual rock types and weighted to their occurrence in the Olkiluoto bedrock [5]. The model concept at $t = 0$ is illustrated to the left.

The shallow bedrock zone (0–150 m b.s.) is characterised by a high frequency of water conducting (wc) fractures and short distances(< 2 m) between pore water samples and the water-conducting fractures. Stable isotope signatures and Cl concentrations of pore water from drillhole OL-KR39, located in the centre of Olkiuoto island, are in equilibrium with fracture groundwater at equal depth (Figs 2 and 3a); the same accounts for Cl and Br. This indicates that the time period since the present-day fracture groundwater began to circulate is sufficient to reach equilibrium between pore water and fracture groundwater, i.e. the time since Olkiluoto emerged from the sea (~3000 a B.P.). In drillhole OL-KR47, which is located directly on the shore line and dips under the Baltic Sea, the shallowest pore water sample is depleted in [18]O compared to the others and also to pore water from OL-KR39, but is still enriched in [18]O and ^{2}H compared to nearby fracture groundwater. The depleted isotope composition indicates the presence of a cold climate or glacial component in the pore water.
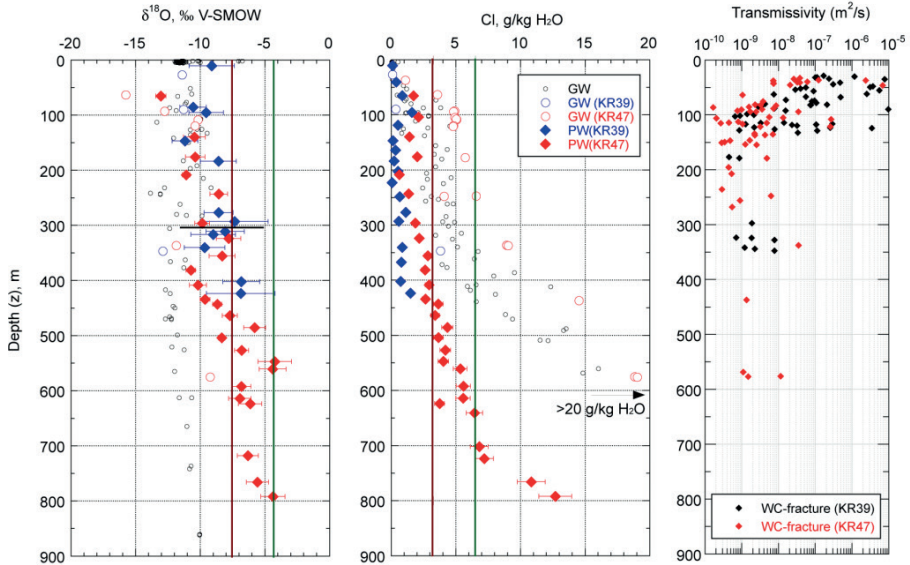
FIG. 2. δ¹⁸O values and Cl concentrations of pore water and fracture groundwater (data from [6]) from the deep boreholes OL-KR39 and OL-KR47as a function of sampling depth and compared to the position of water conducting fractures and their transmissivity (right). The red and green lines indicate average compositions of Baltic and Littorina Sea water.

Such a component is, however, present in different proportions compared to that of the nearby sampled fracture groundwater which is based on a stronger depletion of ^{18}O and ^{2}H, but still has Cl concentrations twice as high as the pore water with the Cl coming from the overlying Littorina/Baltic seawater (Figs 2 and 3a). This further implies that the OL-KR47 pore water contains another type of dilute component, but with an enriched isotope signature. Because the location of the pore water sample has been submerged under seawater since the last cold climate stage, which inhibits recent warm climate meteoric infiltration, this component must be older than the cold climate or glacial component in the fracture groundwater. Pore water from a depth of 140 m in drillhole OL-KR47 has stable isotope ratios enriched in ^{18}O and ^{2}H compared to the sample above, and slightly depleted compared to samples taken in drillhole OL-KR39 (Figs 2 and 3a). The different isotopic signatures combined with the transient state between pore water and groundwater with respect to Cl and the position of the drillhole under the sea, indicates the preservation of a different meteoric water component compared to that observed in pore water of borehole OL-KR39 at similar depth. The data suggest the preservation of a pre-Holocene meteoric warm climate fresh water component in the pore water of borehole OL-KR47, which is no longer observable in that of borehole OL-KR39. The transient state with respect to the stable isotopes and Cl concentrations between pore water and fracture groundwater, and the short distances between the two reservoirs, suggests that the circulation of
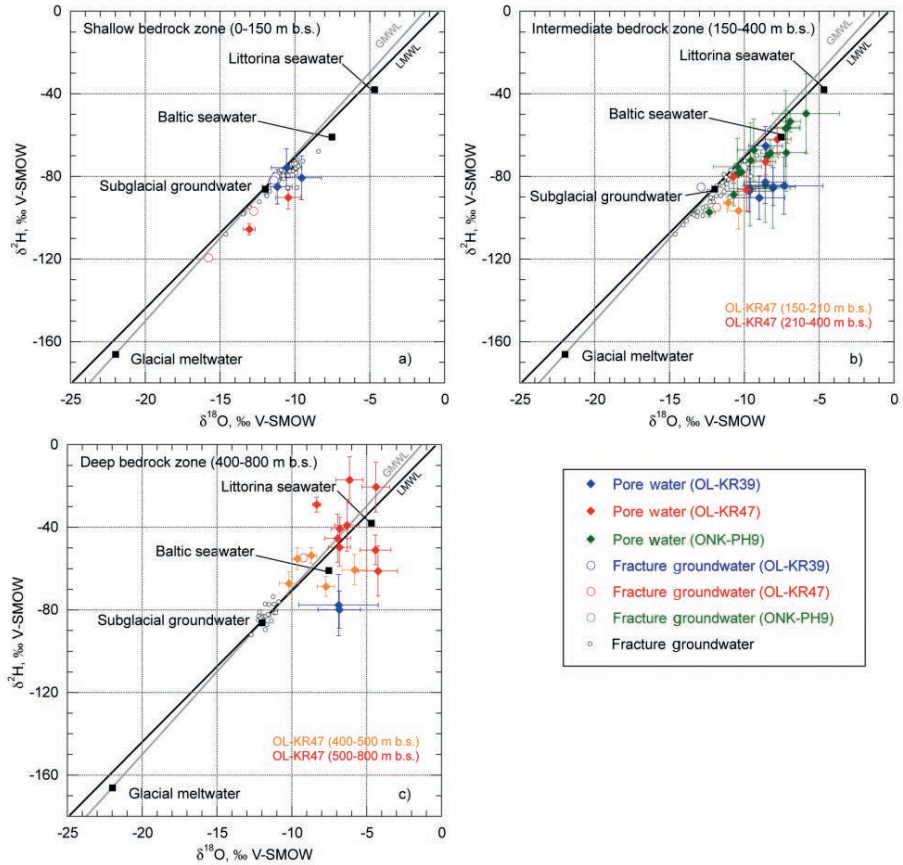
FIG. 3. $\delta^{18}O$ versus δ^2H signatures of pore water from the deep boreholes OL-KR39, OL-KR47 and the horizontal bore-hole ONK-PH9 compared to those of fracture groundwater and surface water (data from Ref. [6]) and sub-divided into shallow, intermediate and deep bedrock zones.

the present-day fracture groundwater in OL-KR47 is in the range of several hundreds to few thousands of years at the most (see Fig. 1).

The intermediate bedrock zone (150–400 m b.s.) is characterised by an intermediate to low transmissive hydraulic regime and strongly variable distances between pore water samples and water conducting fractures (< 2 to almost 50 m). Pore waters are generally enriched in ^{18}O and ^2H compared to the corresponding fracture groundwaters and a transient state is established (Fig. 2). Intermediate zone pore water from OL-KR39 plots further to the right of the LMWL than pore water from borehole OL-KR47 (Fig. 3b). The difference in the isotopic composition of pore waters from the two locations is in agreement with the different Cl and Br concentrations, and suggests the presence of one (or more) old dilute warm climate component(s) in

the pore water. This component is present in higher amounts in pore water from OL-KR39 compared to that from OL-KR47 at equal depth. Its preservation is, however, largely independent of the distance between the pore water sample and the water conducting fractures. This indicates a long term influence of dilute meteoric water during a warm climate period in the range of several tens to few hundreds of thousands of years (see Fig. 1).

In the very low transmissive deep bedrock zone (400–800 m b.s.), the distances between pore water samples and water-conducting fractures are between 5 and >> 50 m. Here, the isotope ratios of pore water become increasingly enriched in ^{18}O and ^{2}H in the first 100 m and remain almost constant at much more enriched ratios compared to shallow and intermediate zone pore waters (Figs 2 and 3c). The difference in the isotopic composition between pore water and groundwater, as well as in the Cl and Br concentrations, becomes larger with increasing depth and a transient state is established. In the δ^{18}O-δ^{2}H diagram most of these deep pore waters tend to plot close to, or to the right of the LMWL above present-day fracture groundwaters and shallower pore waters. In combination with the Cl concentrations, this also indicates the influence of warm climate meteoric water in the deep fracture systems. The transient state between pore water and fracture groundwater with respect to stable water isotopes and chloride is independent of the strongly variable distances between pore water samples and the nearest water conducting fractures. This indicates that warm climate meteoric components were present in the deep fracture systems over time periods in the range of several hundreds to millions of years.

The warm climate meteoric water components observed and preserved in pore water below 150 m b.s. had to infiltrate during times when Olkiluoto was ice free and above sea level. Such conditions occurred, for example during the Eemian interglacial (128–117 ka B.P.), most probably during the Holsteinian interglacial (414–398 ka B.P.) and possibly previous interglacials, as well as during the Tertiary [11, 12]. The possible presence of an old meteoric water of warm climate origin is also consistent with pore water studies carried out in Sweden [13].

5. CONCLUSION

Isotopic and chemical data of pore water residing in the low-permeable crystalline rock matrix indicate continuous interaction with nearby fracture groundwater. The interaction appears to occur mainly by diffusion so that the pore water acts as an archive for the palaeohydrogeological evolution of a site. At the Olkiluoto investigation site, the comparison of isotopic and chemical signatures of pore water with those of sampled fracture groundwaters reveals the presence of warm climate meteoric water components in the rock matrix below 150 m of depth, which are no longer detectable in the present-day fracture groundwaters. Combined with the transport

properties of the non-fractured rock matrix and the distances between pore water sample and the nearest water conducting fractures, it can be shown that these dilute warm climate water components must have circulated in the fracture system over relative time periods in the range of hundreds of thousands of years to a few thousands of years before present.

REFERENCES

[1]   EICHINGER, F.L., WABER, H.N., SMELLIE, J.A.T., Characterisation of Matrix Pore Water at the Olkiluoto Investigation Site, Finland, Posiva Working Report 2006–103, Posiva OY, Olkiluoto, Finland (2006).

[2]   EICHINGER, F., HÄMMERLI, J., WABER, H.N., DIAMOND, L.W., SMELLIE, J.A.T., Characterisation of Matrix Pore Water and Fluid Inclusions in Olkliuoto Bedrock from Drilling OL-KR47, Posiva Working Report 2010–58, Posiva OY, Olkiluoto, Finland (2010).

[3]   EICHINGER, F., HÄMMERLI, J., WABER, H.N., DIAMOND, L.W., SMELLIE, J.A.T., Chemistry and dissolved gases of matrix pore water and fluid inclusions in Olkiluoto bedrock from borehole ONK-PH9, Posiva Working Report 2011-XX, Posiva OY, Olkiluoto, Finland (2011).

[4]   EICHINGER, F., Matrix pore water – fracture groundwater interaction in crystalline bedrock based on natural tracers: An archive of long term hydrogeological evolution, PhD-thesis, University of Bern, Bern, Switzerland (2009).

[5]   KÄRKI, A., PAULAMÄKI, S., Petrology of Olkiluoto, Posiva report 2006–02, Posiva OY, Olkiluoto, Finland (2006).

[6]   POSIVA, 2009, Olkiluoto Site Description 2008, Posiva report 2009–01, Posiva Oy, Olkiluoto, Finland (2009).

[7]   PITKÄNEN, P., PARTAMIES, S. AND LUUKKONEN, A., Hydrogeochemical Interpretation of Baseline Groundwater Conditions at the Olkiluoto Site, Posiva Tech. Rep. 2003–07, Posiva, Helsinki, Finland (2004).

[8]   RÜBEL, A.P., SONNTAG, CH., LIPPMANN, J., PEARSON, F.J., GAUTSCHI, A., Solute transport in formations of very low permeability: Profiles of stable isotope and dissolved noble gas contents of pore water in the Opalinus Clay, Mont Terri, Switzerland, Geochim. Cosmochim. Acta **66** (2002) 1311–1321.

[9]   WABER, H.N., SMELLIE, J.A.T., Characterisation of Pore Water in Crystalline Rocks, App. Geochem. **23** (2008) 1834–1861.

[10]   WABER, H.N., GIMMI, T., SMELLIE, J.A.T., Effects of drilling and stress release on transport properties and porewater chemistry of crystalline rocks, J.Hydrol. **405** (2011) 316–332.

[11]   LUNKKA, J.P., JOHANSSON, P., SAARNISTO, M., SALLASMAA, O., "Glaciation of Finland", Quaternary Glaciations – Extent and Chronology (EHLERS, J., GIBBARO, P.L., HUGHES, P.D., Eds) Elsevier, Amsterdam (2004) 93–100.

[12]   WOHLFARTH, B., BJÖRCK, S., FUNDER, S., HOUMARK-NIELSEN, M., INGOLFSSON, O., LUNKKA, J.-P., MANGERUND, J., SAARNISTO, M., VORREN, T., Quaternary of Norden, Episodes, **31** (2008) 73–80.

[13]   LAAKSOHARJU, M., SMELLIE, J., TULLBORG, E-L., GIMENO, M., MOLINE-RO, J., HALLBECK, L., MOLINER, J., WABER, N., Bedrock hydrogeochemistry Forsmark, SKB R 08–47, Svensk Kärnbränslehantering AB, Stockholm, Sweden (2008).

SUBSURFACE WATER AS NATURAL CO_2 SINK

M. GILLON [a,b], F. BARBECOT [a], E. GIBERT [a], M. MASSAULT [a]

[a] Centre National de la Recherche Scientifique (UMR CNRS 8148-IDES),
   Interaction et Dynamique des Environnements de Surface,
   Université Paris 11, France

[b] Centre National de la Recherche Scientifique (UMR UAPV-INRA EMMAH),
   Environnement Méditerranéen et Modélisation des Agro-Hydrosystèmes,
   Université d'Avignon et des pays de Vaucluse,
   Avignon, France

Abstract

In aquifer recharge areas, groundwater mineralization acts as an important sink for CO_2 (assessed at 100 Mt_{CO_2}/a on a European scale). An isotopic study of C fluxes in the unsaturated zone of a sand carbonate aquifer shows that the physical and geochemical processes controlling CO_2 abstraction induce changes in the isotopic composition of both dissolved and matrix carbonates. An integrated record of these fluxes toward the aquifers is evidenced through isotopic investigation of the recharge areas. It is evidenced that the unsaturated zone represents an archive of pristine conditions, and would help to quantify downward C fluxes and environmental changes related to this CO_2 abstraction process.

1.   INTRODUCTION

One of the most important sinks for CO_2 exists naturally in the aquifer recharge area. This CO_2 abstraction, although very important in terms of flux (assessed at 100 Mt/a on a European scale) has not yet been well quantified. CO_2 produced by the vegetation cover takes part in water mineralization during aquifer recharge. This sink of CO_2 as well as its variability has an incidence on the global C cycle turnover. The CO_2 abstraction process via groundwater mineralization depends on several factors such as groundwater infiltration rate, climatic conditions and properties of pedogeological layers of the unsaturated zone.

In order to highlight geochemical and physical processes induced by the CO_2 abstraction, study of C fluxes in the unsaturated zone between all carbon phases (matrix carbonates, dissolved inorganic carbon -DIC-, and CO_2 gas) has been performed using C-isotopes in a sand carbonate aquifer (Astian sands, France).
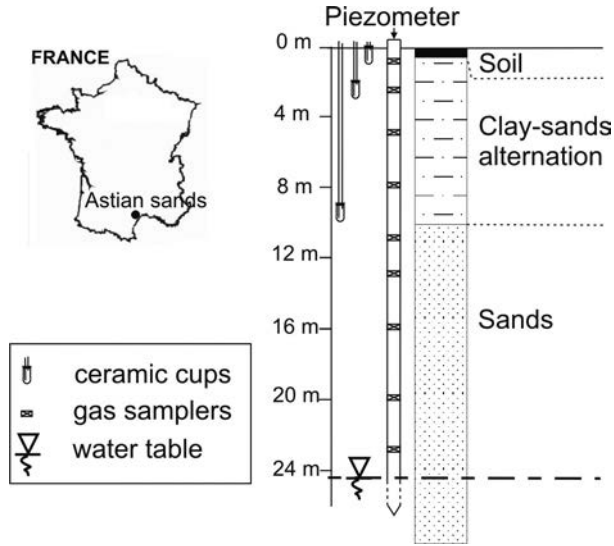
FIG. 1. Location, geological profile and equipment of the study site.

2. METHODS

2.1. Site description and equipment

The Astian sands are a 3 Myr old marine sand carbonate aquifer, located in southern France (Fig. 1). The site is an outcrop of sands, covered by grassland or forest (oaks, beeches, chestnut tree) belonging to the C3-plant group [1]. A 25.5 m thick unsaturated zone profile of the aquifer was equipped with a water/gas permanent sampler at different depths (Fig. 1). Matrix samples were taken at intervals of 0.05 to 2 m on a vertical profile down to the water table. For a complete description of the profile and of the equipment, see [2] and [3].

2.2. Analytical methods

All samples (gas, water and carbonate) were analysed for ^{13}C and ^{14}C. For ^{13}C analyses, the carbon species (i.e. CO_2, TDIC and carbonates) were converted into CO_2 by direct acidification, and the ^{13}C contents of carbon species were measured by mass spectrometry (SIRA) at the IDES Laboratory (University of Paris Sud, France). The ^{13}C content is reported using conventional δ (‰) notation, as a deviation from the V-PDB (Vienna-Belemnite from the Pee Dee formation, North Carolina, USA). For ^{14}C analyses, graphite sources were prepared from the carbon species (i.e. CO_2, TDIC and carbonates) in the IDES Laboratory, and measured using an accelerator mass spectrometry (ARTEMIS accelerator of the UMS LMC14 of INSU-CNRS,

Gif-sur-Yvette, France). The ^{14}C content is expressed as a percentage of modern carbon (pMC) normalized to a $\delta^{13}C = -25‰$.

2.3. Modelling approach

The [13]C–[14]C-transfer in the unsaturated zone depends on (1) the CO_2 production, (2) the CO_2 diffusion, (3) the water advection, and (4) the isotopic exchanges between CO_2-DIC-carbonate. All these processes are characterized by different parameters such as CO_2 production P, the diffusion coefficient of CO_2 D and DIC-carbonate exchange flux ϕ. Each of these parameters can evolve with time, depending on environmental conditions. A numerical approach is thus developed in order to study the [13]C–[14]C transfer in the unsaturated zone and the impact of change of these parameters on the [13]C–[14]C content of CO_2, DIC and carbonate in the unsaturated zone. All previous processes are considered in the study and the calculations are solved by spatial and temporal discretization in one dimension [4].

3.   RESULTS AND DISCUSSION

The DIC in the groundwater of the Astian sands aquifer ranges between 4 and 6 mmol/L. The recharge rate being estimated to 120 mm/a [5], the calculated annual flux of C as DIC reaching the water table is equal to $\sim 0.5 \pm 0.2$ mol·m^{-2}·a^{-1}. Both CO_2 and carbonates contribute to this flux in equal proportions [6]. This implies that ~ 0.25 mol·m^{-2}·yr^{-1} of CO_2 is abstracted from the unsaturated zone during
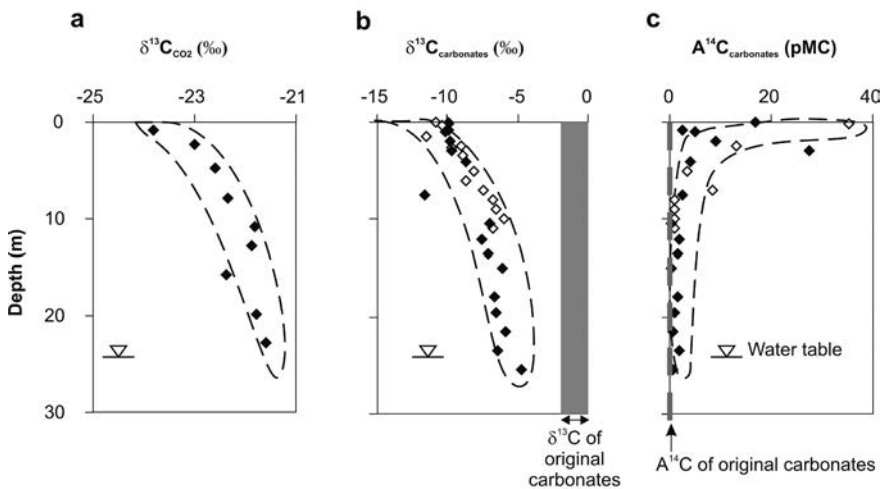
FIG. 2. Evolution of (a) ^{13}C content ($\delta^{13}C_{CO2}$) of CO_2 gas, (b) ^{13}C content ($\delta^{13}C_{carbonates}$) of carbonates and (c) ^{14}C activity ($A^{14}C_{carbonates}$) of carbonates, in the unsaturated zone of the Astian sands. Solid diamonds, profile 2005; open diamonds, profile 2002.

groundwater mineralization. The amount of DIC in percolating water depends on re-charge rate and unsaturated zone-CO_2 partial pressure, which is controlled by root respiration and bacterial activities. These CO_2 pressures can be 100 times higher than those of the atmosphere.

A simple addition of C produced via the dissolution of CO_2 plus carbonates would not have any effect on the isotopic signatures of these two C sources. How-ever, assuming that recharge has been constant for the last 10 kyrs [7], and knowing that the field measured $\delta^{13}C$ of soil-CO_2 (0–1 m below ground level) and of ground-water-DIC are –24.0 ± 0.4‰ and –12.5 ± 0.4‰ vs V-PDB respectively, depth-trends of C-isotopes reveal a dynamic exchange (geochemical and isotopic) between CO_2, carbonate and DIC (Fig. 2). CO_2 dissolution generates a ^{13}C-depleted DIC while car-bonate dissolution contributes to its enrichment.

As a feedback process, continuous C exchanges between liquid, solid and gas lead to ^{13}C-enrichment of CO_2 and to precipitation of a ^{13}C-depleted/^{14}C-enriched sec-ondary calcite compared to the original carbonates, at equilibrium with DIC [8]. Car-bon dissolution–precipitation fluxes at the water–carbonates interface have been cal-culated according to the isotopic compositions of the original matrix and secondary calcite. Results are ranging between 1×10^{-8} and 1×10^{-7} $mol \cdot m^{-2} \cdot yr^{-1}$ [3]. Although very small, this flux of secondary carbonates on unsaturated zone bedrock particles should have recorded the CO_2 abstraction process over time.

In order to study the impact of environmental changes on these isotopic evo-lutions, two parameters related to environmental conditions have been tested using the numeric approach: the CO_2 production P and the diffusion coefficient of CO_2
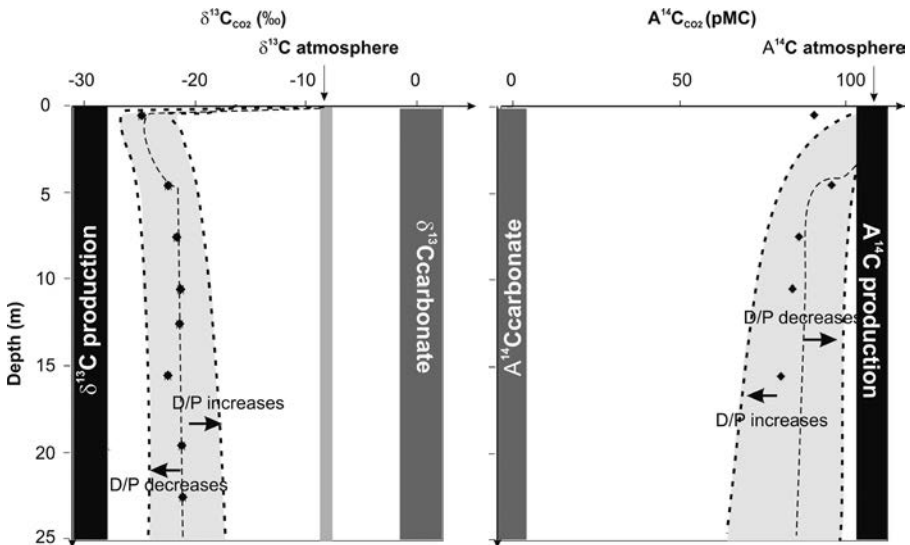
FIG. 3. Impact of the variations of CO_2 diffusion and CO_2 production on the isotopic composition of CO_2 in the unsaturated zone. Solid diamonds, samples collected in February 2006.

D. Both an increase of CO_2 diffusion from soil to atmosphere and/or a decrease of CO_2 production support the exchange between CO_2-DIC-carbonate that then induces the ^{13}C enrichment and ^{14}C depletion of soil CO_2 with the same impact for secondary calcite (Fig. 3). These conditions can occur during a dry period characterized by low water content, one of the parameters controlling CO_2 diffusion and CO_2 production. At the opposite, a decrease of CO_2 diffusion from soil to atmosphere and/or an increase of CO_2 production limit interactions with carbonates. Therefore, the isotopic compositions of CO_2 and of secondary calcite in the unsaturated zone highlight environmental conditions and are sensitive to their changes. Isotopic study of secondary calcite in the unsaturated zone would help to understand environmental change impact on CO_2 abstraction process from pristine conditions recorded on the matrix to modern ones displayed by gas CO_2 distribution.

Since the total amount of abstracted CO_2 through unsaturated zone depends essentially on the extent of recharge areas, the mass balance of the C-fluxes have to be more deeply investigated and quantified in relation with groundwater infiltration, seriously and continuously reduced by the urbanisation and drained surfaces. Knowing that urbanisation surfaces cover ~5% of European area and that the rising-up of urbanized and drained lands has reached ~10% in Europe [9, 10] between 1990 and 2000, the restriction of the CO_2 abstraction process by more than 9 t $CO_2 \cdot km^{-2} \cdot a^{-1}$ [10] would have insidiously enhanced atmospheric CO_2 concentration.

4.   CONCLUSION

During the recharge of groundwater, C-isotopic exchanges occur between CO_2, DIC and carbonates inducing changes in the ^{13}C–^{14}C content of these carbon species. These isotopic exchanges depend on environmental conditions (temperature, water content), and consequently ^{13}C–^{14}C content must be sensitive to environmental changes. The secondary calcite records environmental conditions and could be used to trace potential changes in C-abstraction (land cover, meteorological conditions) in comparison with the modern situation displayed by CO_2.

REFERENCES

[1]   DEINES, P., "The isotopic composition of reduced organic carbon", Handbook of Environmental Isotope Chemistry, Vol. 1 (FRITZ, P., FONTES, J.Ch., Eds), Elsevier, New York, (1980) 329–406.

[2]   GILLON, M., BARBECOT, F., GIBERT, E., MARLIN, C., MASSAULT, M., "Carbon -13 and carbon-14 contents of groundwater located in sandy aquifer outcrops: driving influence of the unsaturated zone", Advances in Isotope Hydrology and its Role in Sustainable Water Resources Management (IHS–2007), Proc. Symp. Vienna, May 2007, IAEA, IAEA-CN–151/126 (2007) 605–612.

[3]   GILLON, M., BARBECOT, F., GIBERT, E., CORCHO ALVARADO, J.A., MAR-
        LIN, C., MASSAULT, M., Open to closed system transition traced through the TDIC
        isotopic signature at the aquifer recharge stage, implications for groundwater ^{14}C dat-
        ing, Geochim. Cosmochim. Acta **73** (2009) 6488–6501.

[4]   GILLON, M., Etude des modes d'acquisition de la signature isotopique en carbone
        des eaux souterraines et préservation du signal environnemental lors de la recharge
        des aquifères, PhD. Thesis, Université Paris sud XI, Orsay, France (2008) 231.

[5]   LEDUC, C., Hydrogéologie de la nappe captive astienne entre Valras et Agde, PhD.
        thesis, Montpellier II Univ., France (1985).

[6]   LANGMUIR, D., Aqueous Environmental Geochemistry, Prentice Hall Inc., Upper
        Saddle River, New Jersey (1997).

[7]   GARNIER, J.M., FONTES, J.Ch., Hydrochimie, géochimie des isotopes du milieu
        et conditions de circulation dans la nappe captive des sables astiens (Hérault), Bul-
        letin du BRGM (deuxième série) section III 3 (1980) 199–214.

[8]   CLARK, I., FRITZ, P., Environmental isotopes in Hydrogeology, Lewis Publishers
        Boca Raton, FL (1997).

[9]   EUROPEAN ENVIRONMENT AGENCY, CORINE Land Cover 2000 (Europe),
        http://www.eea.europa.eu/data-and-maps/data/corine-land-cover-2000-raster-2
        (2000)

[10]   INSTITUT FRANÇAIS DE L'ENVIRONNEMENT, Superficie drainée pour
        l'agriculture en France en 2000, http://eider.ifen.fr/Eider/tables.do (2000).

DISTRIBUTION OF TRITIUM AND [137]CS IN SOUTH INDIAN OCEAN WATERS — IMPLICATIONS OF WATER TRANSPORT PROCESSES

P.P. POVINEC [a], M. AOYAMA [b], J. GASTAUD [c], Y. HAMAJIMA [d],
K. HIROSE [e], M. JEŠKOVSKÝ [a], I. LEVY [c], J.A. SANCHEZ-CABEZA [f],
I. SÝKORA [a]

[a] Comenius University,
  Faculty of Mathematics, Physics and Informatics,
  Bratislava, Slovakia

[b] Meteorological Research Institute,
  Tsukuba, Japan

[c] International Atomic Energy Agency,
  Marine Environment Laboratories, Monaco

[d] Kanazawa University,
  Low-Level Radioactivity Laboratory,
  Nomi, Japan

[e] Sophia University, Faculty of Science and Technology,
  Tokyo, Japan

[f] Universitat Autonoma de Barcelona,
  Bellaterra, Spain

Abstract

The World Ocean, and specifically the Indian Ocean, plays a significant role in the better understanding of the climate. The distribution of global fallout ^{3}H, ^{14}C, ^{90}Sr, ^{129}I and ^{137}Cs in the seawater of the Indian Ocean, after their main injection from atmospheric nuclear weapons tests during the 1960s, have been investigated. Results obtained in the framework of the SHOTS (Southern Hemisphere Ocean Tracer Studies) project are evaluated and compared with previously published data. The enhanced ^{3}H and ^{137}Cs levels observed in the south Indian Ocean indicate transport of water masses labelled with these radionuclides from the Central Pacific Ocean via the Indonesian Seas to the Indian Ocean. The observed surface gradients and presence of several water masses in the south Indian Ocean makes this ocean one of the most dynamic parts of the World Ocean.

1.   INTRODUCTION

Global fallout radionuclides have been frequently used in oceanic studies [1]. They were injected onto the ocean surface from the atmosphere after large scale US and former USSR atmospheric nuclear weapons tests carried out mainly during the 1950s and early 1960s. Mapping of this deposition revealed that the major injection on the ocean surface occurred at the mid-latitudes of the western North Pacific [2]. Global fallout radionuclides have been measured since the 1950s, originally with the aim of assessing radiological impact from nuclear weapon tests. Later they were used as transient tracers to investigate oceanographic processes [1]. The collected radionuclide data have been recently stored in marine radionuclide databases (GLOMARD/MARIS [3, 4], and HAM [5]).

We shall focus in this paper on two global fallout radionuclides, namely tritium and ^{137}Cs. Tritium is an ideal tracer of water motion because it is directly incorporated into the water molecule. However, its short half-life (12.32 a) restricts its use to studies of relatively short term transport processes. Tritium is produced naturally by interactions of cosmic ray particles with nitrogen and oxygen in the upper atmosphere. Tritium has also been released in large quantities from nuclear reprocessing facilities, mainly in Sellafield (UK) and in La Hague (France) [6]. However, the largest amounts of tritium were produced in atmospheric nuclear weapons tests. The tritium from global fallout in atmospheric moisture peaked in 1963, when it was almost 1000 times higher than its natural cosmogenic concentration. The penetration of bomb tritium from surface waters into deeper layers of the ocean has been used to study pathways and time scales of deep and bottom water formation [7, 8]. ^{137}Cs (half-life 30.17 a) is a fission product of only anthropogenic origin. It was released in large quantities during atmospheric nuclear weapons tests, as well as from nuclear reprocessing facilities [6]. It is found in the seawater of the open ocean mostly in a dissolved phase, following well the movement of water masses. Its removal from the water column is mainly due to diffusion and radioactive decay [1]. Large volume water sampling, needed for analysis of ^{137}Cs, was a limiting factor for its wider applications in large scale oceanic studies.

GEOSECS programme [9, 10] carried out during the 1970s, was the first large scale project devoted to the investigation of the distribution of global fallout tritium and ^{137}Cs in the ocean basins. Tritium was also one of the most important players used during the most comprehensive tracer programme WOCE (World Ocean Circulation Experiment), which was carried out during the 1990s [11]. Both programs covered the World Ocean. The International Atomic Energy Agency's Marine Environment Laboratories (IAEA-MEL) carried out the WOMARS (Worldwide Marine Radioactivity Studies) programme during the 1990s [12], which was one of the most comprehensive open ocean studies of anthropogenic radionuclides in the water column. Recently results from the SHOTS (Southern Hemisphere Ocean Tracer Studies) have considerably improved our understanding of radionuclides in the Southern

Hemisphere oceans. It was the first time that many radionuclide tracers were used in such a large scale project producing high density radionuclide data for water profiles. Results of several international and national studies have been published for the Indian Ocean [13–17]. In this paper we present results for the south Indian Ocean obtained during the SHOTS project and compare them with some previous measurements.

2.   SAMPLING AND ANALYTICAL TECHNIQUES

2.1.   Waters samples

Water samples included in the SHOTS project were collected during the round the globe BEAGLE 2003 expedition, organized by JAMSTEC (Japan Agency for Marine-Earth Science and Technology) [18–19], which sampled seawater along 20–30 °S latitude covering the Pacific, Atlantic and Indian Oceans. The Indian Ocean transect was carried out December 2003–January 2004. The transect consisted of two parts: (1) Leg I4 from the African coast to the Madagascar coast along 25°S (the WOCE leg I4); (2) Leg I3 from the Madagascar coast to Port Louis and then to the Australian coast along 20°S (the WOCE leg I3). Surface seawater and water column samples were collected at 22 stations, with sampling spacing of around 2.5°. Surface water (around 80 L) was collected 5 m below the ocean surface by a pumping system. Water column samples (from 5 to 20 L) were collected using a Rosette multisampling system and Niskin bottles. All water samples were filtered through a membrane filter (Millipore HA, 0.45 μm pore size) immediately after sampling.

2.2. Analytical techniques

Tritium in seawater samples was analysed mass spectrometrically at the University of Bremen using a ^{3}He ingrowth method. ^{3}H concentration is given in Tritium Units (1 TU is the isotopic ratio of one ^{3}H atom to 10^{18} protium (^{1}H) atoms, equivalent to 118 mBq/L of water). The ^{3}He ingrowth method can measure ^{3}H levels down to 0.01 TU (precision at 1 σ is around 0.005 TU). ^{137}Cs was concentrated in seawater samples by adsorption onto AMP (ammonium molybdophosphate) using a method described in detail elsewhere [20]. ^{137}Cs activities were determined by low level γ–spectrometry with high efficiency HPGe detectors in MRI, Kanazawa University, University of Bratislava and IAEA-MEL [20]. Intercomparison exercises and regular analysis of Certified Reference Material IAEA–381 (Irish Sea water [21]) were organized between participating laboratories to ensure quality and management of high precision data. Recent analytical developments in analysis of very low concentrations of ^{137}Cs in underground laboratories allowed us to determine ^{137}Cs concentrations in relatively small seawater samples (10 L) with high sensitivity and precision, had not

been possible before. Thanks to these new developments it was possible to reach a high ^{137}Cs data density, which allowed us to draw a detailed picture of the spatial and depth distribution of ^{137}Cs in the Indian Ocean.

3.   RESULTS AND DISCUSSION

The distribution of global fallout tritium and ^{137}Cs in seawater of the south Indian Ocean along 20 °S is presented in Fig. 1. The elevated tritium and ^{137}Cs levels in surface waters are well visible, especially in the case of ^{137}Cs, where the data density is better. The highest surface tritium levels (0.7 TU) were detected at around 40°E, 60°E and 100°E and the minimum at around 80°E. The tritium transect is thus copying the cross-section of the subtropical gyre [17]. The central part of the gyre, outside of the main streams, should have the lowest tritium concentrations, which is confirmed by observation of lower tritium values (0.5 TU) at around 80°E. Surface water
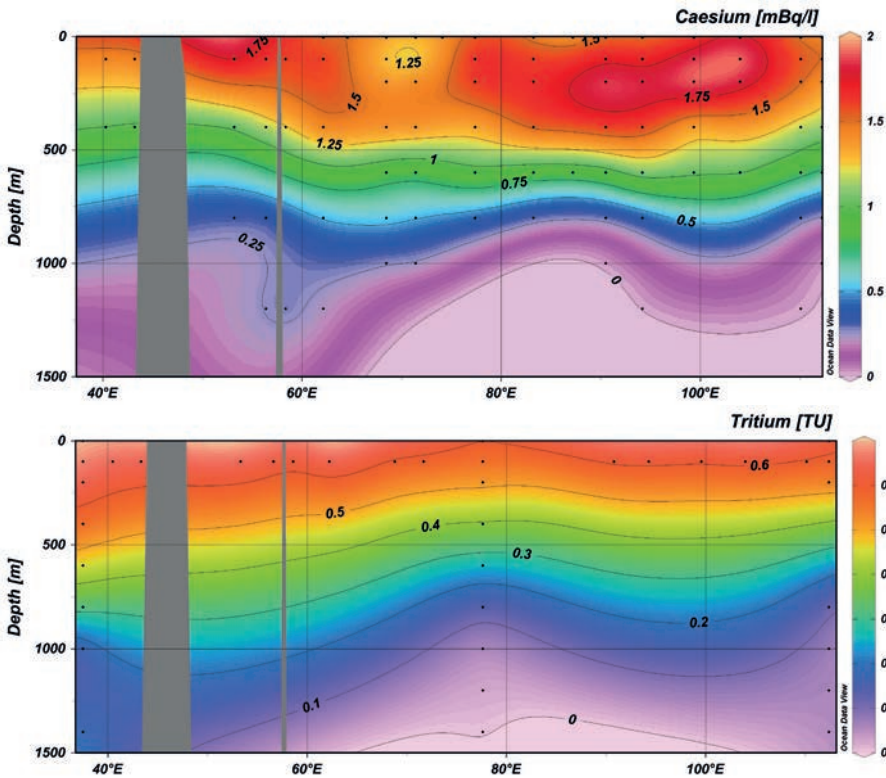
FIG. 1. [137]Cs (top) and [3]H (bottom) in in the water column of the South Indian Ocean along 20°S. Elevated ^{137}Cs and ^{3}H levels are well visible in surface and subsurface waters.

samples collected in 1998 as a part of the Indian Ocean transect [22] also showed higher ^{3}H levels around 30°S, comparable with those presented in Fig. 1. Also WOCE tritium data (1995) shows surface maxima at around 110°E (1.2 TU) and 63°E (1.1 TU), and the surface minimum at 75°E (1 TU).

The ^{137}Cs transect along the 20°S latitude also clearly depicts a presence of two cores of higher ^{137}Cs concentrations at 100°E and 60°E. The subsurface (100–200 m water depth) maximum of ^{137}Cs concentration near 100 °E is the highest level observed in southern hemisphere seawater, and of the same level as the maximum ^{137}Cs concentration observed in North Pacific surface water [23], as well as in the western subtropical Pacific Ocean [24]. As expected, the intrusion depth of ^{137}Cs is deeper in the eastern south Indian Ocean stations and shallower in the western stations, in agreement with the main circulation patterns.

The elevated tritium and ^{137}Cs levels found in the south Indian Ocean must be therefore due to transport of water masses from the western subtropical Pacific Ocean via the Indonesian Seas to the South Indian Ocean. Recent oceanographic measurements [25] suggest that aproximately 10^7 m^3/s of water flow from the Pacific Ocean into the Indian Ocean through the Indonesian seas. The experimental results have recently been confirmed by modelling exercises carried out using an oceanic general circulation model [26].

The observed tritium and ^{137}Cs surface maxima in Fig. 1 correspond to the main stream of the Indonesian throughflow to the south Indian Ocean subtropical gyre, which is situated at 20°S and 40°S. Due to the circulation of tritium and ^{137}Cs in the gyre, and their physical and biogeochemical properties (half-lives over 10 years, both stay in seawater in a dissolved form), elevated concentrations of these radionuclides are maintained in the subtropical gyre. The gyre acts therefore as a reservoir, accumulating radionuclides in the region on a time scale of several decades. As there is only a weak transport of water masses labelled with ^{137}Cs from the south Indian Ocean via the Agulhas Current to the south Atlantic Ocean [27], the south Indian Ocean subtropical gyre acts as a reservoir of dissolved pollutants transported from the Pacific and Indian Oceans, as well as from the Mediterranean Sea [17].

A major contamination of ocean by pollutants has occurred in the northern hemisphere, in which most human activities take place. The obtained results therefore have important implications for the protection of the marine environment against contamination from land based sources, as well as for climate change studies.

4.   CONCLUSIONS

The distribution of global fallout tritium and ^{137}Cs in the seawater of the south Indian Ocean, along 20 °S, about five decades after its main injection from atmospheric nuclear weapons tests on the ocean surface, is presented and discussed. The elevated tritium and ^{137}Cs levels observed at the ocean surface indicate a transport of

water masses from the subtropical West Pacific via the Indonesian Seas to the Indian Ocean. Although the differences in tritium concentrations alongside 20 °S are smaller than in the case of ^{137}Cs, the tritium transect has similar features to the ^{137}Cs transect.

The subtropical gyre in the south Indian Ocean has been maintaining higher tritium and ^{137}Cs levels in surface and subsurface waters in the gyre. The obtained results have implications for the protection of the marine environment against contamination from land based sources, as well as for climate change studies.

ACKNOWLEDGEMENTS

REFERENCES

[1]   LIVINGSTON, H.D., POVINEC, P.P., A millennium perspective on the contribution of global fallout radionuclides to ocean science, Health Phys. **82** (2002) 656–668.

[2]   AOYAMA, M., et al., Re-construction and updating our understanding on the global weapons tests ^{137}Cs fallout, J. Environ. Monitor. **8** (2006) 431–438.

[3]   POVINEC, P.P., et al., Spatial distribution of ^{3}H, ^{90}Sr, ^{137}Cs and ^{239,240}Pu in surface waters of the Pacific and Indian Oceans – GLOMARD database, J. Environ. Radioact. **76** (2004) 113–137.

[4]   POVINEC, P.P., et al., "The marine information system", Isotopes in Environmental Studies, (Proc. Conf. Monaco, 2004), (P.P. POVINEC, JA SANCHEZ-CABEZA, Ed.), IAEA, Vienna (2006) 68–69.

[5]   AOYAMA, M., HIROSE, K., Artificial Radionuclides database in the Pacific Ocean: Ham database, TheScientificWorldJOURNAL **4** (2004) 200–215.

[6]   LIVINGSTON, H.D., POVINEC, P.P., Anthropogenic marine radioactivity, Ocean and Coastal Management **43** (2000) 689–712.

[7]   WEISS, W., ROETHER, W., The rates of tritium input into the oceans, Earth Planet. Sci. Lett. **49** (1980) 435–446.

[8]   ROETHER, W., "Studying thermohaline circulation of the ocean by means of tracer data", Ocean Processes in Climate Dynamics (MALANOTTE-RIZZOLI, P., ROBINSON, A.R., Eds), Kluwer Academic, Dordrecht (1994) 157–171.

[9]   BROECKER, W.S., et al., The distribution of bomb tritium in the Ocean, J. Geophys. Res. **91** (1986) 14331–14344.

[10]   OSTLUND, H.G., BRESCHER, R., Tritium Laboratory Data Report No. 2. University of Miami, Miami, USA (1982).

[11]   SCHLOSSER, P., et al., "Transportation and age of water masses", Ocean Circulation and Climate (G.J. SIEDLER, J. CHURCH, J., GOULD, J., Eds), Academic Press, London (2001) 431–452.

[12]   POVINEC, P.P., et al., ^{90}Sr, ^{137}Cs and ^{239,240}Pu concentration surface water time series in the Pacific and Indian Oceans. WOMARS results, J. Environ. Radioact. **81** (2005) 63–87.

[13]   MIYAKE, Y., et al., Contents of ^{137}Cs, plutonium and americium isotopes in the Southern Indian Ocean waters, Pap. Meteorol. Geophys. **39** (1988) 95–113.

[14]   POVINEC, P.P., et al., Anthropogenic radionuclides in the Indian Ocean surface waters – the Indian Ocean transect 1998, Deep Sea Res. II **50** (2003) 2751–2760.

[15]   MULSOW, S., et al., Temporal (^{3}H) and spatial variations of ^{90}Sr, ^{239,240}Pu and ^{241}Am in the Arabian Sea: GEOSECS Stations revisited, Deep Sea Res. II **50** (2003) 2761–2776.

[16]   POVINEC, P.P., et al., ^{137}Cs water profiles in the South Indian Ocean Water – an evidence for accumulation of pollutants in the subtropical gyre, Progr. Oceanogr. **891** 4 (2011) 17–30.

[17]   POVINEC, P.P., et al., Tracing of water masses using a multi isotope approach in the southern Indian Ocean, Earth Planet. Sci. Lett. 302 (2011) 14–26.

[18]   UCHIDA, H., FUKASAWA, M., (Eds.), WHP P6, A10, I3/I4 Revisit Data Book Blue Earth Global Expedition 2003, Vol. 1, 2, Aiwa Printing Co., Ltd., Tokyo (2005).

[19]   UCHIDA, H., FUKASAWA, M., (Eds.), WHP P6, A10, I3/I4 Revisit Data Book Blue Earth Global Expedition 2003. Vol. 3, Aiwa Printing, Tokyo (2007), see also www.jamstec.org.

[20]   LEVY, I., et al., Marine anthropogenic radiotracers in the Southern Hemisphere: New sampling and analytical strategies, Progr. Oceanogr. **89** (2011) 120–133.

[21]   POVINEC, P.P., et al., Certified reference material for radionuclides in seawater IAEA–381 (Irish Sea water), J. Radioanal. Nucl. Chem. **251** (2002) 369–374.

[22]   POVINEC, P.P., et al., Anthropogenic radionuclides in the Indian Ocean surface waters – the Indian Ocean transect 1998, Deep-Sea Res. II **50** (2003) 2751–2760.

[23]   POVINEC, P.P., et al., IAEA'97 expedition to the NW Pacific Ocean – results of oceanographic and radionuclide investigations of the water column, Deep-Sea Research II **50** (2003) 2607–2637.

[24]   AOYAMA, M., et al., Cross equator transport of ^{137}Cs from North Pacific Ocean to South Pacific Ocean (BEAGLE2003 cruises), Prog. Oceanogr. **89** (2011) 7–16.

[25]   GORDON, A.L., et al., Cool Indonesian throughflows as a consequence of restricted surface layer flow, Nature **425** (2003) 824–828.

[26]   TSUMUNE, D., et al., Transport of ^{137}Cs into the Southern Hemisphere in an Ocean General Circulation Model, Prog. Oceanogr. **89** (2011) 38–48.

[27]   SANCHEZ-CABEZA, J.A., et al., Transport of North Pacific ^{137}Cs labelled waters to the south-eastern Atlantic Ocean, Prog. Oceanogr. **89** (2011) 31–37.

ISOTOPE HYDROLOGY 1
(ATMOSPHERE, SURFACE WATERS AND
WATER QUALITY)

ON THE ISOTOPIC ALTITUDE EFFECT OF PRECIPITATION IN THE NORTHERN ADRIATIC (CROATIA)

Z. ROLLER-LUTZ [a], D. MANCE [a], T. HUNJAK [a], H.O. LUTZ [a,b]

[a] Stable Isotope Laboratory,
Medical Faculty, University of Rijeka,
Rijeka, Croatia,
roller@medri.hr

[b] Physics Faculty,
Bielefeld University,
Bielefeld, Germany

Abstract

The upper (northern) Adriatic is very rich in precipitation. This input into the water system and its stable isotope composition is a basic factor, knowledge of which is required for proper use and management of water resources. The geomorphology of the region (e.g., mountains of 1400 m next to the sea) can cause specific local conditions. The isotopic composition of precipitation has been measured in various locations at different altitudes. For $\delta^{18}O$ this 'altitude effect' is found to lie around $-0.2‰ /100$ m; its exact value depends on the specific location and the season. The δ^2H values and the d-excess vary correspondingly.

1.   INTRODUCTION

The use and protection of the karst aquifers in the border area of Slovenia and Croatia presents a problem since it is strongly influenced by the transboundary hydrological situation. Three out of seven catchment areas between the Kvarner and the Trieste bay belong to transboundary aquifers [1], while the geomorphology (e.g., mountains of up to 1400 m next to the sea) causes specific local conditions. Rijeka, the third largest city in Croatia, is located in this region, and her water supply needs special attention. Evidently, the management of the region's water resources requires a broad knowledge of all related aspects including the precipitation as input into the water system. Besides meteorological data, isotopic tracers are an important tool to understand and quantify such complex problems. The isotopic composition of precipitation is primarily determined by the passage of the water into and through the atmosphere. As the air mass passes over the continent preferentially the heavy
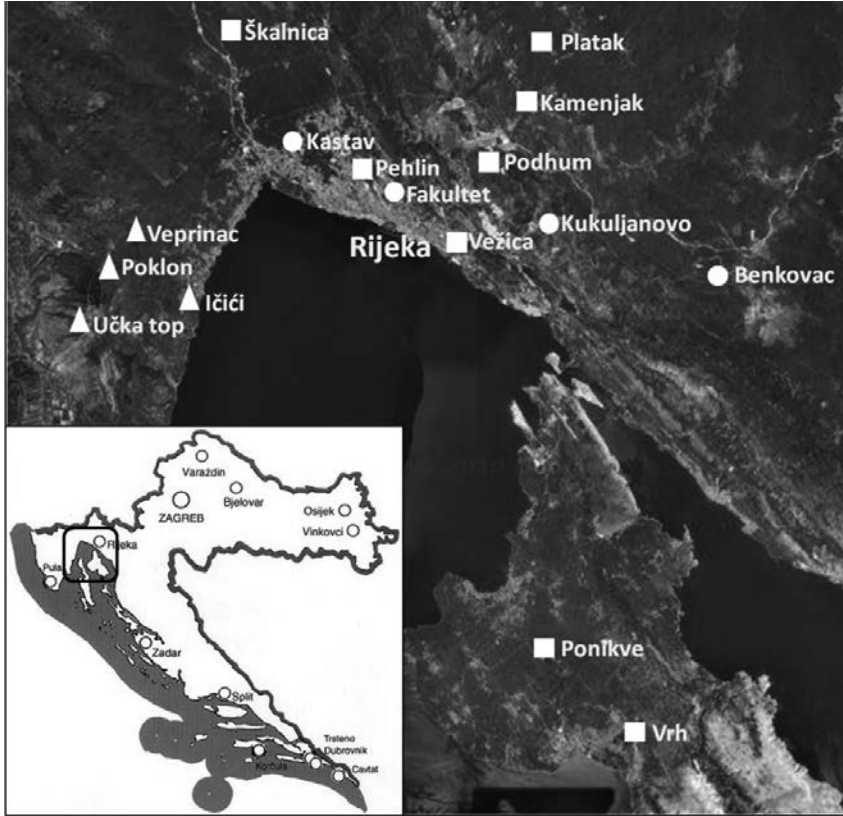
FIG. 1. The upper Adriatic and the precipitation collection stations (■ — recently installed stations; ●, ▲ — stations with isotope record of two full years).

isotopes rain out due to fractionation; as a consequence, the remaining vapour and thus also the further precipitation experience a progressive depletion of the heavy isotopes along the way, and, as is well known, such a mostly temperature related depletion occurs also with increasing altitude. Since only scattered information exists about the isotopic composition of precipitation in our region of interest [2, 3], the Stable Isotope Laboratory (SILab, Rijeka University) has initiated a network of precipitation collection stations on the upper (Northern) Adriatic, i.e. in the Rijeka region (Fig. 1). In this paper we will report on the altitude effect of the isotopic composition of precipitation in this area. The isotopic composition of a water sample is usually expressed by abundance ratios R (^{2}H/^{1}H and ^{18}O/^{16}O, respectively) in terms of the δ-values, δ (‰) = (R_{sample}/$R_{standard}$ − 1) × 10^3, with $R_{standard}$ the abundance ratio of an internationally accepted standard (e.g., the Vienna Standard Mean Ocean Water, VSMOW). Ref. [3] gave a mean value of −0.3‰ /100 m for δ^{18}O of precipitation in the area of interest here; however, as we shall see, the situation is more complicated and depends on the location and the season.

2.   SITE DESCRIPTION

Croatia is located in southeast Europe, bordering on the Adriatic Sea. Generally, the islands and the coast have a Mediterranean climate. From autumn until spring, Icelandic cyclones can cause weather instability, frequently accompanied by secondary Mediterranean cyclogenesis with strong southerly winds along the coast and heavy precipitation, the sirocco. In summer, Azorean and Siberian anticyclones can result in rather stable conditions, often with strong, dry northerly winds — bora — at the seaside. In the northern Adriatic the amount of precipitation during the year is quite considerable. Thus, by the Thornthwaite classification, the climate is mostly humid, while in the mountainous hinterland of the Kvarner Gulf and the wider region of Rijeka orographic effects can intensify the precipitation to over 1500 mm/a and the climate is perhumid [4]. This orographic diversity has an important influence and can cause strong variations within short distances of a few kilometers. For example, between Istria and the Rijeka region the Učka Mountain massive rises up directly from the sea to about 1400 m a.s.l. and is responsible for occasional very heavy local precipitation. Other highlands and mountain chains between the flat Pannonian plain in the north and the sea provide a rather efficient divide and somewhat mitigate weather exchange. Average temperatures show quite pronounced regional variations: in winter they range from –2°C inland with snow in the mountains to 5°C along the coast and in summer they range from 15°C to 25°C, respectively.

3.   SAMPLING AND ANALYSIS

In the northern Adriatic, our network comprises at present 16 stations. Since several stations have been installed only recently (square symbols in Fig. 1), we will show here only the data of those eight stations which cover two complete years (circles and triangles). They are located at different altitudes in the center of Rijeka (Fakultet, 28 m) and the hinterland of Rijeka (Kukuljanovo, 281 m; Kastav, 350 m; Benkovac, 873 m), what is called below 'Kvarner', as well as on Mount Učka (Ičići, 2 m; Veprinac, 484 m; Poklon, 927 m; and on the top of Učka, 1381 m), 'Učka' in the following. We will display the data for the two regions separately since the Učka stations are very close together; therefore, they are particularly well suited to determine altitude effects without local influences. A new type of collector is used, which allows the storing of the precipitation for weeks and even months without noticeable evaporation and associated fractionation. The performance of the collector has been studied in detail and will be published in a separate paper. Monthly samples are brought to the Stable Isotope Laboratory SILab at Rijeka University where they are analysed for their isotopic composition. δ^2H and $\delta^{18}O$ are measured in a Thermo-Finnigan DeltaplusXP isotope ratio mass spectrometer using a combination of dual inlet and equilibration unit as periphery. The samples are equilibrated with H_2 and
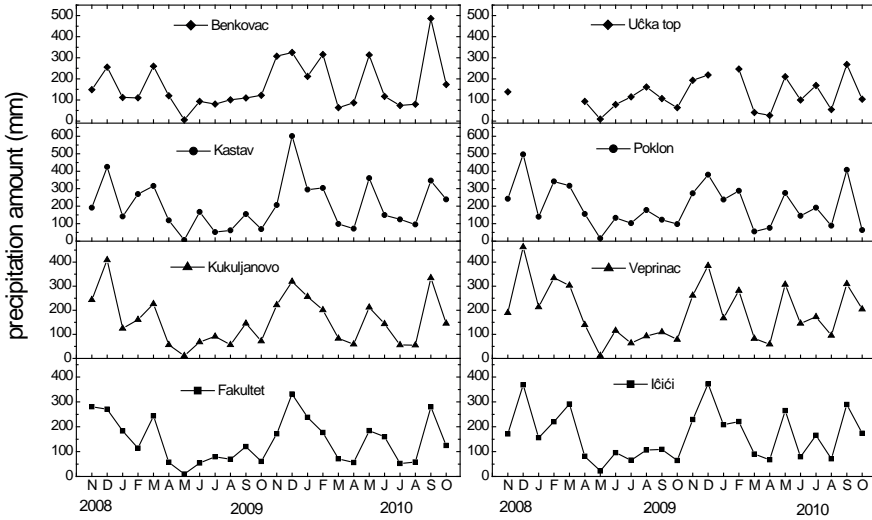
FIG. 2. Precipitation amount at four stations. Left: Kvarner region; right: Učka Mountain.

CO_2, whereby their isotopic composition is transferred to these gases and then analysed in the mass spectrometer. The precision of the δ-values thus determined is 1‰ for δ^2H and 0.1‰ for $\delta^{18}O$. The required working standards were produced by collecting waters of different δ-values and storing them under nitrogen gas in stainless steel barrels. They were calibrated through comparison with IAEA standards.

4.   RESULTS AND DISCUSSION

The rather large precipitation amounts in Rijeka and some stations in the general area are displayed in Fig. 2. The general behaviour shows strong winter maxima and weak precipitation in summer; secondary maxima e.g. in May and September 2010 are characteristic for the variable character of the local climate. Occasionally, some local orographic events emphasize this general behaviour (e.g. Kastav in winter 2009/2010).

At all eight stations, the $\delta^{18}O$ values (Fig. 3) vary between maximum values (around −4‰) in the warm season and minimum values (around −12‰) in the cold season; the exact values depend on the location. δ^2H (not shown) follows $\delta^{18}O$ and varies between around −20‰ and −70‰.

From the data we have extracted the altitude dependence (Fig. 4) of the precipitation weighted mean $\delta^{18}O$ values, separately for the warm (April-September) and the cold season (October-March). In both sets of stations, as expected, the winter data are shifted to more negative values, while the slopes are practically identical
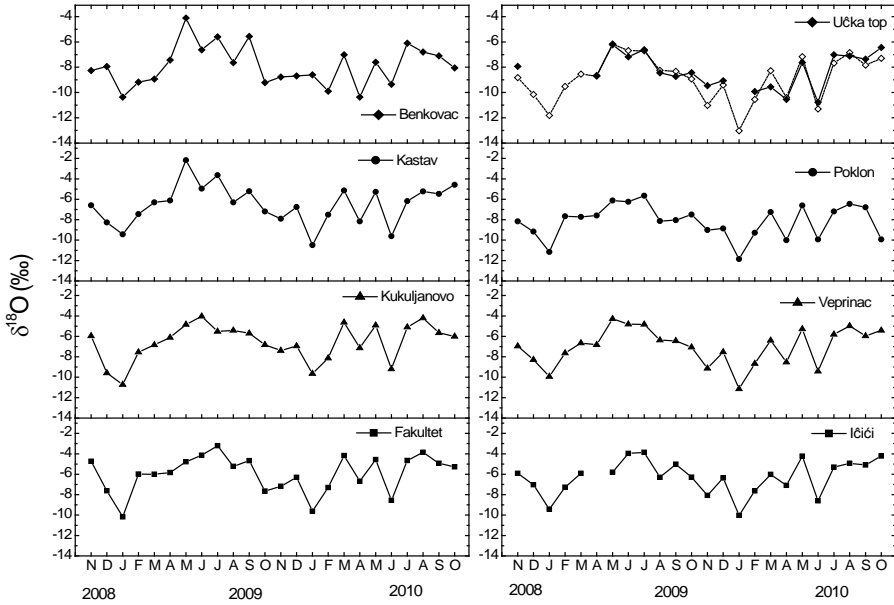
FIG. 3. Precipitation $\delta^{18}O$ in the Kvarner region (left) and on Učka (right).
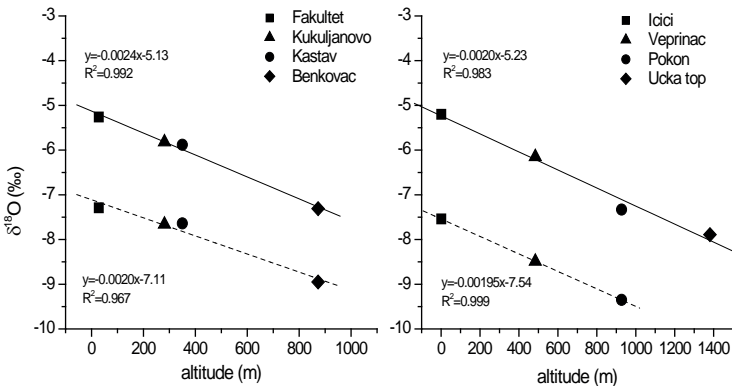
FIG. 4. $\delta^{18}O$ altitude effect of the weighted means for the warm (solid lines) and the cold season (dashed) lines.

(Učka) or slightly different (Kvarner). The yearly averaged $\delta^{18}O$ altitude effects (ca. −0.2‰ /100 m for Učka and −0.22‰ /100 m for the Kvarner) are considerably weaker if compared to the −0.3‰ /100 m as given earlier in Ref. 3. For the station on the top of Učka a few winter data had to be eliminated due to ice formation. However, using the data from a lower-lying station (e.g. Veprinac) where no ice formation occurred, and applying the respective altitude relation as shown in Fig. 4, the Učka
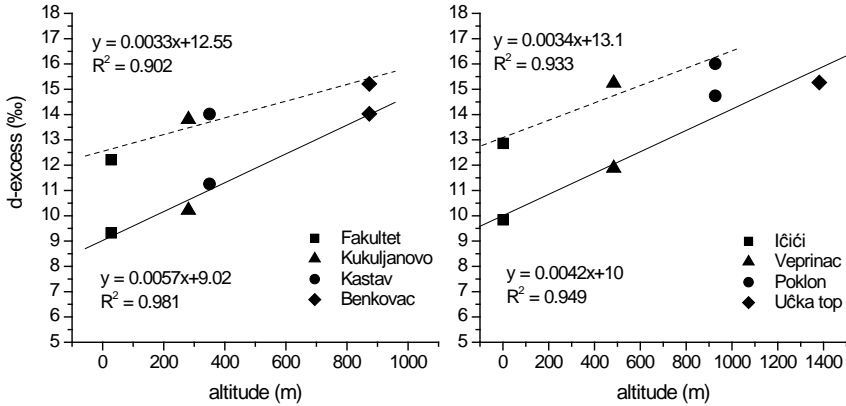
FIG. 5. Altitude effect of the precipitation-weighted mean d-excess for the warm (solid lines) and the cold season (dashed lines).

data including the missing months can be reconstructed (broken curves in Fig. 3). The agreement with the actually measured values is rather good.

The linear relationship between δ^2H and $\delta^{18}O$ (the Local Meteoric Water Line, LMWL) has been determined as $\delta^2H = 7.11\,\delta^{18}O + 6.75$ and $\delta^2H = 7.05\,\delta^{18}O + 5.16$ for Učka and Kvarner, respectively. Both LMWLs are close to the Global Meteoric Water Line (GMWL, $\delta^2H = 8\,\delta^{18}O + 10$ [5]). Slopes and intercept are somewhat smaller if compared to the 2001–2003 data for Portorož and Kozina on the western side of Istria [3]. As suggested in Ref. [3], such a temporal change might indicate a change to warmer (and possibly less humid) climate conditions. Since local influences (evaporative enrichment of falling rain drops beneath the cloud base, snow formation, etc.) may follow different fractionation rules, the LMWL is more of a descriptive characteristic [6]. The deuterium excess $d = \delta^2H - 8\,\delta^{18}O$ appears to be a better indicator [7]. For example, it is generally thought to be useful in identifying the origin of the precipitating air mass: Atlantic air masses have a d-excess typically of around 10‰, while Mediterranean air masses are characterized by a larger d-excess [8]. In the cold season d-excess is generally higher and shows a significant altitude effect, too, at least partly related to the altitude dependence of the temperature. This may require further study.

5.   CONCLUSION

The paper presents the isotopic composition of precipitation collected in a station network on the Northern Adriatic. The $\delta^{18}O$ values decrease with increasing altitude. The slope of this relation depends on the season and on the location; generally it

is, however, somewhat smaller than the one reported in Ref. [3] for the Western side of Istria. Also the d-excess shows a significant altitude effect in that it increases with increasing altitude. To our knowledge, this is the first time that a systematic measurement of an altitude dependent d-excess has been reported.

ACKNOWLEDGEMENTS

REFERENCES

[1]   HORVAT, B., RUBINIC, J., Annual runoff estimation – an example of karstic aquifers in the transboundary region of Croatia and Slovenia, Hydrol. Sci. **51** (2006). 314–324.

[2]   KRAJCAR BRONIĆ, I., VREČA, P., HORVATINČIĆ, N., BAREŠIĆ, J., OBELIĆ, B., Distribution of hydrogen, oxygen and carbon isotopes in the atmosphere of Croatia and Slovenia, Arh Hig Rada Toksikol **57** (2006) 23–29.

[3]   VREČA, P., KRAJCAR BRONIĆ, I., HORVATINČIĆ, N., BAREŠIĆ, J., Isotopic characteristics of precipitation in Slovenia and Croatia: Comparison of continental and maritime stations, J. Hydrol. **330** (2006) 457–469.

[4]   ZANINOVIĆ, K., GAJIĆ-ČAPKA, M., PERČEC TADIĆ, M., et al., Climate Atlas of Croatia, Državni hidrometeorološki zavod, Zagreb (2008).

[5]   CRAIG, H., Isotopic variations in meteoric waters, Science **133** (1961) 1702–1703.

[6]   GAT, J.R., "Some classical concepts of isotope hydrology", Isotopes in the water cycle (AGGARWAL, P., GAT, J.R., FROEHLICH, K.O., Eds), Springer, Dordrecht (2005) 127–137.

[7]   DANSGAARD, W., Stable isotopes in precipitation, Tellus **16** (1964) 436–468.

[8]   ROZANSKI, K., ARAGUAS-ARAGUAS, L., CONFIANTINI, R., Isotopic patterns in modern global precipitation, Geophys. Monogr. **78** (1993) 1–36.

STABLE ISOTOPES IN PRECIPITATION OVER INDONESIA MARITIME CONTINENT

K. ICHIYANAGI [a,b], R. SUWARMAN [a], M.D. YAMANAKA [b]

[a] Graduate School of Science and Technology,
Kumamoto University, Japan

[b] Japan Agency for Marine-Earth Science and Technology (JAMSTEC)

Abstract

Daily variability of stable isotopes in precipitation was observed at 6 stations in the Indonesian Maritime Continent from 2000 to 2006. The annual mean $\delta^{18}O$ at Bukit Kototabang (GAW), Jambi, and Makassar are heavier than those for others. The precipitation amount effect was observed only at Denpasar and Makassar. There are 2 groups resulting from the Local Meteoric Water Line; (1) slope is nearly 7.0 and high d-excess more than 10 at GAW, Denpasar, and Manado, (2) slope is around 7.4 and low d-excess less than 7.5‰ at Jambi, Makassar, and Palau. Seasonal variability of $\delta^{18}O$ and d-excess were classified into three patterns. There are no seasonal variations in $\delta^{18}O$ and d-excess at GAW and Jambi, but clear seasonal variations at Denpasar (DPS) and Makassar (MKS). Due to the amount effect, $\delta^{18}O$ in precipitation is high when the precipitation amount is low from May to October. In contrast, the amount effect is not significant and d-excess is constant throughout the year in Manado and Palau. The $\delta^{18}O$ in precipitation at 2 stations located in Sumatra Island corresponded with the Madden-Jullian Oscillation index, while those for the other 4 stations in more easterly locations did not. This finding indicates that water vapour evaporated from the Indian Ocean can reach the Island of Sumatra, but can't reach more easterly locations.

1. INTRODUCTION

Stable isotopes in meteoric precipitation are strongly influenced by the water vapour source and trajectory history and can be used to reconstruct atmospheric circulation. The Global Network of Isotopes in Precipitation (GNIP) operated by the International Atomic Energy Agency (IAEA) has been conducting a worldwide survey of monthly isotope content in precipitation since 1961 [1]. However, there are few stations in the Indonesian Maritime Continent (IMC) and the sampling interval is monthly. Therefore, spatial and temporal distributions of stable water isotopes in precipitation over IMC are not so much understood.

Since 2001, the daily precipitation in Asian Monsoon regions has been sampled and stable isotopes (deuterium and oxygen-18) in precipitation have been analysed
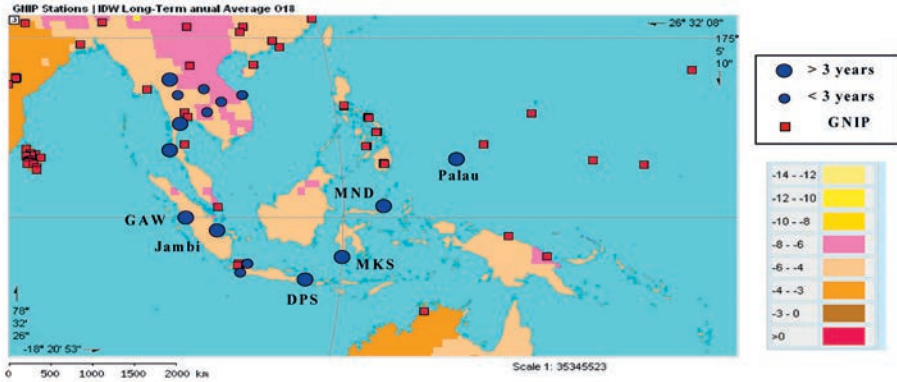
FIG. 1. Locations of the precipitation sampling sites by JAMSTEC and GNIP.

by the Institute of Observational Research for Global Change, Japan Agency for Marine-Earth Sciences and Technology (IORGC/JAMSTEC) [2, 3]. Fig. 1 shows locations of the sampling sites by JAMSTEC and also by GNIP. There are a few GNIP stations in the IMC, so the main objective of our sampling is to interpolate the spatial distributions and temporal variability of stable isotopes in precipitation. Furthermore, the influences to the precipitation isotopes from the Madden-Jullian Oscillation (MJO) are also considered.

2. SAMPLING AND ANALYSIS METHOD

Daily rainfall sampling sites are 5 stations in Indonesia, 7 stations in Thailand, 1 station in Vietnam, and 1 station in Palau, but we focus on the Indonesian Maritime Continent in this study. Table 1 summarized the sampling site, period and basic characteristics in precipitation isotopes. In this study, we use 5 stations in Indonesia and 1 station in Palau. Isotopic compositions of samples were analysed by a MAT–252 analyser with a water equilibrium device at the laboratory of the Ecological Research Center of Kyoto University (samples from 2001 to 2003) and IORGC/JAMSTEC (samples after 2004).

TABLE 1. SUMMARY OF THE SAMPLING SITES AND ISOTOPIC CHARACTERISTICS

Station	Period	Annual $\delta^{18}O$ (‰)	Amount effect (r^2)	δ^2H–$\delta^{18}O$ relationship (r^2)
GAW	Apr 2001–May 2007	–8.32	–0.0071 (0.15)	$\delta^2H = 7.98\,\delta^{18}O + 13.03$ (0.98)
Jambi	Apr 2001–Dec 2005	–6.26	–0.0113 (0.23)	$\delta^2H = 7.44\,\delta^{18}O + 5.55$ (0.97)
DPS	Nov 2002–Sep 2006	–4.56	–0.0105 (0.49)	$\delta^2H = 8.08\,\delta^{18}O + 13.73$ (0.98)
MKS	Nov 2002–Sep 2006	–7.50	–0.0061 (0.43)	$\delta^2H = 7.32\,\delta^{18}O + 6.24$ (0.96)
MND	Nov 2002–Dec 2006	–6.07	–0.0027 (0.07)	$\delta^2H = 7.96\,\delta^{18}O + 11.63$ (0.99)
Palau	Dec 2001–May 2007	–4.68	–0.0072 (0.21)	$\delta^2H = 7.47\,\delta^{18}O + 7.21$ (0.97)

3.   RESULTS

3.1. Amount effect and LMWL

Station Name, observation period, annual mean $\delta^{18}O$, amount effect (slope between $\delta^{18}O$ and precipitation amount), and relations between δ^2H and $\delta^{18}O$ (LMWL; Local Meteorological Water Line) are shown in Table 1. The annual mean $\delta^{18}O$ ranged from –4.56 to –8.32‰. The ^{18}O values at GAW, Jambi, MKS, and MND are relatively more negative (less than –6.0‰) than those at DPS and Palau (more than –5.0‰). The precipitation amount effect is observed with statistical significance only at DPS and MKS. The slope is –0.0105 in DPS and –0.0061 in MKS. The slope and intercept of LMWL are ranged from 7.32 to 8.08 and from 5.55 and 13.73, respectively. There are 2 groups resulting from the LMWL (δ^2H–$\delta^{18}O$ relationship in Table 1); 1) slope is nearly 7.00 and high d-excess more than 10 at GAW, DPS, and MND, 2) slope is around 7.40 and low d-excess less than 7.5 at Jambi, MKS, and Palau.

3.2.   Seasonal variability

The monthly mean $\delta^{18}O$ and d-excess values at 6 JAMSTEC stations were compared to those of GNIP in Fig. 2. Seasonal variability of these stations can be classified into 3 groups. There are no seasonal variations in $\delta^{18}O$ and d-excess at GAW, and there are bimodal peaks at Jambi. These seasonal patterns resemble those of GNIP at Jakarta, Jayapura, and Singapore, while there are clear seasonal variations in $\delta^{18}O$ at DPS and MKS. Due to the amount effect, monthly $\delta^{18}O$ in precipitation is high when the monthly precipitation amount is small from May to October. This seasonal pattern resembles that of GNIP at Darwin and Madang. In contract, $\delta^{18}O$ from May to October is low at MND and Palau. The amount effect is not significant and monthly
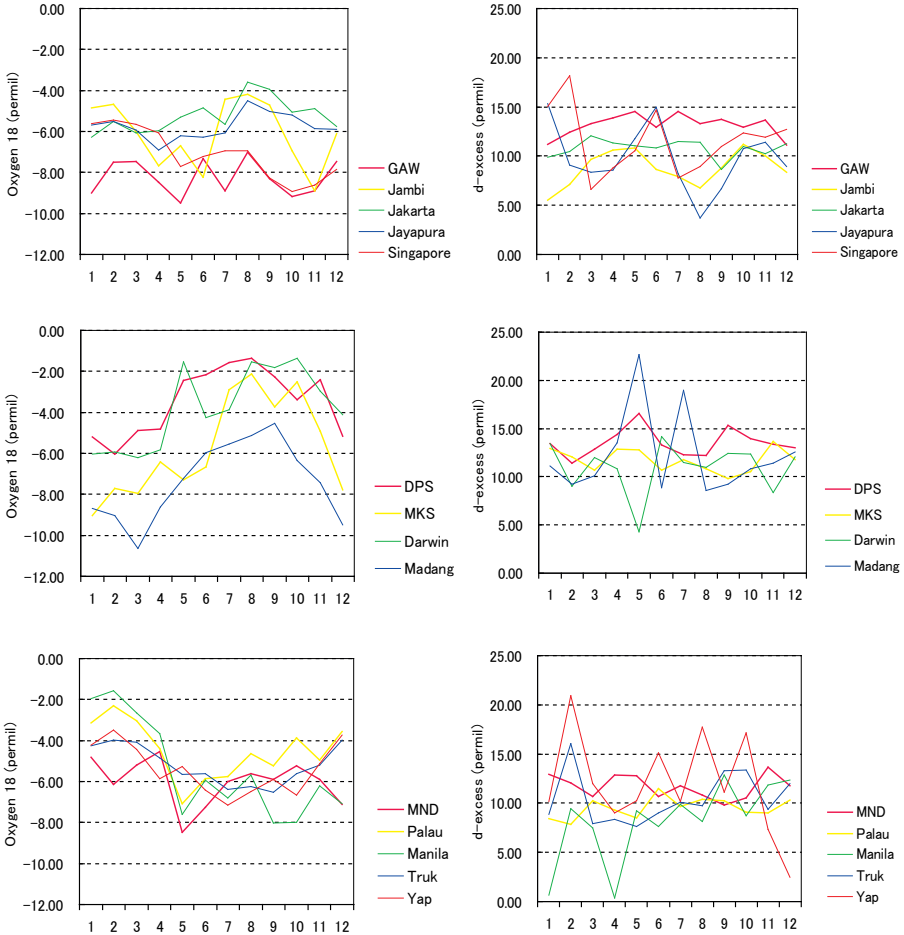
FIG. 2. Seasonal variability in monthly δ18O and d-excess in precipitation over IMC and surrounding area.

d-excess values are almost constant throughout the year in these stations. This seasonal pattern resembles those of GNIP at Manila, Truk, and Yap, which are located on islands in the Western Pacific.

4, DISCUSSIONS

To consider the relationship between δ18O in precipitation and the Madden Julian Oscillation (MJO), δ18O observed in precipitation was compared with the pentad MJO index produced by the Climate Prediction Center of NOAA (downloaded from http://www.cpc.ncep.noaa.gov/products/precip/CWlink/daily_mjo_index/pentad.
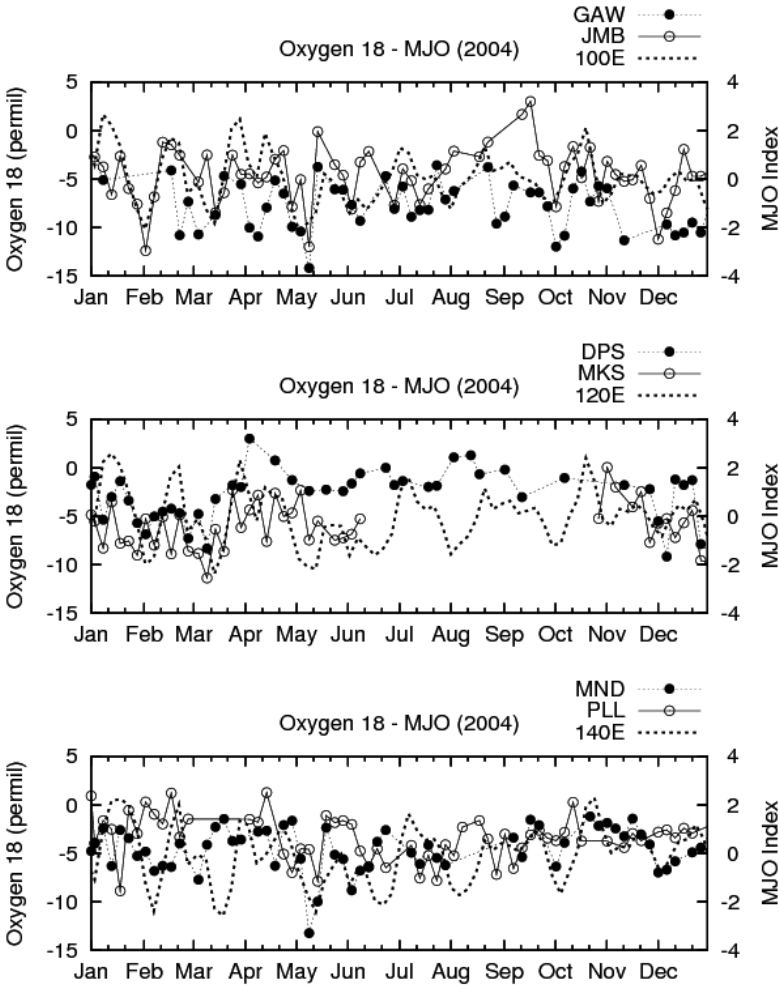
FIG. 3. Time series of pentad δ¹⁸O in precipitation and MJO index at 6 stations observed in 2004.

html). A time series of pentad $\delta^{18}O$ in precipitation and MJO index at 6 stations in 2004 were shown in Fig. 3. Variability in $\delta^{18}O$ at GAW and JMB in Sumatra Island corresponds with the MJO index (upper panel), while other 4 stations which are located more easterly in the Indonesian Maritime Continent (IMC) are not corresponding (middle and lower panels).

Based on the estimation of water vapour origins by using coloured moisture analysis [4], precipitable water at GAW and JMB stations was mostly occupied by water vapour evaporated from the Indian Ocean. However, precipitable water at other 4 stations was mostly composed of water vapour evaporated from the Java Sea and the Pacific Ocean [5].

These findings indicate that water vapour evaporated from the Indian Ocean related to the MJO can only reach the Island of Sumatra in the western part of the IMC. Then, Indian Ocean origin was replaced by the water vapour evaporated from the Java Sea and the Pacific Ocean. Therefore, there are no correlations between $\delta^{18}O$ in precipitation and the MJO index at 4 stations located in the more easterly part of the IMC.

5.   CONCLUDING REMARKS

Stable isotopes in precipitation observed at 6 stations in the IMC were compared in their seasonal variability with the GNIP stations. There are 2 groups resulting from the Local Meteoric Water Line, while seasonal variability in $\delta^{18}O$ and d-excess in precipitation can be classified into 3 patterns. Due to the amount effect, $\delta^{18}O$ in precipitation is high when precipitation amount is low at only DPS and MKS. However, the amount effect is not significant at the other 4 stations. To consider the relation with the MJO, pentad $\delta^{18}O$ in precipitation at only GAW and JMB stations located in Sumatra Island corresponded with the MJO index. However, the other 4 stations located in the more eastern part of IMC were not significant.

REFERENCES

[1]   INTERNATIONAL ATOMIC ENERGY AGENCY/WORLD METEOROLOGIC ORGANIZATION, Global Network of Isotopes in Precipitation, The GNIP Database (2006) http://www.iaea.org/water.

[2]   LARGE-SCALE HYDROLOGICAL CYCLE RESEARCH GROUP, IORGC, JAM-STEC, Ten-year Summary of the Observational Research (1999–2008), Japan Agency for Marine-Earth Science and Technology, Yokosuka, Japan (2008) 165.

[3]   KURITA, N., et al., The relationship between the isotopic content of precipitation and the precipitation amount in tropical regions, J. Geochem. Exp. **102** (2009) 113–122.

[4]   YOSHIMURA, K., et al., Colored moisture analysis estimates of variations in Asian monsoon water sources, J. Meteor. Soc. Japan **82** (2004) 1315–1329.

[5]   ICHIYAANGI, K., "Observational Study of Stable Isotopes in Precipitation over the Tropical Asia", Application of Stable Water Isotopes to Meteorology (YOSHIMURA, K., et al., Eds.)", Kisho Kenkyu Note, 220, Met. Soc. Japan (2009) 15–32 (in Japanese).

STABLE ISOTOPIC COMPOSITION OF RAINFALL IN WESTERN CAMEROON

B. KETCHEMEN-TANDIA, S. NGO BOUM, C.R. EBONJI SETH ,
G.R. NKOUE NDONG, C. WONKAM
Université de Douala,
Douala, Cameroon

F. HUNEAU
Université de Bordeaux,
EA Géoressources & Environnement,
Talence, France

H. CELLE-JEANTON
Clermont Université,
Clermont-Ferrand, France

Abstract

Monthly rainfall collected at the Douala station (Western Cameroon) from 2006 to 2008 was analysed for oxygen-18 and deuterium content. The dataset, which is now integrated into the GNIP database, was compared to the local groundwater record in order to define the input function of regional hydrosystems. The isotope data displays a wide range of values from –0.59 to –6.14‰ for oxygen-18 and from –7.75 to –38.8‰ for deuterium, closely following the GMWL (Global Meteoric Water Line), suggesting that rain formation processes occurred under isotopic equilibrium conditions between the condensate and the corresponding vapour. No significant evaporation tendency was found. The comparison with the previous studies in the area provides a realistic pattern of isotope concentrations in both surface and groundwater throughout Cameroon.

1. INTRODUCTION

This paper discusses the results of the analysis of monthly rainfall collected at the Douala station (south-western Cameroon) for three years. Isotope data on rainfall are scarce for the Central African Region, although stable isotopes of water are very useful tracers in hydrological, hydrogeological and hydroclimatological studies. A good understanding and characterization of isotope contents of precipitation is of major importance for using isotope data as an input function of water systems or for describing atmospheric circulation patterns and air mass trajectories. The isotopic composition of rainfall in Tropical Central Africa has been studied by Fontes

and Olivry [1] and Gonfiantini et al. [2] who focused on the Mount Cameroon area. These studies showed an altitude gradient of approximately –0.16‰ per 100 m for oxygen-18 and the evolution of the isotopic content of rainfall along the slopes. Ref. [3] focuses on the factors controlling the variations of deuterium and oxygen-18 in rainfall collected throughout Southern Cameroon, from Kribi to Moloundou. They suggested that the altitudinal variations of the weighted mean oxygen-18 content of precipitation in coastal areas are controlled by the continuous extraction of vapour from the atmospheric reservoir as rain according to the Rayleigh distillation model. In the area farther than 230 km from the Atlantic coast, the recycling of continental moisture influences the isotopic composition of the rainfall.

In addition, the stable isotope records from the rainfall of the Douala station was compared to some available isotope data from groundwater from the previous studies on the Cameroonian territory [4–15]. The Douala record was compared with the Sahelian GNIP station of N'Djamena (Chad), bordering northern Cameroon, as well as the Atlantic GNIP station of Sao Tome (São Tomé e Príncipe).

2. STUDY AREA

Cameroon has four distinct topographical regions — the south, a coastal plain with dense equatorial rain forests; the centre, the Adamawa Plateau, consisting of a region with elevations reaching about approximately <1300 m.a.s.l.; the far north where the savannah gradually descends to the marshland surrounding Lake Chad; and the west, consisting of high, forested mountains of volcanic origin, where the highest peak in western Africa (4095 m.a.s.l.) is situated. The climate of Douala is of equatorial type influenced by the monsoon during summer (July to September) with maximum rainfall in September and with approximately 174–200 rainfall days per year. There are two distinct seasons: a dry season from November to June and a rainy season from July to October. The meteorological data (1951–2009) from the Douala Observatoire station (4°00'N, 9°44'E, 9 masl) show that the average annual rainfall is 3867 mm with monthly values ranging from 755 mm in August to less than 40 mm in December and January, thus 75% of precipitation falls from June to October. The annual relative humidity is about 82% (1971–2009) with variations from 88% in the full rainy season to 80% in the dry season. The average annual temperature is 27.7°C. The average annual evapotranspiration — pan evaporation method — (1971–2004) is estimated to be around 1235 mm.

The southern Cameroon, including the region of Douala (Fig. 1), is covered by dense moist forest vegetation and is crossed by several rivers. The rainfall regime over the Cameroon rain forest is mainly governed by the northward migration of the intertropical convergence zone (ITCZ). In the Cameroon rainforest, there are two rainy seasons, namely the winter rainy season from March to June and the summer rainy season from August to November. An important hydroclimatological feature to
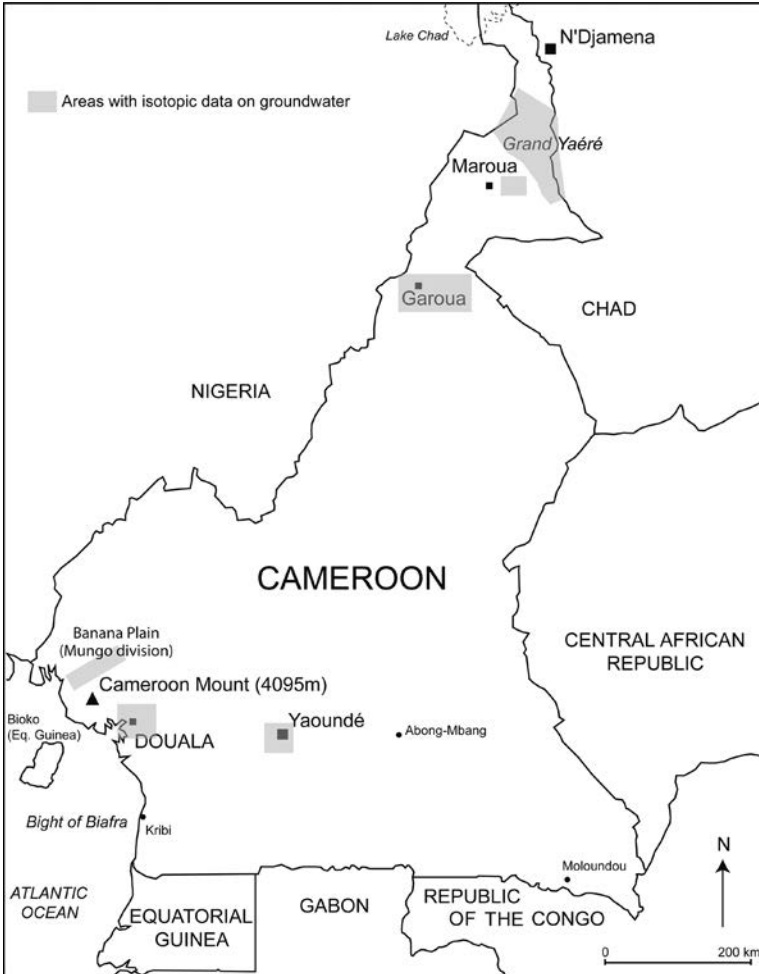
FIG. 1. Location of the study area and references to isotope data: Cameroon Mount [1, 2], Grand Yaéré [4, 11], Banana Plain [5], Garoua [6], Maroua [7], Douala and Yaoundé data are from IAEA CMR/8/008 project.

be noted in this region is the influence of dense forest vegetation on the water cycle [3], approximately 60–75% of precipitation falling over the African rainforest are recycled as continental moisture.

Northern Cameroon, located in the Sudano-Sahelian zone, has a very different climatological regime. The climate is characterized by a marked dry season (from October to March) and a wet season (from May to September) in relation to the latitudinal oscillations of the ITCZ where the Harmattan wind, dry Saharan air masses, and the monsoon, fresh and wet air masses from the Gulf of Guinea, meet. The wet

season is linked to the northward migration of the ITCZ, which reaches its extreme northern limit in July–August around a mean latitudinal position of 20–23°N [3].

The combination of the equatorial climate and the closeness of the ocean causes fractional distillation of the vapour masses (conditions of Rayleigh), according to Ref. [1]. This mechanism partly reduces annual thermal amplitudes and the variation of the isotopic composition of precipitation.

2. SAMPLING AND ISOTOPE MEASUREMENTS

Total precipitation events were collected on a monthly basis at the Douala HYDRAC station (4°1'48''N/9°43'48''E/18 m) from July 2006 to November 2009, representing 34 rainwater samples, which corresponds to 97% of the total rain amount. Samples were collected at the end of each month in a raingauge. Paraffin oil was added to the rain container in order to prevent evaporation during the sample collection. Hydrogen and oxygen isotope analyses were conducted by employing the standard CO_2 equilibration and the zinc reduction techniques respectively, followed by analysis on a mass spectrometer, at the Isotope Hydrology Laboratory of the IAEA (Vienna, Austria). All oxygen and hydrogen analyses are reported in the usual δ notation relative to Vienna Standard Mean Ocean Water (VSMOW), where δ = [(RS/RSMOW)–1] × 1000; RS represents either the $^{18}O/^{16}O$ or the $^2H/^1H$ ratio of the sample, and RSMOW is $^{18}O/^{16}O$ or the $^2H/^1H$ ratio of the SMOW. Typical precisions are ±0.1‰ and ±1.0‰ for the oxygen and deuterium respectively.

3. RESULTS AND DISCUSSION

Values of $\delta^{18}O$ and δ^2H vary from –0.59 to –6.14‰ and from 7.75 to –38.80‰ respectively. The weighted mean values in stable isotopes are –3.55 $\delta^{18}O$‰ and –16.67 δ^2H‰ for the whole period of sampling. These values are close to the ones of the IAEA GNIP stations of Sao Tome (–3.27 $\delta^{18}O$‰, –16.44 δ^2H‰; 1962–1976) and N'Djamena (–3.68 $\delta^{18}O$‰, –19.46 δ^2H‰; 1965–1978), which has the longest records available in the region.

Fig. 2 shows a plot of δ^2H versus $\delta^{18}O$ for rainwater samples collected in Douala from 2006 to 2009; the N'Djamena and Sao Tome weighted mean values are also reported. The Douala meteoric water line is expressed as: $\delta^2H = (8.17 \pm 0.40) \delta^{18}O + (12.76 \pm 1.38)$, n=34. The weighted mean values of Sao Tome and N'Djamena fall on the GMWL whereas the weighted mean value of Douala is on the Douala meteoric water line, above the GMWL. Deuterium excess (d-excess) values of Sao Tome and N'Djamena are close to 10‰, but Douala's d-excess is 11.7‰. The higher value of d-excess could be explained by a continental source of vapour related either to the non-fractionating transpiration from vegetation or to the fractionating evaporation
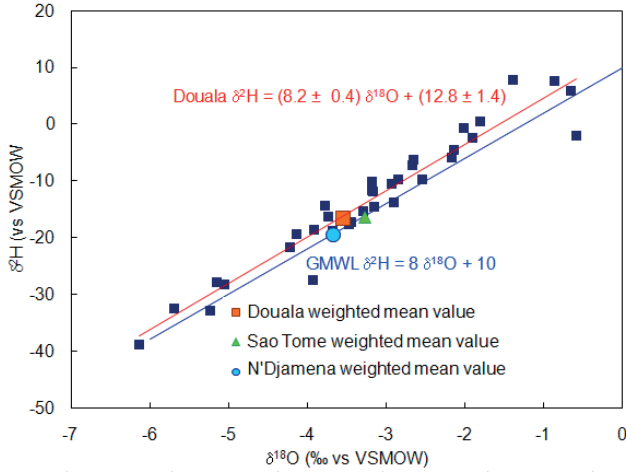
FIG. 2. δ^2H versus $\delta^{18}O$ for rainwater samples collected in Douala for the 2006 to 2009 period.
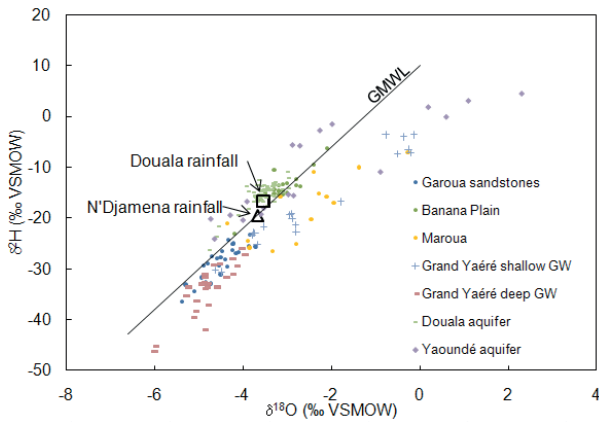
FIG. 3. δ^2H versus $\delta^{18}O$ for groundwaters of Cameroonian aquifers.

from water bodies [8, 12]. Transpiration is supposed to add vapour to the atmosphere which tends to offset the continental effect by lowering the expected depletion of $\delta^{18}O$ values but not modifying the d-excess value. However, due to the abundance of equatorial rain forests and the saturated atmosphere, the humid vegetation can act as water bodies and contribute to isotopic content through the evaporation from the surface of the vegetation cover.

The comparison of stable water isotope values in rainfall with those of groundwater in the Douala region and more generally those of the whole Cameroon territory towards the Chad Lake can be helpful to fingerprint the evolution of the isotope signal in rainfall across Central Africa.

Fig. 3. presents the evolution of the δ^2H versus $\delta^{18}O$ relationships in different aquifers of Cameroon. Data are provided for the Garoua sandstones aquifer [6], the Maroua Plain [7], the Banana Plain [5], the Grand Yaéré Plain [4], the city of Yaoundé [this study] and the city of Douala [this study]. The variety of δ^2H and $\delta^{18}O$ data illustrates the great diversity of the Cameroonian climate with depleted isotope data without evaporation pattern for the Northern deep aquifers (Garoua, Grand Yaéré deep groundwaters). The isotope values of groundwaters in the Douala City and the Banana Plain aquifer are in good agreement with those of rainfall. The groundwaters from the Maroua Plain and the Grand Yaéré shallow aquifers show a strong influence of the evaporation processes towards enriched values. The isotope data in the city of Yaoundé also exhibit a very developed evaporation influence over the isotope signature of groundwater which is probably related to the shallow structure of the Yaoundé aquifer [9, 10].

4.   CONCLUSION

This study is the first isotope analysis of precipitation in Douala, Cameroon. The precipitation collected at this GNIP station is strongly influenced by the adjacent Atlantic Ocean but probably also shows a supply of recycled continental moisture to the atmospheric vapour reservoir originating from the equatorial rainforest. The weighted mean isotope values of precipitation calculated for the 2006–2009 period is well reflected by the stable isotopes measured in local groundwaters in Douala City and the Mount Cameroon region. Isotope tracers are of major importance to evaluate the groundwater dynamics in Cameroon in order to undertake appropriate conservation measures for better water resource management. Indeed, strong anthropogenic impacts are present either in southern Cameroon [13] or in the Lake Chad vicinity [14, 15].

REFERENCES

[1] FONTES, J.C., OLIVRY, J.C., Composition isotopique des précipitations de la région du Mont Cameroun, ONAREST Report (1977) (in French).

[2] GONFIANTINI, R., ROCHE, M.A., OLIVRY, J.C., FONTES, J.C., ZUPPI, G.M., The altitude effect on the isotopic composition of tropical rains, Chemical Geology **181** (2001) 147–167.

[3] NJITCHOUA, R., SIGHA-NKAMDJOU, L., DEVER, L., MARLIN, C., SIGHOMNOU, D., NIA, P., Variations of the stable isotopic compositions of rainfall events from the Cameroon rain forest, Central Africa, J. Hydrol. **223** (1999) 17–26.

[4] KETCHEMEN, B., Etude hydrogéologique du Grand Yaere (Extrême Nord du Cameroun), synthèse hydrogéologique et étude de la recharge par les isotopes de l'environnement, Master's Thesis, Univ. Cheikh Anta Diop, Dakar (1992) (in French).

[5] AKO, A.A., SHIMADA, J., ICHIYANAGI, K., KOIKE K., HOSONO, T., EYONG, G.E.T., ISKANDAR, I., Isotope hydrology and hydrochemistry of water resources in the Banana Plain (Mungo-Division) of the Cameroon volcanic line, J. Environ. Hydrol. **18** (2009).

[6] NJITCHOUA, R., DEVER, L., FONTES, J.C., NAAH, E., Geochemistry, origin and recharge mechanisms of groundwaters from the Garoua Sandstone aquifer, northern Cameroon, J. Hydrol. **190** (1997) 123–140.

[7] NJITCHOUA, R., NGOUNOU NGATCHA, B., Hydrogeochemistry and environmental isotope investigations of the North Diamaré Plain, northern Cameroon, J. African Earth Sci. **25** (1997) 307–316.

[8] TAUPIN, J.-D., COUDRAIN-RIBSTEIN, A., GALLAIRE, R., ZUPPI, G.M., FILLY, A., Rainfall characteristics (δ^{18}O, δ^2H, ΔT and ΔH$_r$) in western Africa: Regional scale and influence of irrigated areas, J. Geophys. Res., D9 **105** (2000) 11911–11924.

[9] FOUEPE TAKOUNJOU, A., NDAM NGOUPAYOU, J.R., RIOTTE, J., TAKEM, G.E., MAFANY, G., MARECHAL, J.C., EKODECK, G.E., Estimation of groundwater recharge of shallow aquifer on humid environment in Yaounde, Cameroon, using hybrid water-fluctuation and hydrochemistry methods, Environ. Earth Sci. **64** (2010) 107–118.

[10] ZEBAZE TOGOUET, S.H., BOUTIN, C., NJINE, T., KEMKA, N., NOLA, M., FOTO MENBOHAN, S., First data on the groundwater quality and aquatic fauna of some wells and springs from Yaounde (Cameroon), Eur. J. Water Qual. **40** (2009) 51–74.

[11] NGOUNOU NGATCHA, B., MUDRY, J., ARANYOSSY, J.F., NAAH, E., SARROT REYNAULT, J., Apport de la géologie, de l'hydrogéologie et des isotopes de l'environnement à la connaissance des "nappes en creux" du Grand Yaéré (Nord Cameroun), Revue des Sciences de l'Eau **20** 1 (2007) 29–43 (in French).

[12] NJITCHOUA, R., et al., Oxygène-18, deutérium et chlorures dans les précipitations à Garoua (Nord-Cameroun): implications météorologiques, C.R. Acad. Sci. Paris **321** (1995) 853–860 (in French).

[13] TAKEM, G.E., CHANDRASEKHARAM, D., AYONGHE, S.N., THAMBIDURAI, P., Pollution characteristics of alluvial groundwater from springs and bore wells in

semi-urban informal settlements of Douala, Cameroon, Western Africa, Environ. Earth Sci. **61** (2010) 287–298.

[14]   NGOUNOU NGATCHA, B., DAIRA, D., Nitrate pollution in groundwater in two selected areas from Cameroon and Chad in the Lake Chad basin, Water Policy **12** (2010) 722–733.

[15]   FANTONG, W.Y., SATAKE, H., AKA, F.T., AYONGHE, S.N., ASAI, K., MANDAL, A.K., AKO, A.A., Hydrochemical and isotopic evidence of recharge, apparent age, and flow direction of groundwater in Mayo Tsanaga River Basin, Cameroon: bearings on contamination, *Environ. Earth Sci.* **60** (2010) 107–120.

ISOTOPIC CHARACTERIZATION OF SNOW, ICE AND GLACIAL MELT IN THE WESTERN HIMALAYAS, INDIA

S.P. RAI, B. KUMAR, M. ARORA, R.D. SINGH
National Institue of Hydrology,
Roorkee, 247 667, India,

Abstract

Precipitation and glacial melt samples were collected at the snout of the Gangotri Glacier, popularly known as Gaumukh, located in the western Himalayas, India. Snow and ice samples were collected from different sites of the Gangotri Glacier. The local meteoric water line (LMWL) developed for the ablation period (May to October) is $\delta^2H = 8.2 \, \delta^{18}O + 17.1 \, (r^2 = 0.99)$, which shows a slightly higher slope and intercept than GMWL. This may be due to local summer connective precipitation occurring under dry climatic conditions and mountainous region moisture recycling with the south-west monsoon. The meltwater line, $\delta^2H = 9.4 \, \delta^{18}O + 37.5 \, (r^2 = 0.96)$, having a significantly higher slope and intercept than the GMWL and LMWL. The main reasons for the higher slope and intercept of meltwater line may be due to the recycling of local vapour with moisture derived from the Western Disturbance moisture whose source is the Mediterranean Sea. The high d-excess values of snow, ice and meltwater indicate that the source of moisture is the Western Disturbances.

1. INTRODUCTION

The Himalayas encompass the world's third largest glacier systems after Antarctica and Greenland, occupying about 15% of the mountain terrain. The glacier systems are classified as mountain or ice caps [1]. Mountain glaciers constitute only about 3% of the glacierized area of earth. In India, there are more than 5000 glaciers on the southern slope of the Himalayas covering an area of nearly 38 000 km^2. The distributions of these glaciers are higher in the north-west than in the north-eastern part of the Indian Himalayas due to the criss-cross mountains, altitude variations and different climatic environment. The three important river systems originating from the Himalayan region are: the Indus System, the Ganges System and the Brahamaputra System, which are significantly fed by snow and glacial melt during the low flow period.

Himalayan glaciers are a sensitive indicator of climate changes, as are the world's other mountain glaciers. The isotopic composition of snow and glacier melt can provide information on atmospheric circulation such as responses to climatic fluctuations, changes in the strength of the south west summer monsoon, and western disturbances. A number of studies have specifically examined $\delta^{18}O$, and to a

121

lesser extent δ^2H, in precipitation and groundwaters from the Himalayan front, e.g. Refs [2–5], the Tibetan Plateu, e.g. Refs [6–15] and southeast Asia, e.g. Refs [16–18]. Other studies revealed that the isotopic composition of modern precipitation provides a conservative tracer for the origin, phase transitions and transport paths of water [19–21]. Streamwater provides a time integrated record of the isotopic composition of precipitation [21–23] and thus a first order measure of broad factors controlling regional scale isotopes of precipitation. Further, the isotopic composition of stream water is helpful to separate out the contribution of snow and glacial melt in the stream discharge with time because different water sources are acting within a river at different seasons [24]. Dalai et al. [25] studied the isotopic composition of the Yamuna River and its relationship with water chemistry. Nizampurkar et al. [26] have studied the climatic changes and ice dynamics of the Dokriani Glacier by dating the ice and measuring the isotopic composition of snow and ice. Kumar et al. [27] have developed the meteoric water line for India and for its various regions. An attempt has been made by Rai et al. [28] and Maurya et al. [29] to separate out the hydrograph of the Bhagiarathi and Ganges rivers using isotopic techniques. No systematic study has been reported on isotopic investigations of the snow, ice and glacial melt of the western Himalayas.

In the present study, rainfall, snow, ice and glacial melt was collected at the snout of the Gangotri Glacier during the ablation period of 2004 and 2005 in order to understand the source of moisture to the western Himalayas using isotopic signatures.

2.   STUDY AREA

The Gangotri glacier is the largest glacier in the western Himalayas. The study area falls in Uttarkashi District of Uttarakhand State (U.K.) between latitude 30° 43'N and 31°01'N and between longitudes 79° 0'E and 79°17'E (Fig. 1). The proglacial meltwater stream, known as the Bhagirathi River, emerges from the snout of the Gangotri Glacier at an elevation of 4000 m. The meltwater is drained through a well defined single terminus of the glacier, known as Gaumukh (the mouth of a cow). Gaumukh is considered the origin of the River Ganges. The main Gangotri Glacier (length: 30.20 km; width: 0.2–2.35 km; area: 86.32 km^2) forms the trunk part of the Gangotri Glacier system. The major glacier tributaries of the Gangotri Glacier system are Raktvarn Glacier, Chaturangi Glacier, Kirti Glacier, Swachand Glacier, Ghanohim Glacier, Meru Glacier, etc. The total catchment area up to the sampling location is about 556 km^2. Out of this, a total area of 286 km^2 is glacierized. The elevation range of the Gangotri Glacier varies from 4000 to 7000 m and the elevation of the study area up to the gauging site lies between 3800 and 7000 m.
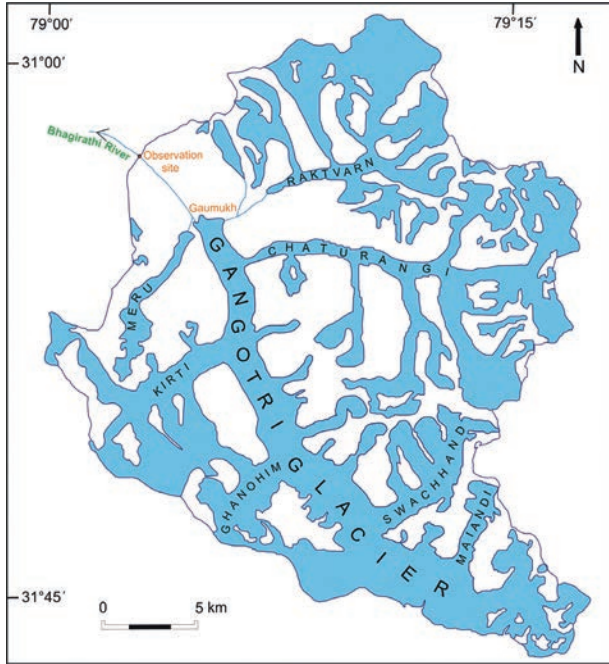
FIG. 1. Location map of sampling site and Gangotri glacierized system in the western Himalayas.

3. SAMPLE COLLECTION AND MEASUREMENT TECHNIQUES

In order to measure the discharge of the river and weather parameters, a hydro-meteorological observatory was established near Bhojwasa by the National Institute of Hydrology (NIH), Roorkee. To measure the $\delta^{18}O$ and $\delta^{2}H$ of precipitation, integrated ten day and monthly samples were collected during an ablation period of years 2004 and 2005 using an ordinary rain gauge. Diffusive and evaporative losses from the rain gauge were avoided by collecting the water daily in a double lidded plastic container while evaporation from storage containers was avoided by sealing the outer cap with paraffin. Meltwater samples were collected from the stream emerging from the Gangotri Glacier snout on a ten day basis for the years 2004 and on a daily basis for the year 2005. Snow and ice samples were collected from the Gangotri glacier.

The isotopic analyses ($\delta^{2}H$, $\delta^{18}O$) of the collected samples were carried out at NIH, Roorkee. $\delta^{2}H$ and $\delta^{18}O$ were measured by Pt–H$_2$ and CO$_2$ equilibration methods respectively, following the standard procedure [30, 31]. To determine $\delta^{2}H$ and $\delta^{18}O$, a three point calibration equation was used with the isotopic water standards V-SMOW, GISP and SLAP (Precision: ±1.0‰ and ±0.1‰ for $\delta^{2}H$ and $\delta^{18}O$, respectively).

4.   RESULTS AND DISCUSSION

4.1. Isotopic composition of rainfall

Fig. 2 shows the plot of δ^2H versus $\delta^{18}O$ for all precipitation samples collected during the ablation period of 2004 and 2005. The Local Meteoric Water Line (LMWL) developed as $\delta^2H = 8.2$ (±0.10) $\delta^{18}O + 17.1$ (±1.53) ($n = 15$, $r^2 = 0.99$) for a complete ablation period shows a higher slope and y-intercept in comparison with the GMWL. It is consistent with the LMWL of the Tuotuohe stations of the Tibetan plateau with a slope of 8.2 and an intercept of 17.5 [10].

The δ^2H and $\delta^{18}O$ values are enriched during the months of May, June and July and depleted during August and September. The most depleted rainfall in terms of the oxygen isotope ($\delta^{18}O$) observed during the month of September in 2004 and 2005 are –23.8‰ and –30.3‰, respectively. Similarly, the most enriched $\delta^{18}O$ values in rainfall observed in the month of June in 2004 and 2005 are –1.7‰ and –3.6‰, respectively. In the months of May, June and July high d-excess and enriched $\delta^{18}O$ in precipitation are due to local summer convective precipitation occurring under dry climatic conditions and resulting from local moisture which was also reported by Tian et al. [32] for the Tibetan plateau. The low d-excess and $\delta^{18}O$ in the month of August and September recorded at Gaumukh indicate change in the source of moisture, which is the southwest (SW) summer monsoon originating from the Bay of Bengal. The SW summer monsoon moves towards the Indo-Gangetic plains reaching up to the western Himalayas with heavy amounts of precipitation which leads to low d in the Indo-Gangetic plains. Further, amounts are released due to uplift of humid air masses resulting in depleted $\delta^{18}O$. The low $\delta^{18}O$ in the months of August and September at Gaumukh indicates that the SW summer monsoon reached up to Gaumukh (3800 m amsl) in the months of August and September during the years 2004 and 2005.
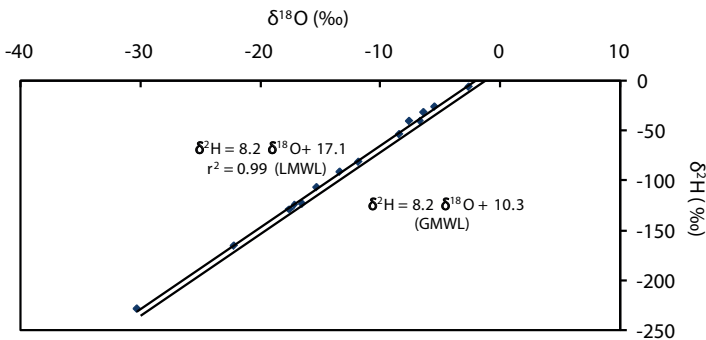
FIG. 2. δ^2H versus $\delta^{18}O$ of precipitation (monthly weighted) during the ablation period 2004 and 2005

TABLE 1. ISOTOPIC VALUES OF SNOW, WESTERN HIMALAYAS

Location	Altitude (m)	$\delta^{18}O$ (‰)	δ^2H (‰)
Chhota Sigari	4050 to 4750	–5 to –9	
Dokriani	4695	–4.5 to –7.2	
	4695	–5 to –23	
	3800	–11.6	–91
	3800	–13.9	–100
	3800	–9.7	–70
Gomukh	3800	–10.1	–70
	3800	–11.7	–86
	3800	–4	–27
	3800	–14	–103

TABLE 2. ISOTOPIC VALUES OF ICE/GLACIER REPORTED BY VARIOUS INVESTIGATORS

Location	Altitude (m)	$\delta^{18}O$ (‰)	δ^2H (‰)	d	Investigators
Rohtang	3748	–18.1	–128	17	
Balacha La	4650	–15.9	–119	8	
Thanglang La	5210	–24.7	–180	18	
Zozilla	3540	–12.2	–90	8	[3]
Khardung La	5629	–17.2	–127	11	
Khardung La	5649	–15.3	–107	15	
Dokriani	4836	–11 to –15.2			[26]
Chhota Sigari	4100 to 4600	–6 to –11			[32]
	4000	–18.5	–132.9	15	
	4000	–13.37	–91.7	15	
	4000	–18.1	–134.3	10	
Gomukh	4000	–14.5	–104.4	16	Present Study
	4000	–13.5	–97.0	16	
	4000	–15	–108.1	16	

4.2. Isotopic composition of snow and ice

The isotopic signature of the fresh snow and surface ice samples collected from different altitudes in the accumulation and ablation zones of the western Himalayan glaciers by various investigators and under the present study from the Gangotri glacier are presented in Table 1 and Table 2.

The results clearly indicate that the fresh snow bears more enriched isotopic signature than the glacier. This is possible as the glacier is formed from the snow that occurs at higher altitude and it also takes several decades in transformation from snow to ice. Based on ^{32}Si and ^{210}Pb radioactivity, the age of the Nehnar, Chhota Shigri and Dokriani glaciers is calculated to be about 500 years, 250 years and 400 years respectively [26]. The depleted $\delta^{18}O$ of these dated glacier snouts revealed that these regions had a cooler atmosphere by a few degree during their formations. High d of these samples reveals that western disturbances are the source of moisture for the precipitation.

4.3. Temporal variation of $\delta^{18}O$ in meltwater

The $\delta^{18}O$ values of meltwater during the month of April to June (pre-monsoon period) are found between –12‰ and –13‰. The $\delta^{18}O$ values gradually deplete further during July to September with an abrupt depletion of $\delta^{18}O$ due to heavy rainfall events during these months (Fig. 3). It has been observed that the isotopic values of melt initially follow the average $\delta^{18}O$ values of snow (–4.0‰ to –14.4‰, Table 1). It suggests that melting of fresh snow dominates in the melt discharge at an initial stage during May and June. Due to melting of snow in the initial phase, the glacier/ice
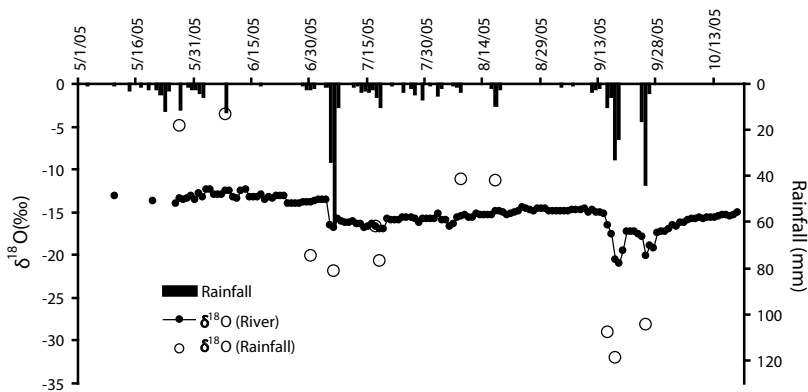
FIG. 3. Variation of $\delta^{18}O$ in meltwater during the ablation period of 2005.

becomes exposed and this results in the subsequent melting of ice, along with snow of higher altitude. The meltwater generated due to the melting of the glacier will bear depleted isotopic signatures. The depletion in isotopic composition of the river starts from the last week of June/first week of July indicating glacier melt dominance in the river discharge. This is the reason that the maximum discharge of meltwater is recorded in the month of July and August at Gomukh [28].

4.4. Isotopic Composition of Meltwater

Fig. 4 shows a $\delta^2 H$ vs $\delta^{18}O$ plot for the meteoric water line developed for the meltwater of Gangotri Glacier at the Gomukh site and the best fit line is $\delta^2 H = 9.4 \pm 0.7\,\delta^{18}O + 37.5 \pm 9.7$, $R^2 = 0.96$, $n = 16$ (2004–2005), which is consistent with LMWL of higher Himalayan snow and glacier with a slope of 8.7 and intercept of 29.9 [3].

The slope and intercept of the meltwater for the study region is similar to that reported earlier by Hren et al. [15], a slope of 10 and intercept of 39 for the stream water of the middle Yarlung region and Zhou et al. [33], a slope of 10.4 and intercept of 41.4 for the snow pack at the altitude of 4860 m of Qilian Mts Glacier. The three main post deposition processes of snow evaporation, melting and refreezing may modify the slope of the meteoric water line but do not cause an increase. Evaporation and refreezing result in a slope decrease and melting has no clear impact on it [34, 35]. The high d-excess reveals that the source of moisture is western disturbances.

5.   CONCLUSIONS

The results reveal that the source of precipitation during the ablation period is local moisture and SW summer monsoon.The high d value of snow, ice and glacial
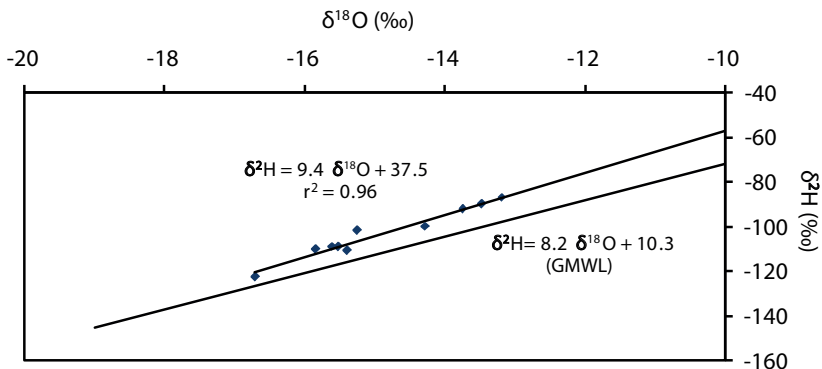
FIG. 4. $\delta^2 H$ versus $\delta^{18}O$ of meltwater (monthly weighted) during the ablation period 2004 and 2005.

melt reveals the source of moisture is western disturbances. The temporal variation in the isotopic composition of meltwater at Gomukh is due to the melting of snow and ice at different altitudes and with an increase in air temperature. The meltwater represents the integrated isotopic signature of snow and ice of different altitudes. The abrupt change in isotopic signature in meltwater is due to the contribution from the SW monsoon to stream discharge as surface runoff. The present study reveals that stable isotopes are very useful in segregating the different components of stream discharge near the snout while conventional techniques have limitations. The long term data of $\delta^{18}O$ of the river near the snout would be useful to study the impact of climate change on the melting of Himalayan glaciers.

ACKNOWLEDGEMENTS

REFERENCES

[1]   ANTHWAL, A., et al., Retreat of Himalayan Glaciers – indicator of climate change, Nat. Sci. **4** 4 (2006) 53.

[2]   AIZEN, V., et al., Isotopic measurements of precipitation on central Asia glaciers southeastern Tibetan, northern Himalayas (Central Tien shan), J. Geophys. Res., 101 D1 (1996) 9185–9196.

[3]   PANDE, K., et al., Stable isotope systematics of surface water bodies in the Himalayan and Trans-Himalayan (Kashmir) region, Earth Planet. Sci. **1109** (2000) 109–115.

[4]   GARZIONE, C.N., et al., Predicting paleoelevation of Tibet and the Himalaya from $\delta^{18}O$ vs altitude gradients in meteoric water across the Nepal Himalaya, Earth Planet. Sci. Lett. **183** (2000) 215–229.

[5]   KARIM, A., VEIZER, J., Water balance of the Indus River Basin and moisture source in the Karakoram and western Himalayas: Implications from hydrogen and oxygen isotopes in river water, J. Geophys. Res. Atmos. **107** (2002) 4362.

[6]   WUSHIKI, H., Some characteristics of stable isotope content in the Himalayan waters, Geological and Ecological Studies of Qinghai–Xizang Plateau (1981) 1671–1676.

[7]   YU, J., ZHANG, H., YU, F., LIU, D., Oxygen isotopic composition of meteoric water in the eastern part of Xizang, Geological and Ecological Studies of Qinghai–Xizang Plateau, Chinese Geochem. **3** (1984) 93–101.

[8]   ZHANG, X., Variation of $\Delta\delta^{18}O/\Delta T$ in precipitation in the Qinghai–Xizang Plateau, Chin. Geogr. Sci. **7** (1997) 339–346.

[9]   ZHANG, X., et al., Variations of stable isotopic compositions in precipitation on the Tibetan Plateau and its adjacent regions, Sci. China (D) **45** (2002).

[10]   TIAN, L., et al., Stable isotope variations in monsoon precipitation on the Tibetan Plateau, J. Meteorol. Soc. Jpn. **79** (2001) 959–966.

[11]   TIAN, L., et al., Tibetan Plateau summer monsoon northward extent revealed by measurements of water stable isotopes, J. Geophys. Res. **106** D22 (2001) 28081–28088.

[12]   TIAN, L., et al., Relation between stable isotope in monsoon precipitation in southern Tibetan Plateau and moisture transport history, Sci. China (D) **44** (2001).

[13]   TIAN, L., et al., Oxygen-18 concentrations in recent precipitation and ice cores on the Tibetan Plateau, J. Geophys. Res. **108** (2003) 4293.

[14]   QUADE, J., et al., Paleoelevation reconstruction using pedogenic carbonates, Rev. Mineral. **66** (2007) 53–87.

[15]   HREN, M.T., et al., $\delta^{18}O$ and $\delta^{2}H$ of streamwaters across the Himalaya and Tibetan Plateau: Implications for moisture sources and paleoelevation reconstructions, Earth Planet. Sci. Lett. **288** (2009) 20–32

[16]   ARAGUÁS-ARAGUÁS, L., et al., Stable isotope composition of precipitation over Southeast Asia, J. Geophys. Res. **103** (1998) 28721–28742.

[17]   LIU, Y., et al., Spatio-temporal variation of stable isotopes of river waters, water source identification and water security in the Heishui Valley (China) during the dry-season, Hydrogeol. J. **16** 2 (2008) 311–319.

[18]   LIU, Y., et al., A model- based determination of spatial variation of precipitation ^{18}O over China, Chem. Geol. **249** (2008) 203–212.

[19]   DANSGAARD, W., Stable isotopes in precipitation, Tellus **16** (1964) 436–468.

[20]   ROZANSKI, K., et al., "Isotopic patterns in modern global precipitation", Climate Change in Continental Isotopic Records (SWART, P.K., et al., Eds), Am. Geophy. Union, Washington, DC (1993) 1–36.

[21]   GAT, J.R., Oxygen and hydrogen isotopes in the hydrologic cycle, Annu. Rev. Earth Planet. Sci., **24** (1996) 225–262.

[22]   FRITZ, P., "River waters", Stable Isotopic Hydrology: Deuterium and Oxygen-18 in the water cycle (GAT, J.R., GONFIANTINI, R., Eds.), IAEA Technical Report, **210** (1981) 177–201.

[23]   KENDALL, C., COPLEN, T.B., Distribution of oxygen-18 and deuterium in river waters across the United States, Hydrol. Process. **15** (2001) 1363–1393.

[24]   DINCER, T., et al., Snowmelt runoff from measurements of tritium and oxygen-18, Wat. Resour. Res. **6** (1970)110–124.

[25]   DALAI, T. K., et al., Stable isotopes in the source waters of the Yamuna and its tributaries: seasonal and altitudinal variations and relation to major cations, Hydrol. Process. **16** (2002) 3345–3364.

[26]   NIJAMPURKAR, V.N., Ice dynamics and climatic studies on Himalayan glaciers based on stable and radioactive isotopes, Intl. Assoc. Hydrol. Sci. Publn. **218** (1993) 355–369.

[27]   KUMAR, B., et al., Isotopic characteristics of Indian precipitation, Wat. Resour. Res. **46** (2010) W12548.

[28]   RAI, S.P., et al., Estimation of contribution of southwest monsoon rain to Bhagirathi River near Gaumukh, western Himalayas, India, using oxygen-18 isotope, Curr. Sci. **97** (2009) 240–245.

[29]   MAURYA, A.S., et al., Hydrograph separation and precipitation source identification using stable water isotopes and conductivity: River Ganga at Himalayan foothills, Hydrol. Process. **25** (2010) 1521–1530.

[30]   EPSTEIN, S., MAYEDA, T., Variations of the $^{18}O/^{16}O$ ratio in natural waters, Geochim. Cosmochim. Acta **4** (1953) 213–224

[31]   BRENNINKMEIJER, C.A.M., MORRISON, P.D., An automated system for isotopic equilibration of CO_2 and H_2O for ^{18}O analysis of water, Chem. Geol. **66** (1987) 21–26.

[32]   NIJAMPURKAR, V.N., et al., Isotopic study on Dokriani Bamak glacier, Central Himalaya: implications for climatic changes and ice dyanamics, J. Glaciol. **48** (2002) 81–86.

[33]   ZHOU, S., et al., Water isotope variations in the snow pack and summer precipitation at July 1 Glacier, Qilian Mountains in northwest China, Chinese Sci. Bull. **52** 21 (2007) 2963–2972.

[34]   ZHOU, S., et al., The effect of refreezing on the isotopic composition of melting snowpack, Hydrol. Process. **22** (2007) 873–882.

[35]   STICHLER, W., et al., Influence of sublimation on stable isotope records recovered from high-altitude glaciers in the tropical Andes, J. Geophys. Res. **106** (2001) 22613–22620.

SPATIAL DISTRIBUTION OF STABLE ISOTOPES OF PRECIPITATION IN KUMAMOTO, JAPAN

M. TANOUE [a], K. ICHIYANAGI [a,b], J. SHIMADA [a]

[a] Graduate School of Science and Technology,
Kumamoto University, Japan

[b] Japan Agency for Marine-Earth Science and Technology

Abstract

To understand the spatial distribution of stable isotopic compositions in precipitation, precipitation samples were collected every two weeks from November 2009 to December 2010 at 6 points in Kumamoto, Japan. The $\delta^{18}O$ and δ^2H of precipitation samples were measured by isotope ratio mass spectrometry (Delta-S) with CO_2/H_2O equivalent method for $\delta^{18}O$ and the chromium reduction method for δ^2H. The range of $\delta^{18}O$ and d-excess (= $\delta^2H - 8\,\delta^{18}O$) in precipitation is from –13.4‰ to –3.5‰ and from 2.6‰ to 35.6‰, respectively. Seasonal variability of $\delta^{18}O$ (d-excess) in precipitation was low (high) in winter and high (low) in summer. The seasonal wind of this study area was dominated by south-westerly in summer (from June to August) and north-westerly in winter (from December to February). These wind regimes indicate seasonal variabilities of the water vapour pathway from the origin. In this paper the trend of inland effect to the $\delta^{18}O$ for both south-westerly and north-westerly are also considered. As a result, significant correlation between distances from the coastal line at south-westerly or north-westerly and $\delta^{18}O$ in precipitation was recognized, particularly from 18 February to 7 March and from 29 September to 19 October in 2010 (statistically significant with 5% level). Furthermore, in order to evaluate the course of precipitation, the column total of water vapour flux was considered in the whole period by using JRA–25 and JCDAS. It is interesting that the inland effect corresponded to the column total of water vapour flux at south-westerly (north-westerly). Hence, it is conceivable that the spatial distribution of $\delta^{18}O$ in precipitation was controlled by a column total of water vapour flux in this area.

1.   INTRODUCTION

Many studies on the spatial distribution of stable isotopes in precipitation, especially in a relationship between the distance from the coastal line and stable isotopes in precipitation, were considered. In Japan, the inland effect of stable isotopic compositions in precipitation has not been studied, except for investigations such as Refs [1, 2]. However, their investigations have reported an inland effect of stable isotopes in precipitation considered by one direction or distance from the shortest coastal

lines. In this study area, Kumamoto, seasonal winds change from the south-westerly wind in summer (from June to August) and the north-westerly wind in winter (from December to February). This evidence shows that there is seasonal variability in the course of water vapour from the origin (where the water vapour evaporated from). Therefore, it is conceivable that the trend of inland effects changes the relationship between the distance from the coastal line and $\delta^{18}O$ in precipitation by the variability of the course of precipitation. Hence the distance from the coastal lines at the south-westerly and the north-westerly was considered. The purpose of this study is to reveal the correlation between distances from the coastal lines at two directions of wind and stable isotopic compositions in precipitation over Kumamoto by analyzing precipitation samples collected on a two-weekly basis.

2.   SAMPLING AND ANALYSIS METHOD

The map of observational stations is shown in Fig. 1. Precipitation samples have been collected from November 2009 to December 2010 in Kumamoto. However the starting date was different. Samples form Kumamoto, Uki and Koushi were first taken on 3 November 2009, whereas Kahoku on 8 December 2009, Matsushima on 9 December while Ohzu was first taken on 21 March 2010. These have been collected approximately twice weekly at 6 stations. The water was sampled a total of 21
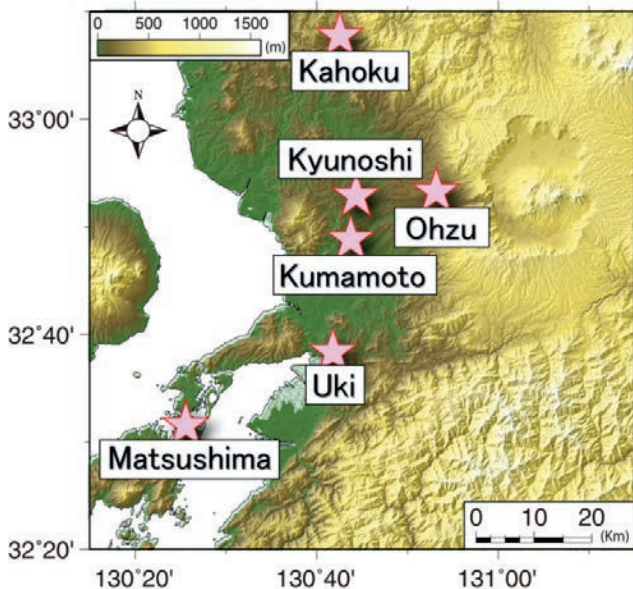
FIG. 1. The map of observational stations in Kumamoto.

TABLE 1. OBSERVATION PERIODS AT THE SAMPLING SITES

Period	Start	End
P01	3 Nov 2009	15 Nov 2009
P02	16 Nov 2009	27 Nov 2009
P03	28 Nov 2009	23 Dec 2009
P04	24 Dec 2009	7 Jan 2010
P05	8 Jan 2010	19 Jan 2010
P06	20 Jan 2010	1 Feb 2010
P07	2 Feb 2010	17 Feb 2010
P08	18 Feb 2010	7 Mar 2010
P09	8 Mar 2010	20 Mar 2010
P10	21 Mar 2010	21 Apr 2010
P11	22 Apr 2010	7 May 2010
P12	8 May 2010	30 May 2010
P13	31 May 2010	10 Jun 2010
P14	11 Jun 2010	1 Jul 2010
P15	2 Jul 2010	29 Jul 2010
P16	30 Jul 2010	15 Aug 2010
P17	16 Augh 2010	9 Sep 2010
P18	10 Sep 2010	28 Sep 2010
P19	29 Sep 2010	19 Oct 2010
P20	20 Oct 2010	4 Nov 2010
P21	5 Nov 2010	26 Nov 2010

times, and each observation period was numbered from P01 to P21. Each observation period is shown in Table 1.

$\delta^{18}O$ and $\delta^{2}H$ of the precipitation samples were measured by isotopic composition mass spectrometry (Delta-S) with a CO_2/H_2O equivalent method for $\delta^{18}O$ and a chromium reduction method for $\delta^{2}H$. Isotopic compositions are expressed by convention as parts per thousand deviations related to Vienna Standard Mean Ocean Water (V–SMOW), that is δ notation (‰). The analytical errors for the standard measurement of $\delta^{18}O$ and $\delta^{2}H$ are better than ± 0.1‰ and ± 1.0‰, respectively.

TABLE 2. THE DISTANCE FROM THE COASTAL LINE TO THE SAMPLING STATIONS

Station	Directions		
	SW[1]	NW[1]	Min[2]
Kumamoto	100.0	126.0	11.5
Uki	85.0	138.0	3.9
Koushi	106.0	121.0	27.9
Kahoku	121.0	99.0	29.7
Matsushima	57.0	129.0	0.0
Ohzu	116.0	130.0	18.9

1   The distance from the coastal lines in km.
2   The distance from the shortest coastal lines in km.

3. STUDY METHOD

3.1. Determining distance from the coastal line

The longest distance from the coastal line to the observational station at south-westerly and north-westerly is Matsushima. Therefore, the standard position of intersection of the coastal line and extended line from Matsushima in a south-westerly and north-westerly direction are determined. Distances from the coastal line to other stations were determined by distance from the vertical line through the standard position to other stations. Distance from the coastal lines at south-westerly and north-westerly on each station is shown in Table 2.

3.2. The water vapour transportation pathway

It is important that the course of precipitation from the water vapour source into this study area can determine the inland effect. Therefore, this paper considered the course of the precipitation. In order to determine the course of the precipitation, this study used column total of water vapour flux by using JRA–25 and JCDAS (meteorological reanalysis datasets). Using the average duration of column total of water vapour flux, the course of precipitation into Kumamoto was evaluated.
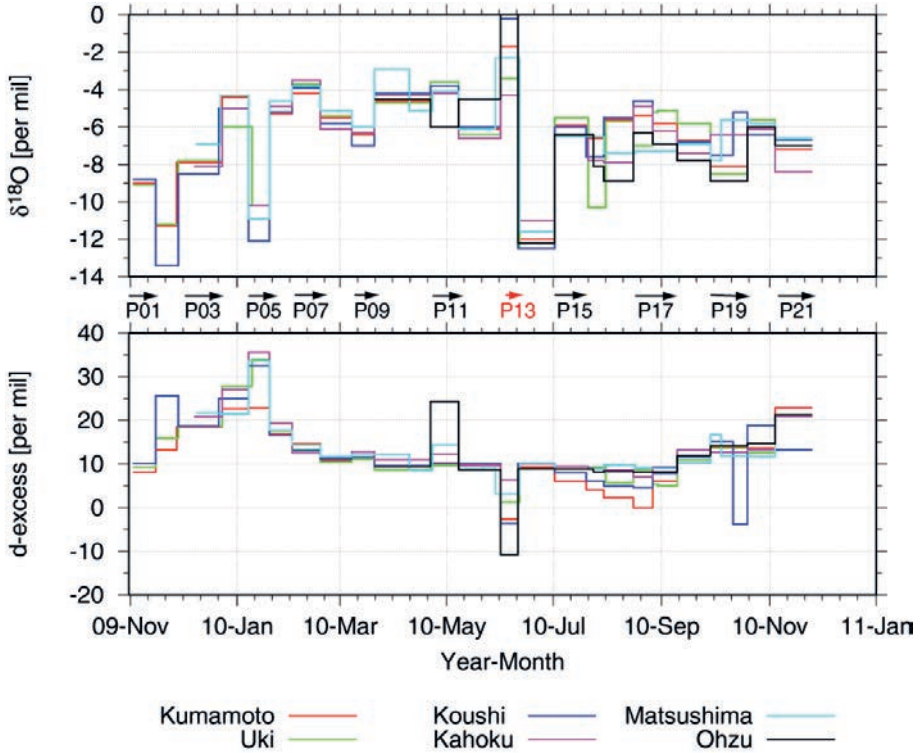
FIG. 2. Time series of stable isotopic compositions.

4.   RESULTS

4.1.   Time series variation of stable isotopic compositions in precipitation

Time series variations of stable isotopic compositions ($\delta^{18}O$ and d-excess) are shown in Fig. 2. The time series of $\delta^{18}O$ presents similar variations at each station from P01 to P14 and from P20 to P21, and a different pattern from P15 to P19. P13 show high $\delta^{18}O$, negative d-excess. P13 is characterized by a lower amount of precipitation and therefore isotope effects due to evaporation are expected. As a result, the range of $\delta^{18}O$ was from −13.4‰ to −3.5‰. The seasonal variation of $\delta^{18}O$ was found to be high in spring (from P06 to P12) and low in P02, P05 and P14.

The time series of d-excess found similar variation form P01 to P12, P14 and from P18 to P21 at each station, and dissimilar variation from P15 to P17. It is conceivable that the time series of similar d-excess at all station were affected by water vapour from the same source area. However, the time series of d-excess from P15 to P17 is different. These indications may be affected by a local precipitation system or a different water vapour source.

At P05 a snow event was observed. Therefore P05 had low δ^{18}O (–12.1‰ ~ –10.2‰) and the highest d-excess (22.8‰ ~ 35.6‰). This characteristic value variation of stable isotopic compositions agrees with the model simulation result of Ref. [3] by using IsoGSM [4]. P14 also had low δ^{18}O values (–12.5‰ ~ –11.0‰) and low d-excess (8.9‰ ~ 10.2‰) by the Baiu front near Kumamoto. The Baiu front occurred in the summer monsoon season over eastern Asia. This characteristic variation of stable isotopic compositions in P14 agreed with Ref. [5].

4.2. Spatial distribution of stable isotopic compositions in precipitation

The correlation between δ^{18}O and the distance from the coastal line at south-westerly or north-westerly direction is shown in Table 3. Mean total column water vapour flux in each period is also shown in Table 3.

Correlation between the distance from the coastal line and δ^{18}O in P08 and P19 is shown in Fig. 3. Significant correlation between the distance from the coastal line at south-westerly or north-westerly and δ^{18}O is found at P08 and P19. This indication shows the inland effect: increasing distance from the coastal line at south-westerly (north-westerly), decreasing δ^{18}O in P08 (P19). Furthermore, it is interesting that the column total of water vapour flux was dominated by south-westerly (north-westerly)

TABLE 3. CORRELATION COEFFICIENTS BETWEEN δ^{18}O AND DISTANCE FROM THE COASTAL LINE IN SOUTH-WESTERLY OR NORTH-WESTERLY DIRECTIONS

Period	P01	P02	P03	P04	P05	P06	P07	P08	P09	P10
Samples	3	3	3	5	5	5	5	5	5	6
WVF	NW	WNW	WNW	WNW	S	SW	WSW	SW	WSW	WSW
corr (SW)	–	–0.76	–0.89	–0.22	–0.12	–0.63	–	–0.95	–0.31	–
corr (NW)	–0.84	–	–	–0.21	–0.12	–	–0.43	–	–0.33	–0.66

Period	P11	P12	P14	P15	P16	P17	P18	P19	P20	P21
Samples	6	6	6	6	6	6	6	6	6	6
WVF	SW	W	W	SW	W	NW	NW	NW	N	NW
corr (SW)	–0.37	–	–	–0.44	–0.23	–	–0.49	–	–0.63	–0.72
corr (NW)	–0.01	–	–0.75	–	–	–0.20	–	–0.91	–	–

The rows are, from the top, as follows: Period, number of samples, WVF: column total of water vapour flux, correlation coefficient at south-westerly and correlation coefficient at north-westerly. About WVF, N: north, W: west, S: south, E: east.
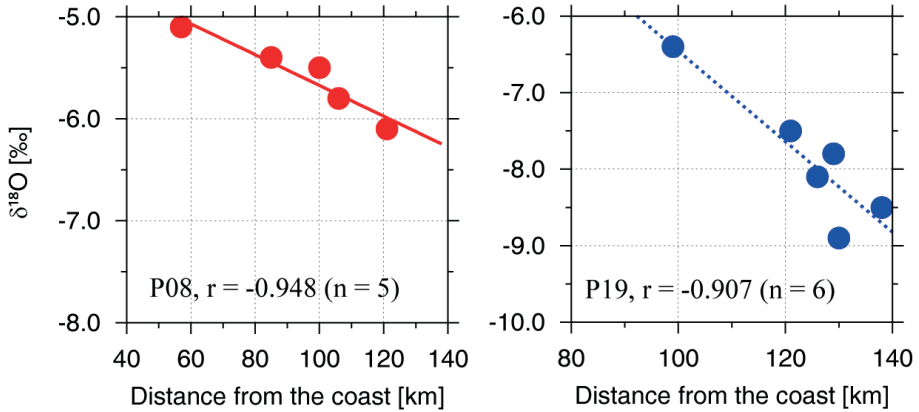
FIG. 3. Correlation between distance from the coastal line and $\delta^{18}O$. Left and right figures show P08 and P19, respectively.

at P08 (P19). Inland effect was involved with the column total of water vapour flux. Namely, it coincided that $\delta^{18}O$ in precipitation decreased along the course of precipitation.

Inland effect at south-westerly (north-westerly) agreed with column total water vapour at south-westerly about for 20%, north-westerly about for 10%. Periods except column total of water vapour flux at south-westerly or north-westerly for about 50%. The remaining 20% do not coincide with inland effect and column total of water vapour flux.

5.   CONCLUDING REMARKS

Inland effect at south-westerly and north-westerly was considered. Inland effect at south-westerly or north-westerly coincides with column total of water vapour at south-westerly or north-westerly. This indication shows the increasing distance from the coastal line, decreasing $\delta^{18}O$ at column total of water vapour flux. That is, the spatial distributions of $\delta^{18}O$ are controlled by the rainout effect.

However, precipitation $\delta^{18}O$ is also affected by the amount effect. Therefore, future study for the spatial distribution of precipitation amount at each period in this study area will be considered.

REFERENCE

[1]   TANIGUCHI, M., et al., Stable isotope studies of precipitation and river water in the Lake Biwa basin, Japan, Hydrol. Process. **14** 3 (2000) 539–556.

[2]   YABUSAKI, S., et al., "Temporal variation of stable isotopes in precipitation at Tsukuba, Ogawa and Utsunomiya City in Japan", Groundwater response to changing climate, CRC Press, Boca Raton, FL (2010) 55–66.

[3]   YOSHIMURA, K., ICHIYANAGI, K., A reconsideration of Seasonal Variation in Precipitation Deuterium Excess Over East Asia, J. Japan Soc. Hydrol. Water Resour. **22** 4 (2009) 262–276 (in Japanese).

[4]   YOSHIMURA, K., et al., Historical isotope simulation using Reanalysis atmospheric data, J. Geophys. Res. **113** (2008).

[5]   ARAGUÁS-ARAGUÁS, L.K., et al., Stable isotope in composition of precipitation over Southeast Asia, J. Geophys. Res. **103** (1998) 28721–28742.

TRITIUM LEVEL IN ROMANIAN PRECIPITATION

C. VARLAM[a], I. STEFANESCU[a], O.G. DULIU[b], I. FAURESCU[a],
D. BOGDAN[a], A. SOARE[a]

[a] Institute for Cryogenic and Isotope Technologies,
  Rm. Valcea, Romania

[b] Faculty of Physics,
  University of Bucharest,
  Magurele, Romania

Abstract

Romania is one of the countries that has no station included in GNIP (Global Network of Isotopes in Precipitation) on its territory. This paper presents results regarding the tritium concentration in precipitation for the period 1999–2009. The precipitation fell at the Institute for Cryogenic and Isotope Technologies (geographical coordinates: altitude 237 m, latitude 45°02'07' N, longitude 24°17'03' E) an was collected both individually and as a composite average of each month. It was individually measured and the average was calculated and compared with the tritium concentration measured in the composite sample. Tritium concentration levels ranged from 9.9 ± 2.1 TU for 2004 and 13.7 ± 2.2 TU for 2009. Comparing the arithmetic mean values with the weighted mean for the period of observation, it was noticed that the higher absolute values of the weighted means were constant. It was found that for the calculated monthly average for the period of observation (1999–2009), the months with the maximum tritium concentration are the same as the months with the maximum amount of precipitation. This behaviour is typical for the monitored location.

1.   INTRODUCTION

Tritium is naturally produced in the atmosphere and from there it enters the hydrological cycle. The tritiated water in the troposphere is rapidly deposited into the ocean or the hydrological system, either by precipitation or by molecular exchange along the water–air interface. It is well accepted that molecular exchange is the main mechanism responsible for removing tritium from the atmosphere and for its deposition into the oceans [1]. Values of tritium concentration prior to nuclear testing are not well known; reports were made only in Canada, showing values between 2 and 8 TU. The concentration of tritium in precipitations increased rapidly in the open atmosphere after the nuclear tests and the recorded data indicated a strong dependence on both location and on season [2]. The level of tritium on the continent

tends to be higher than the level on the coast or in the middle of the ocean, due to the dillution of tritium concentration from the atmosphere with the lower concentration from the oceans. There is also a major seasonal difference caused by the interaction of the stratosphere with the troposphere.

The Experimental Pilot Plant for Tritium and Deuterium Separation is an experimental project within the national nuclear energy research programme and is part of the National Institute for Cryogenics and Isotopic Technologies. The present work presents the variation of tritium concentration in precipitations over a ten-year period, 1999–2009, at our institute, and also a comparison with data recorded over different periods in other countries reported by the Global Network of Isotopes in Precipitation (GNIP). Establishing the level of tritium is an important component of the environmental radioactivity monitoring programme.

2.   DATA REGARDING FALLOUT DURING THE PERIOD 1999–2009

The climate of Romania is determined primarily by its geographical location (midway between pole and equator) and by its location on the continent, approximately 2000 km from the Atlantic Ocean, 1000 km from the Baltic Sea, 400 km from the Adriatic Sea and riparian to the Black Sea. The relief induces significant modifications first of all due to its altitude and second of all due to the orientation of mountain chains: temperature drops depending on height and increase of precipitation quantities at high altitudes. Valley corridors and depressions are responsible for deviations of air currents, temperature inversions (with persistent frosts during winter) or on the contrary, warming due to the 'foehn effect' in early spring.

Taken as a whole, the Romanian climate is temperate continental moderate, making the transition between that of Western Europe (dominated by ocean influences), that of Eastern Europe (highly continental, often excessively), and that of Southern Europe, Mediterranean. In Romania, there are three climate types: mountain type, cool (2–6°C), with heavy precipitations (700–1200 mm) and strong winds; warmer type (6–10°C annual average), reduced precipitations but enough for forest vegetation (500–700 mm); and plains type consisting of low hills with high average temperatures (10–11°C in Romanian Plain and Dobrogea), but with reduced precipitations and frequent droughts.

During the monitoring period of precipitations, 1999–2009, Romania went through years of extremes in terms of rainfalls. The period of September 2006 and July 2007 was considered one of the driest periods, with an average of 379 mm, a value which may be compared with the period September 1945–July 1946, when an average of 438.5 mm was recorded (1940s drought). One must not forget the period 1999–2002, a dry period with values below the average calculated for the period 1960–1990. The average level of precipitations during the entire winter of year 2002 did not exceed 40 mm in the North and 20 mm in the South. This period had

TABLE 1. PRECIPITATION AMOUNT IN RM. VALCEA FOR THE PERIOD 1999–2009

Year	Jan (mm)	Feb (mm)	Mar (mm)	Apr (mm)	May (mm)	Jun (mm)	Jul (mm)	Aug (mm)	Sep (mm)	Oct (mm)	Nov (mm)	Dec (mm)	Total (mm)
1999	34.4	45.3	38.1	120	63.1	90	84.7	122.6	37.5	45.1	41.9	63.2	785.9
2000	17.1	7.6	22.7	48.2	21.1	0.7	74	4.1	59.5	0.7	24.7	35.1	315.5
2001	40.7	64.1	36.4	54.6	26.3	198.7	137.5	63.4	112.4	42	29.5	11.2	816.8
2002	1.8	2.9	1.2	35.8	33.6	205	123.7	87.4	114.8	52.8	38.6	89.9	787.5
2003	65.8	16.4	2.5	69.7	68.5	44.2	138.2	35.9	81.9	131.2	35.2	14.1	703.6
2004	56.1	49.2	27.1	6.1	69.9	21.4	103.8	86.8	51.4	30	125.9	28.6	656.3
2005	55.1	50.2	39.2	56.1	138	75.4	187.8	212	124.8	9.2	43.7	66.5	1058
2006	43	2.7	73.8	78	61.7	112.8	59	109.2	82	39.4	11.7	21.7	695
2007	42.4	5	58.1	0.2	91.9	54	24.2	167.1	131	92.8	83.7	28.1	778.5
2008	11.6	3.2	10.9	92.2	85.8	47.4	52.6	0	79.4	48.2	25.5	69.1	525.9

unexpected implications, especially for the following year, 2003, when a minimum of 1520 m³/s (3–5 September) was recorded for the Danube in Bazias. This low level resulted in the shut down of the Nuclear Power Plant at Cernavoda. The period 2004–2005 lies at the opposite end, with an average of 818.4 mm, well above the average of 633.7 mm calculated for the period 1901–2007.

The level of precipitations recorded at the monitored location at our Institute (altitude 237 m, latitude 45°02'07' N, longitude: 24°17'03' E) presented the particularities of the Oltenia region of which Rm. Valcea is a part. Oltenia is located in the south-east of Romania; as such, it is under the influence of the barrel centres from the Mediterranean Sea, Atlantic Ocean, Russian Plain, north Africa, Scandinavian peninsula and even Greenland. Atmospheric circulation from west and east is prevalent in Oltenia. The position of the Sub-Carpathian and Carpathian Mountains related to the penetration directions of air masses driven by the main barrel centres which influence the area has repercussions on the average temperature distribution which decreases from the north part of the region to the south part (Dr. Tr. Severin, 11.7°C, Dragasani, 10.4°C). For Rm. Valcea, the average temperature is around 10°C, with average monthly temperatures between –5.2°C for January and 27.4°C for July (data recorded in the period 1961–1990). The average level of precipitations recorded in the same period (1961–1990) for Rm. Valcea was 698.5 mm, with a maximum of over 90 mm in May and July and a minimum of around 36 mm in January and March. The average level of precipitations for the period 1999–2009 was 708.9 mm, with 1.5% above the normal level for this location (Table 1).

As a general characteristic, it is noted that the national general trend may also be applied for the location Rm. Valcea. The drought period 1999–2002 had its maximum in the year 2000 when it registered the lowest quantity of precipitations (315.5 mm), whereas 2006 and 2007 (a dry period for Romania) shows values close to normal and even higher. The maximum annual quantity was recorded in the year 2005 (1058 mm), considered rainy also at the national level, and the year 2008 was characterized by a high deficit of precipitations for Rm. Valcea (approx. 25% of normal values for this location).

3.   SAMPLING AND MEASUREMENT

Precipitation sampling involves several strict rules in order to avoid the change of sample isotopic composition. The sampling strategy both of rain and of snow depends generally on the aim of the research. For example, sampling may be performed monthly, weekly, and daily or even every hour. Regardless of the period of time between samplings, recording the precipitation quantity is absolutely necessary, so that the weighted mean for the isotopic composition may be calculated. A short period of time between samplings provides the maximum of information and eliminates the risk of evaporation.

Precipitation sampling at our institute was performed with a typical rainwater collector [3]. Taking into account the rules stated above, it was decided to collect each individual precipitation in a month, the quantity corresponding to the collecting interval to be recorded, to be stored at low temperatures and at the end of the month to prepare both the individual precipitation for tritium concentration determination and the weighted mean of monthly precipitation which was measured under the same conditions as individual precipitation. The tritium concentrations average present in individual precipitation was calculated for each month and was compared with the tritium concentration determined in the monthly composite precipitation. This double-check allowed the use of recorded results even for results where uncertainty exceeded 25%.

The samples were measured by the liquid scintillation method [4] with a Quantulus spectrometer 1220, for 1000 min/sample; the liquid scintillation cocktail used was an OptiPhase Hisafe 3 (initial producer Wallac Oy, today PerkinElmer) or UltimaGold LLT or UltimaGold uLLT (initial producer Canberra Packard, today PerkinElmer). The ratio of water sample: scintillate was the same no matter what cocktail was used i.e. 8:12 mL, in Canberra Packard-type polyethylene vials of 20 mL. Depending on the type of scintillate used, the efficiency ranged from 24.32% (OptiPhase Hisafe 3) to 25.05% (UltimaGold LLT) and 25.90% (UltimaGold uLLT). The background recorded for the tritium free water sample also varied, from 0.628 CPM (OptiPhase Hisafe3), to 0.846 CPM (Ultima Gold LLT) and 0.689 CPM (UltimaGold uLLT). The deuterium depleted water was used as tritium free water, obtained in our

institute, having a concentration of 15 ppm D/D+H [5]. The best performances were obtained using UltimaGold uLLT, the determined limit of detection being 5 TU (confidence level, k = 2). The variation of the tritium level presented below was calculated both for the annual arithmetic mean and for the weighted annual mean according to WMO/IAEA recommendations [6].

4. LEVEL OF TRITIUM CONCENTRATION IN PRECIPITATIONS, 1999–2009

The variation of tritium concentration during the period 1999–2009 for Rm. Valcea is noisy in terms of the maximum annual value, Fig. 1.

May, June, July and August are months with maxima of tritium concentration for the monitored period, with values ranging between 17.2 ± 2.2 (July 2006) and 24.4 ± 2.3 (May 2008). The annual arithmetic average of tritium concentration in precipitations for the period 1999–2009 showed a variation of 9.9 ± 2.1 TU (2004) and 13.7 ± 2.2 UT (2008). The values of annual weighted mean ranged between 10.9 ± 2.1 TU (2004) and 15 ± 2.2 TU (2008). Analyzing the calculated averages, Fig. 2, the higher absolute values of weighted mean than the arithmetic ones may be identified, therefore the possibility of a dependency between precipitations quantity and tritium concentration can be investigated.

The correlation coefficient between the tritium concentration values and the precipitation quantity was calculated using the formula

$$r = \frac{1}{n} \frac{\sum_i \left(x_i - \overline{x} \right)\left(y_i - \overline{y} \right)}{\sqrt{\dfrac{1}{n}\sum \left(x_i - \overline{x} \right)^2}\sqrt{\dfrac{1}{n}\sum \left(y_i - \overline{y} \right)^2}}$$
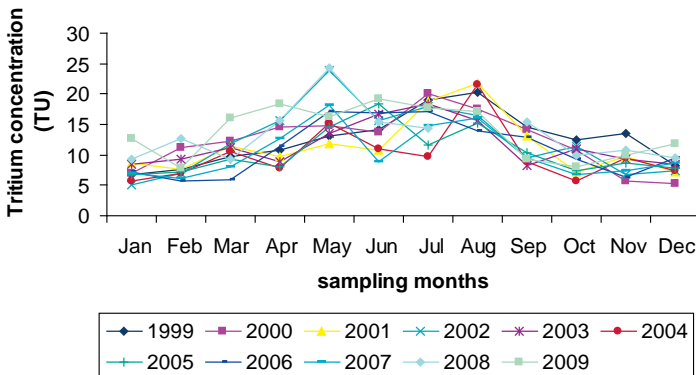
FIG. 1. Annual evolution for tritium concentration in precipitations at Rm. Valcea in the period 1999–2009.

where x_i is monthly tritium concentration, and y_i is the monthly amount of precipitation. An increasing trend for the correlation coefficients, a function of the number of years monitored for the location Rm. Valcea, is observed (shown in Fig. 3), its range being between 0.54 (which is the correlation coefficient for only one year) and 0.81 (the value calculated for the eleven years monitored). It is expected that once we have more available data, the correlation coefficient will increase close to 1, which is an eigenvalue of the observations' correlated sequence.

Fig. 4 shows the monthly averages calculated for the amount of precipitations and tritium concentration in precipitation for the monitored period in the Rm. Valcea location. A similar evolution of the two curves can be noticed. The monthly average maxima in precipitation also represent the monthly average maxima of tritium concentration for the monitored period 1999–2009.
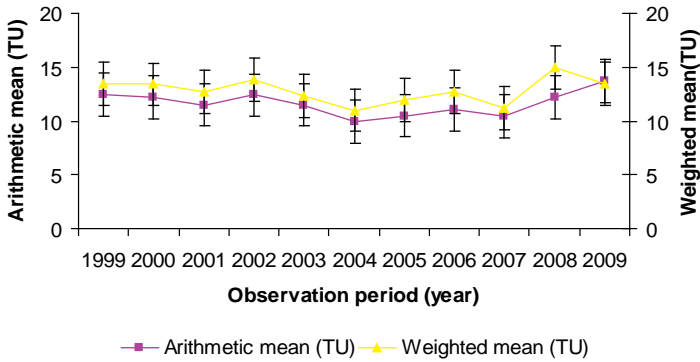
FIG. 2. Arithmetic and weighted mean of tritium concentration during 1999–2009 period in the Rm. Valcea location.
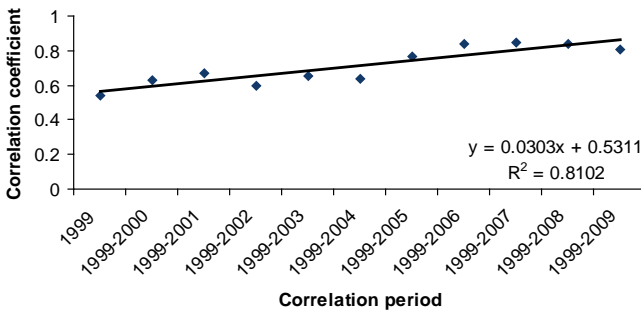
FIG. 3. Evolution of correlation coefficient between the monthly tritium concentration and the monthly amount of precipitation in the Rm. Valcea location.
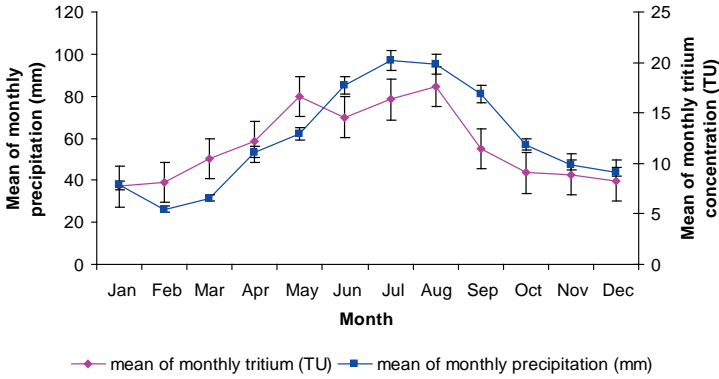
FIG. 4. Monthly average of tritium concentration and amount of precipitation during 1999–2009 period in Rm. Valcea location.

5.   CONCLUSIONS

Tritium is the only conservative tracer used to determine the age of water because it is the only radioactive isotope which can bind to its molecule. All other techniques are based on dissolved constituents whose abundance in water is controlled by physical, chemical and biological processes. Unfortunately, the natural level of tritium is very low and its half-life is relatively low when compared to other natural radionuclides, therefore the period for its use is quite limited.

A normal behaviour of tritium level in precipitations was noticed for the monitored location, with maximum values during warm months and minimum values during cold months. The monthly quantity of precipitations in the same location was monitored and reported in parallel, the data also being used as an annual tritium pulse in order to study the unsaturated area of the soil for this location, or as a level of reference to evaluate the impact of nuclear activity which takes place in this area (The Cryogenic Pilot for Tritium and Deuterium Separation from Heavy Water).

Measured values may also be used nationwide, if we take into account the absence of a GNIP station in Romania. Arithmetic annual averages for Rm. Valcea and Vienna Hohe Warte (location with the most complete records from the GNIP database), Fig. 5, are the same taking into account the reported uncertainties. An average of around 11 TU (11.66 TU for Rm. Valcea and 10.81 TU for Vienna) is specific for the two locations for the monitored period. In these circumstances, the calculated average values in Rm. Valcea location was 11.66 TU for the monitored period 1999–2009, much lower than that measured for Ottawa (another location with complete records to 2007 year), of 17.9 TU. Fig. 5. Regarding the level of tritium in precipitation at the Rm. Valcea location for the period 1999–2009, another particularity was also identified for the tritium monthly average and precipitations: the months with the maximum in tritium concentration are also the months with the maximum in quantity of precipitations.
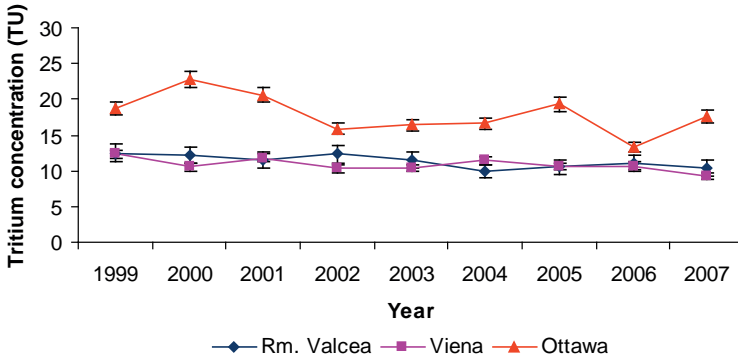
FIG. 5. Evolution of tritium annual weighted mean for Rm. Valcea, Vienna and Ottawa for the period 1999–2007, GNIP processed data (http://nds121.iaea.org/wiser).

REFERENCES

[1]   OSTLUND, H.G., BERRY, E.X., Modification of atmospheric tritium and water vapour by Lake Tahoe, Tellus **22** (1970) 463–465.

[2]   MICHEL, R.L., "Tritium in the Hydrological Cycle", Isotopes in the Water Cycle, Past, Present and Future of a Developing Science (AGGARWAL, P.K., GAT, J.R., FROEHLICH, K.F.O., Eds) Springer (2005) 53–67.

[3]   INTERNATIONAL ATOMIC ENERGY AGENCY, Measurement of radionuclide in food and the environment, Technical Reports Series no. 295, Vienna (1989).

[4]   INTERNATIONAL ORGANIZATION FOR STANDARDIZATION, Water Quality — Determination of tritium activity concentration — Liquid scintillation counting method, first edition, ISO 9698, Geneve (1989).

[5]   VARLAM, C., STEFANESCU, I., DULIU, O., FAURESCU, I., POPESCU, I., Applying direct liquid scintillation counting to low level tritium measurement, J. Appl. Radiation and Isotopes **67** 5 (2009).

[6]   INTERNATIONAL ATOMIC ENERGY AGENCY, Statistical Treatment of Data on Environmental Isotopes in Precipitation, Technical Reports Series no. 331, IAEA, Vienna (1992) 781.

WHAT AFFECTS THE ISOTOPIC COMPOSITION OF PRECIPITATION — A NEW INTERPRETATION?

A. DODY
Nuclear Research Center, Negev,
Beer Sheva, Israel

Abstract

Rainfall events were sampled in high resolution for stable isotope analyses during four rainy seasons in the Central Negev of Israel. Each sample is equivalent to 1–2 mm of rain. High variability in the isotopic composition was found in fractions of rain during storms. Two modes of isotopic distribution were found. The first is a wave shaped distribution, where isotopic compositions showed enriched to depleted graded changes and vice versa. The second mode is a step function where each rain cell displayed a constant $\delta^{18}O$ value, but varied greatly from the other rain cells. New interpretation suggests that during the transport of the air parcel system three processes can occur. The first process is a complete blending among the rain cells. The second is a partial isotopic mixing between the rain cells. Finally the third case is when each rain cell maintains its own isotopic values separate from the other rain cells. The third case of no mixing showed unexpected results due to the high air turbulence, vertically and horizontally. There was no evidence of complete mixing among the rain cells of identical air parcel systems. The processes in the air parcel trajectory itself suggested here is put forward as a new way to explain the changes in the isotopic composition during the rain.

1. INTRODUCTION

In principle, stable isotopes in atmospheric water are used as tracers in order to improve our understanding of the hydrological cycle. There are a large number of observations of stable isotopes in precipitation with monthly time resolution all over the globe [1]. It is well known that temperature, altitude, latitude and continental attributes affect isotopic composition [2]. Others, like Refs [3, 4] suggest additional parameters such as evaporation, relative humidity (RH) and sea surface temperature (SST). Based on Ref. [5] the isotopic composition is relatively uniform over a wide area on any particular day, but differs appreciably from storm to storm. Later on, Refs [6] and [7] showed in their study in the same geographical area that isotopic composition differs dramatically even in a single rain cell. Ref. [8] discussed the affect of the trajectory of stable isotopes in water vapour in the eastern Mediterranean. They calculated the air parcel trajectory based on the RH as measured in the last point. Ref. [9] also mentioned generally the effects of the synoptic trajectory on isotopic

composition. Ref. [10], which was based on the isotope data of Ref. [6] mentions the local parameters such as rain intensity which influence the isotopic composition in a single rain spell. It is obvious today that in order to improve our understanding of the fractionation process under atmospheric conditions, sampling in high resolution is needed. Only few measurements are available such as in Refs [4, 11]. This study presents high resolution sampling of isotopes in precipitation under desert conditions. Unfortunately, at that time of the research (early 1990s), the sampling of precipitation for isotopes was done with no regard to the synoptic trajectory and its processes. Later, Ref. [10] analysed part of the data from Ref. [6] with respect to the trajectory of the water vapours. The average annual precipitation of 86 mm varied from 20 to 191 mm, and was distributed during 20 rainy days per season on average [12]. The research ran during four rainy seasons.

All of the rain samples were analysed at the International Atomic Energy Agency (IAEA). Samples of three rain storms were analysed at both the IAEA Laboratory in Vienna and at the Niedersächsisches Landesamt für Bodenforschung (NLFB) Laboratory in Hannover, Germany. A standard deviation of ± 1‰ for δ^2H and ± 0.1‰ for $\delta^{18}O$ are acceptable accuracies for δ^2H and $\delta^{18}O$ analyses, respectively.

The aim of this work is to present a new interpretation explaining how isotopic composition varies during a single storm.

2.   METHODOLOGY

A mechanical sequential rain sampling with high resolution in time was used to collect approximately 250 to 500 mL of water equivalent to 1–2 mm of rain, respectively [13]. The novel approach to this method is that once an assigned volume of water is collected, the self-potential energy of the loaded containers is used to operate a mechanical seal for isolating the rain sample from the atmosphere. The sampler has 20 rain bags allowing the collection of rain water from a storm in amounts of 20 to 40 mm. A detailed description of the sampler was presented in Ref. [13].

3.   RESULTS

Eight storms were monitored and sampled during four rainy seasons from 1990 to 1993. All data are shown in detail in Ref. [9]. The isotopic composition of rainfall (RF) varied dramatically from enriched to depleted and vice versa in each storm. Two modes of $\delta^{18}O$ distribution during the rain were characterized:

- Wave shape distribution (Fig. 1). The $\delta^{18}O$ is changed gently from enriched to depleted values and vice versa.
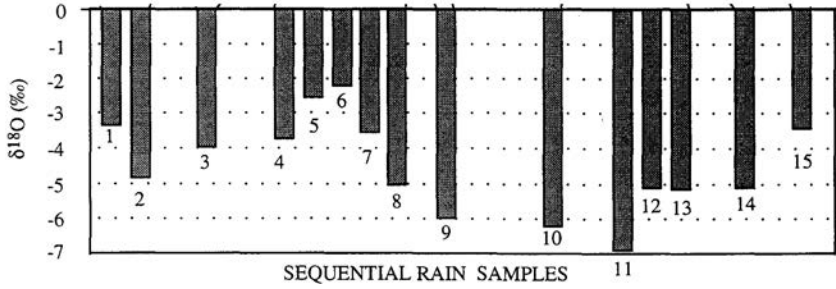
FIG. 1. Wave shape distribution of $\delta^{18}O$ during the rain.
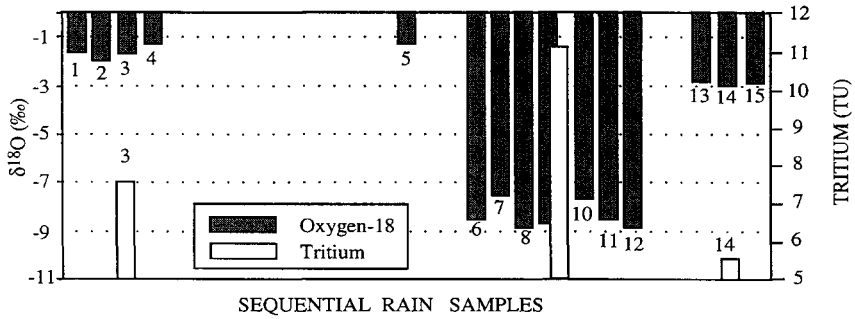
FIG. 2. Constant $\delta^{18}O$ values in each rain cell. Different tritium values between the rain cells.

- Step function, where each rain cell has constant $\delta^{18}O$ values but is significantly different between them (Fig. 2). Changes can also be seen in the tritium values between the rain cells.

4. THE PROBLEM

In a given area and rain storm, the variability in the changes in isotopic composition during a single storm as shown in Figs 1 and 2 could not be explained by simple changes in the air temperature, RH and SST. There must be other processes involved.

5. DISCUSSION

Based on Ref. [8], a change in 12 °C in the SST reveals a change of less than 1‰ for $\delta^{18}O$ (Fig. 3b). In our data (Fig. 2), the difference in the isotope values between two rain cells is around 7‰ for $\delta^{18}O$, which is equivalent to a change in 84 °C of the SST while assuming a linear correlation. This is, of course, not acceptable.
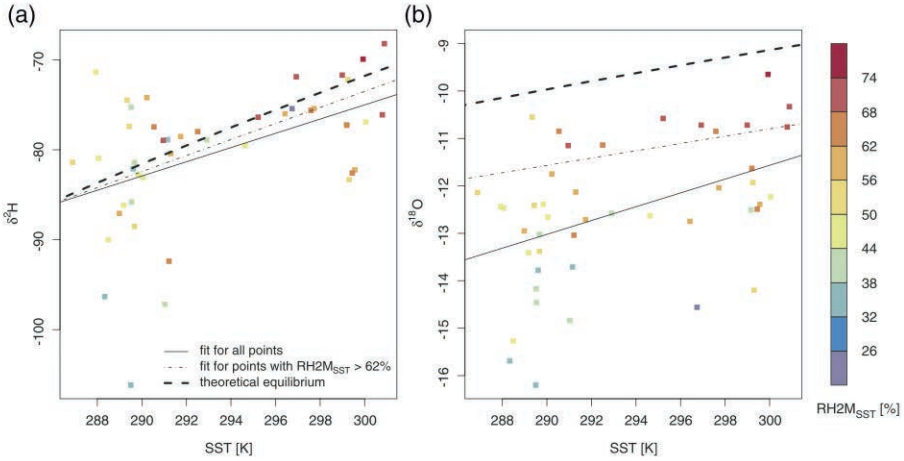
FIG. 3. *Measured values of $\delta^2 H$ and $\delta^{18} O$ plotted against average SST at humidity uptake (after Ref. [8]).*

Moreover, the change in SST in the Mediterranean Sea between winter and summer is 18°C, which means that in average the change per day is around 0.1°. Therefore in a given single storm, the effect of SST on the isotopes' values is negligible. Thus, we should look for a better explanation.

Significant differences in the isotopic composition due to variations in the synoptic conditions (both in terms of the source of the water vapours and the trajectory of the rain cell) were reported previously by Refs [14–16] and [8].The new interpretation describes the processes occurring in the air parcel system along the trajectory. Each of the individual rain cells may represent a small amount of rainfall with a specific isotopic composition. The rate at which the rain storm progresses in a specific location induces the isotopic composition of precipitation at the sampling point, as well as the rate of temporal change in the isotopic variations. Ref. [10], which partly analysed the data this article is based on, claimed that the isotopic composition of a single rain spell is related primarily to the origin and trajectory of the air parcel system. This state supports the second mode of no mixing between the sequential rain spells (Fig. 2). The first mode wave shape distribution (Fig. 1) is explained by Ref. [10] as being due to local parameters, especially rain intensity. The present paper suggests that the waveshape distribution is a result of mixing between two or three sequential rain spells. It must be stated here that based on Ref. [6] no correlation was found between rain intensity versus isotopic composition, as explained by Ref. [10].

a. partial mixing between the cells

Origin of the air parcel system

b. no mixing between the cells

Legend

⬤ enriched water vapours

◌ depleted water vapours
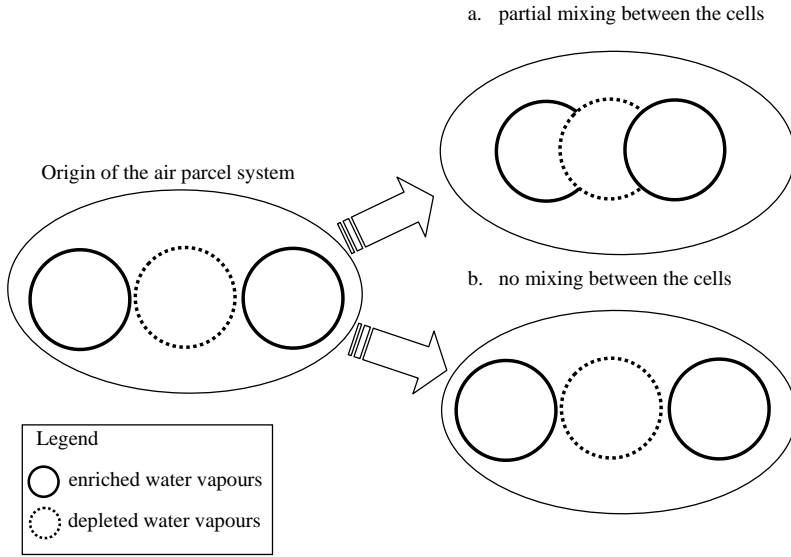
FIG. 4. Air parcel system contains rain cells with different isotopic compositions showing: (a) partial mixing between the rain cells; (b) no mixing between the rain cells.

6.   CONCLUSIONS

Air parcel systems combine different rain cells from different origins. The isotopic composition of each rain cell is determined by meteorological conditions when it joins the synoptic system. A new interpretation suggests that the isotopic composition in precipitation is also controlled by the processes in the synoptic system, such as mixing or not, between sequential rain cells. The isotopic composition of each rain cell can be saved along the trajectory with no mixing although air turbulence may be high both vertically and horizontally.

REFERENCES

[1]   SCHOTTERER U., OLDFIELD, F., FROHLICH, K., (GNIP) Global Network for Isotopes in Precipitation, IAEA (1996) 47.
[2]   CLARK I., FRITZ P., Environmental Isotopes in Hydrogeology, Lewis Publishers, Boca Raton, FL (1997).
[3]   CAPPA C.D., HENDRICKS, M.B., DEPAOLO, D.J., COHEN, R.C., Isotopic fractionation of water during evaporation, J. Geophys. Res. **108** D16 (2003) 4525.
[4]   GAT, J.R., KLEIN, B., KUSHNIR, Y., ROETHER, W., WERNLI, H., YAM, R., SHEMESH, A., Isotopic composition of air moisture over the Mediterranean Sea: An index of air-sea interaction pattern, Tellus **B55** (2003) 953–965.

[5]   LEVIN M., GAT, J.R., ISSAR, A., "Precipitation, flood and groundwaters of the Ne-
        gev highlands: An isotopic study of desert hydrology", Arid zone hydrology: Inves-
        tigation with isotopic techniques (Proc. Meeting Vienna, 1978), IAEA (1980) 3–22.

[6]   DODY, A., Isotopic composition of rainfall and runoff in small arid basin with im-
        plication for deep percolation, Ph.D dissertation, Ben Gurion University of the Negev
        (1995).

[7]   ADAR, E.M., DODY, A., GEYH, M.A., YAIR, A., YAKIREVICH, A., ISSAR,
        A.S., et al., Distribution of stable isotopes in arid storms, I. Relation between the dis-
        tribution of isotopic composition rainfall and in the consequent runoff, J. Hydrogeol.
        6 1 (1998) 50–65.

[8]   PFAHL, S., WERNLI, H., Air parcel trajectory analysis of stable isotopes in water
        vapour in the eastern Mediterranean, J. Geophysi. Res. **113** D20104 (2008).

[9]   DODY, A., Adar, E., Geyh, M., Stable Isotopes of Rainfall and Runoff in Small Arid
        Basin, LAP LAMBERT Academic Publishing (2010).

[10]   GAT, J.R., Adar, E., Alpert, P., Inter and intra storm variability of the isotope compo-
        sition of precipitation in southern Israel: Are local or large factors responsible? Study
        of Environmental Change using Isotope Techniques (Proc. Conf. Vienna, 2001),
        IAEA, Vienna (2001) 41–53.

[11]   BARRAS, V.J.I., SIMMONDS, I., Synoptic control upon $\delta^{18}O$ in southern Tas-
        manian precipitation, J. Geophys. Res. Lett. **35** L02707 (2008).

[12]   ZANGVIL, A., DRUIAN, P., Upper air trough axis orientation and spatial distribu-
        tion of rainfall over Israel, International J. Climatology **10** (1990) 57–62.

[13]   ADAR, E., KARNIELI, A., SANDLER, B.Z., ISAAR, A.S., LANZMAN, L., A me-
        chanical sequential rain sampler for isotopic and chemical analysis, IAEA Final Re-
        port, contract no. 5542/Ro/RB (1991).

[14]   GAT, J.R., "The isotopes of hydrogen and oxygen in precipitation", Handbook of En-
        vironmental Isotope Geochemistry (FRITZ P., FONTES J.CH., Eds), Vol. 1 (1980).

[15]   LEGUY, C., et al., The relation between the 18-O and deuterium contents of rain
        water in the Negev desert and air-mass trajectories, Chem. Geol. **41** (1983) 205–218

[16]   RINDSBERGER, M., MAGARITZ, M., CARMI, I., GILAD, D., The relation be-
        tween air mass trajectories and the water isotope composition of rain in Mediterra-
        nean Sea area, Geophys. Res. Lett. **10** (1983) 43–46.

DEUTERIUM EXCESS OF WATERS IN SLOVENIA
Preliminary results

M. BRENČIČ, A. TORKAR
Faculty of Natural Sciences and Engineering,
University of Ljubljana,
Ljubljana, Slovenia

P. VREČA
Jožef Stefan Institut,
Department of Environmental Sciences,
Ljubljana, Slovenia

Abstract

In climatic and hydrological studies, deuterium excess has proven to be a useful parameter; therefore this parameter has been investigated in the waters of Slovenia — positioned in Central Europe. All the data were acquired from publicly available data sources (e.g. journals, databases). Data were collected for four different parts of the water cycle: precipitation, surface water, groundwater and water in the unsaturated zone. For precipitation the value for deuterium excess ranges between –19.9‰ and 28.8‰ with the median at 10.1‰. Surface water has the minimum at 2.9‰, the maximum at 22.4‰ and the median at 13.2‰. Values for groundwater vary between –17.7‰ and 34.9‰ with the median at 11.8‰. Median for deuterium excess for the unsaturated zone is 15.1‰ and the values are between –2.8‰ and 17.6‰.

1. INTRODUCTION

1.1. Theoretical basis

Deuterium excess is defined as d-excess = $\delta^2H - 8\,\delta^{18}O$ [1] where δ^2H and $\delta^{18}O$ are the isotopic compositions of water molecules. It has shown potential in climatic studies for tracing past and present precipitation processes. It is also a measure of the relative proportions of δ^2H and $\delta^{18}O$ in water and can be visually depicted as an index of the deviation from the global meteoritic water line (GMWL) in the 2D space defined by the coordinates δ^2H and $\delta^{18}O$. In natural conditions, d-excess correlates with physical conditions such as humidity, air temperature and water temperature and the chemical status of water.

During circulation through the hydrological cycle, the isotopic composition of water changes as a consequence of equilibrium, diffusion and kinetic fractionation. The processes in the atmospheric part of the water cycle, from evaporation from

the ocean surface to cloud condensation and precipitation, are well elucidated by the Craig and Gordon [2] model. Equilibrium fractionation and kinetic effects are reflected in the slope of the GMWL with a value of 8. During equilibrium isotope fractionation in the hydrological cycle from ocean source water to water in another compartment (e.g. clouds) the isotopic composition changes along the line. The assumption of evaporation taking place into the atmosphere of 75% humidity above the ocean accounts for a d-excess value of 10‰ in atmospheric moisture [2] which confirms the world average for meteoric waters [2]. Both the slope of the GMWL and the global d-excess value justified Dansgaard's [1] definition. In higher saturation states of the atmosphere above the ocean, d-excess is lower; therefore, some paleo-groundwaters show lower d-excess values than present groundwater [2].

If additional transport and fractionation processes are present during such a process, d-excess differs from that of the liquid vapour transition under equilibrium conditions. In the natural environment, such waters are positioned on the line with a slope reduced relative to the equilibrium line of the GMWL [2]. The isotopic composition of residual water from evaporation is positioned along the line below the GMWL and evaporated water is positioned above the GMWL. In deep and extensive aquifers, geochemical processes can also influence the isotopic composition of water. In mineral and thermomineral waters, aquifers might exchange with CO_2 and H_2S.

1.2. Starting points

In the literature very large number of oxygen and hydrogen stable isotope studies on various components of the hydrological cycle can be found. They depict various processes such as infiltration, water retention in the hydrological compartments, recharge processes as well as many other relevant hydrological phenomena. However, only occasionally are studies interested in the stable isotopic characteristics of the whole hydrological cycle in the particular geographical area.

Slovenia is positioned in the area where the precipitations are predominantly the consequence of the mixture of Mediterranean and Atlantic air masses. When precipitations infiltrate these processes they influence the isotopic characteristics of the groundwater and surface water bodies. A large part of the country is represented by carbonate rocks intersected with tectonic depressions where extensive alluvial aquifers are formed and filled mainly with carbonate clastic sediments. Carbonate aquifers are characterised with deep and extensive vadose zones. In the north-eastern part of the country mixing of shallow and deeper paleo-groundwater is present.

In the present study our attempt is to collect all the available data on hydrogen and oxygen stable isotope characteristics of various components of the hydrological cycle in the area of Slovenia and its near surroundings. The idea is to analyse the ranges and (statistical) distributional characteristics of the stable isotope characteristics of water in the natural environment with particular emphasise on the d-excess

values. Therefore, we have try to collect, review and analyse all the available stable hydrogen and oxygen data from the scientific literature and other publicly available data sources (e.g. research reports, diploma and doctoral theses) as well as data from online resources. An attempt was made to collect data where for the particular sample both hydrogen and oxygen data are accessible. Surprisingly, in spite of the fact that many stable isotope studies of hydrological cycle components were performed and reported, complete data sets are difficult to obtain and are relatively scarce. Several older data sets are lost. Therefore, it is also difficult to reanalyse and reinterpret older interpretations.

In the present paper we are representing ongoing work in collection and database construction of available stable hydrogen and oxygen data from the area of Slovenia. Preliminary statistical analyses of d-excess values are performed and illustrated by descriptive statistics and exploratory statistical diagrams. Hydrological compartments are divided into four groups; precipitation, groundwater, vadose zone water and surface water.

2. METHODS

Data were collected from the scientific literature, online resources and other publicly available data sources. References are not cited due to the limited space. They were included in the electronic database constructed in the Excel™ spreadsheet programme.

All d-excess values, descriptive statistics and empirical distribution functions were calculated by Excel™. The statistical distribution of d-excess values is also represented by univariate kernel density estimation [3]. Normal kernel density procedure with automatic bandwidth selection was applied. All kernel density calculations were performed in R environment [4] with package KernSmooth [5].

3. RESULTS

3.1. Complete data sets

The total number of collected data is 1285. The range of d-excess values is between –19.9‰ and 34.9‰ with the median value of 12.4‰ and average of 12.0‰. Empirical distribution function (EDF) is given on the left side of Fig. 1 and the kernel density estimate on the right side. The later was calculated with the bandwidth of 0.494. Distributions show strong leptokurtic distribution with long tails and bumps on the left hand side of the distribution indicating polymodal distribution where actual distribution is representing a mixture of different distributions.
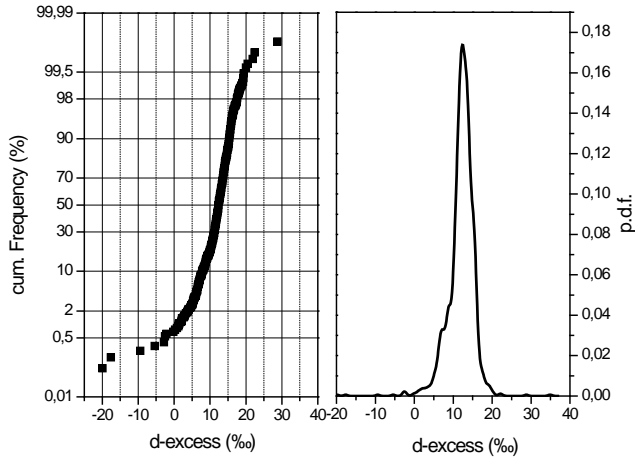
FIG. 1. *Empirical distribution and kernel density estimate of the whole set of data.*
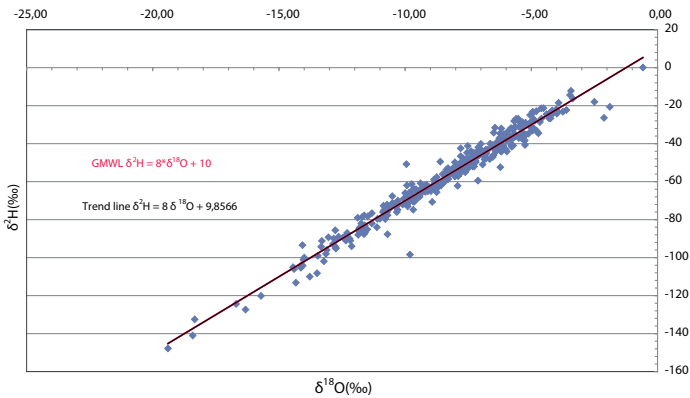
FIG. 2. *δ^2H vs $\delta^{18}O$ contents for precipitation in Slovenia.*

3.2. Precipitation

Precipitation data are mainly represented with the data from Ljubljana precipitation station and stations from the southwestern coastal part of Slovenia. Precipitation data are represented in the δ^2H and $\delta^{18}O$ space (Fig. 2) showing the most regular patern among analysed groups. The GMWL and trend line are nearly identical. For percipitation 362 data were collected; the data have minimum –19.9‰ and maximum 28.8‰. The median value is 10.1‰.

Empirical distributions represented on Fig. 3 are showing symmetry with a heavy tail on the left hand side. The kernel density calculated with the banditdh of 1.027 shows a strongly leptokurtic shape.
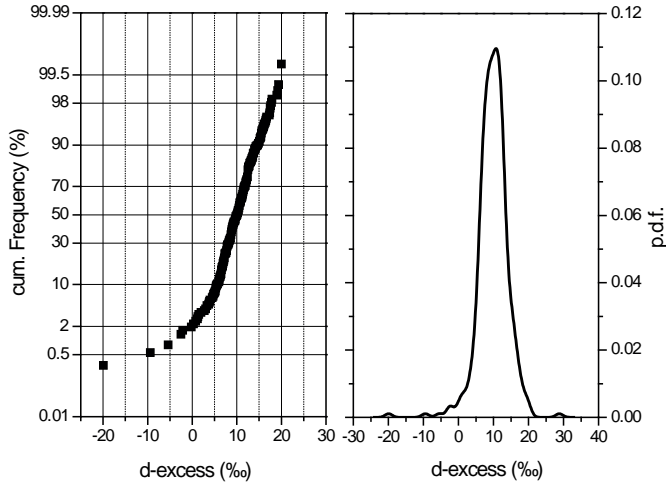
FIG. 3. Empirical distribution and kernel density estimate of the precipitation data.
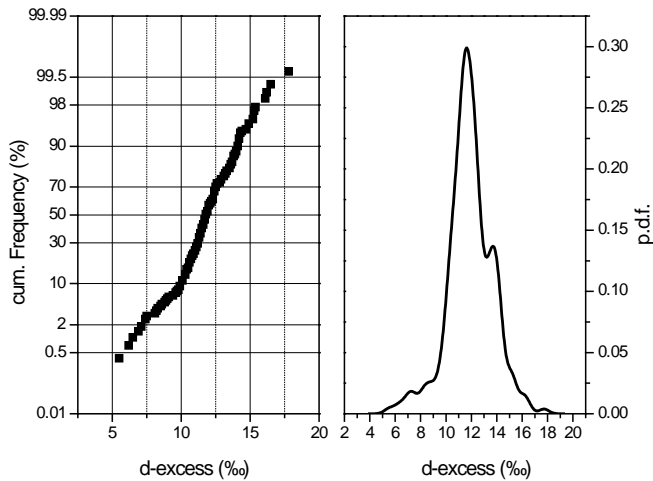
FIG. 4. Empirical distribution and kernel density estimate of the groundwater data.

3.3. Groundwater

Groundwater is represented with 274 data. The d-excess values are between a minimum of –17.7‰ and maximum of 34.9‰. The median value is 11.8‰. The empirical distribution shows asymmetry with the mixture of different parent distributions which is apparent from the kernel density (bandwidth of 0.383) estimate where at least three groups can be seen from the shape of the curve (Fig. 4).

3.4. Vadose zone water

For this part of the hydrological cycle 104 data were collected. This is the smallest data group in the data set with a very irregular data distribution in $\delta^2 H$ and $\delta^{18}O$ space (Fig. 5). The majority of data are above the GMWL and others are showing evaporation processes. Discrepancies between GMWL and vadose zone waters are probably the consequence of the fact that the majority were sampled in karstic areas
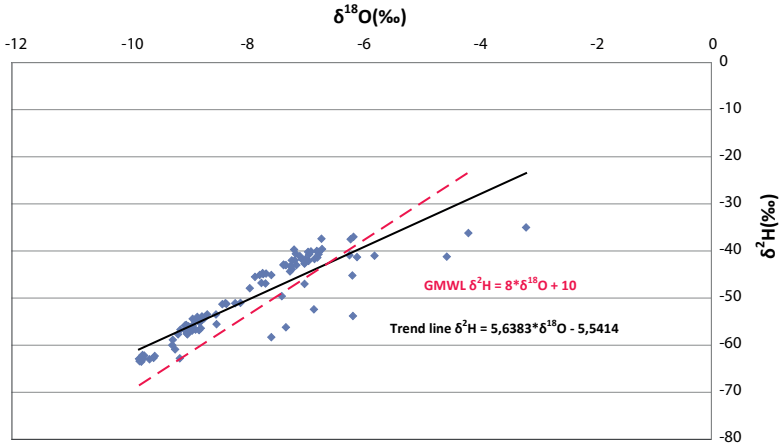
FIG. 5. Vadose zone data in $\delta^2 H$ and $\delta^{18}O$ space
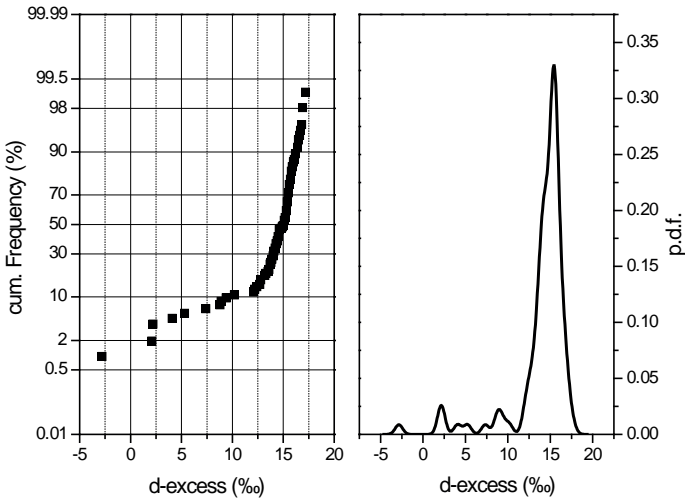
FIG. 6. Empirical distribution and kernel density estimate of the vadose zone data.
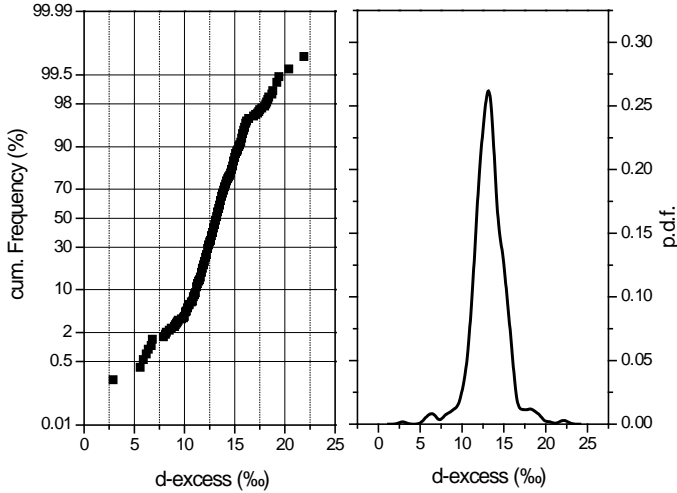
FIG. 7. Empirical distribution and kernel density estimate of the surface water data.

where the vaodse zone is thick. Deuterium excess for the unsaturated zone has a minimum of –2.8‰ and maximum of 17.6‰ with a median value of 15.1‰.

The irregularity of the data is also visible from empirical distribution diagrams (Fig. 6). A long left tail is clearly visible, probably consisting of a separate distribution. The right part of the EDF also shows in the kernel density estimate (bandwidth 0.444) irregularity caused by a mixture of parent distributions.

3.5. Surface water

For surface water 545 data were collected. d-excess for surface water ranges between 2.9‰ and 22.4‰ with the median value at 13.2‰. Empirical distribution is symmetrical with relatively long tails clearly visible in the kernel density estimate (bandwidth 0.494) (Fig. 7).

4. CONCLUSIONS

Preliminary interpretations and calculations of exploratory statistics show differences among groups of water originating from different compartments of the hydrological cycle. A comparison of the median values of d-excess values of precipitation with values among other groups shows relatively large differences. In all cases the median values of d-excess are higher than in the group of precipitation data. In the distributional diagrams it is also visible that data sets consist of different groups.

Further evaluation of the data set is needed. In the next step a more critical approach to available data sets must be applied, especially for very high or low d-excess at the tails of empirical distributions. Further efforts will also be made to close gaps in the data set. Analysis will be followed with further statistical procedures (e.g. hypothesis testing). However, at this stage we can conclude that differences of d-excess and stable hydrogen and oxygen composition of water components in the region of Slovenia are important for showing different processes in the hydrological cycle.

ACKNOWLEDGEMENTS

REFERENCES

[1]   DANSGAARD, W., Stable isotopes in percipitation, Tellus, **16** (1964) 436–468.
[2]   GAT, J.R.,   Isotope hydrology – A study of the Water Cycle, Imperial College Press (2010).
[3]   WAND, M.P., JONES, M.C., Kernel Smoothing, Chapman & Hall/CRC (1995) 212.
[4]   R DEVELOPMENT CORE TEAM, R: A language and environment for statistical computing, R Foundation for Statistical Computing, Vienna, http://www.R-project.org.
[5]   RIPLEY, B., KernSmooth: Functions for kernel smoothing for Wand & Jones (1995), R package version 2.23–3 (2009), http://CRAN.R-project.org/package=KernSmooth.

DEVELOPMENT AND EVALUATION OF A METHODOLOGY FOR THE GENERATION OF GRIDDED ISOTOPIC DATASETS

A.A. ARGIRIOU [1], V. SALAMALIKIS
University of Patras, Department of Physics,
Laboratory of Atmospheric Physics,
Patras, Greece

S.P. LYKOUDIS
National Observatory of Athens,
Institute of Environmental and Sustainable Development,
Athens, Greece

Abstract

The accurate knowledge of the spatial distribution of stable isotopes in precipitation is necessary for several applications. Since the number of rain sampling stations is small and unevenly distributed around the globe, the global distribution of stable isotopes can be calculated via the generation of gridded isotopic data sets. Several methods have been proposed for this purpose. In this work a methodology is proposed for the development of 10´ × 10´ gridded isotopic data from precipitation in the central and eastern Mediterranean. Statistical models are developed taking into account geographical and meteorological parameters as regressors. The residuals are interpolated onto the grid using ordinary kriging and thin plate splines. The result is added to the model grids, to obtain the final isotopic gridded data sets. Models are evaluated using an independent data set. The overall performance of the procedure is satisfactory and the obtained gridded data reproduce the isotopic parameters successfully.

1.   INTRODUCTION

The significance of the stable isotope composition of precipitation in hydrological and climate studies is well known [1]. This composition varies both in time and space and its determination requires a dense measurement network that in most places around the globe does not exist. Lack of isotopic information can be addressed by modelling. Modules for determining the isotope content of precipitation have been included in global circulation models with considerable success. An alternative approach is statistical modelling. Several studies address the generation of gridded isotopic data sets by combining regression and geostatistical methods [2–8]. In this

---

[1]   University of Patras, Department of Physics, Laboratory of Atmospheric Physics, Patras, Greece

work we attempt to create annual and seasonal gridded stable isotope ($\delta^{18}O$ and δ^2H) data with a 10′ × 10′ resolution for the area of the central and eastern Mediterranean.

2. DATA AND METHODS

The area of interest extends between 30°N–55°N and 5°E –45°E. Stable isotopic composition of precipitation, precipitation amount, temperature and vapour pressure data were obtained from the GNIP [9] and the ISOHIS [10] databases, but also from other sources [5, 6]. Most stations dispose of data after a limited number of years, sometimes after only one year. Testing the data for trends did not reveal any systematic patterns [11], therefore all data can be used, irrespective of the period they cover. Monthly gridded climatologies of elevation, temperature, precipitation amount and relative humidity with a 10′ × 10′ resolution were obtained from the CRU CL 2.0 data set [12]. Vapour pressure was calculated through temperature and relative humidity using the Hyland and Wexler formula [13].
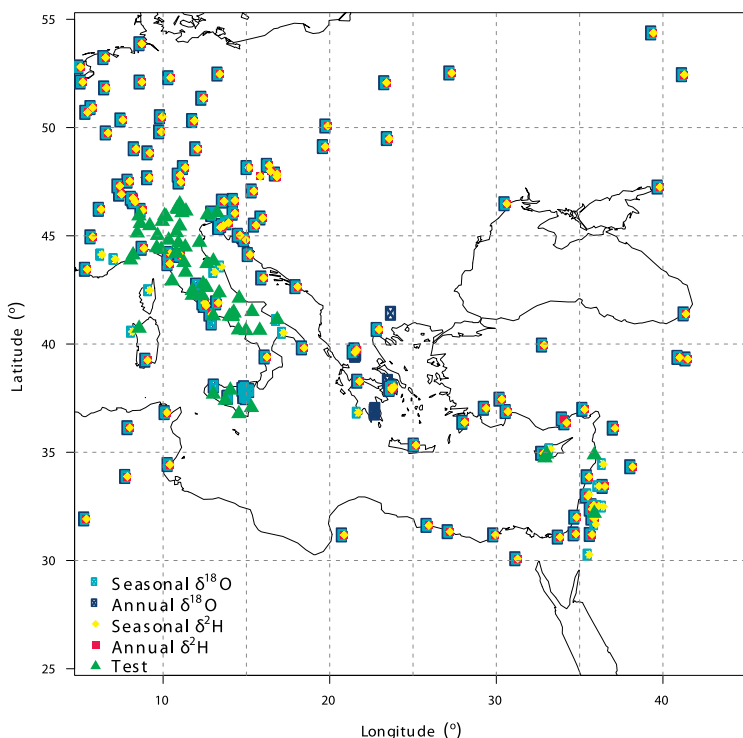
FIG. 1. Area of interest and stations with seasonal and annual isotope data ($\delta^{18}O$ and δ^2H).

Annual and seasonal values according to typical calendar seasons were calcu-
lated: December–January–February (DJF), March–April–May (MAM), June-July-
August (JJA) and September–October–November (SON). For the isotopic param-
eters weighted seasonal and annual means were calculated, arithmetic means for
temperature and vapour pressure and sums for precipitation amount. Fig. 1 represents
the measurement sites included in the annual and seasonal isotopic data sets.

Gridded isotope data are calculated using a hybrid regression–geostatisti-
cal procedure. All interpolation algorithms (kriging, radial basis functions, splines,
squared inverse distance, triangulation etc.) estimate the value at a given location
where measurements do not exist as a weighted sum of data values at surrounding
locations. Due to the sparseness of the isotope data, map precision may be improved
using ancillary information in the interpolation methods. The ancillary spatial infor-
mation can be introduced by creating regression empirical models. The regression
model attempts to derive explicit relationships between isotopic values and param-
eters that are closely related to them. These parameters should be available with a
resolution higher than that of the isotope values and must be strongly correlated with
them. In order to capture the advantages of both the regression and the interpolation
approach, a combined procedure was used which includes the following steps: (a) a
regression model is built to estimate the stable isotopic values, (b) the model is ap-
plied to gridded data of the desired resolution for the generation of a gridded data set
of modelled isotopic values, (c) the model's residuals are interpolated onto the same
grid for the production of a gridded data set which comprises the residual interpo-
lated isotopic values, (d) the two data sets are added to reproduce the final gridded
isotopic data.

The initial Bowen–Wilkinson method [3] included only latitude and altitude
as independent variables. In this work, except for the BW regression model which
provides a point of reference for the Bowen–Wilkinson methodology, various com-
binations of geographical and meteorological variables were used for the creation of
the empirical regression models. The following models were tested:

$$\delta X = f\left(lat, lat^2, alt\right) \tag{1}$$

$$\delta X = f\left(lat, lat^2, lat^3, long, long^2, long^3, alt, alt^2, alt^3\right) \tag{2}$$

$$\delta X = f\left(lat, alt, t, p\right) \tag{3}$$

$$\delta X = f\left(t, t^2, t^3, p, p^2, p^3, vp, vp^2, vp^3\right) \tag{4}$$

where X ^{18}O or ^{2}H, *lat* latitude (°), *long* longitude (°), *alt* altitude (m), *t* tempera-
ture (°C), *p* precipitation amount (mm), and *vp* vapour pressure (hPa).

Eq. (1) represents the BW model. Equation (2) is a model which comprises only
topographical regressors (GEO). Model (3) is a simple 1st order model (SIM) while

model (4) is a combination of meteorological parameters (MET). The BW and SIM models were fitted using multiple linear regression and the remaining models were tested using stepwise linear regression in order to eliminate statistically insignificant contributions. Their performance was assessed via statistical indicators. The models were applied to gridded data with $10' \times 10'$ resolution in order to generate gridded modelled data of isotope values. The residuals of the models were interpolated using two interpolation methods, the stochastic method of ordinary kriging, and the deterministic method of thin plate smoothing splines. For ordinary kriging, the spatial correlation structure of the residuals was defined using an exponential variogram plus a nugget effect except for the season JJA where a linear variogram plus a nugget effect was used. The modelled data grids and the grids from the interpolation of the model's residuals are added for the generation of final gridded isotopic data sets. The overall procedure — the creation of the regression models and the interpolation of the residuals — was performed with the open source language R. The success of each gridded isotopic data set in reproducing the stable isotopic composition of precipitation was assessed comparing the actual point values to the value of the closest grid cell. We created an independent data set for the validation of the grids produced which contained data from published works that were not included in the GNIP–ISOHIS database [6]. The gridded data sets were compared with the independent validation data set using simple statistics.

3.   RESULTS

3.1. Regression Models

As mentioned above, stepwise linear regression was used to obtain robust models and to avoid erroneous predictions when the models were applied to gridded data sets. The final independent variables retained in each model were determined via a stepwise procedure. It was found that the parameters lat^2 and longitude are significant regressors for the empirical models of both isotopic parameters. Longitude assists the determination of the south-eastern tilt of the isotopic composition. This is the result of the different vapour sources across the study area. Temperature and precipitation amount are also significant and they are included in the regression models. The overall assessment of the regression procedure was performed using simple statistics. It was found that the correlation coefficient is lower in the warm period than in winter. Models with only meteorological parameters as independent variables provided higher correlation coefficients regardless of the season concerned. Models using meteorological parameters outperform those based solely on geographical parameters according to their statistical assessment. It is therefore necessary to insert meteorological parameters into the empirical models.

3.2. Gridded data sets

The produced gridded data set, which is a combination of a model and the residual interpolation method, is evaluated in terms of rMAE and rRMSE calculated point wise, using as a reference the independent validation data set. For ^{18}O, the grids produced using the geostatistical method of ordinary kriging present better results from the grids produced by thin plate smoothing splines apart from the model SIM. The statistical indexes, rMAE and rRMSE, for the ordinary kriging method range between 9.8%–11.63% and 12.24%–14.69% respectively. On the other hand, for δ^2H, different results arise from the values of the statistical indexes.

The isotope values of the independent validation set are plotted against the grids produced of each regression model for both isotopes (Fig. 2). For both isotopic parameters, the correlation coefficients for grids based on ordinary kriging interpolation are higher than those based on the other geostatistical method. The models with solely meteorological parameters are unable to estimate successfully the isotopic composition, as indicated by the low values of the correlation coefficients. However, the combination of geographical and meteorological parameters is successful as shown from the overall assessment of the statistical indexes and correlation coefficients. Models with geographical parameters reproduce better the isotopic composition of precipitation compared with the models with only meteorological parameters. This effect occurs in mountainous regions where the values of the gridded data are not high enough resulting in excessively depleted values.

On the basis of the above, the grid obtained from the initial Bowen–Wilkinson model by applying ordinary kriging, using elevation and altitude, and the grid obtained from model SIM of the method thin plate smoothing splines should be the best choices for estimating annual $\delta^{18}O$ gridded values. The best grid for annual δ^2H is obtained from the SIM model for both interpolation methods. Finally, the best grids for the two isotope parameters are provided by BW and SIM models using ordinary kriging.

$$\delta^{18}O = -4.78 - 0.34lat + 0.017lat^2 - 0.0019alt$$
$$\delta^{18}O = -6.00 - 0.077lat - 0.015alt + 0.21t - 0.005p \qquad (5)$$
$$\delta^2H = -13.22 - 1.14lat + 0.009alt + 1.42t - 0.02p$$

Fig. 3 presents the gridded $\delta^{18}O$ and δ^2H data produced by the models of the above equations. The produced distributions seem to capture the characteristics of the isotopic composition of precipitation that are associated with temperature changes. Topography induced isotopic depletion is well represented in all major mountainous areas and is easily discernable on the isotope maps. A distinct disadvantage of this approach is that it does not interpolate over a spherical surface. As a result of the planar interpolation, the isotope maps suffer from edge effects, or discrepancy between matching edges. Due to the sparseness of isotope stations in many parts of
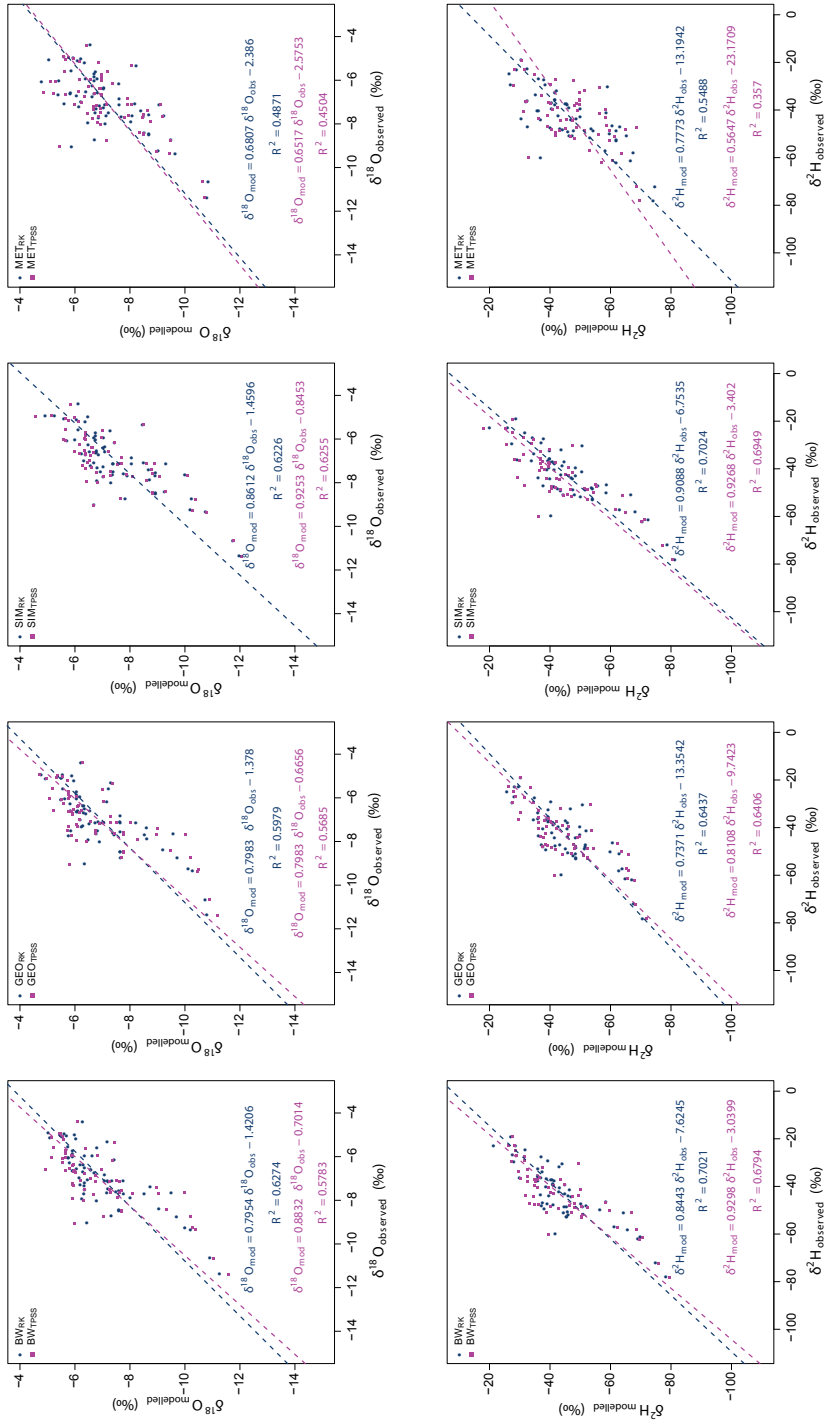
FIG. 2. Correlation between gridded and observed δ¹⁸O and δ²H for the validation data set.
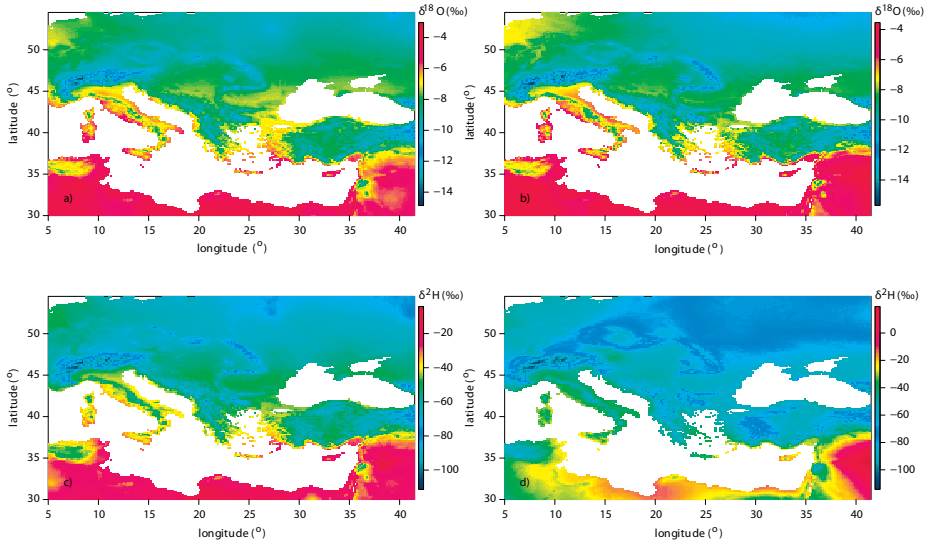
FIG. 3. Gridded composition of precipitation: (a) $\delta^{18}O_{OK}$ BW, (b) $\delta^{18}O_{TPSS}$ SIM, (c) δ^2H_{OK} BW and (d) δ^2H_{TPSS} SIM

the area of interest, the isotope values are not significantly different. This effect is present in the Balkans, Ukraine, southern Russia and north Africa.

4.   CONCLUSIONS

The overall performance of the procedure used for the generation of 10′ × 10′ gridded data sets of the isotopic composition of precipitation across the central and eastern Mediterranean was found to be satisfactory. The obtained isotope data reproduces the isotopic parameters successfully. The correlation coefficients are high for the isotope regression models ranging between 0.63% and 0.85%. The models provide higher correlation coefficients especially when meteorological parameters are added. Models using only meteorological parameters present better goodness of fit statistics than those using only geographical data.

The thin plate smoothing splines method used for first time for the interpolation of isotope data gives satisfactory results. The best grids for the Thin Plate Smoothing Splines method and for both isotopic parameters, are provided by the simple model SIM, which uses the latitude, elevation, temperature and precipitation amounts as independent variables. On the other hand when ordinary kriging is used it is the BW model that provides the best grids for the annual $\delta^{18}O$ and the SIM model for annual δ^2H.

Due to the variation of limited data in several parts of the study area the isotopic composition in these parts does not vary significantly. Also, the use of smoothed gridded data sets in the regression models may produce erroneous results, especially in those regions where no isotope data are available. Thus local effects cannot be described by the overall model.

REFERENCES

[1]   GAT, J.R., Oxygen and hydrogen isotopes in the hydrological cycle, Ann. Rev. Earth. Planet. Sci. **24** (1996) 225–262.

[2]   BIRKS, S.J., GIBSON, J.J., GOURCY, L., AGGARWAL, P.K., EDWARDS, T.W.D., Maps and animations offer new opportunities for studying the global water cycle, Eos Trans. AGU Electronic Supplement **83** (2002) 37.

[3]   BOWEN, G.J., REVENAUGH, J., Interpolating the isotopic composition of modern meteoric precipitation, Water Resour. Res. **39** (2003) 1299.

[4]   BOWEN, G.J., WILKINSON, B., Spatial distribution of delta O–18 in meteoric precipitation, Geology **30** (2002) 315–318.

[5]   DOTSIKA, E., LYKOUDIS, S., POUTOUKIS, D., Spatial distribution of the isotopic composition of precipitation and spring water in Greece, Global and Planetary Change **71** (2010) 140–149.

[6]   LYKOUDIS, S.P., ARGIRIOU, A.A., Gridded data set of the stable isotopic composition of precipitation over the eastern and central Mediterranean, J. Geophys. Res. **112** (2007).

[7]   MEEHAN, T.D., GIERMAKOWSKI, T.J., CRYAN, P.M., GIS-based model of stable hydrogen isotope ratios in North American growing-season precipitation for use in animal movement studies, Isotopes Environ. Health Stud. **40** (2004) 291–300.

[8]   Van der VEER, G., VOERKELIUS, S., LORENTZ, G., HEISS, G., HOOGGEWERFF, J.A., Spatial interpolation of the deuterium and oxygen-18 composition of global precipitation using temperature as ancillary variable, J. Geochem. Explor. **101** (2009) 175–184.

[9]   INTERNATIONAL ATOMIC ENERGY AGENCY, WORLD METEOROLOGICAL ORGANIZATION, Global Network of Isotopes in Precipitaion: The GNIP database v.12/2005, IAEA, Vienna, http://isohis.iaea.org.

[10]   INTERNATIONAL ATOMIC ENERGY AGENCY, Isotope Hydrology Information System: The ISOHIS datbase v.12/2005, IAEA, Vienna, http://isohis.iaea.org.

[11]   LYKOUDIS, S.P., ARGIRIOU, A.A., Temporal trends in the stable isotopic compo-
        sition of precipitation: a comparison between the eastern Mediterranean and central
        Europe, Theor. Appl. Clim. **105** (2010) 199–207.

[12]   NEW, M., LISTER, D., HULME, M., MAKIN, I., A high resolution dataset of sur-
        face climate over global land areas, Clim. Res. **21** 1 (2002) 1– 25.

[13]   HYLAND, R.W., WEXLER, A., Formulations for thermodynamics properties of
        the saturated phases of H_2O from 173.15 K to 473.15 K, ASHRAE Trans **89** 2A
        (1983) 500–519.

MODELLING AND MAPPING OXYGEN-18 ISOTOPE COMPOSITION OF PRECIPITATION IN SPAIN FOR HYDROLOGIC AND CLIMATIC APPLICATIONS

J. RODRÍGUEZ-ARÉVALO, M.F. DÍAZ-TEIJEIRO,
Centro de Estudios y Experimentación de Obras Públicas (CEDEX),
Madrid, Spain

S. CASTAÑO
Geological Survey of Spain (IGME),
Madrid, Spain

Abstract

A simple multiple regression model based on two geographic factors (latitude and elevation) has been developed that reproduces reasonably well the spatial distribution of the current mean oxygen-18 isotope composition in precipitation over Spain. In a preliminary analysis, additional geographic and climatic factors do not improve the performance of the model. A continuous digital map of oxygen-18 isotope composition in precipitation has been produced by combining the polynomial model with a digital elevation model using GIS tools. Application of the resulting map to several groundwater case studies in Spain has shown it to be useful as a reference of the input function to recharge. Further validation of the model, and further testing of its usefulness in surface hydrology and climatic studies, is ongoing through comparison of model results with isotope data from the GNIP database and from isotope studies in hydrogeology and climate change taking place in Spain.

1. INTRODUCTION

The amount weighted $\delta^{18}O$ and δ^2H mean values of precipitation have been routinely used as baseline information to represent the long term isotopic composition of infiltration water in hydrogeology studies. In many case studies, this type of reference isotope information has been obtained by interpolation of the series of isotope data obtained from long term surveillance in nearby stations of the IAEA-WMO GNIP database. Normally, these data have been combined with short term series of isotope data obtained either from precipitation sampled in local meteorological stations of ad-hoc sampling programmes, or from shallow groundwater sampled in springs and wells. Local Meteoric Water Lines (LMWL) and linear correlations between altitude and δ^2H and $\delta^{18}O$-values have been drawn as conceptual and graphical aids from the isotope side in the interpretation of hydrologic problems. These correlations provide gross approximations, though they have proven to be highly useful to identify

groundwater recharge areas, assess different runoff components, trace the origin of contaminants and define conceptual models for flow and transport [1–3].

Isotope applications in the environmental sciences have increased in the last decades to include the study of climate and ecosystems, which have raised the need to take a closer look at the spatial distribution of the isotopic composition of precipitation. This has motivated the development of models of the relationship between isotope composition and geographic and climate parameters [4] that have led to the development of high-resolution maps of isotope composition in precipitation with the aid of geostatistics and the recently available Geographic Information System (GIS) tools.

In Spain, the existence of a network for isotopes in precipitation, in operation now for more than a decade, has provided a series of data of high enough quality that could serve to analyse the nature and extent of the isotope effects of geographic and climate factors. The study of these factors and the application of GIS tools resulted in a model and a continuous map of the spatial distribution of the stable isotope composition in precipitation. A number of isotope studies in hydrogeology and climate change being performed in the country have provided the isotope information of other components of the hydrologic cycle with which the model has been compared. This information gives the opportunity to check the usefulness of such maps to provide isotope baseline information for hydrology and climate studies, and to identify their limitations.

2. SPANISH NETWORK FOR ISOTOPES IN PRECIPITATION

The Spanish network for isotopes in precipitation (Red Española de Vigilancia de Isótopos en la Precipitación, REVIP) provides composite monthly samples of precipitation collected since 2000 at 16 meteorological stations. The stations have a wide geographic distribution, and are located in the main hydrographical basins, in areas representative of the different climatic zones in Spain. The REVIP is managed by the Centro de Estudios y Experimentación de Obras Públicas (CEDEX), in collaboration with the Agencia Estatal de Meteorología (AEMET).

A first study of the factors controlling the isotopic composition of precipitation and groundwater in Spain was performed in 1994 [5] and provided a general framework for the interpretation of isotopic analyses for hydrogeology and related fields in this country. It also pointed out a lack of systematic isotope analyses of samples from meteorological stations evenly distributed through the whole national territory. REVIP, which was designed in order to fill this gap, has already provided a series of more than ten years of systematic isotope information in precipitation that supports the modelling exercise performed in this paper [6].

3. MODELLING ^{18}O COMPOSITION OF PRECIPITATION: FROM GLOBAL
    TO LOCAL SCALE

The Spanish territory includes a wide range of different climate environments (Atlantic, Mediterranean, Subtropical, Continental), and is a mountainous terrain with peaks higher than 3000 m a.s.l. This situation favours the application of stable isotope techniques in hydrology, allowing the study of the influence of different factors in the isotopic composition of meteoric waters in many areas of the country.

δ^{18}O and δ^{2}H values in precipitation obtained from the analysis of composite monthly samples collected for the period 2000–2006 from the REVIP were used to study the spatial distribution of isotope contents over Spain and to identify the main geographical and climate factors that control this distribution. The δ^{2}H–δ^{18}O relationship of the long term weighted means is in good agreement with the GMWL, showing d-excess values only slightly above 10‰, which indicates the relevance of air masses of Atlantic origin as the main source of water vapour over the Iberian Peninsula. This is also supported by the study of the latitude, elevation and continental effects, and the spatial distribution of Tritium concentrations in precipitation [6].

In a first step [7], the spatial variation in δ^{18}O in REVIP stations was compared with the results of previous models that describe, with a good approximation, δ^{18}O values in precipitation at the global scale as a function of latitude and altitude [4]. A bias towards more positive δ^{18}O values was observed for the isotope composition of precipitation from the REVIP stations, particularly for the REVIP coastal stations (elevation < 200 m), compared to those for GNIP stations located at similar latitudes. These differences may derive from the influence of the positive δ^{18}O signature that the warm Gulf Stream may imprint to European precipitation, as suggested in [4].

Therefore, a local model of the relationship between ^{18}O in precipitation and latitude and altitude was obtained through a one-step non-lineal regression, which reproduces noticeably well the observed variations in Spanish precipitation. An exception was made for Tenerife (Canary Islands) which belongs to a different climatic region. Consideration of additional geographic (distance to the sea) and climatic factors (continental effect) did not improve the performance of the model.

4. MAPPING ^{18}O COMPOSITION OF PRECIPITATION IN SPAIN

The polynomial model obtained has been used to produce a continuous digital map of δ^{18}O in precipitation in Spain, by applying GIS tools to a digital elevation model in several steps that include: (1) the adequate transformation of geographic information from raster (digital elevation model) to vector format using ESRI ArcGis; (2) the projection from UTM to geographical coordinates; (3) the application of the regression equation to the geographic information produced previously; and (4) transformation of geographic information from vector back to raster format [8].
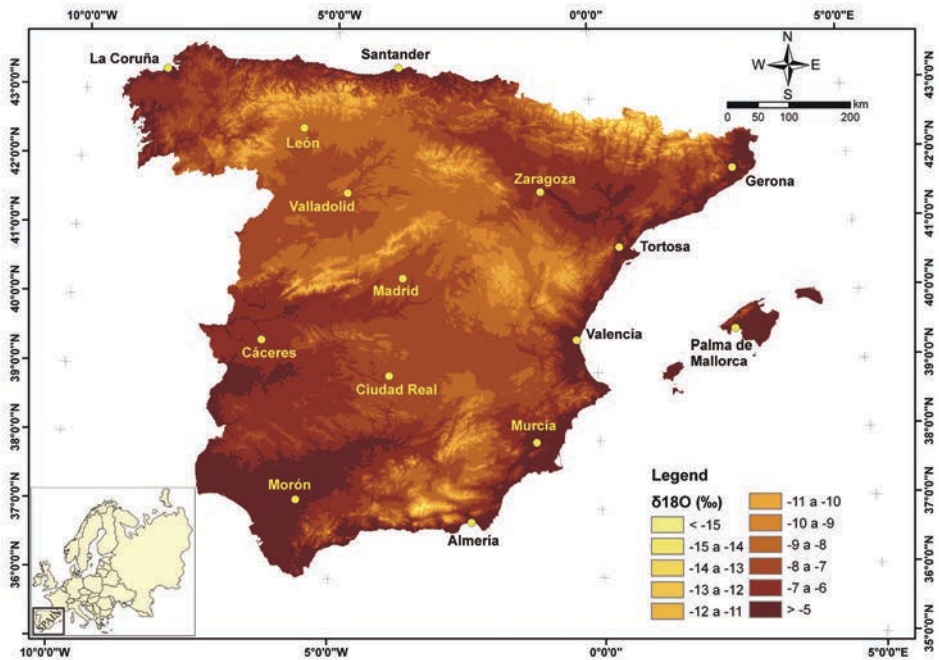
FIG. 1. Continuous digital map of the δ¹⁸O distribution in peninsular Spain and the Balearic islands. Location of the 15 peninsular stations of the REVIR is shown.

The resulting map is shown in Fig. 1, in which isotope values in precipitation are shown for pixels of 500×500 m.

5. EXAMPLES OF APPLICATION TO HYDROGEOLOGY AND CLIMATE STUDIES

The isotope model and the resulting map of $\delta^{18}O$ distribution in precipitation have been applied to several case studies in Spain that cover a range of different geographic and climatic areas. Comparisons between the modelled $\delta^{18}O$-values in precipitation and the $\delta^{18}O$ values observed in surface and groundwaters were made in order to check the assumptions made in the model and to test the usefulness and the limitations of the map as a tool to easily provide baseline isotope information in these areas.

The methodology developed provides a digital layer of the continuous spatial distribution of $\delta^{18}O$ values in precipitation that, combined with other layers of interest in hydrology (cartographic entities such as lithology or permeability) using GIS technologies, allows the assigning of different isotope characteristics to the precipitation

174
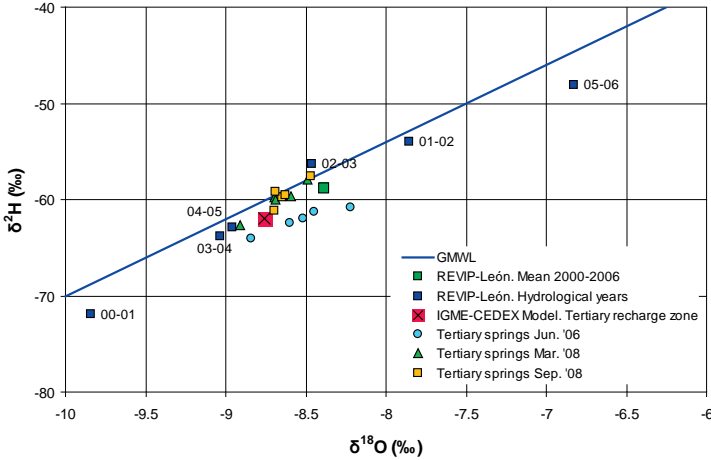
FIG. 2. Comparison of the δ¹⁸O values measured in groundwaters in the city of Burgos against the modelled values in precipitation for the outcropping areas of the geological formations as the potential source of these waters.

input in different potential source areas and compare these against the observed isotope composition of surface and ground waters. Two examples are shown in this paper, in northern Spain, in the surroundings of the city of Burgos, and in a warmer location in central Spain, the Tablas de Daimiel National Park.

Isotope information in precipitation is scarce in the vicinity of Burgos city, where the origin of groundwater is of concern. $\delta^{18}O$ values in groundwater for tertiary aquifers in the area for the years 2006 and 2008 compare well with the modelled composition of precipitation (Fig. 2). Annual and interannual means (period 2000–2006) of $\delta^{18}O$-values in precipitation for León, a nearby REVIP station, are also shown in Fig. 2 for comparison, and highlight the use of the modelled values as a better reference for the area. One of the limitations of the long term model is its difficulty to simulate temporal variations. Modelling for different periods of time may solve this problem.

In the Tablas de Daimiel wetlands, both the origin of surface water and the extent of the trace of evaporated surface water in groundwater are under study. One of the objectives of the studies is to have some water isotope information from the pond water that could be used in correlations with stable isotope data from the sediments in research for climate change. Annual mean (for the period 2000–2006) of $\delta^{18}O$ values in precipitation for Ciudad Real, the closest REVIP station to the area, as well as the isotope composition of surface water in the area sampled at the Cigüela ditch are shown in Fig. 3. All surface water samples fall in an evaporation line that crosses the Global Meteoric Water Line in a point that compares well with both the modelled
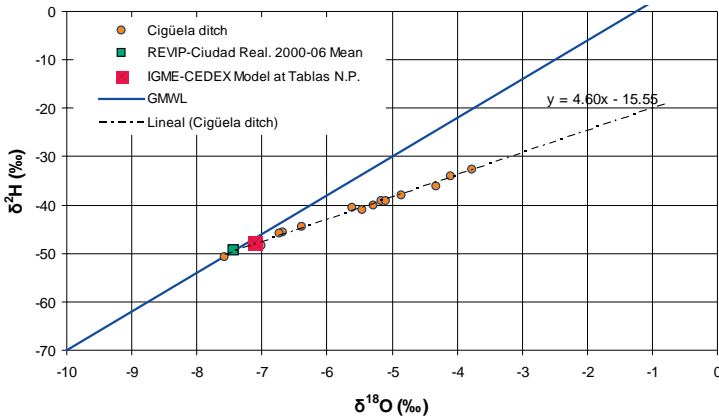
FIG. 3. Comparison of the $\delta^{18}O$ values measured in surface waters in Daimiel National Park against the modelled values in precipitation in the area.

isotopic composition of precipitation in the area and the isotopic composition of precipitation from the closest REVIP station.

6. CONCLUSIONS: LIMITATIONS OF THE REGRESSION MODEL AND FUTURE DEVELOPMENTS

The results obtained so far show a good fit between modelled stable isotope values and those measured in surface and groundwaters from different aquifers and recharge areas. The model seems to provide integrated isotope values for precipitation in areas where direct sampling in meteorological stations is lacking, to trace the sources of water in peninsular Spain. The GIS tools applied to a continuous digital layer of spatial isotope are able to provide accurate information at detailed scales that are not affordable by other means.

These promising results, obtained when the global model was modified to take into account the circumstances of the local scale in this region, are due to the rather simple climatic situation of the country in which the Atlantic Ocean is the main source of water vapour and westerly winds are predominant over the Iberian Peninsula in the long term.

Notwithstanding this, future developments, aimed at further testing the model, are proceeding in order to compare the results of the model with a larger data set of isotope information combining: (1) more recent data from the Spanish network for isotopes in precipitation (REVIP) not yet included in the model; (2) data from the GNIP database for neighbouring countries; (3) isotope data of groundwaters from different sites in Spain covering a wider set of geographic and climatic situations; (4)

isotope information from the Spanish network for isotopes in rivers initiated in 2009; and (5) isotope data of leaky reservoirs.

The validity of the modelling strategy has to be tested case by case before it is applied at the local scale, as far as it depends on the climate and hydrogeological situation of the region under study. Favourable factors for the applicability of these models are the existence of a single or a main source of water vapour for precipitation, and a traceable trajectory of the fronts producing precipitation. Finally, it is important to perform a rigorous comparison between modelled and observed isotope composition of precipitation and other components of the hydrologic cycle in order to test the model and to assess its limitations.

REFERENCES

[1]   INTERNATIONAL ATOMIC ENERGY AGENCY, Stable Isotope Hydrology: Deuterium and Oxygen-18 in the Water Cycle, Technical Report Series No. 210, IAEA, Vienna (1981).

[2]   INTERNATIONAL ATOMIC ENERGY AGENCY, Guidebook on Nuclear Techniques in Hydrology, Technical Report Series No. 91, IAEA, Vienna (1968).

[3]   CLARK, I., FRITZ, P., Environmental Isotopes in Hydrogeology, Lewis Publishers, Boca Raton, Florida (1997).

[4]   BOWEN, G.J., WILKINSON, B.H., Spatial distribution of $\delta^{18}O$ in meteoric precipitation, Geology 30 4 (2002) 315–318.

[5]   PLATA, A., Composición isotópica de las precipitaciones y aguas subterráneas de la Península Ibérica, Monografías, CEDEX, Madrid (1994) (in Spanish).

[6]   DÍAZ-TEIJEIRO, M.F., RODRÍGUEZ-ARÉVALO, J., CASTAÑO, S., La Red Española de Vigilancia de Isótopos en la Precipitación (REVIP): distribución isotópica espacial y aportación al conocimiento del ciclo hidrológico, Ingeniería Civil **155** (2009) 87–97 (in Spanish).

[7]   DÍAZ-TEIJEIRO, M.F., RODRÍGUEZ-ARÉVALO, J., PÉREZ, J.E., CASTAÑO, S., ARAGUÁS, L. "Factors controlling the stable isotopic composition of recent precipitation in Spain", Proc. Int. Symposium Advances in Isotope Hydrology and its Role in Sustainable Water Resources Management (IHS–2007), Vol. 1. IAEA, Vienna (2007) 239–249.

[8]   RODRÍGUEZ-ARÉVALO, J., CASTAÑO, S., DÍAZ-TEIJEIRO, M.F., MARCOS, L.A., VÁZQUEZ-MARROQUÍN, M., Modelo de distribución espacial continua de $\delta^{18}O$ en la precipitación en la provincia de Burgos, Desarrollo de la metodología y aplicación en hidrología, Geogaceta **43** (2007) 79–82 (in Spanish).

MODELLING THE SPATIAL ISOTOPE VARIABILITY OF PRECIPITATION IN SYRIA

Z. KATTAN, B. KATTAA
Department of Geology,
Atomic Energy Commission of Syria (AECS),
Damascus, Syrian Arab Republic.

Abstract

Attempts were made to model the spatial variability of environmental isotope (^{18}O, ^{2}H and ^{3}H) compositions of precipitation in Syria. Rainfall samples periodically collected on a monthly basis from 16 different stations were used for processing and demonstrating the spatial distributions of these isotopes, together with those of deuterium excess (*d*) values. Mathematically, the modelling process was based on applying simple polynomial models that take into consideration the effects of major geographic factors (Lon.E., Lat.N., and altitude). The modelling results of spatial distribution of stable isotopes (^{18}O and ^{2}H) were generally good, as shown from the high correlation coefficients ($R^2 = 0.7$–0.8), calculated between the observed and predicted values. In the case of deuterium excess and tritium distributions, the results were most likely approximates ($R^2 = 0.5$–0.6). Improving the simulation of spatial isotope variability probably requires the incorporation of other local meteorological factors, such as relative air humidity, precipitation amount and vapour pressure, which are supposed to play an important role in such an arid country.

1. INTRODUCTION

The knowledge of spatial and temporal distribution patterns of the environmental isotope (^{2}H, ^{3}H, ^{18}O) compositions in local rainfall forms a primary background data for the proper use of these natural tracers in assessing water resources in terms of recharge origin, replenishment rate, evaporation, mixing process, water–mineral interactions, residence times, and interconnection between the different aquifer systems [1–4]. The application of such isotopes could also provide useful information in evaluating the significance of climate change on local and global scales [5–6].

Climatically, Syria belongs to an arid and semi arid region, and thus it suffers from shortage and intensive imbalance problems in its water resources. As a consequence of the global climate change, the situation of water budget in the country has been dramatically complicated during the last three decades. Therefore, a sharp, continuous and increasing demand of water to cover the different uses was marked, and it has become extremely difficult to fulfill this remarkable deficit in the water budget without finding new water resources. The data of the above mentioned environmental

isotopes of precipitation from selected meteorological stations in Syria was compiled in order to be used later for a better assessment of the availability of water resources in the country, as well as for solving a number of hydrological, hydrogeological, and geochemical problems. This study is initiated to provide the results of modelling the spatial isotope variability of precipitation in Syria.

2.   SAMPLING AND ISOTOPE ANALYSES

Rainfall samples were generally collected from a network covering 16 different stations distributed mostly in the western part of the country (Fig. 1). Sampling from all the stations was made on a monthly basis during different periods, from December 1989 to April 2009. Rainfall samples, collected twice a day, were transferred to a tightly stoppered container to accommodate the monthly amount of precipitation. Paraffin oil was added to the collected samples in order to minimize the effect of evaporation. At the end of the month, three bottles were filled for chemical and isotopic analyses. A bottle of 50 mL was filled for the determination of $\delta^{18}O$ and δ^2H, and the subsequent analyses of samples collected before 2003 were performed in the isotope hydrology lab of Jordan by using a Finnigan Mat delta E mass spectrometer. Rainfall samples collected after 2003 were isotopically analysed in the labs of the Syrian Atomic Energy Commission (AECS) by using a Finnigan Mat DELTA^{Plus} mass spectrometer.
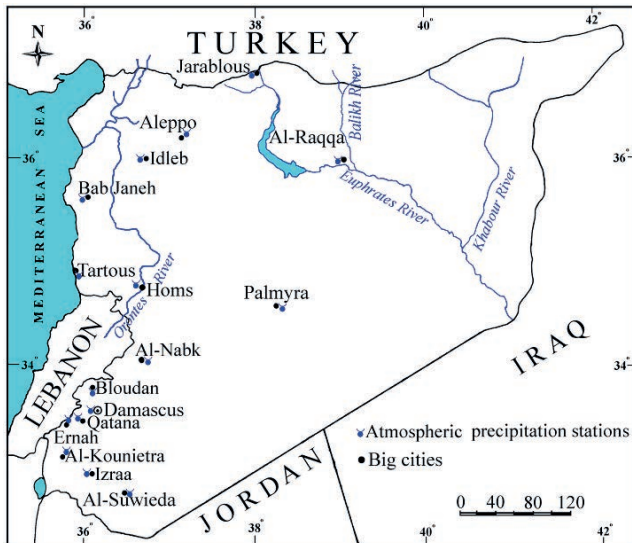
FIG. 1. Location map showing the network of atmospheric precipitation sampling stations in Syria.

A bottle of one litre capacity was filled with rain water for tritium determination, and the related analyses of this radioactive isotope were performed after electrolysis enrichment in the Jordanian lab by using a Packard 3253 liquid scintillation counter (LSC). In the case of analyses conducted in the AECS labs, tritium measurements were performed also after electrolysis by using a Quantulus 1220 LSC instrument. A third bottle of half a litre was filled for carrying out chemical analyses (not discussed in this paper). Measurement accuracy for $\delta^{18}O$ and δ^2H and tritium are $\pm 0.1‰$, $\pm 1.0‰$, versus VSMOW, and $\pm 1\,TU$, respectively.

3. RESULTS AND DISCUSSION

3.1. Characteristics of environmental isotopes

The rainfall isotopic data, compiled for processing and illustrating the spatial isotope variability of precipitation in Syria by using GIS and SURFER software, includes the following parameters: precipitation amount, air temperature, relative humidity, concentrations of stable isotopes (^{18}O and ^2H) and tritium (^3H), together with the deuterium excess (d) values, defined as [7]:

$$d = \delta^2H - 8\,\delta^{18}O \tag{1}$$

The weighted means of isotopic composition for the different monitoring stations were calculated using the following equation [8]:

$$\delta_w = \sum_i^n [P_i \delta_i] / \sum_i^n [P_i] \tag{2}$$

where:
δ_w = weighted mean;
P_i = amount of monthly precipitation;
δ_i = isotopic composition of rainfall for the month i.

The results of the weighted means show that the stable isotope compositions are primarily affected by altitude. Thus, the rainfalls of Bloudan, as the highest station (altitude = 1540 m.a.s.l) were the most depleted in heavy stable isotopes ($\delta^{18}O$ = –8.76‰ and δ^2H = –47.80‰). In contrast, the rains of the coastal station (Tartous) were the most enriched in these isotopes (δ_w = –5.82‰ and –27.90‰ for $\delta^{18}O$ and δ^2H, respectively). As Ernah station is lower in its altitude by ≈110 m than Bloudan, its weighted means were slightly enriched compared with those of Bloudan (Fig. 2). Similarly, the weighted means for Palmyra station, situated in the central Syrian desert, were also enriched (δ_w = –5.81‰ and –28.7‰ for $\delta^{18}O$ and δ^2H, respectively), and very close to those of Tartous.
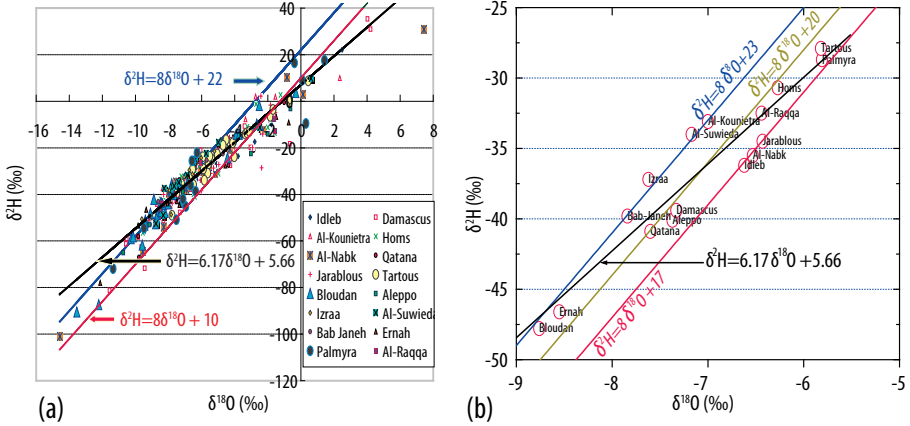
FIG. 2. Relationships between δ^2H and $\delta^{18}O$ values of all rainfall samples collected from the different stations in Syria (a) and of δ^2H and $\delta^{18}O$ values of these samples (b).

Most of the sample points representing all rainfall samples collected from the different stations are distributed between the Mediterranean Meteoric Water Line (MMWL), defined by Ref. [9]: $\delta^2H = 8.\delta^{18}O + 22$ and the Global Meteoric Water Line (GMWL), defined as [7]: $\delta^2H = 8.\delta^{18}O + 10$ (Fig. 2a). Samples situated outside of this range refer mostly to rainfalls affected by evaporation or to samples of low rainfall amounts. The δ^2H–$\delta^{18}O$ relationship of the weighted means of $\delta^{18}O$ and δ^2H concentrations of monthly precipitation samples, generally permits the distinguishing between three different groups (Fig. 2b):

(1) The stations of Bloudan, Ernah, Bab Janeh, Izraa, Al-Suwieda, Al-Kounietra that fit the MMWL ($d = 22$) or a closer regression line with an intercept of $d \approx 23$ instead of $d = 22$;

(2) The stations of Qatana, Aleppo, Damascus, Al-Raqqa, Homs and Tartous that fit a line of $d = 20$;

(3) The remaining interior stations (Idleb, Al-Nabk, Jarablous and Palmyra) fitting a line of $d = 17$.

The equation of the least squares regression line fitting all of the rainfall data is given by:

$$\delta^2H = (6.17 \pm 0.12)\,\delta^{18}O + (5.66 + 0.74) \tag{3}$$

with $R^2 = 0.916$ and $N = 290$

This linear regression, conducted on the analysis of 290 precipitation samples yielded a slope of 6.17 and an intercept of 5.66, with a good correlation coefficient ($R^2 = 0.916$). However, this line differs remarkably from that ($\delta^2H = 8.26\,\delta^{18}O + 19.3$,
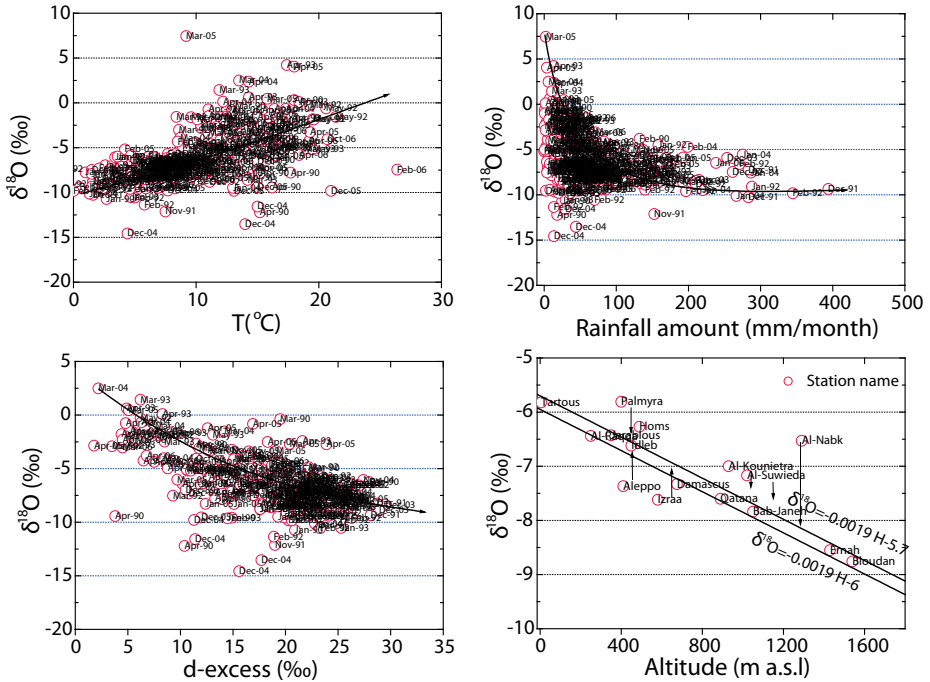
FIG. 3. Relationships between δ¹⁸O and air temperature values (a), between δ¹⁸O values and rainfall amounts (b), between δ¹⁸O and deuterium excess values (c) of all rainfall samples, and between the weighted means of δ¹⁸O and altitude values for the different stations in Syria (d).

with $R^2 = 0.96$ and $N = 43$), defined for the precipitation in Syria collected only during a single rainy season 1989–1990 [10].

The isotopic composition of rainfall is highly scattered between the different stations as a result of many local climatic (temperature, precipitation amount, evaporation and storm trajectory) and topographic (altitude) factors [10]. The interrelations between the different parameters of all rainfall samples were statistically studied and analysed. The plots of δ¹⁸O and δ²H concentrations versus air temperature values clearly show enrichments in the concentration of these stable isotopes with increasing air temperature values (Fig. 3a). Contrariwise, the plots of δ¹⁸O and δ²H concentrations versus precipitation amount values, and δ¹⁸O and δ²H concentrations versus deuterium excess values represent depletions in the concentrations of both isotopes with the increased amount of precipitation and increased *d*-excess values (Fig. 3b and 3c). The altitude effect is represented by a progressive depletion of heavy stable isotopes of about 1.3‰ and 0.19‰ per 100 m for δ²H and δ¹⁸O, respectively (Fig. 3d).
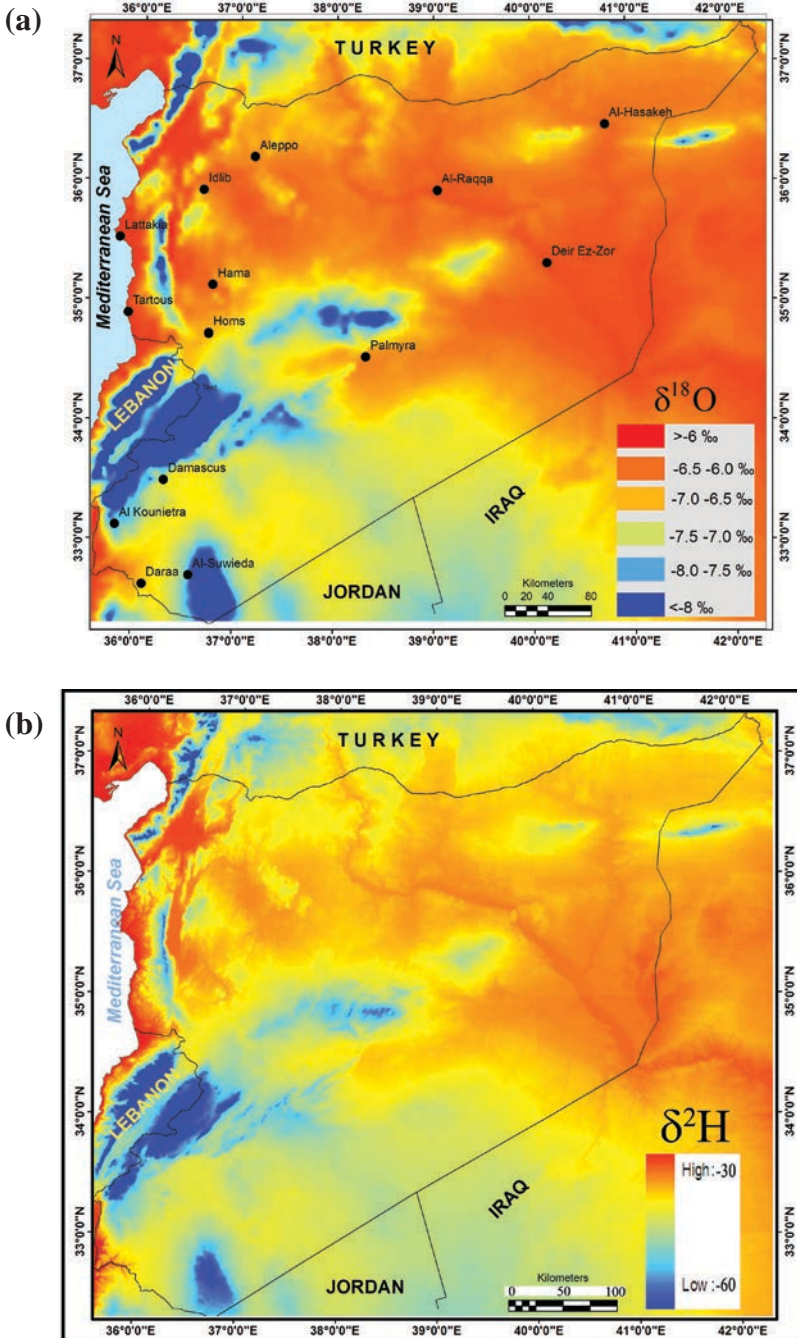
FIG. 4. Modelled spatial distributions of $\delta^{18}O$ (a), δ^2H (b) d-excess (c) values (‰, VSMOW) in Syrian rains, together with those of the tritium content in Syrian precipitation during 2006.

FIG. 4 (cont.). Modelled spatial distributions of $\delta^{18}O$ (a), $\delta^{2}H$ (b) d-excess (c) values (‰, VSMOW) in Syrian rains, together with those of the tritium content in Syrian precipitation during 2006.

185

3.2. Modelling the spatial isotope variability

Modelling the spatial isotope variability of rainfall represents a feasible alternative method for estimating the stable isotope records of certain months or years not yet available or only available for a small number of stations across the world [11]. Extensive efforts have been recently made to model the isotope variability of precipitation by correlating the available data for certain stations with the major geographic parameters (Lon.E., Lat.N., and altitude) to produce high-resolution gridded isotopic data [11–12]. Attempts were made to model the spatial isotope variability of precipitation in Syria. The available data on the environmental isotopes (^{18}O, ^{2}H and ^{3}H) and d-excess (d) values of precipitation in the country were compiled and used in conjunction with other major geographic parameters for processing and gridding the isotopic data of Syrian rainfall in order to be applied later in the GIS plotting methods. Mathematically, this analysis is conducted on the basis of empirical relationships and geostatistical methods. This paper focuses on the creation of acceptable grids of annual weighted means of δ^{18}O, δ^{2}H, deuterium excess (d) values and ^{3}H (only for 2006) of precipitation in Syria. The expressions of the simple polynomial models providing the best gridded isotopic data for the above mentioned isotopic parameters are:

$$\delta^{18}O = 5.2E - 10(lon.E) + 2.56E - 10(lat.N) - 8.53E - 7(alt.)^2 - 6.80 \qquad (4)$$
with $R^2 = 0.794$

$$\delta^{2}H = 5.48E - 7(lon.E) + 9.7E - 8(lat.N) - 5.32E - 6(alt.)^2 - 35.84 \qquad (5)$$
with $R^2 = 0.697$

$$d\text{-}excess = -6.77E - 6(lon.E) + 1.04E - 6(lat.N) - 0.002(alt.) + 24.24 \qquad (6)$$
with $R^2 = 0.483$

$$^{3}H = 3.13E - 5(lon.E) + 3.29E - 10(lon.E)^2 - 0.36 \qquad (7)$$
with $R^2 = 0.566$

The modelling results of spatial distributions of the stable isotopes (^{18}O and ^{2}H) in Syrian rainfall (FIG. 4 a and b) that were generated using the software Arc–GIS–9 were rather good ($R^2 = 0.7 - 0.8$), and clearly reflect the observed isotope variability. The concentrations of these isotopes become more depleted over the high altitude areas and more enriched in the interior lands. However, the maps produced for the distributions of deuterium excess (d) values (all data) and tritium content (only for the data of 2006) that were mapped by using a recent SURFER version (10) were most likely approximates, as can be seen from the moderate correlation coefficients ($R^2 = 0.48 - 0.57$), calculated between the observed and predicted values for the adjusted algorithms. Improving the simulation of the spatial isotope variability requires

most probably the incorporation of other local meteorological factors, such as relative air humidity, precipitation amount, vapour pressure and potential evaporation, that could play an important role in such an arid country. The spatial distribution of *d*-excess values permits the observation that this parameter is high and more than 20‰ in the south-western part of Syria, and gradually decreases towards a value of ≈15‰ in the north-eastern part of the country. The distribution of tritium content is represented by a progressive enrichment in the concentration of this radionuclide with the increasing distance from the coast.

4.   CONCLUSION

The results obtained through the generation of gridded data sets for the isotopic compositions of precipitation in Syria should be considered as approximate and still in need of improvement by adopting more robust models by incorporating other local meteorological factors, such as relative air humidity, precipitation amount, vapour pressure and potential evaporation, that could play an important role in such an arid country. However, despite the fact that no models were adjusted for the above mentioned meteorological parameters, which could be supposed to produce better goodness of fitting than those using the geographical parameters, the obtained modelling results were promising and able to produce acceptable data sets for filling the gap of missed isotopic data of precipitation for certain stations or data set records in the country, not yet covered by the current running programme of monitoring the isotopic composition of rainfall in Syria. The maps of spatial isotope variability in Syrian precipitation could provide better insights and understanding of various hydrological and geochemical processes.

REFERENCES

[1]   CLARK, I., FRITZ, P., Environmental Isotopes in Hydrogeology, Lewis Publishers, Boca Raton, FL (1997) 328 p.
[2]   KENDALL, C., MCDONNELL, J.J., "Isotope tracers in catchment hydrology", (KENDALL, C., MCDONNELL, J.J., Eds), Elsevier Science, Amsterdam (1998) 839 p.

[3]   GAT, J.R., et al., "Environmental isotopes in the hydrological cycle. Principles and applications", IHP-V, Technical Documents in Hydrology (MOOK, W.G., Ed.), No. 39, Vol. II: Atmospheric water. Paris: UNESCO (2001) 113 p.

[4]   AGGARWAL, P.K., GAT, J.R., FROEHLICH K., (Eds), Isotopes in the water cycle, Past, Present and Future of a Developing Science, Springer, Dordrecht (2005) 381 p.

[5]   INTERNATIONAL ATOMIC ENERGY AGENCY, "Deuterium excess in precipitation and its climatological significance", Study of environmental change using isotope techniques, IAEA, Vienna, C&S Papers Series 13/P (2002) 54–65.

[6]   ROZANSKI, K., et al., "Isotopic patterns in modern global precipitation", Geophysical monograph **78** (1993) 1–3.

[7]   DANSGAARD, W., Stable isotopes in precipitation, Tellus **16** (1964) 436–468.

[8]   YURTSEVER, Y., GAT, J.R., Atmospheric waters, Stable isotope hydrology, Deuterium and oxygen-18 in the water cycle, Technical reports series No 210, IAEA, Vienna (1981).

[9]   NIR, A., "Development of isotope methods applied to groundwater hydrology" (Proc. Symp. on Isotope Techniques in the Hydrological Cycle), Am. Geophys. Union Monogr. Series, No 11 (1967).

[10]   KATTAN, Z., Chemical and environmental isotope study of precipitation in Syria, J. Arid Environ. **35** (1997) 601–615.

[11]   LYKOUDIS, S., ARGIRIOU, A., Gridded dataset of the stable isotopic composition of precipitation over the Eastern and Central Mediterranean, J. Geophys. Res. **112** (2007).

[12]   BOWEN, G.J., et al., Global application of stable hydrogen and oxygen isotopes to wildlife forensics, Oecologia **143** (2005) 337–348.

TOWARD A MECHANISTIC UNDERSTANDING OF DEUTERIUM EXCESS AS A TRACER FOR EVAPOTRANSPIRATION

CHUN-TA LAI
Department of Biology,
San Diego State University,
San Diego, CA, USA

Abstract

An understanding of atmospheric water vapour and its isotopic composition is useful for modelling effects of terrestrial evapotranspiration on regional hydrologic cycles. Previous studies showed diurnal and vertical patterns of water vapour isotope ratios (δ^2H_v and $\delta^{18}O_v$) consistently observed in an old growth coniferous forest. Using a box model and a mass balance approach to simulate 'isoflux of d-excess', the effect of evapotranspiration on the d-excess in atmospheric water vapour is quantitatively demonstrated. The results suggest that d-excess can be mechanistically utilized to identify processes that contribute to the diurnal variation in atmospheric moisture. These new findings have implications for larger-scale predictions of precipitation across the terrestrial landscape. In this paper, I report the initial results of the δ^2H_v and $\delta^{18}O_v$ measurements using a cavity enhanced spectroscopy instrument. These recent data are consistent with the pattern observed by the conventional sampling method, providing new opportunities for studying d-excess as a tracer for evapotranspiration.

1. INTRODUCTION

Water recycling over continents plays an important role in the global climate. Modelling studies showed that, on average, terrestrial evapotranspiration contributes no less than 40% of precipitation on land [1]. The relative contributions of transpiration and evaporation from soil or water surfaces, however, remain largely uncertain. In that regard, stable isotope analyses of precipitation and atmospheric water vapour provide a unique and complementary approach to validate satellite based estimates [2–3].

Atmospheric water vapour contains fewer amounts of heavier water isotopes (^2H and ^{18}O) relative to the source water. This is because under the same temperature, saturation vapour pressure is lower for heavier isotopes than for their lighter counterparts. A second effect that augments the fractionation during evaporation is the kinetic (diffusional) difference between masses. In the case of surface water loss via vegetation (transpiration), this preferential loss of heavier water isotopologues results in enriched ^2H and ^{18}O contents in leaf water. The leaf water ^{18}O signal was used to

study biosphere–atmosphere water and carbon dioxide exchange processes spanning from ecosystem to global scales [4–6]. The net effect of vegetation on the isotopic composition of water vapour and its feedback to atmospheric moisture cycling is not very well understood.

Our knowledge regarding the effect of surface evapotranspiration on the ^{2}H and ^{18}O variation in atmospheric water vapour has been limited by the lack of uninterrupted water vapour isotope measurements. Conventional methods for vapour ^{18}O measurements require cryogenic trapping (usually with liquid nitrogen or dry ice), which limits the number of sample collections in the field [7]. New laser techniques that offer near continuous measurements of water vapour isotopes provide a means to overcome this observational challenge [8–10], and are poised to provide new insights into vapour isotope variation. This paper builds on previous research in which diel δ^2H_v and $\delta^{18}O_v$ measurements were made during short summer field campaigns in an old growth coniferous forest in the Pacific Northwest of the United States. Beginning in September 2010, hourly δ^2H_v and $\delta^{18}O_v$ measurements have been made available by a cavity enhanced spectroscopy analyser at this site. This paper presents a summary of instrument performance, the sampling and calibration protocol, and initial results consistent with previous findings reported by Refs [11–12].

2.   MATERIALS AND METHODS

2.1. Study site

The study site is located within the Wind River Experimental Forest, an old growth (~500 years in age) coniferous forest in the southern part of the State of Washington, U.S.A (45°49.227' N 121°57.125' W; elevation = 371 m). This region is characterized by a maritime Pacific climate with dry summer and wet winter periods. The mean annual temperature is 8.7°C, and mean annual precipitation is 2467 mm with < 5% falling between June and August; hence a significant decline in surface soil moisture occurs through the summer (Fig. 1). Stand leaf area index was estimated as 8.6, with ~56% distributed in the middle and upper canopy. Soils were classified as sandy loams of volcanic origin. The dominant overstorey species are *Pseudotsuga menziesii* (Douglas fir), *Tsuga heterophylla* (western hemlock) and *Thuja plicata* (western red cedar). There is a diverse group of understorey species, which includes western hemlock, *Acer circinatum* (vine maple), *Abies amabilis* (Pacific Silver fir), and *Taxus brevifolia* (Pacific yew). The average tree height was 52 m for Douglas fir and 19 m for western hemlock.
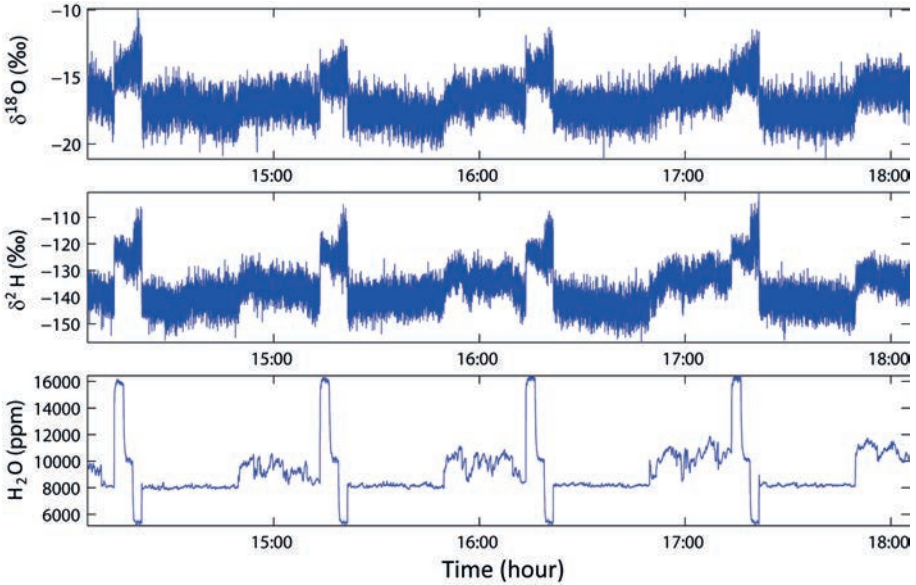
FIG. 1. An example of the uncorrected δ¹⁸Ov, δ²Hv and water vapour concentrations sampled at 2 Hz. Each hour, the ambient air was sampled from 4 inlets, each for 10 minutes. References gases were introduced at 3 concentration levels (5500, 10000 and 16000 ppm), each for 260 s.

2.2. Previous δ^2H_v and $\delta^{18}O_v$ research in Wind River Forest

Lai et al. [11] observed a midday depression (3 to 4‰ more negative compared to the rest of the day) in the average, within canopy $\delta^{18}O_v$ in this old growth coniferous forest. This diurnal pattern was confirmed by the observations in a follow-up experiment in which δ^2H_v and $\delta^{18}O_v$ within and above the canopy were measured every 3 hours for 3 consecutive days [12]. Their results suggest that water vapour isotope ratios are influenced by the combined effect of atmospheric entrainment from the upper atmosphere, transpiration and evaporation from the forest floor. Lai et al. [11] developed a simple canopy box model that has been shown to adequately explain the observed temporal δ^2H_v and $\delta^{18}O_v$ patterns [12].

2.2.1. Atmospheric Water balance in Forest

Atmospheric H_2O balance within a forest can be written as:

$$M_c \frac{dv_c}{dt} = F_+ - F_- + F_T + F_E \qquad (1)$$

where M_c represents the number of moles of air in the column per unit ground area, v_c is the average mole fraction of water vapour in the column, F represents component fluxes; F_+ is one-way flux of water vapour entering the canopy, F_- is the flux of water vapour leaving the top of the canopy, and F_T and F_E are fluxes of transpiration and evaporation, respectively. A mass balance equation can also be written for water isotopologues ($H_2^{18}O$ and HDO) as

$$M_c \frac{dR_c v_c}{dt} = R_+ F_+ - R_- F_- + R_T F_T + R_E F_E \tag{2}$$

where R represents the heavy to light isotope ratios for oxygen or hydrogen isotopologues (i.e. $H_2^{18}O/H_2^{16}O$ or HDO/H_2O). The subscripts c, $+$, $-$, T and E represent water fluxes and R values in the canopy air column, of the atmosphere above, of air venting out of the column, transpiration flux and evaporation flux, respectively. Multiplying Eq. (1) by R_c and subtracting from Eq. (2), an 'isoflux' mass balance equation that describes the time evolution of the isotope composition of water vapour within plant canopies can be derived:

$$M_c v_c \frac{d\delta_c}{dt} = (\delta_+ - \delta_c)F_+ + (\delta_T - \delta_c)F_T + (\delta_E - \delta_c)F_E \tag{3}$$

Previous research in the Wind River Forest relied on the conventional cryogenic trapping method [7] for sample collection. Beginning in September 2010, an off-axis integrated cavity output spectroscopy instrument (Los Gatos Research Inc., Mountain View, CA, USA) was installed for in situ, uninterrupted δ^2H_v and $\delta^{18}O_v$ measurements. In this paper, I report the initial results from the spectroscopy instrument. The instrument first underwent a suite of tests in the laboratory before being deployed in the field. Laboratory experiment showed that with careful calibrations, the LGR analyser was able to produce accurate (± 0.02‰ for $\delta^{18}O$, ± 0.2‰ for δ^2H) and precise (± 0.3‰ for $\delta^{18}O$, ± 3.0‰ for δ^2H) measurements [13]. Here I will focus on results derived from the field experiment conducted in the Wind River Forest in September 2010.

2.3. Spectroscopy analyser for measuring δ^2H_v and $\delta^{18}O_v$

Ambient air was drawn from 3 different heights (1 m, 10 m and 60 m) through 6.35 mm diameter PTFE tubing using a diaphragm pump at a flow rate of 0.5 L/min (KNF Neuberger Model UN811 KNI, 115V, 60Hz). A customized heated PTFE tube (Clayborn Lab, Truckee, CA, USA) was separately installed at 1 m to evaluate the potential cooling effect that may cause condensation in the 3 unheated tubes. All 4 tubes were routed into a manifold housing solenoid values (Clippard single-sided 6-station manifold and EV, normally closed, 2-way, manifold mount, 12V) inside a dry shack below the crane tower. A datalogger (CR3000, Campbell Scientific Inc, Logan, UT, USA) controls the switching of the solenoid values. The solenoids were
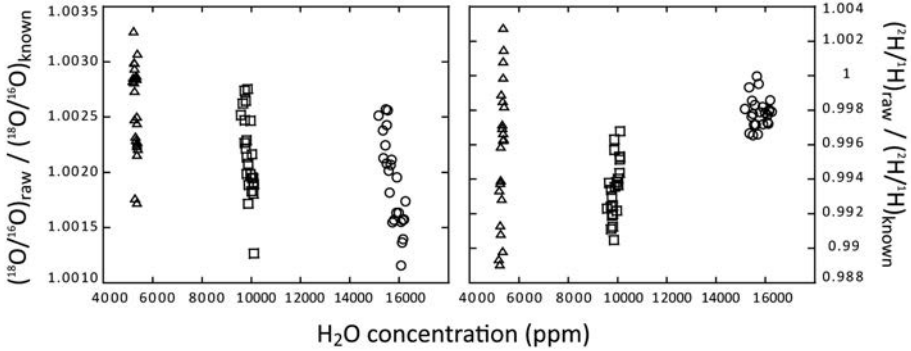
FIG. 2. Hour-to-hour variability of the WVISS-generated reference gases on a typical day. Reference gases were introduced into the water vapour isotope analyser at 3 concentration levels in a 20-minute calibration window at hourly intervals.

coordinated to pass ambient air for 10 minutes from each of the 4 tubes into the LGR water vapour isotope analyser. This leaves 20 minutes per hour for calibration. Fig. 1 shows an example of the uncorrected $\delta^{18}O_v$, δ^2H_v and water vapour concentrations sampled at 2 Hz by the LGR water vapour isotope analyser.

The hourly, online calibration was made possible by accompanying a Water Vapour Isotope Standard Source unit (WVISS, Los Gatos Research) with the analyser. The WVISS uses a nebulizer to inject a miniscule water droplet from a large reservoir of reference water into a heated chamber, providing complete vaporisation without fractionation of the reference water. With a WVISS, reference gases and ambient air can be run in parallel, performing in situ, unattended calibrations, suitable for long term data acquisition. In this study, we used a 3 point calibration protocol that spanned a range of water vapour concentrations that bracketed those observed in the ambient air. Reference gases were introduced at 3 concentration levels (roughly at 5500, 10 000 and 16 000 ppm), each for 260 s, to generate a 2nd order polynomial calibration curve every hour. Ambient air sampled within the hour was then calibrated based on the hourly calibration curves. This regular calibration duty cycle was found necessary in the laboratory experiment [13]. Under field conditions, the WVISS generated reference gases showed large hour-to-hour variability (Fig. 2). The behaviour of the variability appeared different for ^2H when compared to ^{18}O. The uncorrected ^{18}O tend to overestimate while uncorrected ^2H tend to underestimate the known isotope ratios in the reference water. The ^{18}O and ^2H showed an hour-to-hour variation in the range of 2‰ and 14‰, respectively, over a 24 hour period. The analyser appeared to perform better for ^2H at higher concentrations but no apparent concentration dependent effect was noted for ^{18}O. These fluctuations in the reference gases lead to the necessity of frequent (no longer than hourly) calibrations of the LGR water vapour isotope analyser.

3. RESULTS AND DISCUSSION

3.1. Observed d-excess near the forest floor

With regular and careful calibrations, high precision δ^2H_v and $\delta^{18}O_v$ measurements were made at hourly intervals from three heights within and above the Wind River Forest canopy. From these continuous data, deuterium-excess, defined by [14] as $d = \delta^2H - 8 \times \delta^{18}O$, was derived for water vapour observed at all heights. Variations in the d-excess have been shown to qualitatively identify the origin of vapour sources [15]. Angert et al. [16] showed seasonal fluctuations in the d-excess value influenced by the evaporation over the Mediterranean Sea based on near surface water vapour samples collected in an eastern Mediterranean location. Rarely diurnal fluctuations in d-excess have been reported.

Fig. 3 shows the comparison of the d-excess values observed at 1 m above the ground between a heated and an unheated sampling tube. There was a high correlation between the two measurements. The unheated tube captures the diel pattern in the d-excess near the forest floor almost identically to that observed from the hot tube (data not shown). I must note that the two sampling tubes were not equal: the hot tube was only 1m long while the unheated tube was about 25 m in length, extended away from the footprint of the dry shack. The 14% difference in the slope of the regression line likely reflects the source difference because of the local heterogeneity. If condensation had occurred, the fractionation effect would have systematically biased the observed d-excess in a more pronounced fashion due to the long pathlength an air
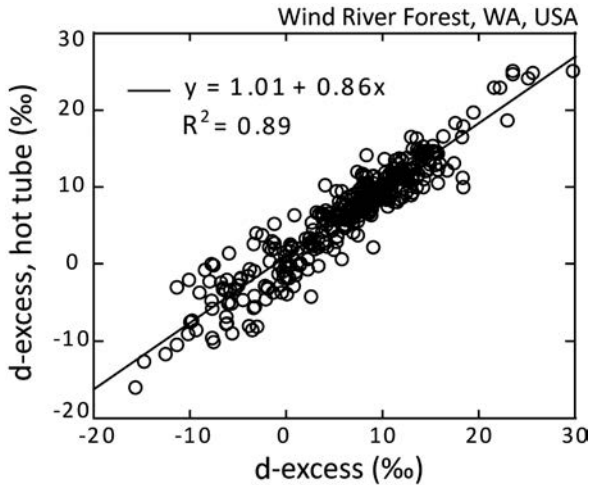
FIG. 3. *Comparison of the d-excess values observed at 1 m above the ground between a heated and an unheated sampling tube (n=168). The comparison includes hourly data collected over a week (September 3–9, 2010; n=168). The 'hot' tube was heated to 5°C above the ambient temperature during the experiment.*

parcel has to travel through the unheated tube. The measured d-excess near the forest floor ranged from –18‰ to 30‰ during this weeklong period, with the majority of the d-excess values clustered between 5‰ and 18‰.

3.2. Observed diel patterns of d-excess in forest canopy

Lai and Ehleringer [12] observed a diel pattern of the d-excess values in atmospheric water vapour from samples collected by cryogenic traps. The d-excess values showed a repeated diel pattern with the lowest values occurring in the early morning and the highest values occurring at midday in a short (3 day) experiment. It is not known whether this diel pattern can consistently be detected and if an optical instrument can reliably capture a similar pattern. Fig. 4 shows the average d-excess values derived from water vapour measurements made near the forest floor and above the canopy.

Similar to the findings reported by Lai and Ehleringer [12], the d-excess values showed a diel fluctuation. The d-excess values ranged from –18‰ in the early morning to over 30‰ at midday during this period. Observations at the two heights showed similar diel patterns, with the d-excess values near the forest floor being slightly lower than those above the canopy on a few occasions.

The initial results shown here are consistent with the previous findings. Using a canopy water balance model (Eq. 3), Lai and Ehleringer [12] demonstrated that atmospheric entrainment appears to drive the isotopic variation of water vapour in the early morning when the convective boundary layer rapidly develops, while evapotranspiration becomes more important in the mid-afternoon as a primary moisture source of water vapour in this forest. With careful and frequent calibrations,
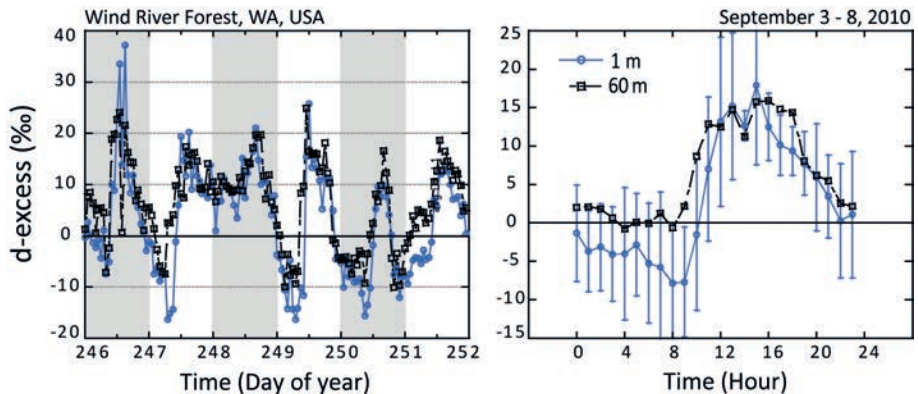
FIG. 4. The average d-excess values derived from water vapour measurements made near the forest floor (1 m) and above the canopy (60 m). The right panel shows the ensemble average from the hourly averages over the 6 days. For clarity, only the data collected at 1 m show 1 S.D. around the mean.

cavity-enhanced spectroscopy isotope analyser enables in situ, high precision monitoring of water isotope ratios, opening new doors for isotope hydrological research.

4.. CONCLUSIONS AND FUTURE RESEARCH

Future research should aim towards a more complete understanding of how land processes influence short term variations in water vapour distribution and its stable isotope contents as continuous, event based water isotope measurements become more affordable. Considerable improvement on our understanding of the biotic and abiotic controls of the ^{18}O and ^{2}H variation associated with evapotranspirational fluxes can be expected. However, careful attention and routine calibrations of laser based instruments are necessary to ensure data quality and compatibility.

ACKNOWLEDGEMENTS

REFERENCES

[1]   VAN DER ENT, R.J., et al., Origin and fate of atmospheric moisture over continents, Water Res. Resour. **46** (2010) W09525.

[2]   GAT, J., Oxygen and hydrogen isotopes in hydrological cycle, Annu. Rev. Earth Planet. Sci. **24** (1996) 225–62.

[3]   WORDEN, J., NOONE, D., BOWMAN, K., Importance of rain evaporation and continental convection in the tropical water cycle, Nature **445** (2007) 528–532.

[4]   FARQUHAR, G.D., et al., Vegetation effects on the isotope composition of oxygen in atmospheric CO$_2$, Nature **363** (1993) 439.

[5]   WANG, X-F., YAKIR, D., Using stable isotopes of water in evapotranspiration studies, Hydrol. Process. **14** (2000) 1407–1421.

[6]   LAI, C-T., RILEY, W., OWENSBY, C., HAM, J., SCHAUER, A., EHLERINGER, J., Seasonal and interannual variations of carbon and oxygen isotopes of respired CO$_2$ in a tallgrass prairie: Measurements and modelling results from three years with contrasting water availability, J. Geophys. Res. **111** (2006) D08S06.

[7]   HELLIKER, B.R., RODEN, J.R., COOK, C., EHLERINGER, J.R., A rapid and precise method for sampling and determining the oxygen isotope ratio of atmospheric water vapour, Rapid Commun Mass Spectrom **16** (2002) 929–932.

[8]   LEE, X., SARGENT, S., SMITH, R., TANNER, B., In situ measurement of water vapour ^{18}O/^{16}O isotope ratio for atmospheric and ecological applications, J. Atm. Ocean. Tech. **22** (2005) 555–565.

[9]   STURM, P., KNOHL, A., Water vapour δ^2H and δ^{18}O measurements using off-axis integrated cavity output spectroscopy, Atmos. Meas. Tech. **3** (2010) 67.

[10]   IANNONE, R.Q., et al., Water isotope ratio (δ^2H and δ^{18}O) measurements in atmospheric moisture using an optical feedback cavity enhanced absorption laser spectrometer, J. Geophys. Res. **115** (2010) D10111.

[11]   LAI, C.-T., et al., Contributions of evaporation, isotopic non-steady state transpiration, and atmospheric mixing on the δ^{18}O of water vapour in Pacific Northwest coniferous forests, Plant. Cell. Environ. **29** (2006) 77.

[12]   LAI, C.-T., EHLERINGER, J.R., Deuterium excess reveals diurnal sources of water vapour in forest air, Oecologia **165** (2011) 213.

[13]   RAMBO, J., et al., On-site calibration and high-precision measurements of water vapour isotope ratios using an off-axis cavity-enhanced absorption spectroscopy, Atmos. Ocean. Tech. **28** (2011).

[14]   DANSGAARD, W., Stable isotopes in precipitation, Tellus **16** (1964) 436.

[15]   GAT, J.R., Atmospheric water balance — the isotopic perspective, Hydrol. Process. **14** (2000) 1357

[16]   ANGERT, A., et al. Seasonal variations in the isotopic composition of near-surface water vapour in the eastern Mediterranean, Tellus **60** (2008) 674.

SEASONAL VARIATIONS IN STABLE ISOTOPE RATIOS OF OXYGEN AND HYDROGEN IN TWO TUNDRA RIVERS IN NE EUROPEAN RUSSIA

E. HUITU [a], E. SONNINEN [b], L. ARVOLA [a]

[a] Lammi Biological Station,
   University of Helsinki, Finland

[b] Radiocarbon Dating Laboratory,
   University of Helsinki, Finland

Abstract

The variability in stable isotope ratios of oxygen and hydrogen ($\delta^{18}O$ and δ^2H values) in river waters in northeast European Russia was studied for the period from July 2007 to October 2008. Exceptional isotope composition in precipitation obtained during the sampling period was clearly traced in the composition of river waters. Water from permafrost thawing did not make a great contribution to river flow.

1.   INTRODUCTION

The two sampled rivers, Usa and Sedyaga, are on the tundra of Komi Republic in northern European Russia (67°N, 62°E) in the zone of discontinuous permafrost. The Usa River has its sources in the polar Urals and runs south into the Pechora River, which drains to the Barents Sea. The whole catchment area of the Usa River is 93 600 km² and the catchment area above the sampling site at the Seida village is 14 100 km². The river Sedyaga is a small tributary of the Usa River with a recharging area of 199 km². The river Sedyaga flows into the Usa River 5 km downstream of the village of Seida, the sampling site of precipitation and local well water.

2.   STABLE ISOTOPE CONTENT

The $\delta^{18}O$ and δ^2H values in both river waters showed distinct seasonal variations similar in both rivers and for both years having their lowest values in spring and early summer and their highest in autumn. The values in May 2008 were for $\delta^{18}O$ –16.1‰ and for δ^2H –113‰ in the large River Usa, and –18.1‰ and –129‰, in the small River Sedyaga respectively. The minimum values coincided with the increased discharge, the input of snowmelt water with low isotope values typical
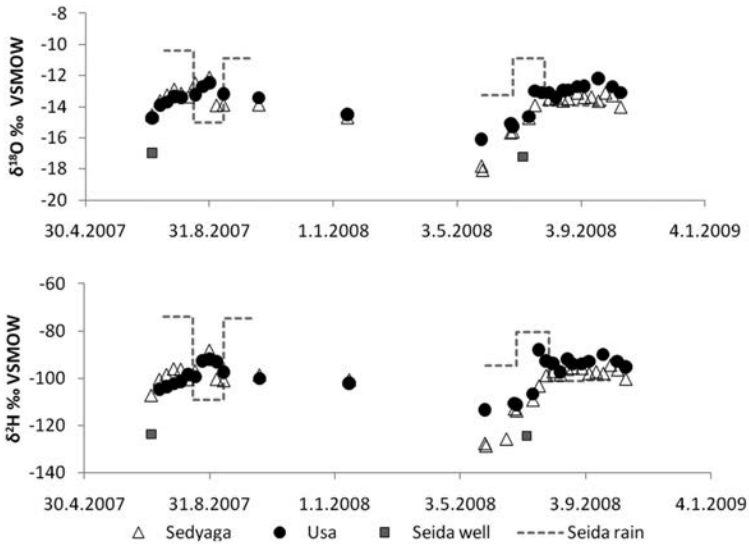
FIG. 1. The $\delta^{18}O$ and $\delta^{2}H$ values in waters sampled from Jul 2007 to Oct 2008 in the river Usa (filled circles) and Sedyaga (open triangles), in monthly accumulated rain (dotted line) and in water from a local well (grey filled squares) collected at Seida, close to the rivers.

for winter precipitation at the middle and high latitudes in continental areas. After the impact of the snow melt pulse later in the summer isotope values in the river waters steadily increased, and at the end of August were in the large River Usa approx.−13.0‰ for $\delta^{18}O$ and approx. −95‰ for $\delta^{2}H$ in both years and in the small River Sedyaga −12.4‰ for $\delta^{18}O$ and −88‰ for $\delta^{2}H$ in 2007, and $\delta^{18}O$ value 1‰ and $\delta^{2}H$ value 9‰ lower in 2008 because of the lower values in precipitation. The highest values observed in late summer could be connected to increased evaporation from river waters and increased input of summer precipitation. The relation between $\delta^{18}O$ and $\delta^{2}H$ values suggests that evaporation has a small role in summer runoff. In addition, exceptional isotope composition in precipitation obtained during the sampling period was traced clearly in the composition of the river waters.

Similar seasonal variations, with low values in spring and increasing values towards the end of summer, have been documented in the isotope ratios of several Arctic rivers [1–3].

3. CONCLUSIONS

The $\delta^{18}O$ and $\delta^{2}H$ values in late summer were clearly higher than the values in the water of a local well, c. −17‰ for $\delta^{18}O$ and −126‰ for $\delta^{2}H$ and in base flow

water, –14.6‰ and –102‰, respectively (sampled in January 2008). Thus water from permafrost thawing did not make a great contribution to river flow.

ACKNOWLEDGEMENTS

REFERENCES

[1]   WELP, L.R., et al., A high-resolution time series of oxygen isotopes from the Kolyma River: Implications for the seasonal dynamics of discharge and basin-scale water use, Geophys. Res. Lett. **32** (2005) L14401.

[2]   HAYASHI, M., et al., Hydrologic functions of wetlands in a discontinuous permafrost basin indicated by isotopic and chemical signatures, J. Hydrol. **296** (2004) 81–97.

[3]   COOPER, L.W., et al., Flow-weighted values of runoff tracers ($\delta^{18}O$, DOC, Ba, alkalinity) from the six largest Arctic rivers, Geophys. Res. Lett. **35** (2008) L18606.

USE OF ISOTOPIC DATA TO DETERMINE INFLUENCE OF SEASONAL EFFECTS IN RIVERS

R.L. MICHEL
US Geological Survey,
Menlo Park, CA , USA

P.K. AGGARWAL, L. ARAGUÁS ARAGUÁS, B. NEWMAN, T. KURTTAS
International Atomic Energy Agency,
Vienna, Austria

Abstract

In 2002 the International Atomic Energy Agency and its Member States initiated a programme for the collection and measurement of isotopes (stable isotopes of water and tritium) in river waters. The purpose of this programme is to establish a long term database (GNIR) similar to the global database currently available for precipitation. These isotopic data provide a baseline for studying parameters in hydrologic basins that can be used to monitor any changes in the basin response due to shifts in future climatic or land use factors. Below, selected ^{18}O and tritium data sets where measurements from several years of routine sampling are available are analysed. A ratio of the average monthly isotopic concentration divided by the average yearly concentration is used to normalize data and makes it possible to compare data from different sites. In general, high flow periods are strongly influenced by younger water whereas baseflow is primarily composed of water of greater age (probably decadal). Using this approach and flow rates, it should be possible to estimate the isotopic concentrations of baseflow. This data set will make it possible to track changes in baseflow concentrations occurring due to future changes in climate or land use.

1.   INTRODUCTION

Water isotopes have been extremely useful in studying physical processes in the hydrosphere. Initial efforts by the International Atomic Energy Agency resulted in the formation of a precipitation network for measuring stable isotopes of water and/or tritium in precipitation that resulted in the Global Network of Isotopes in Precipitation (GNIP). The database available in GNIP has provided an input function for studies of physical processes in hydrologic sciences [1]. In hydrology, both the stable isotopes of water and tritium have been used extensively since the 1960s to study issues related to water sources, flow paths, timescales and other physical processes [2, 3].

For many hydrological studies, particularly in urban and agricultural areas, the source of the water is not precipitation but river water. In particular, it was noted that in surface water hydrology, long term databases provide useful information about hydrologic parameters of rivers and lakes [4–9]. In 2002 the International Atomic Energy Agency and its member states initiated a programme for the collection and measurement of isotopes in river waters [10]. The purpose of this programme is to establish a long term database (GNIR) similar to the global database currently available for precipitation. These data are providing a baseline for studying parameters in hydrologic basins and monitoring any changes in the basin response due to shifts in climatic or land use factors. Below we discuss some of the initial findings of this programme.

2. GLOBAL DISTRIBUTIONS

There is a significant variation of isotopic values with latitude, with tropical latitudes having the heaviest isotopic range and polar rivers being the lightest. Most of the present GNIR data (>80%) comes from stations in the Northern Hemisphere. Fig. 1 shows a plot of D versus ^{18}O for all the data from the database divided into 3 groups, >20°N, 20°N–20°S and >20°S. The northern rivers are uniformly lighter than the two other groupings. The >20°S group is somewhat biased to the heavier isotope ratios due to the sampling of some rivers in arid areas where large evaporation effects occur. Equivalent systems make up a much smaller fraction of the rivers sampled in the Northern Hemisphere. However, it is evident that rivers in the equatorial
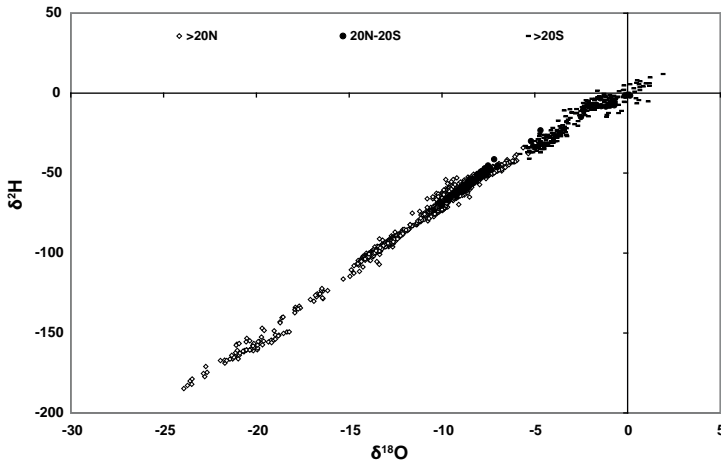
FIG. 1. Plot of $\delta^{18}O$ versus δ^2H for the rivers in the GNIR data base. Plot is broken out into three latitude bands: >20°N, 20°N–20°S and >20°S. All values in ‰.
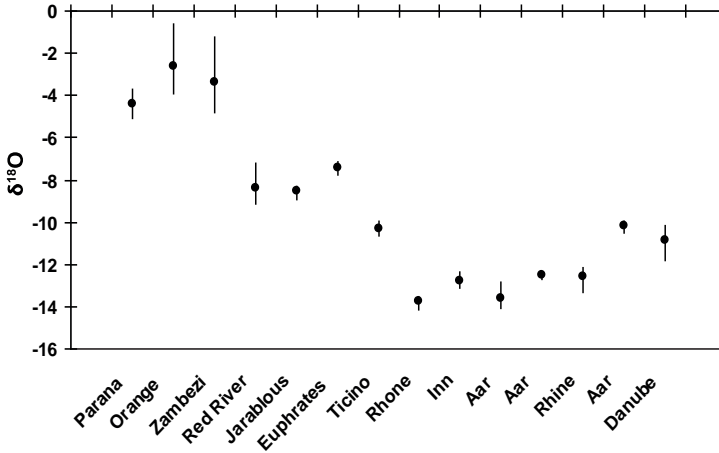
FIG. 2. δ¹⁸O (‰) for selected stations in the GNIR programme with maximum and minimum values. Stations are arranged by latitude with the most southern station (Parana in Argentina) on the left.

region and Southern Hemisphere tend to be heavier due both to heavier precipitation and evaporation factors. Another factor that influences the Southern Hemisphere data is the lack of large continental land masses at higher latitudes in the south. Thus the oceanographic influence will be much higher in many of these areas resulting in a heavier isotopic concentration range in precipitation.

A group of stations which have sufficiently long records of stable isotope data on a monthly basis have been plotted together in Fig. 2. The plot shows the average ¹⁸O values over the period when measurements were made with the range of monthly average values demonstrated by the bars. The southernmost station (Parana) is on the left with stations becoming more northern as they go to the right (the distance between points on the graph do not represent distance). The rivers between the Ticino and the Danube are essentially from a very small latitudinal range in Central Europe. Thus, they have similar isotopic values which are much more depleted than the southern rivers. The Aar at Thun is dominated by Lake Thun and shows little variation. The range for the Euphrates River at Jarablous and the Euphrates Dam are also damped by upstream impoundments. This has a major impact on the isotopic values and variations in this river as stated in Ref. [11]. The heaviest stations are in arid areas of Africa, the Zambezi and Orange Rivers, and they also have the widest range of monthly average values.

3.   APPROACH

One approach to determining if similar processes are impacting rivers from different latitude ranges and climatic regimes (and thus isotopic ranges) is to normalize

the data. This is done by calculating the average yearly isotopic ratio from monthly data for the period of measurements. The average isotopic value for each month over the years of measurement is also calculated. Then the average monthly value is divided by the yearly average. Monthly isotopic ratios will vary due to changes in the relative influence of baseflow and precipitation in the total flow. The influence of these factors in a given month can vary from year to year. The use of several years of measurements will dampen out the occasional outlier and give a truer picture of the general yearly variations in isotopic values for the river. Ratios greater than one are more negative than average, indicating lighter isotope values for those months. Conversely numbers less than one indicate a heavier isotopic value for those months. The same approach can be applied to tritium data with a correction made for the general decline of tritium concentrations with time. This correction is especially relevant in the Northern Hemisphere where the influence of the bomb-tritium pulse is still noticeable. This approach also provides a method to compare the ^{18}O and tritium values from the same river system.

4.   RESULTS

4.1. Global comparison

The above approach has been carried out for ^{18}O from a selected range of rivers in the programme encompassing several different continents. Three of the rivers are shown in Fig. 3: the Danube River at Vienna, Austria, the Parana River in Argentina, and the Zambezi River at Victoria Falls. In general, the wet season will have the highest flow and the greatest ratio (i.e. the lightest stable isotopic ratio) and the dry season will have a stable isotopic composition closer to that of baseflow (generally a heavier isotopic ratio). The Zambezi, which is subject to extremes in evaporation and during the wet seasons, shows the highest variance of the ratio as to be expected from Fig. 2. The other two rivers have much smaller variations with the highest ratios seen during the period of highest flow. The other two rivers have a smaller variation in the ratios, but still have distinct seasonal variations over a period of several years.

Fig. 4 is a similar plot for three rivers from Central Europe, the Danube at Vienna and the Aar at Brugg and at Thun.

4.2. Combined use of tritium and stable isotopic ratios

The same approach of using the ratio of the monthly concentration divided by the average yearly concentration can be applied to normalize tritium data with the provision that the general decline in tritium concentrations over time be taken into account and no contamination from nuclear power plants is present. The tritium ratios can then be compared to the stable isotope ratios. An example of these
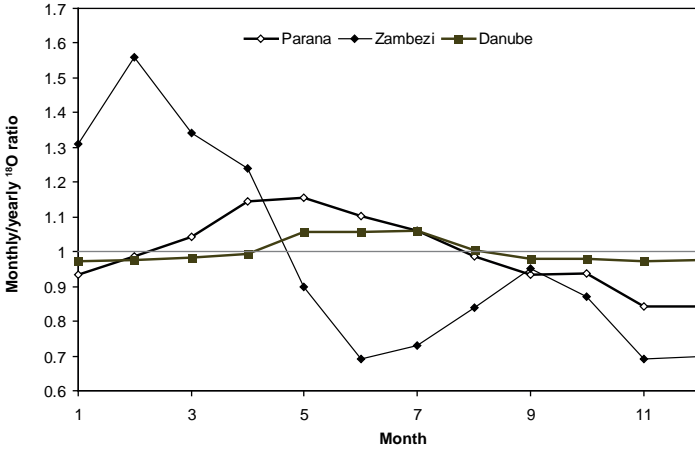
FIG. 3. Ratio of the monthly values of δ¹⁸O divided by the yearly values of δ¹⁸O. Stations are on the Danube River at Vienna, Austria; the Parana River in Argentina; and the Zambesi River at Victoria Falls. Results are plotted monthly.
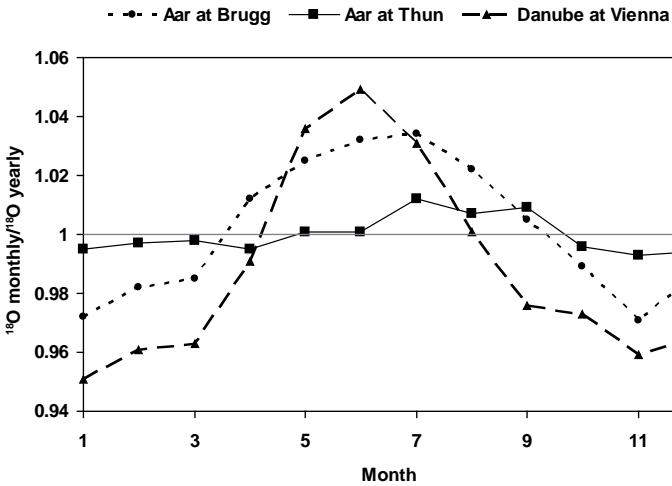
FIG. 4. Monthly isotopic ratios divided by yearly isotopic ratios for three rivers in Central Europe: the Aar at Brugg, the Aar at Thun, and the Danube at Vienna. Results plotted monthly.

comparisons can be seen in figures 5a and 5b which compares the monthly ratios of tritium and ¹⁸O for the Ticino River in Switzerland and the Colorado River at Cisco, Utah over a time span of several years. Both rivers are in the Northern Hemisphere and have several similarities. Stable isotopic ratios are lightest in the spring and early summer due to the influence of snow melt and spring rains which tend to be depleted isotopically. Tritium concentrations are also lowest in the spring. This is due to the influx of younger water from snow and recent rains which has a lower tritium
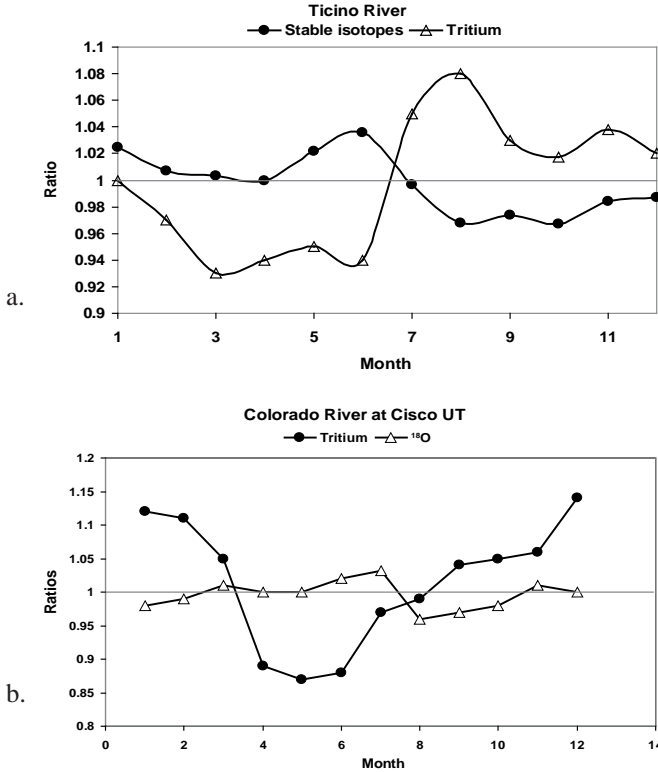
FIG. 5. (a). Ratios for monthly $\delta^{18}O$ and tritium divided by the respective yearly average for the Ticino River at Riazinno in Switzerland. (b). Ratios for monthly $\delta^{18}O$ and tritium divided by the respective yearly average for the Colorado River at Cisco, Utah

concentration than baseflow for most Northern Hemisphere rivers [9]. The baseflow is generally composed of water that has been retained in the basin at timescales in the order of a decade and reflect the higher concentrations found during the earlier part of the tritium transient. The changes in the ratio are dependent on the onset of snowmelt or the increase of flow due to precipitation. Thus the ratios vary inversely using this methodology. The trend in the above figures can be expected to apply to most rivers in the Northern Hemisphere except where a significant impoundment of the river water occurs upstream of the sampling location.

Fig. 6 is a plot of the ratio of (monthly tritium/yearly tritium) versus the ratio of (monthly $\delta^{18}O$/yearly $\delta^{18}O$) for five Swiss rivers where approximately 7 years of data are available for both isotopes. All rivers have similar climatic and flow regimes. For all five rivers it is evident that higher tritium values tend to occur at the same time as heavier ^{18}O values. Using these results with proper flow data it may be possible to obtain a better fit of the two isotopic ratios. Knowing the tritium concentration of baseflow, it is possible to use various models to estimate the mean age of the waters
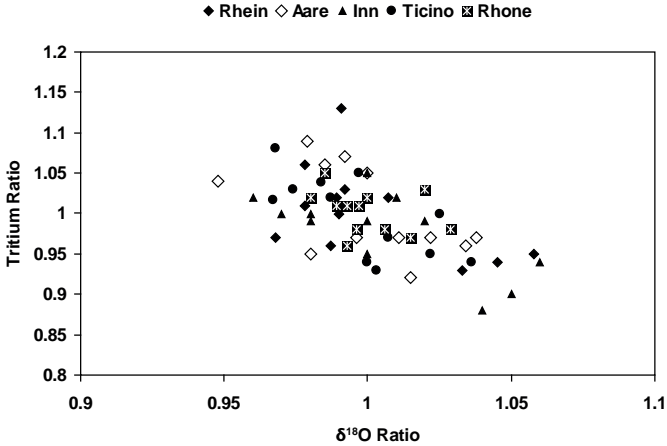
FIG. 6. $\delta^{18}O$ ratios versus tritium ratios for five Swiss rivers. All rivers have very similar climatic and flow regimes with snow melt in spring supplying waters lighter in ^{18}O and lower in tritium.

that comprise baseflow. It has generally been found that baseflow ages have a decadal range [4–9]. The existence of a strong seasonal signal during baseflow for these five rivers suggests that it is also composed of waters with a decadal age range. It may be possible to estimate the tritium and ^{18}O concentrations of baseflow for these five rivers from this data set. While the value of ^{18}O for baseflow will not determine age, it is an important parameter to obtain. It is possible that values for ^{18}O of baseflow will change in the coming years due to climate or land use perturbations. If there is a perturbation, changes will occur to concentrations in baseflow at a rate dependent on the mean age of baseflow obtained from the tritium data. Monitoring over long time spans will allow researchers to assess whether changes are occurring and try to relate them to forcing factors such as temperature and the amount of precipitation.

To properly use these data, it is important that the measurements are of high quality and the frequency of measurements be sufficient to delineate any seasonal variations.

5. CONCLUSIONS

Long term isotopic databases from GNIR have been analysed using a method to normalize observations over different climatic regimes. It is seen that consistent yearly variations of this ratio occur related to flow rates and the input of snowmelt or seasonal rainfall. Water from snowmelt and rainfall tends to be lighter in ^{18}O causing the seasonal effect seen. A similar situation is seen for tritium where the younger waters found in snowmelt or seasonal rainfall are lower in tritium. The baseflow

which is the predominant source of water at certain times of the year will gener-ally have a higher tritium concentration and heavier $\delta^{18}O$ values. With flow data it should be possible to estimate the tritium concentrations and $\delta^{18}O$ values of baseflow. The tritium data will give an estimate of the mean age of the baseflow. If these types of data are continuously monitored over time, changes in isotopic concentrations in baseflow due to climate or land-use factors can be determined. To properly use this method, it is necessary to obtain high quality data, preferably on a monthly basis, for the targeted basin.

REFERENCES

[1]   INTERNATIONAL ATOMIC ENERGY AGENCY, Statistical treatment of data on environmental isotopes in precipitation, Technical Report Series 331, IAEA, Vienna (1992) 781.

[2]   CRAIG, H., GORDON, L.I., "Deuterium and oxygen-18 variations in the oceans and marine atmosphere", Stable Isotopes in Oceanographic Studies and Paleotem-peratures, Lischi and Figli (1965) 9–130.

[3]   SUESS, H.E., Tritium geophysics as an international research project, Science **163** (1969) 1405–1410.

[4]   BROWN, R.M., Hydrology of tritium in the Ottawa Valley, Geochim. Cosmochim. Acta **21** (1961) 199–216.

[5]   ERIKSSON. E., Atmospheric tritium as a tool for the study of certain hydrologic aspects of river basins, Tellus **15** (1963) 303–308.

[6]   MICHEL, R.L., Residence times in river basins as determined by analysis of long term tritium records, J. Hydrol. **130** (1992) 367–378.

[7]   MICHEL, R.L., Tritium hydrology of the Mississippi River basin, Hydrol. Process. **18** (2004) 1255–1269.

[8]   MICHEL, R.L., "Tritium in the hydrologic cycle", Isotopes in the Water Cy-cle, Past, Present and Future of a Developing Science (AGGARWAL, P., GAT, J., FROEHLICH, K., Eds), Springer, Dordrecht (2003) 53–66.

[9]   RANK, D., ALDER, L., ARAGUAS, L.A., FROEHLICH, K., ROZANSKI, K., STICHLER, W., "Hydrological parameters and climatic signals derived from long term tritium and stable isotopes time series of the River Danube", Isotope Techniques in the Study of Environmental Change (Proc. Int. Conf. Vienna, 1997), IAEA, Vienna (1998) 191–205.

[10]   GIBSON, J.J., et al., Isotope studies in large river basins: A new global research focus, EOS **83** (2002) 613–617.

[11]   KATTAN, Z., Estimation of evaporation and irrigation return flow in arid zones us-ing stable isotope ratios and chloride mass-balance analysis: Case of the Euphrates River, Syria, J. Arid Environ. **72** (2008) 730–747.

USE OF ISOTOPIC TECHNIQUES FOR THE ASSESSMENT OF HYDROLOGICAL PROCESSES IN WETLANDS (CIÉNAGA COLOMBIA)

T. BETANCUR, D. SANTA, P. PALACIO, C. PALACIO, B. WILLS,
D.Á. HOYOS
Universidad de Antioquia, Medellín, Colombia

Abstract

The Ciénaga Colombia wetland is located in the Bajo Cauca Antioqueño region where the 'Man' river flows into the Cauca River. Hydrological processes on the Ciénaga Colombia wetland are complex because of the interactive effects of both local and regional elements, associated with a typical tropical wet climatic regime. In this groundwater dependent wetland hydrological studies have been conducted, including hydrochemical analyses and isotope tracers, to describe and understand the interactions between groundwater and surface water, not only for the wetland itself but also for the entire catchment area. Rain samples (five year record) were used to obtain the LML: $\delta^2H = 8.03\,\delta^{18}O +9.9$. The evaporation line is: $\delta^2H = 5.9\,\delta^{18}O - 7.3$. According to the analyses, both groundwater and surface waters have the same isotopic signatures. Unsustainable land use practices along with current and predicted global environmental changes may cause negative impacts on the hydrological functioning of the region, affecting primarily, but not exclusively, evapotranspiration-recharge processes and the sustainability of the entire system.

1.   INTRODUCTION

The study 'Hydrochemical and Isotopic techniques for the assessment of hydrological processes in the wetlands of Bajo Cauca, Antioquia', conducted by the University of Antioquia in the framework of a cooperative project with the International Atomic Energy Agency (IAEA) evaluated groundwater flow and dynamics in the vicinity of the Ciénaga Colombia wetland in the Bajo Cauca Antioqueño region using hydrochemical and isotopic techniques. Because Ciénaga Colombia is a groundwater controlled wetland, our work dealt with the validation of a hydrological model including the interaction between surface waters and groundwater.

2.   DESCRIPTION OF THE AREA STUDIED

The catchment area of Ciénaga Colombia is located in the lower basin of the Man River in northwestern Colombia (Fig. 1). The physical geography of the area
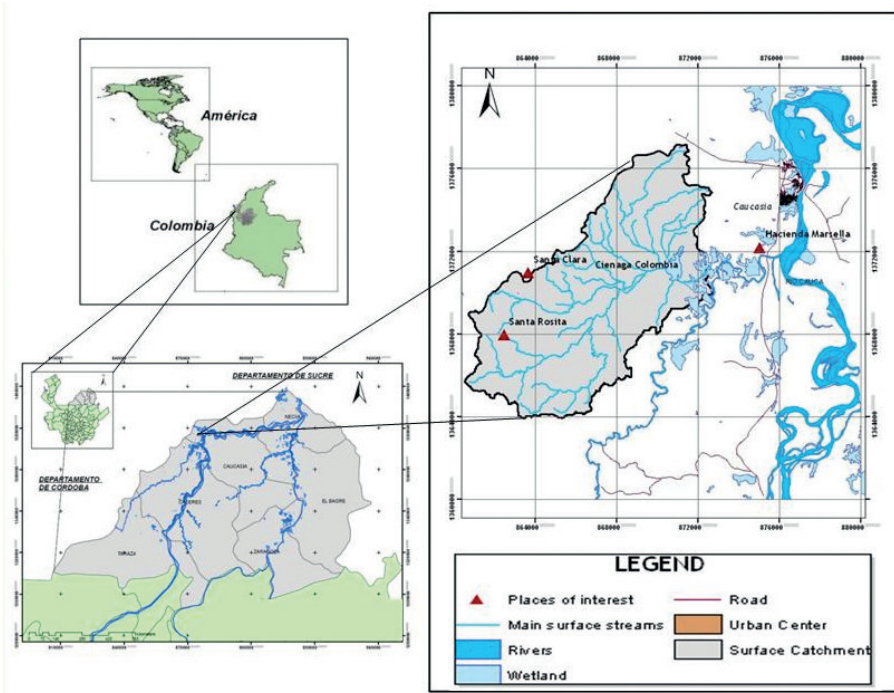
FIG. 1. Location of the study area.

corresponds to a smooth topography with both flat and sloping areas, the slopes reaching a maximum of 7%, covering an area of approximately 84 km^2. The average temperature in the basin of the Ciénaga stream is 27ºC. The rainfall pattern is unimodal, with a wet season between April and November and a dry season between December and March. Average annual rainfall is 2800 mm. These conditions correspond to a humid tropical climate.

The Ciénaga Colombia wetland is part of the drainage basin of the Ciénaga stream, a tributary from the right bank of the Man River which flows to the east of the river Cauca, one of Colombia's most important rivers. The dimensions of the wetland vary seasonally, the water covering an area of about 2 km^2 and reaching a depth of more than 4 m in the rainy season, while during the summer the surface is reduced to 0.6 km^2, and a depth of 0.6 m. Ciénaga Colombia depends on groundwater. It maintains the water level during the dry season due to the contribution of the base flow from a regional unconfined aquifer.

3.   METHODOLOGY

   Wetlands are areas of marsh, fen or peat land, or surfaces covered by water, be they natural or artificial, permanent or temporary, static or flowing, fresh, brackish or salt water, including areas of marine water with a low tide depth of less than six metres. Wetlands are among the most productive regions in the world. They are cradles of biological diversity and sources of water and primary productivity in which numerous species of plants and animals including birds, mammals, reptiles, amphibians, fish and invertebrates depend on for survival.

   Wetlands declared as strategic ecosystems by an intergovernmental treaty (Convention on Wetlands, Ramsar) are surface systems whose existences depend in many cases on interaction with groundwater. According to Custodio [1], wetlands that rely on groundwater are those whose water comes partially, predominantly or only from groundwater. The dynamics of the water bodies in the catchment area of a wetland are studied using hydrological techniques that allow the development of early conceptual models which will then be tested, adjusted or validated by applying other analytical methods which may include numerical modelling, hydrochemistry and hydrology.

   Because natural systems are subject to processes of variability and change over time at a pace that is based on seasonal cycles which sometimes include abnormal periods, there is always more to learn, and systems should therefore be monitored on a continuous basis. In general terms, monitoring has been defined as the continuous observation of the environment using standardized methods [2]. It is recommended that monitoring activities of the relevant groundwater be integrated and coordinated with those of surface water, precipitation, evaporation and soil based on the recognition that the hydrological cycle is the conceptual basis for strategies of integrated water resource management [3].

   Bravo [4] states that the monitoring networks are intended to measure a variable that changes in space and time using a limited number of measuring stations distributed over the region of observation in a way to best capture the spatial variability of the variable of interest. Several authors [4–7] agree that the starting point for the design of a monitoring network is the knowledge of the study area and a clear definition of the information to be collected.

   Since 2007, the University of Antioquia, in the framework of an agreement with the IAEA, has been operating a monitoring network of groundwater levels with monthly water level readings with accuracy to the centimetre; within the same system there is also a monitoring network of hydrochemical and isotopic variables, for which water samples are collected during the rainy and dry seasons. The network consists of 5 rainfall stations, 22 groundwater stations and 6 surface water points (Fig. 2). Hydrochemical variables analysed include major and minor ions, as well as ^{18}O and ^{2}H. Sampling was carried out following the protocols defined by certified laboratories and the IAEA.
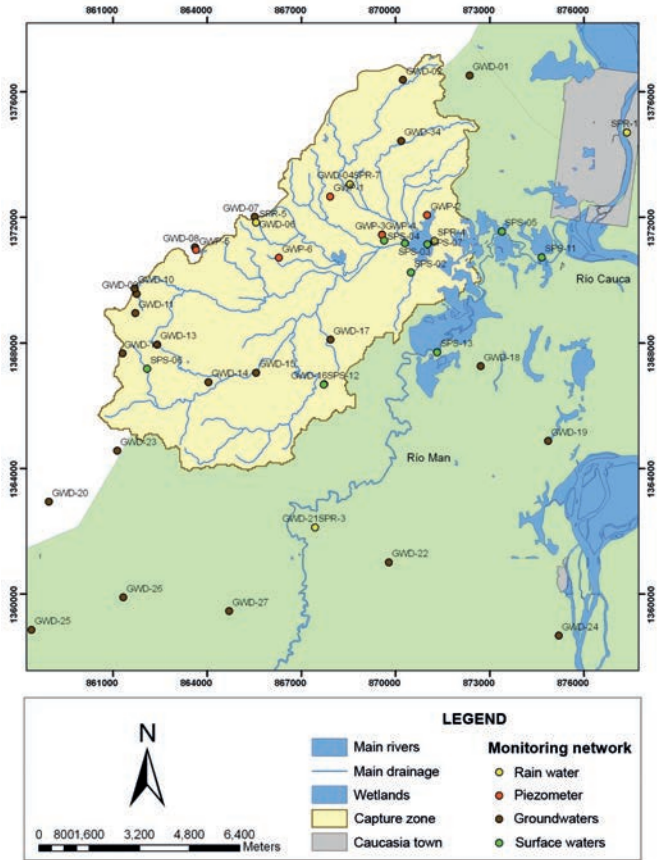
FIG. 2. Monitoring network in the study area.

Chemical analyses were carried out at the Environmental Quality Laboratory at Corantioquia using ion chromatography and atomic absorption methods. Isotopic analyses were made in LaGeo laboratory in El Salvador using mass spectrometry and at the National University of Mar del Plata in Argentina using laser spectroscopy methods.

4. HYDROLOGICAL PROCESSES IN THE CIENAGA COLOMBIA WETLAND

The data collected during the course of this study were used to model, on a monthly basis, potentiometric surfaces providing evidence of the interaction between surface and subsurface components of the hydrological cycle at the Ciénaga creek basin. These maps indicate a constant groundwater flow towards the wetland.
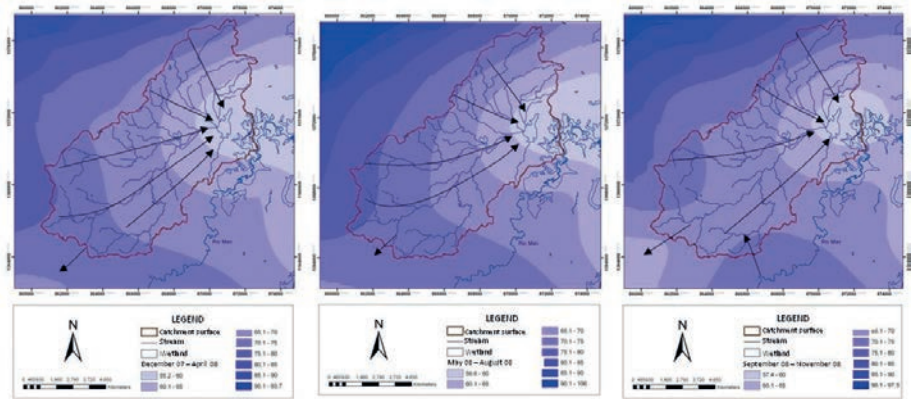
FIG. 3. Groundwater–surface water interactions.

For some time during the year, some surficial currents act as hydrogeological boundaries. The trends studied during three periods with similar characteristics allowed us to characterize the overall groundwater flow pattern (Fig. 3), which shows the changes of the groundwater drainage system towards the south of the Ciénaga creek basin.

5. HYDROCHEMISTRY

The description of the hydrochemistry of the Ciénaga Colombia water system is based on the chemical analysis obtained during seven field campaigns conducted from September 2007 to March 2010. Fig. 4 shows the diagram of chemical signatures, including all results which met the condition of an ionic balance with error lower than 10%. Table 1 summarizes the chemical results.

Surface waters sampled at different sampling sites have shown over time the predominance of chemical signature Ca–Mg–Na–HCO_3, with variations in the abundance of cations. Only four rain samples were analysed, one of which shows the chemical signature Na–HCO_3, the others being Ca–HCO_3. Groundwater in the catchment area of the wetland Ciénaga Colombia shows wide variation in chemical signatures. Looking back over time, it is shown that most groundwater corresponds to the chemical signatures Ca–Na–Mg–HCO_3, however, some sites are excluded from the general trend: Jalisco and La Bonita (Na–HCO_3), piezometer North Ciénaga (Na–HCO_3–Cl), Mirador Las Brisas, Guarumal, Jesusalen and Santa Clara (Na–Mg–HCO_3–Cl). During sampling in November 2009 and March 2010 water samples collected at Siberia were of the type Na–Ca–Mg–Cl–HCO_3. The change of the dry to the rainy season is reflected in the refreshing of the chemical composition,

TABLE 1. BASIC CHEMICAL PARAMETERS OF THE SAMPLES

Water parameter	Surface water						Rain						Groundwater					
	Max	Min	Range	Avarege	Std Dev	Count	Max	Min	Range	Avarege	Std Dev	Count	Max	Min	Range	Avarege	Std Dev	Count
pH	7.59	3.95	3.64	7.03	0.56	41	6.56	5.89	0.67	6.23	0.47	2	8	4.95	3.05	6.56	0.73	73
EC (μS/cm)	115	21.1	93.9	60.52	27.03	38	72.5	7.1	65.4	39.8	46.24	2	1612	16	1596	273.32	333.18	76
Bicarbonate (mg/L HCO_3)	95.2	11.1	84.1	38.82	17.05	48	47.8	2.9	44.9	24.69	23.7	4	974	2.61	971.39	148.91	196.09	92
Chloride (mg/L Cl^-)	5.87	1.5	4.37	2.54	0.98	27	1.52	1.52	0	1.52		1	278	1.67	276.33	23.3	46.74	89
Sulphate (mg/L SO_4^{2-})	9.84	0.0001	9.84	3.32	3.31	11	0.0001	0.0001	0	0		1	27.8	0	27.8	3.06	7.55	27
Nitrate (mg/L NO_3 –N)	2.38	1.3	1.08	1.73	0.38	8	0.62	0.62	0	0.62		1	44.9	0.92	43.09	4.61	6.77	42
Calcium (mg/L Ca)	17.7	0.99	16.71	5.44	3.4	48	13.5	0	13.5	6.38	6.97	4	98.5	0.0045	98.4955	19.44	20.18	92
Magnesium (mg/L Mg)	11.4	0.448	10.95	3.25	1.93	48	0.317	0.024	0.293	0.12	0.13	4	54.4	0.263	54.137	10.11	13.03	92
Iron (mg/L Fe)	3.41	0.167	3.24	0.72	0.66	48	0.133	0.03	0.103	0.08	0.07	2	3.372	0.026	3.346	0.33	0.6	65
Potassium (mg/L K)	3.95	0.472	3.48	1.74	0.72	48	0.25	0.029	0.221	0.15	0.1	4	5.67	0.056	5.614	1.84	1.29	92
Sodium (mg/L Na)	9.64	1.912	7.73	4.09	1.81	48	1.59	0.22	1.37	0.66	0.64	4	301	1.002	299.998	33.28	57.46	92
Silica (mg/L Si)	12.8	0.36	12.44	7.55	2.41	48	1.29	0.65	0.64	0.86	0.37	3	29.3	3.25	26.05	12.51	6.32	92
TDS (mg/L)	218	27	191	68.39	38.99	28	72	72	0	72		1	1375	13	1362	250.14	275.08	43
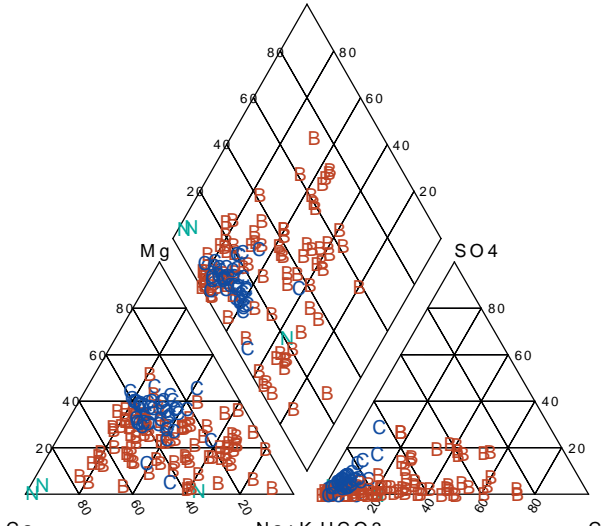
FIG. 4. Piper diagram with all collected data (N — precipitation, B — groundwater, C — surface water).

indicating that mixing must take place between groundwater and water recharged by rainfall.

The spatial variation of total dissolved salts (TDS) and chloride was analysed using Stiff diagrams, and taking into consideration changes in flow along the flow lines [8]. Rainwater usually belong to the calcium bicarbonate type, while surface waters show the presence, in addition to calcium, of sodium and magnesium, classifying them as mixed bicarbonate waters. The source of Na and Mg ions can be attributed to base flow contributions from the aquifer. The chemical characteristics of water from the Ciénaga Colombia wetland are Mg–Na–HCO_3, suggesting that its water, enriched by the rain, is heavily dependent on the base flow. Finally, the relationship between the water of the swamp and the groundwater located to the east of the wetland (site Dynasty, GWD–05), indicates that the interconnection between the groundwater and the wetland is intermittent. The thermodynamic validity of these processes was tested by conducting inverse modelling exercises using the code Netpath [8].

6.   ISOTOPE HYDROLOGY

Thirty six isotopic analyses were conducted on rainwater samples collected at a local station over more than three years. The local meteoric water line was defined as $\delta^2H = 8.03\,\delta^{18}O+9.9$ (Fig. 5), which coincides with the global meteoric line [9, 10]. The calculated mean weighted mean isotopic values of precipitation in the area are:

TABLE 2. SYNTHESIS OF ISOTOPIC DATA FOR THE DIFFERENT WATER
TYPES

	^{18}O rain (‰)	δ^2H rain (‰)	$\delta^{18}O$ surface water (‰)	δ^2H surface water (‰)	$\delta^{18}O$ groundwater (‰)	δ^2H groundwater (‰)
Number	29	29	75	75	121	121
Max.	–0.1	7.8	4.2	5.8	–4.7	–33.4
Min.	–12.3	–89.0	–9.5	–66.6	–10.6	–73.5
Range	29.0	29.0	13.7	72.4	5.9	40.1
Average	–6.8	–44.8	–6.0	–42.4	–6.9	–47.1
Stand. Dev.	3.3	26.2	2.8	16.6	0.8	5.5
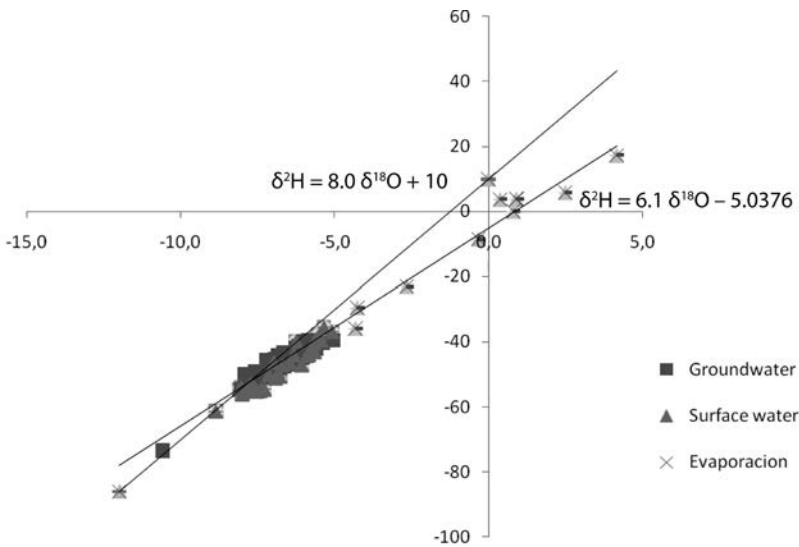
FIG. 5. $\delta^{18}O$ vs δ^2H relationship.

$\delta^{18}O = -5.9$‰ and $\delta^2H = -57$‰. An evaporation line for surface waters was found to
follow the line $\delta^2H = 6.1\delta^{18}O - 5.0$. Excluding the results of the enriched samples,
the range of variation for $\delta^{18}O$ is reduced to the range –7.4 to –5.1‰ (Table 2), while
the values for March ranged from –8.5 to 2.5‰.

Most groundwater samples recorded in each field study show short intervals
that represent a small range of variation. In fact, seldom are variations of more than
2.0 units in δ^2H seen. Two specific situations were registered at the piezometer Adua-
na where a smaller value than the other samples was recorded during February 2009.

7. CONCLUSION

All in all, the evidence shows that surface water (except in March) and underground water have the same isotopic imprint, which highlights the relationship between them via inputs from the subsurface environment in the form of base flow to surface currents and to the wetland.

ACKNOWLEDGEMENTS

REFERENCES

[1]   CUSTODIO, E., Aspectos hidrológicos de los humedales que dependen del agua subterránea, 1ª Reunión Internacional de Expertos sobre la Regeneración Hídrica de Doñana (2001) 20– 26 (in Spanish).

[2]   UNITED NATIONS EDUCATIONAL, SCIENTIFIC AND CULTURAL ORGANIZATION, Water quality surveys, Studies and reports in hydrology, Paris

[3]   VARGAS, N., Monitoreo de Agua Subterránea, Subdirección de Hidrología – IDEAM (1978) 10 (in Spanish).

[4]   BRAVO, L., El diseño de redes de monitoreo: teoría y aplicaciones, Universidad Simón Bolívar, Departamento de Cómputo. Caracas, Venezuela (2007) (in Spanish).

[5]   DIAZ, M., Una metodología alternativa para el diseño de una red de monitoreo nueva en aguas subterráneas para fines de manejo con casi ninguna información, Instituto de Geofísica, UNAM, México D.F (2000) 8 pp (in Spanish).

[6]   MOLERIO, L.F., TORRES, J.C., Métodos geomatemáticos de diseño y optimización de redes de monitoreo de aguas subterráneas, Ingeniería Hidráulica y Ambiental, Vol. XXIII, No. 2 (2002) 38–45 (in Spanish).

[7]   MARTÍNEZ, D., Modelación hidrogeoquímica, Curso de hidrogeoquímica CARSUCRE, Sincelejo (2008) (in Spanish).

[8]   SANTA, D., Identificación de interacciones hidrológicas entre el humedal Ciénaga Colombia y el acuífero libre del Bajo Cauca antioqueño mediante la utilización de técnicas hidroquímicas, Trabajo de investigación: Universidad de Antioquia, Medellín (2009) 118 (in Spanish).

[9]   PALACIO, P., BETANCUR, T., Identificación de fuentes y zonas de recarga a un sistema acuífero a partir de isótopos estables del agua, Gestión y Ambiente **10** (2007) 167–181 (in Spanish).

[10]   BETANCUR, T., Una aproximación al conocimiento de un sistema acuífero tropical, Caso de estudio: Bajo Cauca antioqueño, PhD Thesis, Universidad de Antioquia, Facultad de Ingeniería (2008) 227 (in Spanish).

STABLE ISOTOPES OF DISSOLVED NITRATE AND BORON AS INDICATORS OF THE ORIGIN AND FATE OF NITRATE CONTAMINATION IN GROUNDWATER
Results from the western Po plain (Northern Italy).

E. SACCHI
Dipartimento di Scienze della Terra e dell'Ambiente,
Università di Pavia, and Istituto di Geoscienze e Georisorse,
CNR, Pavia, Italy

C.A. DELCONTE
Istituto di Geoscienze e Georisorse,
CNR, and Dipartimento di Scienze della Terra e dell'Ambiente,
Università di Pavia, Italy

M. PENNISI
Istituto di Geoscienze e Georisorse,
CNR, Pisa, Italy

E. ALLAIS
ISO4 s.n.c.,
Torino, Italy

Abstract

Stable isotopes of dissolved nitrates and boron represent a powerful tool, complementary to existing monitoring data, enabling the identification of nitrate sources, the assessment of their relative contribution to nitrate pollution and the quantification of nitrate transport and removal processes. This contribution aims to present groundwater isotope data obtained in an area of 15 000 km^2 of the western Po plain. Nitrate isotope data show that synthetic fertilisers and anthropogenic organic matter are the main sources of contamination. $\delta^{11}B$ allows the discrimination between manure derived and sewage derived contamination. Results indicate that even in agricultural areas, contamination from sewage exists. Samples from the suburban area of Milan, where sewage was considered the most likely source of contamination, show instead a $\delta^{11}B$ typical for cattle manure. This study demonstrates that the attribution of the contamination to a source based solely on present-day land use may lead to inappropriate conclusions.

1. INTRODUCTION

Nitrate concentration in surface and groundwater is an environmental concern. Nitrate pollution may be attributed to point sources, such as landfills, septic tanks or factory farming. Agricultural regions commonly suffer diffuse water pollution, which, in contrast, cannot be attributed to a precise source. Rather, it is the cumulative effect of day to day activities over large areas, including the application of synthetic fertilisers, manure spreading and sewage sludge disposal.

Distinction between different sources of nitrates in groundwater can be made by coupling hydrochemistry with the isotopic signature of oxygen and nitrogen in the nitrate molecule (e.g. Refs [1, 2] and references therein). The combination of $\delta^{15}N_{NO3}$ and $\delta^{18}O_{NO3}$ data allows the evidencing of cumulative effects in regional contamination problems and, in addition, the recognition of nitrification and denitrification processes. However, nitrate isotopes do not allow the distinguishing of manure derived and sewage derived nitrates, since these sources have overlapping isotopic signatures. In this case, the combined use of $\delta^{15}N_{NO3}$, $\delta^{18}O_{NO3}$, and $\delta^{11}B$ [2, 3] is powerful to distinguish nitrate sources, assuming that these compounds comigrate in many environmental settings [4]. Indeed, manure and sewage have high concentrations of boron and distinct $\delta^{11}B$ imprints [3, 5]. In addition, while redox conditions control the N isotope evolution, B isotopes are not sensitive to this process [4].
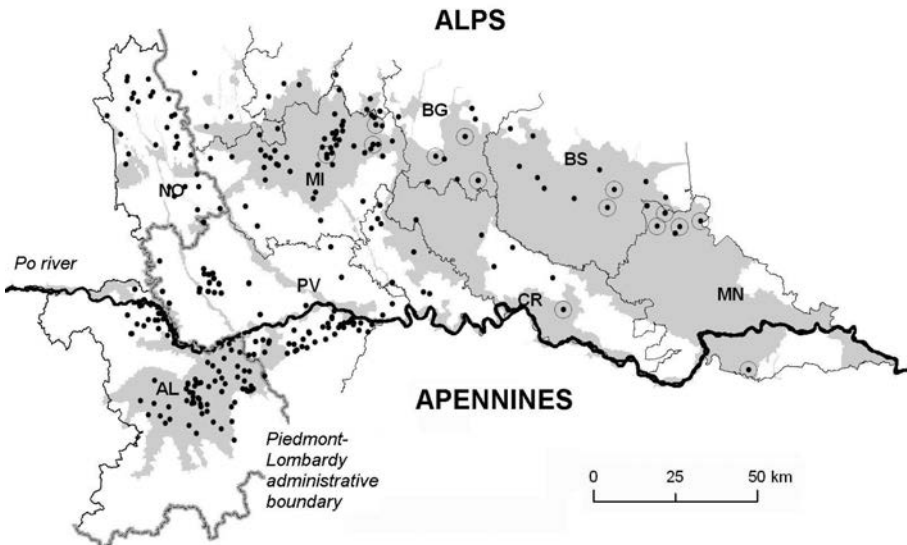
FIG. 1. Map showing the investigated area and the locations where nitrate isotope data are available (black dots). Grey areas highlight NVZ. Circles evidence samples used for B isotopic determinations. AL = Alessandria; BG = Bergamo; BS = Brescia; CR = Cremona; MN = Mantua; MI = Milan; NO = Novara;PV = Pavia.

The Po plain supports most of the agricultural and industrial activities of northern Italy, and hosts several large urban settlements, all associated with groundwater exploitation and pollution. The implementation of the Water Framework Directive (2000/60/EC) and the Nitrate Directive (91/976/EEC) has lead to the designation of large areas as vulnerable to nitrate pollution (Nitrate Vulnerable Zones, NVZ), where the use of fertilisers, especially manure, is restricted. These remedies seem not to be very effective because nitrate pollution may originate from other, unaccounted for, sources (e.g. domestic). The unambiguous identification of the nitrate sources becomes therefore crucial for the application of local, source oriented remedies.

The area covered by this study is of approximately 15 000 km^2, crossing the Po plain from N to S in correspondence to the Piedmont-Lombardy administrative boundary (Fig. 1). The shallow alluvial aquifer, of Quaternary age, is constituted by gravels and sands, and has higher clay contents only in the south eastern part. Groundwater flow in the phreatic aquifer is directed towards the Po river, and is oriented N-S in the pre-alpine sector and S-N closer to the Apennines. Agricultural land use includes corn, wheat and rice fields.

2. METHODS

Groundwater data obtained since 2005 (see Ref. [6] and references therein) were compiled in a single geo-referenced database, containing more than 300 records and including natural outflows, agricultural wells, and wells used for human consumption. The geochemical database includes anion concentrations (nitrate, chloride and sulphate) and stable isotopes of dissolved nitrates ($\delta^{15}N_{NO3}$ and $\delta^{18}O_{NO3}$). Based on these data, some samples were selected for B content and isotope determinations.

Nitrate isotopes were mostly determined by IRMS, and samples were prepared and purified according to the method described by [7]. Uncertainties (1σ) are $\pm 0.5‰$ for $\delta^{15}N_{NO3}$ and $\pm 1‰$ for $\delta^{18}O_{NO3}$. Boron concentration was determined by ICP-AES. Boron isotope analyses ($\delta^{11}B$) were performed by MC-ICP-MS at ALS Scandinavia AB, Sweden, with an uncertainty of ± 0.4 to $\pm 1‰$.

3. RESULTS AND DISCUSSION

3.1. Nitrate isotopes

Groundwater samples show a wide range of nitrate concentrations, deviation from 10 mg/L up to 180 mg/L being observed from the mean value of about 30 mg/L. The variation measured on the isotopic composition of $\delta^{15}N_{NO3}$ and $\delta^{18}O_{NO3}$ is also significant, ranging from $-10‰$ to $+28‰$, and from $+2‰$ to $+23‰$, respectively. On the diagram $\delta^{18}O_{NO3}$ vs $\delta^{15}N_{NO3}$, several sources and processes can be evidenced
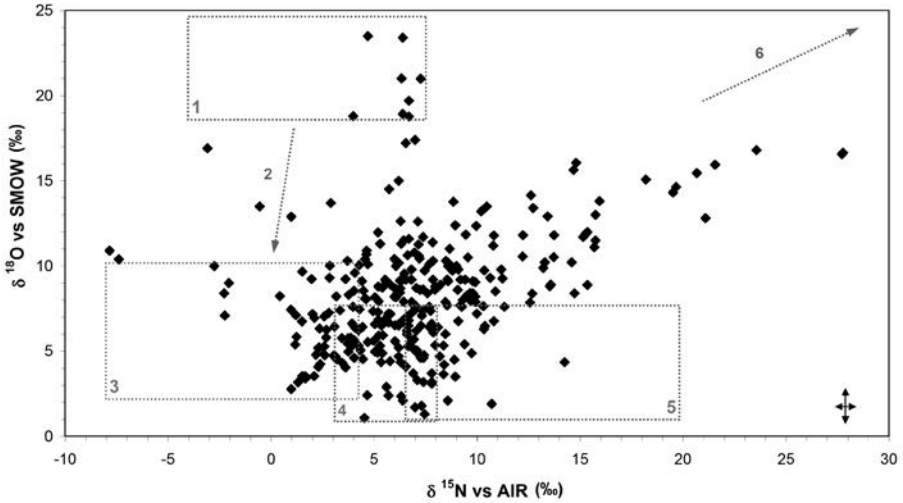
FIG. 2. Stable isotope composition of dissolved nitrates in groundwater from the investigated area. 1) Synthetic fertilisers; 2) Evolution during nitrification; 3) Mineralised synthetic fertilisers; 4) Soil organic matter and contamination from mixed sources; 5) Anthropogenic organic matter (sewage and manure); 6) Evolution during denitrification. Modified after Ref. [11].

(Fig. 2). Nitrate concentrations being higher than 10 mg/L, samples falling in the compositional field of soil organic matter, are likely to record a mixed contamination from both synthetic fertilisers and anthropogenic organic matter. Some samples show an isotopic composition highly enriched by denitrification, reaching up to 80% reduction of the original content.

According to the geographical distribution of the samples, a regional map is produced, highlighting the more vulnerable areas for groundwater resources. In the western part of the investigated area (Alessandria and Novara provinces, north of Milan) the isotopic signature of synthetic fertilisers is dominant. A detailed discussion on this area is reported by Ref. [8]. In the Lomellina area (Pavia province, central western plain) the artificial recharge associated with rice cultivation represents a preferential pathway for the input of exotic substances to groundwater; in this area, the input of nitrogen compounds is highly reduced by denitrification [9]. In the suburban area of Milan, isotopic data fall in the field of contamination by mixed sources or by anthropogenic organic matter; this is attributed to an input from an obsolete and leaking sewage network [10]. An anthropogenic organic matter contamination is also observed in the north eastern part of the plain (Bergamo, Brescia and Mantua provinces) and attributed to manure spreading, according to the local land use (mostly agricultural). Finally the south eastern part of the plain is characterised by clay rich soils favouring denitrification, as also testified by the low nitrate concentration

in groundwater. Indeed, this zone is listed as 'vulnerable to nitrate' mostly due to the high contents found in its surface water.

Combining the information provided by nitrate isotopes with land use and other soil parameters, groundwater contamination results are governed by:

(1) The hydraulic characteristics of the unsaturated zone: clay rich soils reduce infiltration and favour denitrification through the establishment of anoxic conditions;
(2) The agricultural input: corn and wheat cultivation seems to be mostly responsible for nitrate contribution to groundwater;
(3) Irrigation practices, mostly conducted by field flooding.

3.2. Boron isotopes

As regulators need to discriminate in an unambiguous way between contamination arising from agricultural practices, such as manure spreading, and contamination from a civil origin, such as leaking septic tanks and sewage network, a B isotopic investigation was undertaken in 2010. Selected samples respond to the following criteria:

(1) They are located in a nitrate vulnerable zone (Fig. 1);
(2) They show a high concentration of nitrates;
(3) The isotopic composition of dissolved nitrate falls in the field of contamination from mixed or anthropogenic organic matter sources, or in the field of denitrification (Fig. 2).

These samples are mostly located in the Alpine foothills, in the Bergamo, Brescia and upper Mantua provinces, which, together with the Cremona province, host the largest cattle raising activities of Lombardy [12]. For comparison, five samples from the suburban area of Milan and two wastewater samples from water treatment plants discharging in the Oglio river (an important Po river tributary flowing in the NVZ of Lombardy) were considered (see also Ref. [13]).

B concentration in groundwater samples is very low, generally ranging from 15 to about 50 µg/L, well below the drinking water limits of 1 mg/L (Dlgs. 152/06). Indeed, several selected samples (including two from the Milan area) could not be analysed because their B concentration was too low. Higher concentrations are measured in wastewater samples (80 and 85 µg/L) and in two groundwater samples (155 and 540 µg/L). The B isotopic composition shows a wide range of values (Fig. 3), varying from –3.8‰ to + 34.5‰.

A $\delta^{11}B$ of +14.6‰, compatible with a natural origin of B [3], characterizes the sample with the lowest B concentration, which is therefore assumed as the 'uncontaminated' endmember. As B concentration rises, the isotopic composition of boron evolves towards both negative values, which are typical for wastewater and sewage, and towards positive values, indicating a contribution from animal manure.
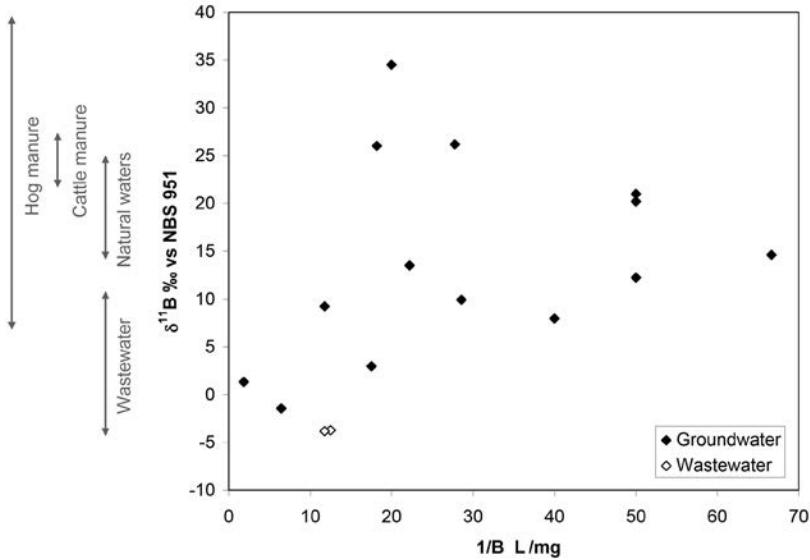
FIG. 3. Boron isotope composition and concentration in groundwater and wastewater samples.

Accordingly, samples can be considered as a mixture in variable proportions of these endmembers.

It is interesting to note that, even in areas mostly devoted to agriculture, a contamination from sewage is observed. Indeed, in rural areas, households are sometimes not connected to sewers, and even when they are, they may not have completely drained out the old septic tanks. Surprisingly, samples from the suburban area of Milan, where sewage was considered the most likely source of contamination, show a $\delta^{11}B$ typical for cattle manure. In this case, nitrates in groundwater are likely related to a contamination occurred in the past, when the area was still mostly devoted to agriculture. This interpretation is consistent with the presence of an isotopic signature of nitrates typical of synthetic fertilisers in the present-day highly industrialised area northwest of Milan, sometimes associated with the presence of pesticides such as atrazine in groundwater.

4.   CONCLUSION

At the regional scale, the impact of intense agriculture activities on groundwater resources is mostly related to the use of synthetic fertilisers. Very little non-point source contamination seems to originate from manure spreading. Peak concentrations in B and nitrates are instead associated with point source pollution and can be attributed to leaking septic tanks or sewage network.

Since synthetic fertilisers and sewage represent the main nitrate sources in the investigated area, the actions undertaken for nitrate pollution mitigation (i.e. limitations to manure spreading) do not target the actual nitrate sources to groundwater.

In addition the present study demonstrates that the attribution of the contamination to a source based solely on present-day land use may lead to inappropriate conclusions, which need instead to be supported by isotopic data as well.

ACKNOWLEDGEMENTS

REFERENCES

[1]   SPRUILL, T.B., et al., Application of classification-tree methods to identify nitrate sources in ground water, Journal Environ. Quality **31** (2002) 1538–1549.

[2]   XUE, D., et al., Present limitations and future prospects of stable isotope methods for nitrate source identification in surface- and groundwater, Water Research **43** (2009) 1159–1170.

[3]   WIDORY, D., et al., Tracking the sources of nitrate in groundwater using coupled nitrogen and boron isotopes: a synthesis, Environ. Sci. Technol. **39** (2005) 539–548

[4]   SEILER, R.L., Combined use of ^{15}N and ^{18}O of nitrate and ^{11}B to evaluate nitrate contamination in groundwater, Appl. Geochem. **20** (2005) 1626–1636.

[5]   KOMOR, S.C., Boron contents and isotopic compositions of hog manure, selected fertilizers, and water in Minnesota, J. Environ. Qual. **26** (1997) 1212–1222.

[6]   SACCHI, E., et al., "Stable isotopes of dissolved nitrates as indicators of the origin and the mechanisms of transport to/removal from groundwater: results from the western Po plain (Northern Italy)", Proc. 16th Nitrogen Workshop, Turin, Italy, 28 June–1 July 2009 (2009) 495–496.

[7]   SILVA, S.R., et al., A new method for the collection of nitrate from fresh water and the analysis of nitrogen and oxygen isotope ratios, J. Hydrol. **228** (2000) 22–36.

[8]   SACCHI, E., et al., "A regional survey on nitrate contamination of the Po valley alluvial aquifer (Northern Italy)" Proc. Int. Symp. on Advances in Isotope Hydrology and its role in Sustainable Water Resources Management, IAEA, Vienna 21–25 May 2007, IAEA-CN–151/34 Vol. 2 (2007) 471–478

[9]   SACCHI, E., et al., "Tracing nitrification and denitrification processes in a periodically flooded shallow sandy aquifer", Proc. Int. Symp. on Advances in Isotope Hydrology and its role in Sustainable Water Resources Management, IAEA, Vienna 21–25 May 2007, IAEA-CN–151/33 Vol. 2 (2007) 461–469.

[10]   ARDUINI, C., et al., "Nitrates in groundwater (Northern Italy): isotopic prospection
         in high vulnerability area", Int. Symp. 'Consoil 2008', Milan, Italy, 3–6 June 2008,
         F205–F215.

[11]   CLARK I., FRITZ P., Environmental Isotopes in Hydrogeology, Lewis Publishers,
         Boca Raton, FL (1997) 328.

[12]   ERSAF-REGIONE LOMBARDIA, Attuazione della Direttiva Nitrati in Lombardia,
         Int. Rep. (2009) 79 (in Italian).

[13]   DELCONTE, C.A., et al., "Evaluation of nitrate sources and transformation in
         the Oglio River watershed" (this volume).

EVALUATION OF NITRATE SOURCES AND TRANSFORMATION IN THE OGLIO RIVER WATERSHED

C.A. DELCONTE
Istituto di Geoscienze e Georisorse, CNR, U.O.S. di Pavia, Italy
and Dipartimento di Scienze della Terra e dell'Ambiente,
Università di Pavia, Italy

E. SACCHI
Dipartimento di Scienze della Terra e dell'Ambiente,
Università di Pavia, Italy and Istituto di Geoscienze e Georisorse,
CNR, U.O.S. di Pavia, Italy

E. ALLAIS
ISO4 s.n.c.,
Torino, Italy

E. RACCHETTI
Dipartimento di Scienze Ambientali,
Università di Parma, Italy

Abstract

In agricultural watersheds, the management of nitrate contamination in rivers requires the understanding of the existing relationships between soil, groundwater and surface water. The reported data correspond to three sampling campaigns, conducted in different seasons on surface water in a Nitrate Vulnerable Zone of Lombardy (Northern Italy). The Oglio River, its tributaries, one spring, and effluents from wastewater treatment plants were sampled to determine N content, speciation and nitrate isotopes. The nitrate content increased along the Oglio River, mostly due to groundwater inputs. In summer, nitrate tended to decrease at the downstream reach, whilst this trend was not clear in autumn and winter campaigns. In summertime chemical and isotopic data suggest the presence of weak denitrification in the Oglio riverbed. Chemical, isotopic data and flow measurements allow the definition of the N fluxes and identification of sources and processes affecting the nitrate concentration in the river.

1. INTRODUCTION

Nitrate contamination in surface [1] and groundwaters [2] is one of the most studied problems of the last years. The environmental impact of this phenomenon

in Europe is highlighted in the Council Directive 91/676//EEC, identifying Nitrate Vulnerable Zones (NVZ) where action must be undertaken in order to reduce pollution caused by nitrates from agricultural sources. In the environment, the presence of a low nitrate concentration in water is often related to a natural origin of this anion. High concentration levels can impair drinking water quality [3] and, in case of surface waters, can contribute to eutrophication [4, 5]. In most cases, high concentrations arise from sources related to human activities, such as agriculture [6] and animal farming. Nevertheless, in watersheds draining urban areas, a contribution from point sources such as effluents from wastewater treatment plants may be present.

The purpose of this study is to investigate the origin of nitrate in the lower Oglio River and in surface waters from its watershed, most of it being designated as NVZ. Since this agricultural watershed is also characterized by the presence of urban settlements and wastewater treatment plants, efficient and effective remedial actions can only be based on a correct source apportionment. With this aim we combined measurements of concentration with measurements of the isotopic composition of dissolved nitrate ($\delta^{15}N_{NO3}$ and $\delta^{18}O_{NO3}$). In addition to source identification, isotope analyses may also evidence the biological processes, (e.g. nitrification and denitrification) [7] that contribute to modify concentration and the chemical form of nitrogen species released in the environment.

2.   MATERIALS AND METHODS

2.1. Study site

The lower Oglio River (Fig. 1) flows for 154 kilometres across the Po Plain of Lombardy (Northern Italy), from the southern end of Lake Iseo to the Po River confluence. The Oglio River receives both natural and artificial tributaries. The most important natural tributaries are the Strone, the Mella and the Chiese Rivers, flowing into the Oglio River after 75, 92, and 123 km respectively.

The Po Plain is an alluvial aquifer mostly deriving from the dismantling of Alpine chain. The substrate is constituted by silicate minerals varying in grain size from coarse to fine from north to south. In the northern sector, the water table depth is approximately 30 m below surface. About 30 km south of the Iseo Lake, the Oglio River flows through an area characterized by the presence of many springs. In this area, indeed, the geological transition from the higher plain (coarser grain size) to the lower plain (finer grain size) occurs, causing the water table to rise to the topographic surface. According to the study realized for the Water Protection Plan of Lombardy [8], the Oglio river is fed by groundwater along most of its length.
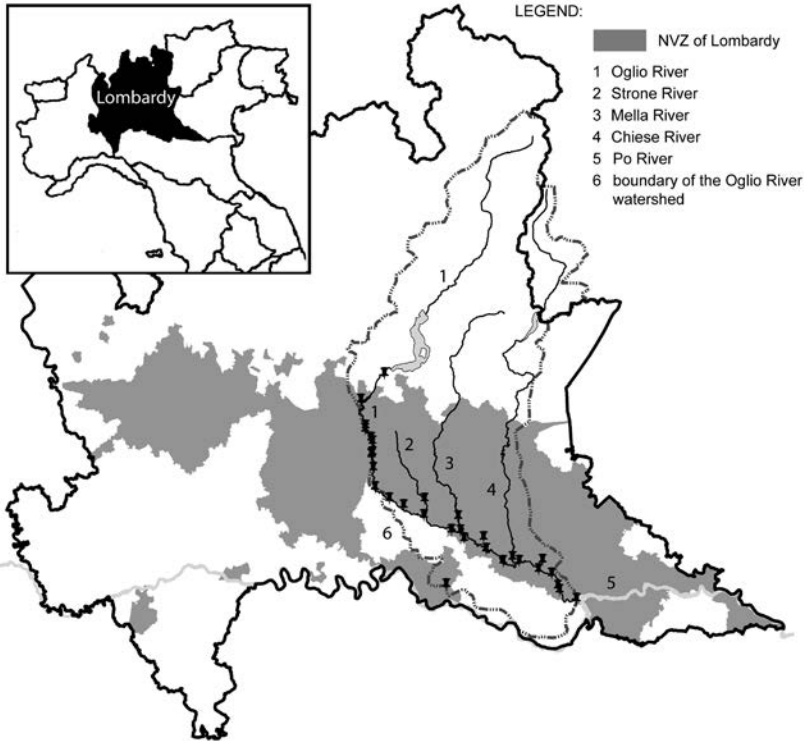
FIG. 1. Location of the study area. The Oglio River watershed is indicated with a dashed line. Black dots indicate the sampling sites of the three campaigns (August 2009, December 2009 and February 2010).

2.2. Sampling and analyses

Three sampling campaigns were performed in August 2009 (summer), December 2009 (late autumn) and February 2010 (winter). Each sampling campaign was conducted during several days. The main Oglio River water course, for its entire length, and its tributaries at the closing section, were sampled. Some samples were also collected from outflows of sewage treatment plants and from two fish farms, for a total number of samples ranging between 69 and 80 for each campaign. Samples were characterized for N species, sulphate and chloride. Based on these results, selected samples were also analysed for $\delta^{15}N_{NO3}$ and $\delta^{18}O_{NO3}$ by IRMS. Isotope analyses were performed using a modified method from Ref. [9]. The analytical precision is $\pm 0.5‰$ for $\delta^{15}N$ and $\pm 1‰$ for $\delta^{18}O$. International standards IAEA N1 and IAEA N3 were used for calibration.

3.   RESULTS

The concentration of N–NO$_3$ in water sampled from the Oglio River shows a wide range of values, spanning from 0.15 up to 7.60 mg\L. Concentrations tend to increase down gradient, with few seasonal differences. It is observed that:

(1)   In the upper part of the river course (0–20 km), the N–NO$_3$ content is rather uniform and lower than 1 mg/L (in summer lower than 0.5 mg/L);

(2)   In the middle part (20–104 km), a steep increase in concentration in all seasons is observed. Summer is characterized by the highest increase in nitrate concentration, occurring between 20 and 50 km (from 0.6 to 7.6 mg/L) and by an almost constant concentration down to 104 km. In winter and autumn, the increase occurs over longer distances, with a similar gradient, although in autumn concentrations are generally higher;

(3)   In the lower part (104 km to closing section) concentration changes are observed. In summer and in winter, the nitrate concentration decreases, whilst in autumn it is variable with no clear tendency.

The number and type of samples selected for the $\delta^{15}N_{NO3}$ and $\delta^{18}O_{NO3}$ analyses is different for the three sampling campaigns. In the autumn campaign water samples of the Oglio River were selected from both upstream and downstream, while summer and winter samples refer only to the middle part down to the closing section.

The isotopic composition of samples collected from the middle up to the closing section of the Oglio River in all seasons seems to be consistent with nitrate originated from natural and anthropogenic organic matter (Figs 2A, 2B and 2C). A contribution from atmospheric deposition or nitrified synthetic fertilizers is found in samples collected upstream, during autumn, which are also characterized by lower nitrate concentrations (Fig. 2B). As expected, water collected from waste water treatment plants shows an isotopic signature typical for anthropogenic organic matter; in one case denitrification is also evident (Fig. 2C). The natural tributaries are characterized by an organic origin of nitrate, but samples do not always cluster with those belonging to the Oglio River.

During autumn, we collected also one sample of spring water outflowing in the upper part of the watershed. This sample (evidenced in Fig. 2B), shows a high nitrate concentration, and an isotopic composition that can be attributed to anthropogenic organic matter. Results are in agreement with those reported in Ref. [10], which analysed 14 lowland springs in the Po River Plain and found that nitrate concentration had a mean value of about 8.4 mg/L. The water samples of the same environments also showed elevated N$_2$O concentrations, indicating a huge N metabolism (denitrification and nitrification).

Fig. 2B also shows the trend of isotopic compositions along the Oglio water course. It is known that the Oglio river is fed by groundwater along its course [8], although this phenomenon is hard to quantify. Mixing of river water with groundwater
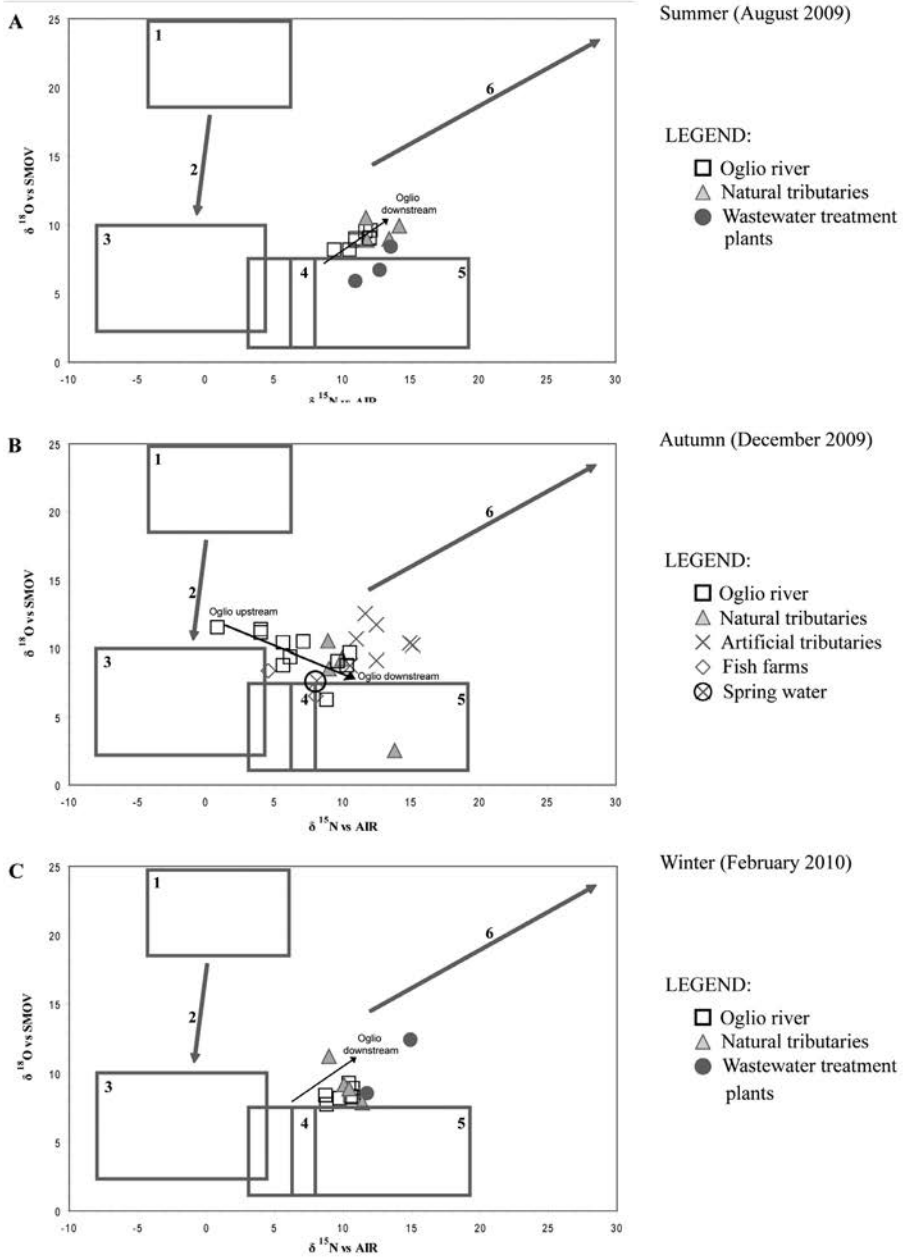
FIG. 2. Isotopic composition of dissolved nitrates. 1= synthetic fertilizers; 2 = nitrification processes on mineralized synthetic fertilizers; 3 = mineralized synthetic fertilizers; 4 = soil organic matter; 5 = animal manure, septic tank effluents, sewage; 6 = evolution during denitrification. Modified after Ref. [7].

233

could explain the upstream variation of nitrate concentrations and isotopic composition observed in autumn.

In the middle and lower part of the watershed, the Oglio river flows through an area where groundwater is poor in nitrate because of the presence of denitrification processes [11]. In the lower part, nitrate concentration in river water is also seen to decrease. Isotope data do not evidence a clear presence of denitrification, especially in autumn and winter, since they tend to cluster and not to align along a denitrification slope. Only in summertime are isotope data slightly better distributed along a denitrification line, and, together with the chemical analyses of nitrate content, suggest the possible presence of this process, even if limited. In the other seasons, based on the available data, it is difficult to prove that the abatement of nitrate concentrations in river water is due to dilution with highly denitrified groundwater.

A nitrogen mass balance, realized for the lower Oglio River basin reported by Ref. [12], suggests an elevated impact of agricultural activities in this watershed. Livestock manure, synthetic fertilizers, biological fixation, atmospheric deposition and wastewater sludge contribute 51, 34, 12, 2 and 1% of total N input, respectively, while crop uptake, ammonia volatilization and denitrification in soils contribute 65, 21 and 14% of total N output, respectively. In the watershed, N inputs exceed outputs by 40 056 t N/a, resulting in an average surplus of 180 kg N·ha^{-1}·a^{-1}. The higher surplus rates were found in municipalites of the middle reach of the Oglio River watershed (>550 kg N·ha^{-1}·a^{-1}) where we measured high nitrate concentrations in riverwater and the isotopic data showed a N origin from anthropogenic organic matter. About 34% of the N surplus is exported annually from the basin through the Oglio River, while the remaining amount (about 27 000 t N/a) undergoes other unaccounted processes within the watershed.

4.   CONCLUSION

The coupled analysis of $\delta^{15}N_{NO3}$ and $\delta^{18}O_{NO3}$ is confirmed as a useful tool in studies regarding the nitrate contamination of surface water. It was also clear that the understanding of hydrology, and the connection among surface and ground water is crucial for the comprehension of environmental behaviour of this contaminant. Therefore surface water data needs to be coupled with those of groundwater. Future efforts will address the combination of chemical and isotopic data with flow measurements, allowing the quantification of the N fluxes and identification of sources and processes affecting the nitrate concentration in the river.

ACKNOWLEDGEMENTS

REFERENCES

[1]   KWANG-SIK, LEE, et al., Tracing the sources of nitrate in the Han River watershed in Korea, using $\delta^{15}N$–NO_3^- and $\delta^{18}O$–NO_3^- values, Sci. Total Environ. **395** (2008) 117–124

[2]   SAVARD, M.M., et al. Nitrate isotopes unveil distinct seasonal N-sources and the critical role of crop residues in groundwater contamination, J. Hydrol. **381** (2010) 134–141

[3]   CAMARGO, J.A., ALONSO, A., Ecological and toxicological effects of inorganic nitrogen pollution in aquatic ecosystems: A global assessment, Environ. International **32** (2006) 831–849.

[4]   HILTON, J., et al., How green is my river? A new paradigm of euthrophication in rivers, Sci. Total Environ. **365** (2006) 66–83.

[5]   SMITH, V.H., SCHINDLER, W.D., Eutrophication science: where do we go from here?, Trends Ecol. Evol. **24** 4 (2009) 201–207.

[6]   SACCHI, E., et al., "A regional survey on nitrate contamination of the Po valley alluvial aquifer (Northern Italy)", Int. Symp. on Advances in Isotope Hydrology and its role in Sustainable Water Resources Management, IAEA, Vienna 21–25 May 2007, IAEA-CN–151/34, Vol. 2 (2007) 471–478.

[7]   CLARK I., FRITZ P., Environmental Isotopes in Hydrogeology. Lewis Publishers, Boca Raton, FL (1997) 328.

[8]   REGIONE LOMBARDIA, "Programma di Tutela e Uso delle Acque, Allegato 3 alla Relazione generale — Classificazione dello stato quantitativo dei corpi idrici sotterranei di pianura", Regione Lombardia, Risorse Idriche (2006), (in Italian), http://www.ors.regione.lombardia.it/resources/pagina/N12032ced450401d4ce6/N12032ced-450401d4ce6/allegato_3.pdf.

[9]   SILVA, S.R., et al., A new method for collection of nitrate from fresh water and the analysis of nitrogen and oxygen isotope ratios, J. Hydrol. **228** (2000) 22–36.

[10]   LAINI, A., et al., Greenhouse Gas (CO_2, CH_4 and N_2O) in Lowland Springs within an Agricultural Impacted Watershed (Po River Plain, Northern Italy), Chem. Ecol. **27** (2011) 177–187.

[11]   SACCHI, E., et al., "Stable isotopes of dissolved nitrate and boron as indicators of the origin and fate of nitrate contamination in groundwater: results from the western Po plain (Northern Italy)", Int. Symp. On Isotopes in Hydrology, Marine Ecosystems, and Climate Change Studies, IAEA, Principality of Monaco 27 March – 1 April 2011, IAEA-CN–186–070 (2011), (this volume).

[12]   SOANA, E., et al., Soil budget, net export and potential sinks of nitrogen in the lower Oglio River watershed (northern Italy), CLEAN **39** (2011) 956–965.

ISOTOPE INVESTIGATIONS OF NITROGEN COMPOUNDS IN DIFFERENT AQUATIC ECOSYSTEMS IN CYPRUS, RUSSIA AND UKRAINE

A. VOROPAEV, S. VOERKELIUS, L. EICHINGER
Hydroisotop GmbH,
Schweitenkirchen, Germany

V. GRINENKO
Vernadsky Institute of Geochemistry and Analytical Chemistry,
Russian Academy of Sciences,
Moscow, Russia

Abstract

The isotope analyses of nitrogen compounds is a powerful tool for the investigation of anrthropogenic influence on the nitrogen cycle in terrestrial and aquatic ecosystems. The isotopic composition of nitrogen and oxygen in nitrates from different groundwater aquifers in Cyprus reflects anthropogenic inputs of nitrogen mainly from industrial fertilizer application in agriculture. Significant denitrification as identified at many sampling sites is an important process, which reduces nitrate concentrations in groundwater. In surface water ecosystems anthropogenic influences and natural environmental changes are detected by the isotopic composition of nitrogen in suspended organic material and in bottom sediments. In the oligotrophic fresh water of Lake Galich in Russia the waste water outflow is a reason for the local increase of $\delta^{15}N$ values in bottom sediments, where the nitrogen and carbon isotopic compositions of unpolluted sediments are very homogeneous. In the Neva estuary in Russia the lateral destribution of $\delta^{15}N$ values in upper layers of bottom sediments reflects changes in the mixing pattern of marine and continental organic matter caused by a flood protection dam building in the Dneprovsko-Bugsky estuary in Ukraine — probably the increasing influence of anthropogenic ^{15}N enriched nutrient load.

1. INTRODUCTION

One of the aspects of human influences on aquatic ecosystems is an increasing input of nitrogen compounds — nitrate and ammonium, which leads to a degradation of water quality. The increase of dissolved inorganic nitrogen content also enhances biological and microbiological processes like nitrification and denitrification in ground and surface water and primary production in surface water. Variations in isotopic compositions of dissolved nitrogen compounds and organic compounds involved in these processes have been used for investigations on nitrogen cycles for

decades. In this paper we present results of case isotope studies which were carried out in different regions and provide information about anthropogenic influence on different aquatic ecosystems, stored in inorganic and organic nitrogen holding compounds from water, suspended organic material and bottom sediments.
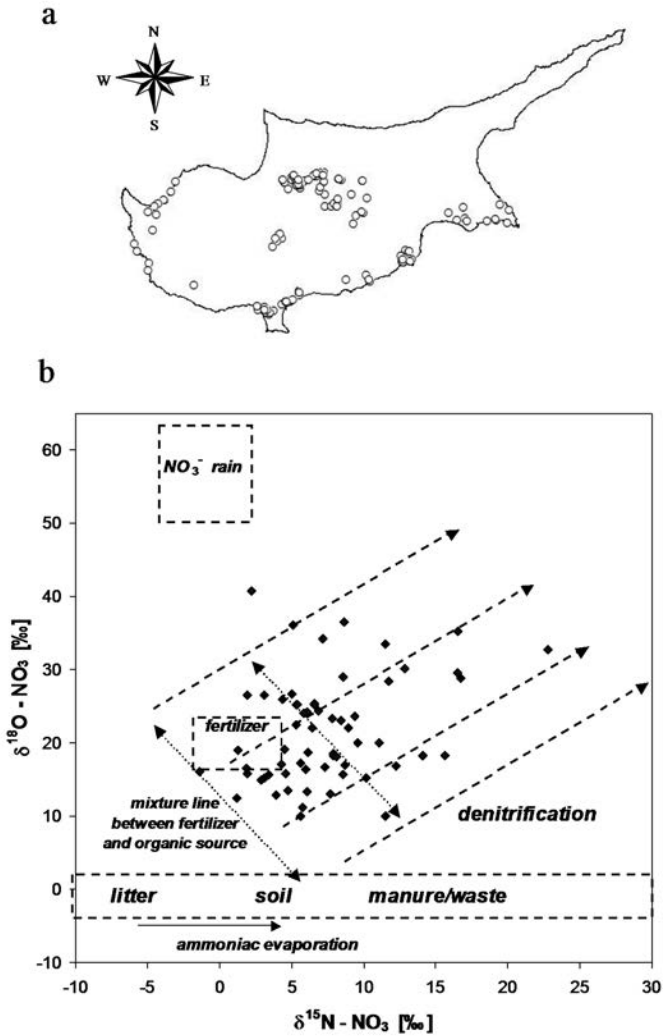
FIG. 1. Sampling point locations (a) and nitrogen and oxygen isotope composition of nitrates in groundwater samples collected in Cyprus - ◆ *(b).*

2.   ISOTOPE STUDIES OF NITRATE IN THE GROUNDWATER OF CYPRUS

An isotope study of nitrate in the groundwater of Cyprus was undertaken on behalf of the Geological Survey Department of Cyprus (GSDC) in 2009–2010. The two groundwater sampling campaigns concerned a number of boreholes in different parts of the island (Fig. 1).

Ten drops chloroform per litre water was added to samples to prevent biological activity. The isotope ratios were measured in the laboratory of Hydroisotop Ltd. in Schweitenkirchen, Germany. Nitrate was isolated as KNO_3 and converted to N_2 and CO_2 through pyrolysis at 550°C with graphite under vacuum. After cryogenic separation gases were analysed using an isotope ratio mass spectrometer 'MAT–251' with a double inlet system. The mass spectrometer was calibrated daily according to international standards ($NO_{\bar{3}}$, USGS 34, USGS 35). Analysed isotope abundance ratios are reported in delta notations ($\delta^{18}O_{NO3}$, $\delta^{15}N_{NO3}$ in ‰) relative to Vienna Standard Mean Ocean Water (V–SMOW) or to air nitrogen.

Groundwater bodies exhibit a wide range of nitrate contents from 1 to 360 mg/L and a wide range of nitrogen and oxygen isotope ratios. All results are presented in Fig. 1 in a $\delta^{15}N/\delta^{18}O$ diagram. Additionally to the results for the samples the value ranges for rain, fertilizers, manure, etc. are displayed [1]. The overall interpretation bears hints towards a two component mixture of fertilizers with low $\delta^{15}N$ values and organic sources which are probably manure from cattle farming or waste water from urbanized areas. One sample suggests the influence of atmospheric nitrate. From these primary isotope signatures dentrification paths can be calculated, which show the different degrees of nitrate dentrification in groundwater. For approximately one fifth of the samples significant denitrification is identified because of increased values of both $\delta^{18}O_{NO3}$ and $\delta^{15}N_{NO3}$. Modelled enrichment paths for signatures of different primary mixtures using the Rayleigh equation are sketched in for better visualisation.

3.   ISOTOPE INVESTIGATIONS OF NITROGEN IN BOTTOM SEDIMENTS AND SUSPENDED ORGANIC MATERIAL IN LAKE AND ESTUARINE ENVIRONMENTS IN RUSSIA AND UKRAINE

Isotope investigations of nitrogen in bottom sediments and suspended organic material in lake and estuarine ecosystems were carried out in 1989–1993 as a part of environmental studies on behalf of the local ecological authorities of Russia.

Sediment cores and surface sediment samples were collected from a ship with gravity corers, cut in 1–2 cm slices and stored in PE bottles in cool boxes until futher processing. The suspended organic material (SOM) was collected by filtration of surface water through a glassfibre filter, dried and stored on the filter in PE bottles in cool boxes. The isotope ratios were measured in the isotope laboratory of the Vernadsky Institute, Russian Academy of Sciences, in Moscow. The SOM samples as well

as bottom sediment samples (bottom sediment samples after acidification with HCL to remove carbonates) were individually combusted with CuO/Cu under vacuum; amounts and isotope ratios of N_2 and CO_2 were measured with isotope ratio mass spectrometer 'MI–1201'. The results were used mainly in internal reports, and are partly still unpublished. Since that time a large number of results from similar and more detailed studies in different regions of the world have been published giving the opportunity for better understanding and interpretation of our data [2–5].

2.1. Lake Galich

Lake Galich is a continental oligotrophic fresh water lake in the Kostroma region of Russia. The lake is about 16 km long from West to East and 6 km wide from South to North. The depth is from 2 to 5 meters, due to low sedimentation and relatively high primary production bottom sediments have high organic contents (C org. 15–60%) and are classified as a sapropel. The samples of bottom sediments were collected in different parts of the lake from the depths 1–50 cm. The sediments imply very homogeneous isotope compositions of nitrogen and carbon ($\delta^{15}N$ = +1.2‰ to +3.7‰, $\delta^{13}C$ = –27.8‰ to –26.4‰) typical for fresh water phytoplankton growing
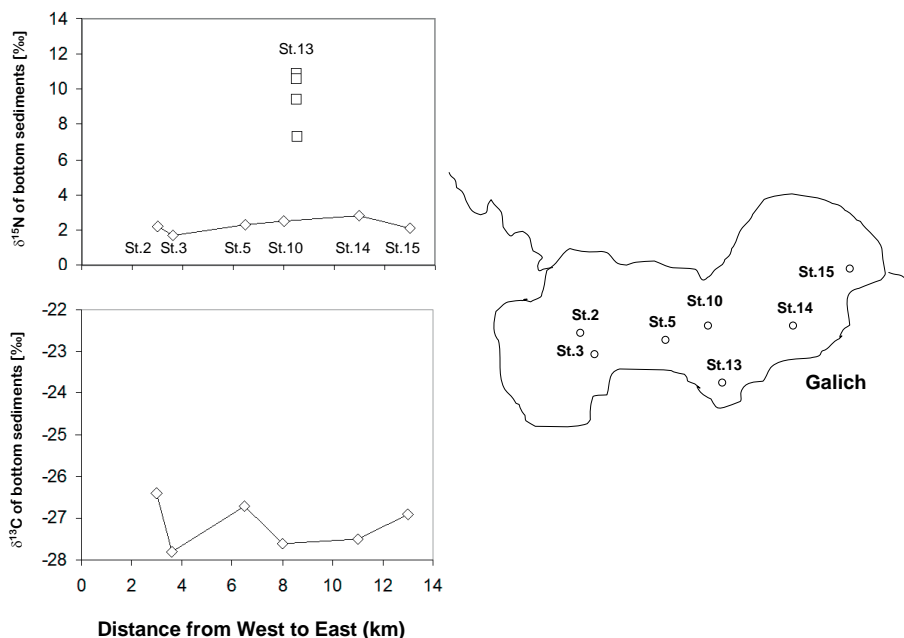
FIG. 2. Station map and isotopic composition of nitrogen and carbon in upper 2 cm of bottom sediments in stations 2, 3, 5, 10, 14, 15 as ◊ and in upper 20 cm in station 13 as □.

without nutrient limitation (Fig. 2). The exception is station 13 near the outflow of the sewage treatment station of the town of Galich. The upper 20 cm of sediments reveal progressive enrichment in $\delta^{15}N$ up to +10.9‰ reflecting debris from uptake by phytoplankton or direct input of nitrogen compounds from urbanised area [6].

2.2. Neva estuary

The Neva estuary represents a transition zone between the Neva river and the Gulf of Finland — a part of the Baltic Sea. The second largest city of Russia, Saint Petersburg, with a population of about 5 million people, is situated in the delta of the Neva and generates a high anthropogenic pressure on the estuarine ecosystem. The flow pattern in this estuary has been essentially changed since 1979 through the construction of a flood protection dam. Bottom sediment samples were collected in 5 stations across the estuary from the depths 1–80 cm. Nitrogen and carbon isotope compositions and carbon and nitrogen contents were measured (Fig. 3a).

The $\delta^{15}N$ and $\delta^{13}C$ values and organic carbon and nitrogen contents demonstrate a general tendency to increase towards the mouth of estuary, especially at depths under 10 cm. In the upper 10 cm of sediments the pattern of $\delta^{15}N$ and $\delta^{13}C$ values is more complicated and demonstrates a progressive upcore increase of $\delta^{15}N$ in Station 2 and progressive decrease of $\delta^{13}C$ in Station 5. Organic carbon concentration in sediments shows a local minimum at Station 2. Assuming the lowest $\delta^{13}C$ (–28‰) and $\delta^{15}N$ (–2‰) values reflect, as in lake Galich, freshwater autochthonous phytoplankton production or allochtonous organic matter that was transported with river water, the progressive enrichment of ^{13}C and ^{15}N content towards the sea reflecting the growing influence of seawater in the lower part of the estuary. The top 10 cm of sediments reflect changes in the mixing pattern in the estuary due to a flood protection dam building since 1979, which leads to an increase of freshwater material in the upper part of the estuary (St. 5.) and the ^{15}N and ^{13}C enriched organic material, characteristic of the marine sections of the estuary, behind the dam in stations 2 and 1 [7].

2.3. Dneprovsko-Bugsky estuary

The Dneprovsko–Bugsky estuary connects the two biggest Ukrainian rivers Dnepr and Bug with the Black Sea. Along the estuary samples of bottom sediments from the depths 1–16 cm, suspended organic material (SOM) and sulphate from surface water were collected at 4 stations (Fig. 3b). The isotope composition of sulphur in surface water sulphate and the isotopic composition of carbon in SOM reflect mixing of sea and fresh water along the estuary with progressive enrichment in ^{34}S in sulphate and ^{13}C in SOM towards the sea. The isotopic composition of nitrogen in the uppermost 1–3 cm of sediments is very close to that found in surface water SOM; the ^{15}N contents of nitrogen decrease with depth/age of sediments in both investigated
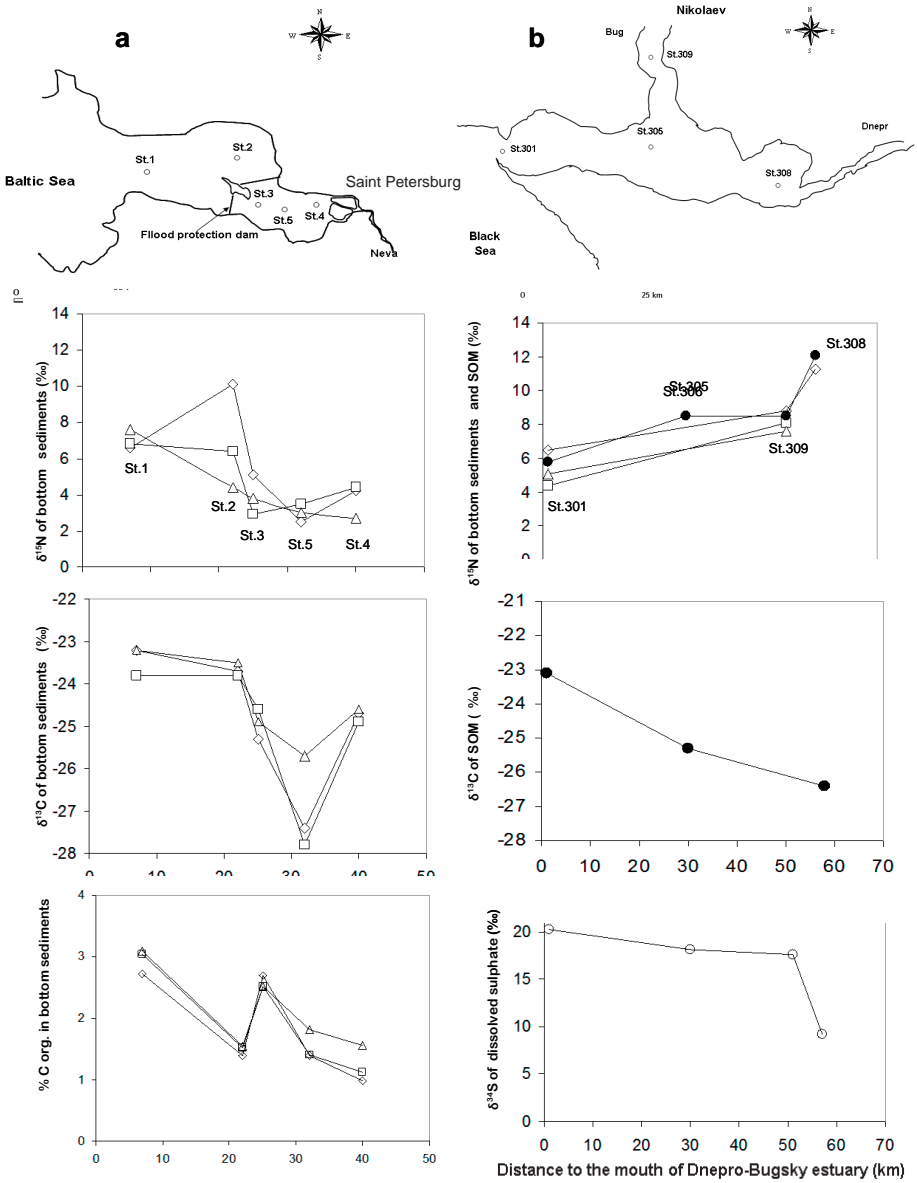
FIG. 3. Station maps and isotope composition of nitrogen, carbon and C org. concentration in bottom sediment cores from different depths: ◊ 0–3 cm, □ 3–7 cm, Δ 7–15 cm, in SOM from surface water- ●, isotope composition of sulphur in dissolved sulphate- ○ , in (a) — Neva estuary and (b) — Dnepro-Bugsky estuary

242

sediment cores. The lateral distribution of δ^{15}N values in SOM and in bottom sediments is quite different to those from the Neva estuary with maximal ^{15}N enrichment up to +12‰ in the upper, fresh water part of the estuary.

3. DISCUSSION

The groundwater of Cyprus is highly influenced by anthropogenic inputs of nitrogen mainly from industrial fertilizer applications in agriculture; other sources such as organic fertilizers, sewages or atmospheric nitrate input are of subordinate importance. Significant denitrification as identified at many samplings is an important process, which naturally reduces nitrate concentrations in groundwater.

In surface water ecosystems isotopic compositions of nitrogen and carbon in suspended organic material, mainly phytoplankton, reflect sources of these elements and processes affecting original isotope signatures. The sinking of particulate material has been shown to provide the preservation of these isotopic signals in the underlying bottom sediments in oceans [8]. The similarity of nitrogen isotope compositions in SOM and the upper 3 cm of bottom sediments, as observed in our study on the Dneprovsko-Bugsky estuary, strongly supports this concept and provides an opportunity to reconstruct the temporal and lateral changes stored in bottom sediment records. In the Neva estuary the δ^{15}N and δ^{13}C values of sediments deeper than 10 cm show an increasing trend from the fresh water part of estuary towards the sea and reflects 'normal' mixing of marine and continental organic matter [9]. The upper 10 cm indicate progressive changes in this mixing process as a result of the building of a flood protection dam. In the Dneprovsko–Bugsky estuary the lateral distribution of δ^{15}N values in SOM and in bottom sediments is inverse to that of the Neva estuary with a maximum in upper fresh water sections, though δ^{34}S in sulphate and δ^{13}C in SOM comply with normal mixing. This effect has also been observed in the Scheldt estuary [10, 2] as a result of incorporation by phytoplankton dissolved in surface water ammonium, which is strongly enriched in ^{15}N because of nitrification in surface water. The increase of δ^{15}N towards the top of sediment cores is probably a result of increasing influence of anthropogenic, ^{15}N enriched, nutrient load in the Dneprovsko-Bugsky estuary, similar to that found in coastal marine sediments of the Baltic Sea [4]. The waste water outflow is a reason for the local increase of δ^{15}N values in bottom sediments in freshwater Lake Galich, where nitrogen and carbon isotope compositions of unpolluted sediments are very homogeneous.

ACKNOWLEDGEMENTS

the Geological Survey Department of Cyprus, Evelthon G. Iacovides und Stalo A. Iacovides from Epsilon Consulting Ltd., Nicosia, Cyprus. The sampling campaign in the Dneprovsko-Bugsky estuary was held under the supervision of Dr. Yury Gursky from Moscow State University. Prof. Dr. P. Horn from Ludwig Maximilian, University of Munich, kindly provided suggestions and stimulating remarks on this manuscript.

REFERENCES

[1]   BÖTTCHER, J., STREBEL, O., VOERKELIUS, S., SCHMIDT, H.-L., Using isotope fractionation of nitrate-nitrogen and nitrate-oxygen for evaluation of microbial denitrification in a sandy aquifer, J. Hydrol. **114** (1990) 413–424.

[2]   DE BRABANDERE, L., et al., $\delta^{15}N$ and $\delta^{13}C$ dynamics of suspended organic matter in freshwater and brackish waters of the Scheldt estuary, J. Sea Res. **48** (2002) 1–15.

[3]   MIDDELBURG, J.J., NIEUWENHUIZE, J., Nitrogen isotope tracing of dissolved inorganic nitrogen behaviour in tidal estuaries, Estuarine, Coastal and Shelf Science **53** (2001) 385–391.

[4]   VOSS, M., LARSEN, B., LEIVUORI, M., VALLIUS, H., Stable isotope signals of eutrophication in Baltic Sea sediments, J. Marine Systems **25** (2000) 287–298.

[5]   ZHANG, J., WU, Y., JENNERJAHN, T.C., ITTEKKOT, V., HE, Q., Distribution of organic matter in the Changjiang (Yangtze River) Estuary and their stable carbon and nitrogen isotopic ratios: Implications for source discrimination and sedimentary dynamics, Marine Chemistry **106** (2007) 111–126.

[6]   VOROPAEV, A., GRINENKO, V., MINEEV, S., "The influence of anthropogenic factors on the isotopic and geochemical parameters of the lake Galich (Kostroma region) during the last decades", Abstracts, XIII Symposium on Isotope Geochemistry, Moscow (1992) 42–43.

[7]   GRINENKO, V., VOROPAEV, A., MINEEV, S., PANTELEEV, G., "Changes in isotopic and chemical composition of bottom sediments in the Neva Gulf, caused by the construction of a flood-protection dam", Abstracts, XIII Symposium on Isotope Geochemistry, Moscow (1992) 56–57.

[8]   ALTABET, M.A., FRANCOIS, R., Sedimentary nitrogen isotopic ratio as a recorder for surface ocean nitrate utilization, Global Biogeochem. Cycles **8** (1994) 103–116.

[9]   OWENS, N.J.P., Variations in the natural abundance of ^{15}N in estuarine suspended particulate matter: A specific indicator of biological processing, Estuarine, Coastal and Shelf Science **20** (1985) 505–510.

[10]   MARIOTTI, A., LANCELOT, C., BILLEN, G., Natural isotopic composition of nitrogen as a tracer of origin for suspended organic matter in the Sheldt estuary, Geochim. Cosmochim. Acta **48** (1984) 549–555.

DETERMINATION, SOURCE IDENTIFICATION AND GIS MAPPING FOR NITRATE CONCENTRATION IN GROUNDWATER FROM BARA AQUIFER

G.M. ELAMI, A.K. SAM, T.I. YAGOB, S.E.M.B. SIDDEEG, E. HATIM, I. HAJO
Sudan Atomic Energy Commission,
Sudan, Khartoum

Abstract

This study was carried out to determine the level of nitrate concentration in well water from Bara aquifer in north Kordofan state (west central Sudan). The analysis was conducted for 69 wells from different villages within the Bara basin. Spectophotometric analysis was used to determine nitrate, nitrite and ammonia. Results revealed that nitrate concentration range was from 9.68 to 891 mg\L in the sampled well with 81% exceeding the maximum permissible limits set for drinking water by WHO and SSMO. Animal waste and organic soil nitrogen were found to be the source of nitrate in these wells as indicated by ^{15}N. The majority of wells with high nitrate are in the north and the north east part of the study area are shown by the GIS predictive map.

1. INTRODUCTION

Nitrogen exists in the environment in many forms and changes forms as it moves through the nitrogen cycle. This cycle operates in both natural and cropland ecosystems. Although nitrate occurs naturally in groundwater, in most cases higher levels are thought to result from overfertilized fields, feed lots, improper disposal of human and animal waste, or improper well construction and well location [1–3]. Due to its high mobility nitrate can be leached through the soil and eventually reach groundwater. Grazed grassland leaching losses were found to be several times greater than for cut grassland because 80% of the nitrogen consumed by grazing animals is returned to the soil as urine or dung [4–6]. Sandy soils under high rainfall or irrigation have high leaching potential. It has been widely documented that high levels of nitrate in drinking water cause blue baby syndrome, cancer and disruption of thyroid function [7–9]. This study aimed to determine NO_3 levels in groundwater drawn from the Bara aquifer in western Sudan and identifying its possible sources using ^{15}N signature.
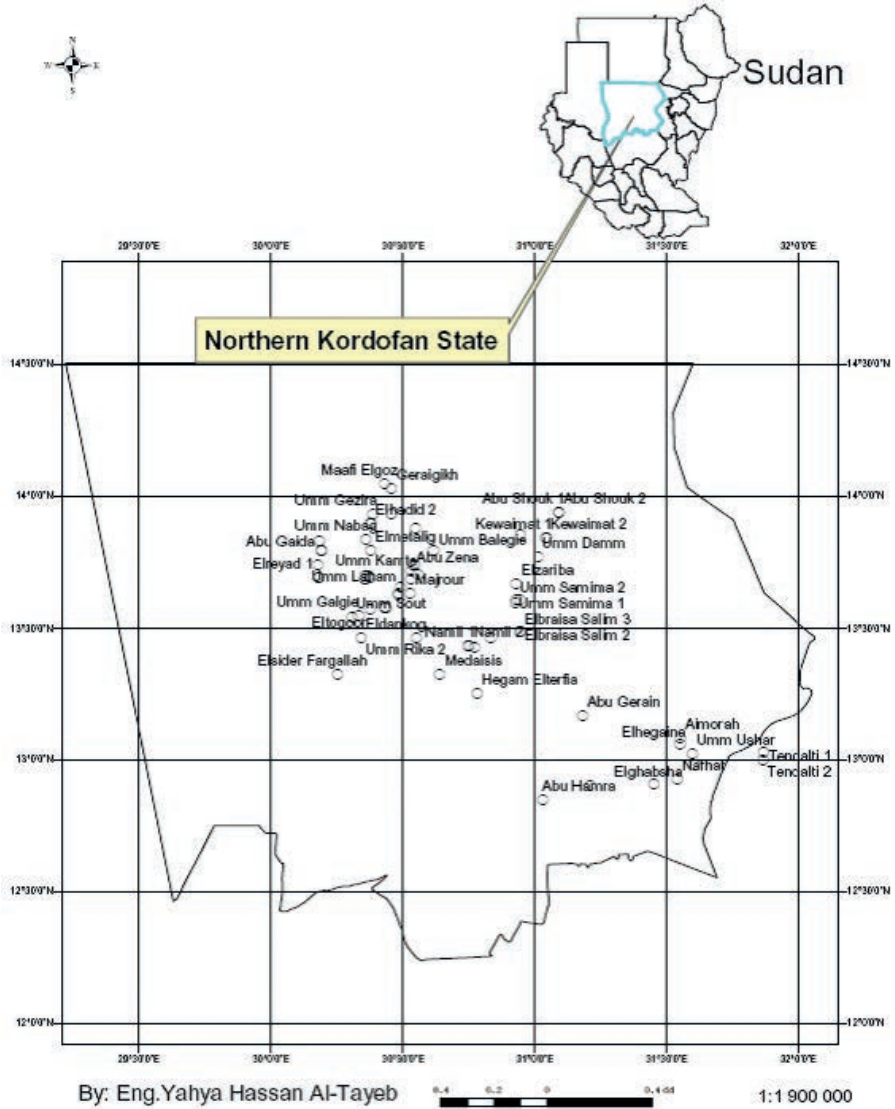
FIG. 1. Map of the study area.

TABLE 1. STATISTICAL SUMMARY OF NITRATE, NITRITE AND AMMONIA CONCENTRATION (mg/L) IN GROUNDWATER SAMPLES COLLECTED FROM WELLS LOCATED IN BARA AQUIFER

Analyse	Sample No.	Min (mg/L)	Percentiles							Max (mg/L)
			10	19	30	50	70	81	90	
Nitrate	69	9.68	28.60	53.68	90.64	146.30	295.90	523.38	631.40	891.00
Nitrite	69	0.01	0.01	0.013	0.03	0.07	0.19	0.327	0.38	9.81
Ammonia	69	0.01	0.01	0.010	0.02	0.05	0.07	0.09	0.11	0.40

2. MATERIAL AND METHOD

2.1. The Study Area

The Bara basin is typical of a shallow aquifer located in a sandy semi-arid zone rich in grazing land and hence heavily populated by livestock which represent the major source of livelihood and showing signs of water quality deterioration [10]. The Bara area suffers from drinking water scarcity and extends from the eastern part of North Kordofan State to the western part of the White Nile State covering an area of approximately 600 km^2 (Fig. 1). It is bounded by longitudes 30°00`W and 32°30`E and latitudes 12°30`S and 14°15`N. It covers vast areas that extend over two climatic zones in the sub-saharan region. The northern zone is a semi arid zone and the southern zone represents a poor savannah zone. The rainfall increases in amount and duration southward; it ranges from 200 mm/a in the North to 450 mm/a in the South where the soil is generally clayey and suitable for agricultural activity.

2.2. Sample collection and analysis

A field trip was conducted during September 2007. General hydrological and theoretical geological observations were noted. A total of 69 water samples were collected from wells in different villages. Sampling locations (wells) were recorded with their coordinates, which were taken with the aid of hand-held GPS. In each well two plastic bottles of 2 liters each were filled; one bottle was reserved for chemical analysis and the other bottle was acidified with 2 mL H_2SO_4 for nitrogen isotope analysis. Immediately after collection the pH, dissolved oxygen and electrical conductivity were recorded using a pH/ion meter (555 Corning Pinnacle), dissolved oxygen meter and conduct meter (Hach Sens ion712 Metrohm), respectively. A spectrophotometer (Hach D.R.4000Comlab) was used for measuring nitrate, nitrite and ammonia concentration, which rely on the cadmium reduction method and mass spectrometer for quantitative analysis of the Nitrogen–15 isotope to identify the source of nitrate pollution.

3. RESULTS AND DISCUSSION

3.1. Nitrate, nitrite and ammonia

The nitrate content of the groundwater samples collected from the study area ranged from 9.68 to 891 mg/L with a medium value of 246.99 mg/L as shown in Table 1. Approximately 81% of the 69 sampled wells showed nitrate levels greater than the maximum permissible limit of 50 mg/L set for drinking water by the Sudanese Standards and Metrology Organization (SSMO) and by WHO limits [11]. The highest values of nitrate were found in wells located north east and west parts of the aquifer as indicated by the GIS predictive map depicted in (Fig. 2). Refs [1, 11]
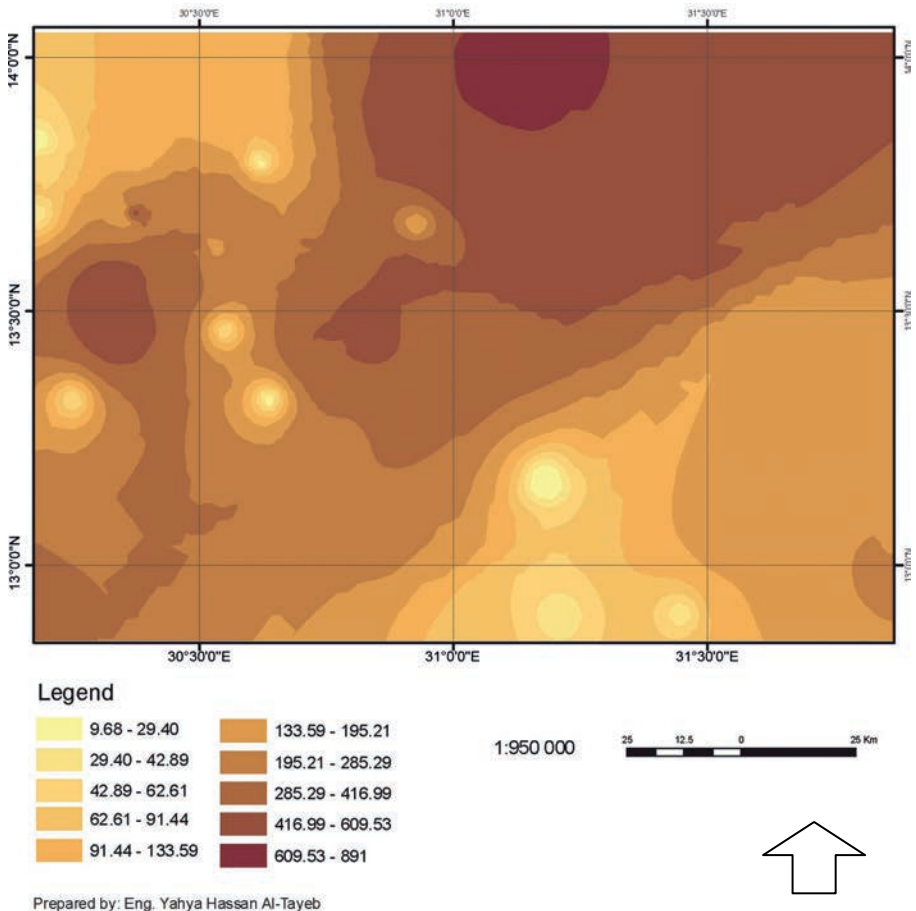
FIG. 2. GIS predictive map of nitrate concentration in Bara aquifer. The highest values of nitrate were found in wells located in the north east and west parts of the aquifer.
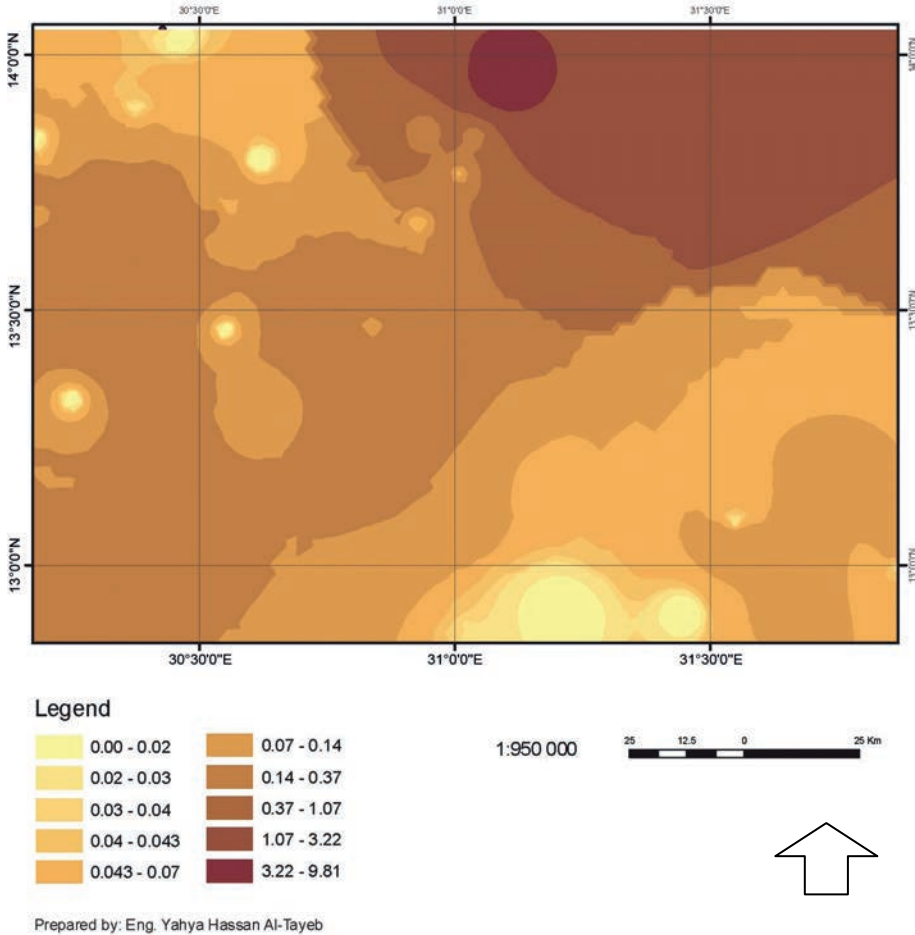
FIG. 3. GIS predictive map of nitrite concentration in the Bara aquifer.

employed the Geographical Information System technology (GIS) for generating regionalized time averaged maps of top aquifer contamination with nitrate from agrochemical fertilizers. In addition, Ref. [1] reported that 95% of the water samples showed nitrate concentrations above the human affected value (3 mg/L NO_3^-) while more than 30% have exceeded the maximum acceptable level (44 mg/L NO_3^-). Costa (2002) reported that nitrate–N concentrations greater than the accepted level for safe drinking water of 10 mg/L were present in 36% of sampled wells and 67% had nitrate concentrations exceeding the background level of 5 mg/L. These results showed that high fertilization and irrigation rates lead to increased hazards of groundwater pollution. Ref. [3] investigated hand pumped wells and dug wells in different areas in Senegal; all the samples from wells are contaminated by high NO_3 contents which
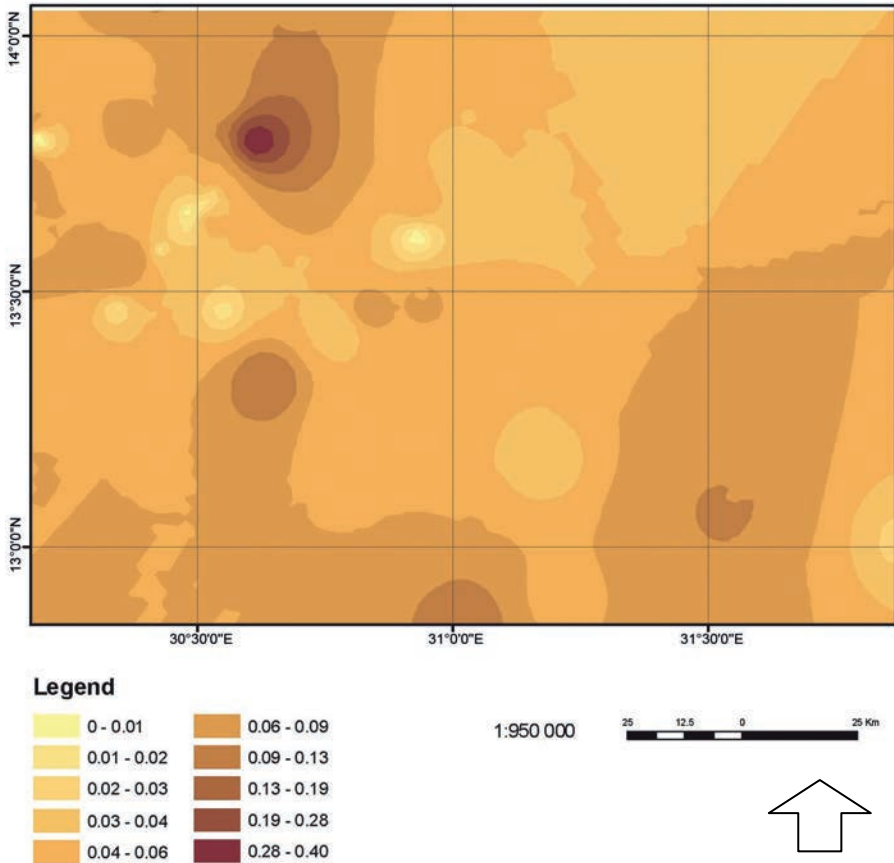
FIG. 4. GIS predictive map of ammonia concentration in the Bara aquifer.

ranged from 100 mg/L to 250 mg/L. The mechanisms of contamination are mainly soil washing and nitrate injection from latrines.

On the other hand, the concentration of nitrite in most of the sampled wells does not constitute a direct problem to consumers as it ranges from 0.01 to 9.81 mg/L with a medium value of 0.07 mg/L. The highest value of nitrite concentration was measured in sample number 66 which was taken from Abu Shouk-2, where the highest value of nitrate concentration was measured. This correspondence gives an indication that nitrite concentration is proportional to nitrate ion concentration and it is also confirmed by the GIS predictive map of nitrite values depicted in Fig. 3. The highest values of nitrite concentrations are mostly found in the northern parts of the area where the water is poorly oxygenated. The nitrite ion is relatively unstable and can be rapidly oxidized to nitrate and is seldom present in well oxygenated or

chlorinated supplies. The recommended guideline values for nitrite in drinking water are 3 mg/L [11] and 2 mg/L (SSMO). Accordingly, the nitrite concentrations for the analysed samples lie far below the maximum levels accepted by both WHO and SSMO with the exception of sample 66 Abu Shouk-2. Traces of nitrite in drinking water may lead to methemoglobinemia in infants, and with long term exposure is a possible cancer risk [9].

The values measured for ammonia concentration in groundwater ranged from 0.01 to 0.4 mg/L with a median value of 0.06 mg/L. According to the WHO [11], the normal concentration levels of ammonia in surface and groundwater should fall below 0.2 mg/L. As such, all the analysed samples showed values below the WHO limit except well no. (28) at Umm Balegie (0.4 mg/L) which is a pipeline station. The sample is collected from the surface as it is well known that ammonia concentration is higher when sampled under these conditions. The SSMO permissible level for drinking water is 1.5 mg/L which is one order of magnitude higher than the maximum value of ammonia concentration measured (0.4 mg/L) in this study. The GIS predictive map for the special distribution of ammonia concentration in the sampled wells is shown in Fig. 4.

3.2. Nitrogen–15 values

Table 2 illustrates the concentration of ^{15}N measured in five representative groundwater samples. The values obtained for $\delta^{15}N$‰ fall within the range of 4.3 to 15.5‰ with a mean value of 7.9‰. The basis for the identification of NO_3 sources using natural abundances of ^{15}N is that as NO_3 originating from different sources has characteristic isotopic ratios. The $\delta^{15}N$ in the range of $+4$ to $+9$‰ indicates original organic N, from animal waste $\delta^{15}N$ is generally greater than $+10$‰ and for N fertilizers typically close to or less than 0‰ [13–16]. The result of this study indicates that nitrate contamination in the Bara basin can be attributed to animal wastes and organic soil nitrogen.

TABLE 2. CONCENTRATION OF ^{15}N IN SOME GROUNDWATER SAMPLES

ID	Depth (m)	Nitrate (mg/L)	$\delta^{15}N$ (‰)
1	NA	698	15.46
2	44	629	4.4
3	34	754	7.3
4	17	400	7.9
5	44	891	4.3
Mean±standard deviations of $\delta^{15}N$ values			7.9±0.6‰

4.   CONCLUSION

Based upon the results obtained in this study, the following concluding remarks can be made:

(1)   Nitrate concentration in 81% of the wells exceeds the maximum permissible limit set for drinking water, and the majority of these wells are located in the north and north eastern part of the study area.

(2)   The ammonia concentration is far below the normal concentration level except in the well No. 28 which is located at Umm Balegie.

(3)   The source of nitrate in the groundwater of the study area is a combination of animal waste and organic soil nitrogen as indicated by $\delta^{15}N$‰ values.

(4)   Further research must consider epidemiological studies as well as devising a monitoring programme for nitrate concentration to evaluate the progress of pollution

(5)   It would be preferable for the local authorities to consider a suitable and affordable method of treatment for reducing nitrate pollution in wells located in north eastern parts of the aquifer.

REFERENCES

[1]   BABIKER, I.S., et al., Assessment of groundwater contamination by nitrate leaching from intensive vegetable cultivation using geographical information system, Environ. Int. **29** (2004) 1009–1017.

[2]   COSTA, J.L., et al., Nitrate contamination of a rural aquifer and accumulation in the unsaturated zone, Agric. Water Management **57** 1 (2002) 33–47.

[3]   TANDIA, A.A., GAYE, C.B., FAYE, A., "Origin, process and migration of nitrate compounds in the aquifers of Dakar Region Senegal", Application of Isotope Techniques to Investigate Groundwater Pollution, IAEA-TECDOC-1046, IAEA, Vienna (1998) 67.

[4]   RYDEN, J.C., BALL, P.R., GARWOOD, E.A., Nitrate leaching from grassland, Nature **311** (1984) 50–53.

[5]   CHO, J.-C., CHO, H.B., KIM, S.-J., Heavy contamination of a subsurface aquifer and a stream by livestock wastewater in a stock farming area, Wonju, Korea, Environ. Pollution **109** (2000) 137–146.

[6]   ALMASRI, N.M., KALUARACHCHI, J.J., Modelling nitrate contamination of groundwater in agricultural watersheds, J. Hydrol. **343** (2007) 211–229.

[7]   VAN MAANEN, J.M.S., et al., Consumption of drinking water with high nitrate levels causes hypertrophy of the thyroid, Toxicology Lett. **72** 1–3 (1994) 365–374

[8]   WEYER, P.J., et al., Municipal drinking water nitrate level and cancer risk in older women: The Iowa Woman′s Health Study, Epidemiology **11** (2001) 327–338.

[9]   KROSS, B.C., Nitrate toxicity and drinking water standards — A review, J. Preventive Medicine **10** 1 (2002) 3–10.

[10]   HAMAD, O.E.-T., EL-BATTAHANI, A., Sudan and the Nile Basin, Aquat. Sci. **67** (2005) 28–41.

[11]   WORLD HEALTH ORGANIZATION, Guidelines for Drinking-water Quality, 2nd edition, Vol. 11, WHO, Geneva (1993).

[12]   FUEST, S., BERLEKAMP, J., KLEIN, M., MATTHIES, M., Risk hazard mapping of groundwater contamination using long term monitoring data of shallow drinking water wells, J. Hazardous Mat. **61** 1–3 (1998) 197–202

[13]   CHEN, J., TANG, C., YU, J., Use of ^{18}O, ^{2}H and ^{15}N to identify nitrate contamination of ground water in a wastewater irrigated field near the city of Shijiazhuang, China, J. Hydrol. **326** 1–4 (2006) 367–378.

[14]   GIRARD, P., HILLAIRE-MARCEL, C., Determining the source of nitrate pollution in the Niger discontinuous aquifers using the natural ^{15}N/^{14}N ratios, J. Hydrol. **199** 3–4 (1997) 239–251.

[15]   KELLMAN, L.M., HILLAIRE-MARCEL, C., Evaluation of nitrogen isotopes as indicators of nitrate contamination sources in an agricultural watershed, Agric. Ecosyst. and Environ. **95** 1 (2003) 87–102.

[16]   CLARK, I., FRITZ, P., Environmental Isotopes in Hydrogeology, Lewis, New York (1997).

CONCENTRATION OF TRITIUM AND MEMBERS OF THE URANIUM AND THORIUM DECAY CHAINS IN GROUNDWATERS IN SLOVENIA AND THEIR IMPLICATION FOR MANAGING GROUNDWATER RESOURCES

M. KORUN, K. KOVAČIČ, J. KOŽAR-LOGAR
Jožef Stefan Institute,
Ljubljana, Slovenia

Abstract

Samples of groundwater were measured in terms of their activity concentration of gamma ray emitters, members of the uranium and thorium decay chains and tritium. The distributions of the number of samples over the measured activity concentrations are presented for ^{238}U, ^{226}Ra, ^{210}Pb, ^{228}Ra, ^{228}Th, ^{40}K and ^{3}H. The distributions have three distinct shapes: log-normal distributions (^{238}U, ^{226}Ra, ^{228}Ra, ^{228}Th), bimodal distributions (^{210}Pb, ^{40}K), and a normal distribution (^{3}H). It appears that the log-normal distributions reflect the dilution of the radionuclides dissolved in the water. The bimodal distributions, being the sum of a log-normal distribution and a distribution having its maximum at the activity concentration of the higher mode, indicate influences from the soil surface, e.g. washout from the atmosphere and fertilizing. The normal distribution indicates mixing with rainwater under circumstances that are characterized by several independent variable parameters.

1.   INTRODUCTION

Slovenia gets a large part of its drinking water from shallow alluvial, karstic and fractured aquifers, which supply more than 97% of the Slovenian population. To manage these groundwater resources properly it is advantageous to know their properties and vulnerability that result from influences on the surface.

It is the aim of this contribution to present the first measurement results of a screening campaign for a characterization of the groundwaters for the activity concentration of natural and anthropogenic beta particle and gamma ray emitters.

In 2009, samples were taken at 58 locations for subsequent tritium measurements. At 49 of these locations, samples for gamma ray spectrometric measurements were also collected. The samples were collected in both the spring and the autumn. Here we present the results of concentration measurements for tritium ^{40}K and ^{210}Pb for all the samples collected. The measurement results for other gamma ray emitters are presented only for the samples collected in the spring.

2.   SAMPLE PREPARATION

The samples for the gamma ray spectrometric measurements were prepared by the evaporation of 50 L of water using forced ventilation, as described in Ref. [1]. However, in spite of filtering the air the dry residue was contaminated by thoron daughters, i.e. thoron with a half-life of 56 s, which passes through the filters and decays in the evaporation cells to its daughter ^{212}Pb with a half-life of 10.6 h. To measure the concentration of ^{228}Th in the dry residue, the daughters from the atmospheric thoron must decay before starting the measurements. In order to allow the daughter to decay before measuring the sample on the gamma ray spectrometer the dry residue samples were aged for at least two days.

The samples for the tritium measurements were prepared using the electrolytic enrichment method, which consists of primary distillation, electrolytic enrichment and secondary distillation. Impurities and other radionuclides that could interfere with the tritium measurements were removed by primary distillation. The electrolytic enrichment was carried out on a 500 mL sample aliquot with a prior addition of sodium peroxide (Na_2O_2). During the electrolysis the samples were subject to a total charge of 1400 Ah and at the end their volume was reduced to approximately 15–20 mL. The samples were neutralized by the addition of lead chloride ($PbCl_2$) and distilled for a second time. The aliquot (8 mL) of the final distillate with a controlled pH was mixed with 12 mL of scintillation cocktail (Ultima Gold LLT, Ultima Gold uLLT or Hi Safe 3) in a 20 mL polyethylene vial. Some 60% of the samples were also prepared for a so-called direct measurement, where the distillate after the primary distillation was mixed with a scintillation cocktail.

3.   MEASUREMENTS

The gamma ray spectrometric measurements are described in Ref. [1]. They were performed on a low activity spectrometer possessing an extended range detector with a beryllium window and a cosmic veto shield. The passive shielding is made up of 15 cm of lead, 10 mm of mercury, 2 mm of cadmium and 2 mm of copper. To measure the concentration of the ^{238}U reliably, the samples were measured twice: at least two days after the evaporation and at least one month later, when the equilibrium between the ^{238}U and its daughter, ^{234}Th, has nearly been achieved. Therefore, the activity concentrations of ^{226}Ra, ^{210}Pb, ^{228}Ra, ^{228}Th and ^{40}K could also be calculated more reliably, as the weighted average of the measurement results obtained from both measurements.

The spectral analysis for the activity calculation of ^{238}U and ^{226}Ra is also described in Ref. [1]. The ^{238}U activity concentration was determined from the peaks at 63 and 92 keV from the decay of ^{234}Th and the peak at 186 keV from the decay of ^{235}U assuming a natural isotopic abundance. The ^{226}Ra activity was calculated from

the peaks belonging to the short-lived ^{222}Rn daughters assuming a disequilibrium between the ^{226}Ra and ^{222}Rn due to its emanation from the sample. The activity concentration of ^{228}Ra was calculated from the peaks at energies of 338 keV, 911 keV and 969 keV, and the activity concentration of ^{228}Th from the peaks at 239 keV, 583 keV and 2615 keV. Coincidence summing effects were taken into account as described in Ref. [2]. The activity concentrations of ^{210}Pb and ^{40}K were calculated from peaks at energies at 46 keV and 1461 keV, respectively.

The tritium measurements were carried out in the Quantulus 1220 liquid scintillation spectrometer. All groundwater samples were measured for 300 min, the spiked samples for 100 min and the background waters for 1000 min. The counting procedures started one day after the sample preparation to avoid any chemoluminiscence. The sequences of all the measurements were performed at least three times. The final results were weighted averages of the activities obtained from measurements after the electrolytic enrichment and direct measurements. The minimum detectable activity for the tritium was approximately 50 Bq/m^3.

4.   RESULTS

Using gamma ray spectrometric measurements the activity concentrations of ^{238}U, ^{226}Ra, ^{210}Pb, ^{228}Ra, ^{228}Th and ^{40}K were measured. The activity of the ^{234}Th was measured as well, but it did not exceed the decision threshold (4 Bq/m^3) in any sample. The distributions of the number of samples over the measurement results are presented in Figs 1–6. The results are presented for samples collected in the first half of 2009, except for the results relating to ^{210}Pb and ^{40}K, where the results for all the samples collected in 2009 are presented. The bins in the figures correspond roughly to

TABLE 1. THE UNCERTAINTIES NEAR THE DETECTION LIMIT AND THE NUMBER OF MEASUREMENT RESULTS, NOT PRESENTED IN FIGS 1–6, AND THEIR AVERAGE

Nuclide	Uncertainty at MDA (Bq/m^3)	Number of measurement results not presented	Average activity (Bq/m^3)
U–238	1	0	—
Ra–226	0.15	2	11
Pb–210	0.5	3	24
Ra–228	0.15	0	—
Th–228	0.05	2	0.9
K–40	1	6	140
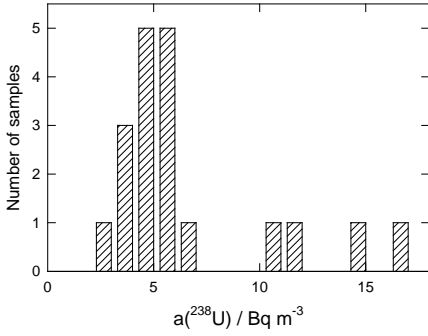
FIG. 1. The probability distribution of the number number of results over the ^{238}U activity concentration.
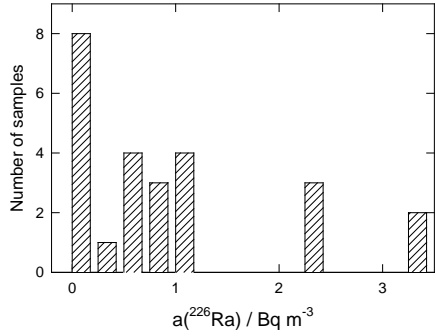
FIG. 2. The probability distribution of the number number of results over the ^{226}Ra activity concentration.
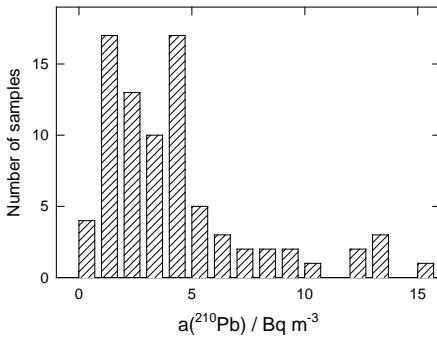
FIG. 3. The probability distribution of the number number of results over the ^{210}Pb activity concentration.
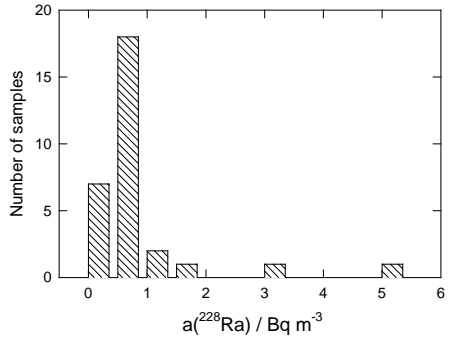
FIG. 4. The probability distribution of the number number of results over the ^{228}Ra activity concentration.
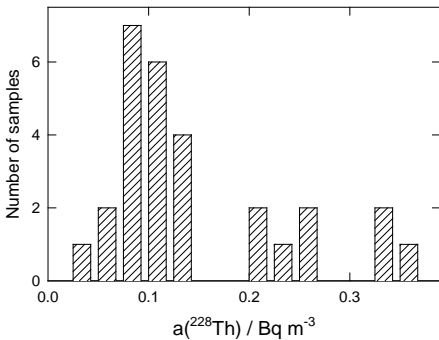
FIG. 5. The probability distribution of the number number of results over the ^{228}Th activity concentration.
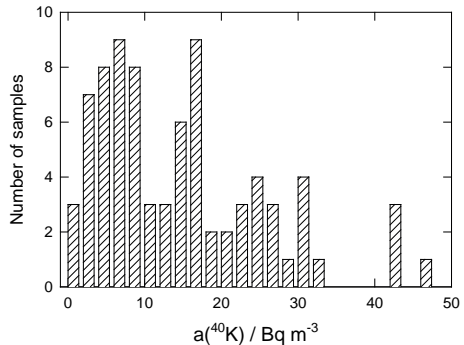
FIG. 6. The probability distribution of the number number of results over the ^{40}K activity concentration.
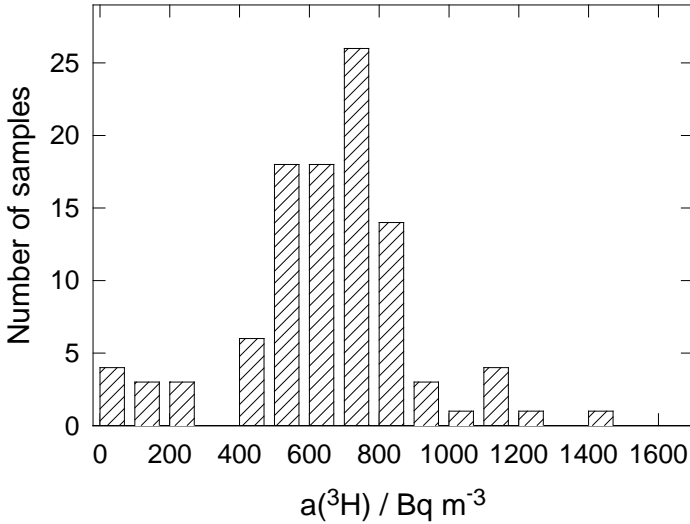
FIG. 7. The probability distribution of the number of results over the 3H activity concentration.

the uncertainties of the measurement results near the detection limit. In Table 1 these uncertainties are given together with the number of measurement results not present in the interval of the activity concentrations presented in the Figs 1–6.

The distribution of the number of samples over the tritium activity concentration is presented in Fig. 7. Here the bin width corresponds, approximately, to the average uncertainty concentration of the activity.

5. DISCUSSION

It is clear from Figs 1–6 that the shapes of the presented distributions fall into three categories: distributions that resemble the shape of the log-normal distribution (^{238}U, ^{228}Ra, ^{228}Th); the distribution for ^{226}Ra, which falls with the activity concentration; and the bimodal distributions (^{210}Pb and ^{40}K). The host material of the Slovenian aquifers are predominantly limestone and dolomite, having a low and fairly uniform activity concentration of the members of the uranium and thorium decay chains. Frequent and large variations in the activity concentrations with respect to the sampling site are therefore not expected. Consequently, the expected shape of the distribution is log-normal, with an average activity concentration given by the solubility of the radionucleus in the water. Thus, more complicated distributions for ^{210}Pb and ^{40}K are, most probably, the result of influences of non-geological factors, caused by e.g. the intrusion of rainwater and the use of fertilizers containing potassium, respectively. For these two radionuclides the distribution is a sum of the log-normal distribution

TABLE 2. MEASUREMENT RESULTS (IN Bq/m^3) OF TWO SAMPLES, EXHIB-
ITING ENHANCED CONCENTRATIONS OF MEMBERS OF THE URANIUM
AND THORIUM DECAY CHAINS

Radionuclide	VP1000	VR2253
^{238}U	2.6 ± 0.3	16.9 ± 1.7
^{226}Ra	16.2 ± 1.0	3.6 ± 0.3
^{210}Pb	8.6 ± 0.5	3.6 ± 0.6
^{228}Ra	1.9 ± 0.2	5.1 ± 0.3
^{228}Th	0.95 ± 0.08	0.82 ± 0.09
^{40}K	18.2 ± 1.5	28.2 ± 2.5
^{3}H	690 ± 100	150 ± 50

and another distribution having its maximum at the mode with the higher activity concentration. The distribution of ^{226}Ra, which does not fall off at low activity concentrations, may reflect difficulties in the spectrum analysis originating from the time dependent background induced by the radon-daughters [1,3].

Among the samples collected, only two exhibit enhanced concentrations of radionuclides. The measurement results for these samples are given in Table 2. It is clear that in the sample VP1000 only the activity concentration of the ^{238}U is not elevated and, in the sample VR2253, the activity concentration of the ^{210}Pb. The catchment of the sample VP1000 consists of Permo-Carboniferous rocks, mainly sandstones. The tritium measurement shows that the water is recent. On the other hand, the sample VR2253 contains older water, with a tritium activity of about 150 Bq/m^3. The aquifier is made of Pliocene unconsolidated sediments, mostly sands and clays.

Where the vulnerability of groundwater resources to influences of anthropogenic pollution is the largest can be inferred from the distribution of the activity concentrations of ^{210}Pb and ^{40}K. In aquifers where the activity concentrations of ^{210}Pb and ^{40}K are close to the maxima at the higher concentration in the bimodal distributions, i.e. 4 Bq/m^3 and 15 Bq/m^3, respectively, the vulnerability may be higher. However, to support this hypothesis additional evidence is needed, e.g. a correlation with the ^{7}Be concentration, the type of aquifer and the concentrations of chemical pollutants.

In the case of tritium the distribution is different compared to the distributions observed in gamma ray emitters. The majority of the samples belong to a normal like distribution with a mean value of approximately 700 Bq/m^3 and a standard deviation of around 200 Bq/m^3. The normal like shape suggests that tritium activities in groundwater are influenced by a number of independent parameters; their variability is reflected in a distribution resembling the shape of a normal distribution. On the other hand, samples having activities less than 200 Bq/m^3 show a distribution,

decreasing with activity concentration, which may resemble a log-normal distribution. These samples could represent groundwaters that were not subject to mixing since the era before atomic bomb testing. In contrast, the activity concentrations falling within the range of the normal distribution may indicate that the corresponding groundwaters are recent.

7.   CONCLUSION

It can be concluded that the relatively homogeneous radioactivity distribution of the Slovenian territory, being dominated by minerals of low concentrations of radioactive substances, is reflected in distributions of activity concentrations of the members of the uranium and thorium decay chains in groundwaters that exhibit a log-normal shape. The more complicated shapes are attributed to the influences from the surface, e.g. the washout of the atmosphere and anthropogenic influences. However, samples can be found with significantly increased activity concentrations, presumably reflecting specific circumstances in the corresponding aquifer.

The bimodal shape of the activity distribution of ^{210}Pb and ^{40}K may reflect influences from the earth's surface on the aquifers and indicate circumstances where the increased vulnerability of groundwater resources to anthropogenic pollution can be expected.

The distribution of the number of samples over the tritium concentration exhibits a symmetrical shape, resembling that of a normal distribution. This shape is attributed to the inflow of rainwater into the aquifers under varying conditions. However, some samples exhibit a low concentration of tritium; these samples are attributed to aquifers with no mixing with the surface water at least since before the period when the atomic bomb tests were performed.

REFERENCES

[1]   KORUN, M., KOVAČIČ, K., Determination of ^{238}U in ground-water samples using gamma ray spectrometry, Appl. Radiat. Isot. **69** 3 (2011) 636–640.

[2]   KORUN, M., MARTINČIČ, R., Activity calculation for voluminous samples in the presence of coincidence summing effects, Nucl. Instr. and Meth. **A 355** (1995) 600–608.

[3]   MAVER MODEC, P., KORUN, M., MARTELANC, M., VODENIK, B., A comparative study of the radon-induced background in low-level gamma ray spectrometers, Appl. Radiat. Isot. **70** (2012) 324–331.

IMPROVING A RADIOISOTOPE MONITORING NETWORK FOR THE HYDRODYNAMIC CHARACTERIZATION OF A KARSTIC BASIN

J.L. PERALTA VITAL[a], R. GIL CASTILLO[a], L. MOLEIRO LEÓN[b],
C. DAPEÑA[c], J. OLIVERA ACOSTA[d], G. FLEITAS ESTEVEZ[a]

[a] Center of Radiation Protection and Hygiene (CPHR),
  Cuba

[b] Environmental Commercial Division (GAMMA),
  Cuba

[c] Institute of Isotope Geochronology and Geology (INGEIS)
  Argentina

[d] Institute of Geodesy and Astronomy (IGA),
  Cuba

Abstract

The paper shows the application of geomathematical tools for the design of a radioisotope monitoring network in order to characterize groundwater dynamics in a karstic basin, a very difficult task to acccomplish due to the complex physical, geographical, geologic and hydrogeological characteristics of karstic basins. The sampling frequency of the network has been optimized according to the analysis of the spectrum of variances. In order to evaluate this optimization, the geomathematical model is compared to the results of the mathematical model AQUIMPE. This model solves the flow equation of groundwater using the finite element method. The results validate the design in order to assess aquifer recharge, residence time of groundwater, vulnerability to pollution and groundwater–surface water interaction in this complex water resource.

1. INTRODUCTION

In 1998, the IAEA, through the Regional Cooperative Agreement for the Advancement of Nuclear Science and Technology in Latin America and the Caribbean, XIII ARCAL [1], sponsored several isotope hydrology investigations addressing the uncertainties of the regional flow system of the Jaruco-Aguacate Basin, Cuba. The main hydrogeological problem of this aquifer appeared in the 1970s, when some springs located in the eastern part of the basin were found contaminated by sugar

263

FIG. 1. Location od the karstic Almendares-Vento watershed.

waste released in a cavern about 20 km to the west. The release took place from the beginning of the century, but without affecting local groundwaters. The pollution happened despite the existance of a groundwater divide between the Jaruco and Aguacate system and the release point. The unexpected event led to the need of defining, with better precision, the position of the groundwater divide between both systems and to study the hydrodynamic regimen of the aquifer. The Almendares-Vento watershed (AVW) (See Fig. 1) is close to the Jaruco-Aguacate watershed, with a similar hydrogeological and geological structure. In the AVW case, it was necessary to identify with more precision the geometry of the aquifer and the transit time of groundwater, the recharge as well as the groundwater dynamics, the residence time, the patterns of groundwater contamination and the role of groundwater–surface water interaction due to the presence of a dam in the basin. The AVW is the main water supply for the city of Havana in the Cuban Republic. The AVW is an unconfined karstic aquifer, extending over 370 km^2 and with underground hydraulic resources estimated at about 278 Mm^3/a. The system presents high vulnerability to groundwater pollution, reflected in a rapid deterioration of groundwater quality. Taking into account the aspects mentioned above and the characteristics of the karstic watershed, it is very important to conduct a detailed study in order to install a radioisotope monitoring network, which will allow evaluation of the current situation of groundwater dynamics in the basin.

2. GENERAL CHARACTERISATION OF THE ALMENDARES-VENTO WATERSHED

2.1. Geology, geomorphology and hydrogeology

The Almendares-Vento watershed (AVW) is formed by carbonated silts of Lower Miocene age. The basin is structurally constituted by sediments of the Paleogene

in the base and filled with a thick series of silts of Neogene age. The geomorphology of the area is characterized by the karstic structure of the fluvial plain. The basin is crossed by the fluvial system of the Almendares River and five other tributaries and other karstic depressions. In the surface, the karst system is manifested by a great diversity of caverns, generally flooded by groundwater [2–4]. Also the large dam Ejercito Rebelde is located in this basin.

The main hydrological parameters of the basin are: transmissivity (1000–5000 m^2/d), permeability (15–200 m/d), thickness of the unsaturated zone (0–25 m), thickness of the saturated zone (80–200 m), static level (less than 25 m), the thickness of the aquifer (300–400 m). Besides, the fundamental hydrological parameters of the Ejercito Rebelde dam have been taken into account: transmissivity (1000–5000 m^2/d), permeability (15–200 m/d), thickness of the unsaturated zone (0–25 m), thickness of the saturated zone (80–200 m), static level (less than 25 m), and thickness (100–200 m). The specific flows in the whole basin range from 10–100 L/s per m of depression. The groundwater levels varies from 2 to 5 m during the year. The maximum oscillation of groundwater level recorded was 8–9 m.

2.2. Trends and regularity analysis of rainfall

For the assessment of the pluviometric regime of the basin before the construction of the Ejercito Rebelde dam, a series of 63 years of the raingauge Hb–26 (1937–1999 period) was used. In the analysis of rain series, the fundamental hydrological paramters studied were the trend and the regularity. The deviations of the long term mean of annual precipitation (1588 mm) were studied into two representative periods of 30–31 years. The humid years and dry years vary in an alternative mode. The first one extended from 1937–1968, with a tendency to increase the precipitation amount, while the second one (1968–1999) has a tendency to decrease. Starting from 1963, the regime was modified, with a trend to increase the number of years below to the average value for the basin, and to increase of the magnitude of the dry period.

2.3. Flooding analysis and possible effects of the flooding

The social-economic expansion of the area, due to the construction of the dam, has been taken into consideration.. The social and economic development of the area has resulted in the occupation of potentially dangerous areas, because of the higher flood levels. The average frequency of extreme event occurrence in the basin is one event every five years, resulting in the affluence of remarkable volumes to the reservoir. The results are endorsed by the use of the AQUIMPE model [2, 4, 5]. This model solved the groundwater flow equation for a two dimensional, non-permanent regime, using the method of finite elements. The average recharge obtained is 3.68 Mm^3/month for a width of 55.86 m and 61.35 m. A value of 5 Mm^3/month was calculated as the infiltration volume at the beginning of the construction of the dam.

This value contrasts with the calculated recharge in its work (3.68 Mm^3/month). The conclusion is that the infiltration volume in the basin has been diminishing.

3. METHODOLOGY USED TO DESIGN THE MONITORING NETWORK IN THE KARSTIC BASIN

The design was carried out taking into account an informative network (sampled on monthly basis), which consists of twelve wells (HV–19, HV–645, AL–4, HV–28, HV–39, AL–5, HV–29, HV–648, AL–6, HV–431, AL–3, AL–7). A time series was obtained using 10 wells, covering the period January 1982 to December 1994. The behaviour of groundwater levels in the wells during the indicated period was the most important parameter for the validation of the series. The validated database was analysed and its characteristics and properties were identified using different statistical techniques. The studies allowed the obtainment of the design of a monitoring radioisotope network for hydrodynamic characterization in the basin.

3.1. Spectral and correlation analysis

The objective was to study, in a quantitative manner, the periodic or stationary components of the series in order to retain the stationary components. The matrix of the lineal correlation coefficients has been interpreted after identifying significant relationships with values of r^2 higher than 0.6. The matrix showed that the lowest correlations were found between wells AL–5, AL–6 and AL–7 with the remaining wells, so there are different behaviour patterns with the rest of the series. In Table 1, the different statistical parameters for each well during the study period are presented.

TABLE 1. STATISTICAL PARAMETERS OF THE TEMPORAL SERIES OF GROUNDWATER LEVELS (IN m)

Statistical parameters	HV–19	HV–28	HV–29	HV–431	HV–645	AL–3	AL–4	AL–5	AL–6	AL–7
Series size	145	145	140	130	124	148	148	148	147	148
Average	47.89	47.44	38.27	48.97	47.85	41.3	46.99	81.54	103.4	78.42
Median	46.89	47.09	41.83	47.77	47.36	40.86	46.18	80.89	103.2	78.13
Variance	11.21	4.46	67.20	10.80	7.44	6.01	14.13	5.89	5.62	4.97
Standard deviation	3.35	2.11	8.20	3.28	2.73	2.45	3.76	2.43	2.37	2.23
Min. value	41.45	43.85	27.4	43.73	41.47	37.75	42.02	78.12	99.22	74.34
Max. value	55.87	53.78	48.97	56.77	54.07	46.26	55.41	87	108.16	84.24

The autocorrelogram technique was used too, in order to obtain the duration of the influence of external stimulus on the system (memory effect), as well as the recurrence of the series. The karstic system can be considered as a filter allowing the input of information, and the flows and piezometric levels can be defined as the role of a random variable [4, 6, 7]. In the autocorrelation, the wells show a high memory effect, taking extreme values, for example, HV–29 well with 28 months and AL–7 well with just 15 months (maximum and minimum times in which the aquifer keeps information of the stimulus).

The variance spectrum technique obtains the recurrence that has influenced the system during the thirteen years of data. The use of this analysis can lead to redefinition of the sampling frequency in the wells. The spectrum of variance density allows the obtainment of a decomposition of the series total variance for different frequencies and shows the random component (period and step of considered time); the variance that corresponds to periodic or stationary phenomena and finally, the variance due to the secular component [7]. As a result, following the approaches mentioned, the sampling frequencies for each well were proposed: monthly HV–28; biannual HV–19; biannual AL–3; biannual AL–4; biannual AL–5; every two months AL–6; every two months AL–7. In the other three wells, it was not possible to obtain the variance spectrum due to the short length of the series.

3.2 Multivariate analysis (main components and cluster analysis)

The multivariate analysis includes two statistical methods: the cluster analysis and the principal component analysis. This analysis allowed the definition of relationships between variables and the factors that affect the system. The cluster analysis is a method of numeric classification based on a measure of the distances among the objective variables. In this case, it was used to establish the most similar patterns resulting in a classification offering the possibility to extrapolate the properties to their nearest neighbours.

The principal component analysis was carried out with the variables that characterize the system.

(1)   Distance to the water intake at Almendares-Vento (DT);
(2)   Total depth of the well (PT);
(3)   Thickness of the unsaturated zone (EZNS);
(4)   Altitude of the bottom of the well (CF);
(5)   Range of water level fluctuation (RF);
(6)   Direction to the next aqueduct (RAP);
(7)   Direction to the water intake at Almendares-Vento (RT);
(8)   Thickness of the aquifer cut (EAC);
(9)   Ground level altitude (CS);
(10) Mean Cota piezometric media (CPM);

(11) Distance to the next aqueduct (DAP);

(12) Distance to the next groundwater line (DDP).

The more relevant variables were obtained using the following matrix (in R form): EAC, RT, PT, CF, DT (first component), CS, RF (second component), EZN, DDP (third component).With this variables, the 86.48% of the series variance is explained, leaving only 13.52% without explanation, due to other factors or variables that have not been included in the analysis.

- **RT (direction to the water intake):** It has a range of variability between 50–297° and this range is appropriate for the location of the wells of the network.
- **PT (total depth):** It should vary between 26–120 m.
- **DT (distance to the water intake):** The wells are located between 3 and 23 km and the distance average will be 13 km. The maximum range cannot be used. The minimum range should fluctuate between 10 and 16 km.
- **CS (ground level altitude):** The altitude level should range between 54 and 113 m, with an average value of 83 m.
- **DDP (distances to the next groundwater line):** The values range from 1.1 to 6.2 km and the average distance 3.5 km.

In the cluster analysis, the matrix (in Q form) was used for the cluster of the wells, obtaining the following cluster: HV–28, HV–29, HV–431, HV–645 (first group), AL–5, AL–6, AL–7 (second group), AL–3, AL–4 (third group).The well HV–19 is not included in the group because it lacks depth information and therefore is not possible to rotate the matrix, but, according to its location and characteristic, it should be associated to the first group, leading to the definition of three areas in the aquifer.

4.   GEOMORPHOLOGICAL VALIDATION OF THE RESULTS

Using geomathematical methods for the exploration of geomorphological variables, these characteristics were correlated with the hydrodynamic features of the basin. Three hydrogeological areas were recognized: (a) north area, (b) centre-east area and (c) centre-west area. The highly karstified surface is the area with maximum groundwater circulation, the articulation relief with the maximum gradient hydraulic and the karstic glacis with the discharge area toward the Almendares-Vento groundwater.

In the analysis of the main components of the 11 variables that have the biggest informative interest, four variables are in relation with the geomorphological characteristics of the basin. With the objective of establishing the geomorphological patterns, a discreet sample of 72 longitudes and azimuth of the geomorphological

alignments was recognized and the patterns that determine the morphologic–structural specific character of the relief and the informative importance in 10 complex genetics form of the relief in the basin were defined. The more relevant attributes were the lineal sectors of the fluvial karstic valleys, since these attributes provide 82% of the obtained information. The azimuth among 10.7º–120º defined two clusters that provide most information in the area. The convergence approach applied on the 8 nodes in the fluvial network allowed the defintion of a fluvial model of the convergent type, developed on three complex relief types. These relief forms provide 39% of the relevant information. In order to determine the informative importance of the relief surfaces and the map of the main components, the calculation of an association Boolean matrix between variables or objects for the lines and the columns of the matrix was carried out. The qualitative attributes obtained for the matrix are: (1) articulation relief, (2) karstic surface of inselberg type, (3) fluvial radial convergent model, (4) karstic corrosive surface, (5) surface of paleo-valleys, (6) non-karstic relief structures, (7) fluvial network station, (8) karstic denudation surface, (9) accumulative-fluvial surface, (10) karstic glacis covered.

With the initial data matrix a likeness matrix was obtained, which indicates the morphogenetic order of each one in the formation of the relief. In Fig. 2 the main components of the geomorphologic surfaces and the three geomorphologic regions in the Basin are presented. These features are the most important to recognise in the relief and the physical properties of the aquifers.

The analysis of longitudes was developed on a sample of 29 individuals and the following summary statistical values were obtained. The summary statistics of the alignments longitudes were: number 72; minimum 0.80; maximum 8.60; mode 1.5; avereage 2.36; median 2.50; range 7.80; variance 1.47; standard deviation 14.92; coefficient of variance 0.51, error of the mean 6.43. The application of the rotational algorithm of discriminate analysis allowed the obtainment of the control matrix of the longitudes as well as other valuable information. This means that just five longitudes control the lineal development in the relief.
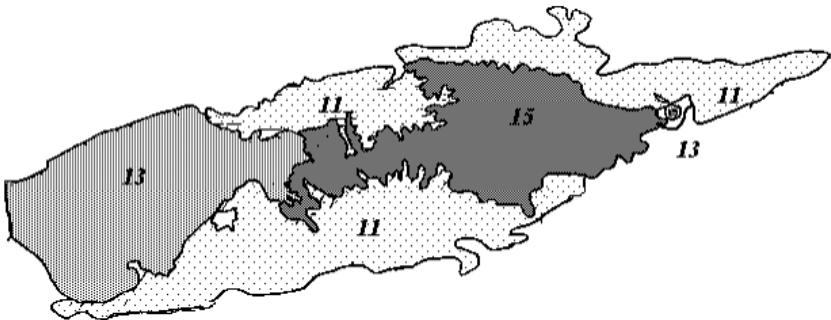
FIG. 2. Map of the principal components of the relief surfaces.

269
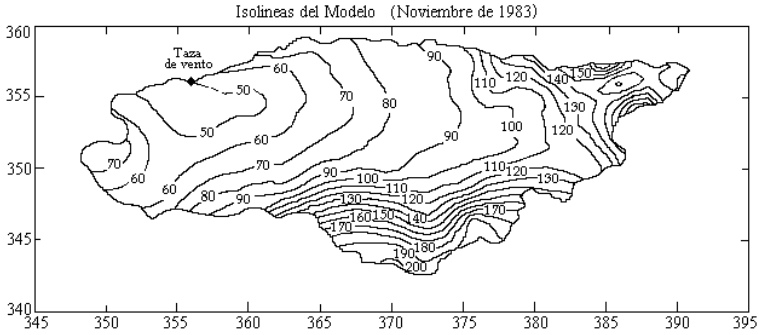
FIG. 3. Map of the mathematical calibration model of the basin.
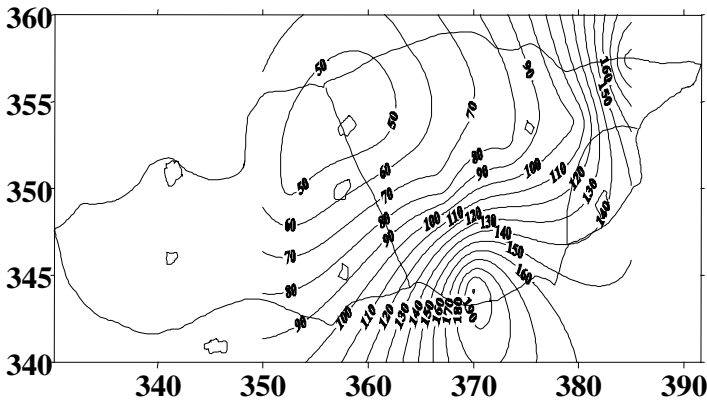
FIG. 4. Map of the optimized monitoring network.

The analysis of azimuthal alignments was based on the same sample taken for the measurements of longitudes. The more common frequencies are in the range 10 to 120, corresponding to the first two quadrants with the directions north-northeast and east-southeast. Morphologically this indicates that tectonics have conditioned the specific morphostructure of the basin. The summary statistic of the azimuthal alignments were: number 72; average 98.5; median 110; minimum 10; maximum 180; error 6.43; lower quartile 60; upper quartile 140; range 170; variance 2858 and standard deviation 53.

Finally the two analysed variables were compared and a regression analysis was carried out. The results showed that no relationship exists between the azimuthal alignments and their longitudes. This situation is only valid for isolated values that are within the confidence interval of the regression curve. These values are: for azimuths of 30°, 150°, 160°, 170° and 180° correlated longitudes of 2 km, for an azimuth of 60° correlated longitudes of 3 km (meaning that these indicative geomorphologic

HIDROISOHIPSAS DE LA RED DE MONITOREO ACTUAL
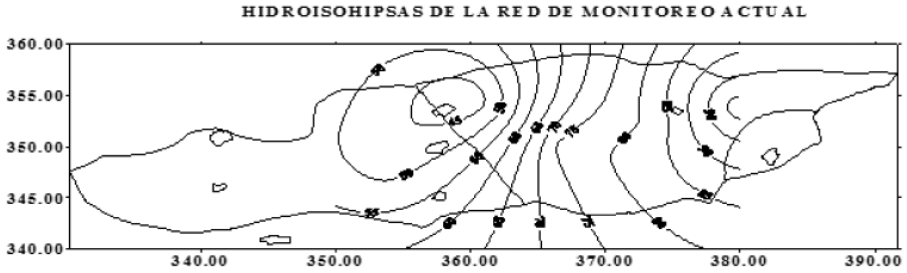
FIG. 5. Map of the Almendares Vento basin with the current groundwater monitoring network.

parameters can not be taken in groups, as geological patterns). The geomorphological results are in agreement with the areas in which the basin has been divided.

The correlation among the three used methods is presented in Figs 3 to 5: the optimization, the mathematical model validation and the geomorphological validation map. The application of all these combined geomathematics techniques [6, 7] allowed the obtainment of an excellent agreement between the water level control line maps of AQUIMPE in the Almendares-Vento watershed (Fig. 3), the water level control line maps of the optimized network (Fig. 4) and the control line maps elaborated with the non-optimized network of the basin (Fig. 5), and the geomorphologic zonation.

5. CONCLUSIONS

The proposed groundwater level monitoring network consist of the following elements (Table 2):

(1) The selected wells are: HV–29 (long record and good correlation with the remaining wells), HV–28, HV–19, HV–645 (high correlation among them and high memory effect), AL–5, AL–6 and AL–7 (good representativeness of the geographical area), AL–3, AL–4 (same memory effect and high correlation).
(2) Due to the great weight that the distance from the wells to the Almendares-Vento Basin water uptake has in the study, a water level device should be included in its surroundings in order to register hydrodynamic changes.
(3) Taking into account the analysis of spectral variances, the sampling frequency of the wells will be: HV–28 (monthly), HV–19 (monthly), AL–5 (monthly), AL–6 (monthly), AL–7 (monthly), AL–3 (monthly), AL–4 (biannual), HV–19 (monthly), HV–645 (monthly), water level recroding system at the Almendares-Vento water uptake (daily).

The geomathematical and statistical study comparison with the results of the mathematical AQUIMPE model, helped to generate the obtained design.

271

TABLE 2. STRUCTURE OF THE PROPOSED TRITIUM MONITORING NETWORK

Water type	Stations	Frequency	Parameter
Rainfall	Raingauge HB–26	monthly	tritium
Aquifer system release water	Almendares-Vento water uptake	monthly	Flow, water level, pH, electric conductivity, major ions and tritium
Groundwater	HV–28, HV–19, AL–5, AL–6, AL–7, AL–3, AL–4, HV–19,HV–645	monthly	Flow, water level, pH, electric conductivity, major ions and tritium
Surface water	Ejército Rebelde dam	monthly	

REFERENCES

[1]   DAPEÑA, C., et al., "Caracterización isotópica de la Cuenca kárstica Almendares-Vento, Cuba. Resultados preliminares", XI Congreso Geológico Chileno, Chile (2006).

[2]   PERALTA VITAL, J.L., et al., "Uso de la hidrología isotópica en la evaluación de una importante Cuenca kárstica Cubana, para la gestión sostenible de sus recursos hídricos". VIII Congreso Latinoamericano de Hidrología subterránea (ALHSUD), Paraguay (2006).

[3]   PERALTA VITAL, J.L., et al, "Isotope hydrology application in Cuba for assessment of water resource management in the most important Basin of Havana City", Advances in Isotope Hydrology and its Role in Sustainable Water Resources Management (IHS–2007), (Proc. IAEA Int. Symp. Vienna, 2007, Vol. 2), IAEA, Vienna (2007) 245–253.

[4]   MOLERIO LEÓN, L.F., ARELLANO, F.D., SURÍ, A,. SANTOS, A., Dinámica de las aguas subterráneas en la cuenca Jaruco-Aguacate, ARCAL XIII-RLA/8/14, Primera Reunión de Responsables de los Estudios de los Recursos y la Contaminación de las Aguas Subterráneas, Inst. Pesquisas Hidr., Univ. Fed. Río Grande do Sul, Porto Alegre, Brasil (1990) 13.

[5]   MOLERIO LEÓN, L.F., Aplicación del método de recesión al estudio hidrodinámico de las fuentes del río Mayabeque, Simposium XXXV, Sociedad Espeleológica, La Habana, Cuba (1975) 67.

[6]   MOLERIO LEÓN, L.F., PORTUONDO LÓPEZ, Y., Técnicas geo-matemáticas aplicadas en hidrogeología, Notas de Clase, CENHICA, Inst. Nacional de Recursos Hidráulicos, Circ. restr. (1997) 69.

[7]   MOLERIO LEÓN, L.F., GUERRA OLIVA, M.G., FLORES VALDÉS, E., ROCAMORA ALVAREZ, E., "Hydrogeological exploration with geomathematical tools in karstic and fissured non-karstic aquifers", Hydrology in the Humid Tropic Environment, (Proc. Symposium, Jamaica, 1996), (JOHNSON, A.I., FERNÁNDEZ-JÁUREGUI, A., Eds), IAHS, Wallingford, UK (1998) 337.

ISOTOPIC INVESTIGATION OF THE ORIGIN OF AMMONIA AND NITRATE IN THE MINERAL SPRING WATERS OF SCUOL (LOWER ENGADINE, SOUTH EASTERN SWITZERLAND)

J. FRITZ [a], F. LEUENBERGER [a], L. EICHINGER [b], W. BALDERER [a]

[a] Eidgenössische Technische Hochschule Zürich,
   Geological Institute, Engineering Geology,
   Zürich, Switzerland

[b] Hydroisotop GmbH,
   Schweitenkirchen, Germany

Abstract

The mineral springs of Scuol-Tarasp are located in the lower Engadine Valley, Graubünden, south eastern Switzerland. In the last century, they have been investigated with respect to their basic chemical parameters. These springs yield a highly mineralized carbon dioxide water, with large quantities of free CO_2. Some of the springs also contain high amounts of ammonia. In order to better understand the origin of the water of the different springs, 13 were investigated, focusing this study on the ammonia content and the isotopic composition of the ammonia in the waters. It results from the study that 7 of the 13 springs contain ammonia. Based on the isotope and chemical results we suggest an origin of that ammonia by natural processes as water–rock interaction within the sedimentary and mantle rocks along the water flow path resulting in the enrichment of ammonia as seen in the investigated spring waters.

1.   INTRODUCTION

1.1. Geology of the investigated region

The springs investigated for this study are located in the villages of Scuol and Tarasp, within the lower Engadine Valley in the Eastern Swiss Alps at an altitude of about 1300 m.a.s.l. The river Inn flows through the valley through a WSW-ENE direction. The Engadine Valley is asymmetric, with steeper slopes on the southern side than on the northern side. The average annual air temperature is 5°C.

The region is located at the border of the Engadine window, where the Austroalpine nappes are partially eroded and the underlying Penninic nappes are exposed. The Penninic nappes consist mainly of 'Bündner schist' and ophiolites. The lowest tectonic unit, which outcrops in the middle of the tectonic window, is

the 'Penninic Bündner schist' unit. It consists of metamorphosed pelagic rocks with black shales and sandy and calcareous phyllites. The Austroalpin S-charl-Silvretta nappe is the highest tectonic unit and consists of a crystalline basement (gneiss) and the overlying paraautochthonous sedimentary cover (consisting of dolomites and limestone). The Tasna nappe between the Silvretta nappe and the Penninic units consists of different imbricated units of crystalline basement and sedimentary cover (granite and gneiss, quartzite, limestone and calcareous phyllites). Of the investigated springs, 11 of the 13 discharge from the Penninic Bündner schist, one discharges from the Penninic ophiolites and one spring ('Sur En', not on the figure) originates from the Scharl-Silvretta nappe.

1.2. Mineral springs

The mineral springs in the Lower Engadine region are known to be CO_2 rich (up to 3000 mg/L) and moderately to highly mineralized. Based on their chemical composition (dissolved cations and anions) Ref. [1] grouped the springs in the region according to their water chemistry in 7 different groups [1–3]. The springs we investigated belong to group 1, 2, 3 and 7, respectively.

The Emeritia, Lucius and Sfondraz springs belong to group 1, which represents the Na-HCO_3-Cl type water. Emeritia and Lucius are the highest mineralized springs, with 15 500–17 700 mg TDS/L. The mineral waters of group 1 contain a 'deep water' component, but its origin is still a subject of discussion.
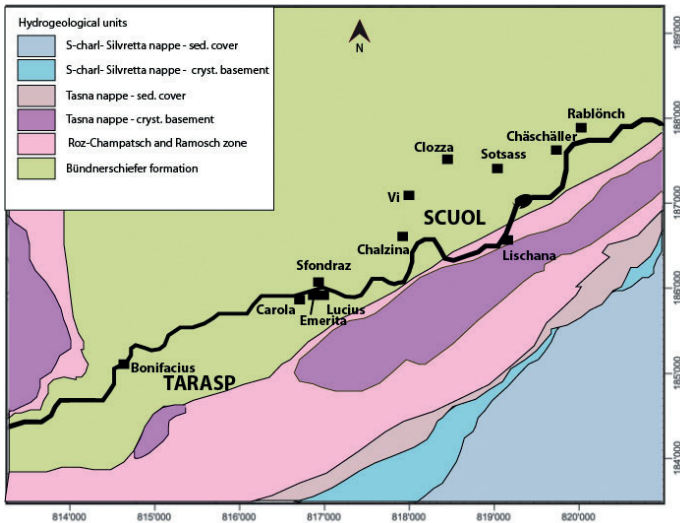
FIG. 1. Map of the springs in the region of Scuol-Tarasp. The numbers at the margins represent the Swiss Topographic Grid (unit: metres) [1].

The Carola and Bonifacius springs belong to group 2, which represents the Na-Ca-HCO$_3$-Cl type water. It can be considered a result of mixing between the two groups 1 and 3.

Rablönch, Chalzina, Sotsass, Clozza and Vi springs belong to group 3, which represents the Ca-HCO$_3$ water type. The springs yield low to medium mineralization (700–3100 mg TDS/L). Tritium data [3, 4] indicate that the water of these springs has a relatively short residence time of less than 5 years.

All mineral springs of the groups 1, 2 and 3 discharge from the Bündner schist formation (Fig. 1).

The Lischana spring belongs to group 7. This water is highly mineralized and was captured by drilling in serpentinite of the Tasna nappe. Its water type is Na-Mg-HCO$_3$-SO$_4$ [2].

The Chäschäller and Sur En[1] springs have not been investigated and classified so far. Chäschäller spring outflows near the Rablönch spring from the Bündner schist formation while the spring Sur En outflows from the S-charl-Silvretta nappe, in a village SW of Scuol and south of the river Inn at an altitude of 1470 m.

Our study focuses on the ammonia content in the spring water. Högl already mentioned that some of the springs in the region contained astonishingly high amounts of ammonia [4]. We analysed the sampled spring waters for their chemical composition as well as for the isotopic composition of the ammonia.

2.   METHODS

Water samples were taken in May and June. They were taken directly from the spring (Sfondraz, Rablönch, Chäschäller, Sur En) or from a spring-fed tap (Emerita, Lucius, Carola, Lischana, Sotsass, Chalzina, Bonifacius, Clozza, Vi). Samples were filtered prior to ion chromatography analysis. Ion chromatography was performed on a DIONEX DX-120 ten days after sampling. The chemical parameters, such as conductivity and temperature as well as the oxygen and pH monitoring were performed directly at the spring locations with standard field instruments (Hach HQ30d and EUTECH INSTRUMENTS/OAKTON Multiparameter PSCTestr 35). For the mass spectroscopy analyses, a Kjeldahl distillation was performed.

3.   RESULTS AND DISCUSSION

Seven of the thirteen analysed springs contain notable amounts of ammonia (Table 1). These are the springs Emeritia, Lucius, Sfondraz and Bonifacius, which

---

[1]   These are not official names of the springs, the two springs are described and named in this way in the Bachelor thesis of J. Fritz

TABLE 1. OVERVIEW OF THE SPRINGS AND THEIR AMMONIA AND POTASSIUM SIGNATURE

Spring name	Group[1]	Water type[2]	NH_4^+ (mEq/L)	K^+ (mEq/L)
Emerita	1	Na–HCO$_3$–Cl	0.45	3.21
Lucius	1	Na–HCO$_3$–Cl	0.50	3.47
Sfondraz	1	Na–HCO$_3$–Cl	0.73	1.78
Bonifacius	2	Na–Ca–HCO$_3$–Cl	0.29	0.64
Carola	2	Na–Ca–HCO$_3$–Cl	n.d.[3]	0.51
Lischana	7	Na–Mg–HCO$_3$–SO$_4$	0.05	1.01
Rablönch	3	Ca–HCO$_3$	0.01	0.14
Chäschäller	–		0.07	0.39
Sotsass	3	Ca–HCO$_3$	n.d.	n.d.
Chalzina	3	Ca–HCO$_3$	n.d.	n.d.
Clozza	3	Ca–HCO$_3$	n.d.	n.d.
Vi	3	Ca–HCO$_3$	n.d.	n.d.
Sur En	–		n.d.	n.d.

[1] groups after Ref. [2]
[2] water type after Ref. [2]
[3] not detectable

are located south of the river Inn, the Lischana spring as well as the two springs Rablönch and Chäschäller, which originate north of the river Inn. All ammonia containing springs exhibit marked amounts of potassium as well.

The minerals springs Emeritia, Lucius and Sfondraz contain high amounts of ammonia (0.45 mEq/L, 0.50 mEq/L and 0.73 mEq/L, respectively) and exhibit ammonia with slightly positive δ–^{15}N values (0.8‰, 0.6‰ and 0.9‰, respectively) (Fig. 2). Bonifacius, with an ammonia value of 0.29 mEq/L has a negative δ–^{15}N–NH$_4$ of –2.5‰. In the two springs Lischana and Chäschäller, the ammonia contents are relatively low but their δ–^{15}N values are by far the highest (2.9‰ and 4.8‰, respectively). In the Rablönch spring, the ammonia content was too low for mass spectroscopy analysis.

The water of the springs Emeritia, Lucius and Sfondraz belong to the water type group 1, with highly mineralized and undiluted 'deep water'[2]. The potassium content of these springs is also relatively high. Sfondraz is less mineralized than the other two springs but it contains the highest amount of ammonia (Table 1, Fig. 2). Due to the fact that the water of these springs is undiluted and due to the long
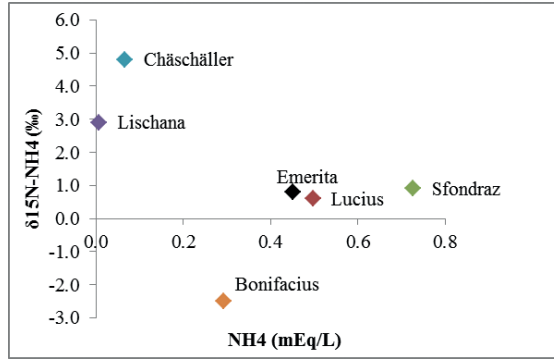
FIG. 2. $\delta^{15}N_{NH4}$ vs ammonia content of the ammonia rich springs ($\delta^{15}N$ relative to air standard).

residence time [3] it is very likely that the ammonia in these waters were formed through interactions with minerals along the water flow path. The correlation with the potassium content indicates that the minerals which served as the ammonia donor are potassium-bearing minerals in which ammonia may partially substitute for potassium. This substitution is likely due to the similar size of ammonia and potassium [5]. The high amount of ammonia can be considered the result of the long residence time of the water or of the interaction with rock that is extremely rich in ammonia. The δ-^{15}N values of the ammonia in these springs are positive. Organic material in sediments shows positive δ-^{15}N values [6, 7] and metamorphosis leads to an enrichment in ^{15}N [8]. Therefore the Bündner schist formation could be the origin of the ammonia in this water.

Ammonia and potassium are lower in the Bonifacius spring than in the first three springs. Bonifacius belongs to group 2 and is therefore probably a mixture between water of the groups 1 and 3. This dilution of type 1 water with type 3 water (which contains none or almost no ammonia) can explain the amount of ammonia in the water of the spring Bonifacius. In contrast, the negative value of the isotopic composition of its ammonia could be an indication for a different origin of the water and therefore a different flow path. Mantle rocks and oceanic basalts show a negative δ-^{15}N value [9, 10]. Such rocks (e.g. from deeper Penninic units) could be considered as the ammonia-donor for this spring.

The spring Carola, which belongs to the same group as Bonifacius, has no detectable amount of ammonia. This is probably due to the generally lower mineralization of the water.

The springs of group 3, except Rablönch, do not contain ammonia. Interestingly, the ammonia containing spring (Rablönch) is the only one of this group that contains potassium, which strongly emphasizes the above mentioned process of water–rock interaction with both the release of ammonia and of potassium ions.

The spring Lischana, which originates from the serpentinite of the Tasna nappe, has a different signature with a highly positive δ-^{15}N value but low ammonia concentration. Its chemical composition differs from that of all the other springs and therefore its ammonia content may be derived from yet another, perhaps higher, metamorphic rock unit.

4.   CONCLUSION

It results from our study that 7 of the 13 springs contain ammonia. Based on the isotope and chemical results we suggest an origin of that ammonia by natural processes as water–rock interaction within the sedimentary and mantle rocks along the water flow path resulting in the enrichment of ammonia as seen in the investigated spring waters.

REFERENCES

[1]   BISSIG, P., Die CO_2-reichen Mineralquellen von Scuol-Tarasp (Unterengadin, Kt. GR), Bull. angew. Geol. **9** 2 (2004) 39–47.

[2]   BISSIG, P., et al., Carbogaseous spring waters, coldwater geysers and dry CO_2 exhalations in the tectonic window of the Lower Engadine Valley, Switzerland, Eclogae Geologicae Helvetiae **99** 2 (2006) 143–155.

[3]   WEXSTEEN, P., JAFFE, F.C., MAZOR, E., Geochemistry of cold CO_2-rich springs of the Scuol-Tarasp region, Lower Engadine, Swiss Alps, J. Hydrol. **104** 1–4 (1988) 77–92.

[4]   HÖGL, O., Die Mineral- und Heilquellen der Schweiz, Verlag Paul Haupt Bern, Stuttgart (1980).

[5]   DEER, W.A., HOWIE, R.A., ZUSSMAN, J., Framework Silicates: Feldspars, 2nd edn, Vol. 4a, Rock-Forming Minerals, Geological Society of London (2001).

[6]   HOEFS, J., Stable Isotope Geochemistry, 5th edn, Springer, Berlin (2004).

[7]   PLESSEN, B., HARLOV, D.E., HENRY, D., GUIDOTTI, C.V., Ammonium loss and nitrogen isotopic fractionation in biotite as a function of metamorphic grade in metapelites from western Maine, USA, Geochim. Cosmochim. Acta **74** 16 (2010) 4759–4771.

[8]   HOLLOWAY, J.M., DAHLGREN, R.A., Geologic nitrogen in terrestrial biogeochemical cycling, Geology **27** 6 (1999) 567–570.

[9]   CARTIGNY, P., BOYD, S.R., HARRIS, J.W., JAVOY, M., Nitrogen isotopes in peridotitic diamonds from Fuxian, China: The mantle signature, Terra Nova **9** 4 (1997) 175–179.

[10]   MARTY, B., HUMBERT, F., Nitrogen and argon isotopes in oceanic basalts, Earth Planet. Sci. Lett. **152** (1997) 101–112.

ISOTOPIC INVESTIGATION OF THE ORIGIN OF NITRATE OF WATERS OUTFLOWING FROM A WASTE DEPOSIT SITE NEAR SCUOL (LOWER ENGADINE, SOUTH EASTERN SWITZERLAND)

M. GSCHWEND [a], F. LEUENBERGER [a], L. EICHINGER [b], W. BALDERER [a]

[a] Eidgenössische Technische Hochschule Zürich,
   Geological Institute, Engineering Geology,
   Zürich, Switzerland

[b] Hydroisotop GmbH,
   Schweitenkirchen, Germany

Abstract

Near the village of Scuol in the Lower Engadine Valley (South Eastern Switzerland) Sot Ruinas, a waste disposal site for domestic and construction refuse, has been in use since the 1960s. It is situated in the vicinity of the Inn River. Over the last years enhanced concentrations of ammonia were found in the outflow of this waste site. But the observed elevated ammonia concentrations could also be a result of natural origin, by inflows of mineral water as observed in the mineral springs of the area. These springs could have acquired their high ammonia content by water–rock interaction with adjacent ultramafic rocks. The isotope analyses were oriented towards the hydrogen, nitrogen and oxygen isotopes on the ammonia, nitrate and nitrogen molecules. The effect of the waste on the outflowing water downstream could be proved by isotope ratios based on chemical processes of the nitrogen cycle and an influence of natural spring water was excluded.

1.   INTRODUCTION

The location of Sot Ruinas was used as disposal site for domestic waste from 1960 to 1984. Since that time only construction materials have been deposited. From 1991 until today a waste sorting plant exists on the former waste disposal site. The Office of Environment of the Canton Graubünden (ANU) approved a rehabilitation need for the waste disposal site in 2008. A preliminary study revealed the possibility of a natural origin of the ammonium due to inflows of mineral water with identical chemical composition as observed in the mineral springs of the area. But this assumption was not based on scientific arguments as the hydrogen, nitrogen and oxygen isotopes on the ammonia, nitrate and nitrogen molecules had not yet been

studied. This study was based on stable isotopes and chemical properties so the influence of the spring water could finally be excluded.

1.1. Geological and hydrological settings

The waste disposal site lies in the 'Bünder schist' [1]. Within the Bünder schist the groundwater is circulating along fractures. [2]. Close to the waste disposal site a serpentinite outcrop is present. This serpentine is a part of an ultramafic complex. Lenses of this ultramafic rock are partly exposed along the Engadine fault (shear zone). These rocks are strongly deformed and nerved with a cleavage system. In
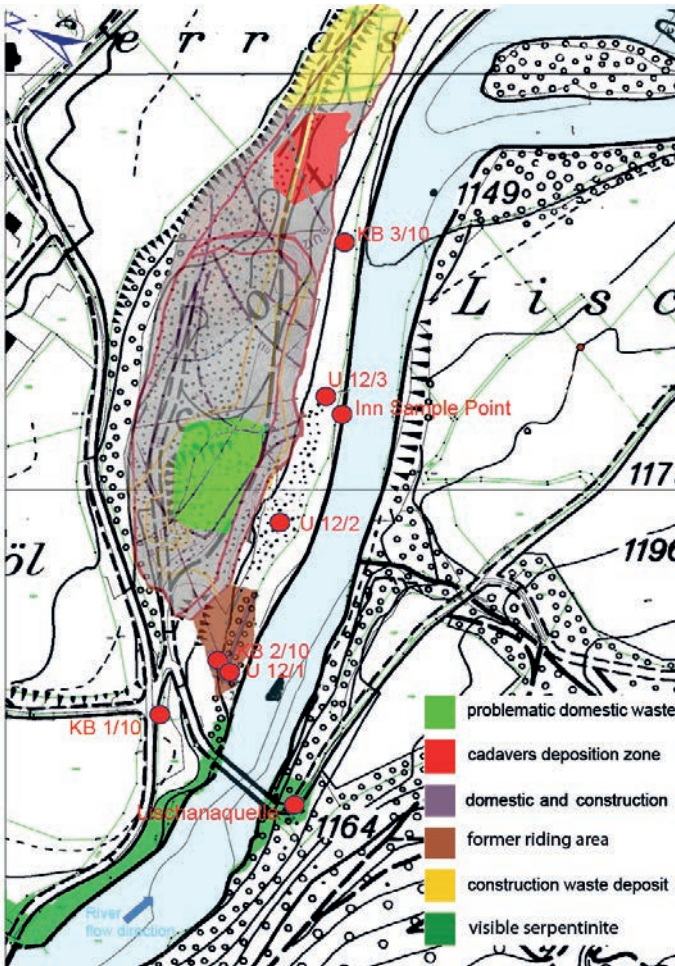
FIG. 1. Different disposal zones identified in the study area [3].

rocks nitrogen is mainly fixed as an ammonium molecule within the crystal lattice of silicate minerals. The ammonium can substitute K in silicate minerals [4].

2. METHODS

At the sample sites in the field, the physical parameters such as temperature, electrical conductivity and pH were directly measured. The dissolved oxygen concentration in mg/L was measured by means of a portable probe based on oxygen luminescence quenching (HACH HQ30d). Water samples were also analysed for their main chemical composition by ion Chromatography (DIONEX DX–120 IC).

3. RESULTS AND DISCUSSION

3.1. Stable water isotopes (^{18}O and ^{2}H)

In the $\delta^2H/\delta^{18}O$ diagram all data points of analysed groundwater are located near the Global-Meteoric-Water-Line (MWL) (Fig. 2). Therefore it can be assumed that the water isotopes are not altered by secondary processes. This can be interpreted as an indication of young meteoric rather than old in origin [5]. Furthermore, since the catchment area of the Inn is situated at a higher mean altitude, its water is more depleted in heavy isotopes because of natural fractionation (altitude effect). The data points of spring waters situated below the MWL may be influenced by a process of evaporation or water–rock interaction. As the values of $\delta^{18}O$ are mainly affected by this process, these points may be backwardly projected onto the MWL parallel to the y-axis [6]. Data points above the MWL result from waters which are enriched in heavy isotopes, as resulting from the gas–water interaction process as e.g. with CO_2 or H_2S (see sample U 12/2, Fig. 1). The water sample, U 12/2, originates from a borehole situated closely below the landfill in a downstream direction where the greatest contamination is assumed to be located. From these investigations further results that the water samples of the boreholes KB 1/10 and KB 2/10 have the lowest mixing component of Inn water. These waters are more enriched in heavy isotopes (Fig. 1). For these waters the mixing ratio with Inn water can be estimated to be approximately 50%.

3.2. Nitrogen and oxygen isotopes of nitrate

As can be deduced from Fig. 3 the initial nitrate formed as a result of nitrification. The origin is not conclusive and could have come from several sources. The possibilities are NH_4^+ fertilizer, organic farmyard manure or nitrogen rich landfill leachate. A denitrification trend is clearly visible, and is most extreme at the piezometer
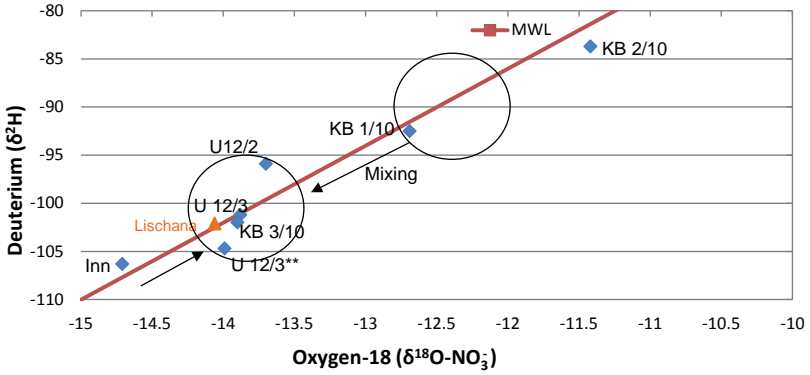
FIG. 2. *δ²H vs δ¹⁸O from the water isotopes.*

a)

b)
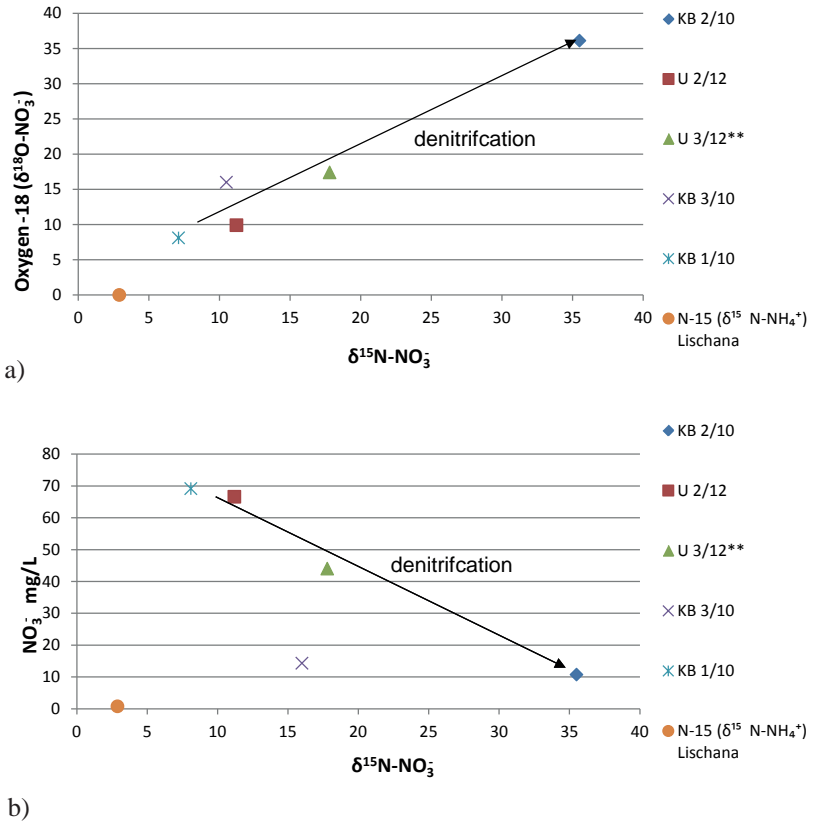
FIG. 3. *δ¹⁵N$_{NO3}$ vs δ¹⁸N$_{NO3}$ (a) and δ¹⁵N$_{NO3}$ vs NO$_3$ concentration in spring water samples.*
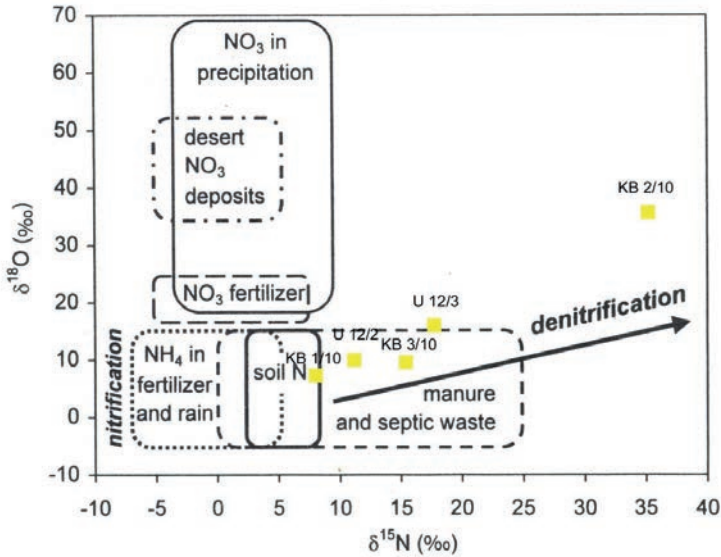
FIG. 4. Origin of the nitrogen and the denitrification trend [7].

KB 2/10. Due to this (denitrification) trend, it can be concluded that microbial processes are at work that are breaking down the nitrate.

3.3. Nitrate source

The source of the nitrate values from KB 1/10 (69.17 mg/L) is not conclusively deducible from the composition of the NO_3^- (Fig. 4). In comparison to the other locations, this one shows the lowest values. If we exclude any influence of the landfill leachate, then the influence of agricultural activities must be substantial. More likely is that the landfill leachate has spread farther than commonly assumed. To quantify the influence of agricultural activities, it would be very helpful to have a drilling sample from the upstream area of the landfill site. In the areas (U 12/2 and U 12/3), where the denitrification does not lead to increased levels of isotopes, the conditions are aerobic.

3.4. Influence of the Lischana spring

As a result of the nitrification of the NH_4^+ to NO_3^-, the nitrate becomes isotopically lighter. This means it is possible to exclude a correlation between ammonium from the Lischana spring and the nitrate. The reason is that the measured nitrate is isotopically heavier than the NH_4^+. The commonly accepted theory is:

$$\delta^{15}N_{NO3} < \delta^{15}N_{NH4} \ [7]$$

This leads to the conclusion that the nitrate cannot come from the ammonium from the Lischana spring. The water of borehole KB 2/10 shows similarities to the Lischana spring in the Schoeller diagram. Due to the isotope composition of the H_2O, this hypothetic relationship can be rejected. Together with the isotope ratios between $\delta^{15}N_{NO3}$ and $\delta^{15}N_{NH4}$, it can be inferred that the ammonium and nitrate of this water do not originate from the mineral spring. Therefore the geogenic influence is very small. This hypothesis can be checked by on the ion concentration of the inferred waters. By an addition of Inn water, assumed to be 50%, the conductivity of the water of the U 12/2 borehole can be calculated as follows:

2[(conductivity U 12/2) − 0.5(conductivity Inn)] = 2578.83µS/cm (undiluted conductivity U 12/2)

This value of the electric conductivity (which is proportional to the total dissolved solids) is far higher than the natural conductivity of groundwater as measured at the undisturbed boreholes and can therefore be seen as a originating from the nitrogen rich landfill leachate.

3.5. Influence of the construction of the waste deposit

The elevated sulphate levels are an indicator that leaching of construction waste deposited in the area is taking place. The different sulphate concentrations analysed in the water samples from the piezometers downstream of the landfill site, at location KB 1/10, clearly show the contamination. This contamination is caused by the deposited construction waste and will only slowly decrease in the near future and as a result will most certainly have a long term influence on the groundwater.

4.   CONCLUSION

To summarize the findings, the contamination of groundwater is caused by the landfill leachate from the construction waste deposit Sot Ruinas. The landfill leachate containing water outflows into the Inn and gets substantially diluted. Therefore the landfill leachate is affecting only to a limited extent the area outside of the landfill site. As the influence of the Lischana spring turns out to be very minor, the source of the ammonium can be traced back to the landfill site. The main goals of this investigation were achieved although the source of the nitrate could not be completely explained. Furthermore the hydrogeological conditions in the area of the landfill site are still not fully understood. The chemical composition of the groundwater in the upstream area of the waste deposit is not known and could only be estimated which further complicates the interpretation of the data. The final recommendation, based on our findings, is not to enlarge the landfill site but to monitor it carefully as it is

already in an aerobic phase, and therefore the nitrate values are a result of the construction waste and will decrease over the next few years.

REFERENCES

[1]   STEINMANN, M.C., Die nordpenninischen Bündnerschiefer der Zentralalpen Graubündens: Tektonik, Stratigraphie und Beckenentwicklung, PhD Thesis, Zurich (1994).

[2]   BISSIG, P., Die CO_2-reichen Mineralquellen von Scuol-Tarasp (Unterengadin, Kt. GR) Bull. angew. Geol. **9** 2 (2004).

[3]   CSD INGENIEURE UND GEOLOGEN AG, THUSIS, "Voruntersuchung und Variantenstudium für eine Deponiesanierung", Deponie Sot Ruinas, für die Gemeinde Scuol (2005).

[4]   MINGRAM, B., BRAUER, K., Ammonium concentration and nitrogen isotope composition in metasedimentary rocks from different tectonometamorphic units of the European Variscan Belt, Geochim. Cosmochim. Acta **65** 2 (2000) 273–287.

[5]   HÖGL, O., Die Mineral- und Heilquellen der Schweiz, Verlag Paul Haupt Bern, Stuttgart (1980).

[6]   INGRAHAM, N.L., "Chapter 3: Isotopic variations in precipitation", Isotope Tracers in Catchment Hydrology (KENDALL, C., McDONNELL, J.J., Eds), Elsevier, Amsterdam (1998) 87–100.

[7]   KENDALL, C., "Chapter 16: Tracing nitrogen sources and cycling in catchments", Isotope Tracers in Catchment Hydrology (KENDALL, C., McDONNELL, J.J., Eds), Elsevier, Amsterdam (1998) 519–576.

ON THE SOURCES OF SALINITY IN GROUNDWATER UNDER PLAIN AREAS. INSIGHTS FROM $\delta^{18}O$, δ^2H AND HYDROCHEMISTRY IN THE AZUL RIVER BASIN, ARGENTINA

M.E. ZABALA [a], M. MANZANO [b], M. VARNI [a], P. WEINZETTEL [a]

[a] Instituto de Hidrología de Llanuras,
   Azul, Argentina

[b] Technical University of Cartagena,
   Spain

Abstract

The Azul River basin, with some 6200 km², is located in the plains of Buenos Aires Province, Argentina. The Azul River flows along 160 km from the Tandilia Range, in the SW, to the Channel 11, in the NE. Average annual precipitation is 1005 mm (1988–2000); mean reference evapotranspiration is 1090 mm. The geology consists of Miocene to recent sediments, mostly sands and silts with some clay and calcrete layers, overlying crystalline rocks and marine sediments. The water table is shallow and groundwater in the aquifer upper 30 m displays an increasing salinity from SW to NE. The previous hypothesis to explain the salinity was infiltration of evapo-concentrated surface water, as the small soil slope in the northern basin (<0.2%) induces rainfall accumulation in lowlands, where water evaporates prior to infiltration. But recent chemical and isotopic data reveal two salinity sources: evaporation of recent recharge water, and mixing with old saline groundwater of yet unknown origin.

1. INTRODUCTION

In large and medium size sedimentary basins groundwater salinity changes in both the horizontal and the vertical direction due to different reasons. In arid and template zones an inverse zonality can be seen, with less saline waters overlain by more saline ones due to evapotranspiration and to dissolution by rain water of salts formed in the soil surface during the dry season. Increased salinity downwards flow can commonly be attributed to growing residence time and/or to upward transfer of deeper, more saline groundwater flows; lateral transfer of groundwater from adjacent basins can also produce horizontal and vertical salinity changes. In plain areas vertical hydraulic gradients are usually very subtle as to identify flow senses and salinity provenances; hydrochemical and isotope tracers are very useful to assess salinity sources in these cases.

2.   GEOLOGY AND CONCEPTUAL HYDROGEOLOGICAL MODEL

The Azul River basin, with some 6200 km², is located in the plains of Buenos Aires Province, Argentina (Fig. 1). The Azul River flows along 160 km from the Tandilia Range, in the SW, to the man-made Channel 11, in the NE, which in turn drains to the Salado River, an afluent of the Paraná River. Average annual precipitation is 1005 mm (1988–2000); mean reference evapotranspiration is 1090 mm [1].

The aquifer is formed by Quaternary-age sediments of the Pampeano and Post-Pampeano formations. These are silts, sandy silts, and clayed silt, overlain by fine sands and silts of various origins, mainly aeolian and fluvial [2]. Calcretes are common at shallow depths within these sediments. According to the U. S. Soil Taxonomy [3] most of the soils in the basin are Paleudol petrocalcic.

Bedrock outcrops occur in the upper basin (SW) and consist of metamorphic rocks, granite, tonalite, migmatite and quartzite [4]. These rocks constitute the lower boundary of the water table aquifer and occur at a depth of 120 m in Azul city. From this city to the northern limit of the basin and beyond, the Quaternary sediments are underlain by the Miocene, wedge shape marine sediments of the Paraná formation, whose maximun thickness is around 750 m under the Salado River basin, to the N of the Azul River basin. In some places of the Azul basin, under the Paraná formation appear the Eocene to Miocene continental sediments of the Olivos formation. While the Olivos formation has usually fresh, good quality groundwater, the Paraná formation has very saline water, even saltier than seawater [5].

The conceptual model to date indicates that in the upper basin (SW) groundwater recharge processes predominate (downward fluxes) and in the NE area groundwater discharge processes, which could be fed by upward fluxes from deeper formations
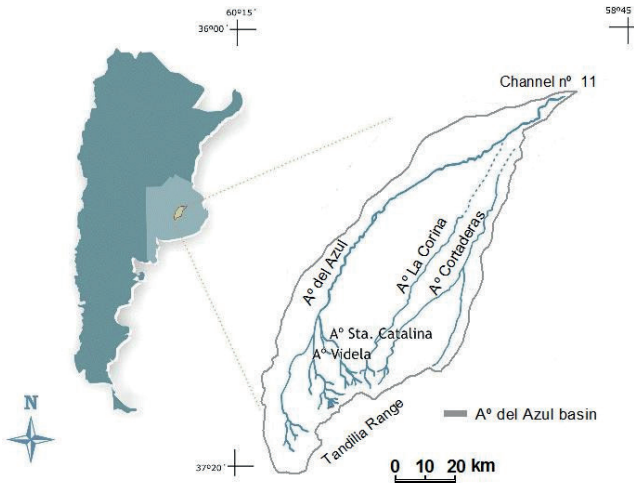
FIG. 1. Location of the study area, the Azul River basin.
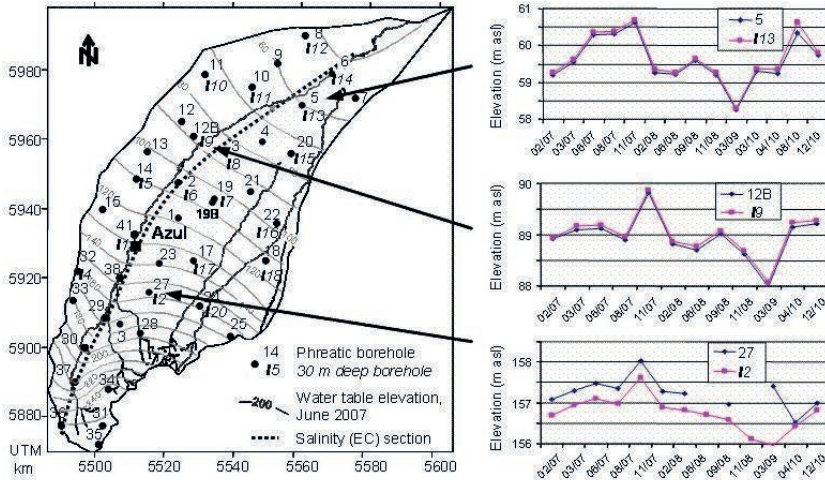
FIG. 2. Water table elevation contour lines; location of boreholes from the two depths monitoring network (3 to 6 m and 30 m depth); piezometric hydrographs at two depths in three representative emplacements. Boreholes 12B and 19B have intermediate depth (around 15 m).

underlain the Quaternary. Also, in this area, due to the shallowness of the water table evaporation–evapotranspiration processes could be produced in the upper layers of the aquifer.

General groundwater flow directions in the upper 30 m of aquifer are from SW to NE, as determined from a two depths monitoring network tapping the phreatic surface (<6 m depth) and the piezometric level at 30 m. But small vertical gradients are observed, which would induce vertical flows dominantly downwards in the S and upwards in the N (Fig. 2).

3. MATERIALS AND METHODS

Chemical analysis of major and some minor components, and isotopic analyses of ^{18}O and ^{2}H in 62 groundwater samples taken in February 2007 were studied to deduce the origin of groundwater composition and to contribute to tracing the groundwater flow pattern.

The samples were taken in a two depths monitoring network of the Instituto de Hidrología de Llanuras (IHLLA). 43 samples are from the phreatic zone network (identified with plain numbers in all figures), which is between 3 and 6 m depth, and 19 samples are from the 30 m depth network (identified with numbers precedeed by I). The monitoring network consists of coupled emplacements covering the whole Azul River basin; the location of the borehole couples is shown in Fig. 2.

4.   RESULTS AND DISCUSSION

The samples shown in this work come from a particular survey (February 2007), but they are reasonnably representative of groundwater composition in the aquifer of the Azul River basin at the two studied depths. This representativity is known from the study of temporal and lateral changes of chemical data from more than 15 surveys performed in the two depths monitoring networks of the IHLLA. Some temporal changes (not shown here) whose origin is under study are observed in the phreatic waters. They seem to mostly obey the recharge history (rainfall and infiltration) prior each sampling survey.

The chemistry of the 30 m depth groundwaters is very stable along time for each particular borehole, and only some minor oscilations have been observed. Any significative chemical change has been observed at reginal scale at both sampling depths.

Groundwater in the aquifer upper 30 m displays an increasing salinity from SW to NE (Fig. 3). Up to now the hypothesis to explain salinity was infiltration of evapo-concentrated surface water, as the small soil slope in the northern basin (<0.2%) induces rainfall accumulation in the lowlands, where water evaporates prior to infiltration. The present work was undertaken to check the salinity sources, among other objectives.

The contents of major and some minor components, as well as some ionic ratios in groundwater at the two observational depths (phreatic water and 30 m), point to two salinity sources: (1) evaporation of recent recharge water (mostly found in the southern sector of the basin); and (2) mixing with saline groundwater of unknown origin (mostly found in the centre and to the N of the basin). The last process
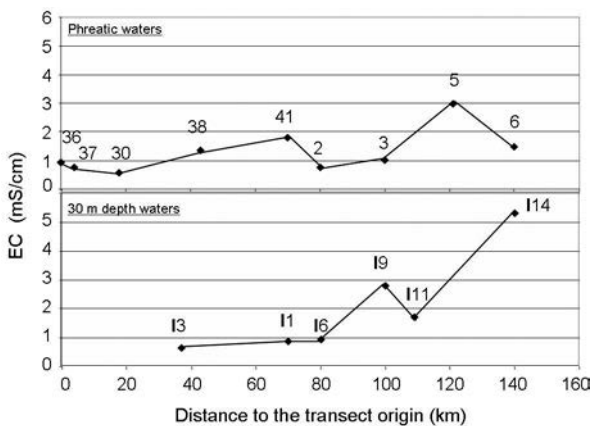
FIG. 3. Horizontal salinity evolution at two depths (phreatic zone and 30 m) in the upper part of the aquifer in February 2007. Transect location and borehole numbers are shown in Fig. 2.
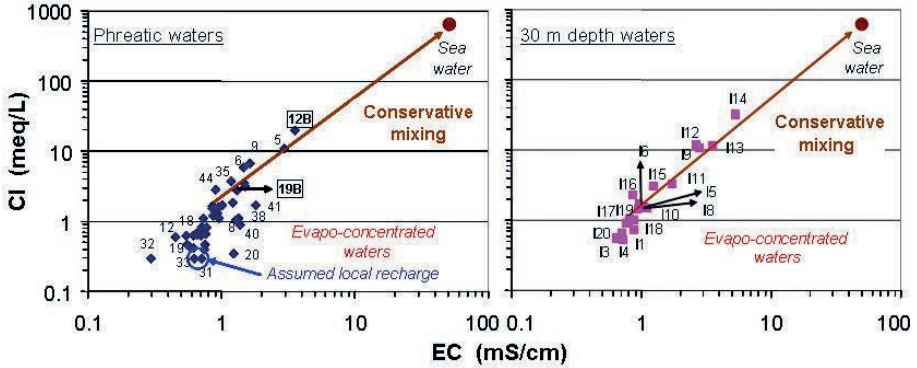
FIG. 4. Cl content evolution in groundwater at the phreatic zone and at 30 m depth in February 2007. Salinity increase in the lowly mineralised waters seems to be the effect of evapotranspiration during infiltration, and may be also from the water table; salinity increase in the most saline waters point to mixing with saline groundwaters similar to seawater. The mixing affects both the shallow (left) and deeper (right) waters. Samples 12B and 19B (left) are from boreholes of intermediate depth (15 m).

contributes to the salinity not only of the 30 m depth waters but also to the phreatic waters (Fig. 4).

The evolution of Na/Cl ionic ratio versus Cl content (Fig. 5) allows us to distinguish two groups of waters, arbitrarily named A and B. Group A waters are mostly found in the southern sector of the basin and at both sampling depths. These waters show a variable Na/Cl ratio but always >>1, while their Cl content does not change. Their salinity is assumed to be the result of local rain infiltration dissolving mostly carbonates and silica, and exchanging Ca–Mg and Na [6].

Group B waters, mostly found to the centre and N of the basin and also at both sampling depths, display a decreasing Na/Cl ratio as Cl increases, approaching Na/Cl ~1. This is assumed to be the result of mixing the type A waters with a saline groundwater different to the locally recharged water and with salinity ratios similar to conventional seawater. They are from boreholes of between 15 m (12B and 19B in Fig. 5, left) and 30 m (I12 and I14 in Fig. 5, right) in depth.

The hydrogeological origin of this saline groundwater has yet to be studied, though the potential candidate is the marine Paraná formation.

The evolution of SO_4/Cl ionic ratio versus electrical conductivity (EC) at the two studied depths points to the existence of reduction processes in most of the phreatic and 30 m depth groundwaters (Fig. 6). But many waters not reduced from both depths seem to show the signature of local recharge mixing with a more saline groundwater.

The $\delta^{18}O$ vs Cl graph (Fig. 7) shows clearly the two salinity sources induced from the chemistry study. Only for reference purposes, the theoretical mixing line between a sea-like salinity groundwater and a fresh groundwater representative of
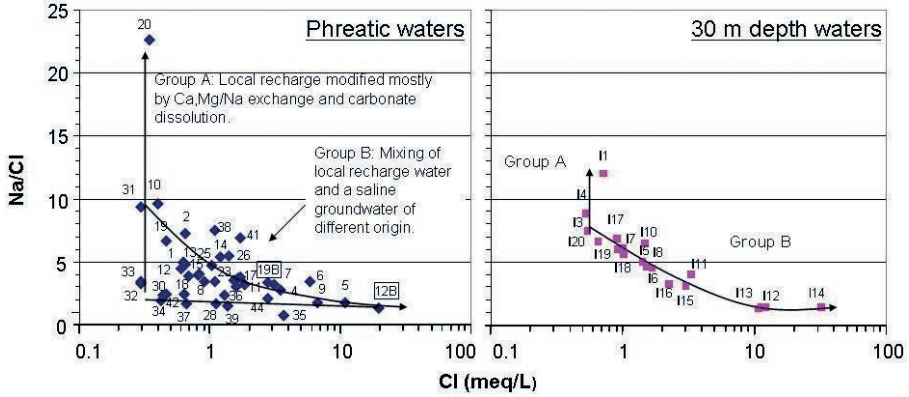
FIG. 5. Na/Cl ionic ratio as a function of Cl content in phreatic and 30 m depth groundwater in February 2007. Numbers refers to the identification of boreholes in Fig 2.
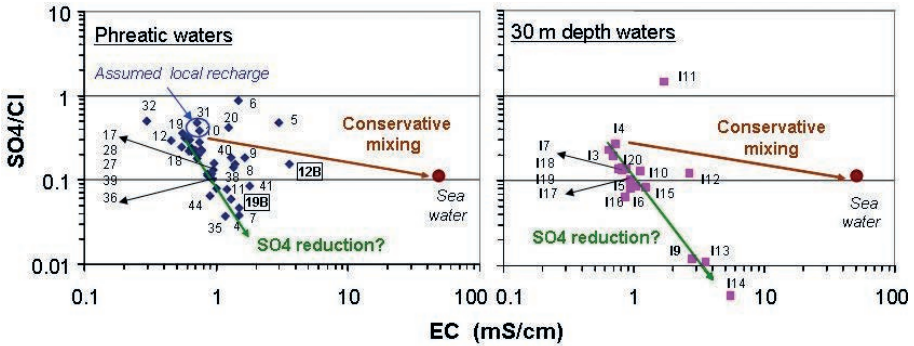
FIG. 6. SO$_4$/Cl ratio evolution versus electrical conductivity in phreatic and 30 m depth groundwater in February 2007. Numbers refers to the identification of boreholes in Fig 2.

local recharge has been drawn. Water from borehole 31 has been chosen as representative of unmodified local recharge, but most probably the real 'fresh' endmember is phreatic groundwater somewhat heavier than average rainfall due to concentration by evapotranspiration. The expected $\delta^{18}O$ signature of local rain in phreatic waters could be around –5.7 to –6.2‰. Also the saline endmember could be saltier than seawater (as it is the porewater of the candidate Paraná formation). Thus, groundwater in many locations and depths (like the phreatic 13, 41, 27, 7, or the 15 m depth 12B, and the 30 m depth I9, I12 and I14) could have their salinity mostly from the saline endmember, with or without the very small effect of evapotranspiration.
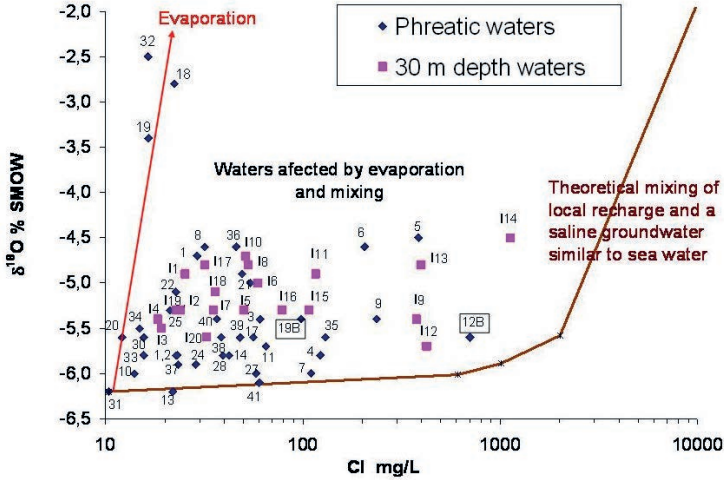
FIG. 7. δ¹⁸O and Cl in February 2007. They support the hypothesis of two salinity sources: evaporation of recent recharge water, and mixing with old saline groundwater with sea-water like salinity. Numbers refers to the identification of boreholes in Fig 2.

5. CONCLUSIONS AND FUTURE WORK

Groundwater salinity in the upper 30 m of the aquifer under the Azul River basin increases form SW to NE, following the flow sense of the river and what was supposed to be the main horizontal component of groundwater flow.

A previous hypothesis to explain this salinity was infiltration of evapo-concentrated surface water, as the small soil slope in the northern basin induces rainfall accumulation in lowlands and evaporation prior to infiltration. But the study of chemical and isotopic data at two different depths (phreatic zone and 30 m) points to the existence of two sources of salinity: (1) evapotranspiration prior to and during recharge, and maybe also from the water table, and (2) mixing of locally recharged water with a saline groundwater of different origin. Mineral dissolution and other processes like cation exchange also contribute to groundwater salinity, but to a minor extent compared to the other sources.

Thus, preliminary results points to the existence of lateral groundwater transfer from deep formations in the northern part of the basin contributing to groundwater salinity, besides evaporation and transpiration in shallower layers. The hydrogeological origin of this saline groundwater is still under investigation, but seems to be the marine sediments of the Paraná formation.

The clear picture shown by the water stable isotopes and by chemical ratios is promising about the successful use of other isotopic tools to assess solute sources and to trace groundwater flow patterns in the large Azul River basin aquifer.

ACKNOWLEDGEMENTS

REFERENCES

[1]   RIVAS, R., CASELLES, V., A simplified equation to estimate spatial reference evaporation from remote sensing-based surface temperature and local meteorological data, Remote Sensing of Environment **93** 1–2 (2004) 68–76.

[2]   FIDALGO, F., DE FRANCESCO, F., COLADO, U., Geología superficial de la llanura bonaerense (Argentina), Proc. VI Argentinean Geological Congress (1975) 103–138.

[3]   SOIL SURVEY DIVISION STAFF, Soil Survey Manual, Soil Conservation Service, U.S. Department of Agriculture, Handbook **18** (1993).

[4]   GONZÁLEZ BONORINO, F., ZARDINI R., FIGUEROA, M., LIMOUSIN, T., Estudio geológico de las Sierras de Olavarría y Azul (Bs. As.), LEMIT, Serie II **63** (1956) 5–22.

[5]   AUGE, M., Regiones Hidrogeológicas — República Argentina: Provincias de Buenos Aires, Mendoza y Santa Fé, Universidad de Buenos Aires, La Plata (2004).

[6]   ZABALA, M.E., MANZANO, M., VIVES, L., "Estudio preliminar del origen del fondo químico natural de las aguas subterráneas en la cuenca del arroyo del Azul", Hacia la Gestión Integral de los Recursos Hídricos en Zonas de Llanura, Vol. 1 (VARNI, M., ENTRAIGAS, I., VIVES, L., Eds) (2010) 249–256.

SPATIAL ISOTOPIC CHARACTERIZATION OF SLOVAK GROUNDWATERS

P.P. POVINEC [a], Z. ŽENIŠOVÁ [b], A. ŠIVO [a], R. BREIER [a],
M. RICHTÁRIKOVÁ [a], P.K. AGGARWAL [c], L. ARAGUÁS ARAGUÁS [c]

[a] Comenius University, Faculty of Mathematics,
Physics and Informatics,
Bratislava, Slovakia

[b] Comenius University,
Faculty of Natural Sciences,
Bratislava, Slovakia

[c] International Atomic Energy Agency,
Isotope Hydrology Section,
Vienna, Austria

Abstract

Žitný ostrov (Rye Island) in the south west of Slovakia is the largest groundwater reservoir in Central Europe (about 10 Gm^3). Groundwater contamination with radionuclides, heavy metals and organic compounds from the Danube River and local industrial and agricultural activities has recently been of great concern. Geostatistical analysis of experimental isotope data has been carried out with the aim of better understanding groundwater dynamics. For this purpose, spatial variations in the distribution of water isotopes and radiocarbon in the groundwater of Žitný ostrov have been evaluated. Subsurface water profiles showed enriched $\delta^{18}O$ levels at around 20 m water depth, and depleted values below 30 m, which are similar to those observed in the Danube River. The core of the subsurface ^{14}C profiles represents contemporary groundwater with ^{14}C values above 80 pMC.

1. INTRODUCTION

Water and specifically groundwater is becoming a strategic raw material of the 21st Century. Therefore it is important to know sources and infiltration areas of groundwater, and to protect it against possible contamination [1–3]. The vulnerability of groundwater to contamination is very high, especially in industrialized countries with high flow rates of contaminants, e.g. from refinery plants, agriculture, etc., which could cause groundwater contamination with radionuclides, heavy metals and organic compounds. The increasing water demand in many regions of the world has

been causing an intensive, and in many cases unsustainable exploitation of water resources [4]. In certain cases large quantities of water are transferred from different catchment areas, or fossil groundwater is intensively used, resulting in a noticeable alteration of the water cycle at regional or local levels [5].

Stable and radioactive isotopes have been extensively used during the last decades as environmental tracers to study the water cycle and to better understand the hydrologic cycle. It has been possible to study the present day distribution of water isotopes in the atmosphere, in rain and river water, in groundwater, and then to trace past isotopic compositions affecting many processes, such as atmospheric circulation, rain and snow formation, groundwater formation, ecology and paleoclimatology of the regions. Isotopes have been used to address key aspects of the water cycle, e.g. the origin, dynamics and interconnections of the different elements of the water cycle [1–9]. Fortunately with the development of the IAEA's Global Network of Isotopes in Precipitation (GNIP) database it has been possible to use isotopes in hydrological, ecological and climate studies, as input functions have been available for many areas of the world [3]. A lot of isotope data have been collected and several regional isotope databases have been developed. The GNIP database (www.gnip.iaea.org) has provided key data for the application of isotopes in hydrology. Recently this monitoring activity has been enlarged to isotopes in the total water cycle. The new isotope database (Isotope Hydrology Information System (ISOHIS), www.isohis.iaea.org) is also covering groundwater data. The ISOHIS together with the GNIP database enables to study the dynamics and spatial characteristics of groundwater [10].

With the development of geostatistical methods of data treatment, based on the application of the Geographical Information System (GIS), it is possible to map the spatial variability of the isotopic composition of water in selected regions of the world. In such a complex system it is possible to trace the origin and pathways of different water masses on the basis of the developed isotopic maps, covering temporal and spatial distribution of hydrochemical and isotope data. Recently new geostatistical tools have been developed to integrate isotope data into a relational database also covering hydrogeology and hydrochemistry, which using GIS would be possible to visualize, and in this way to create temporal-spatial isotope maps of groundwater [11, 12]. Such an integrated attempt will gather new information on the temporal and spatial variability of groundwater, on its dynamics, on anthropogenic and climatic impacts, and on its vulnerability.

Slovakia has an important position in this respect as the largest groundwater reservoir in Central Europe is situated at the Žitný ostrov (about 10^{10} m³). Stable isotopes [13, 14] and radiocarbon [15] have been applied in a few groundwater studies in Slovakia, however, integrated research has not yet been done, which would cover the groundwater regions in their full complexity. Previous isotope hydrology work in Slovakia, e.g. on mineral and thermal waters [15] have contributed to the understanding of origin of these waters, however, temporal and spatial information has been missing, which could better characterize specific groundwater localities, groundwater

ages, infiltration areas, recharging characteristics of groundwater reservoirs, the danger of their contamination, climatic changes, etc. — all important facts for the protection and a reasonable exploitation of groundwater from the long term perspective.

In the framework of the IAEA Coordination Research Project on 'Geostatistical analysis of spatial isotope variability to map the sources of water for hydrology studies' in 2007 we started a pilot study on the development of geostatistical tools for mapping the spatial isotope variability of groundwater in Slovakia. The constructed isotope maps will be used to trace the origin of groundwater in the region, to identify areas where additional isotope data are required, and to evaluate, assess and better manage resources of groundwater in the region. In the areas where limited isotope data are available, new sampling campaigns and isotope analysis will be carried out over the Slovakian territory, and new data will be merged with the compiled Central Europe groundwater database. Geostatistical analysis will be carried out with the aim of establishing temporal and spatial variations in the distribution of water isotopes. A new hydrological isotope database will be developed for Slovakia and Central Europe on the basis of previous studies, as well as using new data collected in the framework of this CRP. Further, possibilities of contamination of the groundwater of Slovakia and their vulnerability to agricultural and industrial activities of neighboring countries (Austria, Czech Republic, Hungary) will be determined. Regimes of groundwater in the most important reservoirs will be studied, further developments in water resources will be estimated, and recommendations will be given to local and regional managements. From the existing and new isotope data obtained in the framework of the project, as well as from other data on the isotopic composition

FIG. 1. Map of Slovakia with Žitný ostrov (an area between the dashed line and the Danube River in the SW of Slovakia).

of groundwater, it will be possible to produce isotope maps of the groundwater of Slovakia, and, after their analysis, to gather new information on groundwater.

In the first paper of these series [15] we discussed the stable isotope distribution and radiocarbon ages of the mineral and thermal waters of Slovakia. Samples of mineral and thermal waters, collected mostly in southwestern and northwestern Slovakia, were analysed for stable isotopes and radiocarbon. The obtained results contributed to the understanding of the origin of these waters. The apparent radiocarbon ages varied within the interval of 32 000 and 9000 a, indicating that groundwater was increasingly flowing mainly during interglacial periods. In this paper we report first results on the spatial radiocarbon and stable isotope ($\delta^{18}O$) variability of groundwater found at the Žitný ostrov in the southwestern part of Slovakia.

2.   HYDROLOGY OF THE ŽITNÝ OSTROV

Žitný ostrov with an area of 1200 km^2 covers the territory of the Danube Plain from Bratislava at the NW to Komárno at the SE (Fig. 1). It is bordered on the north by the river Malý Dunaj (Small Danube), and on the east by the river Váh. The territory of the Žitný ostrov is of great economical significance as it represents the largest reservoir of groundwater in Central Europe (about 10^{10} m^3, which represents potential ~18 m^3/s). In 1987 the territory of Žitný ostrov was declared the National protected water resources territory of Slovakia. There are several groundwater sources situated at the Žitný ostrov which deliver drinking water to Bratislava as well as to many other places in southwestern Slovakia.

The territory of Žitný ostrov also has an important social value with several protected regional areas. Because of its location and good soil and climatic conditions it is the most important agricultural region of Slovakia. The most important Slovak water power plant, called Gabčíkovo (established in 1992), is also located on the Danube River, producing 720 MW of electricity. The Gabčíkovo water system has considerably influenced the hydrology of the region, as well as the Danube River shipping conditions. The Gabčíkovo plant with Čunovo reservoir, the inlet and outlet canals have had positive impacts on regional groundwater conditions. Due to the back water effect of the Čunovo reservoir, the level of groundwater in the region of Bratislava has increased by about 2 m, which has positively influenced all the ecosystems in the region.

From the geomorphology point of view, the Žitný ostrov belongs to the Danube Plain in which several wetplains are located. The relief is made of bottom lands, consisting mainly of fluvial, proluvial wetplain and eolic fluvial relief. The territory represents a flat terrain 136–129 m above sea level. The average precipitation during 1951–1980 was between 528 and 580 mm. The average evaporation from the soil surface at Žitný ostrov for the time interval between 1961 and 1990 was 450–500 mm. A total potential evaporation was between 700 and 800 mm. From the geological

298

point of view the Danube basin is divided by a system of longitudinal and transversal faults, separating the areas on a system of rafts, which were and still are sinking with different intensity.

The groundwater regime of the Žitný ostrov is a result of interactions between Danube water (and other surface waters in the region) and groundwater in the region, as well as between precipitation and evaporation. The Danube River feeds groundwater in the region at all its water levels at the Žitný ostrov. A general trend in the flow of groundwater is mostly following the main rivers in the region (Danube on the south-west, Malý Dunaj on the north and Váh on the east). Precipitation is influencing the groundwater regime especially during summer, in connection with elevated flow rates in rivers, and also by increasing the groundwater level (with different delays depending on the distance from the river). After operation of the Gabčíkovo water plant (monitoring between 1993 and 2002), groundwater levels have increased in the Bratislava region, at the upper part of the Žitný ostrov, and in the direction to Malý Dunaj. A decrease in groundwater levels has been observed from the beginning of the inlet channel up to the end of the outlet channel (its connection with the Danube River).

3.   SAMPLES AND ANALYTICAL METHODS

The sampling strategies were determined by the main objectives of the project which include the development of a relational isotope database of the groundwater of Slovakia, determination of the catchment areas of groundwater at the Žitný ostrov, and contribution to the protection of groundwater against contamination from surface waters (e.g. from the water system of Gabčíkovo), from agricultural fertilizers and industrial products (e.g. oil products from the Slovnaft refinery located in Bratislava, and radionuclides from the Nuclear Power Plant in Jaslovské Bohunice situated on the Váh River). Three sampling campaigns (2008–2010) were carried out, visiting over 50 boreholes. Groundwater samples were taken from different horizons. Water samples for radiocarbon analysis (~50 L) were collected directly from the boreholes. Bicarbonates were extracted as soon as possible by precipitation with barium chloride. $BaCO_3$ produced was stored in polyethylene containers and transported to the laboratory [16]. During groundwater sampling in situ measurements of basic physical and chemical parameters (groundwater temperature, air temperature, pH, electrical conductivity (EC), oxidation reduction potential (E_h), concentration of dissolved oxygen, and oxygen saturation) were carried out as well.

Laboratory analyses included: analysis of stable isotopes (^2H, ^{18}O, ^{13}C), preparation of gas fillings and ^{14}C activity measurements. The $\delta^{18}O$ data are reported in ‰, relative to (Vienna Standard Mean Ocean Water (VSMOW). For ^{14}C analysis of groundwater samples carbon dioxide was released from barium carbonate by addition of H_3PO_4. Methane synthesized from carbon dioxide was then used as a filling

gas of the low level proportional counter [17, 18]. In addition to each water sample, samples of background and of radiocarbon standard (oxalic acid ^{14}C standard from the National Institute of Standards and Technology, Gaithersburg, USA) were also measured. ^{14}C results are expressed as percent modern carbon (pMC) relative to the NIST ^{14}C standard. All ^{14}C data were corrected for δ^{13}C.

4. RESULTS AND DISCUSSION

Spatial distribution of δ^{18}O in surface and subsurface waters with a longitude of the Žitný ostrov area is presented in Fig. 2. While the bottom samples are depleted in δ^{18}O values, generally below –10.5‰ (similar to the Danube values), the subsurface core observed at around 20 m water depth shows enriched δ^{18}O values between –10.0‰ and –9.5‰. However, the surface samples (up to 10 m water depth) show again depleted δ^{18}O values, close to the values observed for the Danube river system. The obtained data are in good agreement with isotope data measured for the Danube river system (values between –10.92‰ and –12.26‰ for the Danube, and between –0.57‰ and –11.39‰ for Malý Dunaj). As expected, the Danube river system is the main source of shallow groundwater observed at Žitný ostrov. It is possible that surface and shallow subsurface waters showing enriched δ^{18}O values may be due to land irrigation, which has been often used in this agriculturally heavily industrialized region.

A subsurface radiocarbon profile of groundwater with a longitude of the Žitný ostrov is shown in Fig. 3. We can see a subsurface core of about 50 pMC at around
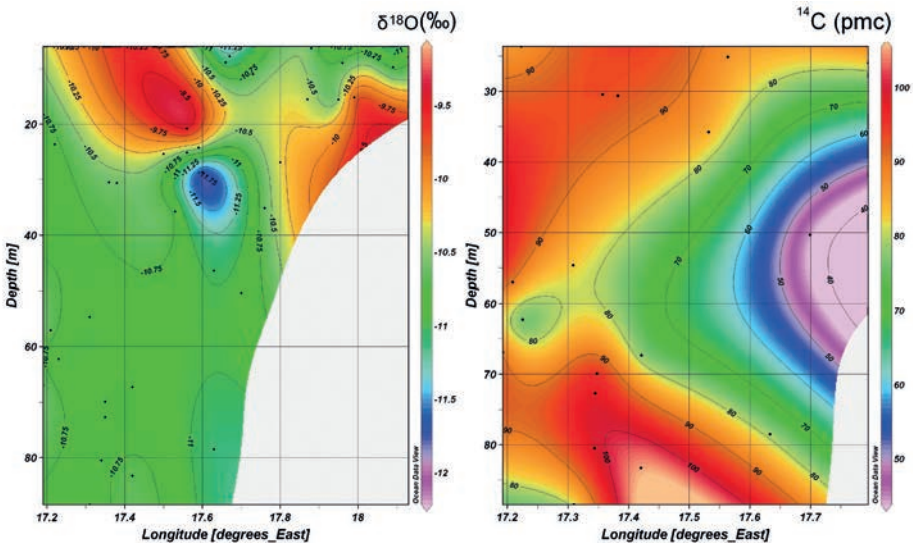
FIG. 2. Vertical distribution of δ^{18}O and ^{14}C in groundwater with a longitude of the Žitný ostrov

60 m water depth, while the surface samples up to 10 m water depth show ^{14}C values above 80 pMC, representing contemporary groundwater.

5. CONCLUSIONS

This has been a first attempt to construct isotope maps and to study the surface and vertical distribution of isotopes in groundwater. More groundwater samples from the Žitný ostrov area will be collected and analysed from surface as well as subsurface horizons, which will help to improve the spatial and profile density of isotope data, and thus contribute to better understanding of the groundwater system on the Žitný ostrov [19]. We hope that this new research approach will improve the capability and efficiency of using isotopic tools for deeper evaluation, more rigorous assessment and more efficient management of water resources in the region.

REFERENCES

[1]   KENDALL, C., McDONNELL, J.J., Isotope Tracers in Catchment Hydrology, Elsevier, Amsterdam (1998).
[2]   FERRONSKY, V.I., POLYAKOV, V.A., Environmental Isotopes in the Hydrosphere, Wiley, New York (1982).
[3]   AGGARWAL, P.K., GAT, J.R., FROEHLICH, K.F.O. (Eds), Isotopes in the Water Cycle, Springer, Heidelberg (2005).
[4]   SANFORD, W., LANGEVIN, C., POLEMIO, M., POVINEC, P. (Eds), A New Focus on Groundwater–Seawater Interactions, Proceedings and Reports Series, IAHS, Wallingford (2007).
[5]   GONFIANTINI, R., FROEHLICH, K.F.O., ARÁGUAS-ARÁGUAS, L., ROZANSKI, K., "Isotopes in groundwater hydrology", Isotope Tracers in Catchment Hydrology (KENDALL, C., McDONNELL, J.J., Eds), Elsevier, Amsterdam (1998).
[6]   RANK, D., et al., "Environmental isotope study at research landfill (Breitenau, Austria)", Proc. Intern. Symp. Isotopes in Water Resources Management, IAEA, Vienna (1995) 379–381.
[7]   DEÁK, J., "Isotope-Hydrogeology Studies in Hungary focusing on the requirements of the EU Water Framework Directive", Proc. Isotopenmethoden in der Hydrogeologie und Wasserwirtschaft, IAEA, Vienna (2003) 1–9.

[8]   SCHIAVO, M.A., HAUSER, S., POVINEC, P.P., Stable isotopes of water as a tool to study groundwater–seawater interactions in coastal south-eastern Sicily, J. Hydrology **364** (2009) 40–49.

[9]   POVINEC, P.P., et al., Characterisation of submarine groundwater discharge offshore south-eastern Sicily, J. Environ. Radioact. **89** (2006) 81–101.

[10]   INTERNATIONAL ATOMIC ENERGY AGENCY, Water and Environment News, Issue No. 22, IAEA, Vienna (2007).

[11]   BOWEN, G.J., WASSENAAR, L.I., HOBSON, K.A., Global application of stable hydrogen and oxygen isotopes to wildlife forensics, Oecologia **143** (2005) 337–348.

[12]   AGGARWAL, P.K., ARAGUÁS-ARAGUÁS, L., Geostatistical Analysis of Spatial Isotope Variability to Map the Sources of Water for Hydrology and Climate Studies, IAEA, Vienna (2006).

[13]   MALÍK, P., MICHALKO, J., MANSELL, S.J., FENDEKOVÁ, M., "Stable isotopes in karstic groundwaters of Veľká Fatra mountains, Slovakia", Proc. Intl Symp. on Isotopes in Water Resources Management, IAEA, Vienna (1995) 248–249.

[14]   MICHALKO, J., Stable isotopes of hydrogen, oxygen and sulphur in the waters of Slovakia, Slovak Geol. Mag. **5** (1999) 63–67.

[15]   POVINEC, P.P., POVINEC, P.P., CHUDY, M., SARO, S., Spatial radiocarbon and stable carbon isotope variability of mineral and thermal waters in Slovakia, Radiocarbon **52** (2010) 1056–1067.

[16]   USAČEV, S., POVINEC, P.P., CHUDY, M., SARO, S., Bratislava radiocarbon measurements I, Radiocarbon **15** (1973) 443–450.

[17]   POVINEC, P.P., Preparation of methane gas filing for proportional ^{3}H and ^{14}C counters, Radiochem. Radioanal. Letters **9** (1972) 127–135.

[18]   POVINEC, P.P., Multiwire proportional counters for low-level ^{14}C and ^{3}H measurements, Nuclear Instruments and Methods **156** (1978) 441–445.

[19]   POVINEC P.P., ŽENIŠOVÁ, Z., BREIER, R., RICHTÁRIKOVA, M., ŠIVO, A., Isotopic tracing of groundwater at Žitný ostrov (SW Slovakia), EPJ Web of Conferences **24** (2012) 03004.

RADIONUCLIDES, HEAVY METALS AND FLUORIDE CONTAMINATION IN AL BAHIRA AQUIFER, YOUSSOUFIA AREA, MOROCCO

T. TAGMA[a], N. WARNER[b], L. BOUCHAOU[a, 1], N. ETTAYFI[a],
Z. LGOURNA[a], S. BOUTALEB[a], A. VENGOSH[b]

[a] Ibn Zohr University,
   Applied Geology and Geo-Environment Laboratory,
   Cité Dakhla, Agadir 80060, Morocco,

[b] Duke University,
   Division of Earth & Ocean Sciences,
   Durham, NC 27708, USA

Abstract

This study investigates the geochemistry and quantity of trace metals and naturally occurring radionuclides (Ra, U) in the shallow groundwater in the western part of the Al Bahira aquifer (Phosphate Plateau) located in west central Morocco. Groundwater is characterized by a wide salinity range (TDS of 540 to 9286 mg/L) and shows systematic linear relationships between the major dissolved constituents. These relationships suggest that the mixing of a single saline source and fresh water controls the quality of groundwater. Fluoride, uranium, selenium, and arsenic concentrations are also correlated with salinity. The activity concentrations of radium-226 exceed the US-EPA drinking water standard. Radium-226 activity in the groundwater is not directly related to salinity and might be affected by other factors such as water temperature. The low ratios of the short lived Ra-224 to Ra-223 (~2) indicate that Ra was derived from a uranium rich source with a low Th/U ratio in the rock source, which is consistent with the U-rich lithology of the aquifer (e.g., phosphate rocks). The high levels of contaminants found in the shallow groundwater samples have important health implications for the local population, as shallow groundwater is used for drinking water in the rural communities northwest of Marrakech and these contaminants pose potential serious health problems (e.g., dental fluorosis, kidney disease, and bone cancer).

1.   INTRODUCTION

The plain of Al Bahira is located in west central Morocco, at 70 km north-western of Marrakech. The aquifer is divided into three parts: eastern, central and

---

1 Corresponding author: lbouchaou@yahoo.fr

the western sections, in which this study has been conducted. In this area, the Al Bahira plain forms a topographical depression surrounded by the Mouissat plateau in the west, the Guentour plateau in the north and the Jbilet massif in the south (Fig. 1-a). The stratigraphy is composed of: (1) underlying Paleozoic schist outcropping in Rhamna and Jbilet; (2) Triassic clay; (3) upper Jurassic marls and limestone of (Mouissat plateau); (4) upper Cretaceous marls and limestone; (5) Eocene limestone, marls and phosphate; and (6) Neogene lacustrine limestone, conglomerate, and marls. The Cretaceous and Eocene formations dip from the north to the south, and bevel against the Jbilet massif [1].

Two aquifers have been identified in the region (Fig. 1b): (1) the shallow aquifer that is composed by the alluvial formations in the eastern part and silts, sandstone,
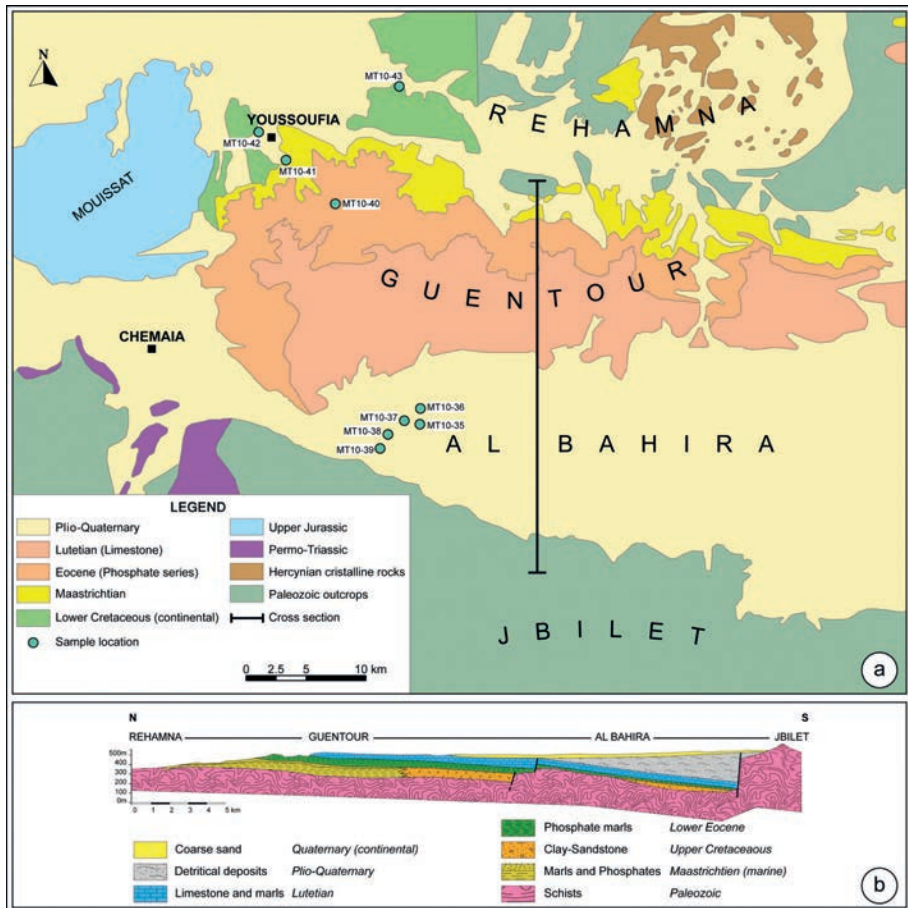
FIG. 1. (a) Geological map of western Al Bahira. The locations of the sampled groundwater are also represented. (b) Cross-section from Rehamna to Jbilet (after [2], modified).

marls and limestone of Plio-Quaternary age in the western part; and (2) the Cretaceous aquifer composed of limestone formations that are common in nearly all the parts of the plain. This aquifer is unconfined where the geological formations outcrop or are shallow. It is captive in areas where it is overlain by thick Plio-Quaternary formations. The groundwater flows to the Tassaout River situated in the extreme east [2].

This area is also known for sedimentary phosphate deposits. Phosphate ore contains naturally occurring radionuclides (mostly uranium) and their daughter radionuclides, such as radium and radon. The International Atomic Energy Agency (IAEA) estimates that Morocco's phosphate deposits contain up to 36 percent P_2O_5 with uranium contents of 150 ppm, with local enrichment in some layers up to 500–600 ppm [3]. Morocco's uranium resources in phosphate deposits were estimated at around 6 million t, which corresponds to twice the world's resources of uranium deposits [3]. Besides radioactive elements, phosphate ore contains hazardous elements including heavy metals (As, Al, Cd, Pb, Co, Cu, Fe, Mn, Mo, Ni, Zn and Hg) and fluorine [4–6]. The adverse environmental impacts of these hazardous elements and radionuclides are of great concern as they can move to the soil or leach to groundwater and ultimately affect humans and animals who consume the this water. Several studies have reported the existence of important clinical problems affecting human and livestock populations in Moroccan phosphate areas and have related these to high concentrations of some of those elements in drinking water but also in air and soil near phosphate plants and manufacturers [7–10]. However, the direct impact of natural phosphate rocks on groundwater has not yet been studied. Therefore the present study has been undertaken to investigate the abundances of radionuclides, heavy metals and fluorine in groundwater associated with natural phosphate rocks of the Youssoufia area, and to assess their potential risk on the local population living in the region.

2.   METHODS

Water samples were collected at the western part of the Al Bahira aquifer. Eight samples of groundwater from private wells and one sample from a municipal well were collected. The locations of the sampling points are shown in Fig. 1a. The water samples were analysed at Duke University (USA) for major and trace elements and also naturally occurring radium. Major and trace elements were measured using inductively coupled plasma atomic emission spectroscopy (ICP-AES) and ion chromatography (IC). Fluoride was measured using a specific electrode and corrected for water salinity. Radium was extracted soon after sampling (the same day) by manganese fiber [11] without prefiltration. ^{226}Ra, and ^{224}Ra–^{223}Ra isotopes were determined respectively by a radon counter [12], and delayed coincidence radium counter [13]. Dissolved oxygen, pH, temperature and conductivity (μS/cm) were measured in the field.

3. RESULTS AND DISCUSSION

3.1. Groundwater chemical characteristics

The salinity of groundwater is determined by the total dissolved solids (TDS) expressed in mg/L. The groundwater of the Al Bahira aquifer is characterized by a wide range of salinity; TDS vary from 540 to 9286 mg/L. Chloride content controls the salinity of groundwater as the Cl/TDS ratio can reach 0.48. The linear correlations between chloride and other major dissolved constituents suggest that water quality is controlled by a simple mixing of two endmembers: (1) saline water dominated by Cl-Na type, and (2) fresh water of HCO_3-Ca type (Fig. 2).
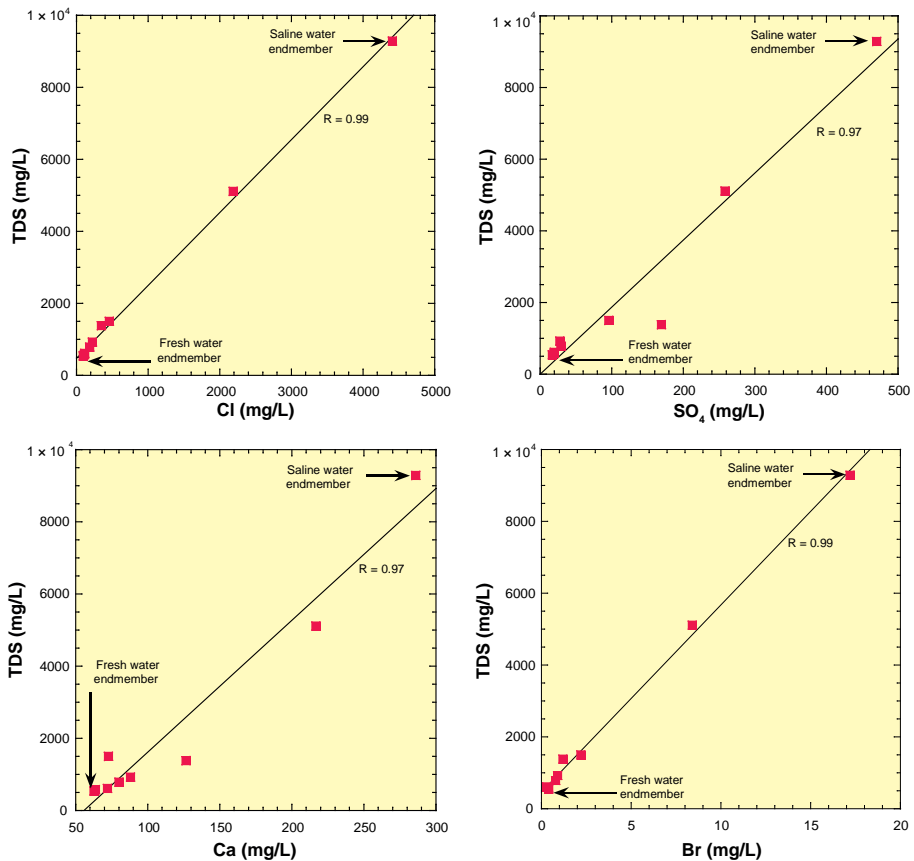
Fig. 2. Linear relationships between major elements and TDS in investigated groundwater. Two endmembers controlling the geochemistry of water are identified: saline water and fresh water.

The data indicate that fluoride concentrations, slightly higher than the allowable limit of 1.5 mg/L of fluoride recommended for potable purposes, have also been observed in the investigated groundwater. The geochemical analysis of the water samples suggests that the salinity is derived from the combination of high cations (mostly Ca and Na) and anions (Cl, SO_4, HCO_3). In particular, the extreme high levels of bicarbonate (>2000 mg/L) suggests an important contribution of organic matter that is converted to dissolved inorganic carbon. The high concentration of nitrate suggests that the groundwater originates from modern recharge possibly with an anthropogenic contribution (agricultural return flows, wastewater). Since the overall salinity is related to the nitrate and bicarbonate concentrations, the salinity might be due to the evaporation of organic and nitrate rich agricultural return flows that infiltrate into the shallow aquifer. Thus, the chemistry of the shallow aquifer might be the result of a mixture of low saline recharge and saline agricultural return flows enriched in fluoride as it is positively correlated to TDS, chloride, calcium, magnesium, bicarbonates, and nitrates, but it is negatively correlated to pH and temperature.

3.2. Trace metals contamination

Table 1 shows trace elements concentration in the investigated groundwater. The maximum contaminant level for each element is also shown. The studied groundwater is highly enriched in several trace metals, such as boron, selenium,

TABLE 1. HEAVY METAL CONCENTRATIONS, EXPRESSED IN PARTS PER BILLION, IN THE AL BAHIRA GROUNDWATER

					Toxic elements					
			Maximum contaminant levels according to WHO standards (ppb)							
Sample code	As 10	B 500	Cd 3	Cr 50	Co –	Fe –	Pb –	Se 10	U 15	Zn –
MT10-35	1.94	120.48	0.09	14.15	0.48	181.22	0.00	2.59	3.09	0.09
MT10-36	2.27	71.19	0.02	9.95	0.41	132.67	0.17	0.51	3.44	0.00
MT10-37	1.77	118.11	0.00	12.85	0.42	162.56	0.00	3.97	3.13	108.11
MT10-38	3.65	742.43	0.05	85.59	1.83	491.64	0.00	54.72	17.55	0.00
MT10-39	6.94	1538.41	0.05	92.13	0.87	606.03	0.54	56.22	22.17	84.33
MT10-40	2.33	75.29	0.00	9.81	0.44	128.22	0.00	2.51	3.67	0.00
MT10-41	4.58	261.54	0.44	14.88	0.56	254.98	0.00	14.76	10.01	6.68
MT10-42	2.13	83.97	0.00	9.70	0.42	150.32	0.11	1.77	3.88	45.20
MT10-43	2.19	223.6	0.23	20.74	1.17	110.64	0.04	19.04	11.93	173.36

uranium, zinc and chromium. The high concentrations of uranium suggest oxic conditions that enable uranium moblization from the rocks. While U does not show a high correlation with salinity, other trace metals have strong relationships with salinity, which suggests that the saline water enhances interactions with the shallow aquifer rocks, presumably phosphates, and results in high concentrations of these elements in the groundwater.

3.3. Radium isotopes

The activity concentrations of radium vary from 0.05 to 1.24 pCi/L for Ra-223, from 0.12 to 2.76 pCi/L for Ra-224, and from 4.1 to 12.5 pCi/L for Ra-226. The latter exceeds the allowable limit of 5 pCi/L USA-EPA drinking water standard (Fig. 3).

The radium-226 activity in the groundwater is not directly related to salinity and might be affected by other factors such as water temperature (Fig. 4). The ratios
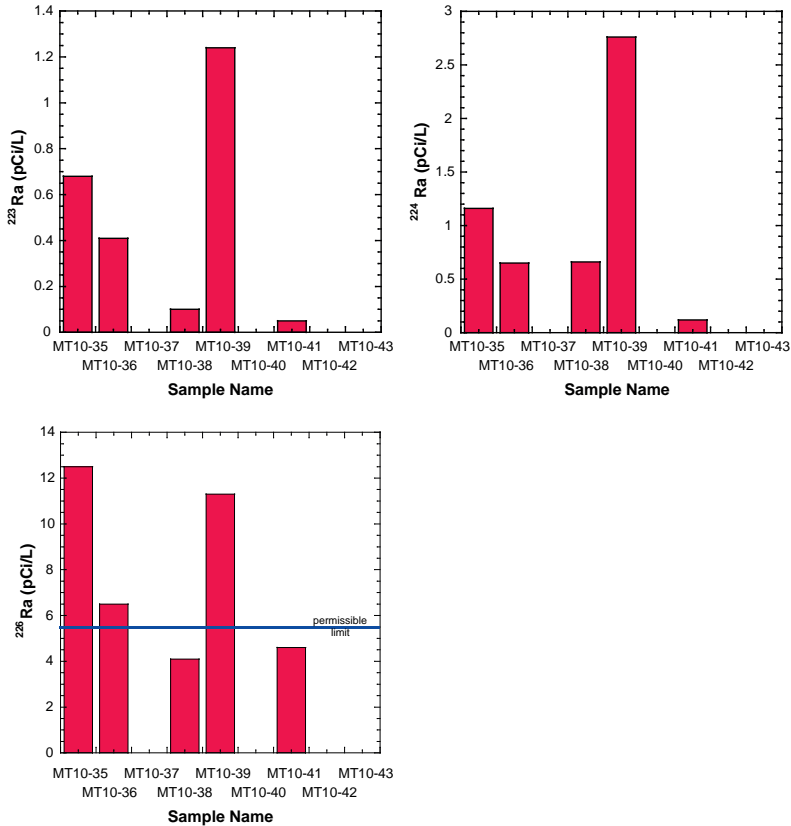
FIG. 3. The activity concentrations of radium-226, radium-224 and radium-223 in the investigated groundwater of the Youssoufia region.
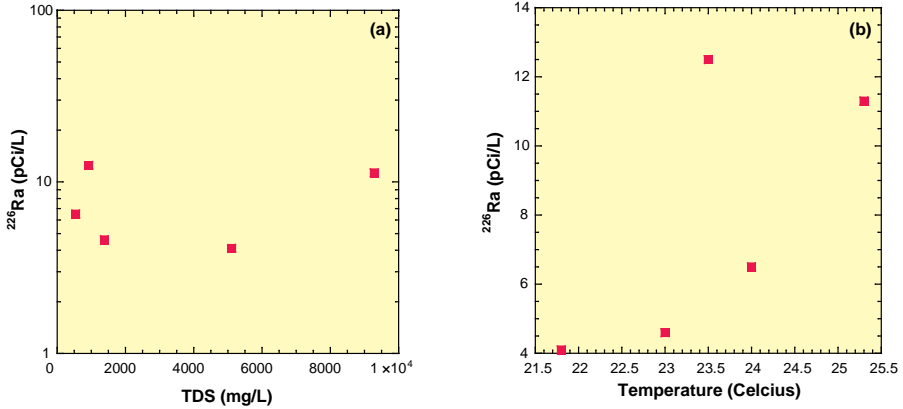
FIG. 4. Relationships between radium-226 and TDS (a), and between radium-226 and temperature (b).

of the short-lived Ra–224 to Ra–223 are low (~2), which indicates that Ra was derived from a uranium rich source with a low Th/U activity ratio in the rock source, probably phosphate rocks.

4. CONCLUSIONS

The water quality and the quality of toxic and radioactive contaminants in the groundwater of the Youssoufia region of western central Morocco were assessed in this study. The results show that the concentrations of radionuclides, several heavy metals and fluoride in the groundwater exceed the allowable drinking water limits for potable utilization and suggest possible sources of these elements. If the groundwater from the study site is used for drinking water for an extended period, these elements could exert adverse effects on human health.

ACKNOWLEDGEMENTS

REFERENCES

[1] BENZAQUEN, M., et al., Bassin de la Bahira-Tadla, étude structurale, Rapport inédit. DMG. Rabat (1963) 14.

[2] INTERNATIONAL ATOMIC ENERGY AGENCY, "Plateau des Ganntour et plaines de la Bahira et de la Tessaoute aval", Ressources en Eau du Maroc, Tome 2, Notes et Memoires du Service Géologique, Rabat, Morocco (1975) 367–392.

[3] INTERNATIONAL ATOMIC ENERGY AGENCY, World Distribution of Uranium Deposits (UDEPO) with Uranium Deposit Classification, IAEA-TECDOC-1629, IAEA, Vienna (2009).

[4] KHARIKOV, A.M., SMETANA, V.V., Heavy Metals and Radioactivity in Phosphate Fertilisers: Short Term Detrimental Effects, USFEC, Ukraine (2000), http://www.fertilizer.org/ifa/publicat/PDF/2000_biblio_126.pdf

[5] KRATZ, S., SCHNUG, E., Schwermetalle in P-Düngern, Landbauforschung Völkenrode, Special Issue **286** (2005) 37–45.

[6] VAN KAUWENBERGH, S.J., Cadmium and Other Minor Elements in World Resources of Phosphate Rock, Proc. Fertiliser Society No. 400, Fertiliser Society, London (1997).

[7] AMRANI, F., Evaluation de la fluorose dentaire dans la région de Khouribga au Maroc, PhD Thesis, Univ. Nancy I, Nancy (2009).

[8] FAYE, B., DIACONO, E., BENGOUMI, M., KESSABI, M., "Hydrotelluric and Industrial Fluorosis Survey in the Dromedary Camel in the South of Morocco", Impact of Pollution on Animal Products, Springer Netherlands (2008) 85–90.

[9] OUFNI, L., MISDAQ, M.A., AMRANE, M., Radon level and radon effective dose rate determination in Moroccan dwellings using SSNTDs, Radiation Measurements **40** (2005) 118–123.

[10] KESSABI, M., ABDENNEBI, E.H., Contribution à l'étude épidémiologique du darmous, Maghreb Vet. **1** (1985) 37–42.

[11] MOORE, W.S., ARNOLD, R., Measurement of ^{223}Ra and ^{224}Ra in coastal waters using a delayed coincidence counter, J. Geophys. Res. **101** (1996) 1321–1329.

[12] KIM, G., et al., Measurement of ^{224}Ra and ^{226}Ra activities in natural waters using a radon-in-air monitor, Environ. Sci. Technol. **35** (2001) 4680–4683.

[13] MOORE, W.S., REID, D.F., Extraction of radium from natural waters using manganese-impregnated acrylic fibers, J. Geophys. Res. **78** (1973) 8880–8886.

ASSESSMENT OF GROUNDWATER QUALITY IN THE WESTERN AQUIFERS OF MAURITIUS USING ISOTOPE TECHNIQUES

D. DINDYAL, R. BRIZMOHUN, J.O.Y. FANNY
National Environmental Laboratory,
Reduit, Mauritius

E. SACCHI
Dipartimento di Scienze della Terra e dell'Ambiente,
Università di Pavia, Italy

Abstract

This contribution reports the results obtained in the IAEA TC project MAR/8/007, initiated in 2007. Fourteen boreholes were sampled during three sampling campaigns (rainy season, winter and summer): analyses include major ions, trace elements, stable isotopes (δ^2H, δ^{18}O and δ^{13}C) and a microbiological assessment (TC and *E. coli*). Results indicate that groundwater quality is generally good. Recharge mostly occurs in the central plateau area, but the increase in nitrates along the groundwater flow and the common presence of *E. coli* indicate that a minor recharge occurs all over the aquifer's extension. Infiltration is rapid and favoured by the presence of vertical fractures in the basalts. Discharge occurs at a lower altitude and is marked by a different stable isotope content and lower nitrates. In addition to validating the general groundwater circulation model, these results show that aquifers are not adequately protected against a possible input of pollutants from the surface.

1. INTRODUCTION

The hydrogeology of basaltic aquifers is a vital topic for water resources management in many locations around the world, especially in developing countries and volcanic islands [1]. Mauritius is heavily dependent on groundwater for drinking purposes: 50% of that demand is satisfied by the system of aquifers. The consumption of water for domestic purposes is about 200 litres per person per day. The growth of industrialisation, the flourishing tourism industry, the increasing use of chemical fertilisers and pesticides, coupled with other human and land based activities may all have an impact on the island's groundwater resources. As the demand for water in Mauritius increases, the risk of groundwater pollution from municipal and industrial wastes rises. It is therefore deemed imperative to characterize the groundwater system and identify existing or potential sources of groundwater contamination.

Isotopic studies on the island funded by the Agency date back to 1976. In 1991–1992, an extensive survey of the isotopic content of the rain, surface and groundwater of the island was carried out in order to assess whether its variability could be used as a tool in groundwater research [2]. The variability of oxygen-18 and deuterium in rain was found to be high, and the patterns showed some regularities. High $\delta^{18}O$ values were obtained during the winter season, when there is low rainfall, and low $\delta^{18}O$ values during summer (high rainfall). In addition, when the rainfall is low, a slight increase in $\delta^{18}O$ values due to the evaporation effect is observed. The comparison of $\delta^{18}O$ and δ^2H values from groundwater and from rainfall indicated that groundwater in Mauritius is mainly recharged during the summer season. Indeed, the $\delta^{18}O$ values of groundwater were found to be typical for summer rain, that is $\delta^{18}O < -2‰$. The previous studies concluded that the regularities and the variability of stable isotopic content of surface and groundwater potentially allowed for the application of isotope techniques in water resources development in Mauritius. With this background and with the quest to identify contamination sources of groundwater, the project MAR/8/007 was initiated in 2007.

The western aquifers of Mauritius were chosen as a study site, following the concern raised about the degradation of the groundwater quality in some selected boreholes. The investigation aims to define groundwater quality, assessing the possible interconnections between aquifers, identifying pollution sources and validating the general groundwater circulation model.

The western aquifers of Mauritius, also known as Aquifer I and II, extend from the plateau area in the centre of the island, with a mean elevation 550–700 m a.s.l, to the sea. The aquifers are constituted by basaltic lava flows, and more specifically by two superposed basalt layers (recent basalts and intermediate basalts), of similar hydraulic conductivity, separated by a thin (< 10m) and discontinuous layer of weathered clayish rocks, behaving as an impermeable layer [3]. It is believed that the aquifers are recharged in the central plateau area, where precipitation is higher than 2500 mm per year. Discharge occurs close to the sea, at a lower altitude, where numerous springs are present. At Flic-en-Flac, a submarine discharge area has been extensively studied in the past also with the involvement of the IAEA (see e.g. Ref. [4]).

Fourteen boreholes tapping Aquifer I and II were sampled during three campaigns (rainy season, winter and summer) and analysed to provide a hydrochemical characterization (major ions, phosphates, Fe and Al) and a microbiological assessment (TC and E.Coli). Stable isotope analyses (δ^2H, $\delta^{18}O$ and $\delta^{13}C$) were performed by the IAEA.

2.   RESULTS

2.1. Hydrochemistry

Conductivity increases from 0.15 mS/cm, close to the recharge area, to about 0.4 approaching the sea. The increase in groundwater mineralization is testified by several
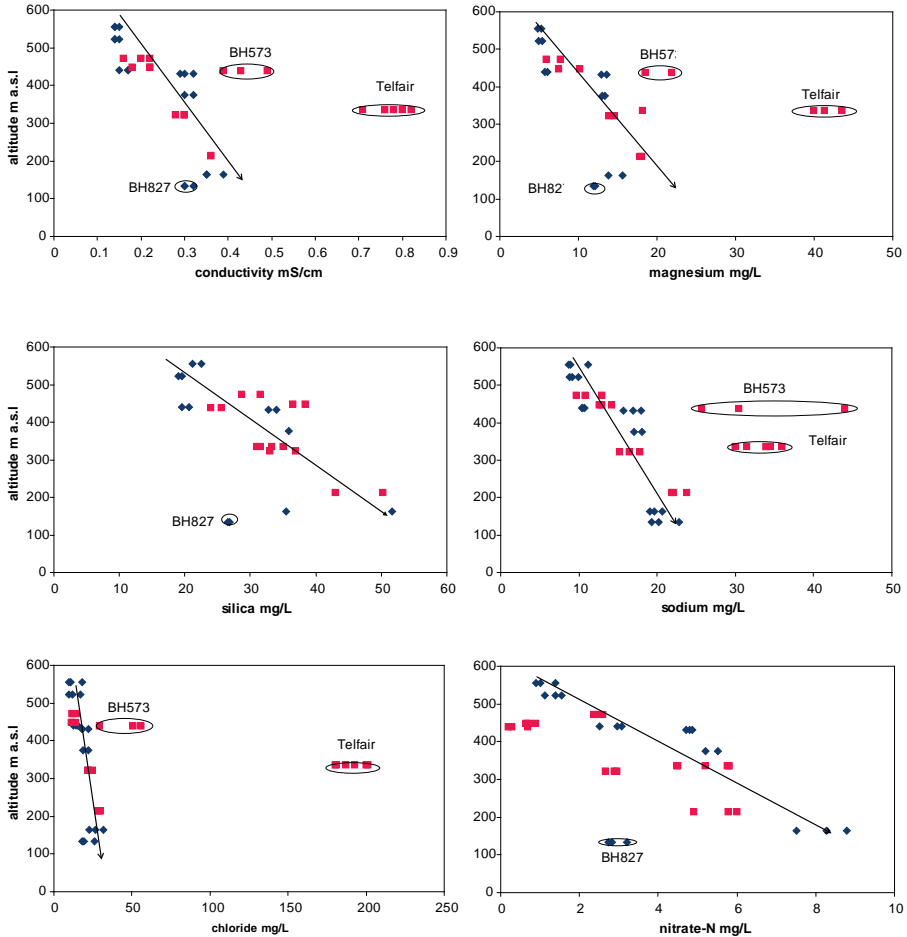
FIG. 1. Observed trends (arrows) of the main constituents in groundwater from Aquifer I (diamonds) and Aquifer II (squares).

parameters (silica, magnesium, calcium), all likely to be of natural origin, since they are derived from the basaltic rocks by water-rock interaction [1, 5]. The two aquifers are not significantly different from the hydrochemical point of view. Water level measurements in static conditions could not be performed. Nevertheless the borehole depth does not exceed 125 m, and therefore borehole elevation can be used as a proxy to indicate groundwater flow. Fig. 1 shows the observed trends of the main constituents in groundwater from Aquifer I and Aquifer II, all gradually increasing downgradient.

Exceptions to these general trends are observed for BH573 (an industrial well of a textile factory), and for boreholes located in Telfair (BH521 and BH531). Differences mainly concern the chloride and sodium content. In the case of BH573, the presence of
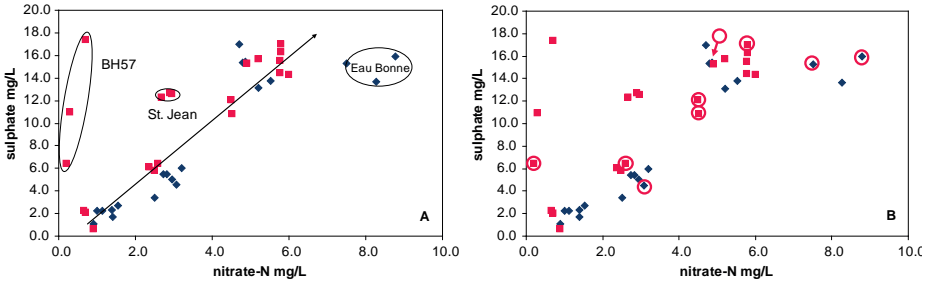
FIG. 2. A: Nitrates and sulphates in groundwater from Aquifer I (diamonds) and Aquifer II (squares). B: Same as above, where circles indicate samples where E.Coli was detected.

these substances is likely to be related to the industrial activity. In the case of the Telfair area, treated wastewater from the textile industry was used in the recent past for field irrigation. The increase in conductivity, Na and Cl of groundwater is also associated with a marked acidification, therefore excluding a marine origin for this contamination.

Unfortunately, the general trend of mineralization increases with distance from the recharge area cannot be attributed solely to natural water–rock interaction and point source pollution. Indeed, a comparable increase in nitrate content is also observed, indicating a widespread input of this constituent coming from the surface. Nitrate-N concentrations reach 8.8 mg/L in the borehole BH247A (Eau Bonne), approaching the limit set for human consumption (10 mg/L). Nitrate contents appear to be lower in Aquifer II than in Aquifer I, at comparable altitudes. This difference cannot be attributed to land use, which is not significantly different between the two aquifers, but rather to the higher protection of Aquifer II with respect to inputs from the surface. Indeed, the geological map of the island shows a widespread presence of weathered intermediate basalts in the area of Aquifer I extension ([3]). The origin of this nitrate input is presently unknown, and multiple sources may exist, as testified by different ratios of nitrates to sulphates content (Fig. 2) and the presence of *E. coli* in several samples [6].

Another exception to the general trends is observed for borehole BH827 (Palmyre), showing a lower mineralization and nitrate content. This borehole is located close to a major fracture affecting the aquifers. It is therefore possible that an upwelling of deeper, less contaminated water occurs along the fracture.

2.2. Stable isotopes

Stable isotopes of the water molecule in groundwater from Aquifer I and Aquifer II are rather homogeneous, ranging from –3 to –4‰ in $\delta^{18}O$ and from –9 to –20‰ in δ^2H. Groundwater data mostly plot above the GMWL (Fig. 3). These results are in good agreement with those presented by Ref. [2] both on rainwater and on groundwater samples. The possible position of the Local Meteoric Water line is indicated in
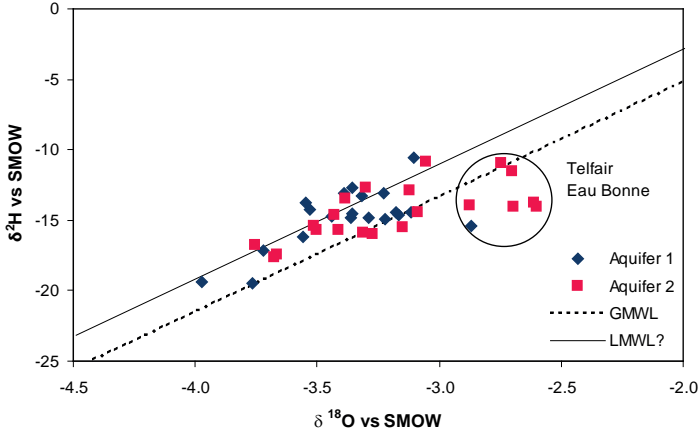
FIG. 3. Stable isotope composition of groundwater from Aquifer I and Aquifer II.
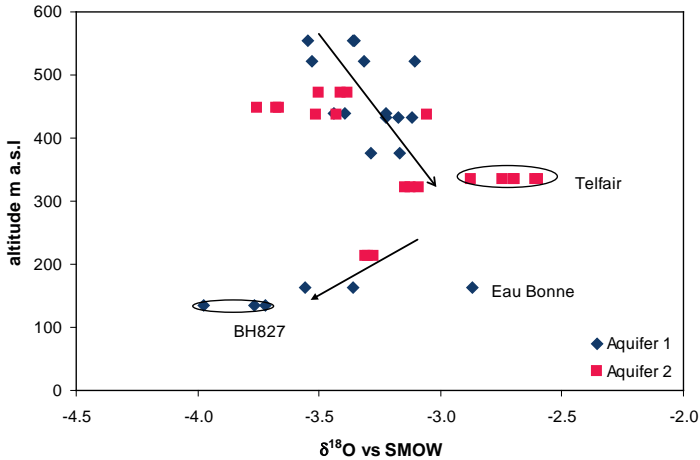
FIG. 4. δ¹⁸O variation with altitude in Aquifer I and Aquifer II.

Fig. 3. Groundwater samples showing an enrichment caused by evaporation are those collected in the Telfair area. These boreholes are affected by the use of industrial efflu-ents for field irrigation, treated prior to reuse by aeration. Also the isotope composition of the Eau Bonne well (only during summer) falls in the field of evaporated water. In this case, a contribution from a small reservoir located uphill, either by leakage or by infiltration of the reservoir water used for irrigation, can be envisaged.

The distribution of $\delta^{18}O$ ratios vs altitude (Fig. 4) shows two different slopes, indicating enrichment along the flow down to about 250 m a.s.l., and depletion at lower altitudes. This confirms the upwelling of deeper water, circulating in the inter-mediate basalts. Indeed this altitude, according to the hydrogeological cross section
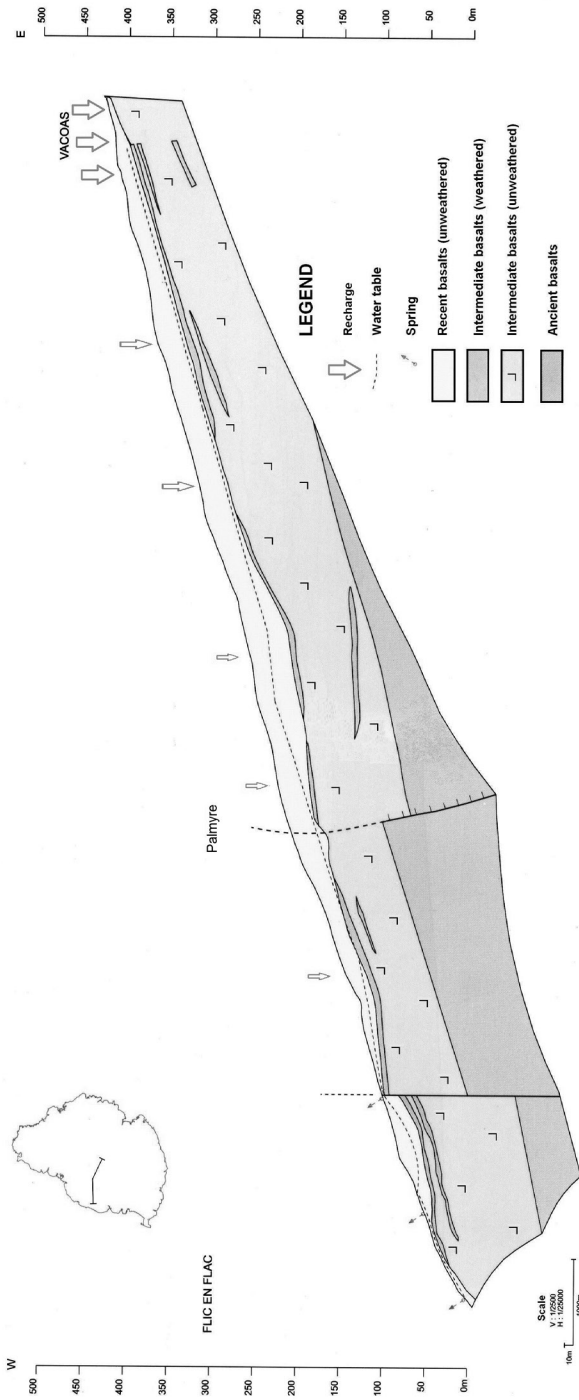
FIG. 5. General groundwater circulation model for Aquifer I and Aquifer II. Modified after Ref. [3].

(Fig. 5), is where natural discharge of the aquifers occurs, favoured by the presence of fractures and by the absence of the impermeable layer separating the recent from the intermediate basalts. This finding is in agreement with the low nitrate content displayed by borehole BH827 (Fig. 1).

$\delta^{13}C$ data range from –20 to –3‰, with large seasonal variations. The most depleted values are found close to the recharge area, while the more enriched values probably reflect the soil CO_2 signature determined by sugar cane cultivation.

3.   CONCLUSION

Aquifer I and Aquifer II are not significantly different in their hydrochemical and isotopic composition, and a possible lateral interconnection between the aquifers cannot presently be assessed using these tools. Groundwater quality is generally good, as testified by a low mineralization. Point source pollution problems have been identified in an industrial well (BH573) and in the Telfair boreholes, which are affected by an input of treated industrial wastewater used for field irrigation. A diffuse pollution problem, testified by a nitrate accumulation along the groundwater flow, is also identified. This seems to mostly affect Aquifer II, Aquifer I being more protected by the widespread presence of weathered intermediate basalts at the surface. Recharge mostly occurs in the central plateau area, but the increase in nitrate contents and the presence of *E. coli* indicate that a minor recharge occurs all over the aquifer's extension. Infiltration is very rapid, as also indicated by Ref. [2], which detected a phase shift of 1–2 months between the isotopic variation in groundwater and rainfall, and attributed the shift to the time of infiltration through the unsaturated zone. The water table can be reached by contamination even at depths of greater than 20 metres, probably because of the basalt vertical fracturing. Discharge of deeper water, circulating in the intermediate basalts, occurs at lower altitude and is marked by different stable isotope contents and lower amounts of nitrates. All data indicate that, although groundwater is generally of good quality, the aquifers are not adequately protected against a possible input of substances from the surface. Therefore the use of treated wastewater of industrial origin for irrigation should be carried out with great caution, by assessing the performance of the treatment process and the fluid quality prior to its use.

The results of the project show how the issue of groundwater monitoring is important to tackle the long term evolution of groundwater quality and to implement correct remedial actions in a timely fashion. This requires the establishment of a groundwater monitoring network covering all the aquifers of the island, especially since new industrial plants will be settled on the island in the future. In this regard, the work performed so far is an excellent starting point. Sampling campaigns should be performed on a regular basis and the investigation should be extended to the other aquifers of the island.

During the ongoing phase of the project, nitrogen isotope analyses are being performed to identify the origin of dissolved nitrates, verify the beneficial effects of the implementation of the sewage collection system and provide indication on the long term sustainability of agricultural practices. The contaminated boreholes in Telfair are also being kept under surveillance; indeed, the use of treated industrial effluents for irrigation has been discontinued and monitoring will help to assess the recovery of groundwater quality. Finally, the investigation now includes another aquifer (Aquifer V) located in the northern part of the island, an area mostly devoted to agriculture and suffering form water shortage during summer.

ACKNOWLEDGEMENTS

REFERENCES

[1]   BERTRAND, G., CELLE-JEANTON, H., HUNEAU, F., LOOCK, S., RENAC, C., Identification of different groundwater flowpaths within volcanic aquifers using natural tracers for the evaluation of the influence of lava flows morphology (Argnat basin, Chaîne des Puys, France), J. Hydrol. **391** 3–4 (2010) 223–234.

[2]   JAGANNATH, R., et al., "Use of isotope techniques in groundwater studies in Mauritius Island", Proc. Int. Symp. on Isotopes in Water Resources management, Vienna, 20–24 March 1995, IAEA, Vienna (1995) 372–374

[3]   GIORGI, L., BORCHIELLINI, S., DELUCCHI, L., La Carte géologique de l'Ile Maurice au 1:50 000, Schéma hydrogéologique, Water Resources Unit, Mauritius (1999).

[4]   BURNETT, W.C., et al., Quantifying submarine groundwater discharge in the coastal zone via multiple methods, Sci. Total Env. **367** 2–3 (2006) 498–543.

[5]   KULKARNI, H., DEOLANKAR, S.B., LALWANI, A., JOSEPH, B., PAWAR, S., Hydrogeological framework of the Deccan basalt groundwater systems, west-central India, Hydrogeol. J. **8** (2000) 368–378.

[6]   TANDIA, A.A., et al., Pollution par les nitrates des nappes phréatiques sous environnement semi-urbain non assaini: exemple de la nappe de Yeumbeul, Sénégal, J. African Earth Sci. **29** 4 (1999) 809–822

PROCESSES AFFECTING GROUNDWATER QUALITY IN THE LA DIGUE AQUIFER, SEYCHELLES

A. ALCINDOR
Public Utilities Corporation, Victoria, Seychelles

E. SACCHI
Dipartimento di Scienze della Terra e dell'Ambiente,
Università di Pavia, Italy

A.E. TAIGBENU
University of the Witwatersrand,
Johannesburg, South Africa

Abstract

This paper presents the results obtained by the Public Utilities Corporation (PUC), within the framework of an IAEA TC project, which aims to evaluate the potential of the La Digue aquifer. Several monitoring activities and hydrochemical and isotopic surveys have been conducted. Results indicate the presence of brackish water at shallow depths, and low redox potentials, attesting to the presence of H_2S and heavy metals. Groundwater quality is affected by the concomitant presence of different adverse factors, namely aquifer characteristics, hydrogeology, and anthropogenic pressure. In addition, seawater penetrates the river course during high tides and infiltrates through the recharge area of the aquifer that is close to the actual pumping station. The positioning of non return high tide gates, an easy and low cost intervention, could enhance groundwater quality. The understanding of the main processes affecting groundwater quality helped in the identification of areas favourable for new wells, located at higher elevations.

1. INTRODUCTION

La Digue is the fourth largest inhabited island of the Seychelles, lying east of Praslin and west of Felicite Island. The island is only 14 km², with most of its surface covered by tropical forests of unparalleled beauty. The steep hill slopes, reaching 333 m a.s.l., are predominantly granitic rocks. In the western part, an oval shaped plateau covers a surface area of 1.87 km², with a mean elevation of 3.5 m a.s.l. (Fig. 1). The plateau is bordered to the east by the sea and to the west by two rivers collecting surface runoff from the hills [1]. The population of about 2000 inhabitants mostly lives in the west coast villages of La Passe and La Réunion, in the plateau

319
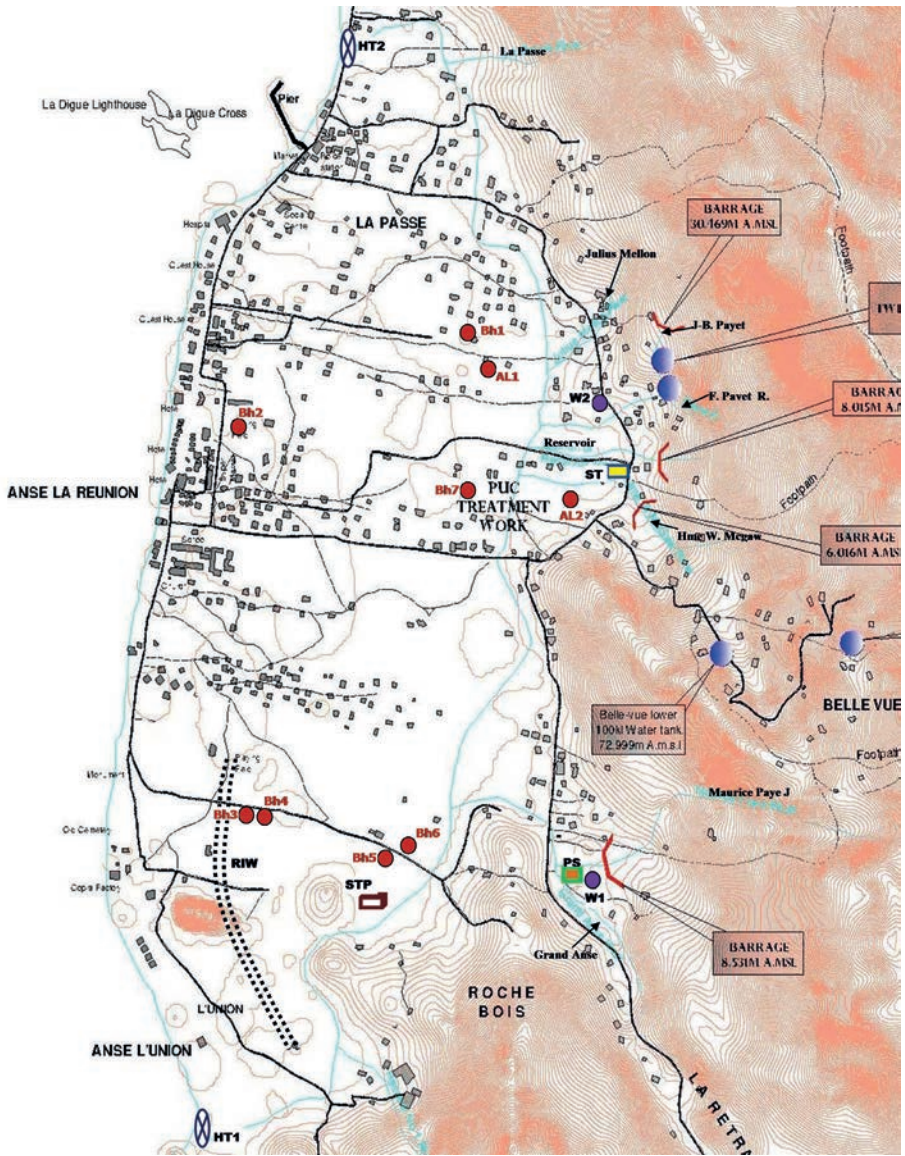
FIG. 1. Location of the investigated boreholes in the La Digue plateau area.

area. The main economic activities of the island are tourism and, to a smaller extent, agriculture.

Traditionally, the Seychelles Islands mostly rely on rain and surface water for human consumption. In the case of La Digue, rain water cannot be stored because of the lack of a suitable topographic setting for dam siting. Therefore, despite

the high precipitation (averaging 1250 mm/a but reaching up to 2400 mm/a in wet years) the island needs to integrate its water supply using groundwater (about 50% of the annual consumption) conjunctively with surface water, supply from the desalination plant and unconventional sources such as rainwater harvesting.

The increasing demand for good quality water for human consumption and for the economic development of La Digue is the main challenge faced by PUC. Following the request of the local counterpart, the IAEA initiated in 2007 a TC project aimed at evaluating the potential of the La Digue aquifer. More specifically, the project objectives are: (a) to understand the reason of the groundwater's undesirable characteristics, namely its elevated hardness and odour, and its rapid decline in quality in recent years; (b) to support the local human capacity in setting up a monitoring programme to keep groundwater quality evolution under control; (c) to assist in the identification of suitable areas for the location of a new pumping station; (d) to evaluate the possibility of increasing recharge by favouring fresh water infiltration and injection of treated water produced by the planned wastewater treatment plant.

2.   HYDROGEOLOGY

The exploited aquifer is constituted by quartz sands and gravels, covered by calcareous sands and gravels, with the total thickness of the deposits varying from 12.5 to 17.5 m. It is mainly recharged by local infiltration on the plateau area and by the rivers bordering the plateau to the east. Several boreholes were drilled on the island to prospect for water [2, 3]. Pumping tests conducted during these surveys indicate transmissivities ranging from 300 to 800 m^2/day, depending on the location, higher close to the ridge and lower on the sea side.

3.   METHODS

In the frame of this study, three expert missions have been conducted, a set of monitoring activities has been implemented and several hydrochemical and isotopic surveys have been carried out. The investigation focusses both on groundwater and surface water, comprising:

(1)   Monthly monitoring of the water level and main hydrochemical parameters (temperature, conductivity, pH, Eh and dissolved oxygen) in wells and piezometers. This activity is performed to assess the seasonal fluctuations of the freshwater–marine water interface, and estimate the amount of freshwater stored underground.
(2)   Three sampling campaigns for groundwater hydrochemical and isotopic characterization. Hydrochemical determinations are major cations and anions, and

trace elements (PO_4^{2-}, Fe and Mn). Isotopic determinations include δ^2H, and $\delta^{18}O$ to provide information on recharge, subsurface evaporation and seawater intrusion. Additionally, $\delta^{13}C$ is determined in order to clarify the role played by decomposing organic matter. Groundwater dating is performed using ^{14}C. The results of this activity provide information on the factors affecting groundwater quality, i.e. apportion between seawater intrusion, water–rock interaction processes and anthropogenic pollution.

(3) Sampling and characterization of river water, using the same hydrochemical and isotopic parameters analysed in the groundwater. This activity defines the quality of the water recharging the aquifer.

(4) Assessment of the inland penetration of seawater through the river channels and in the marsh area, by measuring the main hydrochemical parameters (temperature and conductivity) of the river water as a function of the distance from the sea and of the tides, in order to estimate the influence of seawater penetration and its possible negative effects on groundwater quality.

4.   RESULTS AND DISCUSSION

Electrical conductivities measured in boreholes are high, ranging from 0.4 to more than 30 mS/cm, and tend to increase with depth. Dominant ions are Ca or Mg and bicarbonate for low mineralized water, while Na and Cl dominate in highly mineralized water. At the end of the rainy season, groundwater isotopic composition is rather uniform ($\delta^{18}O = -3.23 \pm 0.19‰$ and $\delta^2H = -16.4 \pm 1.7‰$ vs SMOW, $n = 17$) indicating a common recharge area. At the end of the dry season, some samples appear to be affected by subsurface evaporation (Fig. 2a). ^{14}C activities range between 77 and 98 pmc ($n = 5$), indicating that groundwater in the aquifer is modern.

Hydrochemical results indicate that the La Digue aquifer indeed hosts groundwater of poor quality. The presence of brackish water is detected at shallow depths and also far inland. In addition, redox potentials are generally low, indicating the presence of H_2S and heavy metals. Groundwater quality is likely to be affected by the concomitant presence of different adverse factors, namely (1) the hydrogeological setting, (2) the poor aquifer characteristics, and (3) human pressure.

4.1.   The hydrogeological setting

In the plateau area, the water table depth is 0.80 to 1.5 m below ground surface and only 1–2 m above sea level. Contour maps indicate that, during the rainy season, the aquifer is recharged by local infiltration and by the two rivers bordering its east side [2]. Seawater intrusion in groundwater is marked by the presence of Na and Cl showing the same ratio as in seawater (Fig. 2b). At the end of the dry season, deep water extracted from the pumping station (BH7) accounts for almost
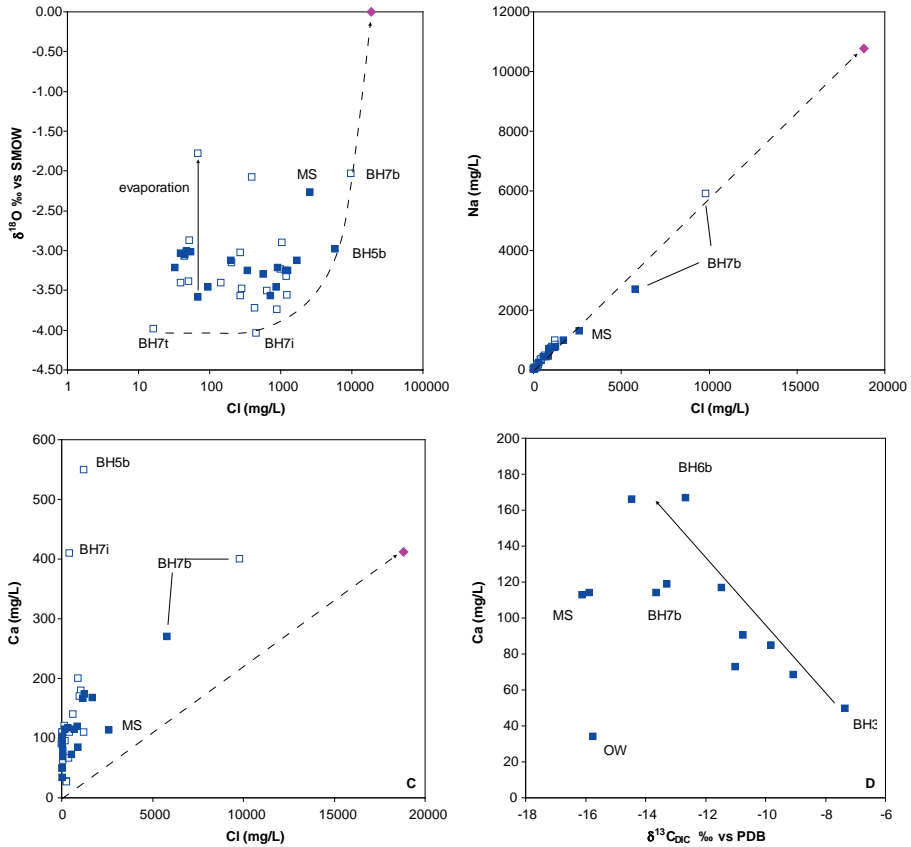
FIG. 2. Hydrochemical and isotopic characteristics of sampled water. BH — borehole, followed by a number and a letter (t — top, i — intermediate, b — bottom) referring to depth; MS — sample collected in the marsh area (Mare Soupape); OW — open well (see Fig. 1 for locations). Full symbols — end of the rainy season (April 2009); empty symbols — end of the dry season (October 2008); diamond — seawater; dashed line — seawater mixing trend.

50% contribution of seawater, based on the chloride mass balance, while at the end of the rainy season the proportion is reduced to 30%. Since the pumping station is located far inland, it raises the question of the route of seawater into this well.

It was observed that seawater penetrates along the ends of the river during high tides. In the past, the river mouths were equipped with non-return high tide gates (HT1 and HT2 in Fig. 1) which would allow excess fresh surface water to discharge into the sea but prevent seawater from penetrating inland. Unfortunately in the nineties the gates ceased functioning and were never replaced. In addition, over the years, most of the streams feeding the rivers were abstracted to satisfy drinking water needs, further reducing the freshwater recharge of the aquifer. Conductivity measurements

performed with increasing distance from the sea, at low tide, indicate that the river water is still highly saline and stratified. Brackish water floods the marsh area located east of the L'Union Reserve (MS in Fig. 2), and is not fully flushed away even during heavy rain events, thereby infiltrating in the recharge area of the aquifer that is close to the actual pumping station. Sulphates contained in seawater are likely reduced to H_2S by the presence of organic rich layers, imparting to groundwater its odour.

4.2. The aquifer characteristics

The shape of the plateau area indicates an origin by infilling of a shallow coastal lagoon (Fig. 1), and the aquifer is constituted by coarse sand, derived from the erosion of the granite relief, covered by carbonate sediments, derived from the dismantling of the barrier reef [2]. The dissolution of carbonates is marked by a strong excess of Ca (Fig. 2c) and a different Ca/Mg ratio with respect to diluted seawater. In addition, a large amount of continental or marine organic matter is contained in the aquifer matrix, imparting a reductive character to infiltrating rain water, as testified by the low Eh values measured and by the strong smell of H_2S. The presence of decomposing organic matter is also marked by low $\delta^{13}C$ values and an inverse relationship with the Ca content (Fig. 2d). Data suggest that the increase in acidity due to the oxidation of the organic matter is buffered by calcite dissolution (arrow in Fig. 2d). The process is evident in groundwater abstracted in the main pumping station (BH7), which is slightly acidic, very hard and shows, in addition, an elevated concentration of heavy metals (Fe, Mn and Al). Treatment by aeration and mixing with water from the desalination plant cannot completely overcome these water quality problems, necessitating the siting of new wells (indicated as W1 and W2 in Fig. 1).

4.3. Human pressure

The plateau area presently hosts most of the small hotels and tourist facilities of the island. Sewage water is not collected and households are only equipped with soakaway and septic tanks. The solid waste disposal site located to the east of HT1 (Fig. 1) is not properly managed, and no recycling programme (paper, plastics, glass) is in place on the island. During the rainy season, the water table level rises, often causing the tanks to overflow. Despite the strong anthropogenic pressure, nitrates are not commonly observed among the main groundwater constituents, possibly because the low redox potential favours denitrification. The isotopic composition of dissolved nitrates analysed in groundwater from BH1 clearly indicates an origin from leaking septic tanks ($\delta^{15}N = -11‰$ vs AIR, $\delta^{18}O = +3.5‰$ vs SMOW); indeed, this borehole is located close to households. On the other hand, NH_4^- is frequently found in groundwater. Its isotopic composition ($\delta^{15}N = -1.2$ and $-1.5‰$ vs AIR) is compatible with an origin from decomposing natural organic matter hosted in the aquifer matrix.

5.   CONCLUSION

This study was successful in identifying the main factors impacting on groundwater quality in the La Digue aquifer. This has ultimately led to the proposition of an easy and low cost intervention to ameliorate the quality of water extracted from the existing pumping station, such as the repair of the high tide gates located at the river mouths. Furthermore, the rivers have to be dredged so that they can hold more flood waters, and hence serve two purposes of flood mitigation and recharge of the aquifer.

Areas favourable for new wells have been identified using three criteira, namely (i) the potential for significant groundwater of reasonably good quality, (ii) the potential for recharge of wells from freshwater sources, and (iii) the ease of integration of these wells to existing pumping stations and sedimentation facilities. Two sites which meet these criteria were identified, located east of the rivers and far from the marsh area, at higher elevation with respect to the plateau area (W1 and W2 in Fig. 1). The aquifer there, although possibly of reduced thickness, is mainly constituted by sands coming from the erosion of the granitic ridge. Groundwater extracted from the open well located close to AL2 shows an acidic pH (6.65), a low conductivity (0.33 mS/cm), a reduced hardness, and a $\delta^{13}C$ isotope ratio typical for recharge areas (OW in Fig. 2d).

Finally, due to its unfavourable natural characteristics and anthropogenic pressure, the use of the plateau aquifer as a storage facility is not without major drawbacks. Rainwater harvesting is an important low cost alternative water source that should be implemented with the support of the government. In addition, in order to preserve groundwater quality, a sewage collection system should be constructed together with a sewage treatment plant, whose location has been identified by PUC. To further enhance recharge of the aquifer, treated effluent from the plant could be injected through recharge wells on the strip of land indicated as RIW in Fig. 1. The reinjection wells will assist in mitigating the saltwater intrusion wedge from the sea.

REFERENCES

[1]   ALCINDOR, H.A., TAIGBENU, A.E., ARAGUÁS-ARAGUÁS, L., JAYAWARDE-
        NA, L.P., "Assessment of groundwater resources on La Digue Island in the Republic
        of Seychelles: A study proposal", Proc. Symp. Advances in Isotope Hydrology and its
        Role in Sustainable Water Resources Management (IHS—2007), 21–25 May 2007,
        Vol 2, IAEA, Vienna (2007) 315–322.
[2]   INSTITUTE OF HYDROLOGY, Groundwater Investigations of Selected Plateaux
        in the Republic of Seychelles, Institute of Hydrology, Wallingford, UK (1978).
[3]   MCCARLEY, S., LINDBERG, J.D., Water Resource Evaluation, La Digue Water
        Supply Development, Water & Sewerage Division, Public Utilities Corporation, Vic-
        toria, Republic of Seychelles (1987).

PRELIMINARY ANALYSIS OF THE ROLE OF WETLANDS AND RIVERS IN THE GROUNDWATER DISCHARGE OF THE GUARANÍ AQUIFER SYSTEM IN NE ARGENTINA

L. VIVES
Instituto de Hidrología de Llanuras,
Universidad Nacional del Centro de la Provincia de Buenos Aires,
Azul, Argentina,
lvives@faa.unicen.edu.ar

L. RODRIGUEZ
Centro de Estudios Hidroambientales,
Facultad de Ingeniería y Ciencias Hídricas, Universidad Nacional del Litoral,
Santa Fe, Argentina

M. MANZANO
Escuela de Ingeniería de Caminos y de Minas,
Universidad Politécnica de Cartagena,
Cartagena, España

A. VALLADARES
Subsecretaria de Recursos Hidricos,
Argentina

P.K. AGGARWAL, L. ARAGUÁS ARAGUÁS
International Atomic Energy Angency,
Vienna, Austria

Abstract

The Guaraní Aquifer System (GAS) is the largest aquifer in South America. Previous regional hydrochemical and isotopic studies suggested that discharge may occur at wetlands and reaches of the Paraná and Uruguay Rivers. Preliminary findings of a project aimed at verifying the discharge hypothesis on the Southern GAS region are presented. The hydrochemical-isotopic composition of 17 samples from surface and groundwater in that area were analysed. Some waters showed chemical facies and isotopic (stable isotope and carbon-14) signatures similar to the formerly identified as GAS+pre-GAS formations. Admixtures between modern and GAS+pre-GAS waters were found at depths between less than 100 m and 200 m. A 96 m deep well located near the Iberá lagoon showed chemical and isotopic composition indicating

presence of GAS waters. The hydraulic gradient favours upward flow near the wetlands, but surface waters seem to originate from local recharge. Investigations continue, incorporating [222]Rn and new sampling sites.

1.   INTRODUCTION

The Guaraní Aquifer System (GAS) is a transboundary aquifer occupying southeastern Brazil, northwestern Uruguay, eastern Paraguay and a portion of northeastern Argentina covering some 1 200 000 km^2 and underlying the Río de La Plata drainage basin in South America (Fig. 1). It is characterized by great variations of relief and diverse climates. The GAS constitutes a strategic water reserve for the four countries. Due to the extraordinary and unplanned increase in aquifer exploitation for diverse uses in the past 30 years, knowing how the aquifer functions is crucial for establishing rational water management plans to assure sustainability.

A multidisciplinary working team recently concluded the 'Environmental Protection and Sustainable Development of the Guaraní Aquifer System' project [1], financed by the Global Environment Facility of the World Bank (GEF–WB) and the International Atomic Energy Agency (IAEA), with the support of the four countries. The project involved a great effort in data acquisition and integration with existing data. However, the resulting hydrogeologic conceptual model is still not robust enough.

Two of the fundamental aspects for the aquifer characterization that carry great uncertainty are the magnitude of the recharge and the location and magnitude of regional discharges. In the construction of the regional groundwater flow model [2], different plausible hypotheses were analysed, mainly related to structural features, aquifer properties and flow system, all typified by a great uncertainty regarding their occurrence and magnitude. Numerical results could not reduce the uncertainties about the magnitude of flows, nevertheless they suggested that a portion of the discharge in the south could occur through selected reaches of the Paraná and Uruguay rivers and their tributaries, and perhaps, through the Iberá wetland system in the southern part of the aquifer within Argentina (Fig. 1).

2.   DESCRIPTION OF THE STUDY AREA

The GAS sedimentary sequence consists of aeolian, and fluvial weakly cemented sandstones beds of Upper Jurassic–Lower Cretaceous age deposited in parts of the tectonic Paraná Basin and Chaco–Paraná Basin [3]. Sandstones range in thickness from a few metres in outcropping areas along western and eastern aquifer boundaries, to more than 600 m at the center of the basin. Upper Cretaceous basalt flows as thick as 1500 m and varying degrees of fracturing/fissuring cover 90% of sandstone
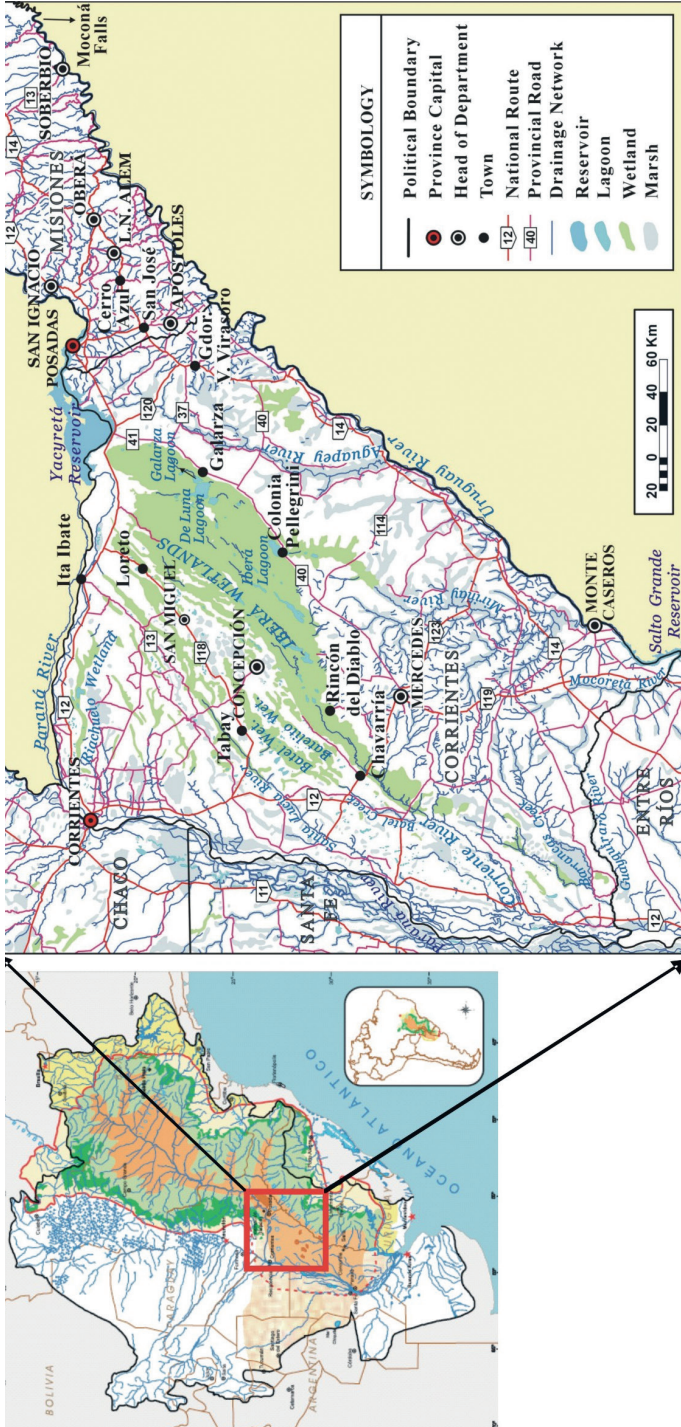
FIG. 1. Location of study area.
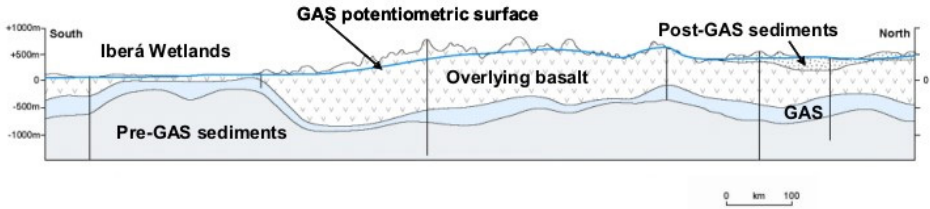
FIG. 2. Simplified GAS stratigraphic longitudinal profile (modified from Ref. [4])

deposits. The stratigraphic sequence completes with Quaternary post-GAS sediments unevenly distributed in space. Fig. 2 shows a simplified longitudinal geologic profiles drawn in the NE-SW direction [4]. In areas of Misiones and Corrientes Provinces (Argentina), the basalt thickness reduces, providing opportunities for the occurrence of discharge/recharge zones.

The GAS ranges from unconfined to semiconfined in recharge areas, becoming increasingly confined towards the centre due to the thickening of overlying basalts. Two main geological structures have exerted a control on aquifer thickness and depth, influencing regional groundwater flow. One of them is the Asunción–Rio Grande Arch shown in Fig. 2. Other tectonic structures and numerous volcanic dykes cut cross the aquifer, but despite these important discontinuities on the local scale, the GAS is considered to be a continuous groundwater body across the entire region (see Fig. 2). Regionally, groundwater flows from the northeast toward the centre of the sedimentary basin and then south. Local recharge/discharge systems have been clearly identified in outcropping areas while regional discharge areas are uncertain. In this work it is assumed that short reaches of the Paraná and Uruguay rivers and the Iberá wetland area located in the southern region of the aquifer could receive GAS water. The study area, in NE Argentina, comprises Misiones and Corrientes provinces.

The Iberá wetland system overlies a large Pliocene-to-present alluvial fan of the Paraná River. The wetland substrate is formed by fine to coarse quartz sands with silt and clay layers corresponding to alluvial sand bars, eolian dunes and fluvial beds. Abandoned beds of anastomosed streams are occupied by large, very shallow and mostly NE-SW elongated lagoons. The system covers 13 200 km^2. To the north and northeast of the Iberá system the sandy formations overlie basalts (Serra Geral formation) with sandstone intertraps (Solari formation), which deepens to the SW; to the west and south they underlie silts and fine sands of the Fray Bentos and Paraná formations. The prevalent hydrological model indicates that the Iberá wetland receives mostly pluvial water, with some shallow groundwater discharge. The whole system drains to the SW, discharging into the Corriente River which, in turn, flows into the Paraná River. The homonymous Iberá lagoon is the most important, covering 52.1 km^2. Galarza lagoon, with its 14.6 km^2, is also a main water body. Water depth at main lagoons ranges from 1.8 to 3 m [5].
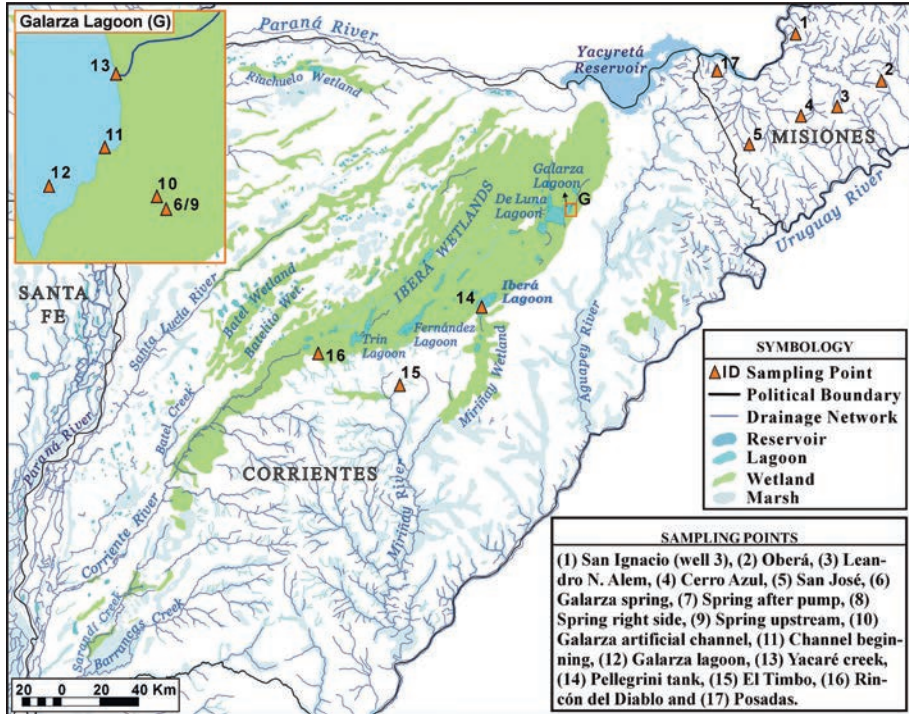
FIG. 3. Location of sampling points.

3. FIELD DATA

In August–September 2009 a field campaign was performed. Seventeen samples were collected: 6 groundwater samples in Misiones, 3 groundwater samples in Corrientes and 7 surface water samples (four from a spring and its close surroundings, one at the mouth of a wetland draining creek into the Galarza lagoon, one at the south part of Galarza lagoon and one at a channel draining into the Galarza lagoon. Data collection points are indicated in Fig. 3. Chemical analysis was performed for all samples as well as the determination of $\delta^{18}O$, δ^2H, ^{14}C, $\delta^{13}C$ and ^3H.

4. RESULTS

The objective of the study is to identify the presence of GAS water in the collected samples, then the main chemical characteristics of the GAS waters are summarized [6].

In the GAS, three basic types of water were identified: (1) hydrochemical facies [Ca/Mg]–HCO_3, always found at outcropping areas; (2) hydrochemical facies

Na–HCO$_3$, found in confined areas of the GAS but near outcropping regions; and (3) hydrochemical facies Na–[SO$_4$/Cl]HCO$_3$, found in confined areas but usually far from recharge areas, or in areas with significant fracturing. Within the facies Na-HCO$_3$ two subgroups were distinguished: (a) with Cl>SO$_4$, (b) with Cl<SO$_4$. Within the facies Na-[SO$_4$/Cl]HCO$_3$ three subgroups were distinguished: (a) with Cl>SO$_4$, (b) with Cl<SO$_4$ and, (c) with a clear dominance of either Cl or SO$_4$.

Therefore, the main conclusions extracted from the GAS Project were:

(1) Waters from the Na–HCO$_3$ type are associated with GAS sandstone formations. The most typical processes within the GAS would be ionic exchange of Ca and Mg in solution for absorbed Na and carbonate dissolution.

(2) Waters from the Na-HCO$_3$ type but with SO$_4$>Cl are associated with GAS but they already have some mixture (difficult to quantify) with more saline formations underlying the GAS, at least in the study area.

(3) Waters from the Na-Cl type are associated with GAS waters that have a higher degree of mixture with more saline formations underlying the GAS.

(4) Little information exists, or at least has been compiled about the chemical composition of pre-GAS formations.

The first step was to draw Piper diagrams (Fig. 4) and Schöeller diagrams. Chemical types described in Fig. 4 were identified in relation to GAS waters.
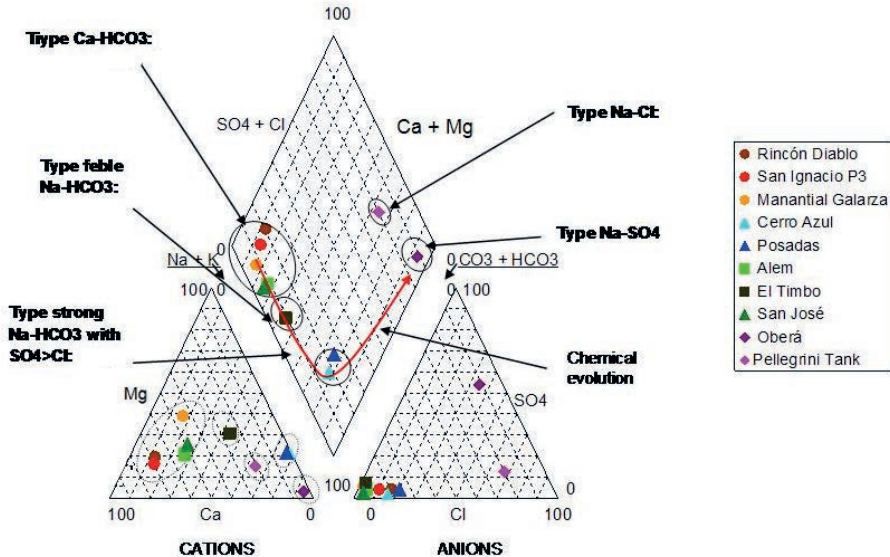
FIG. 4. Piper diagram of Iberá-Misiones water samples collected in Aug–Sep 2009.
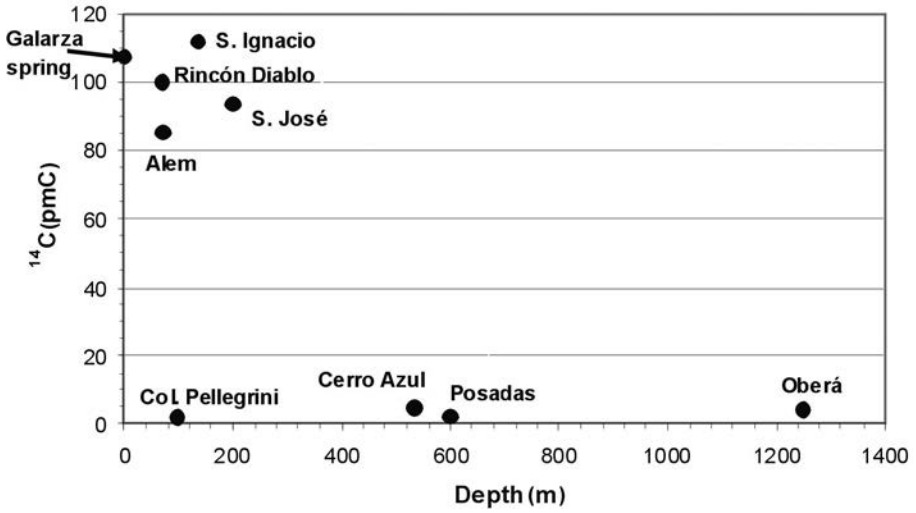
FIG. 5. ^{14}C versus well depth in groundwater samples collected in NE Argentina.
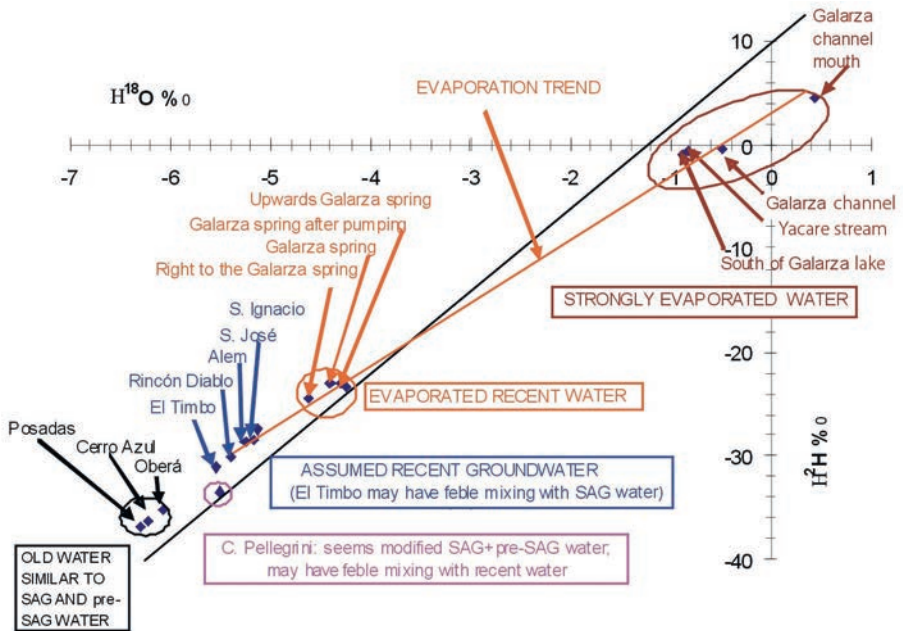
FIG. 6. Relationship between $\delta^{18}O$ and δ^2H groundwater samples collected during the Aug–Sep 2009 field campaign

Of all samples, only Rincón del Diablo, the southwesternmost sample to the south of the wetland, seems to represent present recharge water (Ca–HCO$_3$ type), without chemical or isotopic composition modifications that could be attributed to mixing with GAS water. Nonetheless, it is more saline than typically expected. Isotopically, it doesn't seem to be enriched by evaporation, therefore its saline nature may reflect a different cause/origin.

According to the isotopic signature, surface waters from Manantial Galarza (Galarza spring), Arroyo Yacaré and its surroundings are probably present, local recharge waters. The rest of the samples seem to be either mixtures between present waters and GAS water (some even with a pre-GAS component), or mixtures of GAS and pre-GAS waters.

Wells that show a mixture of recent water and GAS water are: San Ignacio, Alem and San José in Misiones Province; El Timbo and Pellegrini Tanque at Iberá, Corrientes Province. Except for the Pellegrini Tanque well, the recent origin of these groundwaters is confirmed by the high carbon–14 activities, sometimes exceeding 100%, indicating they are present day waters (see Fig. 5). However, the ionic ratio Na/Cl >1 in all samples, indicating the contribution of waters whose cationic contents are modified through ionic exchange. This is more clearly seen as an indicator of GAS waters, but is most probably the result of locally recharged waters flowing through silty and clayed formations, very common in the Iberá shallow substrate. Alem in Misiones, and El Timbo, in Iberá, also show SO$_4$/Cl >1, which is more clearly seen as an indicator of contribution from pre-GAS waters. An analysis of ^{14}C for
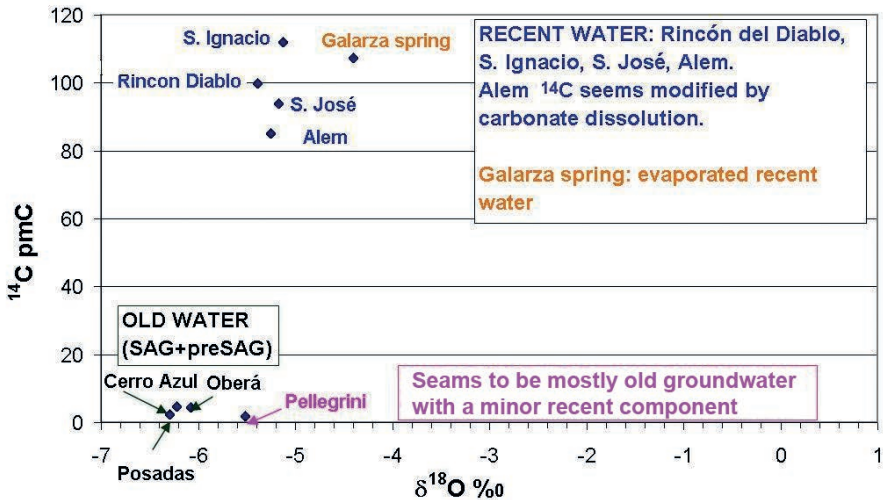
FIG. 7. Relationship between $\delta^{18}O$ and ^{14}C groundwater samples collected during the Aug–Sep 2009 field campaign.

El Timbo is not available, nonetheless it is expected to have a signature coherent with these waters.

Fig. 5 also includes deep GAS wells in Misiones (Cerro Azul, Posadas and Oberá). Surprisingly, Col. Pellegrini (or Pellegrini tank), a 90 m well near the Iberá lagoon, has a similar ^{14}C and δ^2H isotopic composition as these wells located about 200 km away. According to the low ^{14}C content, the absence of tritium and the low values of δ^{18}O and δ^2H, it is very old water. Hydrochemistry indicates moderately saline water of the Na-Cl type. However, the ionic ratios Na/Cl and SO$_4$/Cl, pH, temperature and a minor presence of tritium, among other indicators, suggest that the water has a modern water component. Besides, δ^{18}O and δ^2H values are somehow heavier than expected, if these waters were as old as the others sampled (see explanation below and Fig. 5 and 6). The hypothesis proposed here is that these are GAS waters and pre-GAS waters evaporated near the water surface, with the presence of a small proportion of recent water.

These water mixtures between GAS water and recent water are found at variable depths, between <100 m and 200 m, in both Misiones Province and in Iberá, Corrientes Province (Fig. 7).

Wells in Misiones (Alem, San José and San Ignacio) are located at the water divide between the Paraná and Uruguay rivers (see Fig. 3), and these two rivers may receive discharge from deep, old waters. The depth of El Timbo well in Iberá is unknown, but this well captures waters chemically and isotopically almost identical to those from Alem and San José wells, located 200 km to the NE. The well at Col. Pellegrini is about 96 m deep. At the time of sampling, the piezometric level at this well was above the surface water level surveyed at Iberá lagoon at a point 200 m away from the well. This vertical hydraulic gradient would favor upward flows in the area, from GAS-like waters towards the Iberá wetland system. In light of this promising result and the objectives of the project, field data collection and analysis must be intensified to verify this main conclusion.

5.   CONCLUSIONS

Results of undergoing hydrochemical and isotopic investigations of groundwater and surface water in Misiones and Corrientes provinces in NE Argentina, and their relationship to the Guaraní Aquifer System waters allow to conclude that some waters sampled during the 2009 campaign in SW Misiones Province and near the Iberá wetland in Corrientes Province have chemical facies that can be assimilated to GAS waters. This, plus the waters' isotopic composition, allows us to propose the hypothesis that many samples show the influence, i.e. evidence of mixture, of GAS waters as well as pre-GAS waters. The findings at Col. Pellegrini well in terms of its water composition and vertical hydraulic gradients in relation to the nearby Iberá Lagoon

would favour upward flows in the area, from GAS-like waters towards the Iberá wetland system.

In light of these promising results and in relation to the objectives of the project, field data collection and analysis must be intensified to verify this main conclusion.

ACKNOWLEDGEMENTS

REFERENCES

[1]   GASP, Guaraní Aquifer System Project, Strategic Action Plan (2009) 415.

[2]   VIVES, L.S., RODRÍGUEZ, L.B., GÓMEZ, A.A., COTA, S.D.S., "Modelación Numérica Regional del Sistema Acuífero Guaraní (Regional numerical modelling of the Guaraní Aquifer System)", Project for Environmental Protection and Sustainable Development of the Guarani Aquifer System, Global Environment Facility (GEF), Technical Report, Montevideo, Uruguay (2008) 144.

[3]   ARAÚJO, L.M., FRANÇA, A.B., POTTER, P.E., Hydrogeology of the Mercosul Aquifer System in the Paraná and Chaco-Paraná Basins, South America, and comparison with the Navajo-Nugget Aquifer System, USA, Hydrogeol. J. **7** (1999) 317–336.

[4]   FOSTER, S., HIRATA, R., VIDAL, A., SCHMIDT, G., GARDUÑO, H., The Guarani Aquifer Initiative — Towards Realistic Groundwater Management in a Transboundary Context, GW-Mate Sustainable Groundwater Management: Lessons for Practice, Case Profile Collection 9, World Bank, Washington DC (2009).

[5]   NEIFF, J.J., "Tipificación de los ambientes acuáticos y de interfase del macrosistema Iberá", Estudio del Macrosistema Ibera (Bonetto, A.A., Ed.), Tomo V(1), Ecología, ICA-CECOAL, Corrientes (1981) 14–43.

[6]   MANZANO, M., GUIMARAENS, M., "Hidroquímica Regional del SAG; Estudio del origen de la composición química de las aguas subterráneas del Sistema Acuífero Guaraní (Regional Hydrochemistry SAG; Study of the origin of the chemical composition of groundwater Guaraní Aquifer System)", Project for Environmental Protection and Sustainable Development of the Guarani Aquifer System, Global Environment Facility (GEF), Technical Report, Montevideo, Uruguay (2008) 223.

EVALUATION OF THE MARINE INTRUSION IN HAVANA PROVINCE GROUNDWATER USING HYDROCHEMICAL AND ISOTOPIC TOOLS

A.M. ALVAREZ[a], D.L. BOMBUSE[a], J.R. ESTEVEZ ALVAREZ[a],
C.A. LUACES[b], J. DE LA CRUZ[b], I.P. GONZÁLEZ[a], M. RODRIGUEZ[a],
A.J. QUEJIDO[c], I. RUCANDIO[c], M. SÁNCHEZ[c], P. GONZÁLEZ[d]

[a] Centro de Aplicaciones Tecnológicas y Desarrollo Nuclear (CEADEN),
   Havana, Cuba

[b] Instituto Nacional de Recursos Hidráulicos (INRH),
   Havana, Cuba

[c] Centro de Investigaciones Energéticas, Medioambientales y Tecnológicas,
   (CIEMAT),
   Madrid, Spain

[d] Centro Nacional de Termalismo,
   Havana, Cuba

Abstract

In the present paper the spatial distribution and temporal evolution of the saline intrusion in the most important aquifer of Havana province is presented. Results were obtained through the application of hydrochemical and isotopic tools. Studies were carried out within the framework of the IAEA Regional Project RLA/8/041. The survey was carried out in 2008 during the dry and rainy seasons. Sampling points were selected according to a monitoring network located along the north–south line following the main groundwater flow direction. Stable isotopes (^{2}H and ^{18}O) were used to identify and characterize the groundwater origin and mixing processes. Changes in the chemical composition of groundwater were shown to be mainly controlled by the groundwater and seawater mixing process, followed by cation exchange reactions and a Ca–Mg precipitation process due to the strong influence of the costal wetland. A gradual decreasing of the spatial and temporal saline intrusion was observed.

1. INTRODUCTION

With a longitude approximately of 120 km and a width of 25 km the aquifer located in the south coast of Havana Province provides about 85% of the water supply for drinking, domestic, industrial and agricultural uses. The climate is characterized

FIG. 1. The hydro-geochemical conceptual model of the aquifer.

by the occurrence of two well differentiated seasons: a dry period in winter time and a wet period in summer. The mean monthly temperature ranges from 24.7 to 26.0 °C. The mean annual precipitation is reported to be between 1300 mm and 1700 mm of which almost 77% occurs in the period of May to October [1].

Due to the presence of the Caribbean Sea, the karstic nature of the aquifer and its overexploitation, marine intrusion phenomena have been documented [2]. The highly developed karstic stage of this region, the existence of a permeable red ferralitic soil and poor superficial drainage are responsible factors leading to the direct infiltration of rainfall in the mountain area, causing this area to be the main recharge mechanism. The above-mentioned indicates that the recharge is conditioned by the rainfall pattern.

In a previous paper, a hydraulic transmissibility varying between 5000 and 50 000 m²/d and a permeability coefficient of about 1.45×10^{-2} m/s was reported by González T. O. and R Feitó [2]. These properties allow a high use of this aquifer (pumping rates are about 100–300 L/s).

A fundamental aspect that characterizes and controls the hydro-geological system of this aquifer is the existence of an adjacent wetland throughout the whole coast, with a width of 2 to 5 km. The hydro-geochemical conceptual model of the aquifer is presented in Fig. 1.

The high volumes of water extraction (3.2 m³/s for domestic and industrial use and about 3.5 m³/s for agricultural uses) during the last 80 years, together with the building of a drainage channel, as well as the decrease of the rainfall, led to a decrease of water resources in this sector of the aquifer, and consequently, to seawater intrusion. At the end of the 1980s, the greatest values of extraction were reached in this territory, increasing the sea intrusion in the aquifer even more. As part of the corrective action plan the South Dike of Havana [3] was built in the area.

This paper reports the results obtained during the spatial and temporal evolution of the marine intrusion phenomena in the most important aquifer of Havana province using hydrochemical and isotopic tools.

2.   METHODS

2.1.   Field survey

The selected area of study (Artemisa–Quivicán) belongs to the South Aquifer of Havana and is located between the following coordinates: N 320–350 and W320–380, covering about 1200 km^2, with absolute altitude ranging between 0 and 324 m a.s.l. and an average topographic elevation of 38m.

However, the survey was only based on the area most affected by the sea intrusion. The sampling points are located along a north–south line, following the main direction of groundwater flow, and an east–west line, close to the Caribbean Sea coastline, enclosing the area of the sea intrusion phenomena reported in previous studies. The selected wells have enough depth and have been completely grooved. Table 1 shows the geographical coordinates, sampling depth, topographic altitude and the distance of each well to the sea. Fig. 1 shows the survey location at the end of the dry (April–May) and the wet season (November–December) of 2008.

Sampling depth was selected according to the patterns of in situ electric conductivity values in each well. The rainfall samples were collected on a monthly base in the Quivican municipality (Fig. 1). A 250 mL sample collector was used during the dry season campaign while a submergible pump was employed for the campaign during the rainy season. In the latter case, more representative results were obtained and therefore most of the reported results of this study refer to this campaign.

2.2.   Hydrochemical analysis

The measurement of physical and chemical parameters was made according to the following approach:

- In situ: Electrical conductivity logging up to a depth of about 60 m, as well as temperature, salinity and total dissolved solids;
- In the field: Alkalinity, electrical conductivity, sample temperature, air temperature, pH, and dissolved oxygen;
- Laboratory: Alkalinity, electrical conductivity, sample temperature, pH, water hardness, major components (Ca^{2+}, Mg^{2+}, Na^+, K^+, Cl^-, SO_4^{2-}), NO_3^-, and some heavy metals (Zn, Cd and Pb).

TABLE 1. SAMPLING POINTS DATA

Sample	Wells	Depth. (m)	Altitude (m)	Distance to the sea (km)
M1, M2	Camacho	20, 40	6	5.50
M3	Santa Ana	10	4.90	4.80
M4, M5	Cala 10	10, 20	1.97	4.14
M6, M7, M8	Alvaro Barba	8, 15, 26	2	2.95
M9, M10, M11	Sotolongo Díaz	15, 30, 40	10.86	9.00
M12, M13, M14	Buffon	15, 30, 40	7.22	12.00
M15, M16, M17	El Punto	30, 40, 53	18.27	13.40
M18, M19, M20	Fajardo	40, 52, 58	32.18	15.00
M21, M22, M23	Amaros	28, 45, 55	23.53	14.60
M24, M25	Rancherita	30, 45	20.12	14.50
M26, M27, M28	El Junco	8, 20, 30	5.56	6.11
M29	Güiro Marrero	30	27.57	12.20
M30, M31, M32	La Juanilla	10, 25, 40	4.88	6.70
M33	Dam La Ruda	0.50	—	—
M34	Ariguanabo River	0.25	—	—
M35	Reservoir Guira	0.50	—	—
M36	WTS *	0.25	—	—
M37	Reservoir Pedroso	0.50	—	—
M38	Caribbean Sea	0.50		
M39	Raingauge	—	—	17.05

*WTS Fresh water transfer system Havana–Matanzas.

The quality of the analytical results was evaluated according to the uncertainty of the ionic balance:

$$E\% = \frac{\left(\sum Cat - \sum An\right) \times 100}{\left(\sum Cat + \sum An\right)} \tag{1}$$

2.2. Instruments and methodologies

Samples were collected using a submergible pump model Comet Combi 24V–4A. A level meter model KLL 100 m, and GPS model Unit Trex Summit were

used as well. In situ EC was measured with a portable Tetracom 197i conductim-eter coupled with a multiparameter electrode model TA 197 LF–100. pH was meas-ured with a CONSORT P902 pH-meter. The determination of chemical constituents and trace metals was performed in the analytical chemistry laboratory of CEADEN whereas the second campaign samples were analysed in CIEMAT, Spain.

The rainwater sample represented a weighted annual sample and was collected in the pre-mountainous region where most of the aquifer recharge takes place [4, 5].

2.3. Isotopes in precipitation

The stable isotopes of oxygen and hydrogen are generally considered to be con-servatively transported in shallow aquifers. Because rainwater quickly infiltrates into the ground due to its hydrogeological characteristics, no significant evaporation of rainwater occurs before or after infiltration. Therefore, groundwater oxygen and hy-drogen isotope data can provide important information on the salinization processes in the coastal aquifers [6].

As there is not enough data on the isotopic composition of the rainfall in Cuba, a Global Meteoric Water Line was used ($\delta^2H = 8\,\delta^{18}O + 10‰$) [7]. The stable iso-topic analysis was made in a stable isotope mass spectrometry laboratory at UNAM, Mexico. A Finnigan Delta Plus XL spectrometer and a Thermo Finnigan MAT 253 spectrometer were used with relative uncertainties of 2‰ and 0.2‰ for deuterium and oxygen-18, respectively

Data evaluation and interpretation was performed using Surfer (Version 8.0), Mapinfo (Version 8.0 CSP), Microsoft®Excel, 2007 and Modelagua (Version 1.0, 2001) [8] software packages.
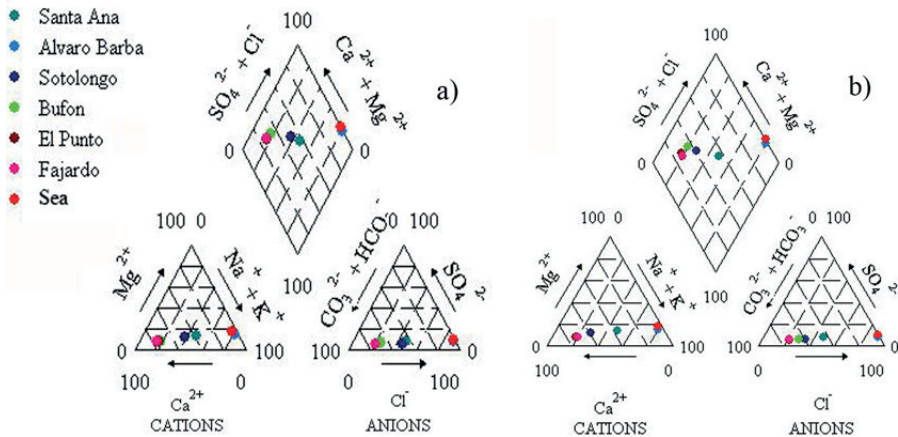
FIG 2. Piper diagram of groundwater sampled along a North-South line at depth of 10 m (a) and 20 m (b).
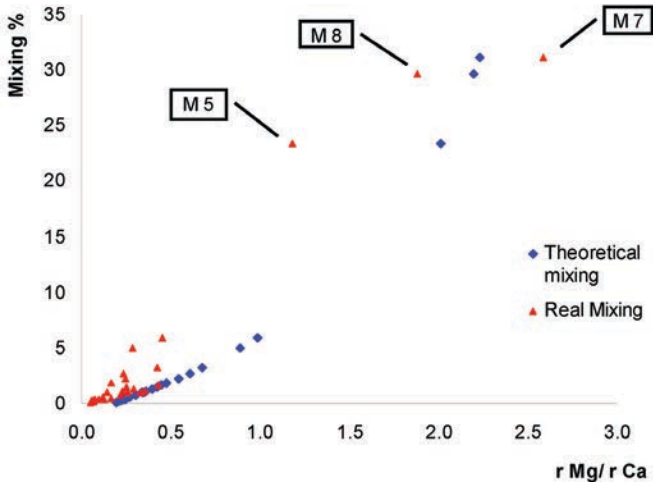
FIG. 3. Relationship between mixing fraction (%) and the rMg/rCa ratio.

TABLE 2. D IONIC VALUES FOR GROUNDWATER SAMPLES

Sample	Dist. Sea (km)	Depth (m)	Mixing fraction (%)	D Na	D Ca	D Mg	D SO$_4$	pH
M6	3.0	8.0	3.2	−2.3	1.4	−0.5	−0.7	7.35
M7	3.0	15.0	31.1	−15.4	−3.1	−8.5	−2.6	8.78
M8	3.0	26.0	29.6	−17.5	−1.5	−8.8	−2.9	9.15
M4	4.1	10.0	5.0	−2.7	2.4	−2.6	−0.6	7.5
M5	4.1	18.0	23.4	−16.5	−1.0	−11.5	−8.7	7.94
M2	5.5	40.0	5.9	−3.5	2.5	−1.6	−0.4	7.55

3. RESULTS AND DISCUSSION

In general, the analytical quality of the results (physical parameters and chemical composition) was suitable, having errors of less than 10%, according to Eq. 1.

The Piper diagram was only employed to carry out the interpretation of the salinity origin of the 10 and 20 m depth wells located on the north–south line flow. Fig. 2 shows that the salinity of the water samples is mainly due to a simple mixture of fresh and seawater [9].

Fig. 3 shows the values of the theoretical and real ionic ratio of Mg/Ca versus the seawater mixing percentage [10, 11], thus the majority of the samples represent a simple mixing process of seawater. However, for a mixing fraction higher
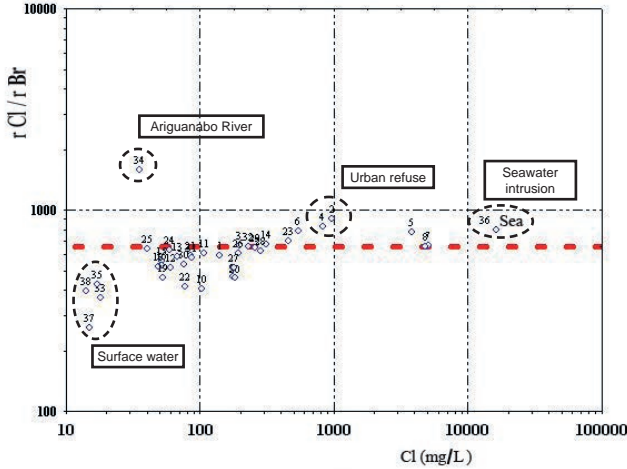
FIG. 4. rCl/Br vs Cl content.

than 3% a hardening process is taking place. This ionic exchange is mainly seen in samples M5 and M8, located near the sea, and also in M2, M4 and M6 collected at the greatest depths.

The result from the sample M7 sample might indicate an increase of Mg content due to dolomite dissolution. However, for a proper interpretation of this process, the use of D ionic is required (Table 2).

For samples M2, M4 and M6 the hardening phenomenon corresponds with the following ionic exchange process: $Na_2X + Ca^{2+} \Leftrightarrow CaX + 2Na^+$ [12].

The lower values of D SO_4 seen in samples M5, M7 and M8 reveal a strong interaction with the wetland. In this case, the sulphate reduction due to bacterial activity increases the bicarbonate content. This process is followed by calcium and magnesium precipitation $CaMg(CO_3)_2$ due to the high pH values. This approach explains the high negative values obtained for D Ca and D Mg. These values are in agreement with those reported by other authors in a previous study [13].

The hydrochemistry of some minor elements, such as Br and Sr, is a good marker of the mixing between fresh water and seawater. The Cl/Br ratios have been used to distinguish salinity of marine and non-marine origin. Because Br and Cl are relatively conservative in hydrological systems, the Cl/Br ratio should be constant when salinization of fresh water occurs by simple mixing of seawater if there is no anthropogenic contamination. The red discontinuous line in Fig. 4 represents the value of this theoretical relationship for seawater.

The evaluation of the relationship rCl/Br vs Cl indicates that the salinization of these groundwaters mainly results from mixing with seawater [14].

In the previous figure it is also observed that the sea intrusion phenomena are more significant on the wells nearest to the coast (M5, M7 and M8) and that
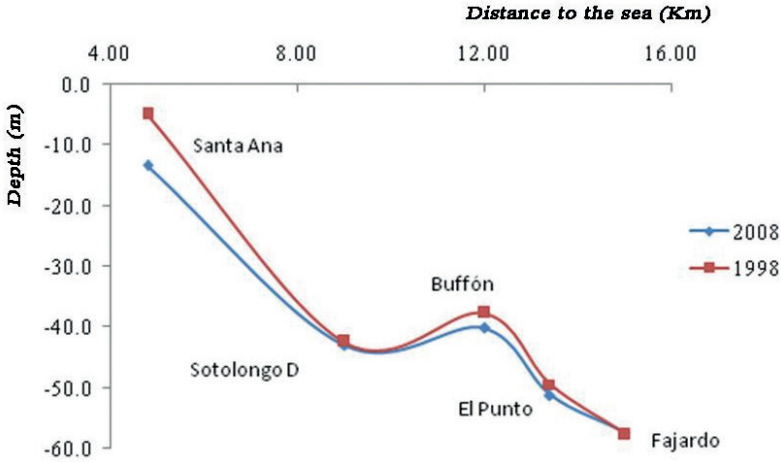
FIG.5. Depth and distance to the coast of the isoline of 1 g/L TDS, from 1998 to 2008.

presumably the origin of the salinity of the samples M2 and M4 are related to urban solid refuse.

In order to evaluate the sea intrusion behaviour during the last ten years, the depth at which TDS values are higher than 1 g/L were plotted for the years 1998 and 2008. Fig. 5 shows an improvement of groundwater quality. The deviation observed between Sotolongo Díaz and El Punto denotes the presence of an active water extraction area, producing a vertical flux of the seawater intrusion.

3.1. Environmental isotopes

The results of δ^2H and $\delta^{18}O$ analyses during the sampling campaigns of 2008 are presented in Figs 6–8. Fig 6 shows that surface waters describe an evaporation pattern, with enriched values of δ^2H and $\delta^{18}O$. However, in the second campaign, during the wet season, this process is less significant.

In Figs 6 and 7 an overlap of the evaporation line and the mixing line is observed. Thus, a proper interpretation of the recharging process in the aquifer is troublesome using this type of diagram (δ^2H vs $\delta^{18}O$).

In general, the environmental isotope analysis demonstrates that the groundwater respond to a pattern of meteoric origin modified by the mixture phenomenon with seawater.

These results suggest that the change in the isotopic composition of these waters is also influenced by recharge water from another origin, even though this well is the nearest to the coast. On the other hand, groundwater discharge takes place in this area, where the wetland has a considerable effect [15].
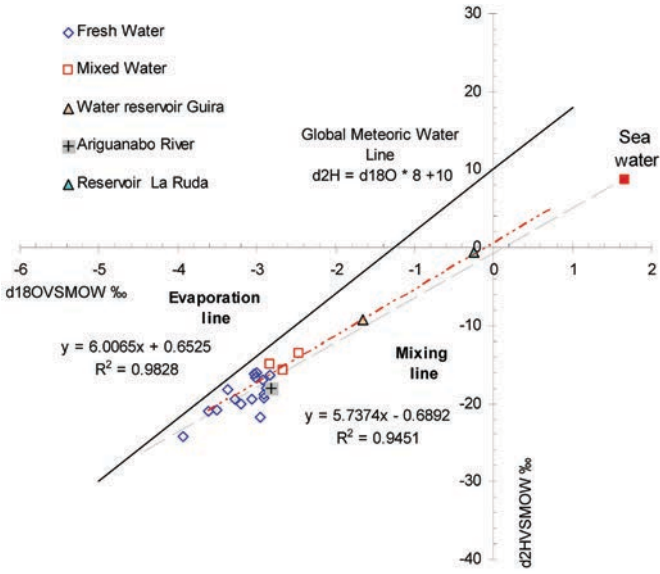
FIG. 6. δ²H vs δ¹⁸O for samples collected in May 2008.
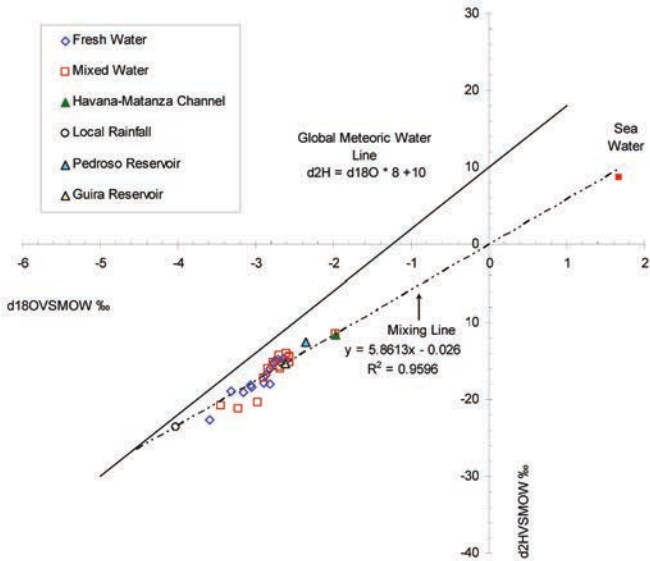
FIG. 7. δ²H vs δ¹⁸O, sampling campaign December 2008.
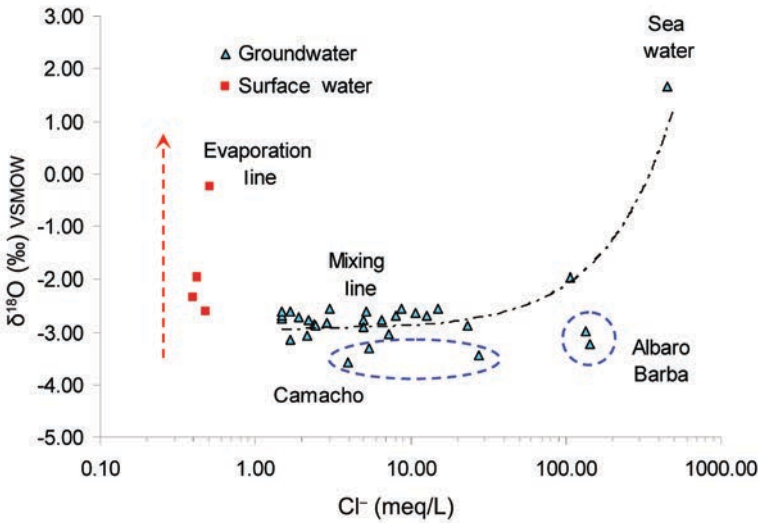
FIG. 8. Relationship between δ¹⁸O and Cl⁻(meq/L) values (campaign December 2008).

The groundwater from Camacho exhibits a similar isotopic fingerprint to that observed in the samples collected from Alvaro Barba at 26m, with values slightly below the mixing line (Fig. 8). Camacho well is located near to the sea intrusion boundary in the east part, at approximately 11 km from the studied north–south profile (see Fig. 1). This result suggests that the waters in this area could have a different origin.

The relationship between the chloride content and δ¹⁸O values corroborates that the origin of groundwater is due to a fresh water–seawater mixing process. The main recharge of the aquifer is subject to rainfall in the region. Moreover, these results agree with previous ones obtained for the Alvaro Barba site.

4.   CONCLUSIONS

The combination of hydrochemical and isotopic tools allowed the assessment of the marine intrusion evolution in the coastal aquifer of the Havana province. The isotopic composition of groundwater revealed the freshwater–seawater mixing process that takes place in the studied area. The measured ²H and ¹⁸O data for the aquifer south-east zone, suggests a contribution of water from different recharge sources. A spatial and temporal improvement of the water quality has been observed over the last 20 years in the South Aquifer of Havana.

REFERENCES

[1]   INSTITUTO NACIONAL DE RECURSOS HÍDRICOS, Segunda comunicación nacional a la convención marco de naciones unidas sobre cambio climático, Línea base de recursos hídricos para el ejercicio de integración sur la habana, Dirección de Cuencas hidrográficas, Delegación provincial de La Habana, Archivo Instituto Nacional de Recursos Hidráulicos (2010).

[2]   FAGUNDO, J.R., et al., Procesos geoquímicos naturales e inducidos por el hombre en acuíferos kársticos costeros, Caso de estudio: Sector hidrogeológico Güira-Quivicán (cuenca sur de la Habana), R. Latino-Americana de Hidrogeología **2** (2002) 71–79.

[3]   JIMÉNEZ, S., Análisis del efecto del Dique Sur Habana en el Acuífero Costera Sur y su entorno, Archivo, Instituto Nacional de Recursos Hidráulicos, Cuba (1999).

[4]   GAT, J.R., Oxygen and hydrogen isotopes in the hydrologic cycle, Annu. Rev. Earth Planet. Sci. **24** (1996) 225–262.

[5]   CLARK, I.D., FRITZ, P., Environmental Isotopes in Hydrogeology, Lewis, Boca Raton, Florida (1997) 328.

[6]   PANARELLO, H.O., DAPEÑA, C., AUGE, M.P., "Mecanismos de salinización del agua subterránea de la zona de La Plata, Buenos Aires, Argentina: su interpretación por medio de los isótopos ambientales", Estudios de Hidrología Isotópica en América Latina 1994, IAEA-TECDOC-835, IAEA, Vienna (1995) 13–27.

[7]   CRAIG, H., Isotopic variation in meteoric waters, Science **133** (1961) 1702–1703.

[8]   FAGUNDO-SIERRA, J., FAGUNDO, J.R., GONZÁLEZ, P., SUÁREZ, M., MELEÁN, C., CENTERVISA, MODELAGUA, Software para determinar el origen de la composición química de las aguas minerales, Registro 08280–08280 (CENDA).

[9]   CHADHA, D.K., A proposed new diagram for geochemical classification of natural waters and interpretation of chemical data, Hydrogeol. J. **7** (1999) 431–439.

[10]   MORELL, I., MEDINA, J., PULIDO BOSH, A., FERNANDEZ-RUBIO, R., Caracterización de la intrusión marina en el acuífero costero de Oropesa-Torreblanca (Prov. de Castellón) en base al estudio de relaciones iónicas, Hidrogeología **1** (1986) 15–31.

[11]   KIM, Y., et al., Hydrogeochemical and isotopic evidence of groundwater salinization in a coastal aquifer: A case study in Jeju volcanic island, Korea, J. Hydrol. **270** (2003) 282–294.

[12]   GONFIANTINI, R., ARAGUAS, L.A., Los isótopos ambientales en el estudio de la intrusión marina, TIAC'88, Tecnología de la Intrusión en Acuíferos Costeros, IAEA, Vienna (1988).

ISOTOPE AND HYDROCHEMICAL STUDY OF SEAWATER INTRUSION INTO THE AQUIFERS OF A COASTAL ZONE IN CUBA

C. DAPEÑA[a], J.L. PERALTA VITAL[b], H.O. PANARELLO[a],
R. GIL CASTILLO[b], D. LEYVA BOMBUSE[b 1], E.I. DUCÓS[a], L. VALDEZ[c],
J. OLIVERA ACOSTA[d], L. MARBÁN[a]

[a] Instituto de Geocronología y Geología Isotópica
(INGEIS, CONICET-UBA),
Buenos Aires, Argentina

[b] Centro de Protección e Higiene de las Radiaciones (CPHR),
La Habana, Cuba

[c] Empresa de Investigaciones y Proyectos Hidráulicos Habana,
La Habana, Cuba

[d] Instituto de Geofísica y Astronomía.
La Habana, Cuba

Abstract

The Artemisa–Quivicán Basin is located in the southern sector of the province of Havana, Cuba. This basin contains the most important aquifer of Havana province. It has a length of nearly 120 km and is 25 km in width. Recharge depends on the precipitation regime and rain infiltrates in a considerable proportion due to the intense development of karstic features. This aquifer is used for water supply to population, industry, and irrigation and is affected by over-exploitation and risk of contamination by saline sea intrusion. The main objective of this study is the isotope and chemical characterization of the aquifer and the delimitation of the area influenced by saline intrusion. Groundwater and river water are of the calcium bicarbonate type except those with evidence of mixture with saline water. Groundwater exhibits a variable proportion of mixture with seawater, indicating the presence of the saline intrusion.

1. INTRODUCTION

The Artemisa–Quivicán basin is located in the southern sector of the province of Havana, Cuba (Fig. 1). It is known as the South Basin ('Cuenca Sur'). The South

---

[1] Present adress: Centro de Estudios aplicados al Desarrollo Nuclear (CEADEN), Cuba

FIG. 1. Location map.

Basin is the most important aquifer of Havana province and it has a length of 120 km and is nearly 25 km in width. Recharge depends on the precipitation regime and rain infiltrates in a considerable proportion due to the intense development of karst. This aquifer is used for water supply to population, industry and irrigation and is affected by overexploitation, depletion and risk of contamination by anthropogenic action and saline sea intrusion. From the economic point of view, this area is one of the most important agricultural zones and one of the main aqueducts that provide water to Havana city (South Basin aqueduct) is located here. This investigation was supported by an International Collaboration Project represented by CPHR, Cuba, and INGEIS, CONICET-UBA, Argentina. The main objective of this work is the isotope and chemical characterization of the aquifer and the delimitation of the sector influenced by saline intrusion.

2. GEOLOGICAL AND HYDROGEOLOGICAL SETTING

Artemisa–Quivicán is an open basin (interconnected with the sea), occupying an extension of 487 km^2. The drainage network is poor due to karst development. The main stream is Ariguanabo River, that infiltrates at San Antonio de los Baños site (Fig. 2, Sample point 12). Groundwater flow is mainly N-S, discharging into the Batabanó Gulf.
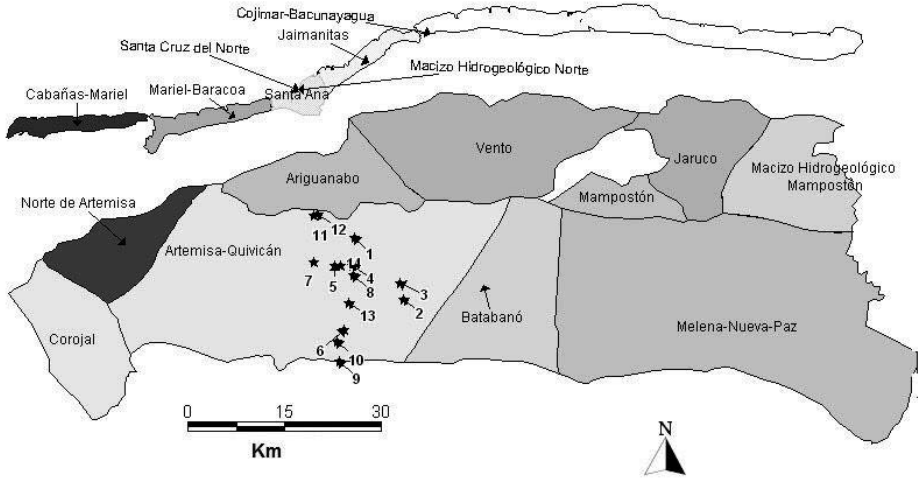
FIG. 2. Map showing the location of sampling sites.

The climate is tropical, moderated by trade winds, and is distinctly divided into a dry season (November to April) and a rainy season (May to October). The annual average temperature ranges between 24.7 and 26.0 ºC. The annual average precipitation is around 1400 mm, mostly occuring during humid months (80%) and extraordinary events like tropical cyclones and hurricanes.

The upper portion of the aquifer (up to 200 m) is represented mainly by the Middle Miocene, intensely karstified limestone of the Guines formation. The lower portion (up to 500 m depth) is represented by the Lower Miocene, karstified and clayey limestone of Cojimar formation. The aquifer is generally unconfined.

2.   MATERIALS AND METHODS

Water sampling was carried out using an optimized monitoring network (Table 1, Fig. 2). From February, 2008, to February, 2009 water samples were collected once a month from 11 wells and the Ariguanabo River, and for a first approach, samples from a rainy season month (October 2008) and from a dry season month (February 2008) were analysed. Precipitation and sea samples were also collected. Temperature, pH and electrical conductivity were determined in the field. Major elements were determined by conventional methods at the Cuban ENAST Laboratory (Empresa de Análisis y Servicios Técnicos Generales) and the Agroambiental Laboratory of INGEIS. It was very complex to obtain monthly seawater samples so published data was used [1]. Environmental isotopes (^{2}H and ^{18}O) were determined using high-precision laser spectroscopy off-axis integrated cavity output spectroscopy [2] at INGEIS

TABLE 1. SAMPLE POINTS LOCATION

No	Sample point	Code	Geographical coordinates		Depth (mbsl)	Altitude (m)
			N	W		
1	Albertina	HSC-537	22° 51′ 16.2”	82° 26′ 37.3”	85	49.89
2	San Agustín	HSC-566	22° 46′ 10.8”	82° 22′ 07.5”	100	23.25
3	Güiro Marrero	HSC-565	22° 47′ 28.4”	82° 22′ 23.2”	97	27.57
4	Fajardo	HSC-539	22° 48′ 58.7”	82° 26′ 47.7”	58	32.18
5	Amaros	HSC-530	22° 48′ 54.7”	82° 28′ 20.1”	90	23.53
6	Sta Ana	HSC-545	22° 43′ 35.5”	82° 27′ 29.4”	11	5.70
7	Rancherita	HSC-523	22° 49′ 15.9”	82° 30′ 13.2”	75	20.12
8	El Punto	HSC-540	22° 48′ 09.7”	82° 26′ 39.6”	60	18.23
9	Cajío Beach				—	—
10	Alvaro Barba	HSC-546	22° 42′ 31.5”	82°28′ 04.4”	34	1.87
11	S. Antonio de los Baños	HSC-521	22° 52′ 59.9”	82° 30′ 17.6”	19	49.52
12	Ariguanabo River	R	22° 53′ 11.9”	82° 30′ 00.2”	—	—
13	Sotolongo Díaz	HSC-542	22° 45′ 49.0”	82° 27′ 02.6”	42	10.86
14	Pluviometric station	H-268	22° 48′ 55.0”	82° 27′ 46.1”	—	21

laboratories. Samples with high salt content were analysed by IRMS. Deuterium in water samples was processed by the procedure indicated in Ref. [3] and ^{18}O was determined using the methodology of Refs [4] and [5], modified by Ref. [6] at INGEIS. Isotope ratios were measured with a triple collector multiport inlet system mass spectrometer Finnigan MAT Delta S. Results are expressed in the usual way, as δ (‰), defined as δ = 1000 (Rs-Rp)/Rp ‰, where δ: isotope deviation in ‰; S: sample; P: international reference; R: isotope relation (^{2}H/^{1}H, ^{18}O/^{16}O). Values are referred to Vienna Standard Mean Ocean Water (V-SMOW) [7]. Uncertainties are ±0.3 ‰ for δ^{18}O and ± 1.0‰ for δ^{2}H.

The rainwater isotope composition was evaluated using monthly composite samples from one collector installed in San Gabriel town (Station H–268, sample point 14, Table 1, Fig. 2). These measurements are supplemented by meteorological information such as mean surface air temperature and amount of precipitation. This information allowed us to estimate the input function (rain isotope content) of the area.
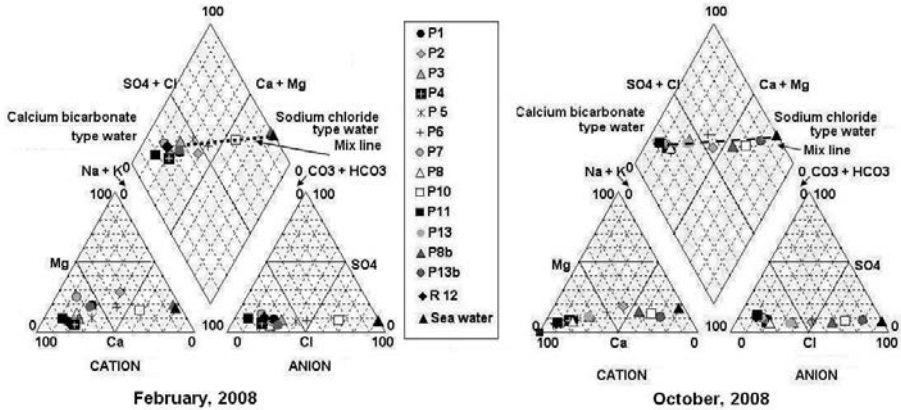
FIG. 3. Piper diagrams.

4. RESULTS

4.1. Chemical composition

Fig. 3 shows the Piper diagrams for groundwater samples (P), Ariguanabo river (R12) and seawater collected on February 2008 and October 2008. Seawater is of the sodium chloride type. Most of the groundwater and river water samples are of the calcium bicarbonate type, but some show a mixture of fresh and seawater types (February 2008 samples P10, P6, P5 and P2, and October 2008 samples P13, P13b, P10, P8, P8b, P6, and P2). The compositions of the latter vary depending on the mixing ratios.

4.2. Isotope Composition

Figure 4 exhibits a conventional $\delta^{18}O$ vs δ^2H scatter plot of all samples, the Global Meteoric Water Line, $\delta^2H = 8\,\delta^{18}O + 10‰$ [8], the Ariguanabo river, the weighted isotope contents of rain in 2008, the individual rains and the Caribbean Seawater. The isotopic composition of groundwater and river water show a meteoric origin. Although the rain isotope record is short, covering about one year of sampling at present, a wide range of values was measured (–7.3 to –1.2‰ for $\delta^{18}O$ and –49 to +1‰ for δ^2H). The weighted average precipitation is $\delta^{18}O = –2.8‰$ and $\delta^2H = –13‰$.

Groundwater shows values between –3.4 to –2.4‰ for $\delta^{18}O$ and –18 to –13‰ for δ^2H. The isotope composition of the Ariguanabo river varies between –2.9 and –2.3‰ for $\delta^{18}O$ and between –15 to –11‰ for δ^2H. In general, sample values are slightly enriched and they fit on an evaporation line. However, not all samples fulfill the evaporation pattern, probably due to mixing mechanisms. Caribbean Seawater values are positive and they were obtained from a measured sample and from
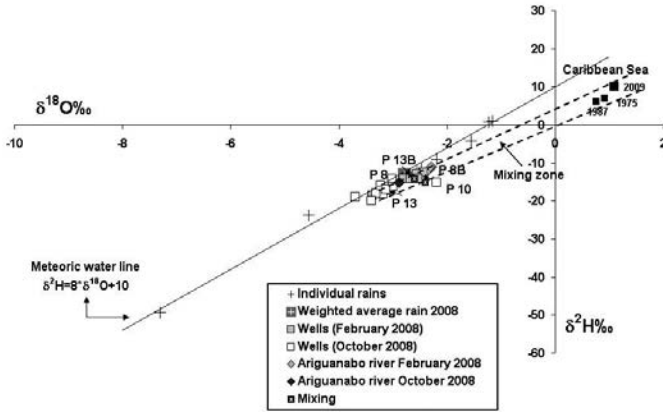
FIG. 4. Scatter plot $\delta^{18}O$ vs δ^2H.
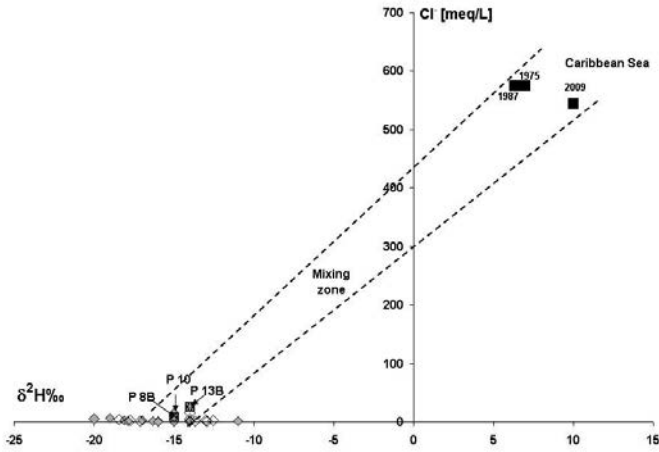
FIG. 5. Chloride vs δ^2H for samples collected in October 2008.

the literature [9]. The relationship between ^2H and ^{18}O provides a clear indication of the mixing process between fresh water and seawater along the straight line of the two mixing poles, with fresh water of the aquifer at one end and seawater at the other end (Fig. 4). In this case, the slope of the line connecting the aquifer and seawater is similar to the line that is based on the evaporation process. The relationship ^{18}O vs chloride of waters samples corroborates the effect of the mixing process (Fig. 5).

5.   CONCLUSIONS

Isotope and chemical results indicate the meteoric origin of waters. Most of the groundwater and river water samples are of the calcium bicarbonate type, but some of them exhibit variable proportions of mixture with seawater indicating the presence of the saline intrusion. Samples were only obtained across a perpendicular line to coast, thus it would be interesting to:

(1)   Check more wells along an east–west transect in order to delimit the extension of the saline intrusion;
(2)   Replace damaged wells;
(3)   Evaluate the chemical and isotopic composition of other potential saline sources, such as irrigation canals, lakes, etc;
(4)   Maintain water precipitation collection for isotope measurement in order to construct a local water line;
(5)   Continue monitoring the water levels and electrical conductivities.

REFERENCES

[1]   GONZÁLEZ HERNÁNDEZ, P., Contribución al Conocimiento Hidrogeoquímico de Acuíferos Cársicos Costeros con Intrusión Marina, Sector Güira-Quivicán, Cuenca Sur de La Habana, Centro Nacional de Investigaciones Científicas, La Habana (2003) 174.
[2]   LIS, G., WASSENAAR, L.I., HENDRY, M.J., High-precision laser spectroscopy D/H and $^{18}O/^{16}O$ measurements of microliter natural water samples, Anal. Chem. **80** (2008) 287–293.
[3]   COLEMAN, M.L., SHEPHERD, T.J., DURHAM, J.J., ROUSE, J.E., MOORE, G.R., Reduction of water with zinc for hydrogen isotope analysis, Anal. Chem. **54** (1982) 993–995.
[4]   EPSTEIN, S., MAYEDA, T., Variation of ^{18}O content of waters from natural sources, Geochim. Cosmochim. Acta **4** (1953) 213–224.
[5]   ROETHER, W., Water–CO_2 exchange set-up for the routine oxygen-18 assay of natural waters, Intern. J. Appl. Rad. Isotopes **21** (1970) 379–387.
[6]   PANARELLO, H.O., PARICA, C.A., Isótopos del oxígeno en hidrogeología e hidrología, Primeros valores en aguas de lluvia de Buenos Aires, Asoc. Geol. Argentina, Revista XXXIX, **1–2** (1984) 3–11.

[7]   GONFIANTINI, R., Standards for stable isotope measurements in natural compounds, Nature **271** (1978) 534–536.

[8]   CRAIG, H., Isotopic variations in meteoric waters, Science **133** (1961) 1702–1703.

[9]   GONFIANTINI, R., Progress Report on the Application of Isotope Techniques to Hydrology in Jamaica, Internal Report, IAEA, Vienna (1975).

[10]   GONFIANTINI, R., SIMONOT, U., "Isotopic investigations of groundwater in the Cul-de-Sac Plain, Haiti", Isotope Techniques in Water Resources Development, Proc. Int. Symp. on the Use of Isotope Techniques in Water Resources Development, Proceedings Series, IAEA Vienna, (1987) 483–506.

NATURAL TRACERS AND ISOTOPE TECHNIQUES TO DEFINE GROUNDWATER RECHARGE AND SALINIZATION IN THE BOU AREG COASTAL AQUIFER (NORTH MOROCCO)

V. RE [a], E. ALLAIS [b], N. EL HAMOUTI [c], R. BOUCHNAN [d], E. SACCHI [e], F. RIZZO [f], G.M. ZUPPI [a,g]

[a] Department of Molecular Sciences and Nanosystems,
University Ca' Foscari, Venice, Italy

[b] ISO4 s.n.c., Torino, Italy

[c] Multidisciplinary Faculty of Nador,
University of Oujda, Nador, Morocco

[d] Laboratory of Physical Phenomena and Natural Risk Modelling,
University of Tangier, Tangier, Morocco

[e] Department of Earth Sciences,
University of Pavia, Pavia, Italy

[f] UNESCO International Hydrological Programme

[g] Institute of Environmental Geology and Geoengineering,
National Research Council, Monterotondo, Italy.

Abstract

The geochemical and isotopic ($\delta^2 H$, $\delta^{18} O$, $\delta^{13} C$, $\delta^{15} N_{NO3}$, $\delta^{18} O_{NO3}$) characterization of the Bou Areg aquifer (North Morocco) based on samples collected during two surveys in November 2009 and June 2010 allowed the identification of runoff from the mountain regions and agricultural return flows as the main sources of aquifer recharge. The high salinization of the aquifer is not only due to the intensive agricultural activities but it is also associated with the natural quality of the catchment. The isotopic signal of dissolved nitrates allowed for the identification of two main sources of nitrogen in the system: (i) fertilizers and (ii) manure and septic effluents. The study, framed within the UNESCO-IHP sub component of the Strategic Partnership for the Mediterranean Large Marine Ecosystem, represents the first isotopic investigation of the area and will serve as a basis for the promotion of robust science based management practices in the region.

1.   INTRODUCTION

Urban and coastal areas in arid and semi arid regions mainly rely on groundwater resources. The continuous utilization of coastal aquifers to respond to human needs can give rise to a deterioration of natural ecosystems, already threatened by climate changes, with possible severe effects on human health and wellbeing. In particular, incessant withdrawal can lead to overexploitation problems (if abstraction exceeds natural replenishment rates) and possible associated saline water encroachment. In addition, salinization problems might be related to other potential sources that must be defined and understood with the aid of appropriate hydrogeochemical techniques [1] to design a sustainable groundwater management programme in the long term.

Within the Strategic Partnership for the Mediterranean Large Marine Ecosystem, UNESCO-IHP subcomponent (Management of Coastal Aquifer and Groundwater), this work applies hydrogeochemical and isotopic tracers to define groundwater recharge and salinization in the pilot case study of the Bou-Areg aquifer [2]. The results will provide criteria to support science based water management practices.

2.   SITE DESCRIPTION

The Bou-Areg coastal plain is located on the Mediterranean shore of Morocco, close to the Spanish enclave of Melilla. The climate of the region is mainly semi arid, but with a general high level of humidity due to the proximity to the sea. The dominant winds have a W–SW direction from November to May and an E–NE direction from May to October [3]. There is no regular rainy season, and regional precipitations are mainly related to Atlantic perturbations, with an average of about 300 mm/a [4].

The catchment area covers a surface of about 190 km^2, and it is limited by the Gourougou volcanic massif (NW), the Beni-Bou-Iffrour volcanic massif and the Kebdana range (SE). The area is also characterized by the presence of the so-called lagoon of Nador, which covers a surface of about 115 km^2. The lagoon is located in the Plio-Quaternary catchment basin of Meilla-Nador. The northern part of the plain is dominated by the presence of minerals such as calcium plagioclase, silica, olivine and pyroxene coming from the Gourougou mountain, while the soils of the southern part are rich in quartz, calcite and clays. In particular, the clay fraction is dominated by illite and chlorite [5], which generally characterize areas at weak pedologic evolution, as young soils or, as in this case, arid and semi arid regions.

The hydrological network is constituted by numerous rivers with temporary flow (*oueds*) and only few permanent ones (the most important of which is the Selouane *oued*). Some *oueds* directly discharge in the lagoon of Nador contributing, together with the underground water flow, to its freshwater and sediment inputs, while all the others do not reach the lagoon because of flow reduction due to evaporative

loss or infiltration in the aquifer. In addition to surface water contribution, sewage and wastewater inputs are also present and are mainly associated with the urban and suburban settlements on the lagoon shore (SE: Kariat Arekman; NW: Beni-Enzar).

3. METHODS

Two sampling campaigns performed in November 2009 and June 2010 allowed for the collection of 40 groundwater samples from private wells in the Bou-Areg aquifer and of two spring samples located close to the lagoon shore. *In situ* measurement involved pH, Eh, Electrical Conductivity, groundwater temperature and alkalinity. Chemical analyses of water samples were performed at the hydrochemical laboratory of CNR-IGAG (Montelibretti, Italy) (November 2009 campaign), and at the hydrochemistry laboratory of the Earth Sciences Department of the University of Pavia, Italy (June 2010 campaign), using ion chromatography. Trace elements analyses (B, Li, Sr) were performed at the Earth Sciences Department of the Pavia University, Italy, using an ICP-AES Jobyn Yvon 24. Br analyses were performed at the CNR-IGG (Pisa) using ion chromatography (Dionex 100). Samples for stable isotope analysis were collected and prepared according to standard procedures [6]. All gases were analysed on a Finningan™ MAT 250 Mass Spectrometer at ISO4 s.n.c., Turin, Italy.

4. HYDROGEOCHEMICAL RESULTS AND DISCUSSION

Groundwater samples in the Bou-Areg area are mainly classified as the sodium-chloride type, with the more enriched waters located in the downstream area, close to the lagoon. The two springs show a chemical composition close to that of groundwater, but with a clear influence of lagoon water, suggesting the occurrence of mixing processes. In addition, the groundwater chemical composition is also influenced by water–rock interaction processes. High alkalinity values registered for most of the wells might reflect elevated concentrations of dissolved inorganic carbon in the aquifer, typical of open system conditions.

All the samples collected in the Bou-Areg aquifer show strong salinization, confirmed by the high concentrations of both Na and Cl (Fig. 1). As a general feature, aquifer salinity increased from November 2009 to June 2010, possibly because of higher leaching of the unsaturated zone, thus recharging the underground system with more dissolved salts [7]. In fact, the salts remobilization from the unsaturated zone is a phenomenon of particular relevance in arid and semi-arid regions, where, after heavy rain episodes, the infiltration is more rapid and stronger.

The chemical composition of dissolved salts in groundwater is slightly different from that of seawater, due to differences in the hydrochemical processes occurring
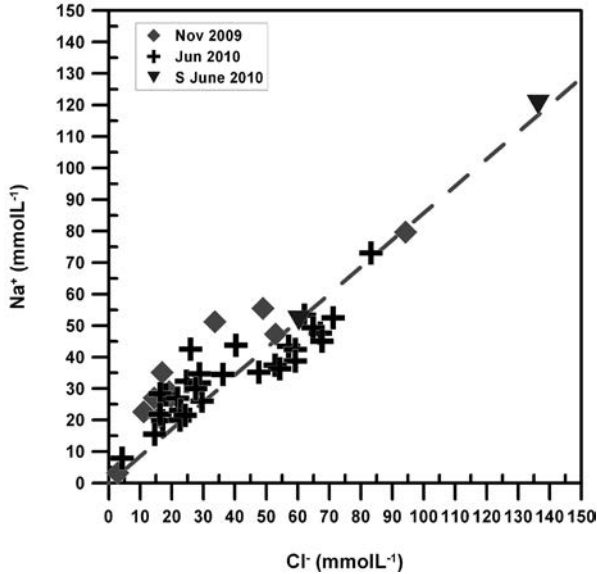
FIG. 1. Plots of sodium versus chloride concentration (in mmol/L) for the samples collected in the Bou-Areg aquifer. The dashed grey line represents the seawater dilution trend.

in those systems. This explains why most of the samples plot above the freshwater–seawater dilution line (Fig. 1). Only few samples have a composition coherent with the progressive dilution with seawater, thus suggesting the possible existence of old seawater intrusion or presence of connate water [4, 8] interacting with the recent recharge in this sector of the aquifer. The aquifer appears to be mainly recharged by mountain runoff. Besides, other sources of local recharge are altering the chemical composition of the studied groundwater, creating a complex system where apportioning natural processes and anthropogenic perturbation is difficult. In this case, isotopes can help to better define the origin of recharge and salinity.

4.1. Groundwater recharge

Stable isotopes of water molecules (Fig. 2) deviate from both the Global Meteoric Water Line (GMWL, [9]) and the Local Meteoric Water Line (LMWL, [10]) suggesting the occurrence of evaporative processes prior to recharge and mixing with external saline sources [6]. The samples that are more enriched in $\delta^{18}O$ (> –5‰) also show relatively higher concentrations of chloride (> 1000 mg/L) and dissolved nitrates (> 50 mg/L). This, associated to the extensive agricultural practices in the area, suggest that agricultural return flows is another important recharge source in

the aquifer [11]. On the other hand, wells with relatively high oxygen-18 values and low chloride concentrations might be associated with mixing with an already evaporated solution (e.g. the irrigation channel water).

4.2. Groundwater salinization

To better understand the pollution sources in the aquifer and the associated recharge process, $\delta^{13}C$ was studied. By comparing carbon-13 and oxygen-18 (Fig. 3) one can notice that the isotopic signal of the oxygen is more uniform, meaning that the waters are affected by the same fractionation processes (evaporation in the aquifer, evaporation during the irrigation processes and water recycling), whereas the carbon isotopic signature is more variable due to interaction with the carbonates system, soil organic matter or pollutants. Two groups of samples can be distinguished: (i) wells of group A (Fig. 3) have a more negative isotopic signal, typical of local recharge remobilizing pollutants in the unsaturated zone, thus changing the isotopic composition of carbon-13, and (ii) wells of group B, showing a tendency towards more positive carbon-13 values. This can be coherent with processes of carbonate dissolution ($\delta^{13}C$ of marine carbonate ~0‰) in intensively irrigated areas; in fact, as carbonate is dissolved, $\delta^{13}C_{DIC}$ will evolve to more enriched values. Of course, how far it evolves and the rate of carbonate dissolution depends on the 'openness' of the system, therefore on the soil CO_2, and possible interaction of photosynthetic uptake (fixation of CO_2 by C3 or C4 plants [6]). For example, C4 plants (e.g. common
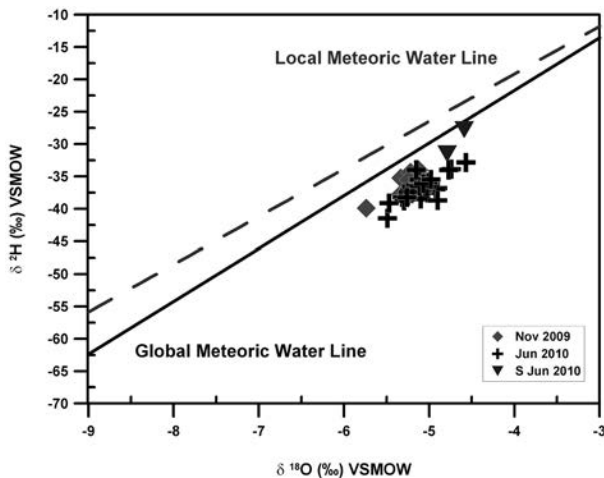
FIG. 2. Water stable isotope content in the Bou-Areg aquifer. Triangles highlight the isotopic composition of the two spring samples. Black and dashed grey lines represent the Global Meteoric Water Line [9]and the Local Meteoric Water Line [10] respectively.
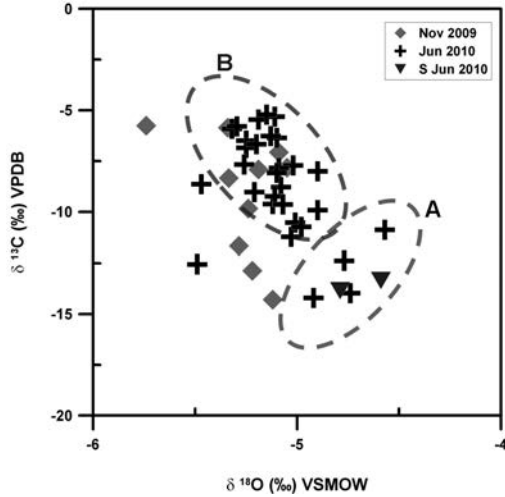
FIG. 3. Isotopic signal of the groundwater in the Bou-Areg aquifer. Plot of $\delta^{13}C$ (‰) versus $\delta^{18}O$ (‰). See text for explanation.
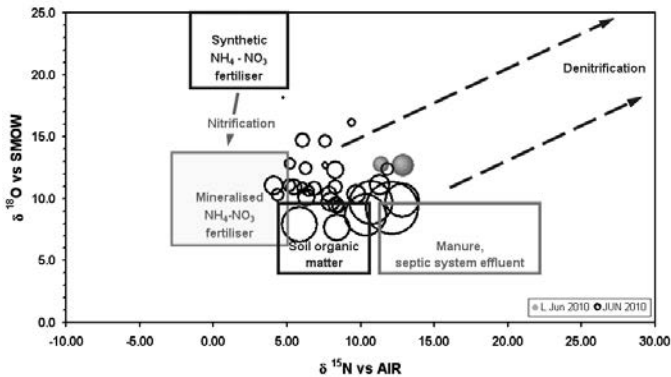
FIG. 4. Isotopic composition of dissolved nitrates $\delta^{15}N$ (‰) for groundwater and spring water samples in the Bou-Areg aquifer. Bubbles dimensions are proportional to the concentration of dissolved nitrate (modifed after Ref. [12]).

agricultural plants like sugar cane, corn and sorghum) have $\delta^{13}C$ ranging from –10 to –16‰, thus coherent with the signal of the Bou Areg water samples.

Experimental findings confirm that for most of the samples the high salinity is given by the coexistence of dissolution processes of evaporative rocks and carbonates from Miocene substratum water–rock interactions, and human impacts due to agricultural return flows. The latter represent the main contribution to groundwater salinization, especially in the central part of the aquifer, as well as one of the main causes of the general increase in nitrate concentrations.

By comparing the obtained isotopic data for groundwater of the Bou-Areg aquifer (Fig. 4), with the isotopic composition of $\delta^{15}N_{NO3}$ in manure, septic system effluents (10–15‰) in soil organic matter (~5‰) and fertilizers (~0‰, [6]), two main sources of nitrogen input to groundwater can distinguished. Two wells, located in the suburbs of the city of Nador and showing the highest dissolved nitrates concentrations appear to be clearly affected by pollution from manure and septic effluents systems (~+12‰), while the other two, located in the central part of the plain, have a signal coherent with mineral fertilizers (~+4‰), thus explaining their high potassium concentrations. As a general feature, most of the wells appears to be a mixing between these two main sources. Despite the fact that their isotopic signal is compatible with the one of soil organic matter ($\delta^{15}N$ ~+4 to +10‰), the mixing origin is more coherent with nitrates concentration quite above the 50 mg/L [6]. For the other wells, mixing processes seem to occur thus affecting the isotopic signal of dissolved nitrate, and the same process appears evident for the two springs.

5.   CONCLUSIONS

Multi-tracer investigation of the Bou-Areg coastal aquifer allowed for a clearer definition of the main sources of groundwater recharge and salinization. Results from this work confirm that human activities are strongly altering the natural characteristics of the Bou-Areg coastal aquifer. This is mainly associated with groundwater exploitation for irrigation practices, and the combined pollution of fertilizers, manure and septic effluents. The improvement of groundwater exploitation, together with the enhancement of sanitation structures and wastewater disposal, will allow the considerable amelioration the quality of the subsurface waters and a better response to climatic and environmental changes in the area.

REFERENCES

[1] INTERNATIONAL ATOMIC ENERGY AGENCY, Isotope Techniques in the Study of Environmental Change, Proc. Int. Symp. on Isotope Techniques in the Study of Past and Current Environmental Changes in the Hydrosphere and Atmosphere, Proceedings Series, IAEA, Vienna (1998) 503–518.

[2] UNITED NATIONS ENVIRONMENT PROGRAMME (UNEP), Strategic Partnership for the Mediterranean Sea Large Marine Ecosystem (MedPartnership), Inception Report, UNEP, Athens (2010) 85.

[3] TESSON, M., Régime hydrologique et hydrodynamique de la Sebkha Bou-Areg (Lagune de Nador, Maroc), Bilan du Printemps 1976, Bulletin du Institut Supérieur des Pêches Maritimes du Maroc **21** (1977).

[4] EL YAOUTI, F., EL MANDOUR, A., KHATTACH, D., BENAVENTE, J., KAUFMANN, O., Salinization processes in the unconfined aquifer of Bou-Areg (NE Morocco): A geostatistical, geochemical, and tomographic study, Applied Geochemistry **24** (2009)16–31.

[5] BLOUNDI, M.K., Etude géochimique de la lagune de Nador (Maroc oriental): Impacts des facteurs anthropiques, PhD Thesis, Ecole et Observatoire des Sciences de la Terre, Centre de Géochimie de la Surface, Université Mohamed V-Agdal, Rabat (2005).

[6] CLARK, I.D., FRITZ, P., Environmental Isotopes in Hydrogeology, Lewis, Boca Raton, FL (1997) 328.

[7] ALLISON, G.B., GEE, G.W., TYLER, S.W., Vadose-zone techniques for estimating groundwater recharge in arid and semiarid regions, Soil Sci. Soc. Am. J. **58** (1994) 6–14.

[8] CHAOUNI ALIA, A., EL HALIMI, N., WALRAEVENS, K., BEEUWSAERT, E., DE BREUCK, W., "Investigation de la salinisation de la plaine de Bou-Areg (Maroc nord-oriental)", Freshwater Contamination, Proceedings and Reports of the Rabat Symposium of the International Association of Hydrological Sciences, (WEBB, B., Ed.), IAHS, Wallingford (1997) 211–220.

[9] ROZANSKI, K., ARAGUÁS-ARAGUÁS, L., GONFIANTINI, R., Isotopic patterns in modern global precipitation, Geophysical Monograph **78** (1993) 1–36.

[10] OUDA, B., EL HAMDAOUI, A., IBN MAJAH, M., "Isotopic composition of precipitation at three Moroccan stations influenced by oceanic and Mediterranean air masses", Isotopic Composition of Precipitation in the Mediterranean Basin in Relation to Air Circulation Patterns and Climate, IAEA-TECDOC-1453, IAEA, Vienna (2005) 125–140.

[11] BOUCHAOU, L., et al., Application of multiple isotopic and geochemical tracers for investigation of recharge, salinization, and residence time of water in the Souss-Massa aquifer, southwest of Morocco, J. Hydrol. **352** (2008) 267–287.

[12] KENDALL, C. "Tracing nitrogen sources and cycling in catchments", Isotope Tracers in Catchment Hydrology (KENDALL, C., McDONNELL, J.J., Eds), Elsevier, Amsterdam (1998) 519–576.

THE USE OF δ^{37}Cl TO EXPLAIN ORIGIN AND PRODUCTION OF SALT FROM THE SALINE SPRING 'FONTE DA PIPA' IN RIO MAIOR (CENTRAL PORTUGAL)

H.G.M. EGGENKAMP, J.M. MARQUES
Centro de Petrologia e Geoquímica,
Instituto Superior Técnico,
Lisbon, Portugal

H. GRAÇA
Centro Hospitalar das Caldas da Rainha,
Caldas da Rainha, Portugal

Abstract

Salt extraction in Rio Maior (Central Portugal) is unique in the sense that salt is exploited from a very saline (134 g/L NaCl) terrestrial spring. This spring receives its salt through meteoric water circulation from nearby hills along a shallow salt diapir. This is shown using δ^{37}Cl, as the composition in dug wells between the mountains and the saline spring is comparable, while δ^{37}Cl in a well to the east is significantly different. Unlike seawater this spring contains nearly pure NaCl, giving us the opportunity to determine δ^{37}Cl values in a natural salt precipitating system beyond the point where (in seawater) potassium and magnesium chlorides start to precipitate. δ^{37}Cl values were determined from brines and by precipitating salt in salt pans with different evaporation stages. Fractionation of up to 1‰ was found. To complement these natural data, evaporation/precipitation experiments are currently being conducted under controlled laboratory conditions. First results of these experiments indicate that during continued evaporation and precipitation δ^{37}Cl continues to decrease.

1. INTRODUCTION

Salt for human consumption can be produced by a number of different processes. At the largest, industrial scale, it is produced using underground dissolution mining of large fossil salt formations, such as the Zechstein in the Netherlands [1]. On a much smaller scale it is produced by evaporating seawater in salt pans along coasts where the (summer) temperature is high enough to evaporate the water and precipitate the salt. As seawater does not consist of pure NaCl, and contains considerable amounts of K, Mg and SO$_4$, which tend to precipitate after NaCl [2], precipitation of salt from seawater has to be stopped before these K, Mg and SO$_4$ salts start to precipitate. In Rio Maior (Central Portugal) a very saline spring ('Fonte da Pipa'/'Fonte

da Bica') is found, and at least since 1177 [3], but probably for a much longer period, it has been used for the extraction of salt. The spring, which is actually a well with its water level at 3.98 m below the level of the salt pans, contains water with a total of 134 g of salt per litre, of which 97% is NaCl, and is referred to in the literature by the two earlier mentioned names, 'Fonte da Pipa' and 'Fonte da Bica' [4]. To produce the salt the water is pumped from the well into preconcentration basins, after which it is guided into shallow concrete salt pans where the solution is evaporated until dryness, which in this case is possible as the solution is a nearly pure NaCl brine.

Very close to the saline spring, one of them as close as 100 m, several fresh water wells are found. Given the proximity of these wells to the saline spring we expected to see some influence of the saline spring into these wells. As there is a very large salinity difference between these freshwater wells and the saline spring there must be a very sharp boundary between the hypersaline and fresh water bodies underground. As the fresh waters are used for watering the fields, pumping large amounts of it could disturb the equilibrium between the two systems, a situation that should be avoided. This justified a study of these systems (saline vs dilute), especially as the geochemistry of this unique system has never been studied before.

Chlorine stable isotopes are used in this study as they are a good proxy of evaporation and precipitation of salt from brines, both marine and terrestrial [5–7]. Cl isotopes fractionate during the precipitation of salt, but do not fractionate during dissolution. Any influence from the saline spring in Rio Maior on groundwater should be indicated with $\delta^{37}Cl$ values which are comparable to that of the saline spring. If the $\delta^{37}Cl$ of a groundwater sample is clearly different, a different origin of the chloride can be concluded. In this paper we show that in the case of Rio Maior we see influences from the saline spring in shallow groundwater. As the spring of Rio Maior contains nearly pure NaCl we also studied the Cl isotope fractionation during precipitation of the salt in the salt pans. In this case we would expect a relatively large fractionation, as no K and Mg chlorides, which show only little fractionation [5], will precipitate.

2.   MATERIALS, METHODS AND RESULTS

2.1. Sampling

Samples have been taken during two one day field trips on the 15th of July and the 29th of September of 2009. During the first field trip the saline spring and the evolving salt precipitates and brines were sampled, while during the second field trip the fresh water wells around the saline spring were sampled.

TABLE 1. MAIN CHARACTERISTICS OF THE WATER AND SALT SAMPLES

Sample	Type	$\delta^{37}Cl$ (‰)	Temp (°C)	pH	Cond. (mS/cm)	TDS (g/L)	Na+Cl as % of TDS
Poço 1	Freshwater well	–0.33	19.9	7.05	1.171	0.855	13
Poço 2	Freshwater well	–0.25	17.4	7.54	1.324	0.881	34
Poço 3	Freshwater well	–0.21	20.7	7.35	1.087	0.722	27
Poço 4	Freshwater well	+0.10	20.0	7.43	0.829	0.550	20
F. da Pipa	Saline spring	–0.22	19.1	6.86	167.1	134	97
RM2	Brine in precon-centration basin	–0.18	24.5	7.54	226	238	98
RM3	Brine in precon-centration basin	–0.15	24.4	7.58	224	228	98
RM4	Brine in saltpan after ca. 1 day	–0.17	30.3	7.42	238	273	97
RM5B	Brine in saltpan after ca. 1 day	–0.42	32.0	7.26	245	265	98
RM6B	Brine in saltpan after ca. 4 days	–0.24	30.2	7.33	246	254	98
RM9B	Brine in saltpan after ca. 4 days	–0.38	32.9	7.42	244	248	97
RM8B	Brine in saltpan after ca. 4 week	–0.51	31.8	7.33	241	285	97
RM7B	Brine in saltpan after ca. 4 week	–1.07	29.6	7.52	242	268	93
RM5P	Prec. from saltpan after ca. 1 day	+0.04				1037	99
RM6P	Prec. from saltpan after ca. 4 days	+0.05				991	99
RM9P	Prec. from saltpan after ca. 4 days	+0.04				926	99
RM8P	Prec. from saltpan after ca. 1 week	–0.20				933	99
RM7P	Prec. from saltpan after ca. 1 week	–0.42				1026	99

2.2. Analytical techniques

Temperature, pH and electrical conductivity of the samples were measured in situ. Cations in the samples have been determined by atomic adsorption (Varian FS280) and anions by ion-chromatography (Dionex ICS-900) in the Laboratório Luís Aires-Barros of the Centro de Petrologia e Geoquímica of the Instituto Superior Técnico (CEPGIST), in Lisboa, Portugal. Chlorine isotope ratios have been measured at Utrecht University, the Netherlands, as described in Ref. [8].

2.3. Results

A basic characterization of the samples can be found in Table 1. It shows the chlorine isotope composition of the samples, as well as the field measurements, which are the temperature, pH and conductivity of the water samples. Further, the total mineralization (the sum of all dissolved solids) and the NaCl content as a percentage of the total mineralization is provided.

3. DISCUSSION

3.1. Relation between the freshwater wells and the saline spring

The saline spring 'Fonte da Pipa'/'Fonte da Bica' is found at the lowest point of a valley (at about 75 to 80 m above sea level [m a.s.l.]) surrounded by relatively low hills. It is found near a northeast–southwest delineating fault with lower Jurassic sediments from the 'Dagorda marls' formation to the west and Miocene and Pliocene sediments to the east [9]. To the west of the saline spring the hills belong to the Candeiros Mountains which are up to 323 m a.s.l. (Mount Conde) and consist of Jurassic karstic limestones. To the east the hills are much lower, up to 160 m a.s.l. (Mount Redes), and consist mostly of Pliocene lignites and diatomites and Miocene sandstones and limestones [9]. For a schematic geological map we refer to Fig. 1.

The chemical compositions of the freshwater wells (Poço 1, 2, 3 and 4) indicate that they are Ca-Na-HCO$_3$ type waters, with very different compositions from the saline spring which is a Na-Cl type water. The Ca-Na-HCO$_3$ type waters are mainly the result of interaction of fresh water with the carbonate (mostly calcitic) rocks.

The δ^{37}Cl values of the five natural waters (four freshwater wells and the saline spring) are very peculiar. Three of the freshwater wells (Poços 1, 2 and 3) have negative δ^{37}Cl values, which are in agreement with the δ^{37}Cl of the saline spring (–0.22‰), while the fourth freshwater well has a positive value (+0.10‰). The fourth well is the only well lying to the east of the fault at which the saline spring issues. This indicates that the chloride in the three wells to the west of the fault has its δ^{37}Cl influenced by the saline spring, while the well to the east does not. This then indicates that
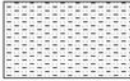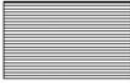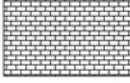
FIG. 1. Schematic geological map of the study region, adapted from Ref. [9].
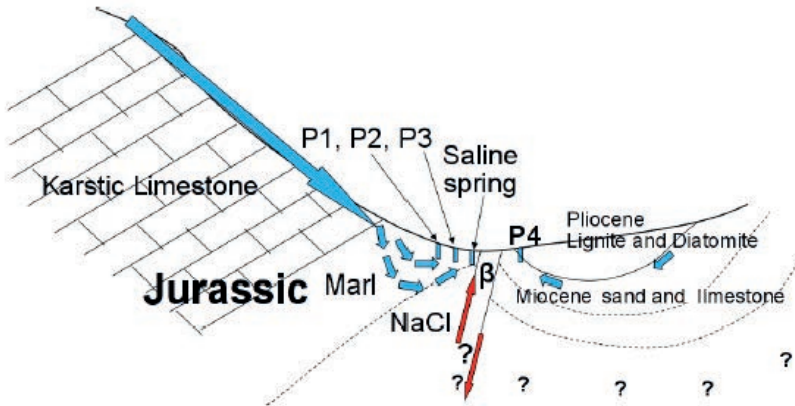
FIG. 2. Preliminary conceptual model for the saline spring at Rio Maior (left is west).

there is no groundwater connection over the fault, and that the water that dissolves NaCl from the salt diapir sampled from the saline spring is coming from the west.

3.2. Development of a preliminary conceptual model for the Rio Maior hydrogeological setting

This multidisciplinary approach, a combination of the geomorphology, geology, geochemistry and isotope hydrology ($\delta^{37}Cl$) of the well's site, gives us the possibility of developing a very preliminary, but nonetheless very satisfying conceptual model for the hydrogeological system around the 'Fonte da Pipa'/'Fonte da Bica'. This system is shown in Fig. 2.

Rainwater from the Candeiros Mountains is flowing relatively close to the surface. If it were circulating deeper it would follow the general geological structure and flow westward, something that is actually happening and is the origin (recharge area) of well known spas such as Caldas da Rainha [10]. Beyond the boundary between the karstic limestones and the marls from the 'Margas da Dagorda' formation the water is circulating deeper and will dissolve NaCl from the salt diapir which is found at most 75 m below the surface [3]. The bottom of the well from 'Fonte da Pipa'/'Fonte da Bica' is actually standing in the caprock of this salt diapir. The water that circulates above the salt diapir, and that will not be in direct contact with it, will stay fresh, and due to the rock characteristics will be of the $Ca-Na-HCO_3$ type, containing relatively low Cl concentrations with the same isotopic composition of the salt diapir. As a small amount of the Cl from the salt deposits will dissolve and disperse into the overlying sediments it will be picked up by the circulating freshwater. The area to the east of the fault consists of much younger sediments and the groundwater that
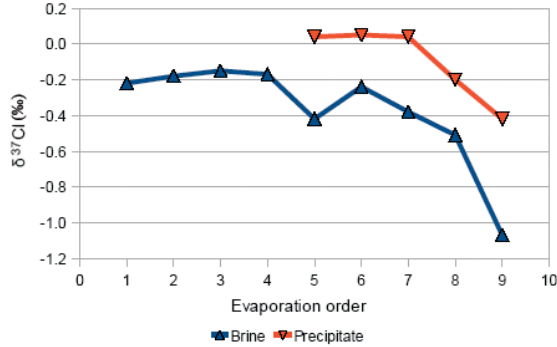
FIG. 3. Chlorine isotope values of brine and co-precipitating salt in the Rio Maior salt pans.

circulates here does not come into contact with the salt at all. The fault actually acts as a good seal between the two systems. For a large part the fault is also (at least in several locations) filled with basaltic intrusions. In this eastern part of the system groundwater is flowing from the hills, starting in the east towards the west.

3.3. Fractionation of Cl isotopes during salt precipitation

Isotope fractionation of the chloride ion during salt precipitation is dependent on the co-precipitating cation [5]. While in the case of NaCl the precipitate has a δ^{37}Cl which is 0.26‰ more positive than the brine, in the case of KCl and $MgCl_2 \cdot 6H_2O$ it is slightly more negative (–0.09‰ and –0.06‰ respectively). In the case of seawater, which contains considerable amounts of K and Mg, which will precipitate as kainite ($K_4Mg_4Cl_4(SO_4)_4 \cdot 11H_2O$), carnallite ($KMgCl_3 \cdot 6H_2O$) and bischofite ($MgCl_2 \cdot 6H_2O$), a minimum δ^{37}Cl of about –0.5‰ can be expected (assuming an original seawater brine with a δ^{37}Cl of 0‰ vs SMOC). However, in the case of 'Fonte da Pipa'/'Fonte da Bica' we have a brine that contains about 97% NaCl, which means that no significant amount of K and Mg chlorides will precipitate. In this case we thus can theoretically expect very low δ^{37}Cl values, provided we are able to sample the very last stage of NaCl precipitation. In the salt pans we could only roughly indicate the age of the evaporating brine and precipitate. According to the manager of the cooperative the salt pans were filled 'one day', 'four days' and 'one week' ago. However, even based upon these rough estimates a very clear picture can be drawn (Fig. 3). As long as no salt has precipitated yet (samples 1 to 4) δ^{37}Cl is constant at –0.2‰. Once NaCl starts to precipitate the isotope composition changes. As expected, the precipitate has a more positive δ^{37}Cl than the brine, and as evaporation progresses both the brine and the precipitate gain lower δ^{37}Cl values. This process is not perfectly systematic in these salt pans as no salt is physically removed, and during the process it occasionally

is mixed to facilitate better evaporation in the salt pan. This mixing of salt will explain the relatively large differences in isotopic composition between the brine and the coexisting precipitate in most sampled salt pans, as the precipitates are a mixture of earlier and later stage NaCl.

Calculations on the theoretical fractionation of chloride which precipitate from modern seawater indicated that a minimum δ^{37}Cl of –0.5‰ could be expected [5, 6]. In our system, only the most evolved sample (RM7B) has a (significantly) lower δ^{37}Cl as is shown in Fig. 3. This indicates that very low δ^{37}Cl values are only reached when the great majority of salt has precipitated, but it also shows that these very negative values can be reached.

3.4. Laboratory experiments on Rio Maior brine evaporation

From two samples, the saline spring and the advanced brine RM8, we are currently conducting progressive evaporation experiments. We slowly evaporate one litre of these samples (at the laboratory temperature of approximately 25 °C) and take subsamples of the brine and precipitate each time when approximately 100 mL of water has evaporated. Then, the salt is removed from the brine, which is allowed to evaporate further. Until now we have been able to analyse just one sample from the experiment with RM8, at the moment when it has evaporated about 75% of the water. In this subsample the δ^{37}Cl has decreased to –1.0‰ (from the original –0.5‰) and the coexisting precipitate has a value of –0.6‰. This first data point indicates that in this system very negative δ^{37}Cl values indeed can be reached.

4. CONCLUSIONS

We have shown that the measurement of stable chlorine isotopes can be a useful tool to determine the influence of a very saline spring on groundwater in its neighbourhood, and this information made it possible to prepare a preliminary conceptual model of the hydrogeological setting of the saline spring and its surroundings. The results obtained so far will be extremely useful for the sustainable management of the dilute groundwater resources in the surroundings of the saline spring 'Fonte da Pipa'/'Fonte da Bica'. We also showed that during precipitation, in salt pans, of terrestrial salt containing little K and Mg, fractionation of Cl isotopes is possible beyond the 0.5‰ that is expected from salt precipitation in seawater. Preliminary laboratory evaporation and precipitation of this type of brine and coexisting precipitate indicate that in such a system very negative δ^{37}Cl values could potentially be found.

ACKNOWLEDGEMENTS

REFERENCES

[1]   HARSVELDT, H.M., "Salt resources in the Netherlands as surveyed mainly by AKZO", Fifth Int. Symp. Salt (COOGAN, A.H., HAUBER, J., Eds), Hamburg, Germany (1980) 65–81.

[2]   BRAITSCH, O., Enstehung und Stoffbestand der Salzlagerstätten, Springer, Berlin (1962).

[3]   SCHMIDT, G., Terrestrische Freiluft-Salinen der Iberischen Halbinsel, Der Anschnitt **53** (2001) 80–87.

[4]   CALADO, C., BRANDÃO, J.M., Salinas interiores em Portugal: o casa das marinhas de Rio Maior, Geonovas **22** (2009) 45–54.

[5]   EGGENKAMP, H.G.M., KREULEN, R., KOSTER VAN GROOS, A.F., Chlorine stable isotope fractionation in evaporites, Geochim. Cosmochim. Acta **59** (1995) 5169–5175.

[6]   EASTOE, C.J., PERYT, T.M., PETRYCHENKO, O.Y., GEISLER-CUSSEY, D., Stable chlorine isotopes in Phanerozoic evaporites, Appl. Geochem. **22** (2007) 575–588.

[7]   TAN, H.B., MA, M.Z., MANG, X.Y, XU, J.X., XIAO, Y.K., Fractionation of chlorine isotope in salt mineral sequences and application: Research on sedimentary stage of ancient salt rock deposit in Tarim Basin and Western Qaidam Basin, Acta Petrol. Sinica **25** (2009) 955–962 (in Chinese with English abstract).

[8]   EGGENKAMP, H.G.M., MIDDELBURG, J.J., KREULEN, R., Preferential diffusion of ^{35}Cl relative to ^{37}Cl in sediments of Kau Bay, Halmahera, Indonesia, Chem. Geol. **116** (1994) 317–325.

[9]   ZBYSZEWSKI, G., MOITINHO DE ALMEIDA, F., Carta Geológica de Portugal, escala 1/50 000, Notícia Explicativa da Folha 26-D – Caldas da Rainha (1960).

[10]   MARQUES, J.M., et al., Assessment of recharge and flowpaths in a limestone thermomineral aquifer system using environmental isotope tracers (Central Portugal), Isot. Environ. Health Studies **46** (2010) 156–165.

ISOTOPES AND RADIONUCLIDES IN
ENVIRONMENTAL STUDIES

HIGH PRECISION STABLE ISOTOPE MEASUREMENTS OF CARIBIC AIRCRAFT CO$_2$ SAMPLES: GLOBAL DISTRIBUTION AND EXCHANGE WITH THE BIOSPHERE.

S.S. ASSONOV [a,b 1], C.A.M. BRENNINKMEIJER [a], T.J. SCHUCK [a], P. TAYLOR [b]

[a] Max Planck Institute for Chemistry,
  Mainz, Germany

[b] Joint Research Centre,
  Institute for Reference Materials and Measurements (JRC-IRMM),
  European Commission,
  Geel, Belgium

Abstract

In 2007–2009 JRC-IRMM, in collaboration with the project CARIBIC (Civil Aircraft for Regular Investigation of the atmosphere Based on an Instrument Container, www.caribic-atmospheric.com), conducted systematic measurements aimed to study the global distribution of CO$_2$ isotopic composition. A large data set for the upper troposphere–lowermost stratosphere and free troposphere was obtained. For the first time it is demonstrated how CO$_2$ isotope signals reflect global scale variability in air mass origin. Tight correlations observed arise either from stratosphere/troposphere mixing or from mixing of background air and air masses affected by CO$_2$ sources and sinks, over long distances and throughout the seasons. The high quality δ^{18}O(CO$_2$) data prove to be a useful tracer reflecting long range CO$_2$ transport and also CO$_2$ exchange with land biosphere and soils. The data provide a benchmark for future comparisons and are available for modelling studies.

1.   INTRODUCTION

The global carbon cycle is extraordinarily complex. The atmospheric CO$_2$ reservoir is coupled to those of vegetation, soils and oceans, and is increasingly burdened by emissions from the combustion of fossil fuel, while at the same time global temperature increases are concomitant with profound changes in vegetation, soils and oceans. To predict future atmospheric CO$_2$ concentrations and changes in the carbon cycle, CO$_2$ fluxes contributing to the global CO$_2$ cycle as well as processes controlling

---

[1] Presently at Institute for Geology, University of Köln, Germany; Email: assonov_sergey@yahoo.com

these fluxes must be understood and quantified. While direct anthropogenic CO_2 input (fossil fuel burning) is rather well quantified by inventories, indirect emissions (deforestation, change of land use, biomass burning) are estimated less precisely. Anthropogenic CO_2 fluxes altogether are much smaller than natural fluxes of photosynthesis, respiration, exchange with biosphere and atmosphere–ocean exchange. However, anthropogenic fluxes result in an atmospheric CO_2 increase that, if allowed to continue unabated, will cause a dangerous degree of climate change accompanied by a host of problems not yet foreseeable. Most changes will result in huge direct and indirect socioeconomical impacts and therefore research focused on better understanding the CO_2 cycle and future predictions is acutely needed. Though modelling is key approach for this purpose [1], models have large uncertainties thus necessitating further research. In particular, models are based on and can be tuned by the use of observational data only. There is a crucial need for observations of CO_2, and this need is addressed by many international programs that measure concentrations, fluxes, and, as in this case, isotopic composition. Isotopic composition measurements are particularly useful for better understanding and quantifying the processes involved. These include mainly photosynthesis, respiration, and, as shown here, the exchange of [18]O between the atmospheric CO_2 reservoir and the water in soils and plant leaves.

In 2007–2009 JRC-IRMM conducted systematic measurements aimed to study the global distribution of CO_2 isotope ratios. This was done in collaboration with the project CARIBIC coordinated by the Max Planck Institute for Chemistry, Mainz, Germany. CARIBIC (http://caribic-atmospheric.com) aims to investigate atmospheric chemistry, transport and composition by measuring many compounds (long and short lived trace gases and aerosols) and air mass characteristics using a large automated instrument container on board a Lufthansa Airbus A340–600 during regular passenger flights. The approach of using commercial aircraft as measurement platforms bridges the gap between ground based measurements and satellite observations. As a result of the extensive measurements at IRMM, there exist, for the first time, systematic data on the distribution of CO_2 isotope signals in the upper troposphere/lowermost stratosphere and tropical free troposphere. Here we demonstrate how these signals reflect global-scale variability in air mass origin. Tight correlations observed arise either from stratosphere/troposphere mixing or from mixing of well-mixed background tropospheric air with air masses affected by CO_2 sources and sinks, both over long distances and also over different seasons. The new data have initiated new findings and also provide a benchmark for future comparisons and modelling.

1.1. The approach

Many observational programmes worldwide aimed at greenhouse gas monitoring covering different geographical scales, from local to regional and global, are based on observation stations and towers at the earth surface. In nearly all cases,
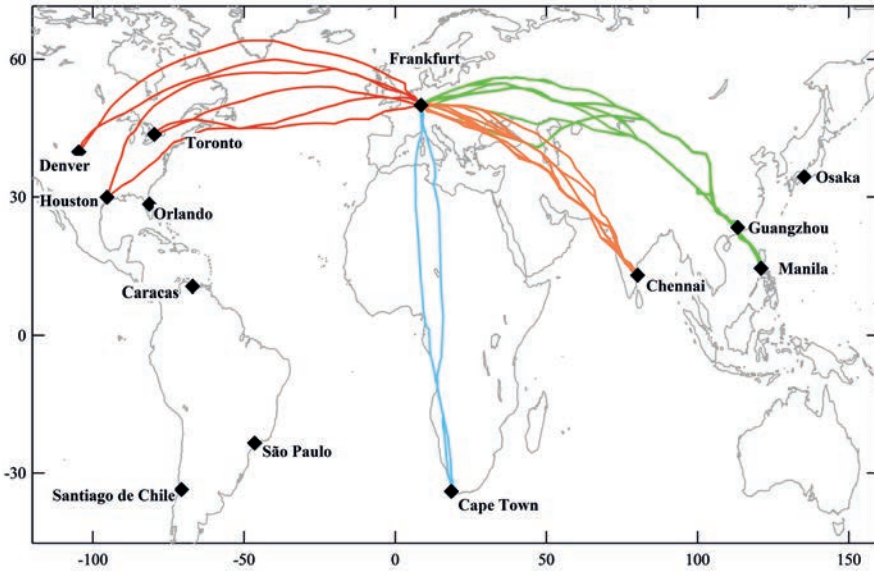
FIG. 1. CARIBIC–2 flight routes where sampling for isotope analysis took place.

planetary boundary layer air is probed. Most of the observation sites are close to CO_2 sources and sinks, whereas only a few stations are on mountains in the free tropo-sphere. There are also a few programmes using ocean ships (e.g. the Pacific Green-house Gas Measurements) and vertical profiling by small research aircraft (NOAA/ ESRL). In particular the use of research aircraft is expensive. Another problem is that global networks cover developing countries (particularly the tropics) only sparsely. Also, much less information is available at altitude, although satellite based obser-vations are continuously being refined. However, satellite observations need to be validated/calibrated by direct measurements. In view of all this, the 13th CO_2 Expert Meeting recommended [2] the promotion of programmes using commercial aircraft (altitudes of ~10 km) providing information about CO_2 and other GHG in back-ground air, in the free tropical troposphere and in the tropopause region, remote from CO_2 sources and sinks.

The project CARIBIC (http://caribic-atmospheric.com) started in 1997 and aims to study atmospheric chemistry and composition by measuring many compounds and species in the upper troposphere around the globe. The CARIBIC–2 (second phase) instrument container, operating onboard an Airbus A340–600 operated by Lufthansa (Frankfurt), conducts monthly flights from Frankfurt to North and South America, China, Japan, and India. The container includes an extended range of instrumentation (O_3, CO, NOx, H_2O and for other species; see http://caribic-atmospheric.com). Dur-ing the period of isotope measurements, the sampling system consisted of two collec-tor boxes each with 14 glass containers being filled with 10 L of air within a minute (giving ~14 km sampling resolution) at regular intervals.
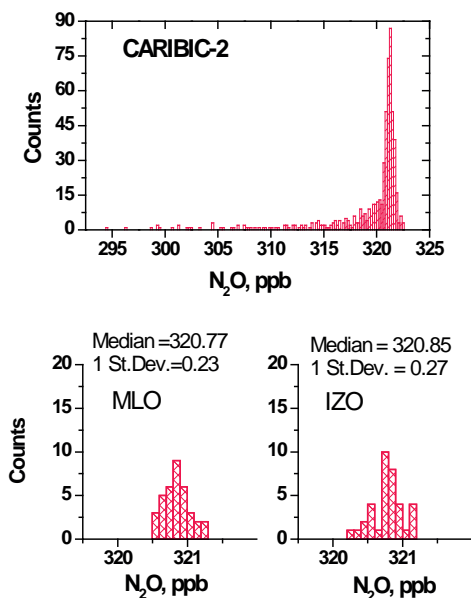
FIG. 2. Distribution of de-trended N_2O data for CARIBIC (left) and stations MLO and IZO (right).

1.2. Measurements.

CO$_2$ isotope analysis was performed on samples taken from April 2007 to Dec 2008 (flight routes shown in Fig. 1). After each flight, CO_2, N_2O, CH_4 and SF_6 were measured at the MPI and then air samples were sent for further analysis to other participating laboratories, including IRMM. Meteorological and other information for these samples are available. A special analytical system was built at IRMM (Geel, Belgium) to perform CO_2 isotope analysis in automated mode. About 500 precise, high quality isotope measurements were made, with a specific focus on data quality and calibration consistency. Special attention was paid to $\delta^{18}O$ (CO_2), as the potential of this signal to provide information on gross CO_2-biosphere exchange fluxes is currently being explored.

2. RESULTS

2.1. Distribution and variability of CO$_2$ isotope signals due to stratosphere/ troposphere mixing

Although air masses are rather well mixed at cruise altitude, a significant variability has been observed both in CO_2 concentrations and isotopic composition. One

cause for observed variability is stratosphere/troposphere mixing. For the interpretation of the CO_2 data in the upper troposphere/lowermost stratosphere mixing region we have developed [3] a new quantitative tracer of mixing stratosphere/troposphere proportions, namely the N_2O distribution. Histograms of detrended N_2O data (i.e. corrected for the N_2O increase) demonstrate a compact peak shape corresponding to tropospheric air masses, with a continuous tailing indicating a stratospheric contribution (Fig. 2 left). The fact that the width of this main N_2O peak agrees well with the N_2O distribution for ground stations in the Northern Hemisphere (Fig. 2 right) means that one can apply N_2O data as a filter to separate signals of purely tropospheric air masses from those affected by stratosphere/troposphere mixing.

By using the N_2O distribution, we demonstrated [3] a regular behaviour of the isotope ratios in the region studied. Namely, CO_2, $\delta^{13}C$ (CO_2) and $\delta^{18}O$ (CO_2) plotted vs N_2O demonstrate (Fig. 3) triangular mixing trends towards the stratospheric component (low N_2O); the latter behaves as a single endmember. Purely tropospheric air masses $(N_2O \geq 320.0$ ppbv) demonstrate large variability in isotopic composition due to seasonality and spatial variability of tropospheric air masses. This variability propagates into the mixing region.

The 'regular' behaviour for $\delta^{18}O$ (CO_2) (Fig. 3) is particularly impressive. The upper trend line indicates a contribution of old stratospheric air (given as the black line in Fig. 3). In the stratosphere $\delta^{18}O$ (CO_2) is modified/increased by reaction between CO_2 and O (^1D) from stratospheric ozone. Influx of such $\delta^{18}O$ enriched stratospheric CO_2 into the troposphere is presently one of the major unknowns in models describing the isotopic composition of atmospheric CO_2 [4]. While most tropospheric air lies below this line, some data points for purely tropospheric air $(N_2O > 320$ ppm) are above this line. These samples contain a contribution of air from the Southern Hemisphere (SH), where $\delta^{18}O$ (CO_2) is systematically higher than in the Northern Hemisphere (NH). Our data also demonstrate that SH air does not take
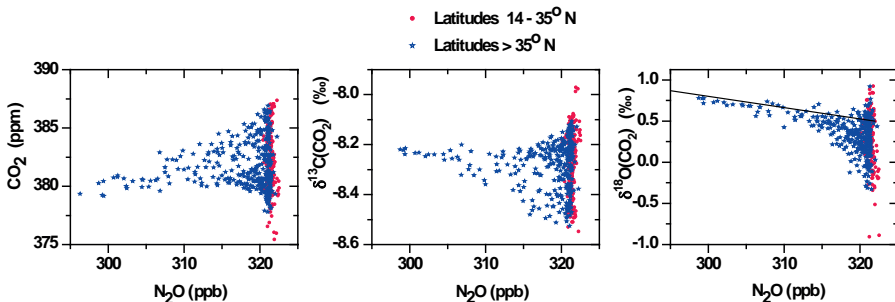
FIG. 3. Stratosphere/troposphere mixing observed for CO_2, $\delta^{13}C$ (CO_2) and $\delta^{18}O$ (CO_2) for CARIBIC.

part in stratosphere/troposphere mixing in the NH which takes place predominantly at latitudes >35 °N.

2.2. Distribution of CO_2 isotope signals in the free tropical troposphere and upper troposphere

Next we analyse the processes responsible for CO_2 isotope distribution in the upper troposphere and free tropical troposphere. As the CARIBIC samples discussed here were taken at latitudes ≥ 14 °N, we limit our analyses to the Northern Hemisphere. We conclude [3] that the measured signals demonstrate a clear seasonality and agree well with the data of remote stations in the NH tropics (Fig. 4), the region where tropical air is uplifted and transported polewards (Hadley circulation). Notably, the CARIBIC data do not show a latitudinal gradient over latitudes 14 °N to 55 °N, in agreement with the circulation pattern. Our data agree well with CO_2 concentration data and their interpretation as published by our colleagues from the JAL CONTRAIL project in Japan (Ref. [3] and references therein).

However, the tropospheric CARIBIC data show larger signal variability than those of tropical NH stations. One reason is that data are plotted for background
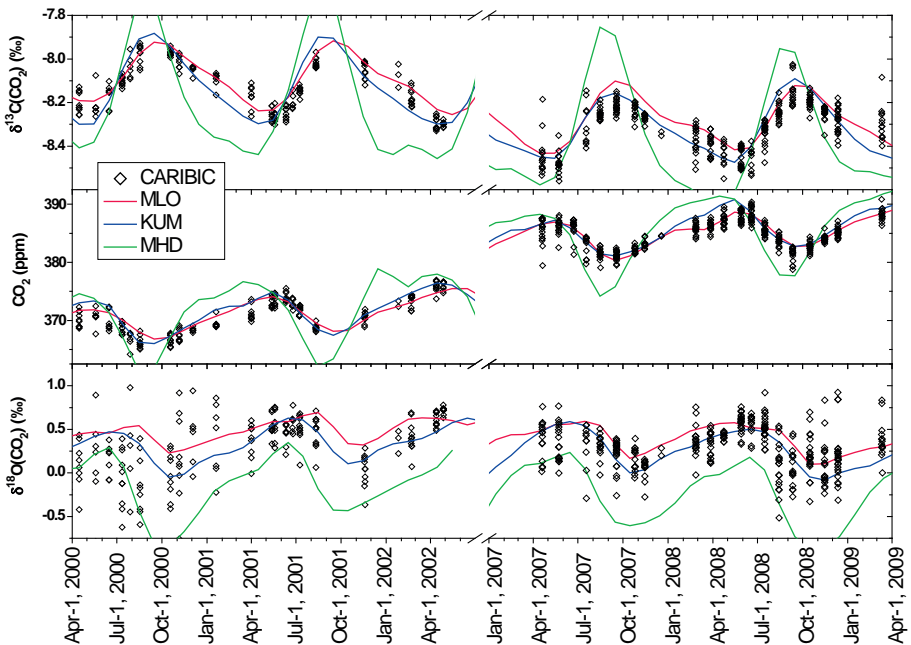
FIG. 4. CARIBIC data together with data for NH stations MLO, KUM, IZO and MHD (data from NOAA). The lines give inter-annual trend at KUM.

February to April 2008

Y=7.82(0.45)*X -28.6(1.2)

August to October 2008

Y=6.46 (0.45)*X -25.1(0.5)
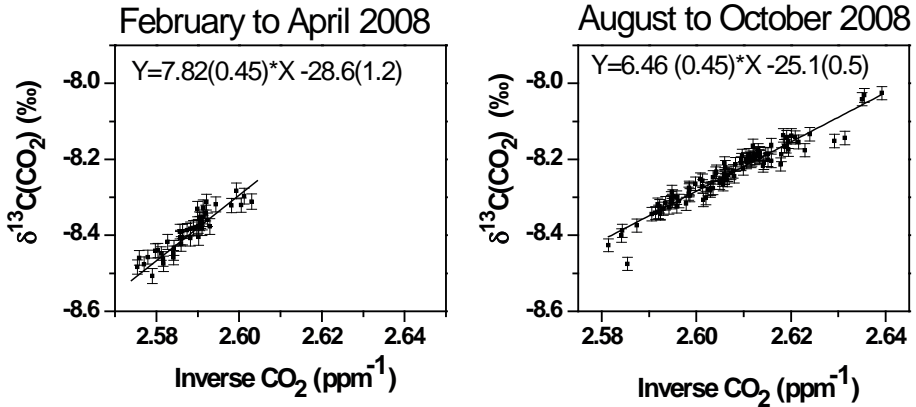
FIG. 5. $\delta^{13}C(CO_2)$ measured over large distances and over several months correlate with the inverse of CO_2 concentrations. Trend lines for different seasons have different slopes.

stations where only homogeneous background air masses are sampled. In contrast, CARIBIC being a moving platform, it sampled a wide range of air masses. Secondly, the plotted stations' data are monthly averages which have already reduced variability. Despite the large distance sampled by CARIBIC and the large temporal range, CARIBIC $\delta^{13}C$ (CO_2) values always demonstrate very tight correlations with CO_2 (Fig. 5). Although the link between CO_2 and $\delta^{13}C$ (CO_2) due to source and sink processes is well known, observing such tight correlations over up to 8000 km distance [3] is surprising indeed. The fact that different seasons demonstrate different slopes of relationships implies different balance of CO_2 sources and sinks over seasons. We also note that such correlations give an independent check for the data quality and absence of sampling artifacts.

One more reason for signal variability is that CARIBIC at times crossed fast uplifted plumes of polluted air and/or air being recently in contact with the earth's surface. This is mostly visible in the variability of $\delta^{18}O$ (CO_2) (Fig. 4) which is sensitive to CO_2 oxygen isotope exchange with water pools of the land biosphere and soils. In particular, a systematic behaviour of $\delta^{18}O$ (CO_2) has been observed in the Indian monsoon plume crossed in 2008 (see below).

2.3. Use of CO_2 data in order to constrain CO_2 exchange fluxes in the Indian summer monsoon

In 2008 CARIBIC flights crossed the Indian summer monsoon plume. Increases in CH_4, N_2O and SF_6 were measured in the uplifted plume, combined with lower CO_2 values. This allowed the estimation of CH_4, N_2O and CO_2 fluxes from the Indian subcontinent in June to September [5]. Negative $\delta^{18}O$ (CO_2) shifts were found,
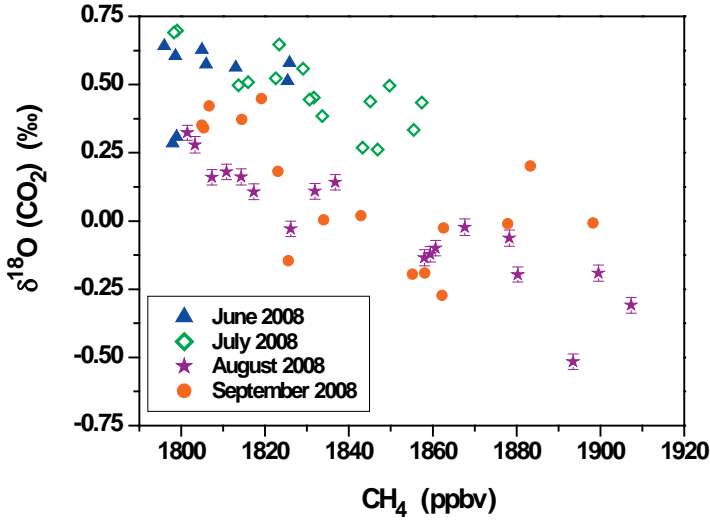
FIG. 6. Correlation between increased levels of methane and negative $\delta^{18}O(CO_2)$ shifts observed during the SW summer monsoon over the Indian region.

correlating with the increase in CH_4 (Fig. 6). That correlation undoubtedly indicates the surface origin of the $\delta^{18}O$ (CO_2) signals.

It is known that $\delta^{18}O$ of air CO_2 is determined by exchange with water pools. The exchange with plant leaves and soils is particularly fast. Plants exchange CO_2 with the atmosphere much faster than net uptake by photosynthesis. Soils and plants also respire CO_2. These gross natural CO_2 fluxes, being sensitive to temperature and climate changes, are difficult to constrain by direct measurements. However, gross natural fluxes may be changed in response to change in atmospheric precipitation and hydrological conditions as well as climate change. This makes understanding and constraining gross fluxes important.

Based on $\delta^{18}O$ (CO_2) shifts observed we develop a formalism linking CO_2-biosphere exchange and respiration fluxes (gross natural fluxes) to the net CO_2 flux. Besides a box model based on the formalism, we have to select boundary conditions such as composition of representative background air masses during the summer monsoon, temperature and $\delta^{18}O$ of precipitation. Despite the large population of India and importance of the monsoon for the region, it appears that $\delta^{18}O$ data of precipitation are scarce, being limited to the IAEA station in Delhi and several case studies. There are no centrally coordinated data for 2008. However, based on some assumptions and reasonably selected boundary conditions, we are able to estimate the ratio [CO_2-exchange & respiration flux]/[net CO_2 uptake flux], e.g. the value for August is estimated around 10. The $\delta^{18}O$ data of precipitation form the largest source of uncertainty in our estimation.

3. CONCLUSIONS

- The combined effort by the Max Planck Institute for Chemistry and the JRC-IRMM has resulted in a unique CO_2 isotope data set for the stratosphere/troposphere mixing region and free tropical troposphere with ~1 month resolution for the period April 2007 through January 2009. These high quality data are available for modelling as well as providing a benchmark for comparison of future atmospheric composition and its changes.

- First analyses of the CARIBIC CO_2 isotope data as based on statistical distribution of signals, tracer–tracer correlations and other available information [3] has demonstrated major reasons for the signal variability. For the first time it is demonstrated that global scale variability in air mass origin are reflected by $\delta^{13}C$ (CO_2) and $\delta^{18}O$ (CO_2). Besides the stratosphere/troposphere mixing, the variability arises from different degrees of mixing of background air with air masses affected by CO_2 sources and sinks. Tight correlations are observed over distances up to 8000 km and also over different seasons, which independently proves a high data quality.

- During the project, several scientific findings were made. Specifically the N_2O distribution is proposed as a quantitative tracer of stratosphere/troposphere mixing and air origin; $\delta^{18}O$ (CO_2) is demonstrated to behave as a sensitive tracer of air mass origin and transport; the approach of how to constrain CO_2-land biosphere exchange & respiration fluxes based on $\delta^{18}O$ (CO_2) data of large uplifted plumes is under development.

ACKNOWLEDGEMENTS

REFERENCES

[1]   INTERGOVERNMENTAL PANEL ON CLIMATE CHANGE, Climate Change 2007: The Physical Science Basis — Contribution of Working Group I to the Fourth Assessment Report of the Intergovernmental Panel on Climate Change, Cambridge University Press, Cambridge (2007).

[2]   WORLD METEOROLOGICAL ORGANIZATION, "Expert Group Recommenda-
        tions", 13th WMO/IAEA Meeting of Experts on Carbon Dioxide Concentration and
        Related Tracers Measurement Techniques, Boulder, Colorado, USA, 19–22 Septem-
        ber 2005, WMO/GAW (2006), http://www.wmo.ch/web/arep/gaw/gawreports.html

[3]   ASSONOV, S.S., BRENNINKMEIJER, C.A.M., SCHUCK, T.J., TAYLOR, P., Anal-
        ysis of ^{13}C and ^{18}O isotope data of CO_2 in CARIBIC aircraft samples as tracers of
        upper troposphere/lower stratosphere mixing and the global carbon cycle, Atmos.
        Chem. Phys. **10** (2010) 8575–8599.

[4]   CIAIS, P., et al., "Remarks on the use of ^{13}C and ^{18}O isotopes in atmospheric CO_2 to
        quantify biospheric carbon fluxes", Stable Isotopes and Biosphere–Atmosphere In-
        teractions (FLANAGAN, L.B., EHLERINGER, J.R., PATAKI, D.E., Eds), Elsevier,
        San Diego (2005) 235–267.

[5]   SCHUCK, T.J., et al., Greenhouse gas relationships in the Indian summer mon-
        soon plume measured by the CARIBIC passenger aircraft, Atmos. Chem. Phys. **10** 8
        (2010) 3965–3984.

AEROSOL CHARACTERIZATION AT THE WMO-GAW STATION OF MT. CIMONE (2165 m a.s.l.) BY ^{7}Be, ^{210}Pb AND PM$_{10}$

L. TOSITTI [a], E. BRATTICH [a,b], G. CINELLI [a,b]

[a] Dipartimento di Chimica 'Giacomo Ciamician',
Laboratorio di Chimica Ambientale e Radioattività,
Università di Bologna,
Bologna, Italy

[b] Dipartimento di Scienze della Terra e Geologico-Ambientali,
Università di Bologna,
Bologna, Italy

Abstract

Measurements of airborne radionuclides ^{7}Be, ^{210}Pb and PM$_{10}$ have been routinely carried out together with aerosol mass concentration at the WMO-GAW station of Mt. Cimone (Northern Apennines, Italy) with the aim of obtaining basic information on aerosol behaviour at this site. Several years of data (the experimental activity was started in January 1998) are presented and discussed in this paper. Aerosol collection is carried out by filtration with a high volume PM$_{10}$ sampler for 48 hours. Activities of ^{7}Be and ^{210}Pb were measured by non-destructive g-ray spectrometry and aerosol mass concentration was determined gravimetrically. A distinct seasonal cycle is observed for ^{7}Be, ^{210}Pb and PM10, with maxima in the summer and minima in the winter. The opposite trend is observed for the activity ratio ^{7}Be/^{210}Pb, used as an indicator of vertical transport. Variability of the three parameters at this site is discussed by means of statistical tools such as t-test analysis classification as well as by back trajectory approach.

1. INTRODUCTION

The importance of environmental radionuclides in the study of atmosphere and climate dynamics has been often emphasized in the course of the last decades, as well documented in the Ref. [1]. Though nowadays the radiotracer method constitutes a niche approach to the comprehension of the planetary complexities, it still deserves attention as it provides a powerful tool for the basic characterization of transfer and transformation mechanisms occurring both at local and large scale. For this reason several radionuclides, namely ^{7}Be, ^{210}Pb, ^{222}Rn and others, are included among the key atmospheric components that are routinely monitored within the WMO-GAW network [1].

Though this is not the suitable place for an historical reconstruction of radiotracer literature in many geophysical as well as radioprotection studies, it is worth noting the steady production of papers in which the environmental radiotracers have been used with the role of quantitative descriptors. Examples can be found in Refs. [2–4].

In this paper we are going to present a brief compendium of the research activity carried out by the University of Bologna in this field since the 1990s. In particular, we will introduce the long term monitoring activity of ^{7}Be, ^{210}Pb in the PM$_{10}$ fraction at Mt. Cimone station, a WMO–GAW station in the Northern Italian Apennines hosting a complex activity of atmospheric research.

2. MATERIAL AND METHODS

2.1. Experimental

^{7}Be, ^{210}Pb and aerosol mass loading in the form of PM$_{10}$ have been measured at Mt. Cimone station since the early 1990s but measurements became regular only since 1998, following the acquisition of a PM$_{10}$ high volume sampler. Since then, sample collection has been accompanied by the acquisition of the mentioned parameters among which the PM$_{10}$ mass loading i.e. one of the standard parameterizations for airborne particulate, ^{7}Be and ^{210}Pb. The choice for PM$_{10}$ sampling relies on the well known size distribution of the radionuclides considered, which tends to populate the fine fraction (< 1.0 mm). Nevertheless, the cutoff chosen allows for the collection of a consistent part of the coarse fraction of aerosols, which may host primordial radionuclides typically found in mineral components, such as soil re-suspension or Saharan dust, detectable by HPGe γ-spectrometry.

At the Mount Cimone station, aerosol sampling is carried out with a time resolution of about 48 hours by means of a Thermo–Environmental PM$_{10}$ high volume sampler (Thermo Environmental Instruments Inc. — Flow rate = 1.13 m^3/min) and using a rectangular glass fibre filter (20.3 cm × 25.4 cm with an effective exposure area of about 407 cm^2). The PM$_{10}$ sampler collects airborne particulate matter with a mean aerodynamic diameter lower than 10 mm that carries the ^{7}Be and ^{210}Pb submicronic particles [5, 6]. ^{7}Be and ^{210}Pb are determined by nondestructive high resolution γ-spectrometry of aerosol samples at 477.6 and 46.7 keV, respectively, using a n-type intrinsic Hyper Pure Ge detector (relative efficiency = 38%; full width at half maximum = 2.03 at 1332 keV). Spectra are processed with a specific software package (GammaVision–32, Ortec). The filter sample is analysed every two days. Radionuclide concentrations are analysed at the Laboratory of Environmental Radiochemistry of Bologna University. The sampled volume amounts to approximately 3250 m^3. The samples are conditioned at a constant temperature (20°C) and relative humidity (30%) in order to determine the aerosol mass loading.

2.2. Measurement Site

Mt. Cimone (44°12' N, 10°42' E) is the highest peak of the Northern Apennines (2165 m a.s.l.), dividing the north of Italy from central Italy and the Mediterranean basin. Besides having a 360° free horizon and being far enough from cities and industrialized areas, MTC has an elevation such that the measurement station 'O. Vittori' lies above the planetary boundary layer during most of the year [6]. Thus the measurements of atmospheric compounds carried out at this site can be considered representative for the south-European free troposphere [7, 8], even though an influence of the innermost layer cannot be completely ruled out, in particular during warm months as for the increased vertical mixing (thermoconvection) and mountain and valley breeze regime [8, 9]. Moreover, MTC can be affected by intense cyclogenic activity often originating in the nearby Gulf of Genoa area [10, 11].

For these reasons, the measurement site can represent a suitable location to investigate the influence of regional and long range transport of polluted air masses on the background free troposphere. Moreover, as being the first high mountain ridge met by North African air masses moving to Italy and Central Europe, measurements activities at MTC can be useful tools to evaluate and to study the impact of mineral dust transport on the properties of atmospheric aerosol [12]. Several scientific programmes have been established at MTC with the scope of studying the chemical physics characteristics of the aerosol [13, 14].

Mt. Cimone station is a WMO–GAW station due to the long term activity of the Italian Air Force in charge for the meteorological service in Italy and responsible
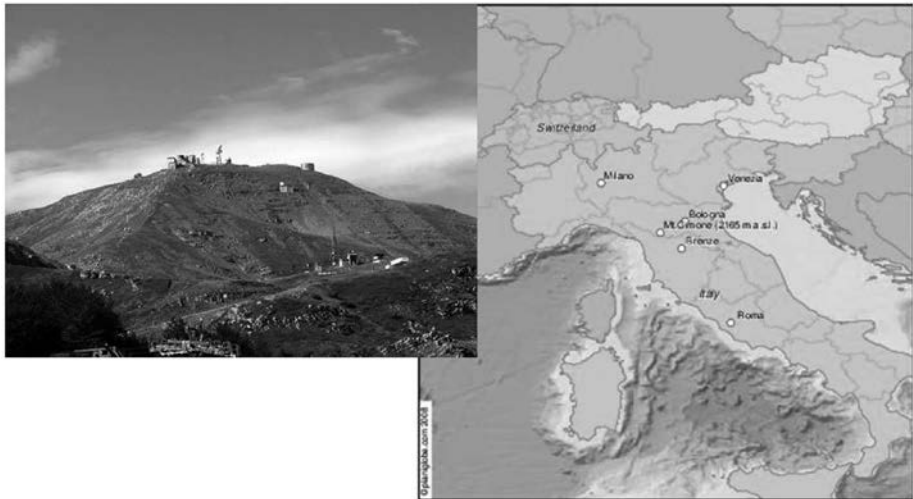
FIG. 1. Photo and map of Mount Cimone.
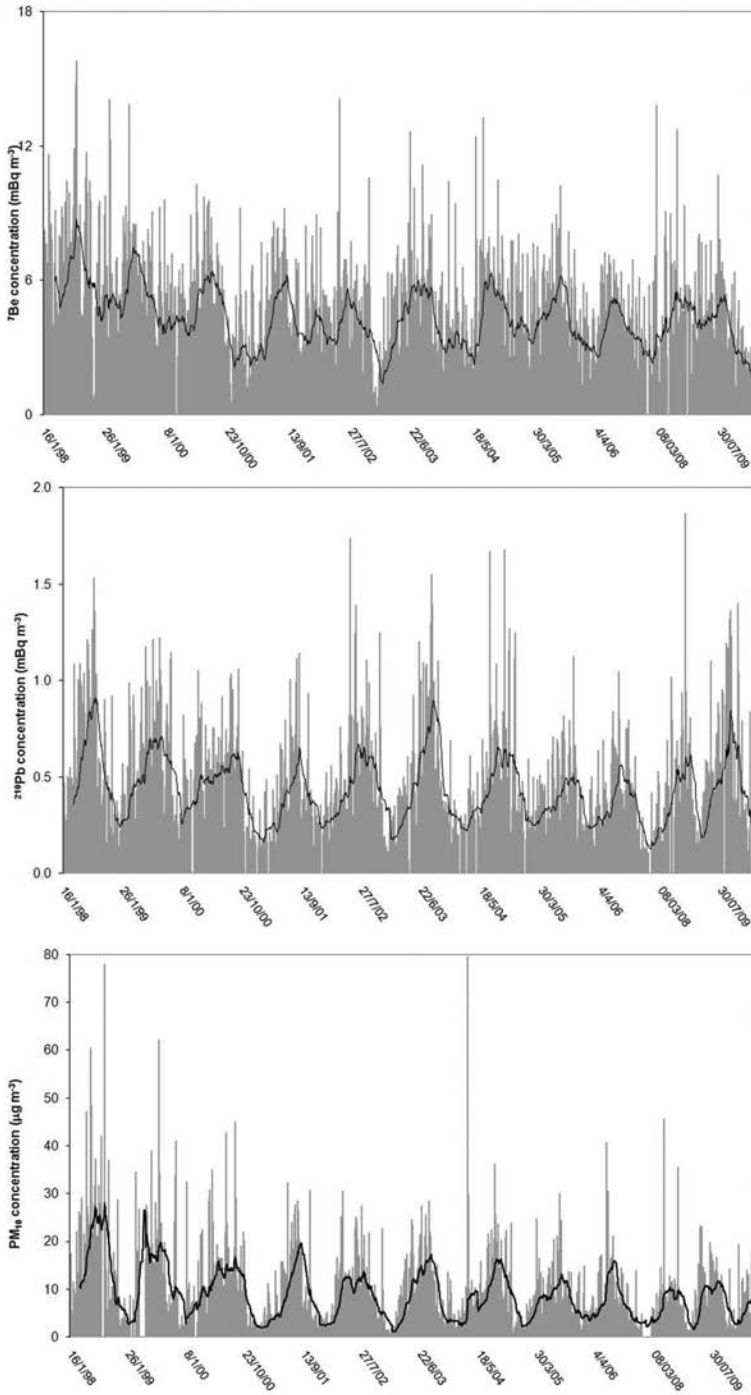
FIG. 2. Time series of ^7Be (mBq/m³), ^{210}Pb(mBq/m³) and PM_{10}(mg/m³).

for the facility which hosts and integrates the research activity led by the Institute of Atmospheric and Ocean Science of the National Council of Research (ISAC–CNR). Besides meteorology, the Italian Air Force — the general bureau for meteorology — manages the collection of atmospheric CO_2 data presently constituting the longest time series of this fundamental greenhouse gas in Europe, dating back to 1979. It is to note that in the past this station served also as one of the Italian monitoring sites for weapon test fallout, an activity discontinued in 1990s. Moreover, the site is considered the most representative WMO–GAW weather station in Italy [15].

3.   RESULTS

In the Fig. 2, time series of ^{7}Be, ^{210}Pb and PM_{10} are shown. We can notice a distinct seasonal cycle for ^{7}Be, ^{210}Pb and PM_{10}, with maxima in the summer and minima in the winter.

Peaks of Beryllium–7 are often associated with downward transport from the upper troposphere or from the stratosphere. This phenomenology, now defined as Stratosphere to Troposphere Exchange (STE), is able to affect ozone budget in the troposphere, and is still a matter of investigation since its mechanism has not been thoroughly elucidated. Nevertheless, research activities carried out at Mt. Cimone within the EU projects VOTALP and STACCATO [7, 9, 16, 17] allowed the discovery that STE events are not limited to the spring–summer period as previously believed, but are scattered throughout the year, at least in the area investigated. In addition a stratospheric index based on the use of ^{7}Be, relative humidity and ozone was introduced in order to quickly identify stratospheric air masses through simultaneous data collected on site [18].

4.   CONCLUSIONS

Vertical motion is characterized by both downward and uplift motion, in order to fulfill hydrostatic conditions in the troposphere. The concurrence of both transports seems to be very well captured by the use of ^{7}Be/^{210}Pb ratio [4].

Other studies in progress concern the identification of transport from Saharan deserts and from contaminated areas such as the Po valley and eastern European areas. In both cases there is a remarkable influence on ozone budget, but in opposite directions: a decrease in the former case and an increase in the latter. We will take advantage of radionuclides such as ^{210}Pb to discriminate between these phenomenologies, which are both characterized by a mass loading increase, but in order to have a more quantitative point of view, massive use of back trajectories will be carried out together with multivariate models. In the meantime collection of samples and their

analysis by HPGe will be continued in order to enlarge the time series and the database available.

ACKNOWLEDGEMENTS

REFERENCES

[1]   WORLD METEOROLOGICAL ORGANIZATION, 1st International Expert Meeting on Sources and Measurements of Natural Radionuclides Applied to Climate and Air Quality Studies, Gif sur Yvette, France, 3–5 June 2003, WMO, Global Atmosphere Watch No. 155, Geneva, Switzerland (2004).

[2]   PAATERO, J., HATAKKA, J., Source areas of airborne ^{7}Be and ^{210}Pb measured in Northern Finland, Health Physics **79** 6 (2000) 691–696.

[3]   LIU, H., JACOB, D.J., DIBB, J.E., FIORE, A.M., YANTOSCA, R.M., Constraints on the sources of tropospheric ozone from ^{210}Pb-^{7}Be-O$_3$ correlations, J. Geophys. Res. **109** (2004) 15.

[4]   LEE, H.N., TOSITTI, L., ZHENG, X., BONASONI, P., Analyses and comparison of variations of ^{7}Be, ^{210}Pb and ^{7}Be/^{210}Pb with ozone observations at two Global Atmosphere Watch stations from high mountains, J. Geophys. Res. **112** (2007) 11.

[5]   PAPASTEFANOU, C., IOANNIDOU, A., Aerodynamic size association of ^{7}Be in ambient aerosols, J. Environ. Radioactivity **26** (1995) 273–282.

[6]   WINKLER, R., DIETL, F., FRANK, G., THIERSCH, J., Temporal variation of ^{7}Be and ^{210}Pb size distributions in ambient aerosol, Atmos. Environ. **32** (1998) 983–991.

[7]   BONASONI, P., et al., Background ozone variations at Mt. Cimone Station, Atmos. Environ. **34** (2000) 5183–5189.

[8]   FISCHER, H., et al., Ozone production and trace gas correlations during the June 2000 MINATROC intensive measurement campaign at Mt. Cimone, Atmos. Chem. Phys. **3** (2003), 725–738.

[9]   CRISTOFANELLI, P., et al., Anomalous high ozone concentrations recorded at a high mountain station in Italy in summer 2003, Atmos. Environ. **41** (2007) 1383–1394.

[10]   BUZZI, A., GIOVANELLI, G., NANNI, T., TAGLIAZUCCA, M., Study of high ozone concentrations in the troposphere associated with lee cyclogenesis during AL-PEX, Beit. Phys. Atmos. **57** (1984) 380–392.

[11]   DAVIES, T.D., SCHUEPBACH, E., Episode of high ozone concentrations at the earth's surface resulting from transport down from the upper troposphere/lower stratosphere: A review and case studies, Atmos. Environ. **28** (1994) 53–68.

[12]   MARINONI, A., et al., Continuous measurements of aerosol physical parameters at the Mt. Cimone GAW Station (2165 m asl, Italy), Sci. Total Environ. **391** (2008) 241–251.

[13]   BALKANSKI, Y., et al., The Mt. Cimone, Italy, free tropospheric campaign: Principal characteristics of the gaseous and aerosol composition from European pollution, Mediterranean influences and during African dust events, Atmos. Chem. Phys. **3** (2003) 1753–1776.

[14]   MARENCO, F., et al., Characterization of atmospheric aerosols at Monte Cimone, Italy, during summer 2004: Source apportionment and transport mechanisms, J. Geophys. Res. **111** (2006).

[15]   WORLD METEOROLOGICAL ORGANIZATION — GLOBAL ATMOSPHERIC WATCH, Report on the measurements of atmospheric turbidity in BAPMo N, Report N 94 (1994) 1–73.

[16]   BONASONI, P., et al., Stratosphere-troposphere exchanges: Case studies recorded at Mt. Cimone during VOTALP project, Phys. Chem. Earth (C) **24** 5 (1999) 443–446.

[17]   CRISTOFANELLI, P., et al., A 6-year analysis of stratospheric intrusions and their influence on ozone at Mt. Cimone (2165 m above sea level), J. Geophys. Res. **111** (2006).

[18]   CRISTOFANELLI, P., et al., Stratospheric intrusion index (SI^2) from baseline measurement data, Theor. Appl. Climatol. **97** (2009) 317–325.

BEHAVIOUR OF U-SERIES RADIONUCLIDES IN AN ESTUARY AFFECTED BY ACID MINE DRAINAGE AND INDUSTRIAL RELEASES

A. HIERRO [1], J.P. BOLÍVAR, F. VACA
Department of Applied Physics,
University of Huelva,
Huelva, Spain

Abstract

The estuary formed by the Tinto and Odiel rivers is an ecosystem of great interest because it is seriously affected by the acid mine drainage (AMD) produced by the high mining activity in the watersheds of these rivers, generating in their waters an extremely low pH (2.5–3.5), and consequently high concentrations of heavy metals and natural radionuclides in dissolution. Secondly, in their estuary there is a large chemical industrial complex, and in particular two phosphoric acid production plants, which use a sedimentary phosphate rock from Morocco as raw material containing at approximately 1.5 Bq/g of U-series radionuclides, which produce annually about 2.5–3 millions of tonnes of a byproduct, called phosphogypsum (PG). PG contains high concentrations of some U-series radionuclides as ^{226}Ra (650 Bq/kg), ^{210}Pb–^{210}Po (600 Bq/kg) or ^{230}Th (450 Bq/kg). Seventeen sampling stations along the end of these rivers and this estuary were selected to study the behaviour of U-series radionuclides in the recent surface sediments and its waters. The most relevant results show a non-conservative behaviour of U-isotopes, precipitating in the zone where large pH changes (3–5) are produced. This behaviour is different from the majority of typical estuaries where only salinity changes are produced, and therefore, a conservative behaviour of uranium is observed.

1.   INTRODUCTION

Estuaries are zones of complex interaction between fluvial and marine processes, where there are large mass exchanges, and big changes in salinity, nutrients, sedimentary conditions and living organisms. These ecosystems may act as geochemical traps of pollutants as heavy metals and radionuclides. The use of radioactive tracers is a valuable tool to analyse the transfer mechanisms between the different system phases: bed sediment–dissolution–particulate in suspension [1, 2].

The estuary formed by the Tinto and Odiel rivers is an ecosystem of great interest due to its being very conditioned by two hydro chemical facts. The first one comes

---

[1]   Present address: Department of Applied Physics, Campus El Carmen, University of Huelva 21071, Spain.

from the fact that both rivers are seriously affected by acid mine drainage (AMD) from long term mining activities developed in the Iberian Pyrite Belt, which produce in these rivers the transport of high amounts of heavy metals and radionuclides due to their extremely low pH (2.5–3.5) [3, 4]. Secondly, in their mouths there is a large industrial complex which includes five phosphate rock processing plants that produce annually about 2.5 million tonnes of a by-product called phosphogypsum (PG), containing enhanced U-series radionuclide concentrations (about 100 Bq/kg of ^{238}U, 650 Bq/kg of ^{226}Ra or 450 Bq/kg of ^{230}Th). Until 1998, about 20% of the generated PG was discharged directly into the estuarine waters, while the remaining 80% was pumped in suspension with seawater (20% PG plus 80% seawater) to be disposed in large piles located on the Tinto river salt marshes. These facts explain that estuary of Huelva is one of the most polluted estuarine systems in the world [5, 6].

It has been demonstrated that hydro chemical characteristics of the water in this estuary suffer two mixture processes: firstly, the salt induced mixture process of water masses. A strong tidal influence controls this mixing process and it has been extensively studied by measuring the changes in the salinity of the mixing water. Specifically the process follows the mixture between seawater (pH over 8 and chlorinity above 21 g/L) and estuarine water (with pH around 6.0–7.0 and chlorinity average over 10–15 g/L). This process is located in Padre Santo and Punta Umbría Channels, but can reach the upper sectors of the estuary (Fig. 1). The second is the pH induced
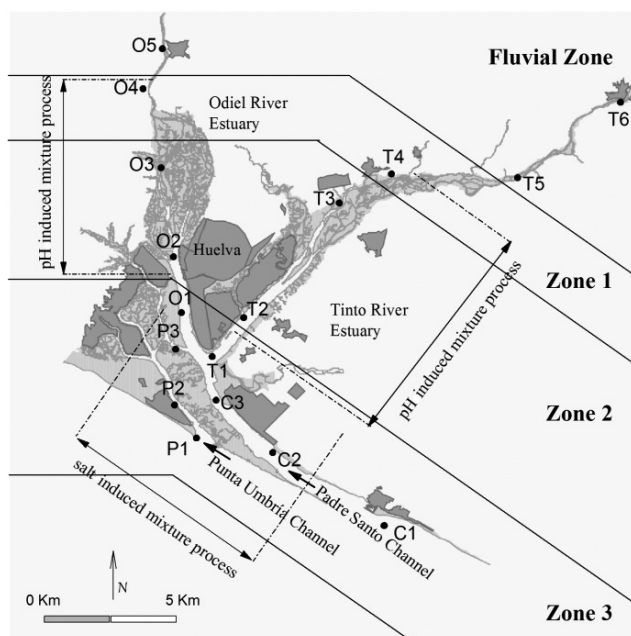
FIG. 1. Map of the estuary of the Tinto and Odiel rivers with the zones and sampling points.

mixture process. This neutralization process results from the mixing of estuarine water (pH= 6.0–7.0) and the fluvial water (pH < 3) containing very high concentrations of dissolved materials, including metals and radionuclides. This neutralization process by dilution of water is restricted to the estuarine areas of both rivers and produces a positive gradient in the pH with a strong directionality outwards from the system [7]. Consequently, the increase of pH leads to the precipitation of heavy metals and radionuclides onto the particulate material.

In previous works [7], these hydrochemical properties of the waters have permitted the division of the estuary into several zones as a consequence of the mixture processes. The fluvial zone is characterized by very low pH due to the acid mine drainage (pH = 2.5–3.5). Zone 1 is the sector where the pH value increases from 2.4 to 4.5 and chlorinity does not rise above 3 g/L (very low content of seawater). Here the processes of neutralization of water is produced in absence of salt-induced mixture giving mainly the precipitation of sulphates, and, as consequence, the scavenging of many heavy metals from the water also occurs. During this process an oxidation of the Fe^{2+} dissolved in the river water into Fe^{3+} takes place, consuming acidity through the following reaction [8]:

$$4Fe^{2+} + O_2 + 4H^+ \rightarrow 4Fe^{3+} + 2H_2O$$
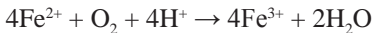
In zone 2 the pH ranges from 4.5 to approximately 7.0, and the chlorinities range from 4 to 15 g/L, close to seawater value. Both parameters have a lineal relation due to the neutralization coming from direct dilution of the water from zone 1 with marine water (pH > 7). Zone 3, which is characterized by slightly basic pH water (above 7.0 and similar to seawater), is where the salt induced mixture process typical of estuarine systems takes place and some dissolved elements such as Cu increase in concentration due to the remineralization produced by saline shock.

Taking into account these facts, the main objective of this work has been to analyse and study the spatial distribution of uranium isotopes in the water masses of the estuary conformed by the Odiel and Tinto Rivers, and to analyse the effect of the estuarine water mixing in it.

2. MATERIALS AND METHODS

2.1. Sampling

Seventeen sampling locations were selected to study the uranium behaviour of this system along the Tinto river estuary, the Odiel river estuary, the Punta Umbría Channel, and the Padre Santo Channel (Fig. 1). We will discuss in this work the sampling campaign done in March 2008 (winter) with low tide. In each sampling station 20 L of superficial water was collected in the centre of the riverbed, and the main

physico-chemical parameters (temperature, pH, electrical conductivity and redox potential) were measured in situ. In addition to the water samples, superficial sediment samples were collected in sediment traps.

These sampling points have been taken in the different zones previously discussed in section 1. The sampling points T6, T5 and O5 belong to the fluvial zone; the points T4 and O4 are included within zone 1; the sampling points O3, O2, T3 and T2 are in zone 2 and the points O1, T1, C1, C2, C3, P1, P2 and P3 belong to zone 3.

2.2. Radionuclide determinations

Alpha emitting radionuclides of U-isotopes were determined by alpha particle spectrometry using ion implanted silicon detectors in geometry with 25% absolute efficiency. Alpha emissions were directly identified in the spectra, ranging the FWHM of the obtained peaks between 30–40 keV [9]. A sequential well established radiochemical method based on extraction chromatography (UTEVA resins) was applied to isolate the radioelements (U, Th and Po) [10].

3.   RESULTS AND DISCUSSION

As we previously commented, the pH, conductivity and chlorinity are the most important parameters used to justify the zoning of the estuary previously discussed
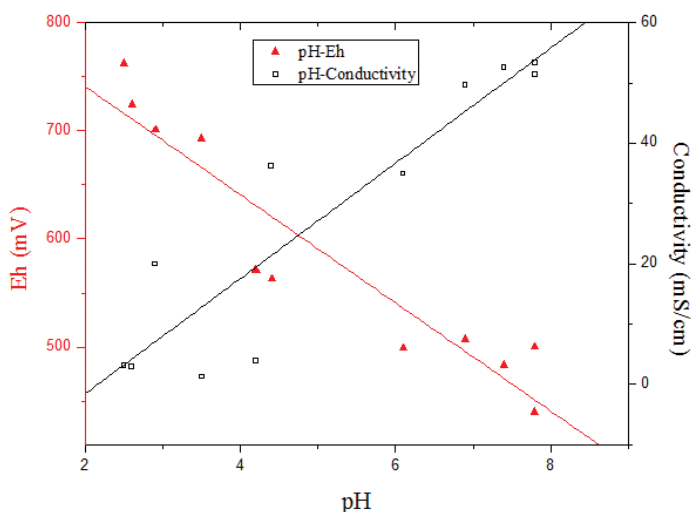
FIG. 2. Variation of redox potential (Eh) and pH.

in section 2. In relation to the pH, in Fig. 2 a progressive increase of these values towards the mouth of the Tinto and Odiel rivers is observed. This fact is due to pH induced and salt induced mixture processes.

Concerning the conductivity, an increase towards the mouth of both rivers in a range from 1.2 to 53 mS/cm is observed and a linear relation is found between conductivity and pH with the equation $C(mS/cm) = (10 \pm 1)pH - (21 \pm 8)$. One of the main features of the systems affected by acid mine drainage is their high dissolved sulphate concentrations [7]. This peculiarity is consistent with the high conductivity values measured in the fluvial zone of both estuaries (O5, T6 and T5), with values between 1–3 mS/cm, which is one order of magnitude higher than for surface waters (0.05–1 mS/cm). Accordingly, as we go towards the mouth of both rivers the values of conductivity increase reaching typical values for marine zones (50 mS/cm) in the Padre Santo and Punta Umbría Channels (Fig. 2).

Both dissolved Cl^- (chlorinity) and pH of waters present a similar pattern, observing in the mixing zone of the Tinto and Odiel rivers greater gradients in chlorinity, where the concentrations of dissolved Cl^- go from 0.05 to 20 g/L. In the Padre Santo and Punta Umbría channels the chlorinity values range from 13 to 16 g/L, closer to the marine values (Fig. 3).

A linear relation is also found between Eh and pH in the Tinto and Odiel river estuary (Fig. 2), as it is expected attending to Nernst's equation. The linear relation indicates that the Eh variation in this system is basically controlled by the pH variation, and, as can be expected, the negative slope implies that the medium is reducing to a higher pH.

The concentrations of ^{238}U determined in the filtered waters are shown in Fig. 3. In the fluvial zone, the concentrations of U-isotopes in the Tinto river (80 ± 2 mBq/L) are higher than in the Odiel river (40 ± 1 mBq/L), since a great burden of uranium is supported by the Tinto river, which shows more acidic water than the Odiel river. While we move towards the mouth of the estuary the pH induced and salt induced mixture process take place and the ^{238}U concentrations decrease. In zone 1 and 2 the lowest values of ^{238}U activity concentration in dissolved matter are reached, 19 ± 1 mBq/L in T2 and 11.1 ± 0.3 mBq/L in O3. These low values are due to the fact that in these zones the pH values are between 4.5 and 6.0 and dissolved uranium is adsorbed by iron hydroxides precipitating onto sediments [11]. For this, the highest values of ^{238}U concentration (1100 Bq/kg) in trap sediments are reached in these zones, which are about fifty times higher than those in unperturbed sediments [12]. In zone 3 the pH increases slowly up to an uniform value typical of seawaters (around 8), being the U concentrations in the range of those found in uncontaminated surface seawaters, 40 mBq/L [13]. A high value of ^{238}U activity concentration (169 ± 4 mBq/L) found in sample T4 can be associated with PG washing by rainwater fallen in this season and transported by the effect of the tides.
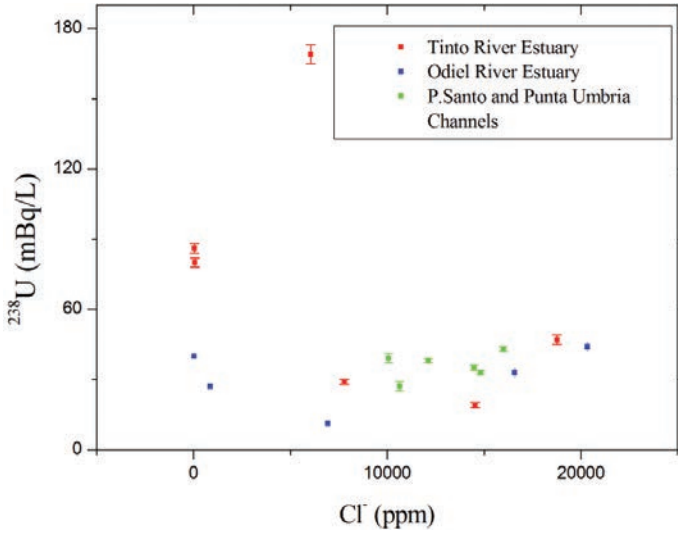
FIG. 3. Variation of ^{238}U activity with chlorinity for dissolved matter.
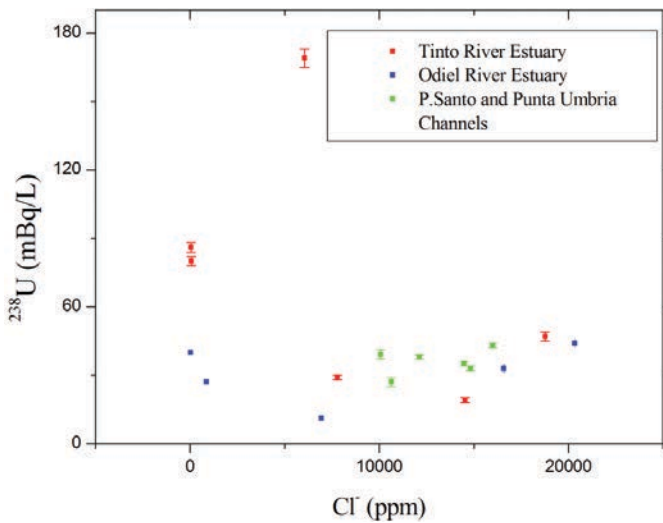
FIG. 4. Variation of ^{234}U/^{238}U activity ratio with pH.

There is not a linear relation between dissolved ^{238}U activity and chlorinity (Fig. 2) and, as we discussed before, when water mixing begins the U precipitates reach lower values than the typical marine ones (40 mBq/L). This fact explains the non-conservative behaviour of U within the study area. So, from the obtained results it is clear that there is a different behaviour of U-isotopes depending on the zones of the estuary and the hydrochemical characteristics of the water previously discussed.

400

Some of the previous conclusions can be ratified by studying activity ratios, being given $^{234}U/^{238}U$ activity ratios in Fig. 4. In the same way as ^{238}U concentrations, the activity ratios $^{234}U/^{238}U$ decrease towards the mouth, varying from 2.25 ± 0.02 to 1.14 ± 0.02 along the study area. The highest values are found in the fluvial zone (T6, T5 and O5), where the $^{234}U/^{238}U$ activity ratio is reported to be as high as 2.3, very high values compared with those of most world river waters, between 1.03 and 1.37 [14]. Values around 3.15 were also found in the Tedori and Kakehashi rivers in Japan, which are also affected by AMD [15]. This excess of ^{234}U in riverwater is primarily derived from the dislocated and easily leachable ^{234}U in mineral grains as well as direct delivery of ^{234}U into the solution phase from recoil. In zone 1 and 2 the values of this activity ratio are around the unity, or slowly higher, which suggest an artificial origin of U-isotope such as phosphogypsum piles situated along the right bank of the Tinto river estuary [16]. And in zone 3 values around 1.14 ± 0.02 are reached, values of $^{234}U/^{238}U$ activity ratio similar to the ones found in unperturbed seawaters [17].

4. CONCLUSIONS

The hydrogeochemical characteristics of the water in both the Tinto and Odiel river estuaries were analysed, with the finding that acid fluvial water and marine water are mixed allowing us to define the intervention of two geochemical processes: a typical process of salt induced mixture bound to a neutralization process of acid water. The temporal and spatial variations of markers as pH and chlorinity regulate the behaviour of both U-isotopes.

The ^{238}U activity concentration at every sampling point decreases towards the mouth of the estuary. In acidic riverwaters from the Tinto and Odiel rivers the $^{238}U/^{234}U$ activity ratios in dissolution present high values (1.6 to 2.3), due to the preferential leaching of ^{234}U from mineral particles in these conditions. But when mixing starts, the values of pH rise and the activity concentrations of U-isotopes decrease in the dissolution phase due to their scavenging onto several metal hydroxides precipitated when the fluvial waters are mixed with the sea/estuarine waters.

And finally, it is possible to affirm that the main pathway of radioactive pollution in the estuary is through the leaching of radionuclides coming from PG piles, and by the entrance of dissolved contaminants (heavy metals and radionuclides) contained in these riverwaters with leached elements from abandoned mines by AMD.

REFERENCES

[1] MIRALLES, J., RADAKOVITCH, O., COCHRAN, J.K., VÉRON, A., MASQUÉ, P., Multitracer study of anthropogenic contamination records in the Camargue, Southern France, Sci. Total Environ. **320** 1 (2004) 63–72.

[2]   YEAGER, K.M., SANTSCHI, P.H., PHILLIPS, J.D., HERBERT, B.E., Suspended sediment sources and tributary effects in the lower reaches of a coastal plain stream as indicated by radionuclides, Loco Bayou, Texas, Environ. Geol. **47** 3 (2005) 382–395.

[3]   GRANDE, J.A., BORREGO, J., MORALES, J.A., DE LA TORRE, M.L., A description of how metal pollution occurs in the Tinto-Odiel rias (Huelva-Spain) through the application of cluster analysis, Mar. Pollut. Bull. **46** (2003) 475–480.

[4]   RUIZ, F., et al., Impact of millennial mining activities on sediments and microfauna of the Tinto River estuary (SW Spain), Mar. Pollut. Bull. **56** (2008) 1258–1264.

[5]   BOLÍVAR, J.P., GARCÍA-TENORIO, R., MAS, J.L., VACA, F., Radioactive impact in sediments from an estuarine system affected by industrial wastes releases, Environ. Int. **27** (2002) 639–645.

[6]   VILLA, M., et al., Contamination and restoration of an estuary affected by phosphogypsum releases, Sci. Total Environ. **408** (2009) 69–77.

[7]   CARRO, B., BORREGO, J., LÓPEZ-GONZÁLEZ, N., LOZANO-SORIA, O., Procesos de mezcla de un estuario afectado por drenaje de aguas ácidas (Ría de Huelva, España), Geogaceta **39** (2006) 115–118.

[8]   YOUNGER, P.L., BANWART, S.A., HEDIN, R.S., Mine Water: Hydrology, Pollution, Remediation, First edn, Kluwer Academic, Dordrecht, The Netherlands (2002).

[9]   AGUADO, J.L., BOLÍVAR, J.P., SAN MIGUEL, E.G., GARCÍA-TENORIO, R., Ra and U isotopes determination in phosphogypsum leachates by alpha-particle spectrometry, Radioactivity in the Environment **7** (2005) 160–165.

[10]   PILVIÓ, R., BICKEL, M., Actinoid separations by extraction chromatography, Appl. Radiat. Isot. **53** (2000) 273–277.

[11]   SARIN, M.M., CHURCH, T.M., Behaviour of uranium during mixing in the Delaware and Chesapeake estuaries, Estuarine, Coast. Shelf Sci. **39** (1994) 619–631.

[12]   HIERRO, A., Natural Radionuclides in Recent Sediments from the Huelva Estuary, Master's Thesis (in Spanish) (2009).

[13]   KU, T.L., KNAUSS, K.G., MATHIEU, G.G., Uranium in open ocean: Concentration and isotopic composition, Deep Sea Res. **24** (1977) 1005–1017.

[14]   SCOTT, M.R., "The chemistry of U and Th series nuclides in Rivers", Uranium-Series Disequilibrium: Applications of Environmental Problems (IVANOVICH, M., HARMON, R.S., Eds) Clarendon, Oxford (1982) 181–201.

[15]   YAMAMOTO, M., SAKAGUCHI, A., KOFUJI, H., Uranium in acidic mine drainage at the former Ogoya Mine in Isikawa Prefecture of Japan, Radioanalytical and Nuclear Chemistry **283** (2010) 699–705.

[16]   BOLÍVAR, J.P., GARCÍA-TENORIO, R., VACA, F., Radioecological study of an estuarine system located in the south of Spain, Water Res. **34** (2000) 2941–2950.

[17]   MOORE, W.S., Amazon and Mississippi river concentrations of uranium, thorium and radium isotopes, Earth Planet. Sci. Lett. **2** (1967) 231–234.

MEDICAL AND OTHER RADIOISOTOPES AS TRACERS IN THE WASTEWATER–RIVER–SEDIMENT CHAIN

H.W. FISCHER, S. ULBRICH, D. PITTAUEROVÁ, B. HETTWIG
Institute of Environmental Physics,
University of Bremen,
Bremen, Germany

Abstract

Medical, natural and other artificial radioisotopes have been followed on their pathway to river sediment employing gamma spectroscopy. Sampling points were situated at a local wastewater treatment plant (inflow, outflow and sludge) and along 70 km of a tidal river (bank sediment). Isotope entry points are assumed to be wastewater for medical isotopes like I–131 and Tc–99m, rain for natural Be–7, and soil erosion for fission generated Cs–137. Medical isotope data reflect the short term dynamics of medical usage, wastewater transport and treatment, and the river system. Be–7 data are influenced by the amount of rainfall on a short time scale, and by the size of the river catchment area and dilution due to tidal effects in the long term. Cs–137 values appear rather constant, behaving similarly to primordial K–40. In conclusion, the investigated radioisotopes offer a variety of possibilities to assess water and sediment dynamics.

1. INTRODUCTION

City wastewater is known to carry considerable amounts of medically used radioisotopes [1, 2]. The mainly used nuclides are ^{99m}Tc for diagnostics and ^{131}I for therapy, which it was possible to follow from day to day in city wastewater in a previous study [3]. The isotopes will reach surface water bodies, normally after passage through a wastewater treatment plant (WWTP). The aforementioned study was able to identify both isotopes in WWTP effluent and primary sludge. ^{131}I could also be detected in the sediment of the river into which the WWTP discharges, in samples taken near the discharge point. Measured ^{131}I concentration levels in WWTP inflow (approx. 0.4 Bq/L), effluent (ca. 0.2 Bq/L) and river sediment (approx. 100 Bq/kg d m. at outflow, approx. 0.5 Bq/kg d m. at a distance allowing for complete mixing with river water) agreed well with predictions from national mean emmission values for medical isotopes and from simple equilibrium radio-ecological models. The question arose whether more detailed data on ^{131}I distribution in sediment would allow more precise modelling, and whether other isotopes also detected in all the sediment samples (^{7}Be, ^{40}K and ^{137}Cs) could provide additional insight into hydrological processes.

2. EXPERIMENT

The study area is, as previously, situated in north-western Germany at about 53°N, 9°E and comprises the tidal section of the river Weser. The river discharges into the North Sea, and due to deepening activities which started at the end of the 19th century it now has a tidal amplitude of more than 2 m in the city centre of Bremen, located about 60 km upstream from the river mouth. In consequence, the river inverts its flow direction about four times in 24 h. Further upstream, tidal effects disappear due to a permanent barrage. A map of the study area is presented in Fig. 1.

Bank sediment samples were taken over a total length of 70 km, including one sample taken upstream of the barrage. Sampling took place at low tide, included material from the upper 5 mm of sediment, and provided sample masses between 70 and 1800 g. Samples were measured by gamma spectrometry applying several high purity germanium detectors of 50% relative efficiency shielded by 10 cm of lead. Samples with masses ranging above 500 g were filled into Marinelli beakers, otherwise 80 ml cylindrical plastic dishes were used. The measurement time was about 24 h per sample. Dry mass was determined by oven drying at 105°C, and reported activities
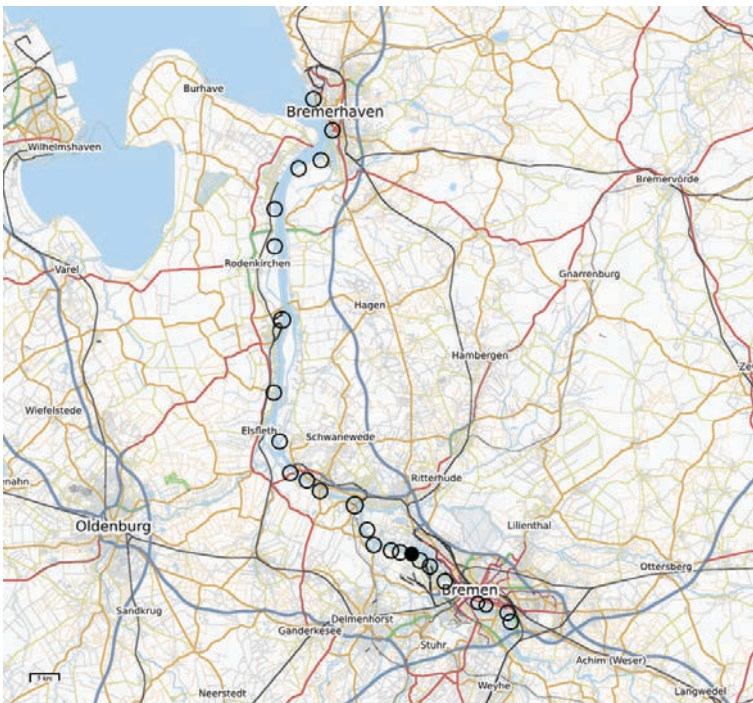
FIG. 1. Geographical map of the study area. Sediment sampling sites are marked by open symbols, the main WWTP is indicated by the filled circle (source: OpenSeaMap, published under CC-BY-SA 2.0).

are related to the sample dry mass. Spectrum analysis was done in a half-automatized way using the commercial software package Genie 2000 (Canberra Industries, Meriden, CA), applying pre-defined nuclide and peak energy libraries. Detection efficiencies applied in spectrum analysis had either been obtained experimentally from spectra collected with standard solutions in identical geometry, or by numerical methods after factory characterization of the detector (LabSOCS software, Canberra Industries, Meriden, CA) [4].

3. RESULTS

3.1. General results

^{131}I was detected over a river length of about 40 km with a maximum at the outflow of the largest WWTP. At that location, ^{111}In und ^{153}Sm could also be detected in one sample. Primordial ^{40}K, cosmogenic ^{7}Be and the fission product ^{137}Cs were found at all sampling sites. The omnipresent members of the natural decay chains have not been treated further in this study. A graphical summary of the data is presented in Fig. 2.
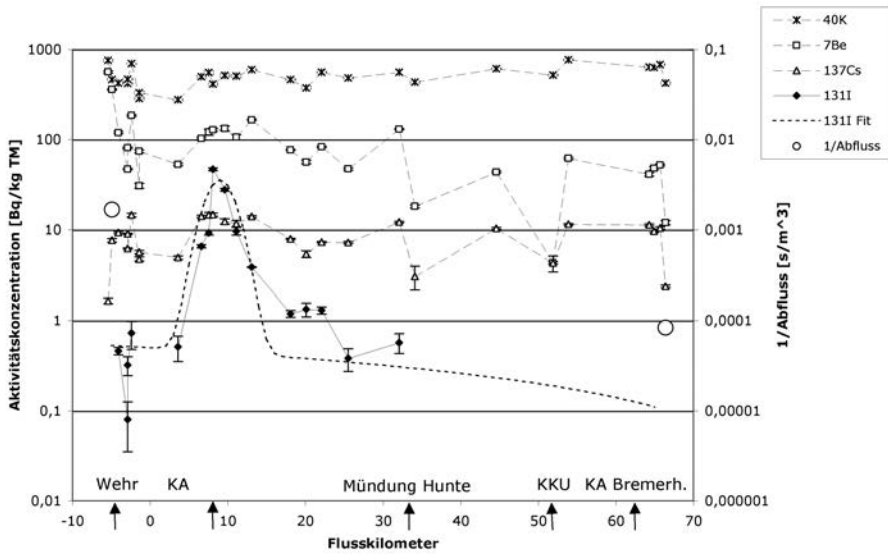
FIG. 2. Plot of the obtained results. The x-axis represents river length with a value of 0 at Bremen city centre at about 53°5'N, 8°48'E. Activity concentrations refer to the left y axis and are plotted as small, connected symbols. Open circles represent data for the reciprocal total river discharge and refer to the right y axis. The first sediment data points at the left for ^{7}Be, ^{40}K and ^{137}Cs represent the sample taken above the barrage. The dashed line represents a purely empirical fit to the ^{131}I data.

3.2. Isotope specific results

^{40}K: data appear relatively constant over the whole river length and correspond to values expected for mineral sediments. Variations are attributed to the relatively unsystematic sampling procedure.

^{137}Cs: values show a behaviour similar to ^{40}K, with similar variations along the river. Above and below the barrage, values vary considerably.

^{7}Be: values decline constantly in the downstream direction. The variation between the samples above and below the barrage is small.

^{131}I: the profile shows a broad peak centred around the WWTP outlet, superimposed over a baseline about two orders of magnitude lower and close to the experimental detection threshold.

3.3. Hydrographic data

The hydrographic conditions in the studied river vary considerably in space and time and might provide additional information helping to interpret isotope data. The tidal property of the river gives rise to a bidirectional transport on a short time scale. In the long term, downstream transport will vary strongly with the very variable, weather and season dependent water flux from upstream. Additionally, total mean water flux in the studied area increases by more than an order of magnitude due to mixing with seawater. Two values for the reciprocal mean flux have been marked in Fig. 2.

4.   DISCUSSION

Based on the experimental data and additional hydrographic information, the preliminary interpretation of the data is isotope specific and is therefore discussed in separate paragraphs.

^{40}K: the data show no sign of a significant variation other than due to unspecific sample variability.

^{137}Cs: the data appear very similar to ^{40}K results, speaking for a homogeneous distribution. As the main ^{137}Cs input source is probably historical fallout onto the land surface with subsequent erosion of particles carrying the isotope from the catchment area of the river, this slow distribution process of the long lived ($T_{1/2} = 30$ a) isotope appears to result in a homogeneous pattern. The concentration step at the barrage might be a sign of separation between the regions upstream and downstream of the barrage.

^{7}Be: the decline of concentration in a downstream direction can be interpreted as a dilution process. As the main isotope input is due to rain, the data should reflect the mixing of river freshwater with seawater. The variations of reciprocal total

discharge and isotope sediment concentration vary by roughly the same factor, as shown in Fig. 2, which support this assumption. The main catchment area of the river (85%) lies upstream of the barrage, so the similarity of the concentration values above and below the barrage is not surprising. Given the short half-life of ^{7}Be (53.4 d), no long term accumulation can be expected and the data should reflect only short and medium term events and processes related to rainfall.

^{131}I: the characteristic concentration profile could be due to a two step process: a fast, small scale mixing of the WWTP effluent with river water, and subsequent transport along the river. An empirical fit is shown as a dashed line in Fig. 2. The concentration ratio at the peak maximum and baseline (about 100) is similar to the ratio between mean river and WWTP discharges, speaking for the applicability of the small scale part of the model. The large scale part should reflect dilution by tidal processes, similar to ^{7}Be. However, ^{131}I data fall below the detection threshold in the downstream direction, excluding quantitative evaluation at the moment.

5.   CONCLUSION

The variety of radioisotopes detectable in the wastewater–river–sediment system of both artificial and natural origin open a fascinating observation window into hydrological processes on different time and length scales. It is envisaged to continue the experimental work and to apply sophisticated models to the refined data.

REFERENCES

[1]   NAKAMURA, A., HAYABUCHI, N., OSAKI, T., OSAKI, S., Output of radiopharmaceutical nuclides of known injected doses from a municipal sewage treatment system, Health Physics **88** (2005) 163–168.
[2]   SUNDELL-BERGMAN, S., et al., Assessing the Impact of Releases of Radionuclides into Sewage Systems in Urban Environment — Simulation, Modelling and Experimental Studies — LUCIA, NKS Report, NKS, Roskilde, Denmark (2007)
[3]   FISCHER, H.W., ULBRICH, S., PITTAUEROVÁ, D., HETTWIG, B., Medical radioisotopes in the environment — following the pathway from patient to river sediment, J. Env. Rad. **100** (2009) 1079–1085.
[4]   MBENE LYSONGE, P., M. Sc. Thesis, University of Oldenburg (2009).

NATURAL AND ARTIFICIAL RADIOACTIVITY IN DRINKING WATER IN MÁLAGA, SPAIN

M.C. FERNÁNDEZ, C. DUEÑAS , E. GORDO , S. CAÑETE
Department of Applied Physics I,
Faculty of Science, University of Málaga

M. PÉREZ
Department of Radiology and Health Physics,
Faculty of Medicine, University of Málaga,

Málaga, Spain

Abstract

The measurement of radioactivity in drinking water permits us to determine the exposure of the population to radiation from the habitual consumption of water. An intensive study of the water supply in the city of Málaga during 2002–2010 has been carried out in order to determine the gross alpha and gross beta activities and natural and artificial radionuclides present in drinking water. A database on natural and artificial radioactivity in water was created. The results indicated that a high percentage of the water sample contains a total gross alpha and beta concentration of less than 0.10 Bq/L and 1 Bq/L, respectively. The main objectives were: (1) to analyse gross alpha and gross beta activities and to know the statistical distributions; (2) to study the levels of natural and artificial radionuclides; (3) to determine a possible mathematical correlation between the radionuclides and several factors.

1. INTRODUCTION

Water has a vast importance for numerous human activities, so that securing supplies of drinking water of a standard quality is becoming more and more difficult. The measurement of radioactivity in drinking water permits us to determine the exposure of the population to radiation from the habitual consumption of water. The occurrence of radionuclides in drinking water gives rise to the internal exposure of humans, directly to the decay of radionuclides taken into the body through ingestion and inhalation and indirectly when they are incorporated as part of the food chain. Since the doses from these pathways are strongly related to the amounts of radionuclides present, an important objective for the radiological protection of the population is the accurate evaluation of the amounts received in the dietary intake.

It is thus indispensable to perform frequent and extensive analyses to guarantee that there is a minimal or zero contamination of drinking water. An exhaustive analysis of gross alpha and beta activities as well as the concentration of gamma emitting radionuclides has been carried out, in compliance with the RD 140/2003, 7 February, whereby standard levels are recommended for background natural radioactivity as well as for that present in water used by humans. From a radiological point of view, these levels are such that water can be considered to be drinkable without the need for any other kind for radiological examination.

2. MATERIALS AND METHODS

The interest of this work lies in the calculation of the index of alpha and beta activities over a period of nine years, from January 2002 to December 2010. The water samples were collected in sterile polythene containers of 10 L capacity every month. This type of container does not alter the general characteristics of the water sample, and is normally recommended for the transport of aqueous samples previous to the measurement of their radioactive content [1]. The sample point was situated in the Faculty of Science of the University of Malaga (4º 28′ 80″ W; 36º 43′ 40″ N) (see Fig. 1). Malaga is the capital of the province of the same name and it is in the southeast zone of the Iberian Peninsula on the Mediterranean coast. The climate in Malaga is warm and temperate with hot summers and little rain (550 mm is the mean annual precipitation level). The geological structure of Malaga is characterized by

FIG. 1. The map of Spain and indication of the sampling location.

predominantly sedimentary rocks (carbonated and detritical) which show a low concentration of radioactive elements [2, 3].

The analytical procedure used to determine the gross alpha activity level was the co-precipitation method with a volume of 500 cm^3 of sample water. This method consists of the selective precipitation of radium isotopes followed by a co-precipitation of the actinoids [4]. Both having been precipitated, they are separated by filtrations and the level of gross alpha activity is measured by a solid SZn(Ag) scintillation counter calibrated with a standard ^{241}Am solution. The zero thickness efficiency was 37%, and the average background 0.015 cpm.

The beta activity is measured with a gas flow proportional counter with a precipitate obtained by evaporation until nearly dry of a maximum volume of sample water of 150 cm^3; the volume was determined by the conductivity values obtained from each of the samples analysed, and was carried out a steel planchet of dimensions appropriate to our detector.

The detection system was a low level gas flow alpha/beta proportional counter model HT1000 CAMBERRA, calibrated with a standard ^{90}Sr /^{90}Y solution. The measured zero thickness efficiency was 32.2%, and the average background 0.51 cpm.

An analysis has also been carried out of radioisotopes by gamma spectrometry using an intrinsic germanium coaxial detector made by CANBERRA with an relative efficiency about 30% to the efficiency of a 3′ × 3′ NaI(Tl) at 25 cm distance. Typical resolution (full width at half maximum) is about 1.3 keV at 46 keV and 2 keV at 1.33 MeV. Careful calibration was carried out using a water standard sample containing a known amount of radioisotopes such as ^{152}Eu, ^{133}Ba, ^{60}Co, and ^{137}Cs uniformly distributed and sealed in Marinelli containers, the same design as those used for the water samples resolution [6]. Samples were counted for 48 h to achieve a higher precision. Owing to the low activity level of most samples, for quality control, instrumental and reagent blanks were measured frequently. Furthermore, for quality control for gamma-spectrometric analysis we participated in international and national intercomparison analyses [7]. This fact allows us to obtain the activity of each of the emission sources that are within of the limits of detection. These limits have been calculated as showing ISO/FDIS 11929 [7].

3.   RESULTS

The results from individual measurements of the gross alpha and gross beta activities were analysed to derive the statistical estimates characterizing the distributions.

Table 1 shows the estimates of the arithmetic mean (AM), geometric mean (GM), standard deviation (SD), dispersion factor of geometric mean (DF), maximum, minimum as well as the percentage of samples with concentration below

TABLE 1. STATISTICAL PARAMETERS OF DIFFERENT MEASUREMENTS

	Date	AM	SD	GM	DF	Max.	Min.	%
Gross α	108	16.53	11.70	12.97	2.08	74.7	1.51	0
Gross β	108	97.06	57.83	80.99	1.87	301	14.2	7.4
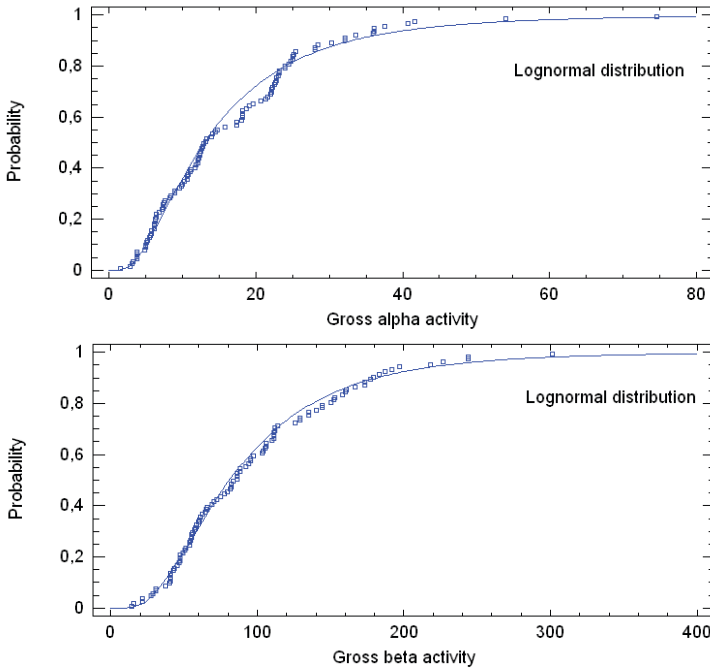
FIG. 2. Normal probability plot.

the minimum detectable (%). These values are given in Bq/L for gross alpha and gross beta activities.

Gross alpha and gross beta activities in the analysed waters follow a log-normal distribution. This is the case for the distribution of all natural radionuclides [5]. Fig. 2 shows that the assumption of a log-normal distribution is justified. Fig. 3 shows that both distributions are log-normal. The chi-squared values obtained by comparing observed frequencies for the logarithm of the original data with our expectations were significant at the 0.05 ± 0.01 level. Assuming these types of distribution, the GM for the gross alpha and gross beta activities should be used to characterize average values. The range of values for gross alpha activity was 73.19 Bq/m^3 and 283.8 Bq/m^3 for gross beta activity.
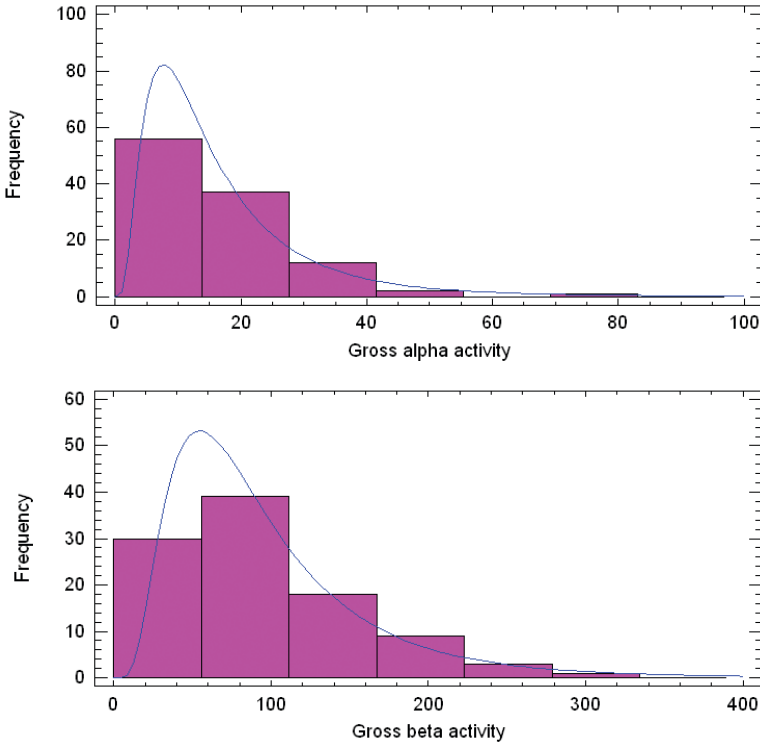
FIG. 3. Frequency histograms of gross alpha and gross beta activities.

Fig. 4 shows the analysis of means (ANOM) of gross alpha and gross beta activities. These plots show each group mean, the centreline at the grand mean, and the decision limits, which determine the groups that differ significantly at the grand mean. If any points are outside the decision limits, it can be concluded that there is a statistically significant difference between the counts.

Fig. 4 shows the same behaviour in gross alpha and gross beta activities. In 2005 there was a change in the behaviour of alpha and beta activities. This year, marked by a severe drought (about 240 mm), a desalination plant comes into operation aimed at improving water quality in the city of Málaga, using a procedure of reverse osmosis to treat brackish water. Thanks to this work it has been possible to increase supply capacity by allowing use of water resources that were previously under-utilized due to its high salt concentration. The variation of gross alpha and gross beta activities in the rest of the years cannot be explained by wet and dry deposition. The gross alpha and gross beta activities in drinking water do not show correlation with bulk deposition.
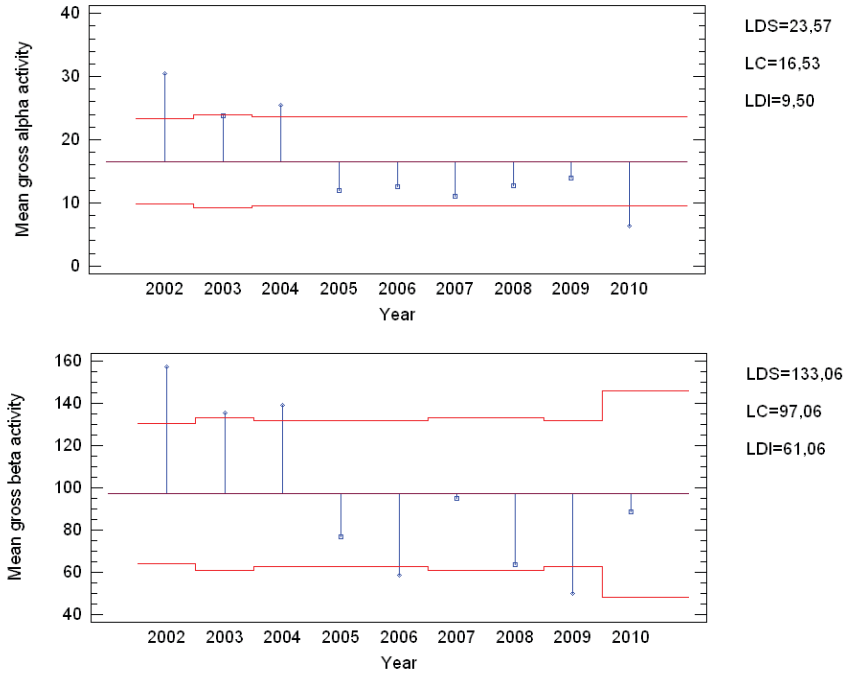
FIG. 4. Analysis of means (ANOM) of gross alpha and gross beta activities.

During the sampling period activity measurements were made with gamma spectroscopy for both natural and artificial sources. The average activity during the sampling periods corresponding to the natural radioisotopes is below the normal level of environmental radioactivity. Only three natural radionuclides have been detected with a frequency of 4.6% (^{40}K), 1.8% (^{214}Pb), and 7.4% (^{214}Bi).

4. CONCLUSIONS

- This paper presents some useful monitoring data for the concentrations of gross alpha and beta drinking water in Malaga, Spain. 100% of all samples collected have concentrations higher than LLD of gross alpha and 92.6% of gross beta.
- The results indicated that 100% of the water sample contains a total gross alpha and beta concentration of less than 0.10 Bq/L and 1 Bq/L respectively and is appropriate for human consumption.

- Gross alpha and gross beta activities in drinking water do not show correlation with bulk deposition so we can't find a mathematical correlation between radionuclides activity and meteorological factors.
- The gamma emitting radioisotopes found were ^{40}K, ^{214}Pb, ^{214}Bi with very low frequency.

REFERENCES

[1]   RODIER, J., L'analyse de L'eau: Eaux naturelles, eaux residuaires, eau de mer, Bordas, Paris (1978).

[2]   AMORÓS, J.L., et al. (Eds), Geología: Manuales de Orientación Universitaria Anaya, Madrid (1979), (in Spanish).

[3]   COTHERN, C.R., Estimating the health risks of Radon in drinking water, J. Am. Water Assoc. **79** 4 (1987) 153–158.

[4]   SUÁREZ J.A., TERÉS, L.P., DE PABLO SANMARTIN, M.A., Procedimientos Radioquímicos: Índice de actividad alfa total en aguas por coprecipitacion, Cuadernos de Investigación, CEDEX 39 (2000).

[5]   COTHERN, C., REBERS, P.A. (Eds), Radon, Radium and Uranium in Drinking Water, Lewis, Chelsea, MI (1990).

[6]   DUEÑAS, C., FERNÁNDEZ, M.C., LIGER, E., CARRETERO, S., Gross alpha, gross beta activities and ^{7}Be concentrations in surface air: analysis of their variations and prediction model, Atmos. Environ. **33** (1999) 3705–3715.

[7]   DUEÑAS, C., FERNÁNDEZ, M.C., GORDO, E., CAÑETE, S., PÉREZ, M., Gross alpha, Gross beta activities and gamma emitting radionuclides composition of rainwater samples and deposition to ground, Atmos. Environ. **45** (2011) 1015–1024.

[8]   INTERNATIONAL ORGANIZATION FOR STANDARIZATION., Determination of the Characteristic Limits (Decision Threshold, Detection Limit and Limits of the Confidence Interval) for Measurements of Ionizing Radiation — Fundamentals and Application, ISO 11929:2010, Geneva (2010).

C AND N STABLE ISOTOPE VARIABILITY IN SOFT TISSUE OF INVASIVE SPECIES *Ficopomatus enigmaticus* (ANNELIDA, POLYCHAETA)

N. CUKROV
Rudjer Boskovic Institute,
Zagreb, Croatia

M. CUKROV
Croatian Biospeleological Society,
Zagreb, Croatia

S. LOJEN
Jozef Stefan Institute,
Ljubliana, Slovenia

Abstract

Ficopomatus enigmaticus (Fauvel, 1923) is a sedentary polychaete. An invasive species, *F. enigmaticus* has been found worldwide, inhabiting coastal brackish waters, lagoons and estuaries of both hemispheres. This tubeworm (Serpulidae) builds calcareous tubes on any hard substrate, with distinctive collar-like rings at irregular intervals, and is relatively easy to identify. It is an efficient suspension feeder, very tolerant and physiologically well adapted to temperature and salinity variations, eutrophic conditions and low dissolved oxygen content. It was introduced to the eastern Adriatic coast recently. Here we report the first record of C and N stable isotope variability in the soft tissue of *F. enigmaticus* from the Krka River Estuary and the Nertva River Delta.

1.   INTRODUCTION

Serpulidae Rafinesque, 1815, is a family of polychaete annelids with calcareous tubes found worldwide from littoral to abyssal depths. Of more than 350 described species of serpulid polychaetes, *Marifugia cavatica* (Absolon & Hrabe 1930) is the only known cave dwelling stygobiotic and freshwater serpulid, five other serpulid; species comprising the genus Ficopomatus are found in brackish water, otherwise serpulids are all marine organisms.

Ficopomatus enigmaticus (Fauvel, 1923), previously known as *Mercierella enigmatica*, is truly cosmopolitan with disjunct distribution. It has been found worldwide inhabiting coastal brackish waters, lagoons and estuaries of warm temperate areas of both hemispheres. The distribution records lie approximately between

the northern hemisphere isotherm of 16 ºC and the 21 ºC isotherm on the southern hemisphere. This tubeworm builds calcareous tubes on any hard substrate. With distinctive collar-like rings at irregular intervals it is relatively easy to identify. It is an efficient suspension feeder, very tolerant and physiologically well adapted to temperature and salinity variations, eutrophic conditions and low dissolved oxygen content.

F. enigmaticus retains particles in the range of 2–16 μm with maximum efficiency, and while both larger and smaller particles were ingested by the worms, the efficiency declined for larger particles [1]. The rates of ingestion and particle clearance by *F. enigmaticus* are among the highest known for serpulid polychaetes. The high filtration rate of this suspension feeder can substantially contribute to water clarity in enclosed embayments like harbours, marinas or lagoons [2, 1].

It probably invaded into the Mediterranean Sea as ship fouling during the First World War [3]. In the Adriatic Sea, *F. enigmaticus* was recorded for the first time in 1934 in the Venice Lagoon in the Northern Adriatic, where it builds huge aggregate 'reefs' today [4, 5]. Along the eastern coast of the Adriatic Sea it is widespread [6–8] as an encrusting organism in many marine communities, especially ports fouling. The fact that populations of *F. enigmaticus* appear near ports suggests that the probable mechanism of introduction was ship fouling or ballast water. Generally, *F. enigmaticus* is considered a fouling nuisance species which negatively affects ships, buoys and harbour structures.

On the other hand, *M. Cavatica* is endemic species of the Dinaric Karst. It is distributed only in subterranean waters of northeastern Italy, Slovenia, Croatia and Bosnia and Hercegovina [9, 10].

Recently phylogenetic analysis places Marifugia as a sister group to a clade of brackish water Ficopomatus species [10]. Aggregations of both species support a higher abundance and diversity of associated fauna between its intertwined tubes [4, 11].

2. STUDY AREA

For the study of *F. enigmaticus* two main populations located in the Krka River Estuary and Neretva River Delta were chosen (Fig. 1).

The Krka River estuary was formed during the Holocene transgression. The estuary has a total length of 22 km and its bottom gradually deepens from 2 m to 42 m. It is a typical karstic highly stratified estuary with a fresh/brackish surface layer flowing seawards, and bottom seawater counter-currently moving upwards. The largest settlement in the region is the town of Šibenik with a large port located in the lower part of the Krka river estuary. *Ficopomatus enigmaticus* has grown in the Krka River Estuary for the last 6 years in the low intertidal to shallow subtidal area.

The Neretva River Delta covers about 20 000 ha of which 12 000 ha are in Croatia. It is constituted of numerous channels. The Port of Ploče is situated near
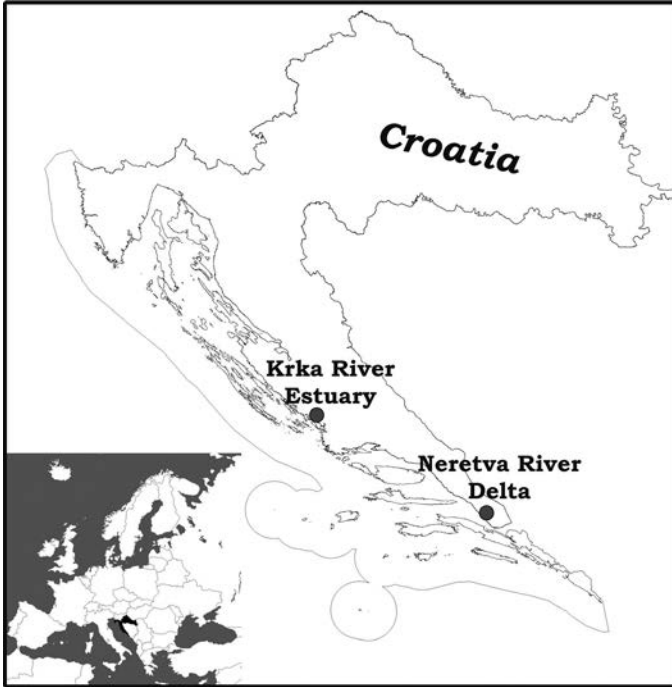
FIG. 1. Map of sampling areas.

the river mouth, and it is one of the largest Croatian ports. The Delta can be divided into three morphological parts: karst area, lowland Delta area and shore. *F. enigmaticus* has appeared in the lowland Delta area and at the shore after Second World War as single specimens or in small aggregates. It mostly occurs at depths of 0.7 m.

3.   SAMPLING AND SAMPLING PREPARATION

Sampling was performed between May and September 2010. Samples were collected manually by a scuba diver. Sampling locations were divided by water salinity into three groups (FW- dominantly fresh water, BW-brackish water with seasonal changes of salinity, MW-marine water).

Particulate organic matter was collected only once, in summer 2010, by filtering seawater through GF/C glass fiber filter. Filters were rinsed with deionized water and dried overnight at 50°C.

Worms were manually extracted from their tubes and dried until constant weight at 50°C. Several individuals (3–20, depending upon availability) were pooled together and homogenized. Particulate organic matter for the isotope analysis of

organic C was treated with 1M HCl to remove carbonate prior to analysis; untreated samples were used for N isotope analysis. Dry samples were analysed using a Europa 20–20 stable isotope analyser with ANCA SL preparation module for solid and liquid samples (Europa Scientific, U.K.). For carbonate C and O isotope analyses, dried sections of colonies were pulverized using agate mortar and pestle and analysed using Varian MAT 250 isotope ratio mass spectrometer after decomposition of 3 mg sample in 100% H_3PO_4 at 25°C for 24 h.

The stable isotopic compositions of carbon, oxygen, nitrogen, and carbonate were determined as heavier isotope to light isotope ratio and reported in ‰ as relative δ values:

$$\delta = (R_{sample}/R_{standard} - 1) \times 1000\ [‰]$$

where R is the $^{13}C/^{12}C$, $^{15}N/^{14}N$ or $^{18}O/^{16}O$ ratio of the sample and the standard. The results for carbon and oxygen are reported relative to V–PDB (Vienna – Pee Dee Belemnite) and nitrogen relative to atmospheric N_2. Samples of soft tissues were analysed in triplicate and were accepted, if the standard deviation was <0.2‰ for both C and N; if the deviation was larger, analyses were repeated until the deviation was within the requested limits. Carbonate samples were analysed in duplicate, with standard uncertainty of 0.1‰ for both $\delta^{13}C$ and $\delta^{18}O$.

4.   RESULTS

Particulate organic matter: the POM was sampled only once, in September 2010, at sites with changing salinity (4 sites in Krka river estuary and one in Neretva river delta) and at one freshwater site (Krka estuary). The $\delta^{15}N$ values ranged from 3.6 to 5‰ for sites with varying salinity and 8.1‰ for the freshwater site, whereas $\delta^{13}C$ values increased from –31.9‰ V–PDB at sites close to the Krka river mouth to –25.1‰ V–PDB at sites closer to the sea; literature data for marine POM in Central Dalmatia show that the seasonal variation in both $\delta^{13}C$ and $\delta^{15}N$ and can range over several permille and that the highest values typically occur in late summer [12, 13]. It is noteworthy, however, that no results are available for the estuarine environment, where intensive mixing of fresh- and seawater occurs, depending upon the temperature and some other physicochemical conditions.

Soft tissues: no data on stable isotope composition of the soft tissues of *M. cavatica* or *F. enigmaticus* worms could be found in the literature. Some $\delta^{15}N$ values were reported for polychaete worms in the Gulf of Aqaba, where it was found that — as intensive filter feeders with high retention capacity — they reflect the $\delta^{15}N$ of POM in their living environment [14]; for unpolluted locations, a mean $\delta^{15}N$ of 3.9‰ was measured, while at locations exposed to fish farm derived effluents, $\delta^{15}N$ values of up to 8‰ were found. Unpublished data for serpulides

from the Bay of Piran in the Northern Adriatic report values between 3.6 and 7‰ V–PDB, depending on the season and distance to the fish farms. The ^{15}N enrichment compared to the particulate organic matter varied seasonally between 2 and 3‰ [14]. The mean δ^{15}N of serpulides analysed in our study was 8.6‰ (*std* = 0.7‰, *n* = 17) in the freshwater environment, 7.8‰ (*std* = 1.7‰, *n* = 26) in the mixed freshwater–saline environment and 8.4‰ (*std* = 0.1‰, *n* = 2) in the marine environment, which means that the N stable isotope composition is rather independent of the salinity. For the observed period, no regular seasonal variation was observed. The obtained values are as expected, considering the δ^{15}N of POM and previously estimated enrichment factor [14]. Much larger variations were observed in the stable isotope composition of organic C in the soft tissues: in freshwater environments, mean δ^{13}C was –31.9‰, however, the standard deviation was 4.7‰ (n = 17); in environments with changing salinity the mean δ^{13}C was –31.0‰ (std = 3.1‰), while in the marine environment the mean δ^{13}C was –32.1‰ with standard deviation of 1.5‰. These values were much lower than those obtained in the unpublished study in the northern Adriatic and the Gulf of Aqaba, where δ^{13}C values typical of those for marine organisms were found (–17 to –22‰ V–PDB). In principle, δ^{13}C values as low as those obtained in our study (down to –37.8‰ V–PDB) at the freshwater site in Krka estuary) could be explained by the uptake of organic matter deriving from methane oxidizing bacteria, which could occasionally derive from the lacustrine environment behind the Skradinski buk waterfall [15]. At the moment, such conclusion can only be speculative since there are other factors which could not yet be taken into account, such as limited water circulation within serpulide colonies, C cycling within soft substrates covering the tubes etc., which could potentially alter the microenvironmental conditions within the colonies and, in particular in freshwater environments, create local hypoxia.

Carbonates: both δ^{13}C and δ^{18}O values of carbonate tubes are related to the salinity of the living environment of organisms: the lowest δ values were determined in the freshwater organisms *M. cavatica* with δ^{13}C between –14.9 and –12.5‰ and δ^{18}O between –10.6 and –9.1‰ VPDB; tubes of *F. enigmaticus* from freshwater environment had δ^{13}C between –14.4 and –6.6‰ and δ^{18}O between –9.4 and –5.7‰ VPDB. These values are very similar to those reported for fossil *M. cavatica* (δ^{13}C = –13.2 to –15.1‰, δ^{18}O = –6.2 to –9.1‰ V–PDB [16]) The lowest values in *F. enigmaticus* were determined in the samples collected just below the waterfall of Skradinski buk, where the river discharges into the estuary; these values match with the δ^{13}C values of dissolved inorganic C in the river which varies seasonally between –8 and –14‰ VPDB, and δ^{18}O of river water (–6.8 to –7.8‰ V–PDB, [17]). Samples collected in the areas with salinity changing seasonally from freshwater to typical marine values (up to 36) had much higher δ values (–6.76 < δ^{13}C < –2.88‰, –4.68 < δ^{18}O < –3.38‰), close to those typical of marine serpulidae tubes determined in the Bay of Koper, Northern Adriatic (δ^{13}C = – 0.3, δ^{18}O = +1.8‰ V–PDB, [16]).

5.   CONCLUSION

The stable isotope composition of serpulide worms in the estuary of the river Krka and Neretva river delta show a large span of $\delta^{13}C$ and $\delta^{15}N$ values; the $\delta^{15}N$ values reflect the stable isotope composition of particulate organic matter in the area, whereas $\delta^{13}C$ values obtained in this study cannot yet be fully explained. The C and O isotope composition of carbonate tubes depend upon the contribution of river-borne dissolved inorganic carbon and its typical $\delta^{18}O$ values and change with the salinity gradient.

REFERENCES

[1]   DAVIES, B.R., STUART, V., DE VILLIERS, M., The filtration activity of a serpulid polychaete population (*Ficopomatus enigmaticus* (Fauvel)) and its effects on water quality in a coastal marina, Estuar. Coast. Shelf Sci. **29** (1989) 613–620.

[2]   BRUSCHETTI, M., LUPPI, T., FANJUL, E., ROSENTHAL, A., IRIBARNE, O., Grazing effect of the invasive reef-forming polychaete *Ficopomatus enigmaticus* (Fauvel) on phytoplankton biomass in a SW Atlantic coastal lagoon, J. Exp. Mar. Biol. Ecol. **354** (2008) 212–219.

[3]   ZIBROWIUS, H., Ongoing modification of the Mediterranean marine fauna and flora by the establishment of exotic species, Mésogée **51** (1991) 83–107.

[4]   BIANCHI, C.N., MORRI, C., Ficopomatus 'reefs' in the Po River Delta (Northern Adriatic): Their constructional dynamics, biology, and influences on the brackish-water biota, Mar. Ecol. **17** (1996) 51–66.

[5]   FAUVEL, P., Annelida polychaeta della Laguna di Venezia, R. Com. Talas. It. Mem. **246** (1938) 1–26.

[6]   CUKROV M., MANCONI, R., CUKROV, N., JALŽIĆ, B., DESPALTOVIĆ, M.,L., Biodiversity in anchialine caves: First record of the tubeworm *Ficopomatus enigmaticus* (Annelida, Polychaeta)" (MOŠKRIČ, A., TRONTELS, P., Eds), ICSB Postojna, Slovenia, ICSB 2010 Abstract Book (2010) 73.

[7]   CUKROV, M., DESPALTOVIĆ, M., ŽULJEVIĆ, A., CUKROV, N., "First record of the introduced fouling tubeworm *Ficopomatus enigmaticus* (Fauvel, 1923) in the eastern Adriatic Sea, Croatia", Rapp. Comm. int. Mer Médit **39** (2010).

[8]   LIPEJ, L., TURK, R., MAKOVEC, T., Ogrožene vrste in habitatni tipi v slovenskem morju – Endangered Species and Habitat Types in the Slovenian Sea, Ljubljana: Zavod RS za varstvo narave (2006).

[9]   BIANCHI, C.N., SANFILIPPO, R., "Policheti Serpuloidei", Grotte Marine: Cinquant'Anni di Ricerca in Italia (CICOGNA, F, BIANCHI, C.N., FERRARI, G., FORTI, P., Eds), Ministero dell'Ambiente e della Tutela del Territorio, Rome (2003) 495–505.

[10]   KUPRIYANOVA, E.K., et al., Evolution of the unique freshwater cave-dwelling tube worm *Marifugia cavatica* (Annelida: Serpulidae), Systematics and Biodiversity **7** (2009) 389–401.

[11]   MATJAŠIĆ, J., "Marifugijska favnula", Treći Jugoslavenski speleološki kongres, Sarajevo, (1963) (in Croatian).

[12]   DOLENEC, T., LOJEN, S., LAMBASSA, Z, DOLENEC, M., Effects of fish farm loading on sea grass Posidonia oceanica at Vrgada Island (Central Adriatic): A nitrogen stable isotope study, Isot. Environ. Helath Stud. **42** (2006) 77–85.

[13]   DOLENEC, T., LOJEN, S., KNIEWALD, G., DOLENEC, M., ROGAN, N., Nitrogen stable isotope composition as a tracer of fish farming in invertebrates *Aplisina aerophoba, Balanus perforatus* and *Anemonia sulcata* in central Adriatic, Aquaculture **262** (2007) 237–249.

[14]   LOJEN, S., et al., δ^{15}N as a natural tracer of particulate nitrogen effluents released from marine aquaculture, Mar. Biol. **148** (2005) 87–96.

[15]   JONES, R.I., GREY, J., Biogenic methane in freshwater food webs, Freshwat. Biol. **56** (2011) 213–229.

[16]   MIHEVC, A., BOSAK, P., BRUNER, P., VOKAL, B., Fosilni ostanki jamske živali *Marifugia cavatica* v brezstropi jami v kamnolomu Črnotiče v zahodni Sloveniji — Fossil remains of the cave animal *Marifugia cavatica* in the unroofed cave in the Črnotiče quarry, W Slovenia, Geologija **45** (2002) 471–474.

[17]   LOJEN, S., et al., C and O stable isotope variability in recent freshwater carbonates (River Krka, Croatia), Sedimentology **51** (2004) 361–375.

ELIMINATION OF ^{137}CS FROM JAPANESE CATFISH ACUTELY CONTAMINATED BY LABELLED FOOD

M.A. MALEK
Atomic Energy Center,
Dhaka, Bangladesh

M. NAKAHARA
Laboratory for Radioecology,
National Institute of Radiological Sciences, Isozaki,
Hitachinaka City,
Ibaraki-ken, Japan

Abstract

The effective half-life of ^{137}Cs in acutely contaminated Japanese catfish was determined. The fish were fed with fish meal incorporated with ^{137}CsCl and then released into aquaria. To assess the ^{137}Cs activity retained in the fish body, the whole body radioactivity of each fish was measured at regular intervals for up to 157 days. The data were plotted with relative counts on the y-axis and corresponding elapsed time on the x-axis. Relative count plotted against elapsed time was found to consist of three components, namely the first fast, second fast and the slow component. The true elimination curves of the first components were calculated by the peeling off method. The effective half-life of the fast components was determined from the slope of the true curves. The effective half-life of ^{137}Cs for the first fast, second fast and the slow component in Japanese catfish was found to be 1.27, 5.76 and 251 days, respectively.

1. INTRODUCTION

The release of radioactive materials to the environment is an inevitable consequence of the use of nuclear energy. One of the major sources of environmental radioactivity is radioactive materials injected into the atmosphere during nuclear weapons or peaceful explosive tests, reactor operations and space application of nuclear energy. In addition, they also gain access into the environment through nuclear fuel fabrication and reprocessing, radioisotope production facilities and other activities such as the use of radioisotopes in medicine, industry and agriculture [1]. Among the radionuclides, radiocaesium has drawn the utmost attention for its long physical half-life, high fission yield [2] and high bioavailability. The Chernobyl accident aroused further interest as a large number of wetland areas were subjected to Chernobyl fallout. Owing to its chemical and physiological similarity with potassium, ^{137}Cs can easily enter into the food chain and has a ubiquitous distribution within the body,

including edible skeletal muscle [3]. Therefore, ^{137}Cs is an important contributor to the internal radiation dose of living bodies [4]. Furthermore, ^{137}Cs is of particular interest to aquatic ecologists because it provides a useful tracer of food web dynamics through the use of ^{137}Cs-based bioenergetics models [5].

Fish is a major source of protein and nutrition and is therefore a potential carrier of radionuclides from the aquatic environment to humans. Because ^{137}Cs is accumulated and concentrated in skeletal muscle, consumption of contaminated fish can be an important pathway for human exposure [6]. There are two modes by which fish can be contaminated: chronically and acutely. In chronic exposure, fish take up radionuclides from their host environment through food, the gills and other ways over a long time. In acute exposure, the radionuclides are introduced to the fish by labelled food, by keeping the fish for a short time in water containing ^{137}Cs or by injecting ^{137}Cs into the fish over a short time [7]. Therefore, the acutely contaminated fish would not be at equilibrium or near the equilibrium state.

After leaving the contaminated area or after ingestion of a single dose, fish eventually lose much of their radioactivity as a result of metabolic processes and through other physiological means of elimination. Therefore, studies on elimination of ^{137}Cs from fish are needed to gather data for the assessment of the expected levels of contamination to predict the time required for fish to be adequately free from [137]Cs [8]. Accurate prediction of radiocaesium elimination is important in gauging the potential health effects of environmental release, as well as estimating the food consumption by free ranging fish. Base line data on each species of fish are essential in formulating a guideline for fish consumption. Many studies have been carried out on the accumulation and elimination of various radionuclides by different species of both marine and freshwater fish, and a comprehensive list of references can be found in the literature [8]. However, there are still a lot of fish species that remain uninvestigated for the baseline data.

Normally, nuclear testing or accidents introduce radioactivity into the aquatic environment for a short time, and a huge amount of contaminant can fall into the environment within a few moments. Fish caught after a short period of contamination can be considered as acutely contaminated disregarding the level of contamination. From a radiation protection as well as a radio-ecological point of view, the effective half-life of ^{137}Cs in the acutely contaminated fish is equally important as the half-life in the chronically contaminated fish. In south Asian countries, many fresh water fish species are available that can remain alive out of water for a long time and furthermore, these fish can also be maintained in small vessels, tanks, buckets or ditches filled with water for a long time. These fish are commonly known as 'zeol' (a Bangla word meaning live) fish. For convenience, people used to catch/collect 'zeol' fish from natural sources and maintain them in small earthen vessels, tanks, buckets or ditches at home for a long time to consume the fish over a period of time. This rural tradition of zeol fish rearing may be a useful tool in protecting people from the ingestion of radionuclides through consumption of contaminated fish. Knowing

the effective half-life of the contaminant radioisotope in the fish, people may be advised to collect the zeol fish from the contaminated aquatic environment and to maintain the fish at home and consume it after a time equal to the effective half-life of the radio-isotope. Therefore, it is prudent to determine the effective half-life of the radioisotope in acutely contaminated fish. The condition maintained in the aquarium to rear the experimental fish in laboratory is almost equivalent to that in a small vessel in a house. Therefore, the data obtained can be treated as the data obtained in field conditions.

Japanese catfish (*Silurus asotus* Linnaeus) is a freshwater fish abundant in Bangladesh, Cambodia, India, Japan, Malaysia, Thailand, and other countries in south and south east Asia and is commonly consumed. The fish has ancillary respiratory organs enabling it to breath air and therefore live out of water. This attribute facilitates handling in the laboratory; the fish can be easily kept under laboratory conditions for a long time. The effective half-life of ^{137}Cs in chronically contaminated Japanese catfish has already been determined [9]. However, experiments have not been conducted for the half-life in acutely contaminated Japanese catfish. Therefore, a research work was undertaken to determine the effective half-life of ^{137}Cs in acutely contaminated Japanese catfish. The purpose of this paper is to report on the elimination of ^{137}Cs in acutely contaminated Japanese catfish and to find out the effective half-life of ^{137}Cs in the fish based on the experimental findings and to compare the half-life with the half-life in chronically contaminated fish.

2. EXPERIMENT

^{137}Cs in chloride form (811.4 kBq/mL on July 4, 2002) was mixed with fresh water. Fifteen fish meal pellets were weighed individually and contaminated with the ^{137}CsCl solution. The ^{137}CsCl solution was poured on the pellets drop by drop so that all pellets were completely moist. The pellets were then dried in air, divided into five groups of three pellets, and placed in small plastic packets and counted for ^{137}Cs activity (Av. 15 Bq/g). Fifteen medium size Japanese catfish (length: 30–39 cm, weight: 350–405 g, age: 2 years, adult fish) were collected from local fisheries and acclimatized in a 200 L aquarium for 3 months. Five fish were selected for the experiment and placed in a plastic bucket containing 10 L fresh tap water with 5 mL of anaesthetic. The fish were immersed in the anaesthetic solution for 4–5 min, until their behaviour indicated that anaesthesia had been attained (unable to remain upright). In order to contaminate the fish, three ^{137}Cs incorporated pellets of a packet were inserted into the stomach through the mouth of the unconscious fish by means of tongs. The ^{137}Cs loaded fish was then weighed, put in a polyethylene bag, placed in a cylinder type plastic scintillation counter and whole body counted for 120 s to

know the initial level of the ^{137}Cs in the fish body. After counting, the fish was released into an aquarium containing 200 L fresh water (non-contaminated), one fish per aquarium.

After the ingestion of the contaminated meal, the fish eventually lost the radioactivity through the undigested food and metabolic processes. To assess the ^{137}Cs activity remaining in the fish body after a period of contamination, fish were counted alive for whole body radioactivity at regular intervals up to 157 days, twice a week for the first 10 weeks and then once a week. On every counting day, fish were removed from the aquarium by fishing net and placed in a bucket, made unconscious and whole body counted following the procedure described above. The water was changed twice a week. The temperature of the water was maintained at $20 \pm 1\,°C$ using heat and refrigeration units. All aquaria were equipped with air pumps to ensure a normal oxygen level in the water.

The background count was measured for 10 min before and after the fish counting and the mean was subtracted from the gross count to obtain the net count. Fish number 5 was found to have disgorged all the pellets 3 hours after the feeding. Since some radionuclide was readily absorbed during the time therefore, the fish was included for further counting. Fish number 4 died at the 12th day, which may be due to food poisoning. Through out the acclimation and the experimental period, the fish were fed non-contaminated commercial high protein rations on each sampling day. In the acclimation period, the pellets were released directly into the aquarium and the fish ate the pellets willingly. In the experimental period, the fish were hand fed while they were out of the water for counting purposes. After finishing the counting, ten pellets were directly inserted into the stomach of the unconscious fish by tongs, one pellet after another. The fish was then released into its host aquarium. The fish regained consciousness within 2–5 minutes.

3.   RESULT AND DISCUSSION

The ^{137}Cs activity remaining in the fish body at different time periods after contamination is plotted in Fig. 2 to show the rate of loss through biological elimination and physical decay, and elimination during the first few days seems to be high. Acutely contaminated fish exhibit artificially high initial losses of administered radionuclides [10]. On close observation of Fig. 1, one may feel that the elimination data points of ^{137}Cs after a single uptake from food for all fish have three different slopes. The 1st slope seems to be over the data points for the period 0–3 days; the 2nd slope is for 3–24 days and the 3rd one is for 24–157 days. Therefore, the slopes of the curves for each fish clearly show that there are three elimination rates involved that could be designated as the first rapid component, second rapid component and the slow component. The curves were fitted to the elimination data on each component separately (Fig. 1).
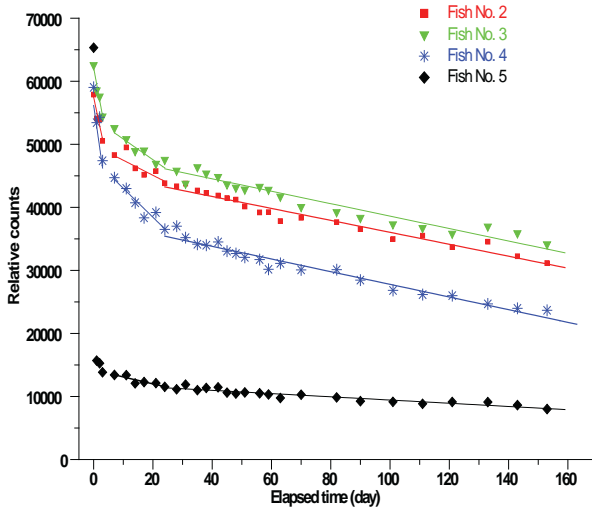
FIG. 1. Data for ^{137}Cs elimination from Japanese catfish after a single dose of ^{137}Cs. The ^{137}Cs activities remaining in the fish body at different times are plotted on the Y-axis against the elapsed time on the X-axis.

The first rapid component is represented by the ^{137}Cs that is not assimilated by the organisms; it is lost by defecation [11–14]. The ^{137}Cs elimination during the second rapid period is driven by release from organs other than muscle, and elimination during the slow component is driven by release from muscle tissue [15]. The data for all components of all fish were well fitted by the equation: $Y = A – MX$ where A is the intercept and M is the slope. All the fitted equations with corresponding values of A and M are shown in Table 1. The predictive power of each individual fish's elimination equation was very high (all $r^2 \approx 0.90$). The data points for the first and second rapid components in Fig. 1 as such the equations fitted to the data points (Table 1) are apparent only. Real elimination rates should be calculated by peeling off the different components. After peeling off, the true elimination rate of the rapid components could be seen [16].

During the period of the first rapid component, elimination due to reasons other than defecation also applies. Therefore, to find the real elimination rate in the first rapid component, data for the two other components must be graphically subtracted from the data obtained during the first rapid component. Likewise, the real elimination rate during the period of the second rapid component should be calculated by subtracting the data for the slow component. The fitted equations for the real first and second rapid components are also given in Table 1. The slopes of the curves of the real first and second rapid components and of the slow component, the effective elimination rate constants λ_{eff} are expressed as :

$$\lambda_{eff} = (\ln C_1 – \ln C_2) / (t_2 – t_1).$$

TABLE 1. EQUATIONS FITTED TO EXPERIMENTAL DATA FOR THE RAPID AND SLOW COMPONENTS AND CORRESPONDING EFFECTIVE HALF-LIVES (DAY) CALCULATED BASED ON THE REAL FIRST AND SECOND RAPID COMPONENTS

Fish No.	1st fast component			2nd fast component			Slow component	
	Apparent	Real	$T_{b\frac{1}{2}}$	Apparent	Real	$T_{b\frac{1}{2}}$	Equation	$T_{b\frac{1}{2}}$
1	2	3	4	5	6	7	8	9
2	$Y = 58655 - 3404.5\,X$	$Y = 1130.8 - 2944.9\,X$	1.289	$Y = 47619.2 - 459.59X$	$Y = 9780.96 - 358.97\,X$	5.300	$Y = 37837.5 - 100.43\,X$	197.59
3	$Y = 57444.5 - 2220\,X$	$Y = 7579.9 - 1981.1\,X$	1.356	$Y = 49865.2 - 238.89\,X$	$Y = 4344.2 - 144.12\,X$	8.822	$Y = 45521 - 94.76X$	270.25
4	$Y = 62106.9 - 2541.1X$	$Y = 7989.9 - 2213.6X$	1.169	$Y = 54117 - 327.71\,X$	$Y = 5634.92 - 229.06\,X$	3.488	$Y = 48482.1 - 98.65\,X$	277.99
5	Vomit out		—	$Y = 14201.1 - 109.77\,X$	$Y = 2000.7 - 842.30X$	5.364	$Y = 12000.4 - 25.54\,X$	258.70
	Av. $T_{\frac{1}{2}} = 1.27 \pm 0.09$			Av. $T_{\frac{1}{2}} = 5.67 \pm 2.25$			Av. $T_{\frac{1}{2}} = 251.13 \pm 36.56$	

Note: 1. Fish No. 1 died on the 12th day and 5 regurgitated the food after 3 hours of feeding
2. Slow components have real part only.

The effective half-life $T_{1/2} = 0.693/\lambda_{eff}$. The $T_{1/2}$ for each component of each fish are shown in Table 1. The average value of the first rapid, second rapid and the slow components of the effective half-life for each adult Japanese catfish were found to be 1.27 ± 0.1, 5.8 ± 2.3 and 251 ± 37 day, respectively (Table 1). Since the physical half-life of ^{137}Cs is rather long (30 years), the biological half-life, in this case, is nearly equal to the effective half-life of the fish. The average $T_{1/2}$ of ^{137}Cs in the chronically contaminated Japanese catfish was determined to be 142 days [9]. It seems like the slow component of the $T_{1/2}$ of ^{137}Cs in acutely contaminated Japanese catfish is almost twice as great as the $T_{1/2}$ of chronically contaminated fish. However, in bluegill (*Lepomis macrochirus*) no difference was found between the $T_{1/2}$ of ^{137}Cs in chronically and acutely contaminated fish [17]. It was reported that chronically contaminated animals eliminated Cs more slowly (longer half-life) than those which are experimentally contaminated by injection or ingestion; the sequence of half time is: chronic $T_{1/2}$ > acute $T_{1/2}$ [18]. It has been observed that the elimination rates of chronically contaminated fish were about 40% longer than expected for acutely exposed fish [10]. In contrast to these reports, acutely contaminated Japanese catfish were found to eliminate ^{137}Cs more slowly than chronically contaminated fish. The reason is not clearly understood. It is unlikely that potential effects of repeated anaesthesia and other factors (such as temperature, water quality etc.) on metabolic rate were responsible for increasing the $T_{1/2}$ of the fish in this study. For acute and chronic contamination, individual fish species may have unique elimination rates, however, data from large scale experiments with various species of fish are required to draw a general conclusion on the matter. It seems that the curves fitted well in the slow components only. In the region of second rapid components, there is much deviation between the experimental data and the fitted curve (Fig. 1). Further, the real first and second rapid component would be calculated by the peeling off method, which is a complex procedure in exponential curve fitting. Therefore, it seems that multicomponent linear regression is a more realistic and straightforward method for calculating the effective half-life in the present experiment.

For fish that receive a single dose of ^{137}Cs, 50–80% of the initial burden is eliminated by a slow component [18]. However, when tissue pools are equilibrated to ambient radiocaesium concentration, nearly 98% of the initial burden is in a slow pool and eliminated by the slow component. Thus, for the purpose of bioenergetics modelling of most fish populations, the slow elimination component is predominant, and the rapid components may be ignored [15]. The variability in elimination rates among the individual fish may be due to body weight, size and physiological condition. It is unlikely that the variation is due to the treatment of the fish during the experiment. The individual elimination rates are more dependent on individual activity patterns, physical condition, age and/or other factors that could not be identified in the study fish, and which may themselves be influenced by body size. It was suggested that the radionuclide elimination rates determined under penned conditions could be used to usefully approximate rate under natural conditions [19]. If the equilibrium of [137]Cs

concentrations of free-living Japanese catfish can be accurately predicted by using the relationship obtained in the penned elimination rate study, the penned elimination data does not accurately reflect elimination under free living conditions. Previously, it was suggested to use the elimination rate to measure the period of maintainance in a consumer's house. The present experimental conditions in the laboratory and the conditions when maintaining the fish in the consumer's house are almost the same. Therefore, the result obtained may be considered as a result obtained in field conditions.

4.   CONCLUSIONS

Due to the experiment being conducted on four animals only, the conclusion drawn on the $T_{1/2}$ of ^{137}Cs in acutely contaminated Japanese catfish seems to be unsound, however, one can gain valuable information from experiments carried out with a limited number of animals particularly when the radioisotope kinetics are checked by making repeated measurements on individuals without sacrificing them [20] and a good approximation on the $T_{1/2}$ of ^{137}Cs in the fish can be obtained from the present study. The present study was performed with 5 adult fish only. Of these five, one fish regurgitated the contaminated food (however it was included in counting for the data for the 2nd rapid and slow components) and a second died on the 12th day of the study. Therefore, the conclusion is based on four fish. A more precise estimate of $T_{1/2}$ of ^{137}Cs in acutely contaminated Japanese catfish should be determined using a large scale study. Besides the acute contamination by ingestion through the stomach, study with injection to blood and muscle is of importance. Possible difference in the results obtained from the studies with different mode of acute contamination might be of interest.

The reason for the large difference between the $T_{1/2}$ of chronically and acutely contaminated Japanese catfish fish needs to be investigated. Within individual species, the $T_{1/2}$ of ^{137}Cs is affected by factors that influence metabolic rate, increasing by a factor of 2 to 3 for each 10°C increase in temperature, and to a lesser degree in proportion to body mass [10, 11, 14, 18, 21]. The temperature in a lake, pond or swamp varies with depth and season. In Japan, the temperature ranges from 37°C in August to below freezing in January/February. Further, handling stress increases the accumulation and retention time and repeated anaesthesia may also disturb the retention time [9]. The age of fish and the acclimatization conditions may also influence the ^{137}Cs elimination rates [10]. The average age of the individual seems more important than the number of animals in the sample, since food uptake ratio, turnover of stable elements and radionuclides and surface to volume ratio can be strongly age dependent [22]. Therefore, an experiment on $T_{1/2}$ of ^{137}Cs at different temperatures with minimum human disturbance and on age and size (old, adult and juvenile) of the fish is recommended.

REFERENCES

[1]   MALEK, M.A., An Investigation on the Uptake Behaviour of Cs–137 in some Freshwater Fish Species Commonly Consumed in Bangladesh, M.Phil. Thesis, Bangladesh Univ. of Eng. & Tech., Dhaka (1990).

[2]   UNITED NATIONS SCIENTIFIC COMMITTEE ON THE EFFECTS OF ATOMIC RADIATION (UNSCEAR), Ionizing Radiation: Sources and Biological Effects, Reports to the General Assembly, United Nations, New York (1982) 211.

[3]   PETERS, E.L., BRISBIN, I.L., Jr, Radiocaesium elimination in the yellow-bellied turtle (Pseudemys scripta), J. Appl. Ecol. **25** (1988) 461–471.

[4]   LEUNG, J.K., SHANG, Z.R., Uptake of ^{137}Cs and ^{90}Sr in rice plants, Health Phys. **84** (2003) 170–179.

[5]   MEILI, M., "The importance of feeding rate for the accumulation of radioactive cesium in fish after the Chernobyl accident", The Chernobyl Fallout in Sweden (MOBERG, L., Ed.), Swedish Radiation Protection Institute, Stockholm (1991) 177–182.

[6]   WHICKER, F.W., HINTON, T.G., NIQUETTE, D.J., STEEL, J., "Health risk to hypothetical residents of a radioactively contaminated lake bed", ER'93 — Meeting on Challenge: Environmental Remediation, Proc. Conf., Georgia: U.S. DOE Savanah River Operation Office, Vol. 1, October 24–28 (1993).

[7]   HASANEN, E., KOLEHMAINEN, S., MIETTINEN, J.K., "Biological half-time of fresh-water fish: perch, roach and rainbow trout", Radioecological Concentration Processes, Proc. Inter. Symp., Stockholm, 1967 (ABERG, B., HUNGATE, F.P., Eds). Pergamon Press, Oxford (1969) 921–924.

[8]   MALEK, M.A., Uptake and elimination of 137Cs by climbing perch (*Anabus testudineus*), Health Phys. **77** (1999) 719–723.

[9]   MALEK, M.A., NAKAHARA, M., NAKAMURA, R., Uptake, retention, and organ/tissue distribution of ^{137}Cs by Japanese catfish (*Silurus asotus* Linneaeus.), J. Environ. Radioact. **77** (2004) 191–204.

[10]   PETERS, E.L., NEWMAN, M.C., 137Cs elimination by chronically-contaminated largemouth bass (Micropterus salmoides), Health Phys. **76** (1999) 260–268.

[11]   KEVERN, N.R., Feeding rate of carp estimated by a radioisotopic method, Trans. Am. Fish. Soc. **95** (1966) 363–371.

[12]   BAPTIST, J.P., PRICE, T.J., Accumulation and retention of cesium-137 by marine fishes, US Fish and Wildlife Service Fishery Bulletin **206** (1962) 177.

[13]   NELSON, D.J., "Cesium, cesium-137 and potassium concentrations in white crappie and other Clinch River fish", Radioecology, Proc. 2nd Nat. Symp. 1969 (NELSON, D.J., EVANS F.C., Eds), Technical Information Service, Springfield, Virginia (1969) 240–248.

[14]   GALLEGOS, A.F., WHICKER, F.W., "Radiocesium retention by rainbow trout as affected by temperature and weight", Radionuclides in Ecosystems, Proc. 3rd Nat. Symp. on Radioecology, 1971 (NELSON, D.J., Ed.), US Atomic Energy Commission Symposium Series, National Technical Information Service, Springfield, VA (1971) 361–371.

[15]   ROWAN, D.J., RASMUSSEN, J.B., The elimination of radiocaesium from fish, J. App. Ecol. **32** (1995) 739–744.

[16]   COMAR, C.L., Radioisotopes in Biology and Agriculture: Principles and Practice, McGraw-Hill, New York (1955).

[17]   KOLEHMAINEN, S.E., The balance of Cs–137, stable cesium, and potassium of bluegill (Lepomis macrochirus Raf.) and other fish in White Oak Lake, Health Phys. **23** (1972) 301–315.

[18]   MAILHOT, H., PETERS, R.H., CORNETT, R.J., The biological half-time of radioactive Cs in poikilothermic and homeothermic animals, Health Phys. **56** (1989) 473–484.

[19]   FENDLEY, T.T., MANLOVE, M.N., BRISBIN, I.L., Jr., The accumulation and elimination of radiocesium by naturally contaminated wood ducks, Health Phys. **32** (1977) 415–422.

[20]   VAN WEERS, A.W., "Uptake of Cobalt-60 from sea water and from labelled food by the common shrimp (Crangon crangon L.)", Impacts of Nuclear release into the Aquatic Environments (Proc. Int. Conf. Vienna, 1975), Proceedings Series, IAEA, Vienna (1975) 349–361.

[21]   UGEDAL, O., JONSSON, B., NJÂSTAD, O., NEUMANN, R., Effects of temperature and body size on radiocesium retention in brown trout, *Salmo trutta*, Freshwater Biology **28** (1992) 165–171.

[22]   FAGERSTRÖM, T., Body weight, metabolic rate, and trace substance turnover in animals, Oecologia **29** (1977) 99–104.

LEAD AND STABLE ISOTOPES IN SEDIMENTS OF BABITONGA BAY: AN OIL SPILL CASE

V.G. BARROS [a], T.M.N. OLIVEIRA [a], G.M. ZUPPI [b], C. VAZ [a]

[a] University of UNIVILLE,
   Department of Environmental Engineering,
   Joinville, Santa Catarina, Brazil

[b] Dipartimento di Scienze Molecolari e Nanosistemi Università Ca' Foscari,
   Venezia, Italy
   and
   Institute of Environmental Geology and Geoengineering,
   National Research Council,
   Monterotondo, Italy

Abstract

The hydrologic complex of Babitonga Bay (Brazil) forms a vast environmental complex, hosting the last great mangrove bulk of the southern hemisphere. Mangroves are among the most productive ecosystems on earth. The effects of an oil spill were studied in Babitonga Bay using lead and carbon isotopes. Samples of the spilled oil were obtained nine months after the accident, as well as sediment and water samples. Thus, the isotopic composition of the oil allowed the tracing of the environmental pollution. Notwithstanding the delay in time, isotopes of lead and carbon allowed the identification of areas where the presence of the oil can be still detected, permitting assessment of the extent of pollution. Contaminated sediments exhibited an isotopic composition ($^{206}Pb/^{207}Pb$ and $^{208}Pb/^{206}Pb$) close to that of the oil spilled. Moreover $\delta^{13}C$ also permitted the ratification of these results. Others isotopes were used but with no contributions. Conclusions are derived in terms of the source of the pollution in the specific area.

1.   INTRODUCTION

Estuarine and transition areas constitute natural reaction zones in which heterogeneous processes may affect the ecological equilibrium due to local changes in the biogeochemical conditions. Besides the natural sources, other inputs provide significant contributions to these areas. In Babitonga Bay (BB) different pollutant sources cause sediment pollution [1], and the major suppliers are: (i) activities at São Francisco do Sul Harbour, (ii) inadequately treated domestic sewage, (iii) industrial activity at Joinville, (iv) other contamination transport from tributaries [2–4]. Estuarine systems are well known as owners of large amounts of organic matter and for this

reason stable carbon isotope composition has been useful in estuary studies [3, 5–8]; and it is a consolidated tracer at these sites. In order to distinguish between anthropogenic and natural inputs, isotopes of lead also represent a potential pollution indicator. It is also reasonably immobile in environmental sinks. In addition, Pb isotopes have the potential to distinguish between Pb originated from natural sources (rocks, soil) and from pollution sources (e.g., fuel combustion, sewage, atmospheric deposition). In the summer of 2008 an accident occurred causing a large oil spill in the BB ecosystems. After nine months a campaign was conducted in order to search for residues of this spill. The major objectives of the present study are to characterize the different isotopic compositions of carbon and lead in BB, especially the product of oil weathering, and to elucidate the origin of Pb and C in sediments. Lead and carbon isotopic compositions were determined in bulk sediments and residues, in order to identify the sources (geogenic or anthropogenic) of different inputs. Lead was chosen as an additional tracer to identify oil origin, due to the fact that the isotopic composition of Pb is not significantly affected by physicochemical fractionation processes [9].

2.   SITE DESCRIPTION

The hydrologic complex of Babitonga Bay (BB) is located 45 km northeast from the city of Joinville, which is the principle city (featuring heavy industry and urbanization) of the Santa Catarina State (Southern Brazil), Fig. 1. The drainage basin of this bay forms a vast environmental complex, where agriculture and shellfish
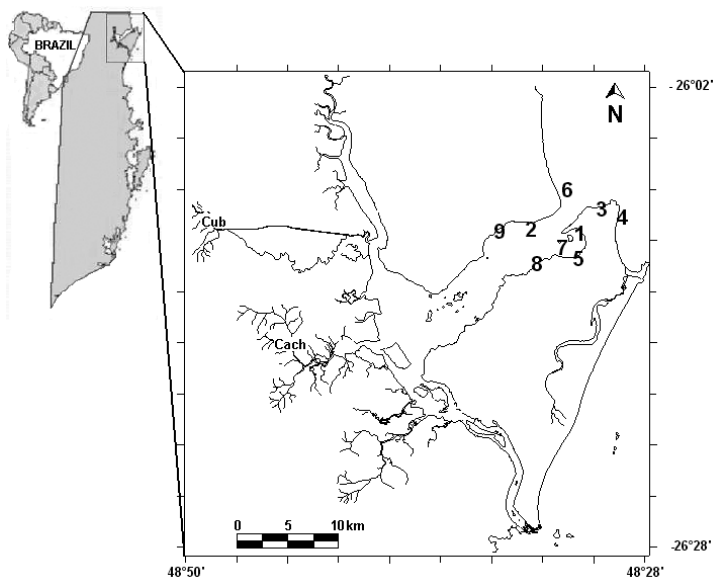

FIG. 1. Hydrological complex of Babitonga Bay and sample sites.

farming, as well as a spectrum of industries, coexist with a unique natural area of Atlantic rain forest. Babitonga Bay, the southern residual mangrove forests of Brazil, is connected to the Atlantic Ocean via an opening with a width of 1850 m and presents a salt wedge circulation system. A significant tidal oscillation brings appreciable water renewal to the whole ecosystem. Tides are mixed exhibiting semidiurnal dominance with diurnal inequalities [10]. The region is characterized by a humid subtropical climate with a rainfall average of 2000 mm/a. There are two distinguishable seasons: summer (from November to April) and winter (from May to October). During summer, the weather is characterized by high temperatures and humidity, with intense precipitation caused by local convection processes strictly controlled by the regional orography. During winter, the influence of polar air masses brings a decline of temperature and precipitation in the region.

3. GEOLOGICAL CONTEXT

3.1. Santa Catarina Granulite Complex

According to Ref. [11] the Santa Catarina Granulite Complex is the oldest tectonic unit in the Catarinense Shield. This complex is composed of tonalitic, granodioritic, and trondhjemitic orthogneisses that were intruded by mafic and ultramafic rocks. Minor occurrences of meta-sedimentary rocks such as quartzites and banded iron formations are also present. The first mantle–crust differentiation of the Santa Catarina Granulite Complex is of Archean age, at 2.8 Ga (TDM model age), and the tectonic stabilization occurred in the Paleoproterozoic, at 1.9 Ga (K–Ar in biotite). The Santa Catarina Granulite Complex was metamorphosed to a granulite facies during two events. The first event occurred at 2675 ± 12 Ma, and the second event occurred at 2168 ± 18 Ma (U-Pb SHRIMP) when the magmatic protoliths crystallized at 2716 ± 17 Ma [12]. Ref. [12] interpreted the Santa Catarina Granulite Complex as a stable craton after 1.9 Ga, and the complex remained an undeformed block during the orogenies of the Brasiliano/Pan-African Cycle (Luis Alves microplate).

4. SAMPLE LOCATION AND METHODS

Sampling was authorized by the public prosecutor (PP) nine months after the oil spill. An additional campaign was made, one month before the one authorized by the PP, in order to take three samples of the oil trapped inside the ship casualty, which remained capsized all this time inside BB. Nine sampling sites were chosen based on the oil slick. The main goal was to identify if the oil was still present in the bay sediments. Sample sites were chosen, by the PP, as a function of the oil stains that were formed after the spill, and were analysed by the Centro de Pesquisas

Geocronológicas, University of São Paulo — USP (Pb isotopes) and Centro de Energia Nuclear na Agricultura, University of São Paulo – USP (C and N isotopes).

5.   RESULTS

The samples analysed represent the surface layer of the sedimentary pile at the sites shown in Fig.1, and Pb and C isotopic composition determined in nine samples defined by the public prosecutor are presented in Table 1.

5.1. Lead

BB has a known history of contamination by heavy metals [1, 4, 13], so analysing Pb concentration would not be interesting, as previous work showed lead concentration in BB sediments [1, 14]. By using Pb isotopic composition differences between Pb from the oil spill and other origins could be spotted. Important isotopic differences are observed between the samples and the geogenic background (Fig. 2). Pb isotopic composition tends to be more radiogenic (high [206]Pb/[207]Pb ratio) in BB sediments – leachate and residual, as well as in the oil collected inside the ship. It is important to mention that BB suffers from the disposal of sewage without treatment, but the impact of this disposal is apparent in the inner part of the Bay [3], whereas samples were collected toward the mouth. The system indicates a simple binary mixing of geogenic with anthropogenic Pb.
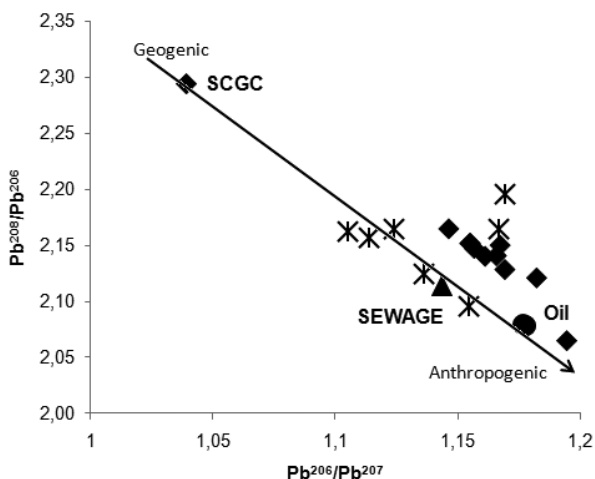

FIG. 2. The relationship between [206]Pb/[207]Pb and [208]Pb/[206]Pb ratios of BB sediments. The linear behaviour suggests a simple binary mixing of geogenic with anthropogenic Pb.

TABLE 1. ISOTOPIC COMPOSITIONS OF BB SEDIMENTS AND OIL SAMPLES

Sample	$^{206}Pb/$ ^{204}Pb	Error % (1σ)	$^{207}Pb/$ ^{204}Pb	Error % (1σ)	$^{208}Pb/$ ^{204}Pb	Error % (1σ)	$^{206}Pb/$ ^{207}Pb	Error % (1σ)	$^{208}Pb/$ ^{206}Pb	Error % (1σ)	$\delta^{15}N$ (‰)	$\delta^{13}C$ (‰)
Oil1	18.654	0.056	15.613	0.058	38.507	0.058	1.195	0.009	2.065	0.008	8.24	−24.57
Oil2	18.347	0.225	15.595	0.223	38.152	0.226	1.177	0.021	2.080	0.013	8.59	−24.15
Oil+seaw	18.416	0.006	15.638	0.006	38.269	0.006	1.178	0.001	2.078	0.002	8.64	−26.31
S1 - L	18.345	0.007	15.688	0.007	39.040	0.007	1.169	0.002	2.128	0.002	nd	nd
S1 - Res	17.783	0.023	15.650	0.025	37.762	0.024	1.136	0.004	2.124	0.002		
S2 - L	17.981	0.008	15.684	0.009	38.918	0.011	1.147	0.002	2.165	0.004	4.22	−24.69
S2 - Res	17.475	0.006	15.544	0.006	37.835	0.006	1.124	0.001	2.165	0.002		
S3 - L	18.333	0.016	15.704	0.017	39.411	0.02	1.167	0.005	2.150	0.009	nd	nd
S3 - Res	22.893	0.004	16.284	0.005	42.810	0.005	1.406	0.001	1.870	0.002		
S4 - L	18.225	0.01	15.692	0.011	38.996	0.012	1.161	0.002	2.140	0.003	nd	nd
S4 - Res	17.468	0.006	15.685	0.005	37.673	0.006	1.114	0.001	2.157	0.001		
S5 - L	18.102	0.006	15.672	0.006	38.942	0.007	1.155	0.001	2.151	0.001	4.92	−21.71
S5 - Res	18.312	0.005	15.695	0.005	39.620	0.005	1.167	0.001	2.164	0.001		
S6 - L	18.566	0.016	15.702	0.015	39.370	0.017	1.182	0.003	2.121	0.002	nd	nd
S6 - Res	18.343	0.01	15.688	0.01	40.276	0.01	1.169	0.002	2.196	0.001		
S7 - L	18.132	0.054	15.696	0.05	39.023	0.053	1.155	0.006	2.152	0.007	10.57	−10.73
S7 - Res	17.310	0.056	15.662	0.056	37.414	0.057	1.105	0.006	2.162	0.005		
S8 - L	18.276	0.056	15.674	0.056	39.115	0.057	1.166	0.004	2.141	0.005	nd	nd
S8 - Res	18.113	0.025	15.686	0.024	37.954	0.024	1.155	0.004	2.096	0.003		
S9 - L	18.163	0.088	15.706	0.096	39.009	0.101	1.157	0.009	2.147	0.012	9.95	−2.07
S9 - Res	19.230	0.023	15.797	0.025	38.369	0.025	1.217	0.005	1.995	0.004		

A different behaviour can be observed among leachate and the residual phase of samples. Leachate presents a Pb isotopic composition which is in general more radiogenic (^{206}Pb/^{207}Pb ratio between 1.1465 and 1.1824) than the residual phase (^{206}Pb/^{207}Pb ratio between 1.1052 and 1.1546), so sediments at sample points present an important anthropogenic input (oil sample presented ^{206}Pb/^{207}Pb ratio 1.1766). In the leachate no important contribution, such as sewage, was observed. According to Refs [15–17], a large amount of the anthropogenic lead added to a sediment can probably be leached from the residue by dilute acid. According to Ref. [18], the influence of organic matter (OM) and iron oxyhydroxide surface can cause reasonable differences between residual and leachate. Lead released from the structures of silicate minerals is isotopically distinct from that released from other sites, demonstrating distinct lead reservoirs. In fact, in BB mangrove sediments have great amounts of OM. Another area of important anthropogenic contribution also can be observed in the vicinities of the Capri Iate Club, with ^{206}Pb/^{207}Pb value as low as 1.1362 for the residue. Considering the influence of São Francisco do Sul Harbour activity, a similar pattern could be expected, with Pb isotopic composition close to that of oil. As oil samples were collected inside the ship, casualty sediment samples tend to match with this oil sampled.

5.3. Carbon and nitrogen isotopes

In order to trace the OM origin, carbon and nitrogen isotopes were used. Unfortunately, sand beaches had no sufficient OM, so it was not possible to detect the carbon isotopic composition due to its low concentration. Mangrove sediments were analysed, and the results are presented in Table 1. Elemental and stable isotope analysis has been used in a large number of studies to determine the spatial and temporal distribution of different sources of organic matter (allochthonous detritus and local phytoplankton) in suspended matter and sediments of estuarine systems e.g. [3, 19]. This approach makes use of the fact that different biochemical pathways, and the degree to which carbon and nitrogen has been reworked, will lead to different isotopic ratios of δ^{13}C and δ^{15}N. When the resulting stable isotope signatures of the different origins are sufficiently dissimilar, it is possible to allocate the sources of organic matter. In this work, in addition to δ^{13}C and δ^{15}N, Pb isotopes were used. Ref. [20] found in BB sediment δ^{13}C values ranging from –22.58‰ to –24.94‰. The more enriched values are observed at oceanward points, suggesting the large contribution of marine organic matter characterized by a typical mean value –21.0‰ [26]. δ^{15}N values of BB sediments range from 3.56 to 6.43‰, and more enriched values are observed oceanward. Oil isotopic composition ranges from 8.24 to 8.64‰ for δ^{15}N and from –26.31 to –24.15‰ for δ^{13}C. Sediment samples collected after the casualty, all of them collected oceanward, presented an isotopic composition varying from –24.69 to –2.07‰ as δ^{13}C, and from 4.22 to 10.57‰ as δ^{15}N. By using isotopes from organic matter just one sample matches with the oil sample. It is important

to reinforce the time elapsed (nine months) since the casualty to the fieldwork. In addition, the successive tides exposing and submerging sample sites, two seasons (summer and autumn), and biogeochemical processes contributed to the isotopic fractionation.

6.   CONCLUSION

BB experiences a hard process of loss of natural features due to recurrent acute and chronic impacts. Particularly in this shipwreck, the slowness of legal bureaucracy brought injury to the environmental impact assessment. Fortunately, previous $\delta^{13}C$ data were available, samples of the spilled oil were collected for analysis (after 8 months) and the $^{207}Pb/^{206}Pb$ and $^{208}/^{206}Pb$ ratio variations between geogenic and oil samples were large. The use of isotopes, such as Pb isotopes, that undergo little fractionation when exposed to weathering and biogeochemical processes, is important and can be an interesting alternative. Despite many difficulties, by using combined isotope tracers it was possible to spot areas were the oil spilled could be identified.

REFERENCES

[1]   CREMER, M.J., MORALES, P.R.D., DE OLIVIERA, T.M.N., Diagnóstico ambiental da Baía da Babitonga, Univille, Joinville, Brazil (2006).

[2]   BARROS, G.V., MAS-PLA, J., OLIVIERA NOVAIS, T.M., SACCHI, E., ZUPPI, G.M., Hydrological mixing and geochemical processes characterization in an estuarine/mangrove system using environmental tracers in Babitonga Bay (Santa Catarina, Brazil), Cont. Shelf Res. **28** (2008) 682–695.

[3]   BARROS, G.V., MARTINELLI, L.A., OLIVIERA NOVAIS, T.M., OMETTO, J.P.H.B, ZUPPI, G.M., Stable isotopes of bulk organic matter to trace carbon and nitrogen dynamics in an estuarine ecosystem in Babitonga Bay (Santa Catarina, Brazil), Sci. Total Environ. **408** (2010) 2226–2232.

[4]   VAZ, C., et al., Use of Artemia salina to identify sites with risk of contamination in the waters of Babitonga Bay, Toxicology Letters **196** 2 (2010) S120.

[5]   DEHAIRS, F., et al., Tracing mangrove carbon in suspended matter and aquatic fauna of the Gautami–Godavari Delta, Bay of Bengal (India), Hydrobiologia **431** (2000) 225–241.

[6]   CARREIRA, R.S., et al., Changes in the sedimentary organic carbon pool of a fertilized tropical estuary, Guanabara Bay, Brazil: An elemental, isotopic and molecular marker approach, Mar. Chem. **79** (2002) 207–227.

[7]   GRAHAM, M.C., EAVES, M.A., FARMER, J.G., DOBSON, J., FALLICK, A.E.. A study of carbon and nitrogen stable isotope and elemental ratios as potential indicators of source and fate of organic matter in sediments of the Forth Estuary, Scotland, Estuar. Coast. Shelf Sci. **52** (2001) 375–380.

[8]   GOÑI, M.A., TEIXEIRA, M.J., PERKEY, D.W., Sources and distribution of organic
        matter in a river-dominated estuary (Winyah Bay, SC, USA), Estuar. Coast. Shelf Sci.
        57 (2003) 1023–1048.

[9]   KOMÁREK, M., ETTLER, V., CHRASTNÝ, V., MIHALJOVIČ., Lead isotopes in
        environmental sciences: A review, Environment International **34** 5 (2008) 562–577

[10]   SCHETTINI, C.A.F., CARVALHO, J.L.B., JABOR, P., Comparative hydrology and
        suspended matter distribution of four estuaries in Santa Catarina State – Southern
        Brazil, Proc. Workshop on Comparative Studies of Temperate Coast Estuaries, Bahia
        Blanca (1996) 29–32.

[11]   GUADAGNIN, F., et al., Depositional age and provenance of the Itajaí Basin, Santa
        Catarina State, Brazil: Implications for SW Gondwana correlation, Precambrian Re-
        search **180** (2010) 156–182.

[12]   HARTMANN, L.A., SANTOS, J.O.S., McNAUGHTON, N.J., VASCONCELLOS,
        M.A.Z., DASILVA, L.C., Ion microprobe (SHRIMP) dates complex granulite from
        Santa Catarina, southern Brazil, Anais da Academia Brasileira de Ciências **72** (2000)
        559–572.

[13]   DE OLIVEIRA, C.R., DOS SANTOS, D., MADUREIRA, L.A., DE MARCHI,
        M.R., Speciation of butyltin derivatives in surface sediments of three southern Bra-
        zilian harbors, J. Hazard. Mater. **181** (2010) 851–856.

[14]   AHMED, H., HÄDER, D.-P., Rapid ecotoxicological bioassay of nickel and cad-
        mium using motility and photosynthetic parameters of *Euglena gracilis*, Environ.
        Exp. Bot. **69** (2010) 68–75.

[15]   CHOW, T.J., et al., Lead pollution: Records in Southern California coastal sedi-
        ments, Science **181** (1973) 551– 552.

[16]   SHIRAHATA, H., ELIAS, R.W., PATTERSON, C.C., Chronological variations in
        concentrations and isotopic compositions of anthropogenic atmospheric lead in sedi-
        ments of a remote subalpine pond, Geochim. Cosmochim. Acta **44** (1980) 149–162.

[17]   KOBER, B., WESSELS, M., BOLLHÖFER, A., MANGINI, A., Pb isotopes in sedi-
        ments of Lake Constance, Central Europe constrain the heavy metal pathways and
        the pollution history of the catchment, the lake and the regional atmosphere, Geo-
        chim. Cosmochim. Acta **63** 9 (1999) 1293–1303.

[18]   GIOIA, S.M.C.L., et al. Sources of anthropogenic lead in sediments from an artifi-
        cial lake in Brasília-central Brazil, Sci. Total Environ. **356** (2006) 125–142.

[19]   CIFUENTES, L.A, et al. Isotopic and elemental variations of carbon and nitrogen in
        a mangrove estuary, Estuar. Coast. Shelf Sci. **43** (1996) 781–800.

[20]   BARROS, G.V., Study and monitoring of biogeochemical process of Babitonga Bay
        catchment — Brazil, using chemical and isotopes approaches, PhD Thesis, Univer-
        sity of Ca' Foscari Venezia, Venice, Italy (2005).

[21]   GUO, L., TANAKA, T., WANG, D., TANAKA, N., MURATA, A., Distributions,
        speciation and stable isotope composition of organic matter in the southeastern Ber-
        ing Sea, Mar. Chem. **91** (2004) 211–226.

LOOKING FOR DAMMING EFFECTS ON THE SEDIMENTATION RATES IN THE ESTUARY REGION OF THE PARAIBA DO SUL RIVER, BRAZIL

C.V.A. WANDERLEY [a], J.M. GODOY [a,b], C.E. REZENDE [c],
M.L.D.P. GODOY [b], Z.L. CARVALHO [b]

[a] Departamento de Química,
Pontifícia Universidade Católica, PUC-RIO,
Rio de Janeiro, RJ, Brazil

[b] Instituto de Radioproteção e Dosimetria, IRD,
Comissão Nacional de Energia Nuclear,
Rio de Janeiro, RJ, Brazil

[c] Centro de Biociências e Biotecnologia,
Universidade Estadual Norte Fluminense Darcy Ribeiro, UENF,
Campos dos Goytacases, RJ, Brazil.

Abstract

The objective of this work is to evaluate the sedimentation rates at Paraiba do Sul estuary and to correlate them with the strong erosion that occurs in Atafona, Rio de Janeiro. The coastal line of Atafona has been regressing in the last 50 years and the sea has destroyed some constructions. There are traces that one of the factors of the situation in Atafona is the disruption of the equilibrium deposition–erosion. The sedimentation rates will show the influence of the river material input and when it happened, enabling the evaluation of the human and natural impacts suffered by the river. The work was based on three transects, north, centre and south, where 10 sediment cores with about 350 sediment samples were collected in January 2010. The sedimentation rates were obtained based on ^{210}Pb dating and the data validated based on the heavy metal profiles and the local anthropogenic impacts records.

1.   INTRODUCTION

Brazil has a great water potential, enough not only for the population's consumption but also for industrial and agricultural purposes, as well as for the generation of electric power. A good example of this potential is the Paraíba do Sul River (PSR) which, together with its affluent, forms the biggest hydrographic basin in the southeastern region, crossing three states, São Paulo, Minas Gerais and Rio de Janeiro, an area of approximately 55 400 km² with 1500 km of extension. The Paraíba

do Sul River estuary is located at a coastal plain formed by the PSR delta in the north of Rio de Janeiro State, near São João da Barra (21°36` S and 41°05` W) (Gonçalves and Carvalho, 2006) [1]. The PSR is one of the most important rivers of the hydrographic basin of this region and has quite varied discharges, mainly due to the dams built along its course.

Anything that happens in the drainage basin will impact direct or indirectly on the rivers. The current situation of the river is worrying, since it has been affected by various forms of degradation along its course: deforestation of the margins, thus causing erosion; use of pesticides; domestic sewage discharge and solid waste, besides the existence of numberless dams, mainly due to the deviation to the Guandu River, where main water supply of the city of Rio de Janeiro comes from. When this detour to the Guandu River was built, in 1952, many reservoirs and plant lift stations were built along the course of the Paraíba do Sul River, among which are Santa Cecília, Santana and Vigário. In 1955 the Guandu River station for impounding and water treatment was built and started to operate, and in 1959 another dam – Santa Branca, at the upper part of the PSR, in the state of São Paulo — was built in order to guarantee the water supply.

The construction of dams on the PSR has reduced the amount of sediment and water coming to the beaches, thus decreasing the strip of sand and increasing the intensity of the erosion [2]. Over the last years this very important river has been suffering a continuous process of modification of its delta, characterized by the sea headway and by the strong erosion of the Atafona beach [3].

Atafona is a town in the São João da Barra district of RJ, Brazil, situated close to the PSR estuary. In the 1950s, this town used to be very popular, with many residences where people went for weekends and summer holidays. Over the last fifty years, Atafona has been suffering with the drying of the river and with the erosion caused by the sea's headway. The coastal line of Atafona is receding, and the advancement of the sea has been destroying most of the litoranean constructions. The retrogradation rate associated to the erosion was estimated at 7.5 m/y, based on photographic data from 1976 and the determination of the front line by GPS in 1996 [2]. Actually, up to this moment, those events have caused the destruction of 183 buildings in 14 squares [4]. The most important cause for this phenomenon is the combination of natural factors, such as wind, waves and tides, with human action.

[210]Pb dating and mass sedimentation rates were determined to investigate the changes in the sediment supply in this region over the last fifty years, aiming for the evaluation of the human and natural impacts on the river's estuarine region.

2. METHODS

The work was based on three transects, north, centre and south and one other point further south at PRS estuary, where 10 sediment cores with 386 sediments
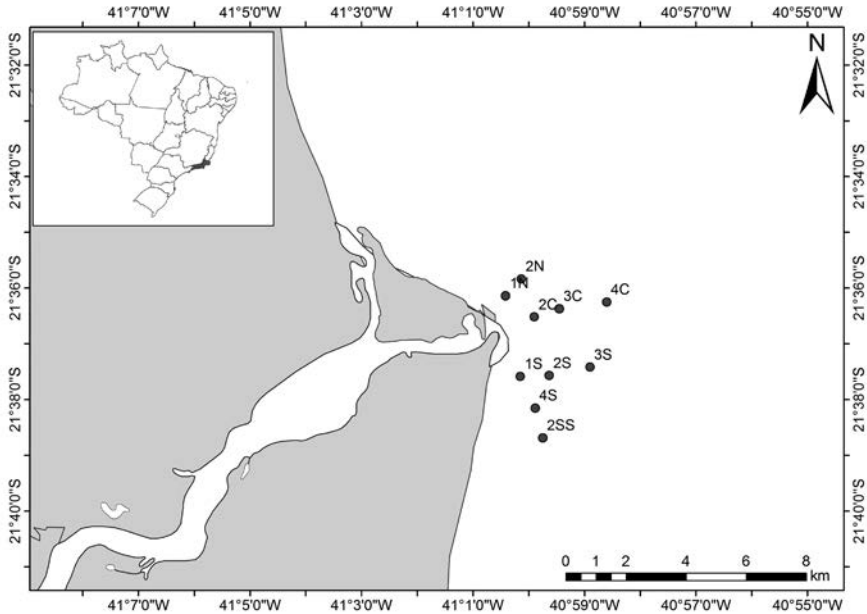
FIG. 1. Selected transects chosen during the 1st sampling campaign.

samples were collected in January 2010 (Fig. 1). The sediment cores were taken with a UWITEC corer and immediately sliced into 1 cm layers.

Once sliced, the samples were weighted and one aliquot was taken for the granulometry determination at UENF laboratories. The remaining fraction was dried at 70°C in an oven with circulating air until they reached a constant weight and were finely ground with a porcelain mortar.

[210]Pb concentrations were determined according to the procedure described by Godoy et al. [5]: Briefly, 3 g aliquots were taken, leached with 40 mL 0.5 M HBr for two hours at 80°C, the obtained solution separated and the residue leached with 40 mL 0.5 M HBr + 1.0 g hydroxylamine hydrochloride for two hours at 80°C. Lead carrier was added to the resultant solution and the mixture transferred to an ion exchange column containing Dowex 1X8, 50–100 mesh. This was followed by a cleaning step with 0.5 M HBr + 1.0 g hydroxylamine hydrochloride and further elution with 1 M HNO_3. Lead is precipitated as chromate and the chemical yield obtained gravimetrically. The concentration of ^{210}Pb is determined based on its daughter decay product, [210]Bi, after two week's ingrowth period, by beta counting on a ten channel low level proportional counter Perkin–Elmer Prof. Berthold LB–750. The detection limit of this technique is 1 Bq/kg for 1000 min counting time.

For elemental analysis, two hundred and fifty milligram aliquots of each sample were taken and totally digested with an acid mixture (0.4 mL $HClO_4$ + 10 mL HNO_3

+ 2 mL HF) in a Teflon digestion vessel, heated to dryness, and the residues were re-dissolved in 40 mL 2% HNO_3. After a 1:10 dilution with 2% HNO_3, the elemental concentrations will be determined by ICP–MS (Perkin–Elmer ELAN 6000) as described in Ref. [6].

The ^{210}Pb method is based on the measurement of the excess or unsupported activity ^{210}Pb, which is incorporated rapidly into the sediment from atmospheric fallout and water column scavenging [7]. Once incorporated into the sediment, unsupported ^{210}Pb decays with depth, equivalent to time, in the sediment column, according to its known half-life. The sediment core chronologies were determined using the Constant Initial Concentration (CIC) model and the Constant Rate of Supply (CRS) model [8–12].

3. RESULTS AND DISCUSSION

3.1. [210]Pb in sediment cores

In order to assess the processes of datation and sedimentation rate changes, a crucial prerequisite is to calculate fluxes, and thus to allow comparison between the study points. The ^{210}Pb fluxes were calculated by using the total [210]Pb$_{excess}$ inventory, as proposed by Appleby and Oldfield [7]. The sampling points located in a south direction from the mouth of the PSR presented values of ^{210}Pb fluxes, 31.0 mBq cm^{-2}·y^{-1}, higher than the sampling points located at the north and centre (Fig. 2). These findings seem to show that the sediment transport is in a southerly direction with the longshore current [13, 14].

The 1S, 1N, 2N, 3S and 4S cores present themselves as a whole mixing zone. This may be due to anthropogenic activities such as trawling, since this is very practiced in the region, and biological activities, due to the presence of polychaetes. Based on these cores' results only the flux of ^{210}Pb of each one could be calculated (Fig. 2).
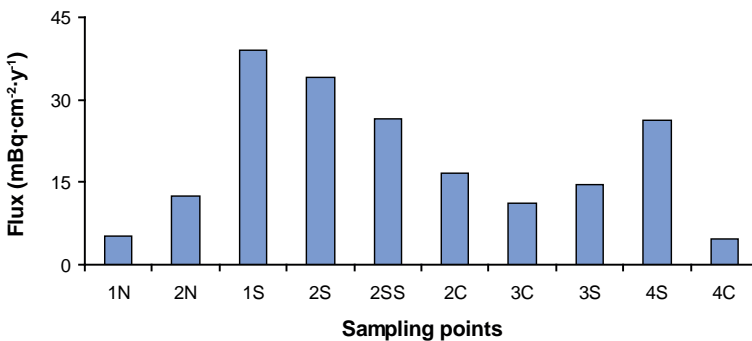

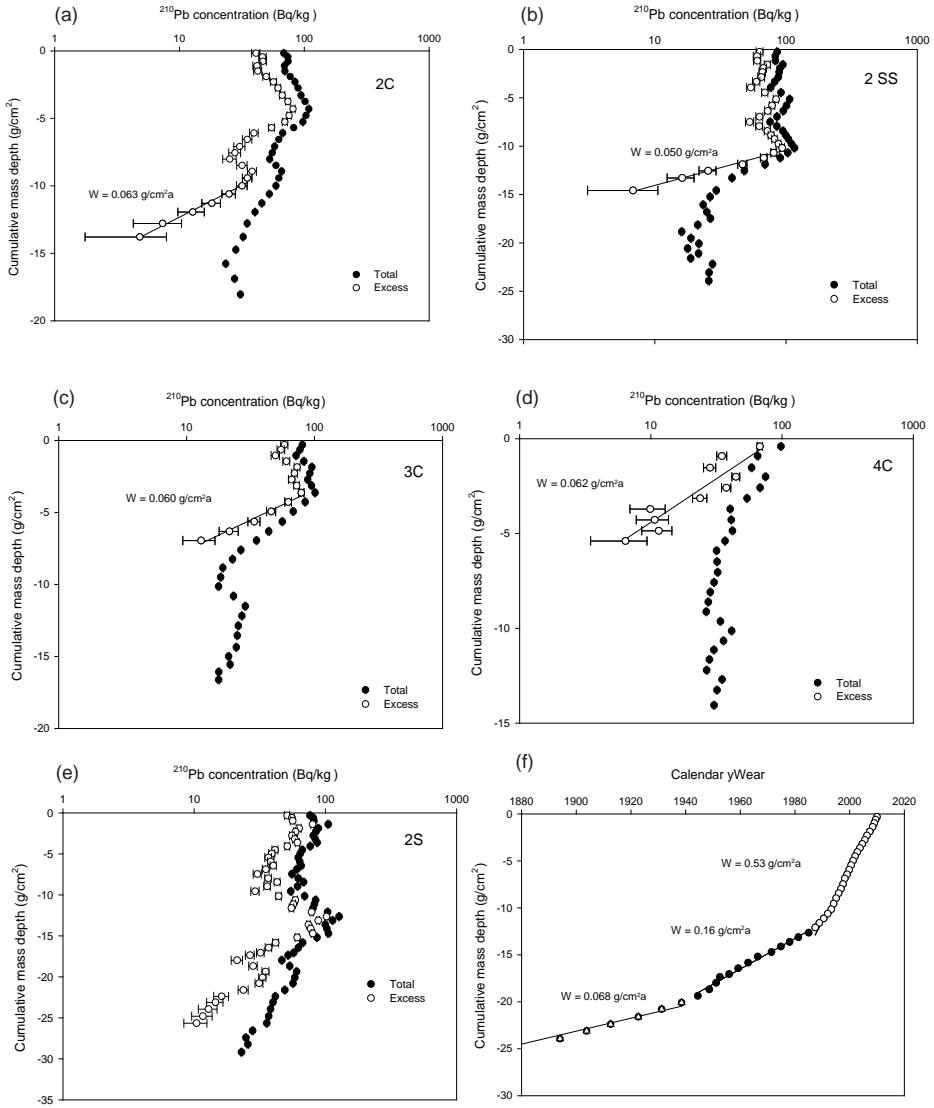*FIG. 2. [210]Pb fluxes at the sampling points.*

FIG. 3. Exponential variation of the ^{210}Pb concentration with depth (Fig. 3a to Fig. 3e), and Fig. 3f represents age and mass depth profile for the sampling point 2S obtained, based on the CRS model.

The 2C and 2SS sampling points showed an exponential variation of the ^{210}Pb concentration with depth. The exponential variation in the 2C core (Fig. 3a) occurred in the deeper layers below 20 cm, where the CIC model was applied, and the sedimentation rate determined was 0.063 g cm^{-2}·y^{-1} for the period before 1950. The sedimentation rate in 2SS point (Fig. 3b) was also obtained through the CIC model with a value of 0.05 g cm^{-2}·y^{-1} below 20 cm before the 1960s. These low sedimentation rates and the dates obtained correlate with construction of the Santa Cecília impoundment in 1955, which brings water from the Paraíba do Sul Basin into the Guandu River, increasing the Guandu river flow from 20 m^3/s to 160m^3/s.

Despite having a surface mixing layer (SML) of up to 8 cm, the 3C core also presented an exponential variation in ^{210}Pb concentration with depth below this. Below the SML, the CIC model was applied and thus determined the sedimentation rate of 0.060 g cm^{-2}·y^{-1} (Fig. 3c).

At the sampling point 4C, the CIC model was applied to the upper layers, until 10 cm, where the sedimentation rate was very low, 0.062 g·cm^{-2}·y^{-1}, and constant over the last 70 years (Fig. 3d). The ^{210}Pb flux was one of the lowest, 5.0 mBq cm^{-2}·y^{-1}, reinforcing the fact that that this region doesn't represent an area highly affected by the river plume as it flows to the south longshore.

A peak of ^{210}Pb concentration appeared in the 2S core at the year of 1985 (27 cm), and the sedimentation rates were determined through the CRS model. Three sedimentation rates were observed: a higher rate of 0.53 g·cm^{-2}·y^{-1} for more recent sediment, until 1985, an intermediate, 0.17 g·cm^{-2} y^{-1} between 1940 and 1985 (27 cm and 40 cm), and a lower rate of 0.07 g·cm^{-2}·y^{-1} for the period before 1940. This mass sedimentation rate of around 0.05–0.07 g·cm^{-2}·y^{-1} seems to represent a baseline value (Fig. 3e–f).

To validate the ^{210}Pb dating, elemental analysis is being made in the 2S core.

4.   CONCLUSIONS

The preliminary results show the beginning of the study, and further research is needed to better estimate accumulation rate changes in these sites. By the way, the second sampling campaign at the PSR estuary was conducted from February 14–18, 2011 to continue this study. At this campaign two new transects were taken: one higher north with 3 sampling points distanced 1km from each other, and the second following the 2SS sampling point where two more cores in this direction were taken at a distance of 1 km from each one, since this region seems to be more affected by the river plume.

Although the elemental analysis will continue to be made to validate the ^{210}Pb dating, the ^{210}Pb dating tool is probably efficient in determining a precise temporal record of sediment changes in this region, allowing for the direct identification of the impact of historical events.

Currently, the region may be undergoing changes due to internal motions arising from the coastal systems, including receiving interference due to recent activity of the future Açu port and also trawling that is very characteristic of the region.

ACKNOWLEDGEMENTS

REFERENCES

[1]   GONÇALVES, G.M., CARVALHO, C.E.V., Particulate heavy metal dynamics in a tropical estuary under distinct river discharge and tidal regimes, Southeastern, Brazil, J. Coastal Res. Special Issue **39** 2 (2006) 1032–1035.

[2]   RIBEIRO, G.P., et al., Análise espaço-temporal no suporte à avaliação do processo de erosão costeira em Atafona, São João da Barra (RJ), Revista Brasileira de Cartografia **56** 2 (2004) 129–138.

[3]   MARTIN, L., et al., "Significado geológico das variações dos graus de arredondamento das areias holocênicas da Planície Costeira do Rio Paraíba do Sul (RJ)", ANAIS DO XXXIII Congresso Brasileiro de Geologia, Rio de Janeiro (1984).

[4]   FIGUEIREDO, A.G., Jr., et al., "Atafona: Avaliação preliminar do processo de erosão costeira", II Simpósio Brasileiro de Oceanografia (2004).

[5]   GODOY, J.M., MOREIRA, I., WANDERLEY, C., SIMÕES FILHO, F.F.M., MOZETO, A.A., An alternative method for the determination of excess ^{210}Pb in sediments, Radiat. Prot. Dosim. **75** (1998) 111–115.

[6]   GODOY, M.L.D.P., GODOY, J.M., ROLDÃO, L.A., CONTI, L.F., Application of multivariate statistical analysis to superficial soils around a coal burning power plant, Journal of the Brazilian Chemical Society **15** (2004) 122–130.

[7]   APPLEBY, P.G., OLDFIELD, F., "Application of lead–210 to sedimentation studies", Uranium-series Disequilibrium: Application to Earth, Marine and Environmental Sciences (IVANOVICH, M., HARMON, R.S., Eds), Oxford Sciences, Clarendon Publications (1992) 731–778.

[8]   KRISHNASWAMY, S., LAL, D., MARTIN, J.M., MEYBECK, M., Geochronology of lake sediments, Earth Planet. Sci. Lett. **11** (1971) 407–414.

[9]   ROBBINS, J.A., EDGINGTON, D.N., Determination of recent sedimentation rates in Lake Michigan using ^{210}Pb and ^{137}Cs, Geochim. Cosmochim. Acta **39** (1975) 285–304.

[10]   GOLDBERG, E.D., "Geochronology with ^{210}Pb", Proc. Symp. on Radioactive dating, Athens, Greece, 19–23 November 1962, IAEA, Vienna (1963) 121–131.

[11]   OLDFIELD, F., APPLEBY, P.G., BATTARBEE, R.W., Alternative ^{210}Pb dating: Results from the New Guinea Highlands and Lough Erne, Nature **271** (1978) 339–342.

[12]   JOSHI, S.R., SHUKLA, B.S., Ab initio derivation of formulations for ^{210}Pb dating of sediments, J. Radioanal. Nucl. Chem. **148** (1991) 73–79.

[13]   KUMAR, V.S., ANAND, N.M., CHANDRAMOHAN, P., NAIK, G.M., Longshore sediment transport rate — measurement and estimation, central west coast of India, Coastal Engineering **48** (2003) 95–109.

[14]   HAMILTON, D.G., EBERSOLE, B.A., Establishing uniform longshore currents in a large-scale sediment transport facility, Coastal Engineering **42** (2001) 199–218.

210PB-EXCESS AND SEDIMENT ACCUMULATION RATES AT THE IBERIAN CONTINENTAL MARGIN

F.P. CARVALHO, J.M. OLIVEIRA, A.M. SOARES
Nuclear and Technological Institute,
Sacavém, Portugal

Abstract

Sediments from the continental shelf, slope, and rise at the continental margin of northern Portugal and the adjacent Iberian abyssal basin were analysed for ^{210}Pb, ^{226}Ra, ^{137}Cs and ^{14}C. Pb–210 derived sedimentation rates at the continental shelf off the Portuguese coast were 0.2–0.6 cm/a. In some cores from fine sediment deposits at the outer shelf, the ^{210}Pb excess continuum was interrupted and sediment layers were missing, suggesting that events such as sediment slides could have occurred. Higher sedimentation rates were determined in locations at the rise of the continental slope, confirming enhanced deposition by sediment slides. In the deeper Iberian Abyssal Basin, using the ^{14}C age of sediment layers the sedimentation rate was determined at 3.2 cm/ka, thus four orders of magnitude lower than at the continental shelf. The spatial distribution of sedimentation rates determined by radionuclide based chronologies, suggested that fine sediments from river discharges are deposited mainly at the outer continental shelf. These deposits may became unstable with time and, occasionally, originate sediment slides that are drained by the canyons and reach the deep sea. The Iberian abyssal basin receives some advective contribution of these sediment slides and the sedimentation rate is one order of magnitude higher than in other abyssal basins of the NE Atlantic Ocean.

1. INTRODUCTION

The use of radionuclides from the uranium decay series in sediment studies goes back to the 1960s, with attempts to date glacier and lake sediments using the ^{210}Pb excess /^{226}Ra chronology [1]. Since then, the method has been largely improved and used to determine sediment accumulation rates in continental shelf areas in many locations [2–5].

At the Iberian Peninsula, the Portuguese northern continental shelf has a wide surface area receiving the outflow of several rivers, including the Douro, Minho, Vouga, and Mondego Rivers (Fig. 1). The shelf is 5 to 80 km wide, and breaks to the continental slope at water depths of between 130 and 190 m. In several zones, the continental shelf is interrupted by underwater canyons, whose formation is not always related to large rivers' outflow. Submarine canyons deeply indent the shelf
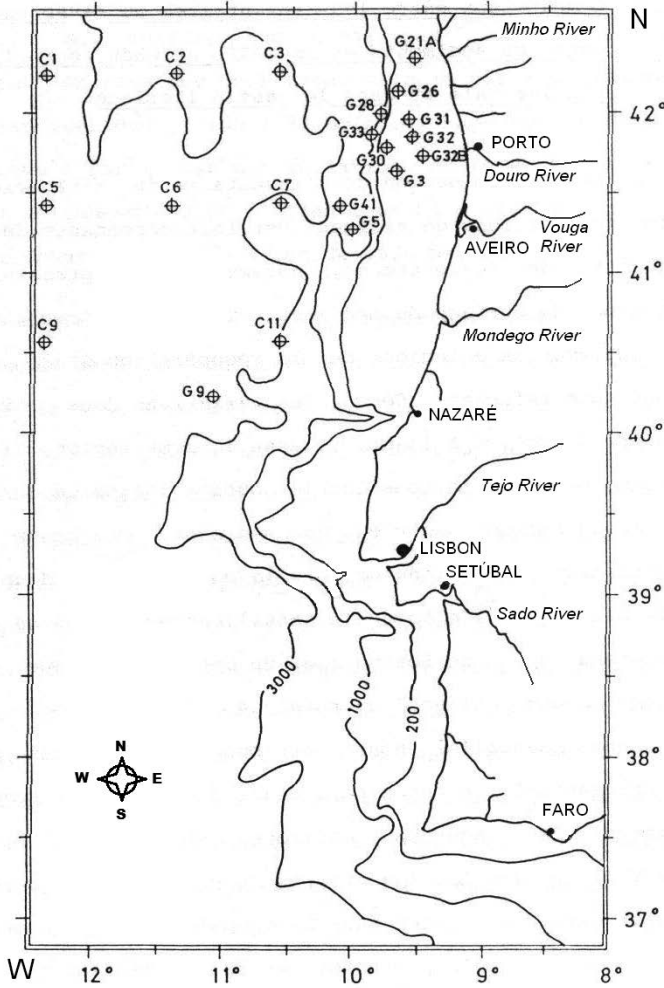
FIG. 1. Continental margin of Portugal and sediment sampling stations.

at the latitude of Porto, Aveiro, Nazaré, and further South near Lisbon and Setúbal. These canyons communicate with the adjacent abyssal basins. At the northern region of this shelf, the Douro River discharges into the sea an average suspended sediment load of 8.6×10^6 m³/a, followed by the discharge of Minho River with 0.4×10^6 m³/a of sediments. Strong coastal currents, with speeds of 0.7–5 km/d mainly oriented in a S-N direction, transport these sediments northwards and distribute them along the continental shelf [6–7].

In the framework of marine geology studies on sediment dynamics on the Portuguese coast, the ^{210}Pb geo chronology method was employed to determine sediment

accumulation rates and to assist with the understanding of sediment transfer process-
es along the northern continental margin of the Iberian peninsula.

2.   MATERIALS AND METHODS

Continental shelf sediments were sampled with a gravity tube corer, weigh-
ing 100 kg in the air, built with stainless steel tube of 1.80 m length provided with
a replaceable 6 cm internal diameter PVC inner liner, and with a sphincter closure
device. Deep sea sediments were collected with a 400 kg weight box corer type sam-
pler, provided with a stainless steel tube penetrator of 50 cm length and 16 cm inter-
nal diameter with a replaceable PVC inner liner, and equipped with a tight closing
device operated by a side arm. Both corers were built in the ITN workshop. Sam-
ples were collected during several oceanographic cruises ('Geomar' and 'Cecir')
performed by the research vessel NRP 'A. Carvalho', operated by the Hydrographic
Institute of Portugal.

Sediment cores were frozen in the PVC inner tubes on board ship and later
sawn in the laboratory from the top to the bottom in slices of 1 or 2 cm in thick-
ness. These sediment layers were weighted for wet and dry weight (oven dry at 60
ºC). Each sediment sample was thoroughly mixed, stored dry in polyethylene tubes,
and aliquots taken for several analyses including grain size determination, organic
carbon, carbonate, and radionuclides.

Sedimentation rates were based on the analyses of lead–210 (^{210}Pb, $T_{1/2}$=22.2 a)
in sediment layers. Pb–210 was determined through the analyses of the polonium–210
alpha emitter (^{210}Po, $T_{1/2}$= 138.4 d), performed after more than one year of sample
storage to ensure the formation of radioactive equilibrium between ^{210}Pb and ^{210}Po.
Po–210 analyses were performed as described earlier [8–9]. In brief, aliquots of
about 0.5 g dry sediment samples were used, and ^{209}Po ($T_{1/2}$= 102 a) was added to
the sample in a Teflon beaker as an internal tracer. The sediment aliquot was covered
with HNO_3 and HCl for complete dissolution on the hotplate, and small volumes of
HF and H_2O_2 were added to dissolve silica and destroy organic matter, respectively.
The dry residue was dissolved in 0.5M HCl, 300 mg of ascorbic acid added, and
polonium spontaneously plated on a silver disc overnight. The measurement of alpha
emissions from both polonium isotopes was performed with silicon surface barrier
detectors in an alpha spectrometer ORTEC EG&G. Chemical recoveries of polonium
were generally better than 90%.

Caesium–137 (^{137}Cs, $T_{1/2}$= 30 a) and radium–226 (^{226}Ra, $T_{1/2}$= 1600 a) were
determined in sediment samples by gamma spectrometry using GeHp solid state
detectors. The sediment aliquots were sealed in tightly closed Millipore petri dish-
es, and measured after formation of radioactive equilibrium between ^{226}Ra and
^{226}Ra daughters.

The analytical quality of the results was tested and ensured through analyses of certified reference materials (e.g., IAEA–384) and periodic participation in blind intercomparison exercises organized by the IAEA with good results [10].

Sedimentation rates were computed using the equation

$$A_{210_{Pbexc}}(n) = A_{210_{Pb\ exc}}(0)\exp(-\lambda n) \tag{1}$$

where $A_{210_{Pbexc}}(n)$ represents the activity concentration (Bq/g dry weight) of ^{210}Pb excess relatively to ^{226}Ra activity concentration in the sediment layer n (cm) below the sediment–water interface, $A^{210}_{Pbexc}(0)$ represents the ^{210}Pb excess in the sediment surface layer, λ is the radioactive disintegration constant of ^{210}Pb, 0.0312/a. [11] In practice, sampling the sea floor with sediment corers produces sediment samples with layers compacted by the corer impact that shortens the sediment core. The correction for sediment compaction and the determination of sediment accumulation by surface area with time can be computed through the equation

$$A_{210_{Pbexc}}(m) = A_{210_{Pbexc}}(0)\exp(-\lambda m/w) \tag{2}$$

where $A^{210}_{Pbexc}(m)$ represents the activity concentration of ^{210}Pb excess (Bq/g) at the mass depth m (g/m^2), $A^{210}_{Pbexc}(0)$ represents the ^{210}Pb excess activity concentration at the water–sediment interface, λ is the radioactive disintegration constant of ^{210}Pb, and w is the sediment accumulation rate (g/cm^{2}a). The mass depth sediment accumulation rate may be converted into a linear sedimentation rate or sedimentation velocity S (cm/a), through $w = Sr$, where r is the in situ sediment density (g sediment dry weight/cm^3 of wet sediment) [11–12].

The upper layers of the sediment cores often showed evidence of sediment mixing caused by bioturbation. The bioturbation, or biodiffusion rate, has the dimensions of a diffusion coefficient and can be computed using the radionuclide distribution in sediments, as described elsewhere [13].

The carbon–14 age of the sediment carbonate fractions were determined in sediment layers of the core C5 from the Iberian Abyssal Basin [13]. The ^{14}C contents were measured using the method of benzene synthesis and the liquid scintillation counting. ^{14}C-ages were calculated following Stuiver and Polach [14].

3.   RESULTS AND DISCUSSION

The radionuclides determined in sediment cores from continental shelf deposits typically displayed three layer zones of interest exemplified in Fig. 2. The upper layer, going down to 5–10 cm below the seawater–sediment interface, displayed generally well mixed sediment with ^{210}Pb and ^{137}Cs concentrations nearly homogenized by
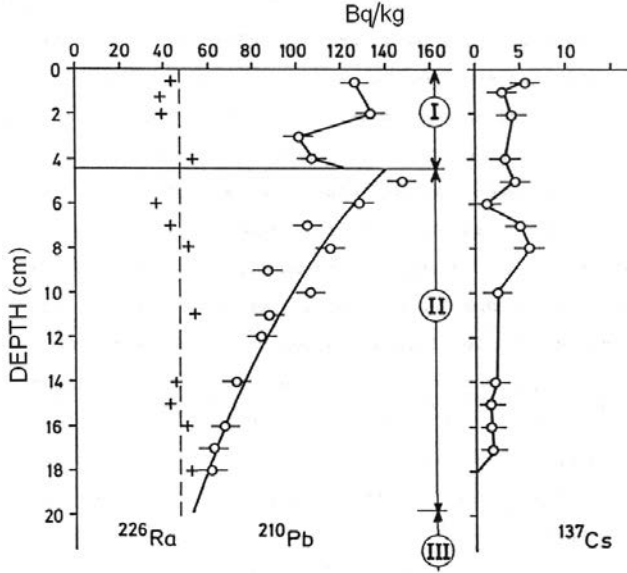
FIG. 2. Activity concentrations (Bq/kg dry weight) in sediment layers of core G32 (Box core). Region I, surface mixed layer; Region II, zone of exponential decrease of ^{210}Pb excess with sediment depth; Region III, ^{210}Pb concentrations leveling off with those of ^{226}Ra.
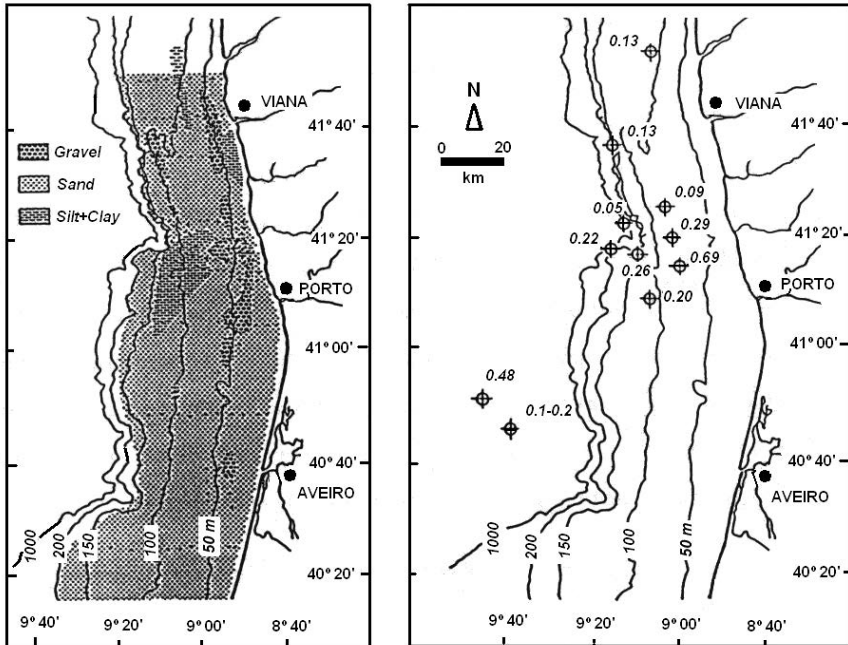
FIG. 3. Northern continental shelf of Portugal. Left: Sediment types and deposits. Right: ^{210}Pb derived sediment accumulation rates (g/cm²a) indicated at the sampling stations.

sediment reworking probably caused by biota. Underneath, an intermediate layer of several cm thickness contained ^{210}Pb excess in relationship to the ^{226}Ra concentration, but the ^{210}Pb excess concentrations decreased exponentially with the depth until leveling off with ^{226}Ra concentrations. In these upper and intermediate layers the ^{137}Cs from radioactive fallout was often measurable and, in undisturbed sediments, displayed a peak of maximum concentration corresponding to the higher depositions of radioactive fallout from nuclear weapon tests that took place around the year 1963. Further below, in deeper sediment layers, the ^{210}Pb excess and ^{137}Cs were not detectable anymore. The region of interest to apply the ^{210}Pb sediment geochronology was the zone of ^{210}Pb exponential decrease, region II in Fig. 2, which slope allows for the determination of sediment accumulation rates.

Sediment accumulation rates based on the ^{210}Pb excess method are shown in Table 1 for sediment cores from the continental shelf, slope and rise. Accumulation rates varied from a maximum of 0.69 g/cm²a (0.55 cm/a) in front of the Douro River mouth, and decreased along the continental shelf following a SE–NW direction to a minimum of 0.09 g/cm²a (0.07 cm/a) (Fig. 3). Comparatively high sedimentation rates, between 0.20–0.29 g/cm²a (0.16–0.22 cm/a), were determined in several cores from fine sediment deposits at the outer continental shelf. This result indicated

TABLE 1. SEDIMENT CORES AND ^{210}Pb EXCESS BASED SEDIMENTATION RATES AT THE CONTINENTAL MARGIN OF THE NORTHERN IBERIAN PENINSULA

Core #		Coordinates		Depth (m)	Sediment accumulation rate (g/cm²a)	Linear sedimentation rate (cm/a)
		Latitude N	Longitude W			
G3	(G)	41° 08.3'	09° 04.5'	100	0.20	0.16
G32	(G)	41° 20.1'	08° 59.4'	75	0.29	0.22
G32	(B)	41° 20.1'	08' 59.4'	75	0.69	0.55
G30	(B)	41° 20.9'	09° 10.3'	635	0.26	0.21
G33	(G)	41° 17.2'	09° 14.7'	520	0.22	0.18
G28	(G)	41° 22.0	09° 11.1'	791	0.05	0.04
G31	(G)	41° 25.5'	09° 01.4'	80	0.09	0.07
G26	(G)	41° 34.7'	09° 14.2'	230	0.13	0.10
G21A	(G)	41° 52.1'	09° 03.6'	103	0.13	0.10
G41	(G)	40° 53.0'	09° 44.6'	2860	0.48	0.38
G5	(G)	40° 48.0'	09° 34.0'	2800	0.1–0.2	0.12

B — box corer; G — gravity corer)

TABLE 2.   CARBON-14 AGE OF THE SEDIMENT CARBONATE FRAC-
TIONS FROM CORE C5 OF THE IBERIAN ABYSSAL BASIN. BP, YEARS
BEFORE PRESENT

Sediment layer (cm)	Lab. Ref.	$\delta^{13}C$ (‰)	^{14}C age (years BP)
0–1	ICEN–263	-1.8	4020 ± 230
2–3	ICEN–271	-1.9	3200 ± 170
3–4	ICEN–272	-0.9	3090 ± 70
4–5	ICEN–275	+0.7	3230 ± 80
5–6	ICEN–280	+0.6	3330 ± 70
6–7	ICEN–281	+1.1	3920 ± 180
7–8	ICEN–282	+1.5	3600 ± 60
9–10	ICEN–283	-1.5	4370 ± 60
11–12	ICEN–284	0.0	5470 ± 110
12–13	ICEN–285	-2.2	5940 ± 60
13–14	ICEN–286	+1.3	6000 ± 70
15–16	ICEN–287	0.0	6000 ± 160
16–17	ICEN–288	-0.1	6450 ± 90

TABLE 3. SEDIMENT CORES COLLECTED IN THE IBERIAN ABYSSAL BA-
SIN. ^{210}PB EXCESS DERIVED BIODIFFUSION COEFFICIENTS (D_B) AND ^{14}C
BASED SEDIMENTATION RATE

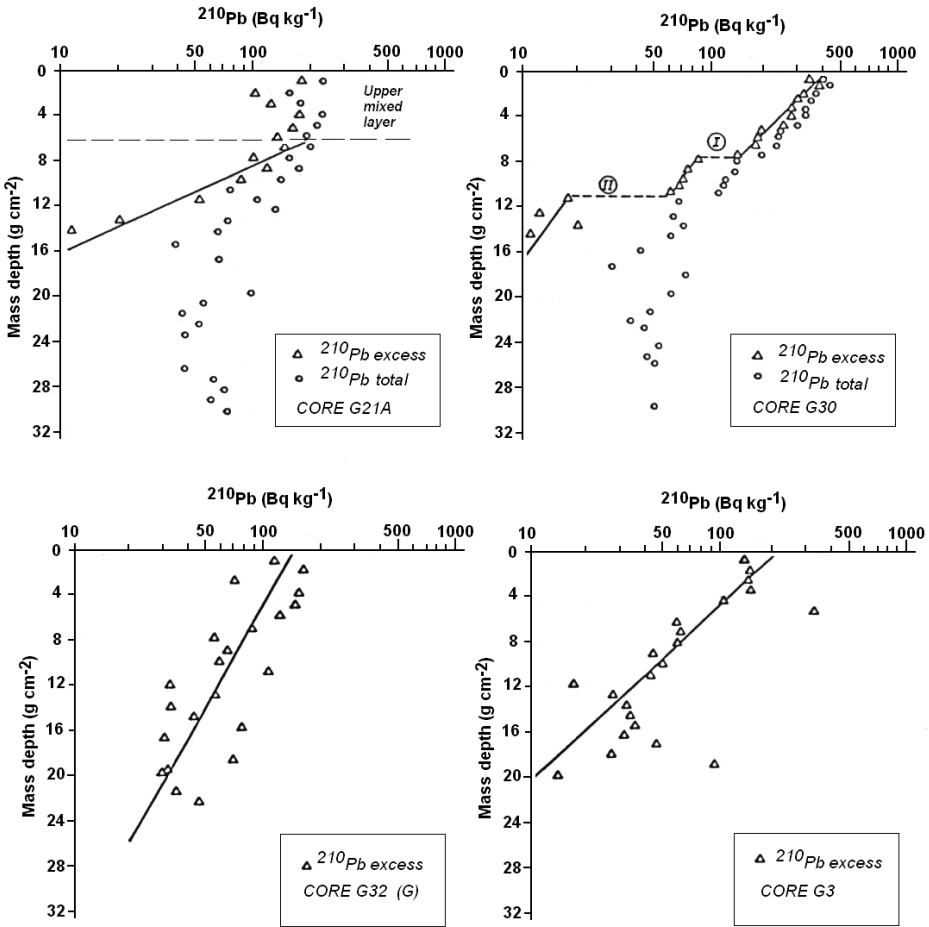| Core #	Coordinates		Depth (m)	Biodiffusion coefficient D_B ($cm^{-2} a^{-1}$)	Sedimentation rate (cm/ka)
	Latitude N	Longitude W			
C 1	41º40'	11º55'	3700	0.64	
C 2	41º40'	10º55'	2750	0.29	
C 3	41º40'	10º05'	3000	0.46	
C 5	40º50'	11º55'	5100	0.09	3.2
C 6	40º50'	10º55'	4500	1.26	
C 7	40º50'	10º05'	2300	0.14	
C 9	40º00'	11º55'	5150	0.16	
C11	40º00'	10º55'	2350	0.16	
x ± 1 SD				0.40 ± 0.37	

FIG. 4. Vertical profiles of ^{210}Pb total and ^{210}Pb excess in sediment cores from the continental shelf. In the core G30, lines I and II indicate gaps in the stratigraphic record likely due to sediment slide events.

that these are zones of current sediment accumulation and not relict deposits of past sedimentation regimes, as previously thought [6–7]. The sediment cores collected at the continental slope displayed low sediment accumulation rates, of 0.05 g/cm^{2}a (0.04 cm/a), probably due to the steep inclination of the sea floor and strong currents along the slope and inside the canyons. Higher sediment accumulation rates, 0.48 g/cm^{2}a (0.38 cm/a), were measured at the continental slope rise in the Aveiro canyon (Fig. 3).

An interesting feature detected in several sediment cores from the continental shelf was the interruption of the ^{210}Pb exponential decay line, and lack of sediment layers in the stratigraphic sediment archive, such as observed in the core G30
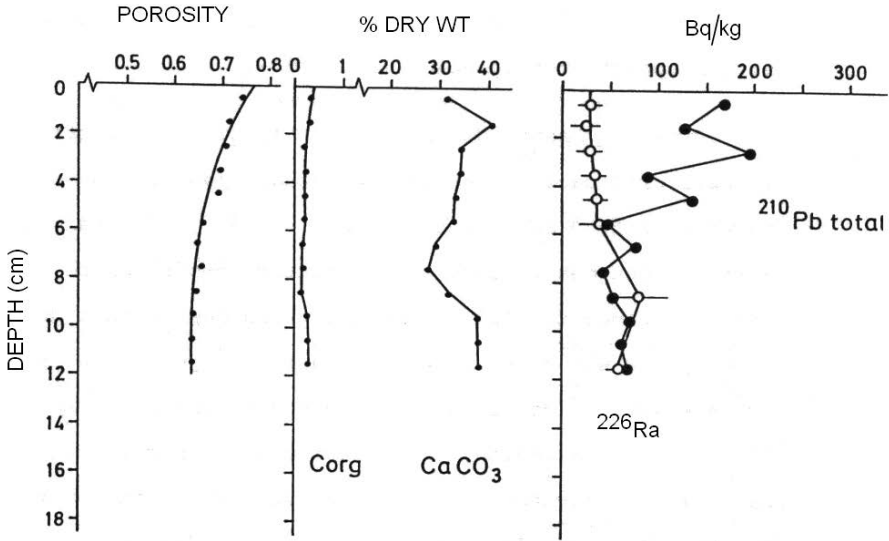
FIG. 5. Sediment core C5 from the Iberian Abyssal Basin (water depth 5150 m): vertical profiles of porosity, organic carbon, calcium carbonate, and radionuclide concentrations (Bq/kg) in the sediment [13].
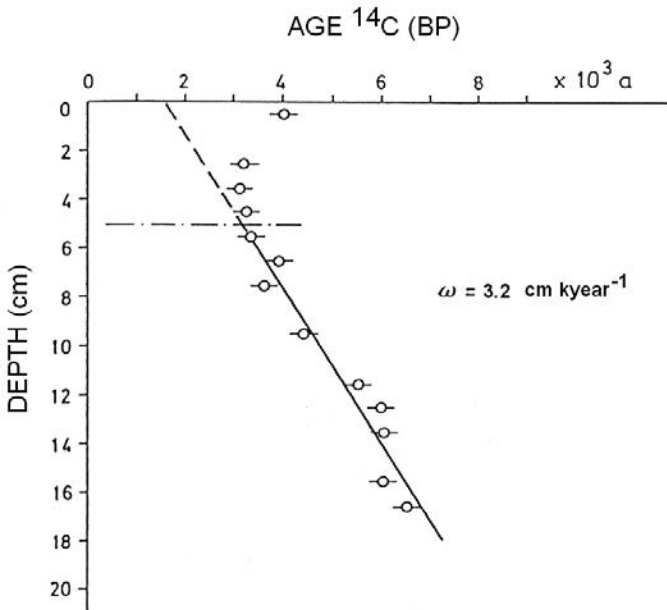

FIG. 6. Carbon–14 age (BP, years Before Present) of sediment layers in the core C5 from the Iberian Abyssal Basin. The average sedimentation rate was determined based on the exponential fit to the layers below the surface mixed layer (dotted line) [13].

collected near the shelf break (Fig. 4). This is interpreted as due to events of post depositional sediment remobilization and transfer through sediment slumps [15].

Sediments collected in the adjacent Iberian abyssal basin were also analysed for radionuclides and, in particular, for ^{14}C dating. Typical vertical profiles of radionuclide activity concentrations in the sediment core C5 of this abyssal basin are shown in Figs 5 and 6. The subsurface ^{210}Pb excess over ^{226}Ra in general goes 6–10 cm deep in the sediment, but the ^{210}Pb excess distribution does not correspond to the true sediment accumulation rate. These deep sea sediment layers are much older than coastal sediments and, based on the ^{14}C age of sediment layers (Table 2), the sedimentation rate was determined at about 3.2 cm/ka, i. e., 4 orders of magnitude lower than sedimentation rates at the outer continental shelf (Fig. 6). The ^{210}Pb excess present in the upper centimetres of the deep sea cores is indeed due to sediment mixing by biological activity, and named bioturbation or biodiffusion. Biodiffusion coefficients averaged 0.40 ± 0.37 cm$^{-2} \cdot$a^{-1} (range 0.09–1.26 cm$^{-2} \cdot$a^{-1}) (Table 3). This biodiffusion is a common feature of deep sea sediments, and it was found in all cores from the Iberian basin we analysed. Similar biodiffusion in deep sea sediments was described for other locations in the NE Atlantic [16–18].

The spatial distribution of the sedimentation rates did show higher values on the continental shelf, followed by intermediate and low values on the continental slope (Fig. 3). Occasionally, higher values were found again at the exit of submarine canyons. In the adjacent Iberian abyssal plain, the sedimentation rate dropped to extremely low values, several orders of magnitude lower than on the continental shelf.

Overall, results suggest that sediments discharged by rivers in the northern continental shelf of Iberia are transported northwards by sea currents. Gravels and sands deposit shortly after the river discharge and, mostly, accumulate along the shore and cover the sea floor of the inner continental shelf. Fine particles, including clay and silt, are transported further away and mainly accumulate with time and continued instability in deposits at the outer continental shelf and at the shelf break (Fig. 3).

Winter storms may easily trigger sediment slumps that can be drained by the canyons out to the deep sea. Sediment slides guided along the canyons seem to deposit again by the canyon exit at the slope rise. In such sites, the ^{210}Pb sediment accumulation rates were indeed high and sometimes even higher than at shelf bottoms. Turbidity currents caused by sediment slides seem to reach also the adjacent abyssal basins. This advective sediment supply to the nearest areas of the Iberian abyssal plain are likely to have increased the sedimentation rate there in comparison with other abyssal areas further away from the European continental margin. For example, the sedimentation rate determined at the Porcupine abyssal plain was reported as 0.14 cm/ka that is one order of magnitude lower than the sedimentation rate determined at the Iberian abyssal plain, 3.2 cm/ka [13].

4.   CONCLUSIONS

Sediment accumulation rates determined by the ^{210}Pb excess method in the northern Portuguese continental shelf ranged roughly from 0.2 to 0.6 cm a^{-1}, which are typical values for coastal regions [2–4]. The spatial distribution of the sedimentation rates allowed the identification of deposition areas for the fine sediments from river discharges at the outer shelf and at the shelf break. These areas, previously thought to be relict deposits from past sedimentation regimes, are currently sediment accretion areas. Some sediment cores also provided evidence that sediment slumps occurred in these areas. Underscoring this interpretation, sedimentation rates at the rise of the continental shelf, in locations with canyons, showed surprisingly high values of sediment accumulation. These discharges of shelf sediments to the deep sea bottoms may have some influence on the sedimentation taking place in the near Iberian abyssal basin. There, the sedimentation rate of 3.2 cm/ka determined by the ^{14}C sediment age, was much lower than at the continental shelf but, nevertheless, was still one order of magnitude higher than at the NE Atlantic abyssal floor at the Porcupine abyssal plain located further away from the European continental margin.

Over geological time, the intense discharges of sediments carried by rivers into the coastal sea off northern Portugal have generated wide deposits of fine sediments at the outer continental shelf. It is hypothesized that over such time scale sediment slides have been frequent events and may have excavated the canyons, which in turn became the actual drainage system of unstable sediments accumulated on the continental shelf. This conceptual model of sediment transport has been suggested for other regions and may be a frequent one in the continental margins around the globe [2–5]. Important aspects to investigate further are the frequency of sediment slides and the mechanisms that trigger them, as well as the quantification of shelf sediment supply to the abyssal basins.

REFERENCES

[1]   GOLDBERG, E.D., "Geochronology with [210]Pb", Proc. Symp. on Radioactive dating, Athens, Greece, 19–23 November 1962, IAEA, Vienna (1963) 121–131.

[2]   CARPENTER, R., PETERSON, M.L., BENNETT, J.T., ^{210}Pb derived sediment accumulation and mixing rates for the Washington continental slope, Marine Geology **48** (1982) 135–164.

[3]   BUESSELER, K.O., LIVINGSTON, H.D., SHOLKOVITZ, E.R., [239,240]Pu and excess ^{210}Pb inventories along the shelf and slope of the northeast USA, Earth Planet. Sci. Lett. **76** (1985) 10–22.

[4]   NITTROUER, C.A., STERNBERG, R.W., The formation of sedimentary strata in an allochthonous shelf environment: The Washington continental shelf, Marine Geology **42** (1981) 201–232.

[5] NEVISSI, A., "Sources and sinks of ^{210}Pb in Puget Sound", Radionuclides: A Tool for Oceanography (GUARY, J.C., GUÉGUÉNIAT, P., PENTREATH, R.J., Eds), Elsevier Applied Science, London (1988) 153–161.

[6] DIAS, J.M.A., NITTROUER, C.A., Continental shelf sediments of northern Portugal, Cont. Shelf Res. **3** 2 (1984) 147–165.

[7] DIAS, J.M.A., Dinâmica sedimentar e evolução recente da plataforma continental Portuguesa setentrional, Tese de Doutoramento, Universidade de Lisboa (1987).

[8] CARVALHO, F.P., ^{210}Pb and ^{210}Po in sediments and suspended matter in the Tagus estuary, Portugal. Local enhancement of natural levels by wastes from phosphate ore processing industry, Sci. Total Environ. **159** (1995) 201–214.

[9] CARVALHO, F.P., OLIVEIRA, J.M., Alpha emitters from uranium mining in the environment, J. Radioanal. Nucl. Chem. **274** (2007) 167–174.

[10] POVINEC, P.P., et al., Reference material for radionuclides in sediment IAEA-384 (Fangataufa Lagoon sediment), J. Radioanal. Nucl. Chem. **273** (2007) 383–393.

[11] ROBBINS, J.A., EDGINGTON, D.N., Determination of recent sedimentation rates in Lake Michigan using Pb-210 and Cs-137, Geochim. Cosmochim. Acta **39** (1975) 285–304.

[12] SCHELL, W.R., "Dating recent (200 years) events in sediments from lakes, estuaries, and deep ocean environments using lead–210", Nuclear and Chemical Dating Techniques — Interpreting the Environmental record, (CURRIE, L.A., Ed.) ACS Symposium Series **176** (1982) 331–361.

[13] CARVALHO, F.P., OLIVEIRA, J.M., SOARES, A.M.M., Sediment accumulation and bioturbation rates in the deep Northeast Atlantic determined by radiometric techniques, ICES Journal of Marine Science **68** (2011) 427–435.

[14] STUIVER, M., POLACH, H.A., Discussion: Reporting of ^{14}C data, Radiocarbon **19** (1977) 355–363.

[15] CARVALHO, F.P., RAMOS, L.A., "Lead–210 chronology in marine sediments from the Northern continental margin of Portugal", Proc. Second National Conf. on Environmental Quality (SANTANA, F., SANTOS, M., COSTA, M., PEREIRA, D., Eds), Vol. 1, Universidade Nova de Lisboa, Lisboa (1990) 143–151.

[16] COCHRAN, J.T., et al., ^{210}Pb scavenging in the North Atlantic and North Pacific oceans, Earth Planet. Sci. Lett. **97** (1990) 332–352.

[17] SMITH, J.N., BOUDREAU B.P., NOSHKIN, V., Plutonium and ^{210}Pb distributions in the northeast Atlantic sediments: Subsurface anomalies caused by non-local mixing, Earth Planet. Sci. Lett. **81** (1986) 15–28.

[18] THOMSON, J., BROWN, L., NIXON, S., COOK, G.T., MacKENZIE, A.B., Bioturbation and Holocene sediment accumulation fluxes in the north-east Atlantic Ocean (benthic boundary layer experiment sites), Marine Geology **169** 1–2 (2000) 21–39.

ISOTOPIC AND RADIOACTIVITY FINGERPRINTING OF GROUNDWATER IN THE UNITED ARAB EMIRATES (UAE)

A. MURAD [a], A. ALDAHAN [a,b], X.L. HOU [c], S. HUSSEIN [a], G. POSSNERT [d]

[a] Department of Geology,
United Arab Emirates University,
Al Ain, UAE

[b] Department of Earth Sciences,
Uppsala University,
Uppsala, Sweden

[c] Risø National Laboratory for Sustainable Energy,
Technical University of Denmark,
Roskilde, Denmark

[d] Tandem Laboratory,
Uppsala University,
Uppsala, Sweden

Abstract

A pilot investigation using radioactivity together with chemical features was conducted to characterize groundwater sampled from wells drilled in fractured Paleogen-Neogen carbonate rocks along the foothill of about 1200 m absl high mountain and wells drilled in Quaternary clastic sediments from a nearby alluvial plain in the southeastern part of the UAE. These two water modes are relatively easily separated by their chloride and EC (salt content) contents and provide an ideal case for testing radioactivity fingerprints. The groundwater of the alluvial plain, which is expected to reflect a short distance precipitation recharge source, indicates a concentration of ^{222}Rn and ^{226}Ra 2–3 orders of magnitude lower than the groundwater of the carbonate rocks. The range of variability for gross alpha is similar, but the gross beta activity indicates only 1 order of magnitude difference between the two water types. The radioactively richer groundwater of the carbonate aquifers compared to the alluvium plane may reflect the signature of deep basinal fluids. These marked differences in radioactivity of the two water modes clearly suggests that radioactive fingerprinting can provide a potential method for the identification groundwater sources in the UAE.
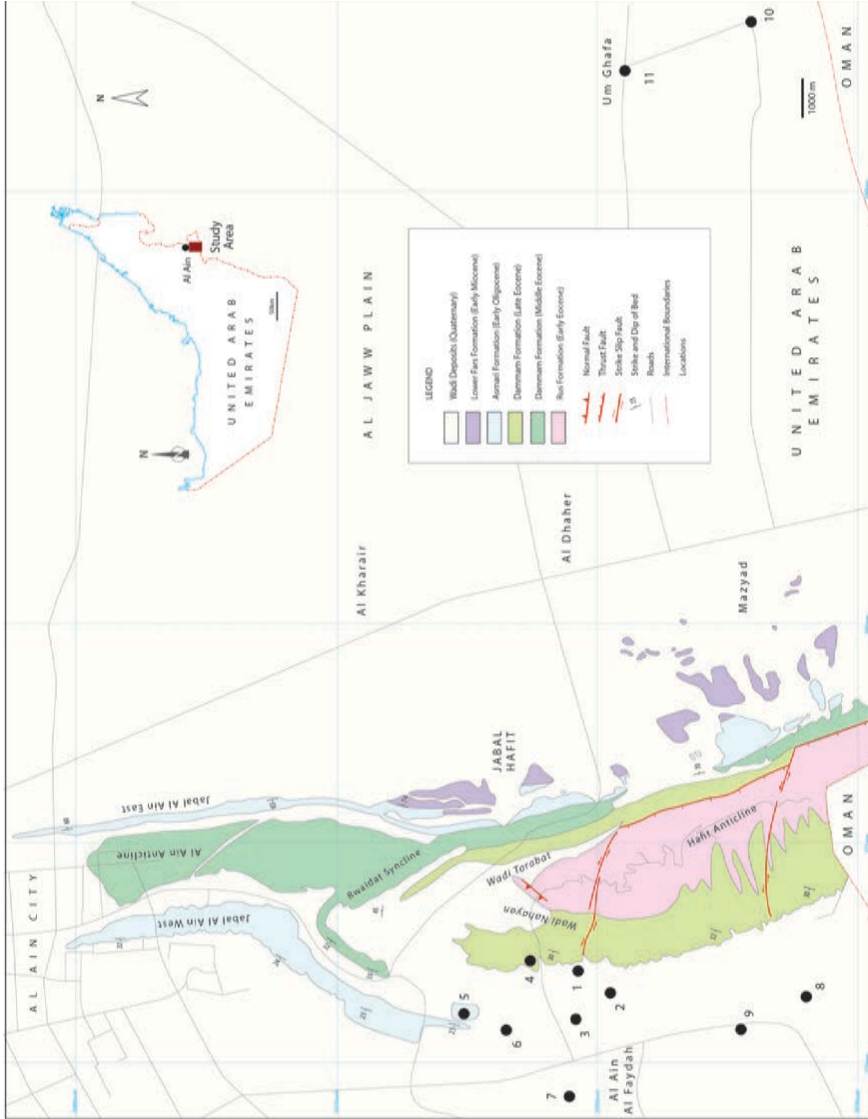
FIG. 1. Map showing the location of the study area and sampling points. Simplified from Ref. [4].

1.   INTRODUCTION

The tremendous demand for groundwater in the United Arab Emirates (UAE) and many other countries worldwide necessitates the use of sophisticated exploration techniques for identification of sources and recharge areas. However, as groundwater penetrates aquifers, many of its primary chemical features may change due to interaction with the aquifer contents. Generally, long residence times and recharge pathways and deeper transport can be fingerprinted in groundwater types, but establishing these features is difficult. Stable and, more recently, radioactive isotopes and total radioactivity data of groundwater can elucidate parameters linked to groundwater sources and recharge areas. In addition, the level of radioactivity in groundwater may reach values that can be judged as unsafe for domestic uses [1, 2].

A pilot investigation of using radioactivity was conducted together with other physical and chemical features to characterize groundwater from southeastern UAE. The water was sampled from wells drilled in fractured Paleogen-Neogen carbonate rocks along the foothill of about 1200 m asl high mountain (Jabel Hafit) and wells drilled in Quaternary clastic sediments from a nearby alluvial plain (Al Jawa Plain) (Fig. 1). Groundwater from the mountain foothill is commonly used for recreational activities, artificial ponds and watering whereas groundwater of the plain region is commonly used for agriculture and household use. Recharge of the groundwater in the alluvium plain is strongly controlled by the amount of rainfall in the Oman Mountains which is reflected by the climatic conditions in the region. Generally, the climate is arid to semi arid [3]. Recharge of groundwater in the carbonate rocks is apparently more complicated and may be related to both large scale deep basinal and a mixed basinal meteoric source as will be discussed later.

2.   SAMPLING AND ANALYTICAL TECHNIQUES

Water samples were collected from 9 wells that penetrate Neogene-Paleogen carbonate rocks and 2 wells that penetrate the Quaternary alluviums (Fig. 1). Measurements of temperature and EC (Electrical Conductivity) were done in the field using a WTW-COND–330I instrument. Each water sample was divided into three portions for radon, total radioactivity and U–Th and total chemistry. For ^{222}Rn measurement, groundwater was directly sampled in a low diffusion LSC vial with 10 mL prefilled with Opti-Fluor O liquid scintillation cocktail (PerkElmer) and the activity was measured using a Quantulus 1220 liquid scintillation counter within10 days from sampling time.

The activity of ^{222}Rn was calculated by using the sum of the counts of ^{222}Rn and two of its short lived radionculides (^{218}Po + ^{214}Po) and was corrected for blank and samples decay. The measurement of other radionuclides and total activity was performed 20–30 days after the sampling. The ^{226}Ra was measured after precipitation

as $Ba(Ra)SO_4$ from 500 mL water using $BaCl_2$ carrier and 20 Bq [133]Ba as a chemical yield tracer. After washing with water, the precipitate was dissolved with 5 mL of 1M EDTA solution (pH=9) in a hot water bath, and the solution was then transferred to a low diffusion LSC vial. Then 10 mL of Opti-Fluor O liquid scintillation cocktail (PerkElmer) was added. After 7 days for ingrowth of [222]Rn from [226]Ra, the vial was shaken, and then counted using Quantulus 1220 liquid scintillation counter for 60 min of each sample and 3 cycles. The result was corrected for blank count rate, ingrowth of [222]Rn from [226]Ra between [226]Ra separation and counting for about 7 days and quenching. For gross alpha and beta measurement, 100 ml of water was evaporated to near dryness and the residue was dissolved with water to a final volume of 5–15 mL. A 4 mL of the concentrated solution was taken to a LSC vial and 16 mL of Ultima Gold LLT scintillation cocktail was added. After mixing and set in dark and cool for 1 hours, the sample was measured using Quantulus 1220 liquid scintillation counter for 60 minutes per sample for 3 cycles. Detection limit in Bq/L was 0.8 ([222]Rn), 0.07 ([226]Ra), 0.16 (gross alpha) and 1.1 (gross beta).

The measurement of [238]U, [235]U, [232]Th and chlorine was performed with ICP-MS after addition of 0.20 mL of 100 mg/mL In(III) (as $InCl_3$) as an internal standard and 10 times dilution with 3% HNO_3 (super pure). The standards of U, Th and Cl were prepared using a similar method as samples by dilution of uranium, thorium and chlorine standard solutions (purchased from the National Institute of Standard technology, USA) with 3% HNO_3 (super pure). Indium solution, as an internal standard, was also added to the standard solution. The concentrations of target analytes (e.g. [238]U, [235]U, [232]Th and [35]Cl) and the internal standard (i.e. [115]In) in the samples and standards were measured using an inductively coupled plasma mass spectrometry (ICP–MS) system (X Series[II], Thermo Fisher Scientific, Waltham, MA) equipped with an Xt-skimmer cone and a concentric nebuliser under hot plasma conditions. The concentrations of [235]U, [238]U, [232]Th and Cl in the samples were measured by comparing with the standard and correction for introduction efficiency using indium internal standard. The detection limits calculated as three times of the standard deviation (3σ) of the processing blank are 0.21 mg/L for Cl, 1.2 mBq/L, for [232]Th, 0.37mBq/L, for [235]U and 0.95 mBq/L for [238]U. A 0.5 mol/l HNO_3 solution was used as a washing solution among consecutive assays. No carry over (memory effect) was observed for consecutive analysis of samples differing in U and Th concentrations up to three orders of magnitude. A least squares regression equation was used to quantify the elemental concentration over the range of 0.01–100 mBq/L for U, 0.002–10 mBq/L for Th and 0.5–5000 mg/L for Cl.

3.   RESULTS AND DISCUSSION

Chemical analyses of the groundwater used in this study suggest that those of the alluvium plain (samples 10 and 11, Table 1) are relatively less saline than

the groundwater in the carbonate rocks (samples 1–9). This result is also clearly shown by the total Cl data which indicate a large difference between the two groundwater modes. These two groundwater modes are also relatively easily separated by their TDS (EC) and temperature and provide an ideal case for testing radioactivity fingerprints. The groundwater of the alluvial plain, which is expected to reflect a short distance precipitation recharge source, indicates negligible ^{232}Th, ^{235}U and ^{238}U concentrations compared to the groundwater from the carbonates (Table 1). The ratio of ^{235}U/^{238}U is, however, comparable to the natural value in all the samples. The results also show a concentration of ^{222}Rn and ^{226}Ra 2–3 orders of magnitude lower in the alluvium plain than the groundwater of the carbonate rocks. The range of variability for gross alpha is similar, but the gross beta activity indicates only 1 order of magnitude difference between the two water types (Table 2). As the groundwater samples were analysed about one month after sampling, the gross alpha and beta activity do not only reflect the concentration of the long lived radionuclides in the groundwater but also the growth of alpha and beta emitting ones resulting from decay during storage time. However, the rather good correlation between ^{226}Ra and gross alpha (Fig. 2) suggests that most of this radioactivity is related to the decay of this isotope and its progenies. Although ^{228}Ra and ^{224}Ra are not measured here, the relatively low activity of ^{232}Th in the samples indicates the relatively low activity of these two radium isotopes compared to ^{226}Ra, which is mainly a decay product of the ^{238}U. It is also apparent that even if the gross alpha values are calculated with subtraction of uranium activity, the final product will be <1% of the total gross alpha activity.

The total uranium activity may not be complete due to the absence of ^{234}U which results from decay of ^{238}U (via ^{234}Th and ^{234}Pa). The low natural abundance of ^{234}U (0.0055%) means that the atomic ratio of ^{234}U/^{238}U is at about 10^{-5}. However, because of the relative shorter half-life of ^{234}U (246 000 a) relative to ^{238}U, the activity level of ^{234}U is at a similar level as that of ^{238}U, i.e. A234U/A238U = 1. Therefore, it was assumed that the activity level of ^{234}U in the groundwater might be at a similar level to ^{238}U which means a relatively insignificant contribution to the total alpha activity in the investigated samples (Table 2).

The sources of gross beta in the analysed groundwater may partly relate to the decay products of ^{238}U and ^{232}Th (via ^{228}Ra– ^{228}Ac–^{228}Th), but the activity of ^{238}U and ^{232}Th is too low to account for the whole gross beta activity. Another possible source is the growth of ^{234}Th and ^{234}Pa during storage, but again the relatively low concentration of ^{238}U in the studied samples cannot support all the gross activity as also shown by the correlation with ^{226}Ra (Fig. 2). Another possible source for the beta activity is ^{40}K which has not analysed here. Accordingly, the relatively high gross beta activity of the samples may suggest the existence of ^{228}Ra that is not related only to storage growth within the sample but incorporation into the groundwater from the surrounding rocks. This interpretation may also apply for the relatively high activity of ^{226}Ra and ^{222}Rn.
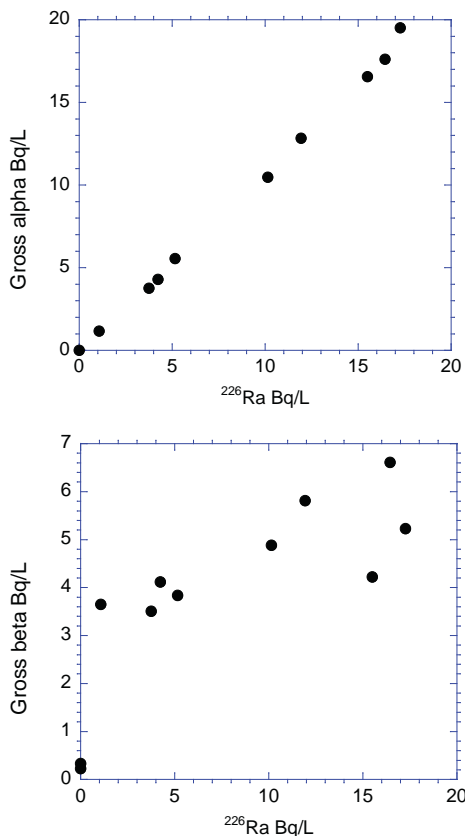
FIG. 2. Correlation of ^{226}Ra with gross alpha (r^2=0.99) and gross beta (r^2=0.80).

4.   CONCLUSIONS AND FUTURE WORK

The radioactively richer groundwater of the carbonate aquifers compared to the alluvium plain may reflect signature of deep basinal fluids extracting their composition from the carbonates. These marked differences in radioactivity of the two water modes clearly suggest that radioactive fingerprinting can provide a potential method for the identification of groundwater sources in the UAE. Groundwater from other parts of the UAE will be investigated using the same methodology to unravel the different sources as well as the effects of mixing and aquifer interaction.

TABLE 1. ANALYSES OF GROUNDWATER SAMPLES COLLECTED FROM THE STUDY AREA

Code	Sample ID	Sampling date	Cl (mg/L)	^{232}Th (ng/L)	^{235}U (ng/L)	^{238}U (ng/L)	^{235}U/^{238}U (10^{-2})	Temp. (°C)	EC (mS/cm)
1	ADD0911078	5/30/2010	3712 ± 12	0.83 ± 0.31	12.33 ± 0.52	1577 ± 11	0.78	49.0	
2	GWW–58	5/30/2010	3986 ± 4	0.75 ± 0.14	11.46 ± 0.42	1476 ± 11	0.77	46.9	11.08
3	ADD0911080	5/30/2010	5233 ± 18	2.53 ± 0.49	15.47 ± 0.37	2042 ± 9	0.76	44.9	14.53
4	ADD0911085	5/30/2010	3742 ± 14	1.67 ± 0.29	11.57 ± 0.28	1469 ± 17	0.78	49	10.43
5	GWW–53	5/30/2010	5011 ± 70	2.17 ± 0.21	39.03 ± 1.69	5139 ± 62	0.76	34.5	14.90
6	ADD0911076	6/2/2010	5293 ± 45	<1	32.45 ± 0.41	4448 ± 16	0.73	34.6	15.26
7	GWW–47	6/2/2010	5074 ± 7	<1	31.80 ± 0.48	4171 ± 16	0.76	32.5	14.85
8	GWW-F	6/2/2010	4502 ± 30	<1	3.44 ± 0.09	429 ± 7	0.80	33.4	12.30
9	GWW-F	6/2/2010	4556 ± 25	<1	3.63 ± 0.16	525 ± 5	0.69	34.8	12.45
10	GWW-Jaw,1	6/7/2010	125 ± 0.6	<1	0.42 ± 0.03	55 ± 0.6	0.76	35.3	0.78
11	GWW-Jaw,2	6/7/2010	72 ± 0.1	<1	0.19 ± 0.01	25 ± 0.4	0.76	33.5	0.55

TABLE 2: ACTIVITY OF GROUNDWATER SAMPLES COLLECTED FROM THE STUDY AREA

Code	^{232}Th (mBq/L)	^{235}U (mBq/L)	^{238}U (mBq/L)	^{222}Rn (Bq/L)	^{226}Ra (Bq/L)	Gross Alpha (Bq/L)	Gross Beta (Bq/L)
1	3.37 ± 1.26	0.99 ± 0.04	19.55 ± 0.14	214 ± 23	15.51 ± 0.79	16.5 ± 2.5	4.22 ± 0.82
2	3.05 ± 0.57	0.92 ± 0.03	18.30 ± 0.14	502 ± 34	17.26 ± 0.92	19.5 ± 3.7	5.23 ± 1.17
3	10.27 ± 1.99	1.24 ± 0.03	25.32 ± 0.12	404 ± 29	11.93 ± 0.63	12.8 ± 2.3	5.81 ± 0.67
4	6.78 ± 1.18	0.93 ± 0.02	18.22 ± 0.21	233 ± 29	16.45 ± 0.85	17.6 ± 3.4	6.61 ± 1.23
5	8.81 ± 0.85	3.12 ± 0.13	64.72 ± 0.77	208 ± 15	3.75 ± 0.19	3.76 ± 0.89	3.51 ± 0.33
6	<0.40	2.6 ± 0.03	55.16 ± 0.20	207 ± 16	4.24 ± 0.23	4.29 ± 0.69	4.12 ± 0.39
7	<0.40	2.54 ± 0.04	52.72 ± 0.20	34 ± 6	1.07 ± 0.07	1.17 ± 0.15	3.65 ± 0.40
8	<0.40	0.28 ± 0.01	5.32 ± 0.09	1181 ± 115	5.15 ± 0.30	5.6 ± 1.3	3.84 ± 0.46
9	<0.40	0.29 ± 0.01	6.51 ± 0.06	1167 ± 121	10.14 ± 0.57	10.5 ± 2.1	4.88 ± 0.42
10	<0.40	0.03 ± 0.00	0.68 ± 0.00	6.97 ± 1.67	0.0021 ± 0.0004	0.01 ± 0.00	0.23 ± 0.02
11	<0.40	0.01 ± 0.00	0.32 ± 0.00	0.16 ± 0.02	0.0021 ± 0.0004	<0.01	0.33 ± 0.03

REFERENCES

[1]   RUBERU, S.R., LIU, Y.-G., PERERA, S.K., Occurrence of ^{224}Ra, ^{226}Ra, ^{228}Ra, gross alpha, and uranium in California groundwater, Health Physics **89** (2005) 667.

[2]   PLASTINO, W., et al., Environmental radioactivity in the ground water at the Gran Sasso National Laboratory (Italy): A possible contribution to the variation of the neutron flux background, J. Radioanal. Nucl. Chem. **282** (2009) 809–813.

[3]   NATIONAL CENTER OF METEOROLOGY & SEISMOLOGY, Climatic Data for major stations in UAE (2009).

[4]   ELLISON, R.A., ARKLEY, S.L.B., WARRAK, M., FARRANT, A.R., Geology of the Al Ain 1:50,000 map sheet, United Arab Emirates, Keyworth, Nottingham: British Geological Survey, (2006).

ASSESSMENT OF POTENTIAL NITRATE POLLUTION SOURCES IN THE MARANO LAGOON (ITALY) AND ITS CATCHMENT AREA USING A MULTI ISOTOPE APPROACH

P. SACCON[a], A. LEIS[a], A. MARCA[b], J. KAISER[b], L. CAMPISI[b],
J. SAVARINO[c], M.E. BÖTTCHER[d], A. EISENHAUER[e], J. SÜLTENFUSS[f],
J. ERBLAND[c]

[a] Joanneum Research Forschungsgesellschaft mbH,
Institute for Water, Energy and Sustainability,
Graz, Austria

[b] School of Environmental Sciences,
University of East Anglia, Norwich,
United Kingdom

[c] UJF-Grenoble 1/CNRS-INSU,
Laboratoire de Glaciologie et Géophysique de l'Environnement,
St.-Martin-d'Hères, France

[d] Leibniz Institute for Baltic Sea Research,
Geochemistry & Isotope Geochemistry Group,
Marine Geology Section,
Warnemünde, Germany

[e] IFM-GEOMAR,
Kiel, Germany

[f] University of Bremen,
Institute of Environmental Physics, Section of Oceanography,
Bremen, Germany

Abstract

The aims of this study were mainly: (i) the identification and differentiation of the main anthropogenic nitrogen sources in the Marano Lagoon (Italy) and its catchment area; and (ii) the assessment of the intra-lagoonal water circulation, the morphological development of the lagoon and its anthropogenic pressure by applying a combined approach of hydrochemical, isotopic and remote sensing techniques. To achieve the aforementioned targets analyses of the stable isotope signatures of nitrate, boron, water and sulphate have been used. Moreover,

the residence times of groundwater were determined by the tritium–helium dating method. To characterize the chemical composition of the different water types the concentrations of the major ions and nutrients as well as the physicochemical parameters have been measured. Remote sensing techniques have been applied to assess the spatial distribution of the most superficial algal flora, water temperature as well as the key environmental and morphological changes of the lagoon since the beginning of the 1970s.

1. INTRODUCTION AND METHODS

The present study represents a novel approach to the determination of potential nitrate sources in a lagoon environment, which, besides the traditional hydrochemical analyses (main ions and nutrients), introduces the isotope signature of nitrate ($\delta^{15}N$, $\delta^{18}O$ and $\Delta^{17}O$), boron ($\delta^{11}B$), water (δ^2H and $\delta^{18}O$), and sulphate ($\delta^{34}S$ and $\delta^{18}O$), the tritium/helium ($^3H/^3He$) isotopic method as well as remote sensing techniques. The stable isotopes in nitrate measured by the denitrifier method have been used to differentiate between different nitrate sources as described in [1] and [2]. Boron isotopes have been used to identify the impact of domestic wastewater to the aquatic system using the LA–MC–ICP–MS method [3]. Use of $\delta^{11}B$ coupled with $\delta^{15}N$ has proved to be an effective means for tracing agricultural nitrate sources (e.g., hog manure, cattle feedlot runoff and synthetic fertilizers) in surface and groundwaters [4, 6]. The stable isotopes in water have been used to calculate mixing ratios between sea and fresh water and to estimate the mean altitude of the recharge area of surface waters. The stable isotopes in sulphate have been adopted to determine both its origin and the marine and terrestrial contributions, while the tritium–helium isotopic method has been used to assess the mean residence time of groundwater (groundwater age). In order to characterize the chemical composition of the different water types, the concentration of Ca^{2+}, Mg^{2+}, Na^+, K^+, NH_4^+, NO_3^-, NO", Cl^-, Br^-, SO_4^{2-}, PO'$^-$, HCO_3^-, total silicon, total phosphorus and total boron have been analysed. Moreover, the physicochemical parameters such as pH, electrical conductivity, dissolved oxygen, salinity and temperature have been measured. In order to identify the origin and the fate of nitrate, a water monitoring network was implemented in the Marano Lagoon and its catchment area. Monitoring involved the collection of water samples from the lagoon, tributary rivers, groundwater upwelling line, groundwater, sewer pipe and open sea on a quarterly interval from 2009 to 2010.

2. STUDY AREA

The Marano Lagoon is located in the Northern Adriatic Sea (north eastern Italy) and it is entirely included in the Province of Udine of the Friuli Venezia Giulia region as represented in Fig. 1.
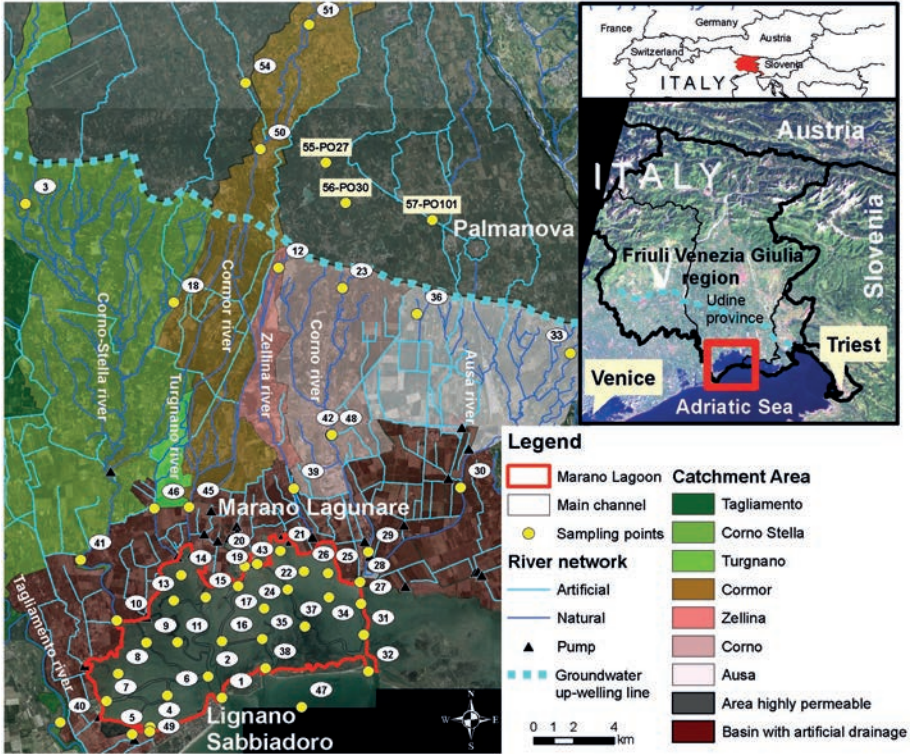
FIG. 1. Study area: Marano Lagoon (red line).

The lagoon has a surface of about 77 km², with a length of nearly 14 km and an average width of 5.5 km. The Marano Lagoon borders the Grado Lagoon to the east, which is the second part of the whole Grado–Marano Lagoon system. In the south the Marano Lagoon communicates to the Adriatic Sea through three lagoon inlets (Porto Lignano, S. Andrea and Porto Buso). A total mean water exchange rate between the lagoon and the Adriatic Sea through the Porto Lignano and Porto Buso inlets are respectively on the order of 1750 and 1500 m³/s. The mean bathymetry in the shallow lagoon areas is around 0.8 m, while in the navigable channels is about 3.2 m. In the south west the lagoon is characterized by the urban and touristic areas of Lignano Sabbiadoro, which is one of the main summer resorts in northern Italy, and by the Aprilia Marittima resort. The artificial channel of Bevazzana is also located in this lagoon sector, and forms a connection between the Tagliamento river and the lagoon. The fishing community of Marano Lagunare is situated in the northern lagoon sector, which is, with its 2007 inhabitants, the main urban centre within the lagoon perimeter. This lagoon sector is also characterized by the discharge of freshwater from its tributary rivers: Stella, Turgnano, Cormor, Zellina, Corno and Ausa.

The groundwater upwelling line divides the Friulian Plain into two units, the Upper Friulian Plain and the Lower Friulian Plain. The mean discharge of the groundwater upwelling line in the left Tagliamento river side is about 80 m³/s which corresponds to a mean discharge per kilometre of about 1.3 m³/s·km⁻¹.

3.   RESULTS

The isotopic composition of different anthropogenic and natural nitrate sources, as well as the values of measured samples, are reported in Fig. 2.

None of the samples fell into the isotopic range typically observed for nitrate originating from synthetic fertilizers. The isotopic composition of nitrate measured in the rivers was in the typical range of animal manure and urban sewage water but in the case that urban sewage water flows directly into the river system the $\delta^{15}N$ values can be much more enriched. This phenomenon has been detected in the Cormor river south of Udine city (sampling points: 50 and 51) and in the Corno river (sampling point 48 at sewer pipe). Moreover these isotopic values fit very well with the high concentration of nitrate, nitrite, ammonium and phosphate measured at the same sampling points. Since nitrite, ammonium and phosphate are typical indicators of local and direct anthropogenic pollution it could be concluded that, in this case, the main nitrate sources come from urban wastewater. Since water circulation in the lagoon is strongly influenced by the seawater (as confirmed by the analyses on the spatial distribution of bromide as well as by the isotopic composition of water)
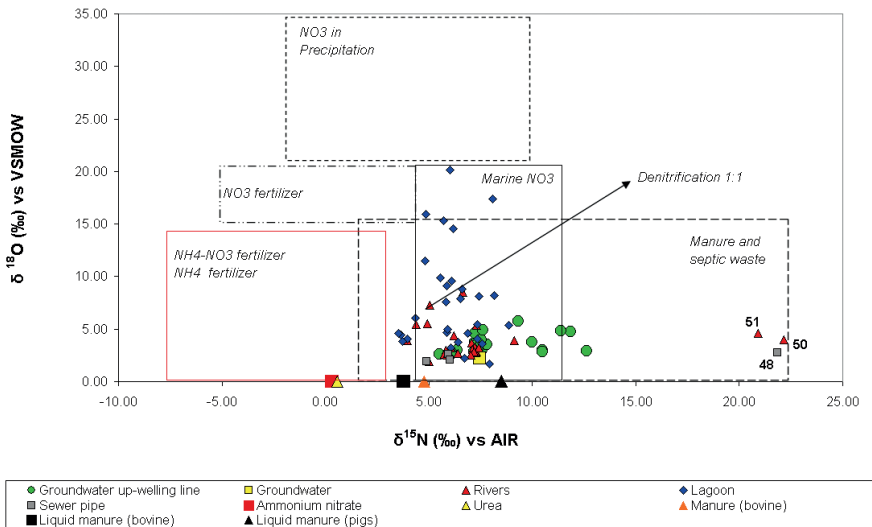

FIG. 2. Nitrogen and oxygen isotopic composition of nitrate (modified after [8]).

and since the $\delta^{18}O$ of seawater is higher than that of freshwater, the nitrate produced in the lagoon from nitrification of ammonium will have a higher $\delta^{18}O$ value. This may mean that nitrate with $\delta^{18}O > 8‰$ mainly originates from nitrification processes within the lagoon itself, especially since the small $\Delta^{17}O$ values (mean 0.65‰, maximum 3‰) indicate an atmospheric nitrate contribution of no more than 3% on average (but up to 10% locally). $\Delta^{17}O$ values of atmospheric nitrate fall in the range of 22 to 35‰, with the corresponding $\delta^{18}O$ values between 50 and 90‰. A contribution of 3% atmospheric nitrate would therefore increase the $\delta^{18}O$ of lagoon nitrate by only about 2‰.

Thus, the isotopic signatures of nitrates detected in the lagoon clearly showed that the nitrate load was not only derived from the agriculture activities but also from other sources such as urban wastewater and nitrification processes in the lagoon itself. To assess the impact of different boron sources in a catchment area an 'endmember mixing model' has been used. The most important pollution endmembers selected for this study were: manure, urban waste water and seawater. Manure has low boron concentrations (<0.1 mg/L and big variations in $\delta^{11}B$ values from 15 to 30‰. Upwelling groundwater is influenced from agriculture and characterized by relative low boron concentrations (0.11 to 0.23 mg/L). This is relatively close to natural background content (below 0.1 mg/L) in northern Italy [7]. The $\delta^{11}B$ values of the upwelling groundwater samples analysed in this study showed large variations from 4 to 22.7‰ (median value 17.7‰).

In contrast, urban wastewater has higher boron concentrations (0.46 to 1.1 mg/L) and lower $\delta^{11}B$ values from 0 to 12.9‰. No significant differences in boron contents and isotopic compositions have been found between raw and treated sewage. Therefore, boron isotope variations can be applied for tracing contamination of groundwater by both raw and treated sewage effluents. The sampled seawater in the Adriatic Sea at sampling point 47 was characterized by a boron content of 4.2 mg/L and a $\delta^{11}B$ value of 40.5‰. Most of the samples plotted within the range of these mixing curves can be explained by ternary mixing among the three endmembers. However, some of the river samples are above the mixing line. This group of data are characterized by low to moderate boron contents (0.1–0.45 mg/L) and high $\delta^{11}B$ values (36.2–39.6‰). From this it can be assumed that the mixing of river water boron with anthropogenic boron from manure and wastewater as well as with boron from seawater is the major factor which determines the distribution of $\delta^{11}B$ in the catchment of the lagoon and in the lagoon itself.

However, the higher boron concentrations in the seawater endmember result in non-linear (hyperbolic) boron concentration versus $\delta^{11}B$ mixing curves. That complicates the identification of the other pollution sources especially in the lagoon itself. Therefore, $\delta^{11}B$ values have been normalized using the bromide concentration in the water as a second tracer for the admixing of seawater. The data plotted in Fig. 3 indicates that most of the samples were influenced by both agriculture and urban waste water pollution sources. Moreover, the data show that in some areas
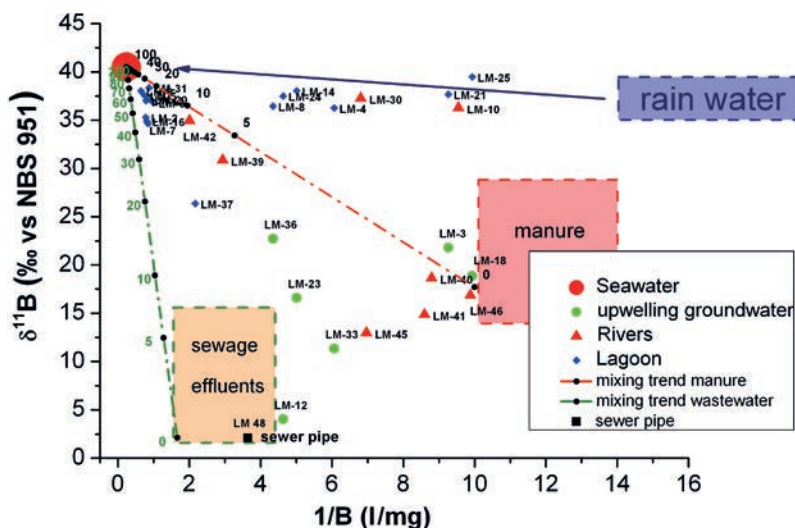
FIG. 3. $\delta^{11}B$ vs 1/B diagram showing normalized boron concentrations and $\delta^{11}B$ values.

of the lagoon the waters are less affected by these pollution sources. This identifies rainwater as an additional mixing endmember.

Sulphate in aquatic ecosystems can be from atmospheric, pedospheric and lithospheric origins. Moreover, sulphur compounds in industrial waste products are an additional source of sulphate. The different sulphates are introduced to the aquatic ecosystem by groundwater discharge to rivers (atmospheric, pedospheric and lithospheric sulphate) and direct mixing with seawater and precipitation (marine and atmospheric sulphate). Therefore sulphur isotopes can be used to trace natural and anthropogenic sources of sulphur in agricultural watersheds as well as in coastal aquifers.

The measured $\delta^{34}S$ and $\delta^{18}O$ values for sulphate at the sampling points 40 (Tagliamento river) were 12.3‰ and 12.9‰ respectively, while at the sampling point 5 (Bevazzana channel) they were 12.5‰ and 11.9‰ respectively, most likely indicating a lithogenic origin, e.g. from the dissolution of Permian evaporites [9]. This is in agreement with ion balance calculations of the dissolved components found at these sites. In contrast, dissolved sulphate at sampling point 6 (lagoon) shows $\delta^{34}S$ and $\delta^{18}O$ (20.6‰ vs V–CDT and 9.3‰ vs V–SMOW, respectively) that are typical for Mediterranean Seawater without indication for net sulphate reduction or an intense reduction–oxidation cycle. The sulphur and oxygen isotope analyses confirm that the waters of the southwestern lagoon sector are influenced by the Tagliamento river. Since 2008 the entire catchment area of the Marano Lagoon has been defined as a nitrate vulnerable zone (NVZ), where an action programme on the reduction of nitrate leaching has been launched. In order to assess the time necessary to expect the effects of the action programme in the NVZ an additional sampling campaign

TABLE 1. RESULTS OF THE ANALYSIS FOR TRITIUM (^{3}H) AND HELIUM ISOTOPES FOR GROUNDWATER DATING

Sample ID	^{3}H (TU)	Excess Ne (%)	^{4}He rad. (ccSTP/kg) Error: 0.2 E–6	^{3}He$_{tri}$ (TU)	Age (years)
55-PO27	4.95 ± 0.1	48	0.0 E–6	0.4	1.3 ± 0.5
56-PO30	5.1 ± 0.1	44	0.0 E–6	0.4	1.4 ± 0.5
57-PO101	4.85 ± 0.1	34	0.0 E–6	1.2	4.0 ± 1.0

Note: The derived data were calculated with assumed infiltration temperature of 10°C, altitude 0 masl and scaled to the sampling date of June 15th 2010.

to estimate the mean groundwater residence time has been carried out in June 2010. Groundwater in the Upper Friulian Plain was sampled at three irrigation wells (Fig. 1: 55–PO27, 56–PO30 and 57–PO101) for ^{3}H–^{3}He dating. The dating method utilized for these analyses is described e.g. by Ref. [10]. The results of the measurements of tritium (^{3}H) and helium isotopes for dating groundwater are reported in Table 1. Ages were calculated with the assumption of piston flow conditions in the aquifer. None of the samples show ^{4}He from radiogenic sources, which is used as an indicator for waters with ages much above 50 years. The concentration of ^{3}H and tritiogenic ^{3}He (^{3}He$_{tri}$) in the samples match the concentration of ^{3}H in precipitation quite well. The portion of excess Ne — compared to solubility equilibrium concentration — is rather high, namely in the order of 34–48% of the equilibrium value. This indicates that a recent equilibration of the dissolved gases in the water with the atmosphere could be excluded. Hence, the low concentration of ^{3}He$_{tri}$ and the derived young ages are a reliable feature of the aquifer.

To explain the groundwater age differences between the first two sampling points (55–PO27 and 56–PO30) and the point 57–PO101 it must be noted that before sampling groundwater at point 57–PO101, the two pumps installed in the irrigation well were running. Therefore, mixed waters between upper groundwater and deeper groundwater layers (older groundwater) have been sampled. In the other two irrigation wells (55–PO27 and 56–PO30) the pumps were out of order for many days, therefore the sampled waters from these two wells were not mixed with deeper water as in the first case.

4.   CONCLUSIONS

The isotopic compositions of different anthropogenic and natural nitrate sources as well as the isotopic signatures of nitrate in numerous water samples collected in the Marano Lagoon and its catchment area have been measured. Nitrates detected in groundwater and along the groundwater upwelling line are mainly related to the use

of manure (both liquid and solid), while other nitrate sources come from urban waste-water as detected in some rivers such as the Cormor and Corno rivers. In the lagoon, the characterization of the origin and fate of nitrate was in general much more difficult to achieve because of complex mixing processes among different water types such as seawater, riverwater and rainwater. However, it was possible to confirm that nitrate can be formed in the lagoon itself by nitrification processes of ammonium coming from both anthropogenic sources as well as from remineralization. Therefore, it can be concluded that the nitrate load in the lagoon, as detected during the monitoring period 2009–2010, was not only derived from agriculture activities but also from other sources such as urban wastewater, nitrification processes in the lagoon itself as well as from atmospheric deposition. Due to the fact that boron represents a co-migrant of nitrate in anthropogenic pollution sources, boron isotopes have been used as an additional tracer to identify different human impacts on aquatic ecosystems. Manure, urban wastewater and seawater were the three endmembers used for this analysis. From the concentration values and from the isotopic signature of boron found in the sampled waters it can be concluded that the distribution of $\delta^{11}B$ in the Marano Lagoon and its catchment area resulted from mixing of anthropogenic boron from urban wastewater and manure (liquid and solid) as well as from boron in seawater. The measured data indicate that most of the samples were influenced by both pollution sources: agriculture and urban wastewater.

Moreover, the data are showing that in some parts of the lagoon the water is less affected by these two pollution sources. Few samples along the groundwater upwelling line could not be explained with the use of the endmember mixing model. Therefore, these samples may be affected by the contamination of a different anthropogenic boron source such as landfill. The isotopic compositions in water have been used to characterize the mean altitude of the recharge area of the freshwater samples as well as to identify the origin of groundwater along the groundwater upwelling line. Additionally the water isotopes were used to identify mixing processes between freshwater and seawater within the lagoon. From these results it was possible to confirm that the sampled water along the groundwater upwelling line comes from local groundwater. The isotopic signature of sulphate confirmed the influence of the Tagliamento river in the western lagoon sector through the Bevazzana artificial channel. Moreover, the analysis conducted in three groundwater irrigation wells in the Upper Friulian Plain has shown that the groundwater age is very young in the range between 1.3 and 4.0 a.

REFERENCES

[1]   KAISER, J., HASTINGS, M.G., HOULTON, B.Z., RÖCKMANN, T., SIGMAN, D.M., Triple oxygen isotope analysis of nitrate using the denitrifier method and thermal decomposition of N_2O, Anal. Chem. **79** (2007) 599–607.

[2]   MORIN, S., et al., Comprehensive isotopic composition of atmospheric nitrate in the Atlantic Ocean boundary layer from 65 °S to 79 °N, J. Geophys. Res. **114** (2009) D05303.

[3]   FIETZKE, J., et al., Boron isotope ratio determination in carbonates via LA-MC-ICP-MS using soda-lime glass standards as reference material, J. Anal. At. Spectrom. (2010) 1953–1957.

[4]   BASSETT, R.L., BUSZKA, P.M., DAVIDSON, G.R., CHONG-DIAZ, D., Identification of groundwater solute sources using boron isotopic composition, Environ. Sci. Technol. **29** (1995) 2915–2922.

[5]   KOMOR, S.C., Boron contents and isotopic compositions of hog manure, selected fertilizers, and water in Minnesota, J. Environ. Qual. **26** (1997) 1212–1222.

[6]   WIDORY, D., et al., Nitrate in groundwater: An isotopic multi-tracer approach, J. Contam. Hydrol. **72** (2004) 165–188.

[7]   TARTARI, G., CAMUSSO, M., Boron content in freshwaters of northern Italy, Water, Air, Soil Pollut. **38** (1988) 409–417.

[8]   KENDALL, C., ELLIOTT, E.M., WANKEL, S.D., "Tracing anthropogenic inputs of nitrogen to ecosystems" (MICHENER, R.H., LAJTHA, K., Eds), Stable Isotopes in Ecology and Environmental Science, Chapter 12, 2nd edition, Blackwell, Oxford (2007) 375–449.

[9]   BÖTTCHER, M.E., The stable isotopic geochemistry of the sulfur and carbon cycles in a modern karst environment, Isot. Environ. Health Stud. **35** (1999) 39–61.

[10]   KIPFER, R., AESCHBACH-HERTIG, W., PEETERS, F., STUTE, M., "Noble Gases in Lakes and Ground Waters in Noble Gases in Geochemistry and Cosmochemistry" (PORCELLI, D., BALLENTINE, C.J., WIELER, R., Eds), Mineralogical Society of America and Geochemical Society of America, Washington, D.C. (2002) 615–700.

TOXIC MICROALGAL BLOOMS: WHAT CAN NUCLEAR TECHNIQUES PROVIDE FOR THEIR MANAGEMENT?[1]

B. REGUERA
Instituto Español de Oceanografía,
Centro Oceanográfico de Vigo, Spain

F. BOISSON
International Atomic Energy Agency,
Environment Laboratories, Monaco.

H.T. DARIUS
Institut Louis Malardé,
Laboratoire de recherche sur les Microalgues Toxiques,
Tahiti, French Polynesia, France

M.-Y. DECHRAOUI BOTTEIN
NOAA, National Ocean Service, Marine Biotoxins Programme,
Center for Coastal Environmental Health and Biomolecular Research,
Charleston, SC, USA

Abstract

Some harmful algal blooms (HABs) produce potent toxins that accumulate in shellfish and fish and represent a major threat to human health, international trade and sustainable coastal fisheries development. In the context of climate change and displacement of endemic toxigenic species (via ship ballast waters and other vectors) to new coastal areas, HABs appear to be more frequent and widespread. The IAEA Marine Environment Laboratory and its partners have been developing and transferring isotopic based analytical methods and instrumentation for monitoring HAB species, their biotoxins, and radiometric dating of sediment cores. The extremely sensitive and robust Receptor Binding Assay (RBA) for toxins associated with Paralytic Shellfish Poisoning (PSP) and Ciguatera Fish Poisoning (CFP) provides an alternative method to the standard mouse bioassay, and radiometric sediment core dating combined with fossil cyst abundance allows reconstruction of the prior history of blooms and their relationship to climate.

---

1. INTRODUCTION

Harmful Algal Blooms (HABs) is a term used by the Intergovernmental Oceanographic Commission (IOC) of UNESCO to designate any microscopic algae proliferation — regardless of their concentration — that is perceived as harmful from a human perspective. HABs pose a serious threat to public health, the exploitation of shellfish and artisanal fisheries, aquaculture and tourist resorts. Some HABs release exotoxins or reactive oxygen species (ROS) in the environment and impact fisheries and aquaculture. Other high biomass HABs lead to water discolorations, anoxic sediments or even skin and respiratory irritations in sunbathers exposed to sea spray containing remains of toxic cells or aerosolized toxins [1]. Here, attention is focused on HAB species that produce potent toxins, which, mainly due to their accumulation, by filter feeding bivalves, find their way through the food chain to humans, causing a variety of gastrointestinal and neurological illnesses, such as: (i) Paralytic Shellfish Poisoning (PSP); (ii) Diarrhetic Shellfish Poisoning (DSP); (iii) Amnesic Shellfish Poisoning (ASP); (iv) Neurotoxic Shellfish Poisoning (NSP); (v) Ciguatera Fish Poisoning (CFP) and (vi) Cyanobacterial Toxin Poisoning.

The socioeconomic impact of toxin producing microalgae (toxic HABs) on shellfish safety has been widely recognized [2]. Shellfish sanitation management requires regular monitoring of the waters of growing and harvesting areas for the detection of potentially toxic microalgae and testing of shellfish tissue to detect and quantify microalgal toxins accumulated by filter feeding bivalves. The impact of HABs is especially dramatic in developing countries where local fish and shellfisheries are an integral part of their diet or where utilization of shellfish resources, shellfish exports and tourism constitute a primary income source. Chronic HABs may cause human fatalities and/or prohibition of shellfish exports to developed counties from the lack of established monitoring programmes and awareness of health and fisheries authorities in these countries [3]. HABs are natural events and the best management practice is to improve prediction of their occurrence. Public health will be safeguarded if monitoring programmes are established which allow early warning of the occurrence of (i) Potentially toxic microalgae in the environment and/or (ii) Phycotoxins in seafood, before they attain concentrations that cause human illnesses or that force regulatory authorities to forbid harvesting and exports. Exports of live shellfish and ship deballasting from transoceanic cargos — both potential carriers of microalgae seeds (cysts) —increased aquaculture activities, tourism in developing countries and regulations on seafood safety have with no doubt led to an increasing impact of HAB events worldwide [1]. Lately, the potential tropicalization of warm–temperate seas due to global warming, and the subsequent spreading of warmwater species to new grounds — i.e. Ciguatera producers detected in the Mediterranean Sea and Atlantic islands — are a new matter of concern [4].

2. APPLICATION OF NUCLEAR TECHNIQUES IN HABS MANAGEMENT AND RESEARCH

In response to the growing interest expressed by its Member States in mitigating and managing HAB events, the IAEA has enlarged its activities to address impacts of HABs on public health. These activities include the selection of cost effective technologies, involving isotopic compounds, to be utilized for technology transfer and capacity building after careful comparison with non-nuclear techniques. A recent example of these initiatives are the IAEA technical cooperation projects (TCP), such as the RLA/7/014 'Designing and Implementing Systems for Early Warning and Evaluation of the Toxicity of Harmful Algal Blooms in the Caribbean Region, Applying Advanced Nuclear Techniques, Radioecotoxicological Evaluations and Bioassays (ARCAL CXVI)". Among the different radionuclide techniques, two emerge as good candidates for application in HAB research and management: (i) the receptor binding assays (RBA) and (ii) sediment dating combined with cyst identification.

2.1. The use of RBA to estimate toxins in seafood and in plankton extracts

Mouse bioassays (MBA) are validated methods used to monitor toxins in seafood. MBA are applied as the basis for warning of the presence of PSP, NSP and other toxins and for prohibiting trade in contaminated seafood products. While it is simple and robust, the method lacks in specificity and sensitivity. Moreover, the use of live animals for product testing is prohibited in many countries and will be discontinued in the European Union by the end of 2014. Reliable, rapid, sensitive and accurate assays for toxins are a requirement for any legal regulatory framework and a powerful tool for screening toxins in sanitation laboratories. The Receptor Binding Assay (RBA) using rat brain membrane preparation and brevetoxin as a radioligand is a simple, sensitive (ppb range) and high throughput method that can be used for early warning of neurotoxins, such as PSP, CFP and NSP toxins in shellfish and fish. The method is based on the specific interaction between the toxins and their pharmacological target, i.e. the voltage gated sodium channel, site 1 for PSP toxins, and site–5 for NSP and CFP toxins. In this assay, a radio labelled toxin ([^{3}H]saxitoxin or [^{3}H]brevetoxin) competes with unlabelled molecules for the sodium channel sites in a rat brain crude membrane preparation. When the binding equilibrium is reached, free [^{3}H]toxins are removed by filtration and collected, while receptor bound [^{3}H]toxins are quantified by liquid scintillation counting. The reduction in [^{3}H] toxin binding is directly proportional to the amount of unlabelled toxin present. A standard curve is generated using increasing concentrations of unlabelled toxin standard; the concentration of toxin in extracts of samples is determined in reference to the standard curve. The assay being employed within IAEA Technical Cooperation Projects (TCP) is a modification of the method of Doucette [5] and uses a 96 well microtiter plate format to minimize error by reducing sample handling and pipetting steps. Hence
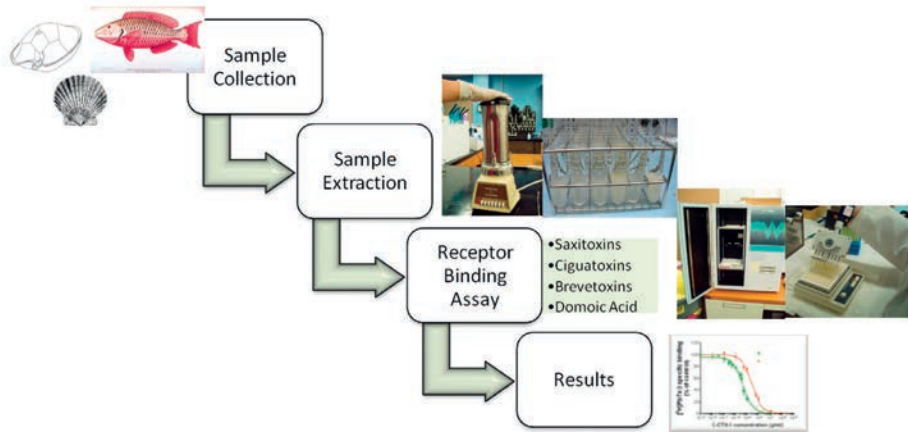
FIG. 1. Simplified scheme of the receptor binding assay method, from sample collection to results.

the receptor binding assay fulfils the requirements of a high throughput, quantitative analysis that reports a summed activity measurement expressed as equivalents of a reference toxin per unit of seafood weight. Thus, the RBA is a functional assay that estimates the toxic potential (toxicity) of the extract, in a manner comparable to the mouse bioassay. The sensitivity and specificity of this high throughput functional assay offers great advantages for a wide range of applications including seafood toxin screening [6,7], environmental monitoring for risk assessment [8] or exposure (zooplankton [9], crabs [10], whales [11], and humans [12, 13]) toxicological studies [14,15], or to guide chemical identification of new toxins [16].

These reports indicate that the RBA method is implemented in research laboratories all over the world, from the Pacific Ocean region (French Polynesia, New Zealand), to North America (USA, Canada), Asia (Malaysia) and Europe (Norway). In addition, over the last decade, the RBA technology has been transferred and implemented through IAEA-TCPs to developing countries in South east asia, Africa and Latin America. The use of the microtiter plate format, in conjunction with microplate scintillation counting, makes the assay potentially suitable for use in a high throughput regulatory setting. The RBA for PSP toxins has been evaluated in an AOAC Single Laboratory Validation [17] and is currently undergoing an AOAC inter-laboratory collaborative trial.

2.2. Dating of sediment cores combined with cyst analysis: looking into the past to redirect the future

Long term data sets (decades, centuries) of phytoplankton, collected with unchanged sampling methods, have to share the same temporal scales (decades,

centuries) as the natural or anthropogenic influences to which they may be related. These kinds of data sets are rare but essential to determine: (i) whether a HAB species has been recently introduced in a new area; (ii) whether blooms of a HAB species are increasing in frequency, intensity and geographic extension, or are just going through normal decadal fluctuations [18].

About 70% of the 100 microalgae species included in the IOC reference list of toxin producing microalgae [19] are dinoflagellates. Species of this group exhibit complex polymorphic life cycles that include a sexual resting cyst stage. At the end of a bloom, resting cysts are accumulated in the sediments and may remain viable and ready to germinate — following a species specific mandatory dormancy period — when conditions in the water column are again favourable for growth. Cysts of some of the most harmful toxin producing dinoflagellate genera (i.e. *Gymnodinium*, *Pyrodinium*) have an organic cover of a highly resistant compound, dinosporin; this substance is responsible for the cyst fossilisation. The fossil cysts or dinocysts, 15–100 μm in diameter, usually preserve well in the sediments and can be identified and quantified in palynological slides [20]**.** From all the above it is easy to guess that fossil records of dinoflagellate cysts constitute a valuable alternative material to study long term changes in HAB populations and help to address some of the previously mentioned issues.

The dinoflagellate *Pyrodinium bahamense* var. *compressum* is the species responsible for the highest number of fatal PSP victims in Central America [3] and the tropical western Pacific [21]. This species is presently confined to tropical, mangrove
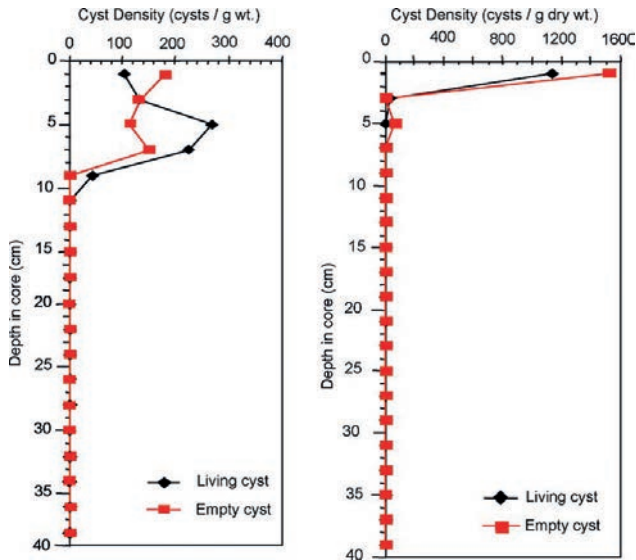

FIG. 2. *Vertical distribution of* P. bahamense *cysts in core 3 (left) and core 4 (right) collected in outer Malampaya Sound, the Philippines (Sombrito, pers. comun.).*

TABLE 1. CRUDE ANNUAL INCIDENCE RATE (IR) OF CFP PER 10000 PEO-
PLE (2007 TO 2010) IN THE FIVE ARCHIPELAGOS OF FRENCH POLYNESIA.
DATA FROM THE CFP DATABASE SHARED BY THE PUBLIC HEALTH DI-
RECTORATE OF FRENCH POLYNESIA AND INSTITUT LOUIS MALARDÉ

Year	2007	2008	2009	2010	IR per archipelago in 2010
Society	63	137	140	159	7
Marquesas	57	108	91	64	71
Australes	41	50	149	107	162
Tuamotu	187	208	164	162	101
Gambier	72	69	71	79	525
Total	420	572	615	571	
French Polynesia (IR/10 000 pop.)	16.2	21.8	23.1	21.2	

fringed coastal waters. Nevertheless, comparison of its present distribution with that in fossil records showed that it had a much wider range of distribution in the past [1]. There is concern that global warming may lead to a range expansion of PSP events caused by *Pyrodinium bahamense*. Temporal variations in the type and abundance of dinoflagellate cysts in Manila Bay, the Philippines, have been established using long ^{210}Pb dated sediment cores; *Pyrodinium bahamense* var. *compressum,* the main PSP toxin producer in the region, may have been present in the area at least since the 1920s [22]. In addition, collection of shorter cores and application of ^{210}Pb derived sedimentation rates and dinoflagellate cyst analyses have been used to understand the inter-annual variability of *Pyrodinium bahamense* blooms in relation to environmental conditions there (Fig. 2).

2.3. Case study: the Ciguatera risk assessment programme in French Polynesia

Ciguatera fish poisoning (CFP), endemic in tropical reef areas, is globally the most common nonbacterial foodborne illness [23]. Toxins are produced by benthic microalgae which live attached to seaweeds or other substrate and are transmitted to humans through herbivorous and carnivorous fishes. At the moment, there is not a realistic, cost effective way to monitor CTXs in seafood and the only possible prevention is to avoid consumption of risk species from risk areas. The Ciguatera risk assessment programme in French Polynesia, a hot spot for CFP events, is based on two main activities (i) Epidemiological survey of marine biotoxin intoxications

throughout the islands and (ii) the microalgal toxin based field monitoring in the lagoons, complemented with awareness education of the local population. French Polynesia has been engaged in a long term epidemiological survey programme of CFP since the 1960s. Since 2007, the Public Health Directorate in collaboration with the Institut Louis Malardé made a new clinical questionnaire available online (http://www.ilm.pf/DeclarationCiguatera) to elucidate the aetiology and prevalence of CFP and to detect new emerging marine intoxications in the region. Since 1973, the number of CFP cases in French Polynesia has decreased but incidences within islands are very variable: e.g. 2 and 1800 cases per 10000 people for Tahiti and Rapa islands respectively in 2009 [24]. Epidemiological data have revealed an increase of CFP since 2009 in the less risky Australes archipelago (Table 1).

This programme has also highlighted the emergence of new forms of marine intoxications from consumption of giant clams in Raivavae Island and of sea urchins in Rurutu Island, probably linked to blooms of marine benthic cyanobacteria [25]. Analyses of clinical questionnaires suggest that the prevalence could be more than double the reported cases [8]. The epidemiological database is updated weekly, and the status of CFP of each island can be followed in real time. Since 2004, a risk assessment for CFP has been conducted on six islands. The study undertaken on Raivavae Island has shown that risky areas of the lagoon have been submitted to the impact of natural and anthropogenic disturbances [26, 27]. Moreover, the population possesses traditional knowledge of the toxic fish species and risky areas of their lagoon.

The RBA analyses applied to laboratory cultures of the toxic dinoflagellate *Gambierdiscus* and to field collected fish samples have led to: (i) the characterization of a highly toxic new strain, *G. polynesiensis* (ii) the addition of two high CFP risk fish species to be avoided by consumers, and (iii) the identification of two safe (toxin free) fishing areas [28]. On Rapa Island, preliminary results suggest contamination of fish by more than one group of toxins: CTXs produced by *Gambierdiscus* spp. and palytoxins (PLTXs) associated with a bloom of *Ostreopsis*. RBA results have shown that fish may contain high level of CTXs and that among the 24 sampling areas, only two to three areas seem to be safe.

The main results of this ciguatera assessment programme were that: (i) The RBA is a suitable tool for multiple biological matrices when the matrix effect is controlled; (ii) the toxin extraction protocol needs to be improved when more than one toxin producer (e.g. *Gambierdiscus* and cyanobacteria) is present due to the diversity of toxins implicated, (iii) RBA values did not vary significantly with fish size or weight (e.g. smaller fish can be as dangerous as big ones), and (iv) herbivorous fish can be at least as toxic as carnivorous fishes. The RBA is a reliable tool for the assessment of ciguatera risk on a given island; results are congruent with epidemiological data and popular knowledge regarding the risk of certain areas and fish species.

3.   CONCLUSIONS

In summary, nuclear techniques developed by the IAEA and its partners have been successfully used as a tool for: CFP risk assessment in French Polynesia, ecology of PSP agents in southeast Asia, and environmental monitoring and mitigation of socioeconomic impacts of HABs. Its implementation for early warning of toxic microalgae and phycotoxins in Latin America and in Africa is in progress.

REFERENCES

[1]   HALLEGRAEFF, G.M., A review of harmful algal blooms and their apparent global increase, Phycologia **32** 2 (1993) 79–99.

[2]   FOOD AND AGRICULTURAL ORGANIZATION OF THE UNITED NATIONS, Marine Biotoxins, Food and Nutrition Papers No. 80, FAO, Rome (2004).

[3]   INTERGOVERNMENTAL OCEANOGRAPHIC COMMISSION OF UNESCO, IV Taller Regional Científico de la COI sobre Floraciones de Algas Nocivas en IOCARIBE-ANCA, Colombia (2007).

[4]   HALLEGRAEFF, G.M., Ocean climate change, phytoplankton community responses, and harmful algal blooms: A formidable predictive challenge, J. Phycol. **46** 2 (2010) 220–235.

[5]   DOUCETTE, G.J., LOGAN, M.M., RAMSDELL, J.S., VAN DOLAH, F.M., Development and preliminary validation of a microtiter plate-based receptor binding assay for paralytic shellfish poisoning toxins, Toxicon **35** 5 (1997) 625–636.

[6]   PLAKAS, S.M., DICKEY, R.W., Advances in monitoring and toxicity assessment of brevetoxins in molluscan shellfish, Toxicon **56** 2 (2010) 137–149.

[7]   COSTA, P.R., et al., Comparative determination of paralytic shellfish toxins (PSTs) using five different toxin detection methods in shellfish species collected in the Aleutian Islands, Alaska, Toxicon **54** 3 (2009) 313–320.

[8]   DARIUS, H.T., et al., Ciguatera risk assessment in two toxic sites of French Polynesia using the receptor-binding assay, Toxicon **50** 5 (2007) 612.

[9]   DAVID, L.S., NICHOLSON, R.A., Quantitation of paralytic shellfish toxins using mouse brain synaptoneurosomes, Chemosphere **55** 10 (2004) 1315–1321.

[10]   JESTER, R., RHODES, L., BEUZENBERG, V., Uptake of paralytic shellfish poisoning and spirolide toxins by paddle crabs (*Ovalipes catharus*) via a bivalve vector, Harmful Algae **8** 2 (2009) 369–376.

[11]   DOUCETTE, G.J., et al., Paralytic shellfish poisoning (PSP) toxins in North Atlantic right whales *Eubalaena glacialis* and their zooplankton prey in the Bay of Fundy, Canada, Mar. Ecol. Prog. Ser. **306** (2006) 303–313.

[12]   GESSNER, B.D., et al., Hypertension and identification of toxin in human urine and serum following a cluster of mussel-associated paralytic shellfish poisoning outbreaks, Toxicon **35** 5 (1997) 711–722.

[13]   HAMILTON, B., et al., Human fatality associated with Pacific ciguatoxin contaminated fish, Toxicon **56** 5 (2010) 668–673.

[14]   BAKKE, M.J., HORSBERG, T.E., Kinetic properties of saxitoxin in Atlantic salmon (*Salmo salar*) and Atlantic cod (*Gadus morhua*), Comp. Biochem. Physiol. C Pharmacol. Toxicol. Endocrinol. **152** 4 (2010) 444–450.

[15]   DECHRAOUI, M.Y., NAAR, J., PAUILLAC, S., LEGRAND, A.M., Ciguatoxins and brevetoxins, neurotoxic polyether compounds active on sodium channels, Toxicon **37** 1 (1999) 125–143.

[16]   HAMILTON, B., et al., Isolation and characterisation of Indian Ocean ciguatoxin, Toxicon **40** 6 (2002) 685–693.

[17]   VAN DOLAH, F.M., et al., Single-laboratory validation of the microplate receptor binding assay for paralytic shellfish toxins in shellfish, J. AOAC Int. **92** 6 (2009) 1705–1713.

[18]   WYATT, T., "Can we detect meaningful changes in Mediterranean phytoplankton?", Phytoplankton responses to Mediterranean Environmental Changes (BRIAND, F., Ed.), CIESM Workshop Monographs 40, CIESM, Monaco (2010) 15–18.

[19]   MOESTRUP, Ø., et al., (Eds), IOC-UNESCO Taxonomic Reference List of Harmful Micro Algae (2009), http://www.marinespecies.org/HAB

[20]   DALE, B., The sedimentary record of dinoflagellate cysts: Looking back into the future of phytoplankton blooms, Sci. Mar. **65** Suppl. 2 (2001) 257–272.

[21]   HALLEGRAEFF, G.M., MACLEAN, J.L., (Eds), "Biology, Epidemiology and Management of *Pyrodinium* Red Tides", (Proc. Management and Training Workshop, Bandar Seri Begawan, May 1989), International Centre for Living Aquatic Resources Management, Manila 1989, Vol. 21.

[22]   SIRINGAN, F.P., AZANZA, R.V., MACALALAD,N.H., ZAMORA, P.B., STA MARIA, Y.Y., Temporal changes in the cyst densities of *Pyrodinium bahamense* var. *compressum* and other dinoflagellates in Manila Bay, Philippines, Harmful Algae **7** 4 (2008) 523–531.

[23]   LEHANE, L., LEWIS, R.J., Ciguatera: recent advances but the risk remains, Int. J. Food Microbiol. **61** (2000) 91–125.

[24]   CHATEAU-DEGAT, M.L., CHINAIN, M., DARIUS, T., DEWAILLY, E., MALLET, H.-P., Surveillance épidémiologique de la ciguatéra en Polynésie française, BEH **48–49–50** (2009) 522–525.

[25]   LAURENT, D., et al., Are cyanobacteria involved in Ciguatera Fish Poisoning-like outbreaks in New Caledonia?, Harmful Algae **7** 6 (2008) 827–838.

[26]   CHATEAU-DEGAT, M.L., Les toxines marines: Problème de santé en émergence, VertigO – La revue en Sciences de l'Environnement **4** 1 (2003) 1.

[27]   HALES, S., KOVATS, R.S., WOODWARD, A., What El Niño can tell us about human health and global climate change, Global Change and Human Health **1** 1 (2000) 66–77.

[28]   CHINAIN, M., HALES, S., KOVATS, S., WOODWARD, A., Ciguatera risk management in French Polynesia: The case study of Raivavae Island (Australes Archipelago), Toxicon **56** 5 (2010) 674–690.

PLUTONIUM IN SOUTHERN HEMISPHERE OCEAN WATERS

K. HIROSE [a], M. AOYAMA [b], J. GASTAUD [c], M. FUKASAWA [d], C.-S. KIM [e],
I. LEVY [c], P.P. POVINEC [f], P. ROOS [g], J.A. SANCHEZ-CABEZA [h], S.A. YIM [i]

[a] Sophia University,
Tokyo, Japan

[b] Meteorological Research Institute,
Tsukuba, Japan

[c] Marine Environment Laboratories,
International Atomic Energy Agency,
Monaco

[d] Japan Agency for Marine-Earth Science and Technology
Yokosuka, Japan

[e] Environment Laboratories,
International Atomic Energy Agency,
Seibersdorf, Austria

[f] Comenius University,
Bratislava, Slovakia

[g] Risø National Laboratory,
Roskilde, Denmark

[h] Universitat Autonoma de Barcelona,
Bellaterra, Spain

[i] Korea Institute of Nuclear Safety,
Daejeon, Korea

Abstract

Plutonium in seawater collected by the BEAGLE2003 cruise was determined using ICP–SF–MS and alpha spectrometry after Fe co-precipitation and radiochemical purification. Levels and distributions of dissolved plutonium activity concentrations in Southern Hemisphere ocean waters are summarized here, including historical data. Pu–239 concentrations in surface water

of the central South Pacific (32.5 °S) in 2003 were around 1 mBq/m^3. The ^{239}Pu concentrations in the Indian Ocean surface waters (20 °S) were similar to that in the South Pacific, whereas the ^{239}Pu concentrations in the South Atlantic surface waters (30°S) were markedly lower than those in the South Pacific and Indian Oceans. The ^{239}Pu vertical profile pattern was similar to that in the North Pacific subtropical gyre, although ^{239}Pu concentrations in the deep South Pacific were significantly lower than those in the North Pacific. One of the dominant factors controlling plutonium distributions in the Southern Hemisphere oceans is biogeochemical processes including particle scavenging.

1.   INTRODUCTION

Most of the plutonium in the major oceans was deposited to the ocean surface by global fallout of the large scale atmospheric nuclear testing in the early 1960s and close-in fallout due to nuclear explosions conducted in the Pacific province in the 1950s [1]. After that, plutonium has been spread to world oceans and transported into ocean interiors by physical (advection and diffusion) and biogeochemical processes [2–4]. Current plutonium distributions in the world oceans reflect injection and oceanic processes which occurred four or five decades after the major injection of plutonium in the early 1960s [1]. Especially in the Southern Hemisphere oceans, plutonium has been important for the elucidation of long term transport processes, which include transport between ocean basins and biogeochemical processes in each basin, because the deposition of plutonium into the Southern Hemisphere oceans was weaker than that into the Northern Hemisphere oceans and the major injection process was only global fallout except for a local contamination due to French nuclear explosions in the subtropical South Pacific [1].

In 2003 and 2004, the Japan Agency for Marine-Earth Science and Technology (JAMSTEC) conducted the Blue Earth Global Expedition (BEAGLE2003), visiting the South Pacific (winter), South Atlantic (late spring) and South Indian (summer) Oceans during the 7-month expedition [5]. This campaign was undertaken within the framework of the SHOTS project (Southern Hemisphere Ocean Tracer Study) [6]. The main aim of this project was to study the distribution of artificial radionuclides in Southern Hemisphere oceans, in conjunction with hydrographical data (temperature, salinity, nutrient concentrations and others) collected with the aim to investigate the response of oceans to climate change.

We present here plutonium concentrations in Southern Hemisphere ocean waters using the BEAGLE2003 data and historical data, and discuss factors which control its distribution in Southern Hemisphere oceans [7–9].

2. DATA

Plutonium data of the BEAGLE expedition are cited from Refs [7–9]. The sampling strategy and analytical procedures of plutonium determination are described elsewhere [6, 10]. Historical data of Southern Hemisphere oceans are cited from the HAM database [11], including the GEOSECS data.

3. RESULTS AND DISCUSSION

3.1. Surface plutonium in Southern Hemisphere oceans

The BEAGLE2003 expedition provided 48 surface plutonium data in the South Pacific Ocean [7], 20 surface plutonium data in the Indian Ocean and 22 surface plutonium data in the south Atlantic Ocean [9] in addition to five vertical profiles of plutonium in the south Pacific ocean [8]. Plutonium (^{239,240}Pu) concentrations in the south Pacific surface waters were determined by alpha spectrometry [7] whereas ^{239}Pu concentrations in the Indian and Atlantic Oceans, and vertical profiles in the South Pacific were measured by Sector Field Inductively Coupled Plasma Mass Spectrometry (SF-ICP-MS)[8, 9]. Unfortunately we cannot obtain information on ^{240}Pu/^{239}Pu atom ratios in the south Pacific, Indian and south Atlantic Oceans because ^{240}Pu, a minor isotope of plutonium, cannot be detected because of the small volumes of the seawater samples [8, 9]. Plutonium inventories in the water columns of the central South Pacific are the same order of magnitude as the cumulative deposition of plutonium [8, 12]. The ^{240}Pu/^{239}Pu atom ratios in the subtropical South Pacific (Rangiroa (14°47'S: 0.166 ± 0.011) were similar to that of global fallout (0.18) [13]. This result implies that there is no transport of Pu from the North Pacific to the subtropical South Pacific, as the plutonium atom ratio is higher in the North Pacific due to close-in fallout from the Pacific Proving Ground nuclear testing conducted in the mid 1950s. Then it is reasonable to assume that the plutonium atom ratio in the South Pacific mid-latitude region is nearly equal to that of global fallout (0.18).

We calculated the ^{239}Pu activity (A(^{239}Pu)) in surface waters of the South Pacific Ocean using the following equation:

$$A(^{239}Pu) = A(^{239,240}Pu)\,(1 + \lambda(^{240}Pu)/\,\lambda(^{239}Pu)\,R_{240/239}\,)^{-1}$$

where $\lambda(^{240}Pu)$, $\lambda(^{239}Pu)$, and $R_{240/239}$ denote decay constants of ^{240}Pu and ^{239}Pu, and atom ratio, respectively. The calculated ^{239}Pu activities in the central South Pacific coincided with that determined by ICP–MS within the analytical uncertainty as shown in Table 1.

TABLE 1. ^{239}Pu ACTIVITY CONCENTRATION (mBq/m^3) IN THE SOUTH PACIFIC SURFACE WATER. COMPARISON BETWEEN ALPHA SPECTROMETRY AND ICP–MS

Location	Alpha spectrometry	ICP–MS
177.67°W	0.96 ± 0.23	0.92 ± 0.12
169.5°W	1.5 ± 0.5	1.02 ± 0.07
163.17°W	1.08 ± 0.18	0.9 ± 0.1
157.33°W	0.66 ± 0.12	0.71 ± 0.06
149.83° W	0.90 ± 0.12*	0.9 ± 0.1

* 147.35 W

The ^{239}Pu concentrations in the South Pacific surface waters ranged from 0.3 to 2.5 mBq/m^3 with an average of 1.1 mBq/m^3. The ^{239}Pu concentrations in the Indian and South Atlantic surface waters ranged from 0.54 to 1.64 mBq/m^3 with an average of 0.86 mBq/m^3 and from 0.13 to 0.66 mBq/m^3 with an average of 0.35 mBq/m^3, respectively [9]. The longitudinal distribution of ^{239}Pu is shown in Fig. 1. Although relatively higher ^{239}Pu concentrations occurred in South Pacific surface waters, the level of surface ^{239}Pu in the South Pacific is similar to that in the Indian Ocean surface waters. On the other hand, the level of surface ^{239}Pu in the South Atlantic is significantly lower than that in the South Pacific and Indian Oceans. In order to elucidate the reason why the surface plutonium in the South Atlantic was markedly lower than that in the South Pacific and Indian Oceans, we analysed temporal changes of surface plutonium in the Southern Hemisphere oceans. Previous results reveal that the apparent half residence time (HRT) of plutonium in surface water in the South Atlantic (9–10 years) [4, 8] is shorter than that in the South Pacific (western South Pacific: 34 years, South Pacific Subtropical Gyre: 19 years, eastern South Pacific: 22 years) and Indian Ocean [7, 8]. We re-examined the temporal change of ^{239,240}Pu concentrations in surface waters in the western South Atlantic and eastern Indian Ocean (latitude band: 15°–35°S) including ^{239,240}Pu calculated from ^{239}Pu in SHOTS data assuming that ^{240}Pu/^{239}Pu atom ratio is equal to that in global fallout. The apparent HRT of surface plutonium in the weatern South Atlantic and eastern Indian Ocean are 12^{+13}_{-5} and 20^{+15}_{-6} years, respectively, which are similar to previous estimates [4, 8] although the apparent HRT of the surface plutonim in the eastern Indian Ocean is longer than the previous estimate [8]. This finding suggests that surface plutonium in the South Atlantic is removed from surface layer faster than that in the South Pacific and Indian Ocean mid-latitude regions.
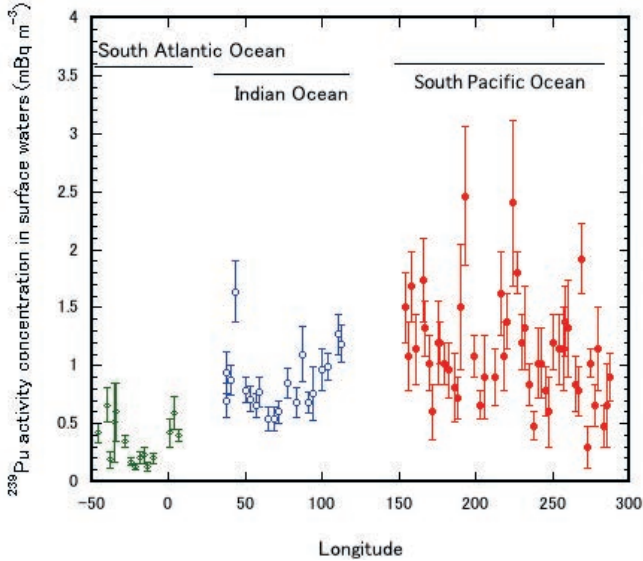
FIG. 1. Longitudinal distribution of ^{239}Pu activity concentration in Southern Hemisphere oceans.

3.2. Vertical profiles of plutonium

Vertical profiles of plutonium in the Southern Hemisphere oceans are scarce. There were several profiles of plutonium in the South Pacific and South Atlantic Oceans determined in GEOSECS. In the BEAGLE2003 expedition, five profiles of ^{239}Pu in the central South Pacific were determined [8]. The results revealed that the ^{239}Pu concentration increased with increasing depth and reached a maximum (4.6 to 6.6 mBq/m^3) at 600–800 m depth, a result similar to those reported by previous studies in the South Pacific [15°S, 148°W] (^{239,240}Pu: 9.2 mBq/m^3) [13]. The ^{239}Pu concentration then sharply decreased from 800 to 1400 m depth and reached a minimum at 2000 m depth. Plutonium is a useful transient tracer of biogeochemical processes in the marine environment. Unfortunately there is no vertical profile of plutonium in the Indian Ocean. In the South Atlantic, the vertical profiles of ^{239,240}Pu were obtained in 1972. The ^{239,240}Pu concentration showed a subsurface maximum, whose depths were shallower than those of the current Pu profiles determined in the Pacific. The results suggest that the ^{239}Pu vertical profiles in the Pacific Ocean are controlled primarily by biogeochemical processes which consist of plutonium uptake by biogenic particles, gravitational sinking of particles and regeneration of plutonium as a result of bacterial decomposition of particles in deeper water [14, 15] although physical processes such as advection, mixing and upwelling contribute to plutonium distributions as well.

In order to extract the biogeochemical processes in the ocean by using transient tracers, it is effective to use the plutonium/^{137}Cs activity ratio because their behaviour in seawater is different [7, 16, 17]. Recently it has been revealed that the [239,240]Pu/^{137}Cs activity ratios in the water columns of the North Pacific, except the equatorial region, exponentially increased with depth from 100 m to 1200 m depth [18] although the vertical profile of the [239,240]Pu concentration in the water column significantly differs from that of [137]Cs. A similar relationship between [239]Pu/^{137}Cs ratio and depth was observed in the South Pacific [8]. We examined the relationship between [239,240]Pu/^{137}Cs ratio and depth in the South Atlantic (GEOSECS). The [239,240]Pu/^{137}Cs ratios in the South Atlantic water columns exponentially increase with increasing depth. The half-regeneration depth obtained from the relationship between [239,240]Pu/^{137}Cs ratio and depth in the South Atlantic, which ranged from 87 to 350 m, correlates with the plutonium maximum layer depth. These findings suggest that the [239,240]Pu/^{137}Cs ratios in the water columns are useful tools to deduce factors which govern the biogeochemical processes.

3.3. Deep water plutonium

Model studies [19] revealed that the plutonium profile from surface to around 2000 m depth is primarily governed by the biogeochemical processes. In fact, good exponential relationships between [239,240]Pu/^{137}Cs ratio and depth are observed at shallower depths than 1500 m [18]. Deeper plutonium, below 2000 m water depths, may be controlled by the direct injection process of fallout Pu and physical processes such as advection and diffusion rather than biogeochemical processes because of weak biological activities in the deep ocean. The North Pacific Deep Water (NPDW), which is characterized as old radiocarbon water from 2000 to 3000 m depth, intrudes into the South Pacific from the North Pacific. We examined a latitudinal distribution of plutonium in 2000 – 3000 m depth in the Pacific using data obtained in the mid 1990s and early 2000s. The result reveals that a gap of [239,240]Pu concentrations exists between the equator and 15°S; high [239,240]Pu concentrations in the North Pacific and low concentrations in the South Pacific. This finding suggests that plutonium in NPDW is an effective tool to trace long term motion of NPDW.

4.   CONCLUSIONS

Plutonium concentrations in Southern Hemisphere oceans were presented and discussed. [239]Pu concentrations in the South Atlantic surface water in 2003 are markedly lower than those of the South Pacific and Indian Oceans. The vertical profiles of [239]Pu in the South Pacific water columns exhibited surface minimum, mid-depth (near 600 m depth) maximum and lower levels in deep waters. This profile can be explained by biogeochemical processes. Good exponential correlations between

the ^{239,240}Pu/^{137}Cs activity ratio and depth exist not only in the North Pacific but also in the South Pacific and South Atlantic Oceans. There is a marked large difference of the plutonium concentration between the North Pacific and South Pacific deep waters, which could be used as a tool to trace deep water motion. These findings suggest that plutonium is a unique transient tracer to elucidate biogeochemical processes and deep water advection.

ACKNOWLEDGEMENTS

REFERENCES

[1]   UNITED NATIONS SCIENTIFIC COMMITTEE ON THE EFFECTS OF ATOMIC RADIATION, "Annex C: Exposures to the public from man-made sources of radiation", Sources and Effects of Ionizing Radiation, UNSCEAR 2000 Report to the General Assembly, United Nations, Vienna (2000) 158–291.

[2]   HIROSE, K., Plutonium in the ocean environment: Its distributions and behaviour, J. Nucl. Radiochem. Sci. **10** (2009) R7–R16.

[3]   LIVINGSTON, H.D., POVINEC, P.P., ITO, T., TOGAWA, O., "The behaviour of plutonium in the Pacific Ocean", Plutonium in the Environment (Kudo, A., Ed.), Elsevier, Amsterdam (2001) 267–291.

[4]   POVINEC, P.P., et al., ^{90}Sr, ^{137}Cs and ^{239,240}Pu concentration surface water time series in the Pacific and Indian Oceans – WOMARS results, J. Environ. Radioact. **81** (2005) 63–87.

[5]   UCHIDA, H., FUKASAWA, M. (Eds.), WHP P6, A10, I3/I4 Revisit Data Book: Blue Earth Global Expedition 2003, Vols 1, 2, JAMSTEC, Yokosuka, Kanagwa, Tokyo (2005).

[6]   AOYAMA, M., et al., "Southern Hemisphere Ocean Tracer Study (SHOTS): An overview and preliminary results", Radionuclides in the Environment: Int. Conf. on Isotopes in Environmental Studies, (POVINEC, P.P., SANCHEZ-CABEZA, J.A. Eds), Elsevier, London (2006) 53–66.

[7]   HIROSE, K., et al., Plutonium and ^{137}Cs in surface water of the South Pacific Ocean, Sci. Total Environ. **381** (2007) 243–255.

[8]   HIROSE, K., et al., Vertical profiles of plutonium in the central South Pacific, Prog. Oceanogr. **89** (2011) 101–107.

[9]   GASTAUD, J., et al., Transport and scavenging of Pu in surface waters of the Southern Hemisphere Oceans, Prog. Oceanogr. **89** (2011) 92–100.

[10]   LEVY, I., et al., Marine anthropogenic radiotracers in the Southern Hemisphere: New sampling and analytical strategies, Prog. Oceanogr. **86** (2011) 120–133.

[11]   AOYAMA, M., HIROSE, K., Artificial radionuclides database in the Pacific Ocean: HAM database, TheScientificWorldJOURNAL **4** (2004) 200–215.

[12]   HARDY, E.P., KREY, P.W., VOLCHOK, H.L., Global inventory and distribution of fallout plutonium, Nature **241** (1973) 444–445.

[13]   CHIAPPINI, R., POINTURIER, F., MILLIES-LACROIX, J.C., LEPETIT, G., HEMET, P., [240]Pu/[239]Pu isotopic ratios and [239+240]Pu total measurements in surface and deep waters around Mururoa and Fangataufa atolls compared with Rangiroa atoll (French Polynesia), Sci. Total Environ. **237/238** (1999) 269–276.

[14]   LIVINGSTON, H.D., ANDERSON, R.F., Large particle transport of plutonium and other fallout radionuclides to the deep ocean, Nature **303** (1983) 228–231.

[15]   HIROSE, K., "Complexation scavenging of plutonium in the ocean", Radionuclides in the Oceans: Input and Inventories, Part 1: Inventories, Behaviour and Processes (GERMAIN, P., GUARY, J.C., GUÉGUÉNIAT, P., MÉTIVIER, H., Eds), Radioprotect.-Colloq. **32** (1997) C2.225–230.

[16]   HIROSE, K., SUGIMURA, Y., AOYAMA, M., Plutonium and ^{137}Cs in the western North Pacific: Estimation of residence time of plutonium in surface waters, Appl. Radiat. Isot. **43** (1992) 349–359.

[17]   YAMADA, M., et al., ^{137}Cs, [239+240]Pu and [240]Pu/[239]Pu atom ratios in the surface waters of the western North Pacific Ocean, eastern Indian Ocean and their adjacent seas, Sci. Total Environ. **366** (2006) 242–252.

[18]   HIROSE, K., AOYAMA, M., POVINEC, P.P., [239,240]Pu/^{137}Cs ratios in the water column of the North Pacific: A proxy of biogeochemical processes, J. Environ. Radioact. **100** (2009) 258–262.

[19]   TSUMUNE, D., AOYAMA, M., HIROSE, K., Numerical simulation of ^{137}Cs and [239,240]Pu concentrations by an ocean general circulation model, J. Environ. Radioact. **69** (2003) 61–84.

ECOLOGICAL STUDIES IN THE COASTAL WATERS OF KALPAKKAM, SOUTHEAST COAST OF INDIA, IN THE VICINITY OF A NUCLEAR ISLAND

K.K. SATPATHY[a], A.K. MOHANTY[a], GOURI SAHU[a], M.V.R. PRASAD[a],
M. SMITA ACHARY[b], S.N. BRAMHA[a], M.K. SAMANTARA[b], S. BISWAS[b],
M. SELVANAYAGAM[b]

[a] Environmetal Safety Division,
Radiological and Environmental Safety Group, REG,
Indira Gandhi Center for Atomic Research,
Tamil Nadu, India

[b] Loyola Institute of Frontier Energy,
Loyola College,
Chennai, India

Abstract

Ecological monitoring of the coastal waters at Kalpakkam, which presently harbour various nuclear facilities, has been in progress for the last four years to create a benchmark dataset on water quality, phytoplankton, zooplankton, fisheries, sedentary organisms and molluscan species diversity. Results indicated a significant impact of monsoonal rain and backwaters on the coastal water quality. About 325 phytoplankton, 140 zooplankton, 350 fish, 130 molluscs and 100 species of sedentary organisms have been catalogued. Two fish species, which are native to Indonesia, were recorded for the first time in Indian coastal water. The study indicated that the coastal water is rich in biodiversity. Similarly, results of studies on costal sediment characteristics indicated the influence of monsoonal rain and backwater discharge. Overall, the study indicated little impact of nuclear activity on coastal water biodiversity and water quality.

1. INTRODUCTION

Organisms exist as part of a complex entity made up of interacting inorganic and biotic elements, to which we apply the term ecosystem. Ecology is the study of relationships between organisms and their surroundings, which is fundamental to the understanding of biology because organisms cannot live as isolated units. The life of organisms is dependent upon, and closely controlled by, the physical and chemical conditions in which they live and the populations of other organisms with which they interact. Physicochemical properties in any aquatic ecosystem play a

significant role in determining abundance, growth and metabolism of the organisms present in it. Phytoplankton, being the chief primary producer, serve as the base of the food chain in the marine habitat and act as a food reserve for primary consumers. Zooplankters form a link in the marine food chain and are considered the primary index at the secondary trophic level. Sedentary organisms, most of which are filter feeders, play an important role in coastal ecosystems for the biogeochemical cycling of elements by siphoning out the decaying organic matter from the water column. They colonize on submerged surfaces and successive colonization takes place due to inter-specific competition and their seasonal breeding pattern, which depends upon the water quality of the region. Among the several invertebrate phyla of the animal kingdom, Mollousca forms one of the major and important phylum. The majority of molluscs live in marine environments and are found to be excellent indicators of pollutions, thus, they are monitored to assess the health of the ecosystem of a region. Fish diversity and abundance, which provides livelihood for sizable populations, is an important component of the food chain process. Coastal and estuarine regions are important sinks for many persistent pollutants and thus, its geo-chemical characteristics can be used to infer the weathering trends, source of pollution and can also help to improve management strategies. Therefore, ecological monitoring of the coastal milieu adjacent to any industrial unit needs assiduous monitoring in order to assess any anthropogenic impact.

2. STUDY AREA

Kalpakkam coast (12°33´N Lat. and 80°11´E Long.) is situated about 80 km south of Chennai (Fig. 1). At present, a nuclear power plant (Madras Atomic Power Station, MAPS) and a desalination plant are located near the coast. MAPS uses seawater at a rate of 35 m^3/sec drawn through an intake structure located inside the sea at about 500 m away from the shore. After extracting heat, the heated seawater is released into the sea. Two backwaters, namely the Edaiyur and the Sadras backwater systems, are important features of this coast. These backwaters are connected to the Buckingham canal, which runs parallel to the coast. During northeast (NE) monsoon and seldom during southwest (SW) monsoon, the two backwaters discharge considerable amounts of freshwater to the coastal milieu for a period of 2 to 3 months. The average rainfall at Kalpakkam is about 1300 mm out of which the bulk of its rainfall (~65%) is received during NE monsoon. The detailed discussion of the study site is given elsewhere [1]. Based on the pattern of rainfall and hydrographic characteristics at Kalpakkam coast, the whole year has been divided into three seasons viz: (1) Summer/post-monsoon (February–May), (2) SW monsoon/pre-monsoon (June-September) and (3) NE monsoon (October–January). Seasonal monsoon reversal of wind that results in consequent change in the circulation pattern and coastal water quality is a unique feature of this coast [2]. The southerly current during NE monsoon

FIG. 1. Study area showing sampling location.

changes to northerly during February–September which coincides partly with the SW monsoon period (June- August).

3.   METHODS

Seawater samples were collected fortnightly in precleaned polythene bottles. Parameters such as temperature, pH, salinity, dissolved oxygen (DO) and turbidity were measured in the field using multi parameter probes (YSI 550). Dissolved micronutrients (nitrite, nitrate, ammonia, silicate, phosphate, total nitrogen and total phosphorous) and chlorophyll-a (chl-*a*) were estimated by spectrophotometry following the standard methods [3]. Phyto- and zooplankton samples were collected using an appropriate conical plankton net with mouth area 0.125 m² (mesh size–55 μm for phytoplankton and 200 μm for zooplankton) fitted with a flow meter (Hydrobios). Qualitative and quantitative analysis of plankton was carried out using a stereo-binocular research microscope (NIKON Eclipse 50*i* and Nikon TS100 with 400 X magnifications). Standard literatures were followed for identification (phyto- and zooplankton) and estimation of density and biomass (only for zooplankton)

[4–6]. Settlement pattern of sedentary organisms was studied by suspending teak wood panels (each $12 \times 9 \times 0.3$ cm) attached to epoxy coated mild steel frames from MAPS jetty. Detailed procedures followed are given elsewhere [7]. Molluscs were collected from the intertidal region during low tides and identified following standard literature [8]. Fish samples were collected from fishermen along the coast at weekly intervals. The morphometric and meristic characters like colour, spots and other important characters were noted in the field. Standard literatures [8–10] were consulted for identification of the fish. Sediment samples were collected onec monthly from
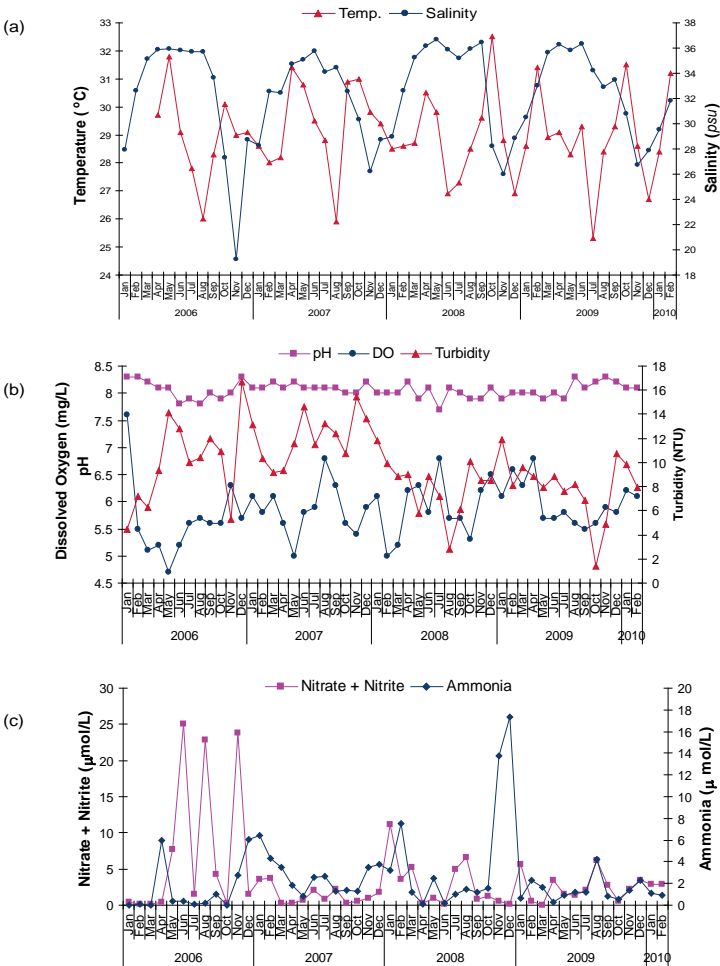
FIG. 2. Seasonal variation in physicochemical parameters in the coastal waters of Kalpakkam (cont. on the next page).

five locations using a Van Veen grab sampler. Sand, silt and clay % were analysed by following standard methods [11]. Metals such as Fe, Cu, Cr, Ni, Pb, Zn and Cd were analysed in ICPMS following standard methods [12].

4.   RESULTS

pH values ranged from 7.7–8.3 in the coastal waters. The observed salinity values ranged from 19.28–36.71 psu. The lowest and highest salinity values were observed during monsoon and summer respectively (Fig. 2a). The DO contents varied between 4.7–7.6 mg/L, with a relatively high concentration during monsoon period (Fig. 2b). Turbidity values ranged from 1.41–16.7 NTU having relatively high values during the summer and monsoon as compared to the rest of the year. Nitrite + nitrate,
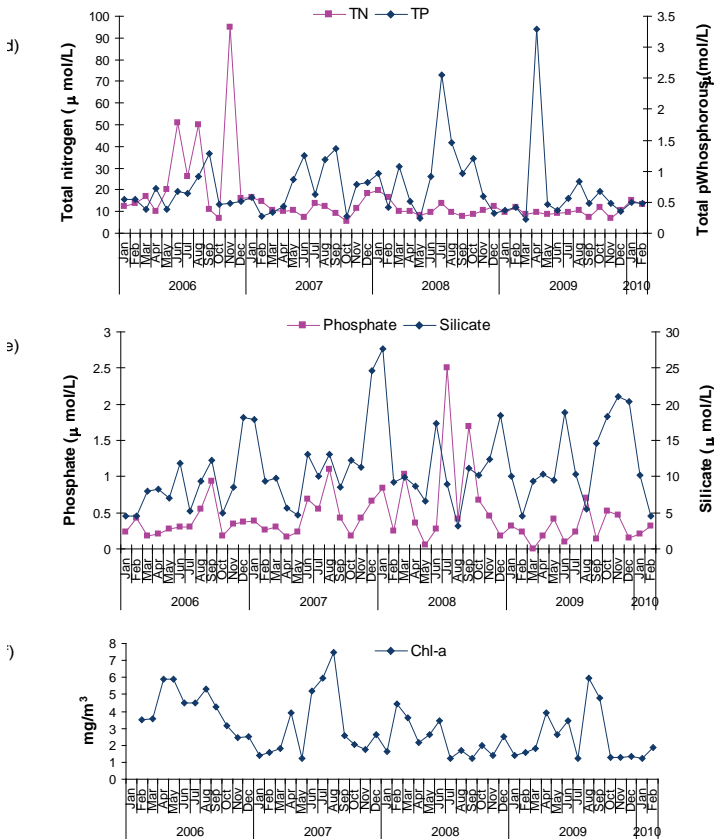
FIG. 2 (cont.). Seasonal variation in physicochemical parameters in the coastal waters of Kalpakkam.

the ammonia and TN concentration varied from 0.04–25.07 µ·mg/L, BDL =17.31 µ·mg/L and 5.29–94.94 µ·mg/L respectively (Fig. 2c, d).

Phosphate and TP concentration ranged from BDL = 2.51 and 0.23–3.29 µ·mg/L respectively and the pre-NE monsoon period registered relatively high values (Fig. 2e). Silicate values ranged from 3.23–27.71 µ·mg/L. Nitrogenous nutrients and silicate values were generally high during the NE monsoon period. Chl-*a* concentration ranged from 1.21–7.47 mg/m with high values during the summer and pre-monsoon (Fig. 2f).

Phytoplankton was found to be qualitatively much diversified in the coastal waters of Kalpakkam. A total of ~325 species have been catalogued during the last four years of study. Out of these, 252 species have been identified. The phytoplankton community constituted 7 groups, namely, diatoms, (111 Centric; 58 Pennate), Dinoflagellates (60), Silicoflagellates (2), Cyanobacteria (5), Chlorophycean members (13), two Haptophycean members (out of which one is Cocolithophore) and one Sarcomastigophora. Phytoplankton density ranged from 0.23×10^5 cells/L to 15×10^5 cells/L with the lowest and the highest coinciding with the post- and pre-monsoon periods respectively (Fig. 3a). Qualitative abundance showed the lowest (85) number of centrics during post-monsoon period and the highest number (105) during the monsoon. Pennates (Lowest: 44; Highest: 56) showed a completely analogous trend with that of the centrics. Dinoflagellates also showed a similar trend to that of diatoms. Qualitatively, the zooplankton community comprised of two major groups, i.e., holoplankton (whole life plankton) and meroplankton (planktonic in the larval stage only). Results showed that, both qualitatively and quantitatively, zooplankton was found to be rich during the pre-monsoon and summer period, which ranged from 2.2×10^5 to 9.9×10^5 per 10 m³ (Fig. 3b). Biomass (g(dry wt)/10 m³) also showed similar trend to that of density (lowest: 0.36 — monsoon; highest: 0.76 — summer). Copepods were abundant throughout the year.

About 100 species of sedentary organisms have been identified. It included 5 species of cnidarians, 12 species of annelids, 8 species of molluscs, 4 species of arthropods, 13 species of other crustaceans, 5 species of ectoprocta, 3 species of flat worms, 3 species of echinoderms and 7 species of tunicates. The density of organisms varied from $0.3–6.9 \times 10^3$ per 100 cm² with peak values during the pre-NE monsoon period (Fig. 4). Biomass did not show any trend and was mainly dependant on the larger organisms such as green mussels and barnacles. It ranged from 3.6–79.3 g per 100 cm². The area coverage was ~100% most of the times, however, it occasionally went down to 75%. Barnacles and green mussels emerged as the dominant macrobenthos in the coastal waters. Barnacles were found almost throughout the year (80% of the total density) with peak density observed during the NE monsoon period. Green mussels showed dominance during the pre-NE monsoon period.

Results of the taxonomic study of marine molluscs, the first of its kind from the Kalpakkam coast, would form a benchmark dataset for future investigations and impact assessments. So far about 130 species of molluscs have been collected, of
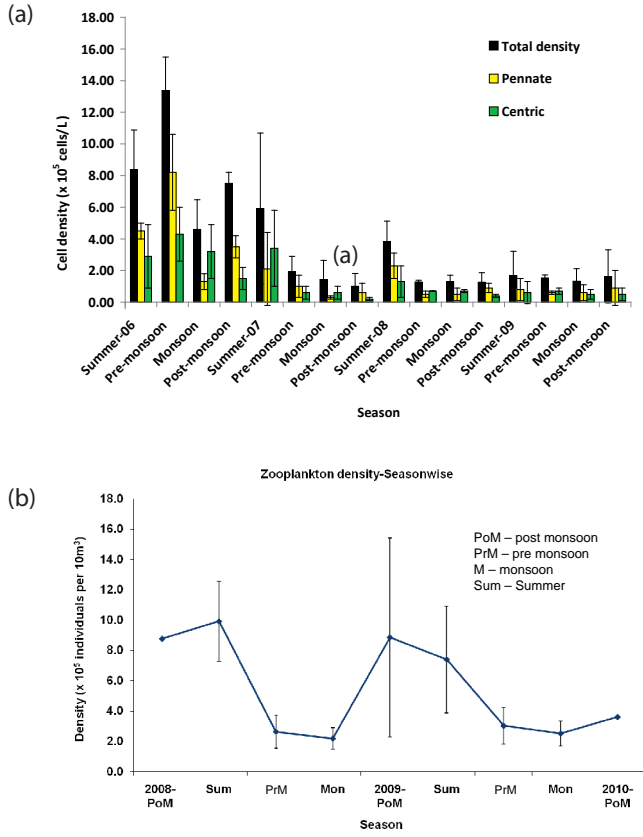
(a)

(b)

FIG. 3. Seasonal variation in total phytoplankton, pennate and centric diatom (a) and zooplankton density (b) in the coastal waters of Kalpakkam
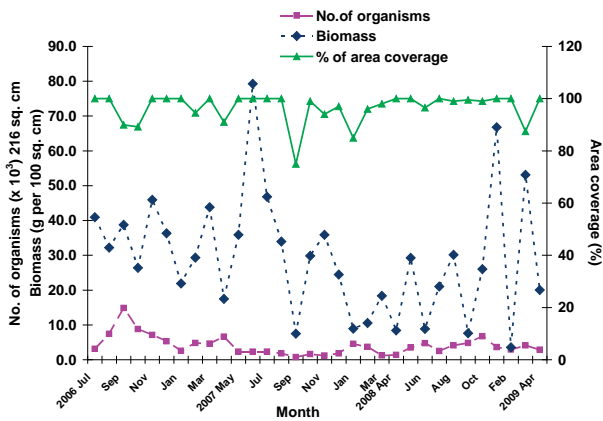

FIG. 4. Variations in density, biomass and area coverage of macrobenthic population on wooden surface exposed to coastal waters at Kalpakkam.
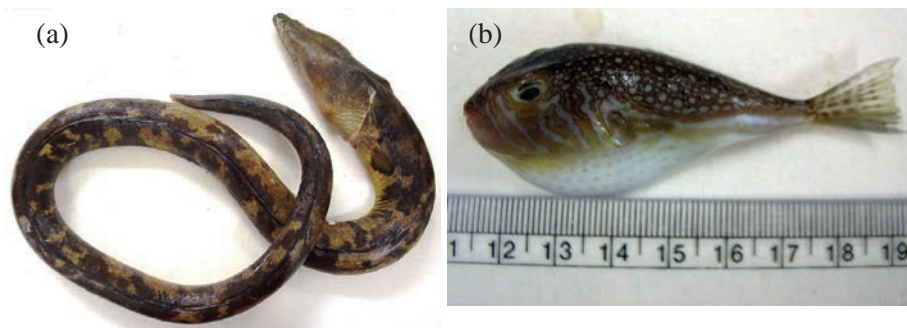
FIG. 5. (a) Brachysomophis cirrocheilos (Bleeker); (b) Torquigener brevipinnis (Regan).

which about 80 species have been identified. Efforts are underway to identify the remaining species. The fishery potential of coastal waters at this location was found to be high. Out of 350 species collected, 250 species of 84 families in 21 orders have been identified so far. The cartilaginous fish comprised only 6.4% of the total species composition. The order Perciformes was the most common with 114 species. The presence of 84 families in itself shows that the area has a rich diversity. Two of them, viz. *Brachysomophis cirrocheilos* (Fig. 5a) and *Torquigener brevipinnis* (Fig. 5b), common to the Indo-West Pacific waters of Papua New Guinea, Indonesia and Australia, are reported for the first time in Indian waters. Additionally, one of the species collected is supposed to be a totally undescribed species and efforts are underway for its confirmation.

Grain size distribution of sediments showed that the inner shelf was carpeted with a mosaic of sand and silty sand with a minor amount of clay (Fig. 6a). The annual average of heavy metal content followed a trend as Fe (0.48%) > Cu (21.3 ppm) > Zn (20.8 ppm) > Cr (12.2 ppm) > Pb (9.1ppm) > Ni (5.2 ppm) > Cd (1.5 ppm) with maximum variation for Fe and minimum variation for Cd (Fig. 6b).

5.   DISCUSSION

The physicochemical and biological properties of the coastal water at Kalpakkam was significantly affected by freshwater input during the NE monsoon. The nutrient rich freshwater diluted the coastal waters during the monsoon leading to an increase in concentration for all the nitrogenous nutrients and DO and a decrease in salinity and chl-*a* content. Phosphorous at this location was found to be of marine origin as its concentration in coastal waters was not affected by the monsoon. Salinity was found to be the most important factor controlling the phytoplankton as well as zooplankton production at this location. The optimum salinity and nutrient concentrations during the summer/pre-monsoon period favoured phytoplankton

(a)

(b)
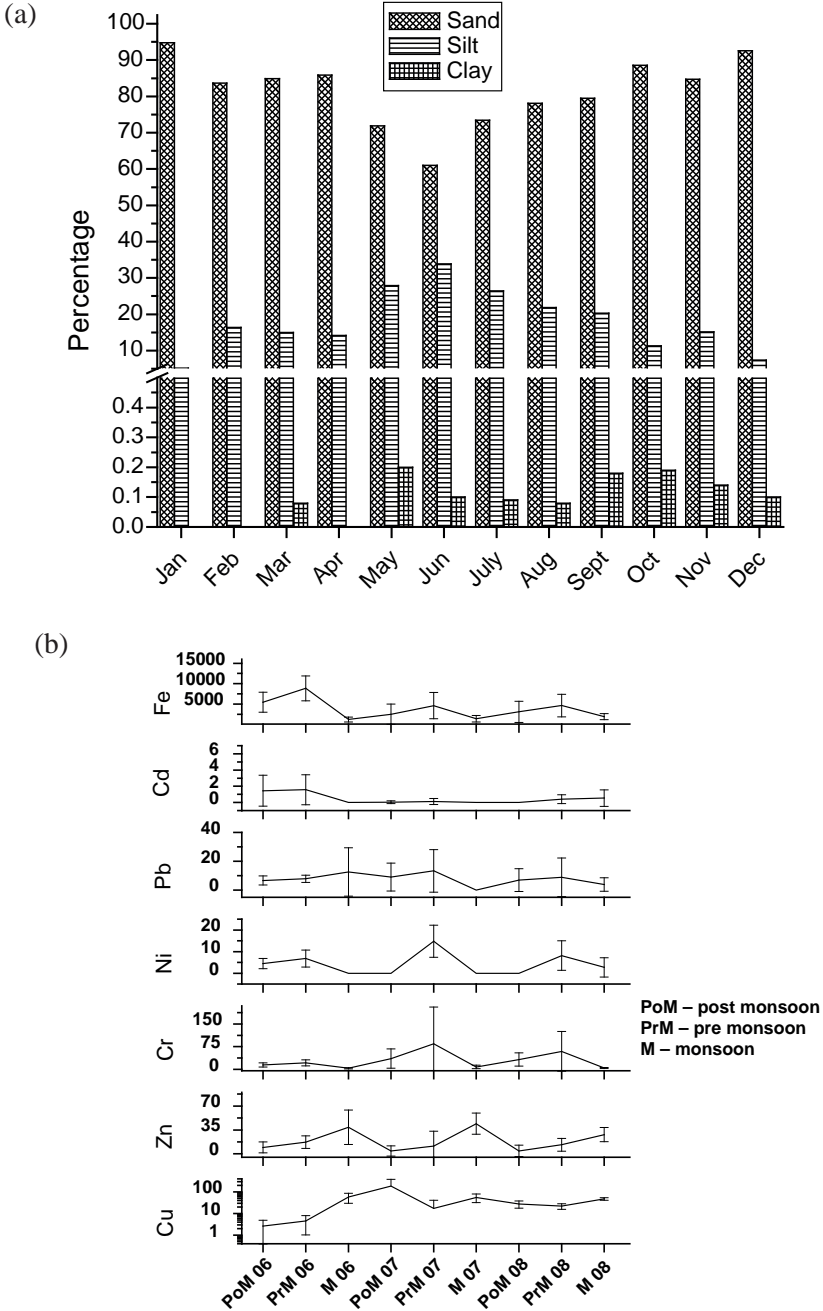
FIG. 6. (a) Variations in sand, silt and clay %; (b) heavy metal concentration (ppm) in the coastal sediments.

growth as compared to the adverse conditions prevailed during monsoon leading to the lowest phytoplankton abundance. A considerable increase (>5 fold) in phytoplankton species composition (325 species) was observed as compared to earlier findings (60 species) [13–14]. Despite such a massive change in floristic composition, a 4–10 times reduction in total cell count was observed during the present study. It is worthwhile to mention here that this coast was devastated by the December 2004 tsunami and studies on coastal water characteristics during the post-tsunami period have shown an increase in turbidity [15], a hindrance for light penetration, which could have led to a reduction in phytoplankton production. Nitrogenous nutrients were found to be limiting for phytoplankton growth during late summer and pre-monsoon periods, whereas the role of silicate and phosphate remained insignificant in this regard. Apart from salinity, temperature and phytoplankton species composition were found to be the dominant factors in determining species composition, standing stock and succession of zooplankton at this location. Concomitant with phytoplankton abundance the zooplankton density showed its peak during the summer and the lowest abundance was observed during the monsoon period. Similarly, the abundance and settlement pattern of benthic organisms at this location was significantly influenced by salinity and chl-*a*. However, due to the relatively clean and unpolluted environment at Kalpakkam, heavy settlement and rapid growth of these organisms was observed throughout the year. Bivalves showed dominance in the mollusc community. Mass mortality of molluscs was observed during the monsoon period. This locality showed a tremendous fishery potential. It is worthwhile to mention here that only about 500 species have been recorded from the entire Tamil Nadu coast against 350 species recorded from this area. The station close to the opening of a backwater showed typically higher values of heavy metal than the other stations pointing to the role of Buckingham canal as the anthropogenic source. Similarly an increase in some of the metal content was noticed during the monsoon period, indicating the role of land runoff and backwaters.

REFERENCES

[1]   SATPATHY, K.K., et al., Variations of physicochemical properties in Kalpakkam coastal waters, east coast of India, during southwest to northeast monsoon transition period, Environ. Monit. Assess. **171** (2010) 411–424.

[2]   VARKEY, M.J., MURTY, V.S.N., SURYANARAYANA, A., Physical oceanography of the Bay of Bengal and Andaman Sea, Oceanogr. Mar. Biol. **34** (1996) 1–70.

[3]   PARSONS, T.R., MAITA, Y., LALLI, C.M., A Manual of Chemical and Biological Methods for Seawater Analysis, Pergamon Press, New York (1984).

[4]   DESIKACHARY, T.V., et al., Atlas of Diatoms, Fascicles III and IV, Madras Science Foundation, Madras (1987).

[5]   KASTURIRANGAN, L.R., A Key to the Identification of the More Common Planktonic Copepoda of India Coastal Waters, Indian National Committee on Oceanic Research, CSIR, New Delhi (1963).

[6]   CONWAY, D.V.P., WHITE, R.G., HUGUES-DIT-CILES, J., GALLIENNE, C.P., ROBINS, D.B., Guide to the Coastal and Surface Zooplankton of the South-Western Indian Ocean, Occasional Publication No. 15, Marine Biological Association of the United Kingdom, Plymouth (2003).

[7]   SAHU, G., et al, Studies on the settlement and succession of macrofouling organisms in the Kalpakkam coastal waters, southeast coast of India, Indian J. Mar. Sci. **40** (2011) 747–761.

[8]   TALWAR, P.K., KACKER, R.K., Commercial Sea-Fishes of India, Zoological Survey of India, Calcutta (1984).

[9]   DAY, F., The Fishes of India, Vol. 1, Today & Tomorrow's Book Agency, New Delhi (1978).

[10]   DAY, F., The Fishes of India, Vol. 2, Today & Tomorrow's Book Agency, New Delhi (1978).

[11]   KRUMBEIN, W.C., PETTIJOHN, F.J., Manual of Sedimentary Petrography, Appleton Century, New York (1938).

[12]   TESSIER, A., CAMPBELL, P.G.C., BISSON, M., Sequential extraction procedure for the speciation of particulate trace metals, Anal. Chem. **51** (1979) 844–851.

[13]   SARGUNAM, C.A., Studies on the Microfouling in the Coastal Waters of Kalpakkam, East Coast of India, with Reference to Diatoms, PhD Thesis, University of Madras, India (1994).

[14]   POORNIMA, E.H., Impact of Thermal Discharge from a Tropical Coastal Power Plant on Marine Phytoplankton, PhD thesis, University of Madras, India (2005).

[15]   SATPATHY, K.K., MOHANTY, A.K., PRASAD, M.V.R., NATESAN, U., SARKAR, S.K., Post-tsunami changes in water quality of Kalpakkam coastal waters, east coast of India with special references to nutrients, Asian J. Water, Env. Pollut. **5** (2008) 15–30.

THE TRANSPORT OF CLOSE-IN FALLOUT PLUTONIUM IN THE NORTHWEST PACIFIC OCEAN: TRACING THE WATER MASS MOVEMENT USING [240]Pu/[239]Pu ATOM RATIO

SANG-HAN LEE
Korea Research Institute of Standards and Science,
Daejeon, Rep. of Korea

GI-HOON HONG, MOON-SIK SUK
Korea Ocean Research and Development Institute,
Seoul, Rep. of Korea

J. GASTAUD
International Atomic Energy Agency,
Marine Environment Laboratory, Monaco

J. LA ROSA
National Institute of Standards and Technology,
Ionizing Radiation Division,
Gaithersburg, Maryland, USA

CHUL-SOO KIM
Environmental Laboratories,
International Atomic Energy Agency,
Seibersdorf, Austria

E. WYSE
New Brunswick Laboratory Argonne,
Illinois, USA

P.P. POVINEC
Comenius University,
Faculty of Mathematics and Physics,
Bratislava, Slovakia

Abstract

[240]Pu/[239]Pu atom ratios in seawater and surface sediment collected from the northwest (NW) Pacific Ocean from 1992 to 1997 were determined using ICP-sector field mass spectrometry (ICP–MS). In whole water columns, the atom ratios of [240]Pu/[239]Pu were higher than

the global fallout ratio (0.18). It is noted that the atom ratios of ^{240}Pu/^{239}Pu in the seawater increase with depth. Such elevated ^{240}Pu/^{239}Pu atom ratios indicate that the close-in fallout plutonium isotopes originating from the Pacific Proving Grounds (PPGs) due to the U.S. tests are prevailing in the seawater in the NW Pacific Ocean. However, the ^{240}Pu/^{239}Pu atom ratios in the surface sediment from the NW Pacific Ocean varied with the sampling locations. As a consequence, this study will provide the information that the water mass along with the current plays a key role in driving the distribution of Pu and in transporting Pu from the PPGs to the far eastern marginal sea in the NW Pacific Ocean.

1.   INTRODUCTION

Plutonium in the marine environment consists mainly of four isotopes: ^{238}Pu ($t_{1/2}$=87.74 a), ^{239}Pu ($t_{1/2}$=2.4119 × 10^4 a), ^{240}Pu ($t_{1/2}$=6.563 × 10^3 a), ^{241}Pu ($t_{1/2}$ = 14.4 a), of which ^{239}Pu and ^{240}Pu are the most important isotopes because of their long half-lives and high abundance. Extensive studies of plutonium isotopes were carried out to evaluate contamination, to understand biogeochemical processes in the water column and to identify the sources of this radionuclide in the northwest (NW) Pacific Ocean [1–6]. Consequently, the major source of plutonium in seawater and sediment in the Northwest Pacific Ocean has been known from the nuclear weapons tests carried out at the Marshall Islands from 1946 to 1958 (global and local fallout), and at Novaya Zemlya Island in the Arctic in the late 1950s and the early 1960s (global fallout) [7]. Furthermore, the North Equatorial Current (NEC) and Kuroshio Current (KC) have been thought to play an important role in transporting the Pu from the PPGs [2, 4] to the far eastern marginal seas including the East Sea/the Sea of Japan and East China Sea. Nevertheless, the overall processes are not well understood because most studies were conducted over small areas and an insufficient number of samples were taken.The atom ratio of ^{240}Pu/^{239}Pu is dependent on the test series, i.e., the weapon's design and explosion yield [8]. The average atom ratios of ^{240}Pu/^{239}Pu from global fallout are 0.176 ± 0.014 to 0.180 ± 0.014 [9, 10]. The elevated ^{240}Pu/^{239}Pu atom ratios (0.21–0.32) were found in soil samples, in seawater and in sediment from the NW Pacific Ocean [3, 11, 12]. Therefore, the ^{240}Pu/^{239}Pu atom ratio is a powerful tool to identify the sources of Pu and to be applied for tracing water masses with the clarification of the transport processes in the ocean. In this study we demonstrate the characteristics of the ^{240}Pu/^{239}Pu atom ratio in the water column and in the surface sediment from the NW Pacific Ocean. The results we describe here provide a synthesis of information on the origin of Pu isotopes in the NW Pacific Ocean and contribute to a better understanding of transport processes in the region.
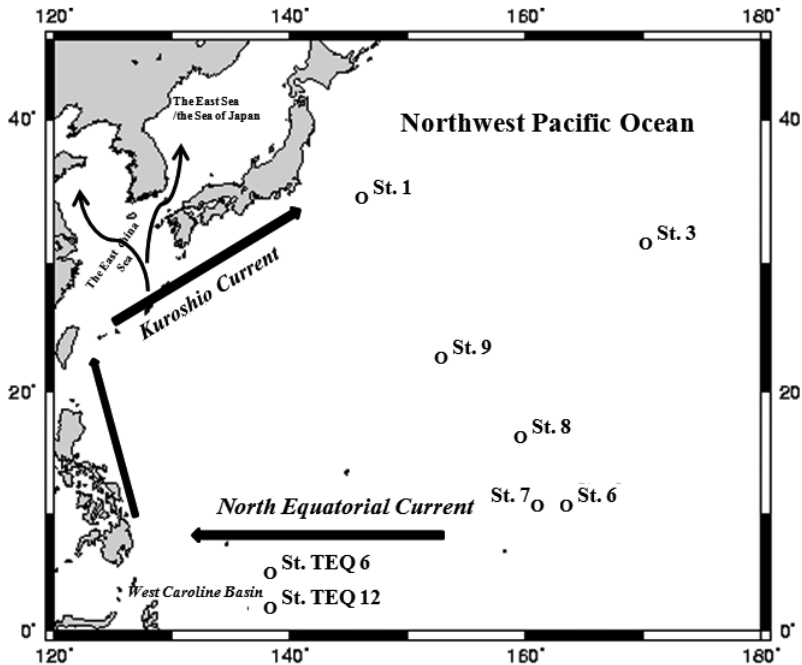
Fig. 1. Seawater and sediment sampling stations from the Northwest Pacific Ocean.

2. METHOD AND MATERIALS

The full details pertaining to this cruise, and the procedures used for processing seawater and sediment samples, and for the analysis of plutonium, are given elsewhere [1, 3, 13–16]. Seawater samples examined in this study were collected using a large volume seawater sampler (500 L 'Gerard Ewing' fiberglass) in 1997 from the NW Pacific Ocean during the IAEA'97 expedition conducted by the International Atomic Energy Agency's Marine Environment Laboratory (IAEA–MEL) in Monaco as a part of the WOMARS (Worldwide Marine Radioactivity Studies) project.

Bottom sediment core samples were collected using a box corer (Ocean Instruments BX640, $40 \times 40 \times 60$ cm) at stations 1, 6, 8, and 9 in the NW Pacific (Fig. 1). Furthermore, two additional bottom sediment samples (TEQ 6 and TEQ 12) were collected from the West Caroline Basin in the West Pacific Ocean in the 1992 expedition conducted by the Korea Ocean Research and Development Institute (KORDI) as a part of the TOGA (Tropical Ocean and Global Atmosphere) project.

3. RESULTS AND DISCUSSION

3.1. Distribution of ^{240}Pu/ ^{239}Pu in the seawater from the NW Pacific Ocean

The results of the atom ratio of ^{240}Pu/^{239}Pu in the seawater collected in the NW Pacific Ocean are presented in Fig. 2. The ^{240}Pu/^{239}Pu atom ratios in the seawater varied from 0.212 ± 0.011 to 0.262 ± 0.008, with a mean of 0.236 at St. 1, from 0.206 ± 0.006 to 0.261 ± 0.008, with a mean of 0.236 at St. 3, from 0.206 ± 0.014 to 0.281 ± 0.008, with a mean of 0.236 at St. 7, from 0.207 ± 0.004 to 0.278 ± 0.008, with a mean of 0.226 at St. 8, respectively. The results are similar to previous studies conducted in the NW Pacific Ocean: 0.24 in the East Sea/the Sea of Japan and Yellow Sea [4], 0.234 from the Sagami Bay [17], 0.242 in the South China Sea [5], 0.204 to 0.260 in the East Sea/the Sea of Japan [18], 0.235 to 0.249 in Rokkasho, Aomori, in Japan [19]. The atom ratios of ^{240}Pu/ ^{239}Pu observed in this study show significantly higher values than the global fallout ratios (0.176 to 0.180), and also these values are higher than those found in the water column in the Northeast Atlantic Ocean [15]. The atom ratios of ^{240}Pu/^{239}Pu from the close-in fallout originating from the US nuclear weapons tests in the early 1950s in the Pacific Proving Grounds (PPGs) in the Marshall Islands have been reported as 0.34–0.36 [5, 11, 20, 21]. Therefore, such high atom ratios shown in the water column in the NW Pacific Ocean indicate that the significant amounts of plutonium isotopes existing in the seawater were contributed by the close-in fallout transported from the Enewetak and Bikini Atolls.

The atom ratios of ^{240}Pu/^{239}Pu in the water column showed the lower values near the surface and tend to increase with depth. Our findings in the NW Pacific water column are different from those observed in the East Sea/the Sea of Japan [4, 6]. In their results, even though the atom ratios of ^{240}Pu/^{239}Pu were higher than that of global fallout, there is no notable variation with depth. However, Buesseler [11] reported similar results in the NW Pacific Ocean to those we obtained, ie., lower atom ratios of ^{240}Pu/^{239}Pu in the surface water and higher ratios in the bottom water (there is no available data in the mid-depth from his results). This might be due to a difference of hydrodynamic condition between marginal seas (East Sea/the Sea of Japan) and the open ocean in the NW Pacific. Since Pu was introduced into the Pacific Ocean mainly by two pulse injections into the seawater in the early 1950s (close-in fallout) with a higher ^{240}Pu/^{239}Pu atom ratio and in the early 1960s (global fallout) with a lower ^{240}Pu/^{239}Pu atom ratio, the ^{240}Pu/^{239}Pu atom ratio in the water column is in a transient state and its ratio should change according to oceanographic, geochemical and biological processes that occur in the water column.

Seoung and Yoon [22] have reported that the large scale vertical mixing due to winter convection occurred easily in the north central East Sea/ the Sea of Japan [4], leading to homogeneity in their results; no variations of ^{240}Pu/^{239}Pu atom ratios were observed.
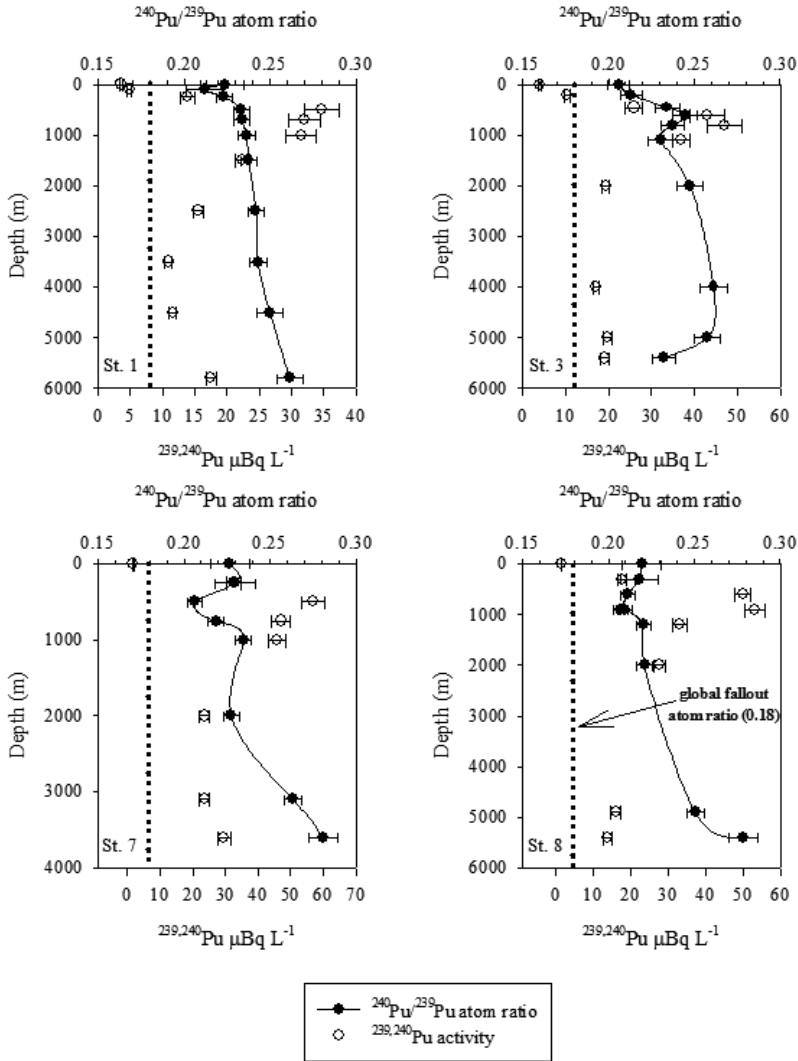
Fig. 2 The atom ratios of $^{240}Pu/^{239}Pu$ in the water column of the Northwest Pacific Ocean (dotted line indicates the mean atom ratio of $^{240}Pu/^{239}Pu$ of global fallout, 0.18).

Although a vertical migration of plutonium is dependent upon the presence of particles because of its particle affinity, most of the plutonium isotopes of the total inventory are still in the water column in the NW Pacific Ocean [1, 3].

Therefore, the specific features of $^{240}Pu/^{239}Pu$ in the water column shown in this study might reflect two pulse injections and the ratios could change with time and with depth by mixing and/or by diffusion in the water column. As a consequence,

the elevated [240]Pu/[239]Pu atom ratio in the deeper water may indicate the presence of enhanced plutonium injection in the early 1950s.

3.2. Evaluation of the relative contribution from the global fallout and the close-in fallout

To evaluate the relative contribution from the global fallout and the close-in fallout, several studies have been attempted to estimate their contributions on the basis of the [240]Pu/[239]Pu atom ratios using a simple mixing model [3, 6, 9, 23, 24] in the seawater and sediment in the NW Pacific.

$$\frac{\text{Pu}_\text{C}(\text{close} - \text{in fallout})}{\text{Pu}_\text{G}(\text{global fallout})} = \frac{R_G - R}{R - R_C} \frac{(1 + 3.68 R_C)}{(1 + 3.68 R_G)}$$

and

$$(\text{Pu activity \%})_\text{C} + (\text{Pu activity \%})_\text{G} = 100$$

where R represents the [240]Pu/[239]Pu atom ratio of the seawater sample observed in this study, R_C represents the [240]Pu/[239]Pu atom ratio from the close-in fallout and R_G represents the [240]Pu/[239]Pu atom ratio of global fallout. The [240]Pu/[239]Pu atom ratio of 0.36 [20] observed at Bikini Atoll is introduced as the representative value of the close-in fallout, and the [240]Pu/[239]Pu atom ratio for global fallout is 0.18 [21]. The results showed that the [239,240]Pu contributed from the close-in fallout source increased with depth, with ranges from 23 to 54% at St. 1, from 19 to 53% at St. 3, from 19 to 64% at St. 7, and from 20 to 63% at St. 8, respectively. These results are comparable to previous estimations [6, 24] in the marginal seas from the NW Pacific Ocean.

4. [240]Pu/ [239]Pu IN SURFACE SEDIMENT FROM THE NW PACIFIC OCEAN

The [240]Pu/ [239]Pu atom ratios in the surface sediment in the NW Pacific Ocean ranged from 0.175 ± 0.002 to 0.287 ± 0.008. As expected from the previous studies [3, 12], the atom ratio of [240]Pu/[239]Pu collected near the PPGs (at St. 8) was significantly higher than the global fallout ratio. However, in the surface sediment collected from St. 9 which is located in the north of PPGs, the [240]Pu/[239]Pu atom ratio decreased slightly (0.199 ± 0.013). St. 1 located in the most northern part of NW Pacific in this study presented the lowest [240]Pu/ [239]Pu atom ratio (0.175 ± 0.002) which is consistent with that of the global fallout ratio [9, 10]. In the West Caroline Basin in the West Pacific Ocean, the [240]Pu/[239]Pu atom ratios are 0.217 ± 0.012 at St. TEQ 6 and 0.183 ± 0.011 at St. TEQ 12, respectively. The distribution of the [240]Pu/ [239]Pu atom ratios in the surface sediments of the NW Pacific shown in this study may be

explained by the water mass movement along with the currents in the NW Pacific Ocean. In the equatorial region, the North Equatorial Current (NEC), is the dominant circulation current which flows westward in the southern boundary of the survey area (PPGs) and on reaching the island of Honshu, its western boundary current becomes the Kuroshio Current [1, 25]. Taking into account this current system and the distribution of the $^{240}Pu/$ ^{239}Pu atom ratios in the surface sediment in the NW Pacific Ocean, the movement of plutonium could be described. Since Enewetak and Bikini Atolls are located within the North Equatorial Current (NEC), the close-in fallout with higher $^{240}Pu/$ ^{239}Pu atom ratio would have travelled westward and fed into the Kuroshio Current (KC) off the Philippines and then turned north flowing along the Japanese islands towards the east [4]. This could also explain that the $^{240}Pu/$ ^{239}Pu atom ratio in the TEQ 6 is different from that observed in the TEQ 12, even though the distance between the two sampling sites is relatively close compared to other stations. While the St. TEQ 6 is located within the NEC, the St. TEQ 12 is located within the Equatorial Count Current (ECC).

5.   CONCLUSIONS

(a)   The atom ratios of $^{240}Pu/^{239}Pu$ observed in the seawater of NW Pacific were considerably higher than the global fallout ratios.
(b)   The high atom ratios shown in the water column in the NW Pacific Ocean were attributable to the close-in fallout transported from the Enewetak and Bikini Atolls.
(c)   The $^{239,240}Pu$ contributed from the close-in fallout source in the NW Pacific increased with water depth, with ranges from 19% to 64%. And the elevated $^{240}Pu/^{239}Pu$ atom ratio in the deeper water may indicate the presence of enhanced plutonium injection in the early 1950s.
(d)   While the atom ratio of $^{240}Pu/^{239}Pu$ in the surface sediment collected near the PPGs was significantly higher than the global fallout ratio, the lowest $^{240}Pu/^{239}Pu$ atom ratio was found in the most northern part of NW Pacific.
(e)   The distribution of the $^{240}Pu/^{239}Pu$ atom ratios in the surface sediments of the NW Pacific could be explained by the water mass movement along with the currents such as the NEC, the KC and the ECC.

REFERENCES

[1]   POVINEC, P.P., et al., IAEA'97 expedition to the NW Pacific Ocean — results of oceanographic and radionuclide investigations of the water column, Deep-Sea Res. II **50** (2003) 2607–2637.

[2]   LEE, S.-H., et al., Distribution of plutonium and americium in the marginal seas of the Northwest Pacific Ocean, Deep-Sea Res. II **50** (2003) 2727–2750.

[3]   LEE, S-H., et al., Distribution and inventories of ^{90}Sr, ^{137}Cs, ^{241}Am and Pu isotopes in sediments of the Northwest Pacific Ocean, Marine Geology **216** (2005) 249–263.

[4]   KIM, C.K., et al., Plutonium isotopes in seas around the Korean Peninsula, Sci. Total Environ. **318** (2004) 197–209.

[5]   YAMADA, M., ZHENG, J., WANG., ^{137}Cs, $^{239+240}$Pu and ^{240}Pu/^{239}Pu atom ratios in the surface waters of the western North Pacific Ocean, eastern Indian Ocean and their adjacent seas, Sci. Total Environ. **366** (2006) 242–252.

[6]   YAMADA, M., ZHENG, J., WANG, Z.L., Temporal variation of ^{240}Pu/^{239}Pu atom ratio and $^{239+240}$Pu inventory in water columns of the Japan Sea, Sci. Total Environ. **408** (2010) 5951–5957.

[7]   LIVINGSTON, H.D, POVICEN, P.P., ITO, T., TOGAWA, O., "The behaviour of plutonium in the Pacific Ocean", Plutonium in the Environment (KUDO, A., Ed.), Elsevier, Amsterdam (2001) 267

[8]   WARNEKE, T., CROUDACE, I.W., WARWICK, P.E., TAYLOR, R.N., A new ground-level fallout record of uranium and plutonium isotopes for northern temperate latitudes, Earth Planet. Sci. Lett. **203** (2002) 1047–1057.

[9]   KREY, P.W., et al., "Mass isotopic composition of global fallout Pu in soils", Transuranium Nuclides in the Environment, Proc. Int. Symp. on Transuranium Nuclides in the Environment, Proceedings Series, IAEA, Vienna (1976) 671.

[10]   KELLEY, J.M., BOND, L.A., BEASLEY, T.M., Global distribution of Pu isotopes and ^{237}Np, Sci. Total Environ. **237–238** (1999) 483–500.

[11]   BUESSELER, K.O., The isotope signature of fallout plutonium in the North Pacific, J. Environ. Radioact. **36** (1997) 69–83.

[12]   MURAMATSU, Y., et al., Measurement of ^{240}Pu/^{239}Pu isotopic ratios in soil from the Marshall Islands using ICP-MS, Sci. Total Environ. **278** (2001) 151–159.

[13]   MOON, D.S., Accumulation of anthropogenic and natural radionuclides in the bottom sediments of the Northwest Pacific Ocean, Deep-Sea Res. II **50** (2003) 2649–2673.

[14]   WYSE, E.J., LEE, S.H., LA ROSA, J., POVINEC, P.P., DE MORA, S.J., ICP-sector field mass spectrometry analysis of plutonium isotopes: Recognizing and resolving potential interferences, J. Anal. At. Spectrom. **16** (2001) 1107–1111.

[15]   LEE, S.H., et al., Determination of plutonium isotopes in seawater samples by Semiconductor Alpha Spectrometry, ICP-MS and AMS techniques, J. Radioanal. Nucl. Chem. **282** (2009) 831–835

[16]   LA ROSA, J., et al., Recent developments in the analysis of transuranics (Np, Pu, Am) in seawater, J. Radioanal. Nucl. Chem. **263** (2005) 427–436.

[17]   YAMADA, M., ZHENG, J., WANG, Z.L. ^{240}Pu/^{239}Pu atom ratios in seawater from Sagami Bay, western Northwest Pacific Ocean: Sources and scavenging, J. Environ. Radioact. **98** (2007) 274–284.

[18]   YAMADA, M., ZHENG, J., Determination of ^{240}Pu/^{239}Pu atom ratio in coastal sur-
       face seawaters from the western North Pacific Ocean and Japan Sea, Appl. Radiat.
       Isot. **66** (2008) 103–107.

[19]   OIKAWA, S., et al., Plutonium isotopes concentration in seawater and bottom sedi-
       ment off the Pacific coast of Aomori sea area during 1991–2005, J. Environ. Radio-
       act. **102** (2011) 302–310.

[20]   DIAMOND, H., et al., Heavy isotope abundances in 'Mike' thermonuclear device,
       Phys. Rev. **119** (1960) 2000–2004.

[21]   KOIDE, M., BERTINE, K.K., CHOW, T.J., GOLDBERG, E.D., The ^{240}Pu/^{239}Pu ra-
       tio, a potential geochronometer, Earth Planet. Sci. Lett. **72** (1985) 1–8.

[22]   SEUNG, Y.-H., YOON, J.-H., Some features of winter convection in the Japan Sea,
       J. Oceanogr. **51** (1995) 61–73.

[23]   WANG, Z.-L., YAMADA, M., Plutonium activities and ^{240}Pu/^{239}Pu atom ratios in
       sediment cores from the East China Sea and Okinawa Trough: Sources and invento-
       ries, Earth Planet. Sci. Lett. **233** (2005) 441–453.

[24]   DONG, W., ZHENG, J., GUO, Q., YAMADA, M., PAN., Characterization of pluto-
       nium in deep-sea sediments of the Sulu and South China Seas, J. Environ. Radioact.
       101 (2010) 622–629.

[25]   WIJFFELS, S.E., et al., Multiple deep gyres of the western North Pacific: A WOCE
       section along 149°E, J. Geophys. Res. **103** (1998) 12985.

NEW RESIN FOR THE SELECTIVE EXTRACTION OF [129]I

A. BOMBARD, S. HAPPEL
TrisKem International,
Bruz, France

A. ZULAUF
NUKEM Technologies GmbH,
Alzenau, Germany

R. STRENG
Radiochemistry, Department of Chemistry,
Philipps-University Marburg,
Marburg, Germany

Abstract

[129]I is an ideal tracer of the marine environment. It has been used for some years particularly in the northeast Atlantic, Nordic seas and Arctic to determine its distribution after its discharges from La Hague and Sellafield reprocessing plants. Various methods for [129]I determination exist. A new resin selective for iodine has been developed, characterized and tested on environmental samples. In order to allow [129]I determination and to obtain accurate and precise results, the samples have to pass a number of sample preparation steps; among these steps are chemical separation and purification. The results of the analysis of seawater samples are presented.

1.   INTRODUCTION

[129]I with a half-life of $16.1(7) \times 10^6$ a (100% β^- decay to [129]Xe, $E_{\beta,max}$: 190.8 keV [1]) is being used as a tracer in the environment [2–4] and particularly in the marine environment [5–7]. Different methods can be used for its determination: NAA [2], AMS [5, 6], ICP-MS [4], γ-X-spectrometry [8] and ß-spectrometry [9]. For most of these methods, a chemical extraction of the iodine/iodide species is performed previous to its measurement. Different schemes are used depending on the type of matrices and the oxidation degree of the iodine, among which liquid–liquid extraction with CCl_4 followed by back extraction in reducing aqueous solutions [4, 6], use of anion exchange resins [2, 3].

An extraction chromatographic resin primarily designed for [36]Cl determination, the so-called CL Resin (TrisKem International SAS, France), was used throughout

523

the experiments. This resin is based on an extraction system selective for noble metals as platinum group elements (PGE) and Ag over a wide range of acid concentrations. The selectivity for halogenides is introduced by loading the CL Resin with silver cations. Halogenide separation is then obtained by elution with suitable complexing agents. Zulauf et al. [10] showed that SCN⁻ and NaOH aqueous solutions were efficient in maintaining ^{129}I retained on the resin while they were eluting all chloride initially loaded. The authors had tested the CL Resin for various environmental matrices, but not for seawater. This paper investigates the use of this resin for iodide extraction and separation from seawater samples followed by its measurement by liquid scintillation counting.

2.   EXPERIMENTAL

2.1.   Reagents and apparatus

All reagents used were analytical grade; 18 MΩ deionized water was used throughout all experiments. CL resin was supplied by TrisKem International and was used as received without further purification. 2 mL of soaked resin were packed into empty columns (TrisKem International). ProSafe HC liquid scintillation cocktail (Meridian Biotechnologies Ltd, UK) was used. LSC measurements were performed using a TriCarb 1600TR (Packard, USA). Seawater samples (taken from the North Sea coast near Nord Beveland, The Netherlands) were spiked with ^{36}Cl and ^{129}I standards, as well as 5 mL aliquots of all reagents used for elutions and rinses, to allow yield determination in all obtained fractions. 5 mL samples of seawater were adjusted as indicated in the procedure section and loaded onto Ag⁺ loaded CL Resin.

2.2.   Procedure

The standard procedure described by Zulauf [10] consists in loading the resin with 20 mg Ag⁺ dissolved in 2 mL1M H_2SO_4 and allowing it to stand for 30 minutes up to 1 hour. The sample, preferably equally adjusted to 1M H_2SO_4, is then loaded on the Ag⁺ loaded CL resin, which is then rinsed with ultrapure water in order to remove traces of acid, as well as potential interferents and matrix elements. Chlorides are eluted with 5mL SCN⁻ solution; the last traces of chlorides are removed with 10 mL 1% NaOH solution. Additionally, it was shown by Zulauf [10] that this rinse increases the iodide yields considerably. Iodides are finally eluted with 5 mL Na_2S solution.

Different load conditions as described below were tested. Chlorine being the main component of seawater (average of 20 g per L), its chemical behaviour was monitored by addition of a ^{36}Cl standard solution in order to detect any interference with ^{129}I separation (cross contamination of the iodide fraction). ^{129}I was added for yield determination and detection of an eventual breakthrough of iodide during

sample load. 3 replicates were performed for each load condition and each radionuclide, ^{129}I and ^{36}Cl. 5 mL of each eluate fraction were mixed with 15 mL liquid scintillation cocktail and measured by LSC for 30 minutes.

Experiment A: CL Resin was loaded with 20mg Ag^+ dissolved in 2 mL 1M H_2SO_4. After allowing it to stand for at least 30 min, seawater samples adjusted to 1M H_2SO_4 were loaded on the resin which was then rinsed with 10 mL ultra-pure water. The resin was further rinsed with 5 mL 0.1M SCN^- and 10 mL 1% NaOH to elute chlorides. Iodide was eluted with 5 mL 0.35M Na_2S.
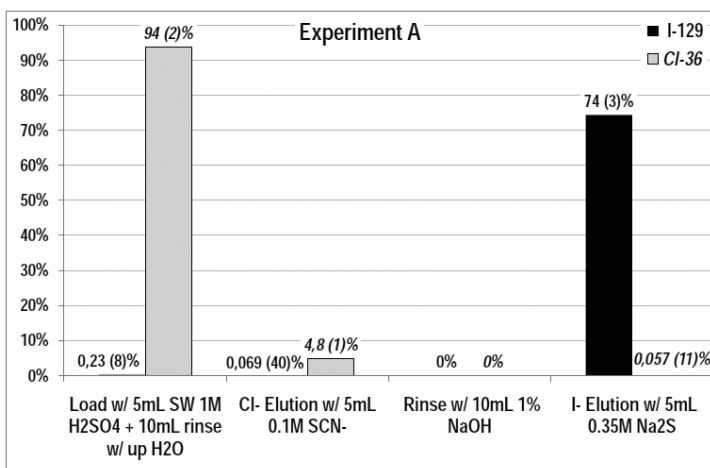
FIG.1. Results of elution study for experiment A.
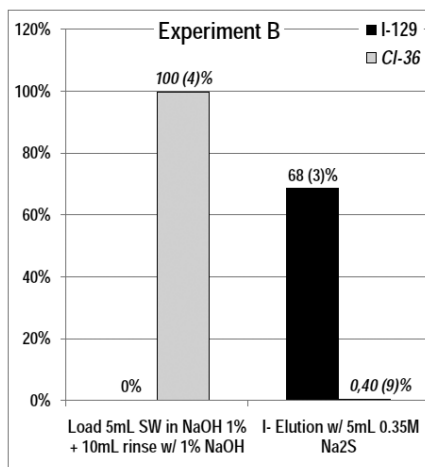
FIG.2. Results of elution study for experiment B.
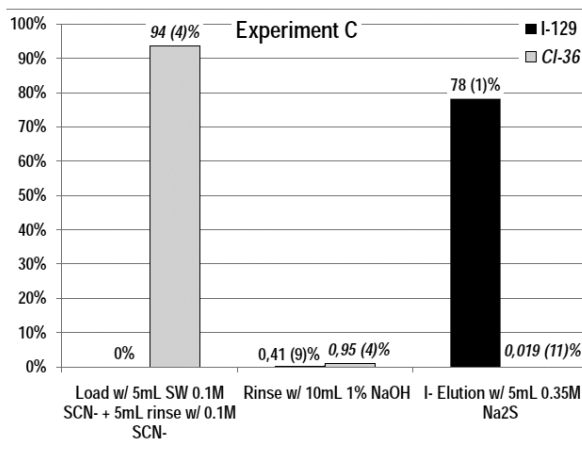
FIG.3. Results of elution study for experiment C.
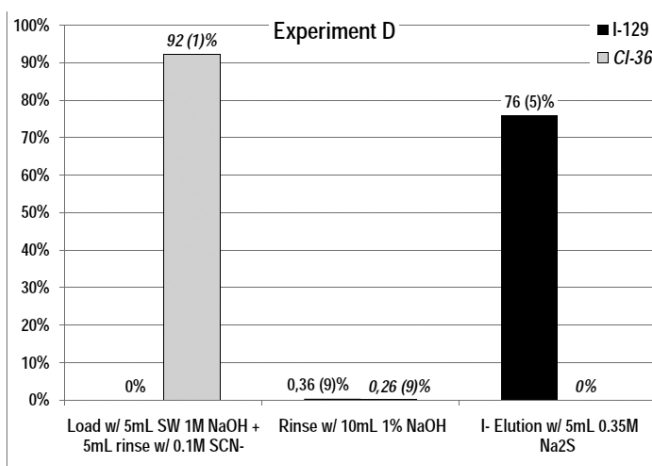
FIG.4. Results of elution study for experiment D.

Experiment B: CL Resin was loaded with 20 mg Ag$^+$ dissolved in 2 mL 1M H$_2$SO$_4$. After allowing it to stand for at least 30 min, the resin was rinsed with 10 mL ultra-pure water, then with 5 mL 0.1M SCN$^-$. Seawater samples adjusted to 1% NaOH were then loaded onto the resin. The resin was then rinsed with 10 mL 1% NaOH for chloride removal and iodide was finally eluted with 5 mL 0.35M Na$_2$S.

Experiment C: CL Resin was loaded with 20 mg Ag$^+$ dissolved in 2 mL 1M H$_2$SO$_4$. After allowing it to stand for at least 30 min, the resin was rinsed with 5 mL ultra-pure water. Seawater samples adjusted to 0.1M SCN$^-$ were loaded onto

the resin. The resin was rinsed with 5 mL 0.1M SCN$^-$ and 10 mL 1% NaOH to elute chlorides. Iodide was eluted with 5 mL 0.35M Na$_2$S.

Experiment D: CL Resin was loaded with 20mg Ag$^+$ dissolved in 2 mL 1M H$_2$SO$_4$. After allowing it to stand for at least 30 min, seawater samples adjusted to 1M NaOH were loaded on the resin which was rinsed with 5 mL 0.1M SCN$^-$ and 10mL 1% NaOH to elute chlorides. Iodide was eluted with 5 mL 0.35M Na$_2$S.

3.   RESULTS AND DISCUSSION

Figs 1 to 4 show the results obtained for experiments A to D. For all experiments, the ^{129}I yields were between 70% to 80%. No ^{129}I was detected in the other fractions (loads or rinses) indicating that no iodide break-through took place, extraction was thus quantitative. Accordingly, either the volume or the S^{2-} concentration of the employed elution step — 5mL 0.35M Na$_2$S — was not sufficient to obtain a quantitative iodide elution, other than described by Zulauf and al. [10, 11] who obtained quantitative recoveries on the different environmental matrices tested; it should, however, be taken into consideration that the authors analysed samples with considerably lower matrix content such as tab water, effluents and 250 mg samples of soil, concrete and filters [11].

Chloride was recovered with a yield between 94–100% in the load or rinse fractions for all experiments. No chloride was found in the iodide fraction. The presence of very high concentrations of chloride did thus not interfere the iodide uptake. For experiment D, the rinse with 0.1M SCN$^-$ was necessary to elute remaining chloride. Previous experiments had shown that without this rinsing step, chloride would have remained fixed on the resin and would have been co-eluted with the iodide fraction.

Seawater samples that were adjusted to 1% and 1M NaOH showed a significant white precipitate that clogged the top frit of the resin, slowing down the flow rate. However, this problem can easily be overcome by filtering the seawater sample before sample loading.

For experiments B, C and D, a black precipitate appeared in the eluted iodide fraction, assumed to be AgS. This behaviour had been observed for seawater sample load solutions with volumes smaller than 5mL as well.

Experiment A also allowed the estimation of the CL Resins capacity for chloride, assuming an average chloride content of 20 g chloride per L of seawater. The capacity found was in the order of 7 mg chloride/g of CL Resin, with is in agreement with Zulauf et al. [10].

The preparation of the column, loading with Ag$^+$ and allowing to stand took about 1h30. The preconditioning, load, rinse and ^{129}I elution took about 2 hours. The iodide eluate was directly mixed with 15 mL of liquid scintillation cocktail. For these experiments, the counting time was 30 minutes.

4. CONCLUSION

The experiments performed indicate the possibility of using CL Resin for the separation of ^{129}I from very salt rich aqueous samples such as seawater. The elution volume and/or the concentration of the sodium sulphide solution used for iodide elution requires more investigation in order to evaluate which minimum volume (or concentration) would be needed to obtain quantitative iodide recovery. The large amounts of chloride present in the samples did not interfere with iodide$^-$ uptake. The overall experiment from Ag$^+$ loading to end of LSC counting took no more than 4 hours with a ^{129}I recovery of 70 to 80%, making this method suitable for emergency measurement, as well as iodide isolation for current determination. Experiments are currently being performed with 20 mL seawater samples on 2 mL columns.

REFERENCES

[1]   LABORATOIRE NATIONAL HENRI BECQUEREL, Recommended Data, Table of radionuclides, accessed 24 March 2011, http://www.nucleide.org/DDEP_WG/DDEPdata.htm.

[2]   SZIDAT, S., et al., Status and Trends of Iodine-129, Abundances in the European Environment, P–4a–229, accessed 24 March 2011, http://www.irpa.net/irpa10/cdrom/00084.pdf.

[3]   SZIDAT, S., et al., Iodine-129: Sample preparation, quality control and analyses of pre-nuclear materials and of natural waters from Lower Saxony, Germany, Nucl. Instr. and Meth. in Phys. Res. **172** (2000) 699–710.

[4]   BIENVENU, P.H., BROCHARD, E., EXCOFFIER, E., PICCIONE, M., Determination of iodine 129 by ICP-QMS in environmental samples, Can. J. of Anal. Sci. Spectrosc. **49** 6 (2004) 423–428.

[5]   HOU, X., DAHLGAARD, H., NIELSEN, S.P., "Application of ^{129}I as A Oceanographic Tracer", Radioactivity in the Environment, Proc. 2nd Int. Conf. Nice, 2005, Norwegian Radiation Protection Authority (2005) 448–451.

[6]   EDMONDS, H., Tracer Application of Anthropogenic Iodine-129 in the North Atlantic Ocean, PhD Thesis, Massachusetts Institute of Technology, Cambridge (1997).

[7]   ALFIMOV, V., ALDAHAN, A., POSSNERT, G., WINSOR, P., Anthropogenic iodine–129 in seawater along a transect from the Norwegian coastal current to the North Pole, Mar. Pollut. Bull. **49** (2004) 1097–1104.

[8]   FRECHOU, C., et al., Direct γ-X-spectrometry with experimental self-absorption correction, J. Environ. Radioact. **70** (2003) 43–59.

[9]   KABAI, E., VAJDA, N., GACA, P., Simultaneous determination of radioactive halogen isotopes and ^{99}Tc, Czechoslov. J. Phys. **53** Suppl. 1 (2003) A181–A188.

[10]   ZULAUF, A., HAPPEL, S., MOKILI, M.B., BOMBARD, A., JUNGCLAS, H., Characterization of an extraction chromatographic resin for the separation and determination of ^{36}Cl and ^{129}I, J. Radioanal. Nucl. Chem. **268** 2 (2010) 539–546.

[11]   ZULAUF, A., et al. 'Characterisation of a Cl- and I- selective resin', Presentation at the TrisKem International users group meeting, 14/09/2010, Chester (UK).

IAEA
International Atomic Energy Agency

Where to order IAEA publications

In the following countries IAEA publications may be purchased from the sources listed below, or from major local booksellers. Payment may be made in local currency or with UNESCO coupons.

AUSTRALIA
DA Information Services, 648 Whitehorse Road, MITCHAM 3132
Telephone: +61 3 9210 7777 • Fax: +61 3 9210 7788
Email: service@dadirect.com.au • Web site: http://www.dadirect.com.au

BELGIUM
Jean de Lannoy, avenue du Roi 202, B-1190 Brussels
Telephone: +32 2 538 43 08 • Fax: +32 2 538 08 41
Email: jean.de.lannoy@infoboard.be • Web site: http://www.jean-de-lannoy.be

CANADA
Bernan Associates, 4501 Forbes Blvd, Suite 200, Lanham, MD 20706-4346, USA
Telephone: 1-800-865-3457 • Fax: 1-800-865-3450
Email: customercare@bernan.com • Web site: http://www.bernan.com

Renouf Publishing Company Ltd., 1-5369 Canotek Rd., Ottawa, Ontario, K1J 9J3
Telephone: +613 745 2665 • Fax: +613 745 7660
Email: order.dept@renoufbooks.com • Web site: http://www.renoufbooks.com

CHINA
IAEA Publications in Chinese: China Nuclear Energy Industry Corporation, Translation Section, P.O. Box 2103, Beijing

CZECH REPUBLIC
Suweco CZ, S.R.O., Klecakova 347, 180 21 Praha 9
Telephone: +420 26603 5364 • Fax: +420 28482 1646
Email: nakup@suweco.cz • Web site: http://www.suweco.cz

FINLAND
Akateeminen Kirjakauppa, PO BOX 128 (Keskuskatu 1), FIN-00101 Helsinki
Telephone: +358 9 121 41 • Fax: +358 9 121 4450
Email: akatilaus@akateeminen.com • Web site: http://www.akateeminen.com

FRANCE
Form-Edit, 5, rue Janssen, P.O. Box 25, F-75921 Paris Cedex 19
Telephone: +33 1 42 01 49 49 • Fax: +33 1 42 01 90 90
Email: formedit@formedit.fr • Web site: http://www. formedit.fr

Lavoisier SAS, 145 rue de Provigny, 94236 Cachan Cedex
Telephone: + 33 1 47 40 67 02 • Fax +33 1 47 40 67 02
Email: romuald.verrier@lavoisier.fr • Web site: http://www.lavoisier.fr

GERMANY
UNO-Verlag, Vertriebs- und Verlags GmbH, Am Hofgarten 10, D-53113 Bonn
Telephone: + 49 228 94 90 20 • Fax: +49 228 94 90 20 or +49 228 94 90 222
Email: bestellung@uno-verlag.de • Web site: http://www.uno-verlag.de

HUNGARY
Librotrade Ltd., Book Import, P.O. Box 126, H-1656 Budapest
Telephone: +36 1 257 7777 • Fax: +36 1 257 7472 • Email: books@librotrade.hu

INDIA
Allied Publishers Group, 1st Floor, Dubash House, 15, J. N. Heredia Marg, Ballard Estate, Mumbai 400 001,
Telephone: +91 22 22617926/27 • Fax: +91 22 22617928
Email: alliedpl@vsnl.com • Web site: http://www.alliedpublishers.com

Bookwell, 2/72, Nirankari Colony, Delhi 110009
Telephone: +91 11 23268786, +91 11 23257264 • Fax: +91 11 23281315
Email: bookwell@vsnl.net

ITALY
Libreria Scientifica Dott. Lucio di Biasio "AEIOU", Via Coronelli 6, I-20146 Milan
Telephone: +39 02 48 95 45 52 or 48 95 45 62 • Fax: +39 02 48 95 45 48
Email: info@libreriaaeiou.eu • Website: www.libreriaaeiou.eu

The International Symposium on Isotope Hydrology, Marine Ecosystems and Climate Change Studies was held from 27 March to 1 April 2011 in Monaco, to commemorate the fiftieth anniversary of the establishment of the IAEA laboratory in the Principality of Monaco. The symposium was jointly organized by the IAEA Water Resources Programme and the IAEA Environment Laboratories. The event also represented the thirteenth edition of the quadrennial Symposium on isotope hydrology and water resources management, which has been regularly organized by the IAEA since 1963. The technical sessions covered aspects related to the use and application of isotope tools in a broad spectrum of scientific disciplines through invited talks, oral and poster presentations and workshops. The five technical sessions covered the following topics: (a) the role of isotopes in understanding and modelling climate change, marine ecosystems and water cycles (b) carbon dioxide sequestration and related aspects of the carbon cycle (c) isotopes and radionuclides in the marine environment, (d) groundwater assessments of large aquifers and (e) analytical methods and instrumentation. These proceedings contain the presentations made at the symposium.

Water Resources Programme

Environment Programme

INTERNATIONAL ATOMIC ENERGY AGENCY
VIENNA